EMERGING INFECTIOUS DISEASES®

CDC
Centers for Disease Control and Prevention

Vectorborne Infections

February 2022

P. R. Morley Horder, designer (1870–1944); J. Starkie Gardner Ltd, fabricator (years active 1884–1976). *Gilded Vectors of Disease*, 1912. Gilded bronze and iron railings. 10.2 in x 10.6 in/26 cm x 27 cm. Images courtesy of Library & Archives Service, London School of Hygiene & Tropical Medicine, London, United Kingdom.

EMERGING INFECTIOUS DISEASES®

Emerging Infectious Diseases is published monthly by the Centers for Disease Control and Prevention, 1600 Clifton Rd NE, Mailstop H16-2, Atlanta, GA 30329-4027, USA. Telephone 404-639-1960; email, eideditor@cdc.gov

EMERGING INFECTIOUS DISEASES®

Vectorborne Infections **February 2022**

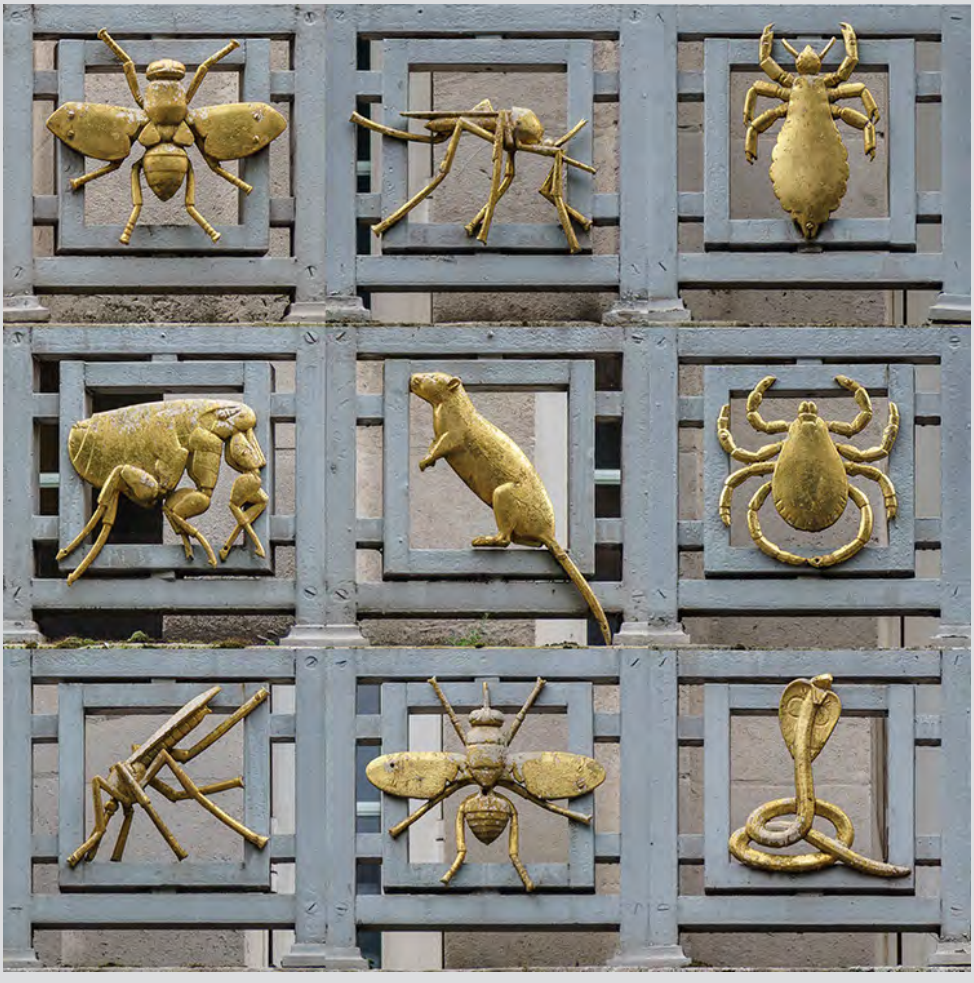

On the Cover

P. R. Morley Horder, designer (1870–1944); J. Starkie Gardner Ltd., fabricator (years active 1884–1976). *Gilded Vectors of Disease*, 1912. Gilded bronze and iron railings. 10.2 in x 10.6 in/26 cm x 27 cm. Images courtesy of Library & Archives Service, London School of Hygiene & Tropical Medicine, London, United Kingdom.

About the Cover p. 495

Perspective

Synopses

Medscape EDUCATION ACTIVITY

EMERGING INFECTIOUS DISEASES®
February 2022

Research

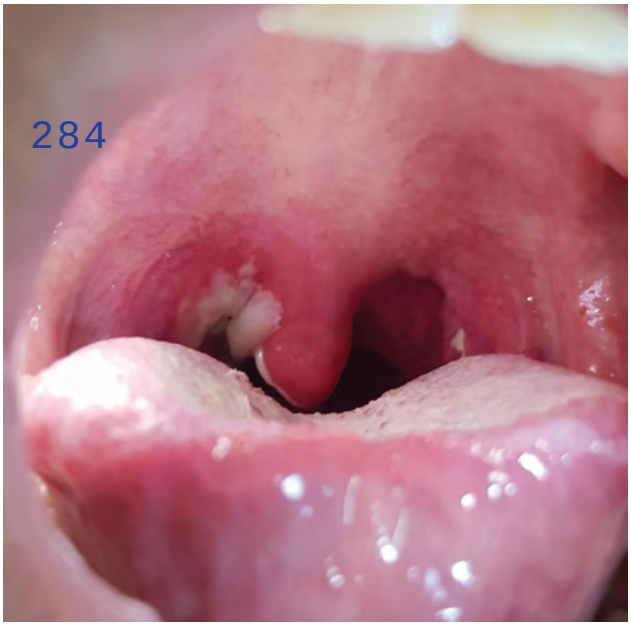

Dispatches

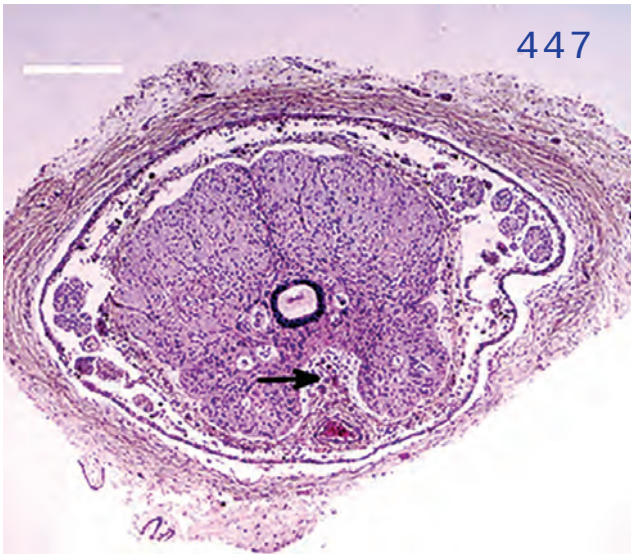

EMERGING INFECTIOUS DISEASES®
February 2022

Research Letters

Comment Letters

Books and Media

About the Cover

Etymologia

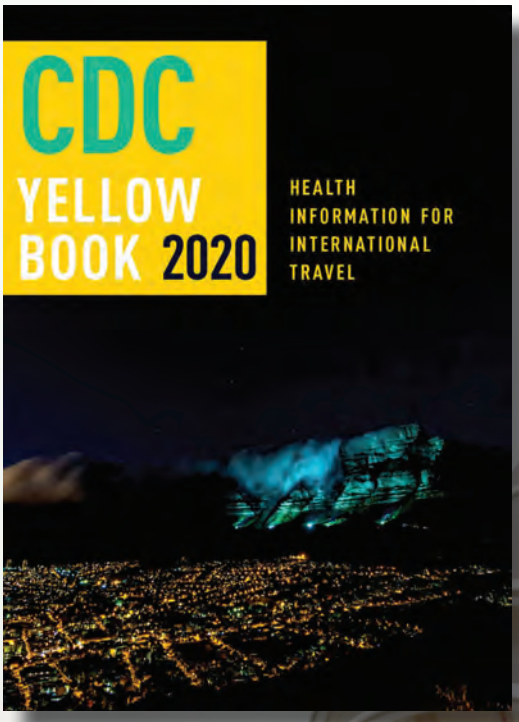

Available Now
Yellow Book 2020

The fully revised and updated CDC Yellow Book 2020: Health Information for International Travel codifies the US government's most current health guidelines and information for clinicians advising international travelers, including pretravel vaccine recommendations, destination-specific health advice, and easy-to-reference maps, tables, and charts.

ISBN: 978-0-19-006597-3 | $115.00 | May 2019 | Hardback | 720 pages

ISBN: 978-0-19-092893-3 | $55.00 | May 2019 | Paperback | 687 pages

Yellow Book 2020 includes important travel medicine updates

- **The latest information on emerging infectious disease threats, such as Zika, Ebola, and henipaviruses**
- **Considerations for treating infectious diseases in the face of increasing antimicrobial resistance**
- **Legal issues facing clinicians who provide travel health care**
- **Special considerations for unique types of travel, such as wilderness expeditions, work-related travel, and study abroad**

OXFORD
UNIVERSITY PRESS

Order your copy at:
www.oup.com/academic

Viral Interference between Respiratory Viruses

Jocelyne Piret, Guy Boivin

Multiple respiratory viruses can concurrently or sequentially infect the respiratory tract and lead to virus–virus interactions. Infection by a first virus could enhance or reduce infection and replication of a second virus, resulting in positive (additive or synergistic) or negative (antagonistic) interaction. The concept of viral interference has been demonstrated at the cellular, host, and population levels. The mechanisms involved in viral interference have been evaluated in differentiated airway epithelial cells and in animal models susceptible to the respiratory viruses of interest. A likely mechanism is the interferon response that could confer a temporary nonspecific immunity to the host. During the coronavirus disease pandemic, nonpharmacologic interventions have prevented the circulation of most respiratory viruses. Once the sanitary restrictions are lifted, circulation of seasonal respiratory viruses is expected to resume and will offer the opportunity to study their interactions, notably with severe acute respiratory syndrome coronavirus 2.

Several respiratory viruses can circulate during the same period and can concurrently or sequentially infect the respiratory tract, leading to virus–virus interactions. At the host level, the course of infection of 1 virus might be influenced by prior or concurrent infection by another virus. Infection by a first virus could enhance or reduce infection and replication of a second virus, resulting in positive (additive or synergistic) or negative (antagonistic) interaction.

Positive virus–virus interaction corresponds to a co-infection that might result in an increased disease severity and pathogenesis (e.g., severe acute respiratory syndrome coronavirus 2 [SARS-CoV-2] and influenza A[H1N1]pdm09 virus) (*1*). Negative virus–virus interaction can be homologous or heterologous depending on whether the 2 viruses belong to the same family or to different serotypes or families. Homologous virus–virus interaction implies that cross-reactive immunity against a first virus prevents infection with a second virus (e.g., among different influenza subtypes or lineages) (*2*). Heterologous viral interference relies on induction of a nonspecific innate immune response by a first virus that reduces or prevents infection and replication of a second virus (e.g., influenza A virus [IAV] and respiratory syncytial virus [RSV]) (*3*). The type of virus–virus interaction (negative or positive) is probably dependent on the respiratory viruses involved, the timing of each infection, and the interplay between the response of the host to each virus. In this perspective, we focus more specifically on viral interference.

Mechanisms of Negative and Positive Virus–Virus Interactions

The more probable mechanism of negative viral interactions relies on the induction of a transient innate immunity by the interfering virus. Structural components of viruses are sensed by pattern recognition receptors in epithelial and immune cells (Figure) (*4*). This recognition triggers the expression of interferon (IFN)–stimulated genes (ISGs) and type I (i.e., IFN-α/β) and type III (i.e., IFN-λ) IFNs. The IFN-α/β receptor is expressed on most cell types, whereas the IFN-λ receptor is predominantly present on epithelial cells of the gastrointestinal and respiratory tracts. Secreted IFNs bind to receptors present at the surface of infected and neighboring cells to amplify the expression of ISGs. This process leads to an antiviral defense program consisting in the production of effectors that directly inhibit viral replication, as well as cytokines and chemokines.

Induction of ISGs by a first virus might limit infection and replication of a second virus, especially if they show a differential ability to induce an IFN response or different degrees of susceptibility to immune mediators. To evade the immune system, respiratory viruses have developed a series of mechanisms that counteract the induction and antiviral action of IFNs, which might influence the type of virus–virus interactions. Influenza viruses and SARS-CoV-2 have

Author affiliation: Centre de Recherche du Centre Hospitalier Universitaire de Québec–Université Laval, Quebec City, Quebec, Canada

DOI: https://doi.org/10.3201/eid2802.211727

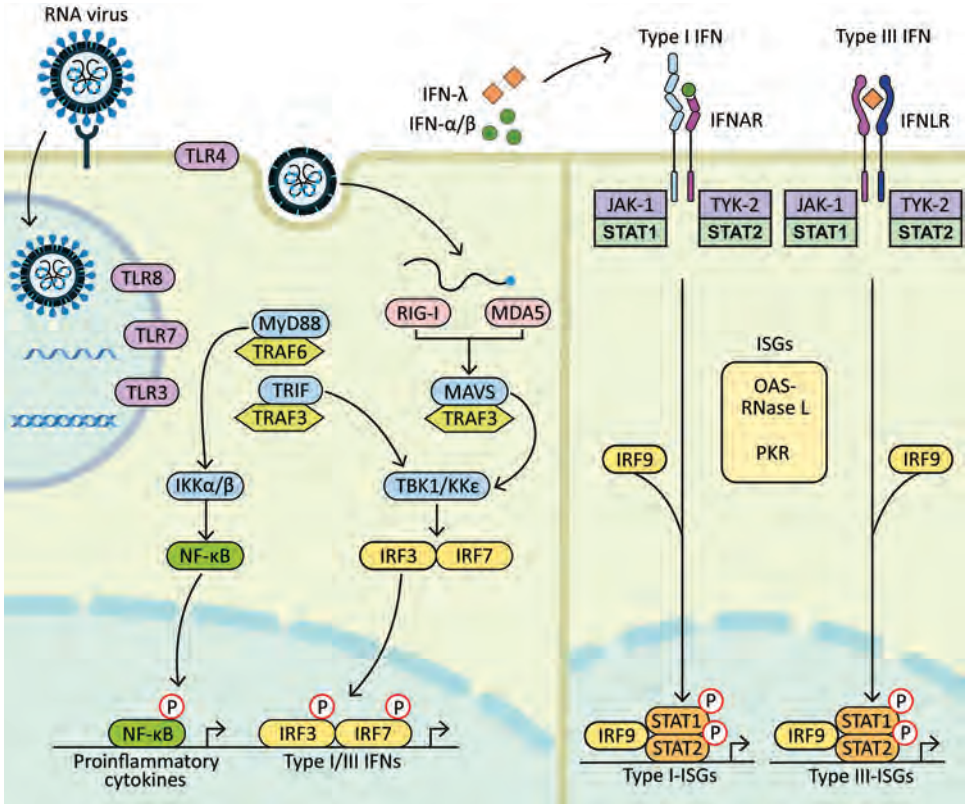

Figure. Diagram showing how components of RNA viruses are recognized by TLRs located at the plasma membrane (TLR4, viral glycoprotein sensing) and in the endosomal compartment (TLR3, double-stranded RNA sensing; TLR7 and TLR8, both single-stranded RNA sensing). Virus replication intermediates and replicated genomes are also recognized by cytosolic RNA sensors, RIG-I, and MDA5. Downstream adaptor proteins, MyD88 for TLR4, TLR7, and TLR8; TRIF for TLR3 and TLR4, and MAVS (for MDA5 and RIG-I) are activated. These activations trigger signaling cascades through TRAF3 and TRAF6; TBK1; and IKKα, IKKβ, and IKKε, which leads to phosphorylation and nuclear translocation of NF-κB, IRF3, and IRF7. These changes result in production of proinflammatory cytokines and type I and type III IFNs. Secreted IFN-α/β and IFN-λ bind to their specific receptors (IFNAR and IFNLR) in infected and neighboring cells. Activation of JAK-1 and TYK-2 leads to phosphorylation of STAT1 and STAT2. After translocation in the nucleus, phosphorylated STAT1 and STAT2 form a complex with IRF9 to induce expression of ISGs, such as OAS-RNase L and PKR, and establishment of an antiviral program. IFN, interferon; IFNAR, IFN-α/β receptor; IFNLR, interferon-λ receptor; IKK, inhibitor of nuclear factor-κB kinase; ISGs, IFN-stimulated genes; IRF, IFN regulatory factor; JAK-1, Janus kinase 1; MAVS, mitochondrial antiviral signaling protein; MDA5, melanoma differentiation-associated gene 5; MyD88, myeloid differentiation factor 88; NF-κB, nuclear factor-κB; OAS, 2′-5′ oligoadenylate synthetase; P, phosphorylated protein; PKR, protein kinase receptor; RNase L, latent endoribonuclease; RIG-I, retinoic acid–inducible gene I; STAT, signal transducer and activator of transcription; TBK 1, TANK binding kinase 1; TLRs, Toll-like receptors; TRAF, tumor necrosis factor receptor-associated factor; TRIF, TIR-domain-containing adapter-inducing IFN-β; TYK-2, tyrosine kinase 2.

developed a broader range of multifaceted strategies to escape IFN induction and signaling than RSV, human metapneumovirus (HMPV) and human rhinovirus (HRV) (Table 1).

At the cellular level, blocking or reduction of cell surface receptors and competition for cellular resources and factors were suggested as mechanisms of negative virus–virus interaction. For instance, the expression of neuraminidase in 293T cells infected with influenza A(H1N1) or A(H3N2) viruses can prevent a subsequent infection with retroviruses pseudotyped with a range of hemagglutinin molecules or a second IAV by removing sialic acid from the cell surface (*9*). Furthermore, replication of RSV was inhibited during co-infection with IAV in MDCK cells by competition for viral protein synthesis and budding from infected cells (*10*).

Other mechanisms leading to reduced or increased viral replication include the down-regulation or up-regulation of the gene promotor of a virus by a gene product of an interfering virus, but these mechanisms have not been yet demonstrated for respiratory viruses. Positive virus–virus interaction could result from the formation of syncytia. For instance, the cell–cell fusion activity of human parainfluenza virus type 2 was shown to enhance the growth of IAV in Vero cells (*11*). Co-infection could also increase disease severity through an overzealous production of IFNs or proinflammatory cytokines or through a reduced secretion of noninflammatory mediators, such as interleukin 10 (*12*).

Viral Interference

The concept of viral interference was described by the research group of Voroshilova in the 1960s (*13*). This group developed live enterovirus vaccines (LEV) consisting of naturally attenuated enteroviruses for the prevention of enteric diseases that are caused by a large number of unrelated enteric pathogens, mainly in children. In addition to LEV's protective effect on

pathogenic enteroviruses, in particular polioviruses, oral administration of LEV in children decreased detection of several unrelated respiratory viruses, such as influenza virus, parainfluenza virus, RSV, HRV, and human adenovirus. This effect was suggestive of a phenomenon of viral interference that could be mediated through the IFN-inducing effect of LEV. During the 1968–1971 fall–winter seasons, large, controlled trials indicated that healthy adults immunized with LEV and oral polio vaccine showed a 2.6-fold and 3.8-fold decrease, respectively, in acute respiratory infections compared with adults who were not immunized (*14*). This study demonstrated that LEV and oral polio vaccine might confer protection against acute viral respiratory infections. However, the interest was dampened by the occurrence of rare cases of circulating vaccine-derived poliovirus (person-to-person transmission) and vaccine-associated paralytic poliomyelitis, a serious side effect.

Advantages and Limitations of Ex Vivo and In Vivo Models

Three-dimensional models consisting of multiple differentiated nasal or bronchial epithelial cells that are polarized and share common characteristics with the human airway epithelium have been commonly used to characterize viral interference (*15*). The permeability and integrity of the reconstituted nasal or bronchial epithelia are ensured by the formation of tight junctions between epithelial cells. Differentiated human nasal or bronchial epithelia are cultured at the air–liquid interface. These epithelia show active beating of cilia and are able to produce mucus. They can be infected by respiratory viruses and secrete IFNs and other immune mediators. Although these ex vivo models are limited by the absence of some immune cells that could contribute to viral interference, they are convenient tools to characterize the mechanisms of virus–virus interaction at the mucosal level.

Animal models that are susceptible to several human respiratory viruses, such as ferrets and golden Syrian hamsters, are also valuable to evaluate the effects of concurrent and sequential viral infections on disease severity, immune response and the mechanisms of virus–virus interaction at the host level (*16*). However, the immune response against human respiratory viruses and the mechanisms of immune evasion might differ between animal models and humans, which constitutes a potential limitation.

Potential Interferences between Respiratory Viruses

A series of potential interferences between different respiratory viruses are demonstrated in epidemiologic studies and at the host level (Table 2). In some cases, the mechanisms involved in viral interference were

Table 1. Evasion mechanisms of human respiratory viruses to type I interferon*

Virus	Viral proteins interfering with interferon induction and signaling	Reference
Human rhinovirus	IFN induction: VPg interferes with viral RNA recognition by RNA sensors; 2A protease reduces cap-dependent translation of cellular mRNA; 2A and 3C proteases cleave MAVS. IFN signaling: 3C protease inhibits activation of antiviral protein complexes.	(*5*)
Human metapneumovirus	IFN induction: G interferes with TLR4 signaling; SH inhibits NF-κB signaling; M2.2 protein interferes with MAVS and inhibits IRF7 phosphorylation. IFN signaling: SH prevents STAT1 phosphorylation.	(*6*)
Respiratory syncytial virus	IFN induction: NS1 inhibits IRF3 phosphorylation, inhibits TRIM25-mediated RIG-I ubiquitination; NS2 binds to RIG-I and reduces IRF3 activation; G reduces IFN-λ production. IFN signaling: NS1 promotes OASL degradation and inhibits IFNAR1 expression; NS1 and NS2 induce STAT2 degradation.	(*5*)
Influenza virus	IFN induction: NS1 interferes with viral RNA sensing by TLR and RIG-I, binds to viral RNA and reduces RIG-I activation, inhibits TRIM25-mediated RIG-I ubiquitination and prevents the export of cellular mRNA to cytoplasm; PB1-F2 and PB2 interfere with MAVS; PA reduces IRF3 activation; M2 protein interacts with MAVS. IFN signaling: NS1 reduces PKR and OASL activation; HA induces IFNAR1 degradation; SOCS inhibits STAT2; NP and M2 protein interfere with PKR activation.	(*7*)
Severe acute respiratory syndrome coronavirus	IFN induction: NSP14 methylates capped RNA transcripts; NSP15 cleaves 5′-polyuridines from viral RNA; NSP16 and NSP10 methylate viral RNA cap; N protein inhibits TRIM25-mediated RIG-I ubiquitination; NSP3 deubiquitinates cellular substrates (possibly RIG-I) and inhibits IRF3 phosphorylation; ORF9b targets MAVS, TRAF3 and TRAF6 to degradation; M protein impedes TRAF3/TBK1/IKKε complex formation; ORF3b might target MAVS; NSP1 promotes cellular mRNA degradation and prevents host mRNA translation. IFN signaling: ORF3a promotes IFNAR1 degradation; NSP1 decreases STAT1 phosphorylation; ORF6 inhibits nuclear translocation of STAT1.	(*8*)

*G, glycoprotein; HA, hemagglutinin; IFN, interferon; IFNAR1, IFN-α/β receptor 1; IRF, IFN regulatory factor; M, matrix; MAVS, mitochondrial antiviral signaling protein; N, nucleocapsid; NP, nucleocapsid protein; NS, nonstructural; NSP, nonstructural protein, OASL, 2′-5′ oligoadenylate synthetase-ribonuclease L; ORF, open reading frame; PA, polymerase acidic; PB, polymerase basic; PKR, protein kinase receptor; RIG-I, retinoic acid–inducible gene I; SH, viroporin protein; SOCS, suppressor of cytokine signaling; STAT, signal transducer and activator of transcription; TANK, TRAF family member–associated NF-κB activator; TBK1, TANK binding kinase 1; TLR, Toll-like receptor; TRAF, tumor necrosis factor receptor–associated factor; TRIM25, tripartite motif containing 25.

Table 2. Potential viral interferences between respiratory viruses*

Interfering virus	Second virus	Observed effect in patients, animal models, and ex vivo systems	Results and statistical significance	Reference
pH1N1	H3N2	Prevents A(H3N2) shedding in ferret model	No H3N2 virus shedding	(*17*)
	IBV	Prevents or delays IBV shedding in ferret model	Peak delayed by 1.8 d (p = 0.014)	(*17*)
IAV	RSV	Reduced likelihood of co-detection in patients	OR 0.11 (95% CI 0.00–0.92)	(*18*)
		Reduced likelihood of co-detection in patients	OR 0.37 (95% CI 0.24–0.57)	(*19*)
		Prevents or delays RSV shedding in ferret model	Peak delayed by 2 d (p = 0.009)	(*3*)
RSV	HMPV	Reduced likelihood of co-detection in patients	OR 0.27 (95% CI 0.09–0.80)	(*19*)
		Reduces HMPV replication in HAEC model	By 1 or 2 log after 5 d (p<0.05)	(*20*)
HRV	IAV	Reduced likelihood of co-detection in patients	OR 0.06 (95% CI 0.01–0.24)	(*18*)
		Reduced likelihood of co-detection in patients	OR 0.08 (95% CI 0.02–0.30)	(*21*)
		Reduced likelihood of co-detection in patients	OR 0.15 (95% CI 0.04–0.53)	(*22*)
		Reduced likelihood of co-detection in patients	OR 0.16 (95% CI 0.09–0.28)	(*23*)
		Reduces IAV replication in HAEC model	>15-fold after 24 h (p = 0.0002)	(*23*)
RSV	HRV	Reduced infection rate with HRV in patients	8% vs. 14% (p<0.049)	(*24*)
		Reduced likelihood of co-infection in patients	OR 0.17 (95% CI 0.09–0.33)	(*18*)
		TCRI study	OR 0.30 (95% CI 0.22–0.40)	(*25*)
		INSPIRE study	OR 0.18 (95% CI 0.11–0.28)	(*25*)
		MAKI trial	OR 0.34 (95% CI 0.16–0.72)	(*25*)
HRV	SARS-CoV-2	Reduces SARS-CoV-2 replication in HAEC model	By 3 log after 48 h (p = 0.006)	(*26*)
			By 3.5 log after 72 h (p<0.0001)	(*27*)

*HAEC, human airway epithelial cells; HMPV, human metapneumovirus; HRV, human rhinovirus; IAV, influenza A virus; IBV, influenza B virus; INSPIRE, Infant Susceptibility to Pulmonary Infections and Asthma Following RSV Exposure (in a region of the southeastern United States); MAKI, trial on the effects of RSV prophylaxis with palivuzimab in healthy preterm infants in the Netherlands; OR, odds ratio; RSV, respiratory syncytial virus; SARS-CoV-2, severe acute respiratory syndrome coronavirus 2; TCRI, Tennessee Children's Respiratory Initiative.

investigated in differentiated human airway epithelial cells and in animal models.

Influenza Virus Types and Subtypes

Influenza A(H1N1) virus reemerged during 1977 and cocirculated with seasonal influenza A(H3N2) before being replaced by the influenza A(H1N1) pdm09 pandemic virus. During the 1977–78 winter season in Japan, the percentage of children infected with H1N1 virus was lower for those infected shortly before with H3N2 virus than for persons who were not infected with H3N2 virus (59% vs. 91%; p<0.05) in 3 schools in which sequential outbreaks were observed (*28*). In a fourth school in which H3N2 and H1N1 virus outbreaks occurred concurrently, the rates of infection for children who had both viruses was lower than in the first 3 schools (2% vs. 21%, 23%, and 31%; p<0.05 for all). This study suggested that 2 mechanisms are at play in cross-subtype protection (i.e., antibody production during sequential outbreaks and viral interference during a mixed outbreak).

During the 2009–2011 influenza A(H1N1)pdm09 virus pandemic, several countries recorded distinct influenza epidemic peaks. During 2009, only pH1N1 virus circulated during the influenza season (weeks 23–36) in most temperate countries of the southern hemisphere. In contrast, a typical seasonal H3N2 peak (week 33) preceded the first pH1N1 wave (weeks 34–38) in South Africa (*29*). During the same year, a small seasonal H3N2 peak (week 34) occurred before the pH1N1 wave (weeks 44–54) and a subsequent influenza B virus (IBV) peak (week 4 of 2010) in Beijing (*30*).

The temporal patterns of the different influenza epidemic peaks suggests a hierarchy between these viruses. The potential interference between influenza subtypes (pH1N1 and H3N2) and types (pH1N1 and IBV) has been evaluated in a ferret model (*17*). The disease outcome (i.e., shedding of co-infecting viruses in nasal wash specimens) varied with respect to the timing of the first and second infections. When the time interval was <3 days, co-infections occurred in almost all ferrets. Interferences between influenza virus types and subtypes were observed when sequential infections were attempted in an interval ranging from 3 to 7 days (Table 2). For this period, the authors suggested that innate immunity and intrinsic antiviral factors mediated by infection of ferrets with the interfering virus may prevent or delay infection and replication of the second virus (*17*). The pH1N1 virus was the most potent inducer of a protective immunity compared with IBV, but H3N2 virus was the less potent. In ferrets sequentially infected with 2 different IBV lineages, innate immunity and cross-reactive protection mediated by an IFN-γ response were involved (*2*).

IAV and RSV

Surveillance of respiratory viral infections in Norway showed that RSV was less frequently detected during influenza epidemics, suggesting viral interference (*31*). An epidemiologic interference between influenza and RSV was also reported during different winter

seasons in other countries (*32*,*33*). During 2002–2017, it was estimated that RSV circulated an average of 6 weeks before IAV in Victoria, Australia (*19*). During the pH1N1 pandemic, the shift in influenza activity was associated with a change in seasonal RSV activity that further supports viral interference (*34*–*38*). Moreover, the probability of co-detecting both viruses was lower than expected from random associations; odds ratios (ORs) were <1 in 2 studies (Table 2), suggesting a negative interaction between IAV and RSV (*18*,*19*). In the ferret model, infection with pH1N1 virus prevented a subsequent infection with RSV for ≤7 days as assessed by viral shedding in nasal wash specimens (Table 2) (*3*). A first infection with RSV reduced the morbidity (i.e., duration of viral shedding and bodyweight loss) associated with a second challenge with pH1N1 virus, but all ferrets were co-infected. Infection of ferrets with pH1N1 virus induced a higher production of cytokines, chemokines, and immune mediators in the respiratory tract compared with RSV. However, both viruses induced only a low number of cross-reactive IFN-γ–producing cells. These data suggest that innate immune mechanisms might be involved in interference between IAV and RSV.

RSV and HMPV

RSV and HMPV co-circulate during winter and spring and can be co-detected in nasopharyngeal swab specimens of patients. Nevertheless, the type of interaction between these 2 pneumoviruses is controversial. A study reported that the likelihood of co-detecting RSV and HMPV in patients was reduced compared with expected values (OR 0.27, 95% CI 0.09–0.80), suggesting that a viral interference could occur (*19*). Differentiated human lung epithelial cells preinfected with RSV were less permissive to HMPV (Table 2), but the opposite was not detected (*20*). HMPV was more sensitive to IFN-α and IFN-λ than was RSV. IFN-α had a stronger antiviral effect on the 2 viruses compared with IFN-λ. The inhibition of HMPV replication by RSV was partially prevented in human lung adenocarcinoma A549 cells deficient for signal transducer and activator of transcription 1, suggesting that viral interference was partially mediated by the host innate immune response. Furthermore, inhibition of HMPV replication by RSV was also greatly reduced by antibodies against IFN-I and IFN-III.

HRV and IAV

Many studies reported that the 2009 autumn epidemic of HRV might have delayed the circulation of pH1N1 in several countries in Europe (*39*–*41*). During 2014, a higher rate of HRV infections might have affected the subsequent influenza summer peak and even prevented the influenza epidemic in Hong Kong, China (*42*). Asynchronous epidemic peaks of HRV and IAV infections in adult patients were recorded during the 2017–2019 winter seasons at Yale–New Haven Hospital (New Haven, CT, USA) (*23*). Furthermore, co-detection of HRV and IAV was lower than expected from random associations; ORs were <1 in several studies (Table 2), suggesting a negative virus–virus interaction (*18*,*21*–*23*). Although mice do not support the complete replication process of HRV, its inoculation 2 days before IAV reduced the severity of influenza disease (i.e., clinical signs and bodyweight loss) and prevented deaths of animals (*43*). In contrast, HRV was less effective at protecting mice when given concomitantly with IAV. The protective effect of HRV was associated with an early but controlled pulmonary inflammatory response that enabled rapid clearance of IAV. Furthermore, infection of differentiated human airway epithelial cells with HRV protected against subsequent IAV or pH1N1 infection for up to 3 days (Table 2) (*23*). HRV infection induced expression of several ISGs, and blocking the IFN signaling pathways with BX795, an inhibitor of TANK binding kinase 1, restored pH1N1 virus replication.

RSV and HRV

Detection of RSV was associated with a reduced probability of co-detecting HRV in clinical specimens (OR 0.17, 95% CI 0.09–0.80), indicating a negative virus–virus interaction (*18*). A negative interaction between RSV and HRV was consistently observed across diverse disease severity patterns, populations, seasons and geographic regions when analyzing 3 cohorts from the United States and the Netherlands (Table 2) (*25*). The rate of HRV infections was lower in children with recent RSV infection compared with children who were not infected (8% vs. 14%; p<0.049) (*24*). However, the median duration of symptoms was longer in children who were co-infected (that possibly occur outside of temporary immunity window) compared with children who had a single RSV infection (14 days vs. 11 days; p<0.02), suggesting an increased disease severity. Furthermore, HRV infections were more common in infants given immunoprophylaxis (palivizumab) against RSV than in infants who did not receive this drug (70.7% vs. 59.4%; OR 1.65, 95% CI 1.65–2.39) (*25*).

HRV and SARS-CoV-2

In contrast to most respiratory viruses, HRV continued to circulate despite the mitigation measures put in place during the COVID-19 pandemic. HRV is a

nonenveloped virus that is more resistant to hydroalcoholic disinfectant (*44*), and its transmission is not prevented by face masks (*45*). Studies showed that previous infection of human bronchial epithelial cells with HRV impairs replication of SARS-CoV-2 (Table 2), but the opposite was not detected (*26*). HRV triggers induction of several ISGs and blocks SARS-CoV-2 replication (*27*). Inhibition of ISG induction by BX795 abrogates the interference mediated by HRV and enhances the replication rate of SARS-CoV-2.

Interactions between Influenza Virus and SARS-CoV-2

SARS-CoV-2 was shown to trigger a broader up-regulation of ISGs, cytokines and chemokines in the human nasal mucosa than pH1N1 virus (*46*). However, contrarily to influenza virus, SARS-CoV-2 fails to induce an early IFN-I and IFN-III response in human lung tissues, leading to a late and vigorous inflammatory response. Thus, the differential innate immune responses induced by SARS-CoV-2 and influenza virus in the upper and lower respiratory tracts might influence the type of virus–virus interactions, depending on which virus will infect first. Sequential infection of golden Syrian hamsters with pH1N1 and SARS-CoV-2 resulted in lower pulmonary SARS-CoV-2 load, suggesting a reduced replication in this tissue (*1*). In contrast, previous infection with SARS-CoV-2 did not affect pH1N1 load in the lungs compared with a single infection. Lung inflammatory damage and disease severity (i.e., clinical scores and bodyweight loss) were higher in animals infected with both viruses compared with a single virus. In this study, both viruses were inoculated into hamsters 24 hours apart, which might have been too short a time to induce interference. In ferrets first infected with influenza virus, there was a lag of 1–2 days before a nonspecific immune response was elicited and during which a co-infection with a second virus was likely to occur (*17*). Thereafter, the host innate immune response correlates with viral shedding in nasal wash specimens, which peaks at 2–3 days and persists for 5–6 days, corresponding to the window period when viral interference occurs. Thus, further studies are needed to clarify the interactions between SARS-CoV-2 and influenza viruses.

Defective Viral Genomes, a Novel Therapeutic Option Based on Viral Interference

Defective viral genomes (DVGs) are produced during replication of RNA viruses and are believed to play a role in adaptation, viral escape, and persistence (*47*). DVGs have severe genomic truncations/modifications and require a full-length helper virus to replicate. DVGs are packaged, forming virus particles that are biochemically and morphologically similar to standard virus. DVGs might hamper the cytopathic effects induced by a wild-type virus. DVGs also rapidly produce cytopathic effects and interfere with replication of other co-infecting homologous or heterologous viruses. DVGs resulting from influenza virus replication can mediate homologous interference by competing with viral genomes for replication or packaging. DVGs might also mediate heterologous interference through production of IFN-I and IFN-III.

The role of DVGs in viral interference is not clearly established, but it is suggested that they could be used as therapeutic interfering particles against respiratory virus infections. In this respect, a first infection of mice with influenza A–based defective interfering virus, which was derived by a single central deletion from the full-length genomic segment 1 of influenza virus isolate A/PR/8/34 (H1N1), prevented disease caused by a second infection with a heterologous IBV (*48*). Protection against IBV was partially alleviated in mice that did not express a functional type I IFN receptor. Furthermore, a first infection with influenza A–based defective interfering virus also protected mice against a second infection with pneumonia virus, a genetically unrelated respiratory virus (*49*).

Conclusions and Perspectives

Recent viral infections of the respiratory tract might induce a refractory period during which the host is less likely to be infected by another respiratory virus. This viral interference requires closely spaced virus co-exposures, implying that both viruses share common ecologic conditions (e.g., cold weather). Factors that could predict an interference between respiratory viruses include the capacity of the interfering virus to induce a rapid IFN response; the degree of susceptibility of the second virus to immune mediators; the extent to which the different viruses counteract the induction and antiviral effects of IFN; and the differential innate immune response patterns triggered by each viruses in the upper and lower respiratory tracts.

The duration of the refractory period at the host level has not been determined, but might correspond to the period of virus shedding and the associated transient innate immune response. Mathematical models that simulate the co-circulation of seasonal IAV and HRV confirmed that the temporary immunity provided by an IFN response might be sufficient to produce the asynchronous epidemic peaks recorded for these 2 viruses (*12*). At the population level, the

concept of viral interference corresponds to an ecologic phenomenon in which the epidemic caused by one virus delays the start or advances the end of the epidemic caused by another virus. These episodes are difficult to demonstrate because the transmission dynamics of respiratory viruses might be influenced by social behaviors for different age groups. The contact rate between persons might also vary according to different periods of the year, such as during school opening and closing. Furthermore, a large proportion of respiratory infections are asymptomatic and do not require testing, thus, excluding this part of the population from studies. Environmental conditions such as temperature and humidity can be confounding factors for viral interference. Prospective epidemiologic studies enabling detection of multiple respiratory viruses in serial nasopharyngeal swab specimens of participants over several epidemic periods would enable demonstration of viral interference. The type of interaction between respiratory viruses producing distinct epidemic peaks should be then confirmed by evaluating their likelihood of co-detection in patients, as well as the mechanisms involved in ex vivo and in vivo models.

The reappearance of H1N1 virus during 1977 and the 2009–2011 pH1N1 pandemic offered the opportunity to study the epidemiologic interactions between the newly circulating virus and seasonal respiratory viruses in northern and southern hemispheres and thus strengthened the concept of viral interference. During the COVID-19 pandemic, nonpharmacologic interventions have prevented the circulation of most respiratory viruses. Therefore, their potential interactions with SARS-CoV-2 could not be determined in epidemiologic studies, except in some reports at the onset of the pandemic. A systematic review and meta-analysis showed that the most common respiratory viruses co-detected with SARS-CoV-2 were influenza viruses, RSV, and HRV (*50*). Once the sanitary restrictions are lifted, the circulation of seasonal respiratory viruses should resume and different types of interactions are expected to occur.

Mathematical modeling predicting the timing and magnitude of epidemics caused by SARS-CoV-2 and seasonal respiratory viruses might improve public health interventions to protect persons at risk for co-infection through introduction of nonpharmacologic measures, adjustment of vaccine schedules, or use of prophylactic agents. Finally, the interfering and immunostimulatory activities of DVGs make them attractive candidates for development of prophylactic broad-spectrum antiviral drugs or vaccine adjuvant, which would be based on the concept of viral interference (*47*).

This study was supported by a Foundation Grant from the Canadian Institutes of Health Research (no. 148361) to G.B. G.B. is the holder of the Canada research chair on emerging viruses and antiviral resistance.

About the Authors

Dr. Piret is a biologist and a project leader at the Research Center in Infectious Diseases at Laval University, Quebec City, Quebec, Canada. Her primary research interests include pathogenesis of infections caused by herpesviruses and Zika virus, emergence of drug resistance, and interactions between respiratory viruses.

Dr. Boivin is an infectious disease specialist and the head of the virology laboratory at the Research Center in Infectious Diseases at Laval University. His primary research interests include pathogenesis of infections caused by respiratory viruses, as well as development of vaccines, antiviral drugs, and immunomodulatory agents.

References

1. Zhang AJ, Lee AC, Chan JF, Liu F, Li C, Chen Y, et al. Coinfection by severe acute respiratory syndrome coronavirus 2 and influenza A(H1N1)pdm09 virus enhances the severity of pneumonia in golden Syrian hamsters. Clin Infect Dis. 2021;72:e978–92. https://doi.org/10.1093/cid/ciaa1747
2. Laurie KL, Horman W, Carolan LA, Chan KF, Layton D, Bean A, et al. Evidence for viral interference and cross-reactive protective immunity between influenza B virus lineages. J Infect Dis. 2018;217:548–59. https://doi.org/10.1093/infdis/jix509
3. Chan KF, Carolan LA, Korenkov D, Druce J, McCaw J, Reading PC, et al. Investigating viral interference between influenza A virus and human respiratory syncytial virus in a ferret model of infection. J Infect Dis. 2018;218:406–17. https://doi.org/10.1093/infdis/jiy184
4. Schneider WM, Chevillotte MD, Rice CM. Interferon-stimulated genes: a complex web of host defenses. Annu Rev Immunol. 2014;32:513–45. https://doi.org/10.1146/annurev-immunol-032713-120231
5. Kikkert M. Innate immune evasion by human respiratory RNA viruses. J Innate Immun. 2020;12:4–20. https://doi.org/10.1159/000503030
6. Soto JA, Gálvez NM, Benavente FM, Pizarro-Ortega MS, Lay MK, Riedel C, et al. Human metapneumovirus: mechanisms and molecular targets used by the virus to avoid the immune system. Front Immunol. 2018;9:2466. https://doi.org/10.3389/fimmu.2018.02466
7. Li C, Wang T, Zhang Y, Wei F. Evasion mechanisms of the type I interferons responses by influenza A virus. Crit Rev Microbiol. 2020;46:420–32. https://doi.org/10.1080/1040841X.2020.1794791
8. Sa Ribero M, Jouvenet N, Dreux M, Nisole S. Interplay between SARS-CoV-2 and the type I interferon response. PLoS Pathog. 2020;16:e1008737. https://doi.org/10.1371/journal.ppat.1008737
9. Huang IC, Li W, Sui J, Marasco W, Choe H, Farzan M. Influenza A virus neuraminidase limits viral superinfection. J Virol. 2008;82:4834–43. https://doi.org/10.1128/JVI.00079-08

10. Shinjoh M, Omoe K, Saito N, Matsuo N, Nerome K. In vitro growth profiles of respiratory syncytial virus in the presence of influenza virus. Acta Virol. 2000;44:91–7.
11. Goto H, Ihira H, Morishita K, Tsuchiya M, Ohta K, Yumine N, et al. Enhanced growth of influenza A virus by coinfection with human parainfluenza virus type 2. Med Microbiol Immunol (Berl). 2016;205:209–18. https://doi.org/10.1007/s00430-015-0441-y
12. Nickbakhsh S, Mair C, Matthews L, Reeve R, Johnson PCD, Thorburn F, et al. Virus-virus interactions impact the population dynamics of influenza and the common cold. Proc Natl Acad Sci U S A. 2019;116:27142–50. https://doi.org/10.1073/pnas.1911083116
13. Voroshilova MK. Potential use of nonpathogenic enteroviruses for control of human disease. In: Melnick JL, editor. Progress in medical virology. Basel: Karger; 1989. p. 191–202.
14. Chumakov MP, Voroshilova MK, Antsupova AS, Boĭko VM, Blinova MI, Priĭmiagi LS, et al. Live enteroviral vaccines for the emergency nonspecific prevention of mass respiratory diseases during fall-winter epidemics of influenza and acute respiratory diseases [in Russian]. Zh Mikrobiol Epidemiol Immunobiol. 1992;11–12:37–40.
15. Rijsbergen LC, van Dijk LL, Engel MF, de Vries RD, de Swart RL. In vitro modelling of respiratory virus infections in human airway epithelial cells: a systematic review. Front Immunol. 2021;12:683002. https://doi.org/10.3389/fimmu.2021.683002
16. Shou S, Liu M, Yang Y, Kang N, Song Y, Tan D, et al. Animal models for COVID-19: hamsters, mouse, ferret, mink, tree shrew, and non-human primates. Front Microbiol. 2021;12:626553. https://doi.org/10.3389/fmicb.2021.626553
17. Laurie KL, Guarnaccia TA, Carolan LA, Yan AW, Aban M, Petrie S, et al. Interval between infections and viral hierarchy are determinants of viral interference following influenza virus infection in a ferret model. J Infect Dis. 2015;212:1701–10. https://doi.org/10.1093/infdis/jiv260
18. Greer RM, McErlean P, Arden KE, Faux CE, Nitsche A, Lambert SB, et al. Do rhinoviruses reduce the probability of viral co-detection during acute respiratory tract infections? J Clin Virol. 2009;45:10–5. https://doi.org/10.1016/j.jcv.2009.03.008
19. Price OH, Sullivan SG, Sutterby C, Druce J, Carville KS. Using routine testing data to understand circulation patterns of influenza A, respiratory syncytial virus and other respiratory viruses in Victoria, Australia. Epidemiol Infect. 2019;147:e221. https://doi.org/10.1017/S0950268819001055
20. Geiser J, Boivin G, Huang S, Constant S, Kaiser L, Tapparel C, et al. RSV and HMPV infections in 3D tissue cultures: mechanisms involved in virus-host and virus-virus interactions. Viruses. 2021;13:139. https://doi.org/10.3390/v13010139
21. Arden KE, Greer RM, Wang CY, Mackay IM. Genotypic diversity, circulation patterns and co-detections among rhinoviruses in Queensland, 2001. Access Microbiol. 2019;2:acmi000075.
22. Mackay IM, Lambert SB, Faux CE, Arden KE, Nissen MD, Sloots TP, et al. Community-wide, contemporaneous circulation of a broad spectrum of human rhinoviruses in healthy Australian preschool-aged children during a 12-month period. J Infect Dis. 2013;207:1433–41. https://doi.org/10.1093/infdis/jis476
23. Wu A, Mihaylova VT, Landry ML, Foxman EF. Interference between rhinovirus and influenza A virus: a clinical data analysis and experimental infection study. Lancet Microbe. 2020;1:e254–62. https://doi.org/10.1016/S2666-5247(20)30114-2
24. Karppinen S, Toivonen L, Schuez-Havupalo L, Waris M, Peltola V. Interference between respiratory syncytial virus and rhinovirus in respiratory tract infections in children. Clin Microbiol Infect. 2016;22:208.e1–6. https://doi.org/10.1016/j.cmi.2015.10.002
25. Achten NB, Wu P, Bont L, Blanken MO, Gebretsadik T, Chappell JD, et al. Interference between respiratory syncytial virus and human rhinovirus infection in infancy. J Infect Dis. 2017;215:1102–6. https://doi.org/10.1093/infdis/jix031
26. Dee K, Goldfarb DM, Haney J, Amat JA, Herder V, Stewart M, et al. Human rhinovirus infection blocks SARS-CoV-2 replication within the respiratory epithelium: implications for COVID-19 epidemiology. J Infect Dis. 2021;224:31–8. https://doi.org/10.1093/infdis/jiab147
27. Cheemarla NR, Watkins TA, Mihaylova VT, Wang B, Zhao D, Wang G, et al. Dynamic innate immune response determines susceptibility to SARS-CoV-2 infection and early replication kinetics. J Exp Med. 2021;218:e20210583. https://doi.org/10.1084/jem.20210583
28. Sonoguchi T, Naito H, Hara M, Takeuchi Y, Fukumi H. Cross-subtype protection in humans during sequential, overlapping, and/or concurrent epidemics caused by H3N2 and H1N1 influenza viruses. J Infect Dis. 1985;151:81–8. https://doi.org/10.1093/infdis/151.1.81
29. Van Kerkhove MD, Mounts AW. 2009 versus 2010 comparison of influenza activity in southern hemisphere temperate countries. Influenza Other Respir Viruses. 2011;5:375–9. https://doi.org/10.1111/j.1750-2659.2011.00241.x
30. Yang Y, Wang Z, Ren L, Wang W, Vernet G, Paranhos-Baccalà G, et al. Influenza A/H1N1 2009 pandemic and respiratory virus infections, Beijing, 2009–2010. PLoS One. 2012;7:e45807. https://doi.org/10.1371/journal.pone.0045807
31. Anestad G, Vainio K, Hungnes O. Interference between outbreaks of epidemic viruses. Scand J Infect Dis. 2007;39:653–4. https://doi.org/10.1080/00365540701253860
32. Nishimura N, Nishio H, Lee MJ, Uemura K. The clinical features of respiratory syncytial virus: lower respiratory tract infection after upper respiratory tract infection due to influenza virus. Pediatr Int. 2005;47:412–6. https://doi.org/10.1111/j.1442-200x.2005.02099.x
33. van Asten L, Bijkerk P, Fanoy E, van Ginkel A, Suijkerbuijk A, van der Hoek W, et al. Early occurrence of influenza A epidemics coincided with changes in occurrence of other respiratory virus infections. Influenza Other Respir Viruses. 2016;10:14–26. https://doi.org/10.1111/irv.12348
34. Gröndahl B, Ankermann T, von Bismarck P, Rockahr S, Kowalzik F, Gehring S, et al. The 2009 pandemic influenza A(H1N1) coincides with changes in the epidemiology of other viral pathogens causing acute respiratory tract infections in children. Infection. 2014;42:303–8. https://doi.org/10.1007/s15010-013-0545-5
35. Mak GC, Wong AH, Ho WY, Lim W. The impact of pandemic influenza A (H1N1) 2009 on the circulation of respiratory viruses 2009–2011. Influenza Other Respir Viruses. 2012;6:e6–10. https://doi.org/10.1111/j.1750-2659.2011.00323.x
36. Green HK, Ellis J, Galiano M, Watson JM, Pebody RG. Critical care surveillance: insights into the impact of the 2010/11 influenza season relative to the 2009/10 pandemic season in England. Euro Surveill. 2013;18:20499. https://doi.org/10.2807/ese.18.23.20499-en
37. Casalegno JS, Ottmann M, Bouscambert-Duchamp M, Valette M, Morfin F, Lina B. Impact of the 2009 influenza A(H1N1) pandemic wave on the pattern of hibernal respiratory virus epidemics, France, 2009.

Euro Surveill. 2010;15:19485. https://doi.org/10.2807/ese.15.06.19485-en
38. Meningher T, Hindiyeh M, Regev L, Sherbany H, Mendelson E, Mandelboim M. Relationships between A(H1N1)pdm09 influenza infection and infections with other respiratory viruses. Influenza Other Respir Viruses. 2014;8:422–30. https://doi.org/10.1111/irv.12249
39. Ånestad G, Nordbø SA. Virus interference. Did rhinoviruses activity hamper the progress of the 2009 influenza A (H1N1) pandemic in Norway? Med Hypotheses. 2011;77:1132–4. https://doi.org/10.1016/j.mehy.2011.09.021
40. Linde A, Rotzén-Ostlund M, Zweygberg-Wirgart B, Rubinova S, Brytting M. Does viral interference affect spread of influenza? Euro Surveill. 2009;14:19354. https://doi.org/10.2807/ese.14.40.19354-en
41. Casalegno JS, Ottmann M, Duchamp MB, Escuret V, Billaud G, Frobert E, et al. Rhinoviruses delayed the circulation of the pandemic influenza A (H1N1) 2009 virus in France. Clin Microbiol Infect. 2010;16:326–9. https://doi.org/10.1111/j.1469-0691.2010.03167.x
42. Zheng X, Song Z, Li Y, Zhang J, Wang XL. Possible interference between seasonal epidemics of influenza and other respiratory viruses in Hong Kong, 2014–2017. BMC Infect Dis. 2017;17:772. https://doi.org/10.1186/s12879-017-2888-5
43. Gonzalez AJ, Ijezie EC, Balemba OB, Miura TA. Attenuation of influenza A virus disease severity by viral coinfection in a mouse model. J Virol. 2018;92:e00881–18. https://doi.org/10.1128/JVI.00881-18
44. Park S, Michelow IC, Choe YJ. Shifting patterns of respiratory virus activity following social distancing measures for COVID-19 in South Korea. J Infect Dis. 2021;jiab231. https://doi.org/10.1093/infdis/jiab231
45. Leung NH, Chu DK, Shiu EY, Chan KH, McDevitt JJ, Hau BJ, et al. Respiratory virus shedding in exhaled breath and efficacy of face masks. Nat Med. 2020;26:676–80. https://doi.org/10.1038/s41591-020-0843-2
46. Alfi O, Yakirevitch A, Wald O, Wandel O, Izhar U, Oiknine-Djian E, et al. Human nasal and lung tissues infected *ex vivo* with SARS-CoV-2 provide insights into differential tissue-specific and virus-specific innate immune responses in the upper and lower respiratory tract. J Virol. 2021;95:e0013021. https://doi.org/10.1128/JVI.00130-21
47. Vignuzzi M, López CB. Defective viral genomes are key drivers of the virus-host interaction. Nat Microbiol. 2019;4:1075–87. https://doi.org/10.1038/s41564-019-0465-y
48. Scott PD, Meng B, Marriott AC, Easton AJ, Dimmock NJ. Defective interfering influenza A virus protects in vivo against disease caused by a heterologous influenza B virus. J Gen Virol. 2011;92:2122–32. https://doi.org/10.1099/vir.0.034132-0
49. Easton AJ, Scott PD, Edworthy NL, Meng B, Marriott AC, Dimmock NJ. A novel broad-spectrum treatment for respiratory virus infections: influenza-based defective interfering virus provides protection against pneumovirus infection in vivo. Vaccine. 2011;29:2777–84. https://doi.org/10.1016/j.vaccine.2011.01.102
50. Musuuza JS, Watson L, Parmasad V, Putman-Buehler N, Christensen L, Safdar N. Prevalence and outcomes of co-infection and superinfection with SARS-CoV-2 and other pathogens: a systematic review and meta-analysis. PLoS One. 2021;16:e0251170. https://doi.org/10.1371/journal.pone.0251170

Address for correspondence: Guy Boivin, Centre Hospitalier Universitaire de Québec-Université Laval, 2705 Boul. Laurier, R-0709, Quebec City, QC, G1V 4G2, Canada; email: guy.boivin@crchudequebec.ulaval.ca

Novel Clinical Monitoring Approaches for Reemergence of Diphtheria Myocarditis, Vietnam

Ho Quang Chanh, Huynh Trung Trieu, Huynh Ngoc Thien Vuong, Tran Kim Hung, Tu Qui Phan, James Campbell, Caitlin Pley, Sophie Yacoub

Diphtheria is a life-threatening, vaccine-preventable disease caused by toxigenic *Corynebacterium* bacterial species that continues to cause substantial disease and death worldwide, particularly in vulnerable populations. Further outbreaks of vaccine-preventable diseases are forecast because of health service disruptions caused by the coronavirus disease pandemic. Diphtheria causes a spectrum of clinical disease, ranging from cutaneous forms to severe respiratory infections with systemic complications, including cardiac and neurologic. In this synopsis, we describe a case of oropharyngeal diphtheria in a 7-year-old boy in Vietnam who experienced severe myocarditis complications. We also review the cardiac complications of diphtheria and discuss how noninvasive bedside imaging technologies to monitor myocardial function and hemodynamic parameters can help improve the management of this neglected infectious disease.

Diphtheria was once a leading cause of childhood death globally, but cases worldwide have been dramatically reduced over the few past decades by mass vaccination campaigns followed by routine childhood vaccination (*1*). More than 22,000 cases of diphtheria were reported globally in 2019, compared with >97,000 cases in 1980, although both figures are likely to be underestimates (*1*–*3*). However, progress has been grossly uneven; although high-income countries rarely see cases, low- and middle-income countries (LMICs), where the disease remains endemic, frequently grapple with outbreaks (*2*). Annual reported cases have been rising in the past decade, increasing by nearly 5 times during 2010–2019 (Figure 1), likely as a result of improved surveillance and reporting systems, sporadic conflict-associated outbreaks, and other global phenomena such as vaccine hesitancy and migration. Diphtheria is particularly likely to reemerge in settings of conflict or political turmoil, as a result of crowding, inconsistent vaccination, and a lack of public health infrastructure to treat cases and stem further spread (*2*). In recent years, several major outbreaks have occurred in fragile settings, including in Haiti, Venezuela, and Yemen and among Rohingya refugees (*4*–*7*). Vaccination coverage in children has stagnated at ≈86% since 2010 (*2*), and pockets of incomplete vaccination are present in all countries (*3*). The effects of coronavirus disease (COVID-19) on vaccination, case management, and surveillance data quality are not yet known but are likely to reduce vaccination rates even further.

In Vietnam, during 2004–2019, annual cases of diphtheria ranged from 6 to 53 cases and showed a clear increasing trend (*8*). In the first 9 months of 2020, a large outbreak of 198 cases was reported, mostly in the central highlands (*8*). Although the estimated vaccination rate for 3 doses of the combined diphtheria, tetanus toxoid, and pertussis vaccine was ≈96% in 2014, maintaining vaccination coverage in mountainous and remote areas remains a challenge (*9*). The national public health program has been further disrupted by the COVID-19 pandemic. Several vaccination campaigns have been delayed or cancelled because of restrictions and ongoing public fear of COVID-19.

A diagnosis of diphtheria is made on the basis of clinical features, pathogen isolation, and presence of diphtheria toxin or of the *tox* gene (*10*). Severe diphtheria is usually associated with cardiac and neurologic complications because of the high affinity of diphtheria toxin with theses tissues (*11*). Antitoxin is

Author affiliations: Hospital for Tropical Diseases, Ho Chi Minh City, Vietnam (H.Q. Chanh, H.T. Trieu, H.N.T. Vuong, T.K. Hung, T.Q. Phan); Oxford University Clinical Research Unit, Ho Chi Minh City (H.Q. Chanh, H.T. Trieu, J. Campbell, S. Yacoub); University of Cambridge, School of Clinical Medicine, Cambridge, United Kingdom (C. Pley); University of Oxford Centre for Tropical Medicine and Global Health, Oxford, United Kingdom (S. Yacoub)

DOI: https://doi.org/10.3201/eid2802.210555

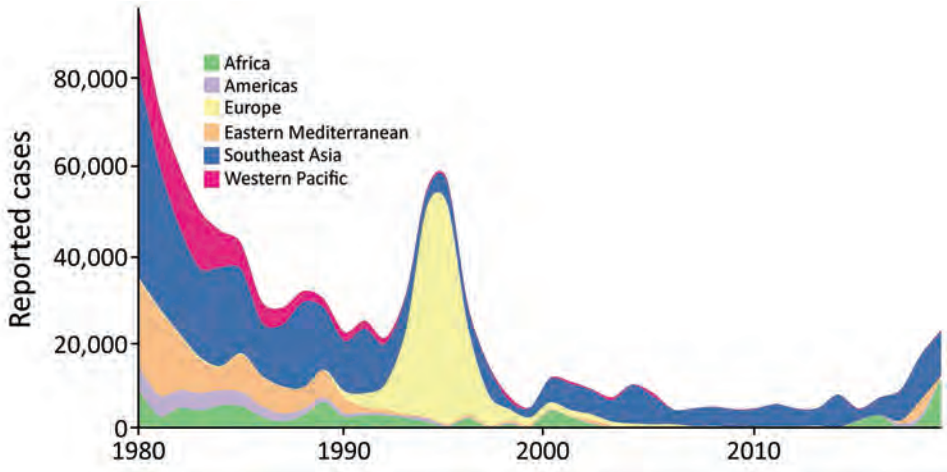

Figure 1. Global and regional epidemiologic trends in reported cases of diphtheria, 1980–2019. Cases shown are those reported to the World Health Organization and the United Nations Children's Fund.

considered the cornerstone of the prevention of severe complications and death and should be readily available. However, a global shortage of diphtheria antitoxin (DAT) is ongoing, which hinders availability in low-resource settings (*12*). In Vietnam, only a few tertiary hospitals have DAT readily available for early treatment. In recent years, the advance in noninvasive bedside monitoring has enabled early detection of deterioration and more timely intervention, which could improve patient outcomes.

In this article, we describe a case referred to our department at the Hospital for Tropical Diseases in Ho Chi Minh City, Vietnam. After late manifestation of severe diphtheria, the case-patient experienced toxin-mediated complications, including diphtheria myocarditis and neuropathy. We review and discuss the cardiac complications of diphtheria, with a particular focus on how noninvasive bedside imaging technologies to monitor myocardial function and hemodynamic parameters can help improve the management of this neglected infectious disease. We also provide results of a literature search for diphtheria myocarditis based on our search strategy and selection criteria (Appendix, https://wwwnc.cdc.gov/EID/article/28/2/21-0555-App1.pdf).

The Case-Patient

In July 2020, a 7-year-old boy was brought a provincial hospital in Kon Tum, a highland area of Vietnam, for a 2-day history of a high fever, poor appetite, sore throat, and a progressively swollen neck. He had no unwell contacts, and the boy's vaccination status was unknown. Clinical examination revealed a swollen neck and pharyngitis with a thick gray pseudomembrane covering the pharynx and tonsils (Figure 2). The patient received a diagnosis of suspected pharyngeal diphtheria and was treated with oral erythromycin (50 mg/kg/d) and prednisolone (5 mg/d). DAT was unavailable. A throat culture yielded *Corynebacterium diphtheriae*. An antibiogram was not available. The Elek test, used to detect the presence of toxigenic *C. diphtheriae* strains, was positive. By day 7 of illness, the patient was afebrile and the pseudomembrane had resolved. His condition deteriorated on day 9 with the onset of chest pain. Cardiac enzymes showed a raised creatinine kinase myocardial band of 60 U/L (reference range 5–25 U/L) and a troponin T level of 3,225.9 pg/mL (reference range <14 pg/mL). An echocardiogram showed normal left ventricular (LV) function and an ejection fraction (EF) of 65.9%. Electrocardiography (ECG) was not performed.

The patient was transferred to our hospital on day 10 with a diagnosis of diphtheria myocarditis. At arrival, he was afebrile, heart rate was 80 beats/min, blood pressure was 85/55 mm Hg, respiratory rate was 24 breaths/min, and oxygen saturation was 98% on room air. No pseudomembrane was visible. Cardiovascular and respiratory examinations were unremarkable. A full blood count revealed a mild leukocytosis of 17.02 k/UL and a neutrophil percentage of 70%. Renal and liver function and coagulation tests were with reference ranges, but troponin I was elevated (14,313.4 pg/mL [reference range <400 pg/mL]). An ECG showed sinus arrhythmia, incomplete right bundle branch block, and QTc prolongation (Figure 3). Cardiac point-of-care ultrasound (POCUS), which was performed early, revealed a mildly reduced EF of 57% and a cardiac output of 3.1 L/min. The result of a repeat throat swab culture was sterile. Because this patient had poor prognostic factors, including presence of a bull neck and cardiac complications, he was given DAT at a dose of 40,000 IU despite the late stage of the illness. We continued him on oral erythromycin.

On day 11, his blood pressure reduced slightly to 80/55 mm Hg, and his heart rate was 90 beats/min. Although the ECG showed sinus rhythm with QTc prolongation (510 ms), POCUS revealed further reduction in EF to 50% and cardiac output to 2.5L/min. We immediately started an infusion of a low dose (3 μg/kg/min) of dobutamine. Troponin I had more than doubled, to 35,705.5 pg/mL (Figure 4). On day 14, the boy became more hemodynamically unstable. We performed serial POCUS to assess the extent of myocardial impairment and guide inotropic support. LV function deteriorated substantially, to an EF of 40% (Figure 4) and cardiac output of 1.54 L/min. ECG showed sinus tachycardia and T-wave inversion (Figure 4). We increased dobutamine to 8 μg/kg/min and added noradrenaline (0.1 μg/kg/min). The need for inotropic support decreased over the next 5 days, and myocardial function improved. His troponin I level normalized on day 21.

On day 39, the patient experienced neurologic symptoms, including dysphagia, dysphonia, and loss of power and sensation in his lower limbs. He subsequently had onset of respiratory distress, requiring intubation for mechanical ventilation on day 47. He gradually recovered and was weaned off the ventilator on day 62. After a week of mobilization and physiotherapy, he was discharged on day 71. At discharge, he still had mild lower limb weakness but was otherwise fully mobile. ECG results were unremarkable, and POCUS showed some residual impairment of LV function (EF of 53% and mild dilation of the left ventricle).

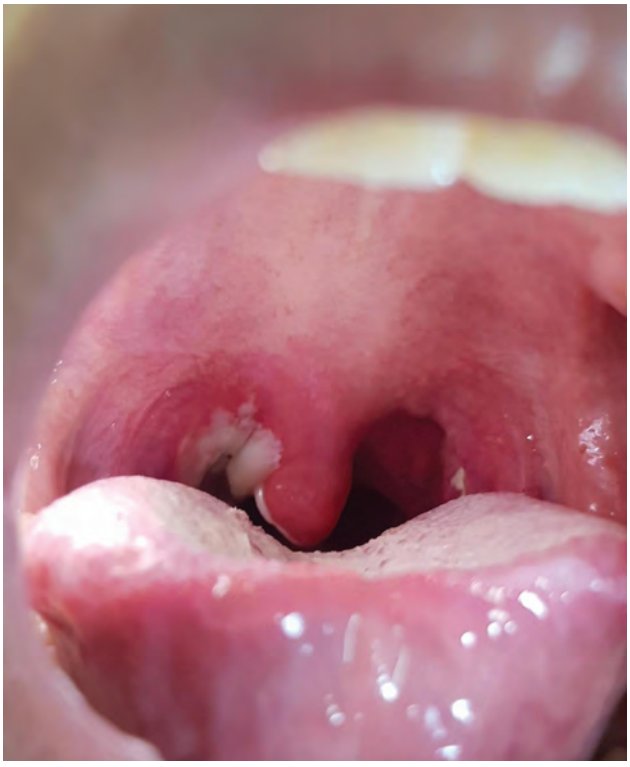

Figure 2. The thick pseudomembrane covering the oropharynx of a 7-year-old boy at admission to a local hospital before his diphtheria myocarditis was diagnosed, Vietnam, 2020.

At a follow-up appointment 2 weeks later, the patient was well, had no cardiac symptoms, and was fully mobile. ECG results were unremarkable, and LV systolic function had improved to 60% (Figure 5), but the left ventricle remained mildly dilated at 4.3 cm.

Diagnosis and Clinical Features of Diphtheria

Corynebacterium spp. are gram-positive, nonmotile rods with a club-like morphology and are aerobic or facultatively anaerobic (*13*). The infectious agents causing diphtheria are toxigenic strains of *C. diphtheriae* and, less commonly, the closely related *C. ulcerans* and *C. pseudotuberculosis*. The World Health Organization laboratory diagnostic criteria require either isolation of *C. diphtheriae* from a clinical specimen or a ≥4-fold rise in antibodies (*10*). The diagnosis should be confirmed by identifying 1 of the 3 species and testing for toxigenicity. The species can be identified with high sensitivity and specificity by using matrix-assisted laser desorption/ionization time-of-flight mass spectrometry. Alternatively, PCR may be used to identify the species and the presence of the *tox* gene. Toxigenicity can be confirmed with the Elek test. Diphtheria can be transmitted through respiratory droplets or direct physical contact with contagious cutaneous lesions (*3*).

Clinical symptoms typically begin 2–5 days after nasopharyngeal infection, and can include sore throat, malaise, cough, hoarse voice, painful swallowing, bloody nasal discharge, and drooling of saliva (*14*). Fever is frequently mild or absent. A gray-white membrane is characteristic, initially covering the tonsils then rapidly spreading to the uvula, soft palate, and posterior wall of the throat. In severe cases, airway obstruction can cause respiratory distress. Systemic disease occurs when diphtheria toxin disseminates in the bloodstream, leading to toxin-mediated damage to the heart, kidneys, and peripheral nerves (*11*). Notably, the heparin-binding epidermal growth factor–like growth factor, which is binding site of the diphtheria toxin, is expressed abundantly on the cell membranes of cardiomyocytes and neurons, enabling the toxic effects of diphtheria in these tissues (*13*). Neurologic disease can involve peripheral polyneuropathy and, less frequently, bulbar palsy.

Once the toxin enters the bloodstream, patients appear toxic, pale, and lethargic. Myocarditis often

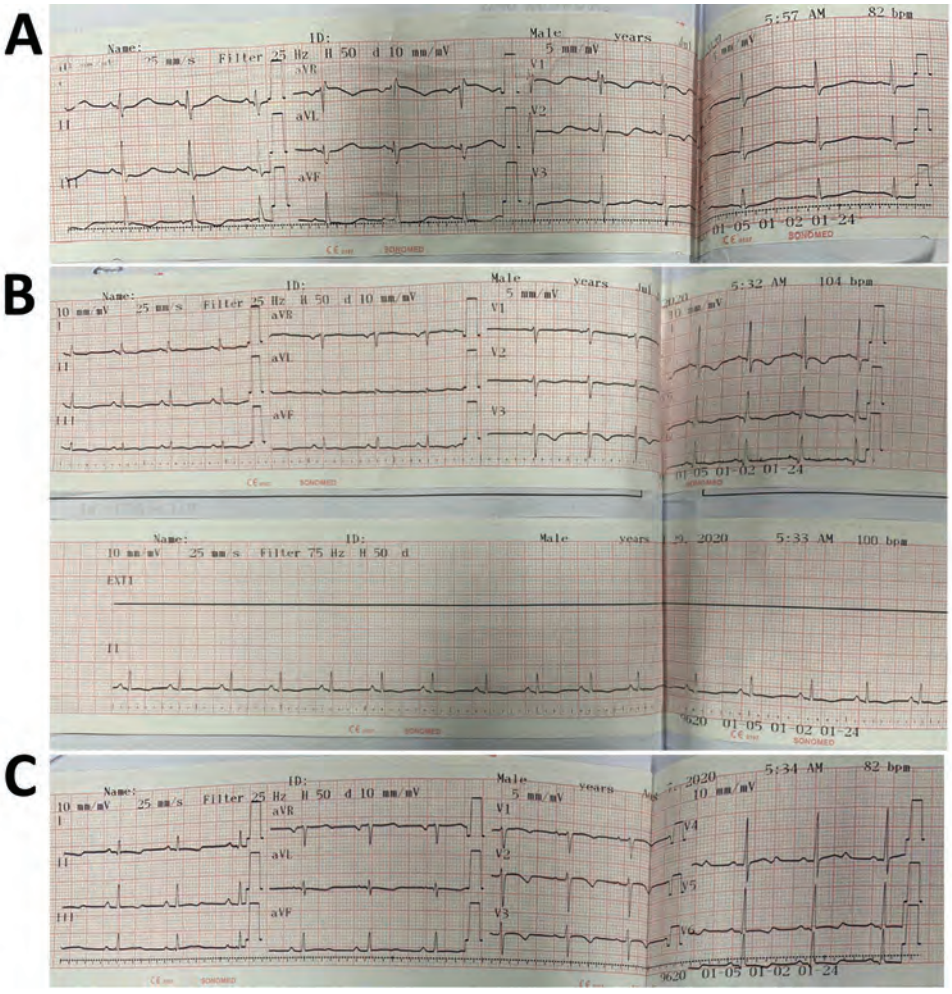

Figure 3. Results of 12-lead electrocardiograms conducted on a 7-year-old boy later diagnosed with diphtheria myocarditis, Vietnam, 2020. A) At hospital admission (day 10 of illness), electrocardiography showed an incomplete right bundle branch block (RSR) in V1–3 with QRS duration of 92 ms), QTc prolongation (519 ms), and ST depression. B) On day 14 of illness, we observed sinus tachycardia with occasional supraventricular premature complexes and T-wave inversion. C) On day 25, we observed widespread T-wave inversion, which persisted even after clinical recovery.

manifests as life-threatening arrhythmias and can be followed by neuritis and paralysis of the limbs, soft palate, and diaphragm, which can persist for weeks to months. Other known complications include otitis media, kidney injury, liver dysfunction, and thrombocytopenia (*13*,*15*). Diphtheria's case-fatality rate ranges from 5% to 17%, but rates have improved with supportive care and DAT (*13*).

Managing diphtheria includes early use of DAT and antibiotics. Mortality rates increase daily with delays in DAT administration, from 4.2% if the disease is treated in the first 2 days to 24% by the fifth day of illness (*12*). A global shortage of DAT persists because of lower demand, resulting in former DAT manufacturers discontinuing production; the shortage is rapidly becoming a public health crisis not only in LMICs but also in high-income settings (*16*). Diphtheria can be treated effectively with several antibiotics, including penicillins, macrolides, oxacillin, clindamycin, rifampin, and tetracycline (*11*). The antibiotics of choice are erythromycin or penicillin for 14 days (*15*). However, resistance to the empirical antibiotics has been reported (*17*,*18*). Patients should be isolated for ≥6 days after the administration of antibiotic therapy or until 2 negative cultures are obtained.

Appropriate supportive care is also important. Tracheotomy is indicated for respiratory distress because of airway obstruction. Steroids can help reduce local inflammation but do not prevent complications (*19*). Patients should still receive primary vaccination if unvaccinated or booster vaccinations after recovery to provide full future protection (*15*).

Cardiac Manifestations

Cardiac complications are common and well documented in diphtheria because of the affinity of the diphtheria toxin for cardiac myocytes and the cardiac conduction system (*20*). Myocarditis is caused by diphtheria toxin–induced degradation of actin filaments, leading to impaired contractile function (*21*). In patients who recover, damaged cardiomyocytes are eventually replaced with fibrotic tissue, which

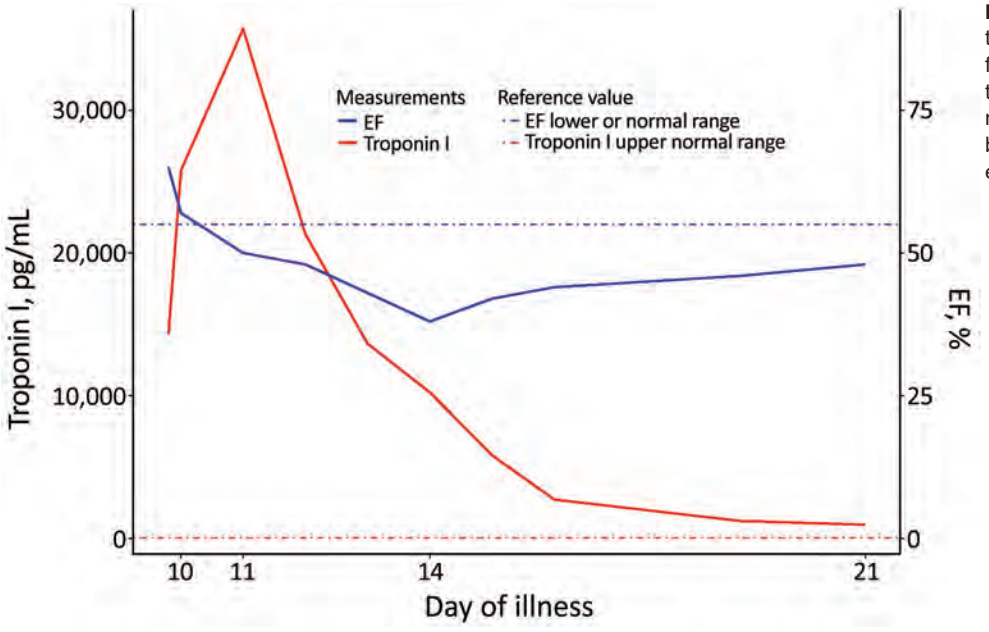

Figure 4. Temporal changes in troponin I levels and ejection fraction measurements during the acute phase of diphtheria myocarditis in a 7-year-old boy, Vietnam, 2020. EF, ejection fraction.

can lead to long-term cardiac sequelae (*13*). Cardiac complications can also occur in patients infected with nontoxigenic strains of *C. diphtheriae* (*22*,*23*).

Cardiac involvement in diphtheria is diverse but most commonly characterized by myocardial dysfunction and arrhythmias and, occasionally, pericarditis and endocarditis (*24*). The presence of a bull neck and the amount of pharyngeal pseudomembrane at admission are potential risk factors for cardiomyopathy (*25*).

Diphtheria myocarditis occurs in 10%–20% of respiratory diphtheria (*13*), although this figure is likely underestimated because cardiac screening is lacking in many endemic settings. Of note, this complication almost exclusively occurs in persons who are unvaccinated or incompletely vaccinated. Myocarditis usually manifests at the end of the second week of infection but in severe infections can manifest earlier (*26*). Diphtheria myocarditis once had a case-fatality rate of 60%–70% (*27*), but recent articles have reported a mortality rate ranging from 0% to 80% (*24*,*25*,*28*–*40*). This large discrepancy can be explained by heterogeneity of diagnostic criteria and immunization status of patients. The utility of modern diagnostic and monitoring methods, such as invasive blood pressure monitoring, continuous ECG monitoring, and point-of-care echocardiography, could also improve diagnosis and management through earlier detection of cardiac dysfunction and subclinical rhythm disturbances. Long-term sequelae in survivors of diphtheria myocarditis are rare, but sudden cardiac death can occur several months after the acute infection, suggesting persistence of a low-grade cardiomyopathy (*28*–*30*).Ventricular ectopics at admission are predictive of poor outcomes. Tachyarrhythmias and bradyarrhythmias are common and can last well into recovery (*28*). We summarized the common features of diphtheria myocarditis from case series, case reports, and observational studies conducted since 1960 (Appendix Tables 2, 3).

Synthesized Findings of Diphtheria Myocarditis Derived from the Literature

Laboratory Biomarkers

Laboratory markers predictive of poor outcome in diphtheria myocarditis include leukocytosis (>25 × 10^9 leukocytes/L [reference range 3.6–11.0 leukocytes]) and elevated aspartate transaminase levels (>80 U/L [reference range 8–33 U/L]) (*24*). Marked elevation of cardiac enzymes is also associated with fulminant cardiac failure (*31*). The troponin I level likely reflects myocardial damage and the severity of the disease; however, the association between troponin I and mortality rates is still unclear (*32*). In our patient, we observed a lag between troponin I levels and EF; as troponin levels began to gradually normalize, EF continued to deteriorate for the next 3 days. Thus, even when active myocardial damage has ceased, myocardial function recovery may take more time, demonstrating the importance of using POCUS in patient monitoring.

ECG Monitoring

ECG abnormalities in diphtheria myocarditis include atrioventricular conduction disturbances, bundle

branch block, ST depression, T-wave inversion, or some combination (*25*,*33*). Prolongation of the QT or PR intervals, sinus arrhythmia, ventricular tachycardia, and supraventricular tachycardia have also been demonstrated (*25*,*33*). Complete heart block is strongly associated with severe disease and higher mortality rates (*25*,*33*). A study recording 24-hour ECGs in severe pediatric diphtheria showed high rates of supraventricular and ventricular ectopic rhythms without evidence of heart failure (*34*). Furthermore, ventricular ectopics on admission were predictive of poor outcomes (*28*). Tachyarrhythmias and bradyarrhythmias are common and can last well into recovery (*28*). Left bundle branch block has been shown to be an independent predictor of long-term risk for death (*35*). Hence, continuous ECG monitoring, where available, should be applied to capture these changes and preempt malignant arrhythmias to improve the overall outcome in patients with severe diphtheria.

Recent advances in medical sensors and data analysis have helped with early diagnosis and close monitoring of patients with critical illness in high-income settings and, more recently, low- and middle-income settings (*36*). These devices hold promise for patients with neglected infections such as diphtheria because of their low cost, noninvasive nature, and potential for sharing findings electronically, thereby enabling remote monitoring in disease outbreak situations (*36*–*38*). An example of this approach is being evaluated for use in treatment of tetanus by applying machine learning techniques to analyze 24-hour ECG waveforms, detected by a novel low-cost wearable patch (*37*). Continuous physiologic monitoring aids in the early detection of deterioration and complications, improving the quality of care. Noninvasive and low-cost devices for continuous physiologic and ECG monitoring would thus be of huge benefit to the clinical management of diphtheria myocarditis and should be considered where available.

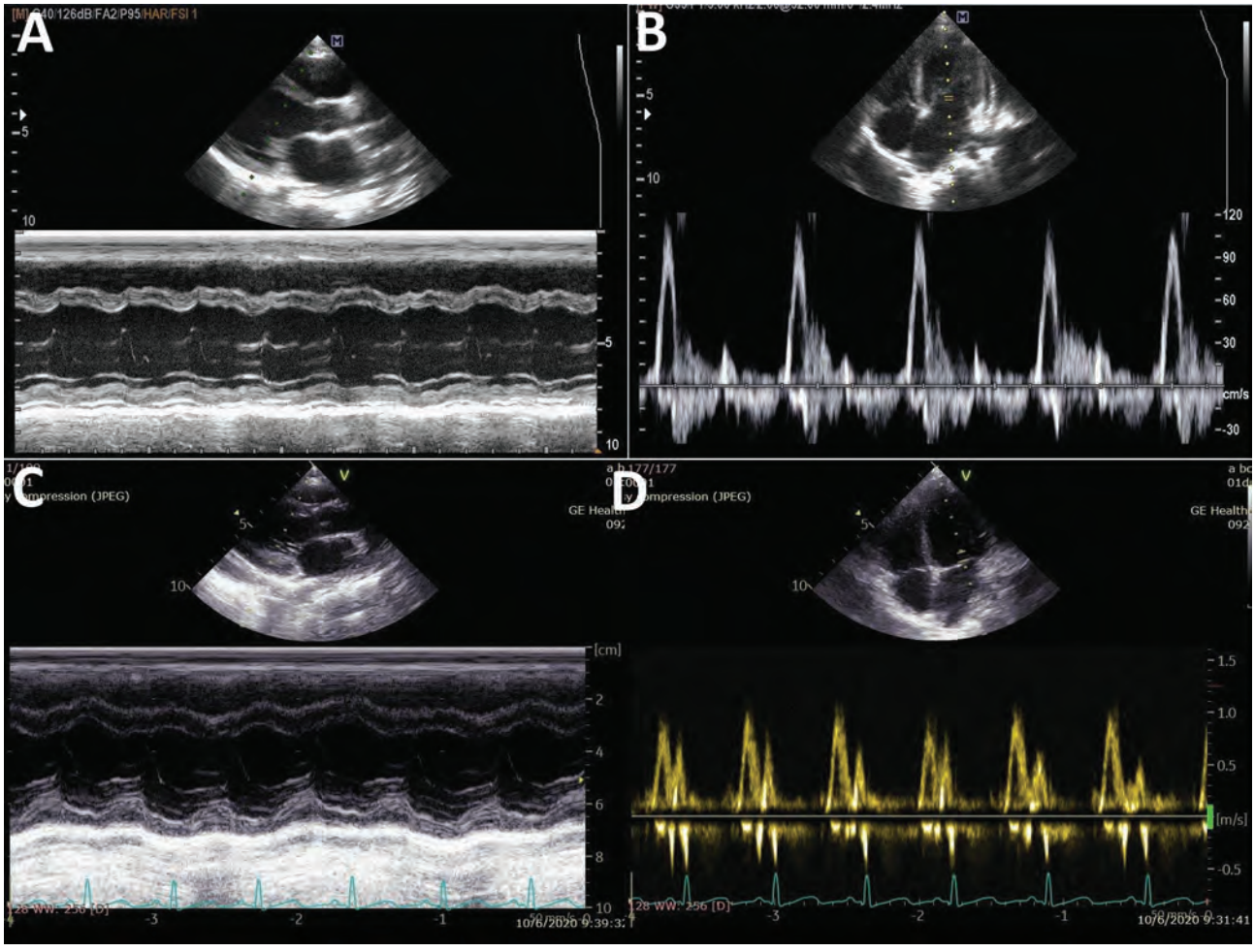

Figure 5. Serial echocardiographic recordings for 7-year-old boy later diagnosed with diphtheria myocarditis, Vietnam, 2020. On day 14 of illness, the M-mode left ventricular ejection fraction decreased to 40% (A) and the E/A ratio was >3.5 (B). At 2-week follow-up after discharge, both left ventricular systolic (C) and diastolic function (D) had recovered.

Echocardiography

Echocardiography is a useful noninvasive tool to assess cardiac function. However, until now, the use of echocardiography in the diagnosis and management of diphtheria has been limited, partly because of a lack of devices and expertise in LMICs. A large knowledge gap regarding echocardiographic findings in diphtheria myocarditis exists (*32*,*39*,*40*). Patients with severe diphtheria can have no clinical evidence of heart failure despite having subtle changes in cardiac function and subclinical dysrhythmias. Abnormalities on echocardiography include both systolic and diastolic dysfunction, characterized by rapid reduction in LV EF (*24*). Other abnormalities visualized on echocardiograms are LV dilation, LV wall thickening, pericardial effusion, and mitral and tricuspid regurgitation (*24*,*39*). Serial myocardial contractility assessment using POCUS can identify early cardiac decompensation and need for inotropic support. In the case of the patient described in this article, the use of POCUS helped attending clinicians detect early deterioration in cardiac function and guide the use of inotropes and fluid resuscitation. Thus, serial cardiac POCUS together with ECG monitoring should be applied to all patients hospitalized with diphtheria because the manifestations of diphtheria myocarditis are variable (*39*). Improved availability of low-cost portable echocardiograms and increasing expertise in many intensive-care units in LMICs, in addition to wearable ECG monitors, means a comprehensive cardiac assessment is now possible and should be applied to diphtheria patients to enable timely interventions and appropriate support (*41*).

Cardiac-Specific Treatment

Current management of diphtheria myocarditis mainly relies on supportive treatment aiming to maintain normal hemodynamic parameters. Antiarrhythmic drugs are usually reserved for sustained tachyarrhythmias. Prophylactic treatment of subclinical arrhythmias is not recommended, but further research into early administration for certain arrhythmias that are at high risk for progression or are associated with poor outcomes is warranted (*28*). Temporary pacemaker insertion can be used in patients with severe diphtheria myocarditis and bradyarrhythmias. The success of temporary pacing depends on the degree of damage to the conduction system and myocardial reserve. One report demonstrated improved survival outcomes of patients with diphtheria myocarditis and complete heart block (*42*). However, pacing did not improve outcomes in severe cases reported in Chile and Thailand (*40*,*43*).

Discussion

The findings of our literature review are well reflected in the clinical journey of this patient, whose vaccination status was unknown. He had swollen neck and extensive pseudomembrane, followed by onset of myocarditis in the second week (day 9), despite a short period of clinical stability. He did not have risk factors for myocarditis, such as leukocytosis and elevated aspartate transaminase, and only minor cardiac rhythm disturbances were present, suggesting a good prognosis. Because DAT was only available in some health facilities in Vietnam, the patient only received DAT on day 10, when he was admitted to our hospital. Whether the use of DAT at such a late time can still alter the progression of myocarditis is unclear. In the case of this patient, myocardial function continued to deteriorate after DAT was administered. We demonstrated that the use of POCUS assisted early detection of myocardial function deterioration, whereas the ECG findings were not as informative in terms of indicating cardiac dysfunction. Moreover, cardiac troponin I levels peaked and fell despite the ongoing cardiac impairment, suggesting a time lag between myocardial cellular damage and functional performance. We therefore recommend continuing close hemodynamic monitoring until myocardial functional recovery can be visualized on echocardiographic examination. Continuous monitoring using the POCUS and low-cost wearables coupled with intelligent technology is now under investigation in our hospital for treatment of other neglected diseases in Vietnam (http://vital.oucru.org). Positive results should encourage the extrapolation of this approach to other LMIC settings.

In conclusion, we report a severe case of diphtheria myocarditis, monitored using serial point-of-care echocardiography, enabling the timely management of the cardiac complications that ensued, which included heart failure and rhythm abnormalities. Serial point-of-care echocardiography, where available, together with serial ECGs and standard-of-care clinical monitoring, should be used in the treatment of all hospitalized patients with diphtheria myocarditis to enable timely intervention to mitigate severe and life-threatening consequences. Noninvasive wearable technology might be of benefit for detecting early signs of deterioration in diphtheria myocarditis. Outbreaks of diphtheria may become more frequent in the future because of the ongoing COVID-19 pandemic and related health service disruption but also because of increased vaccine hesitancy in many countries. The increasing availability of portable ultra-

sound and low-cost monitoring devices in Vietnam and other LMICs should now mean these methods can be used as standard of care in managing diphtheria myocarditis. Access to supplies of DAT, particularly in vulnerable settings, needs to be prioritized, and awareness of diphtheria, including its potential complications and management, should be raised for frontline health workers globally. Finally, full diphtheria vaccination provides the best protection against all complications of diphtheria.

Acknowledgments

We thank the Pediatric Intensive Care Unit staff at the Hospital for Tropical Diseases for their help and support. Written informed consent was obtained from the parents of the patient.

Author contributions: H.Q.C. and H.T.T. were the physicians managing the patient and wrote the case report and some of the review sections. H.N.T.V., T.K.H., and T.Q.P. were the physicians managing the patient and commenting on the manuscript. C.P. conducted the literature search, wrote sections of the manuscript, and read and edited the manuscript. J.C. wrote sections of the manuscript and reviewed the manuscript. S.Y. conceptualized and reviewed the manuscript. All authors reviewed, edited, and approved submission of the manuscript.

About the Author

Dr. Chanh is a research physician at Oxford University Clinical Research Unit and also holds an honorary position at the Pediatric Intensive Care Unit at the Hospital for Tropical Diseases in Ho Chi Minh City, Vietnam. His research aims to improve the quality of management and monitoring for children during an episode of critical illness in low- and middle-income countries through rigorously conducted research and innovative technologies.

References

1. World Health Organization. Diphtheria reported cases. 2020 [cited 2020 Aug 15]. https://apps.who.int/immunization_monitoring/globalsummary/timeseries/tsincidencediphtheria.html.
2. Clarke KEN, MacNeil A, Hadler S, Scott C, Tiwari TSP, Cherian T. Global epidemiology of diphtheria, 2000–2017. Emerg Infect Dis. 2019;25:1834–42. https://doi.org/10.3201/eid2510.190271
3. World Health Organization. Diphtheria vaccine: WHO position paper—August 2017. Wkly Epidemiol Rec. 2017;92:417–35.
4. Page KR, Doocy S, Reyna Ganteaume F, Castro JS, Spiegel P, Beyrer C. Venezuela's public health crisis: a regional emergency. Lancet. 2019;393:1254–60. https://doi.org/10.1016/S0140-6736(19)30344-7
5. Dureab F, Al-Sakkaf M, Ismail O, Kuunibe N, Krisam J, Müller O, et al. Diphtheria outbreak in Yemen: the impact of conflict on a fragile health system. Confl Health. 2019;13:19. https://doi.org/10.1186/s13031-019-0204-2
6. Clerville J. Diphtheria outbreak, Haiti, 2014–2017: an epidemiological profile and a case fatality rate trend analysis. Int J Infect Dis. 2018;73:274–5. https://doi.org/10.1016/j.ijid.2018.04.4041
7. Rahman MR, Islam K. Massive diphtheria outbreak among Rohingya refugees: lessons learnt. J Travel Med. 2019;26(1). https://doi.org/10.1093/jtm/tay122
8. General Department of Preventive Medicine. Update on diphtheria and key preventive measures. 2020 [cited 2021 Jan 20]. https://vncdc.gov.vn/files/article_attachment/2020/9/2-cuc-ytdp-bai-trinh-bay-bach-hau-hoi-nghi-pcd-1992020-new.pdf
9. Nguyen CTT, Grappasonni I, Scuri S, Nguyen BT, Nguyen TTT, Petrelli F. Immunization in Vietnam. Ann Ig. 2019;31:291–305.
10. World Health Organization. WHO-recommended surveillance standard of diphtheria. 2014 [cited 2020 Aug 15]. https://www.who.int/immunization/monitoring_surveillance/burden/vpd/surveillance_type/passive/diphtheria_standards/en
11. MacGregor R. *Corynebacterium diphtheriae*. In: Mandell G, Bennett J, Dolin R, editors. Mandell, Douglas, and Bennett's principles and practice of infectious diseases. Philadelphia: Churchill Livingstone Elsevier; 2009. p. 2687–93.
12. Truelove SA, Keegan LT, Moss WJ, Chaisson LH, Macher E, Azman AS, et al. Clinical and epidemiological aspects of diphtheria: a systematic review and pooled analysis. Clin Infect Dis. 2020;71:89–97. https://doi.org/10.1093/cid/ciz808
13. Sharma NC, Efstratiou A, Mokrousov I, Mutreja A, Das B, Ramamurthy T. Diphtheria. Nat Rev Dis Primers. 2019;5:81. https://doi.org/10.1038/s41572-019-0131-y
14. Murphy JR. *Corynebacterium diphtheriae*. In: Baron S, editor. Medical microbiology. Fourth edition. Galveston (TX): University of Texas; 1996 [cited 2020 Sep 2]. https://www.ncbi.nlm.nih.gov/books/NBK7971
15. Centers for Disease Control and Prevention. Diphtheria. In: Hamborsky J, Kroger A, Wolfe C, editors. Epidemiology and prevention of vaccine-preventable diseases. Washington, DC: Public Health Foundation; 2015. p. 107–17 [cited 2020 Aug 16]. https://www.cdc.gov/vaccines/pubs/pinkbook/dip.html
16. World Health Organization. Diphtheria anti-toxin (DAT) supply issues: brief review and proposition. 2017 [cited 2020 Aug 16]. https://www.who.int/immunization/sage/meetings/2017/april/3_Diphtheria_anti_toxin.pdf
17. Barraud O, Badell E, Denis F, Guiso N, Ploy M-C. Antimicrobial drug resistance in *Corynebacterium diphtheriae mitis*. Emerg Infect Dis. 2011;17:2078–80. https://doi.org/10.3201/eid1711.110282
18. Floros P, Gunaratne DA, Chang A, Coman WB. A rare case of toxigenic diphtheria tonsillitis resistant to penicillin causing sepsis and death. Australian Journal of Otolaryngology 2018;1:29 [cited 2020 Aug 20]. http://www.theajo.com/article/view/4117
19. Thisyakorn U, Wongvanich J, Kumpeng V. Failure of corticosteroid therapy to prevent diphtheritic myocarditis or neuritis. Pediatr Infect Dis. 1984;3:126–8. https://doi.org/10.1097/00006454-198403000-00009
20. Hadfield TL, McEvoy P, Polotsky Y, Tzinserling VA, Yakovlev AA. The pathology of diphtheria. J Infect Dis. 2000;181(Suppl 1):S116–20. https://doi.org/10.1086/315551

21. Burch GE, Sun SC, Sohal RS, Chu KC, Colcolough HL. Diphtheritic myocarditis. A histochemical and electron microscopic study. Am J Cardiol. 1968;21:261–8. https://doi.org/10.1016/0002-9149(68)90328-7
22. Kanungo R, Vijayalakshmi N, Nalini P, Bhattacharya S. Diphtheria due to non-toxigenic *Corynebacterium diphtheriae*: a report of two cases. Indian J Med Microbiol. 2002;20:50–2.
23. Tiley SM, Kociuba KR, Heron LG, Munro R. Infective endocarditis due to nontoxigenic *Corynebacterium diphtheriae*: report of seven cases and review. Clin Infect Dis. 1993;16:271–5. https://doi.org/10.1093/clind/16.2.271
24. Loukoushkina EF, Bobko PV, Kolbasova EV, Kazakova LV, Krasnov VV, Shipova LG, et al. The clinical picture and diagnosis of diphtheritic carditis in children. Eur J Pediatr. 1998;157:528–33. https://doi.org/10.1007/s004310050871
25. Kneen R, Nguyen MD, Solomon T, Pham NG, Parry CM, Nguyen TT, et al. Clinical features and predictors of diphtheritic cardiomyopathy in Vietnamese children. Clin Infect Dis. 2004;39:1591–8. https://doi.org/10.1086/425305
26. Christie AB. Diphtheria. In: Infectious diseases: epidemiology and clinical practice. Volume 2. New York: Churchill Livingstone; 1987. p. 1192–205.
27. Hoyne A, Welford NT. Diphtheritic myocarditis: a review of 496 cases. J Pediatr. 1934;5:642–53. https://doi.org/10.1016/S0022-3476(34)80043-1
28. Bethell DB, Nguyen MD, Ha TL, Le TNM, Nguyen QD, Day NP, et al. Prognostic value of electrocardiographic monitoring of patients with severe diphtheria. Clin Infect Dis. 1995;20:1259–65. https://doi.org/10.1093/clinids/20.5.1259
29. Begg N. Diptheritic myocarditis: an electrocardiographic study. Lancet. 1937;229:857–60. https://doi.org/10.1016/S0140-6736(00)83448-0
30. Kneen R, Pham NG, Solomon T, Tran TM, Nguyen TT, Tran BL, et al. Penicillin vs. erythromycin in the treatment of diphtheria. Clin Infect Dis. 1998;27:845–50. https://doi.org/10.1086/514959
31. Samdani S, Jain A, Meena V, Meena CB. Cardiac complications in diphtheria and predictors of outcomes. Int J Pediatr Otorhinolaryngol. 2018;104:76–8. https://doi.org/10.1016/j.ijporl.2017.10.032
32. Lakkireddy DR, Kondur AK, Chediak EJ, Nair CK, Khan IA. Cardiac troponin I release in non-ischemic reversible myocardial injury from acute diphtheric myocarditis. Int J Cardiol. 2005;98:351–4. https://doi.org/10.1016/j.ijcard.2003.10.062
33. Ledbetter MK, Cannon AB II, Costa AF. The electrocardiogram in diphtheritic myocarditis. Am Heart J. 1964;68:599–611. https://doi.org/10.1016/0002-8703(64)90268-6
34. Havaldar PV, Sankpal MN, Doddannavar RP. Diphtheritic myocarditis: clinical and laboratory parameters of prognosis and fatal outcome. Ann Trop Paediatr. 2000;20:209–15. https://doi.org/10.1080/02724936.2000.11748136
35. Celik T, Balta S, Ozturk C, Yildirim AO, Iyisoy A. Qrs prolongation and long-term prognosis in patients with dilated cardiomyopathy: reflections from diphteritic myocarditis. Int J Cardiol. 2016;212:295. https://doi.org/10.1016/j.ijcard.2016.03.092
36. Ming DK, Sangkaew S, Chanh HQ, Nhat PTH, Yacoub S, Georgiou P, et al. Continuous physiological monitoring using wearable technology to inform individual management of infectious diseases, public health and outbreak responses. Int J Infect Dis. 2020;96:648–54. https://doi.org/10.1016/j.ijid.2020.05.086
37. Tadesse GA, Zhu T, Le Nguyen Thanh N, Hung NT, Duong HTH, Khanh TH, et al. Severity detection tool for patients with infectious disease. Healthc Technol Lett. 2020;7:45–50. https://doi.org/10.1049/htl.2019.0030
38. Rodriguez-Manzano J, Chia PY, Yeo TW, Holmes A, Georgiou P, Yacoub S. Improving dengue diagnostics and management through innovative technology. Curr Infect Dis Rep. 2018;20:25. https://doi.org/10.1007/s11908-018-0633-x
39. Groundstroem KW, Molnar G, Lumio J. Echocardiographic follow-up of diphtheric myocarditis. Cardiology. 1996;87:79–81. https://doi.org/10.1159/000177065
40. Washington CH, Issaranggoon Na Ayuthaya S, Makonkawkeyoon K, Oberdorfer P. A 9-year-old boy with severe diphtherial infection and cardiac complications. BMJ Case Rep. 2014 Nov 20:2014;bcr2014206085. https://doi.org/10.1136/bcr-2014-206085
41. Turner HC, Van Hao N, Yacoub S, Hoang VMT, Clifton DA, Thwaites GE, et al. Achieving affordable critical care in low-income and middle-income countries. BMJ Glob Heal. 2019;4:e001675. https://doi.org/10.1136/bmjgh-2019-001675
42. Dung NM, Kneen R, Kiem N, Bethell DB, Phu NH, Solomon T, et al. Treatment of severe diphtheritic myocarditis by temporary insertion of a cardiac pacemaker. Clin Infect Dis. 2002;35:1425–9. https://doi.org/10.1086/344176
43. Stockins BA, Lanas FT, Saavedra JG, Opazo JA. Prognosis in patients with diphtheric myocarditis and brady arrhythmias: assessment of results of ventricular pacing. Br Heart J. 1994;72:190–1. https://doi.org/10.1136/hrt.72.2.190
44. Kazemi B, Tahernia AC, Zandian K. Motor nerve conduction in diphtheria and diphtheritic myocarditis. Arch Neurol. 1973;29:104–6. https://doi.org/10.1001/archneur.1973.00490260048009
45. Ismail D, Utomo U, Suharjanto S. Serum transaminase in diphtheritic myocarditis. Paediatr Indones. 1976;16:89–93. https://doi.org/10.14238/pi16.3-4.1976.89-93
46. Wahab AS, Sastroamidjojo P. A selective study of clinical diphtheric myocarditis. Paediatr Indones. 1973;13:24–30. https://doi.org/10.14238/pi13.1.1973.24-30
47. Prasodo AM, Narendra M, Joernil A, Wahjoenarso, Kaspan F. Congestive heart failure in diphtheric myocarditis. Paediatr Indones. 1976;16:71–80. https://doi.org/10.14238/pi16.3-4.1976.71-80
48. Kole AK, Roy R, Kar SS, Chanda D. Outcomes of respiratory diphtheria in a tertiary referral infectious disease hospital. Indian J Med Sci. 2010;64:373–7. https://doi.org/10.4103/0019-5359.100340
49. Celik T, Selimov N, Vekilova A, Kursaklioglu H, Iyisoy A, Kilic S, et al. Prognostic significance of electrocardiographic abnormalities in diphtheritic myocarditis after hospital discharge: a long-term follow-up study. Ann Noninvasive Electrocardiol. 2006;11:28–33. https://doi.org/10.1111/j.1542-474X.2006.00062.x
50. Choremis C, Leonidas J. Serum transaminases in diphtheritic myocarditis. Their relation to electrocardiographic findings. Acta Paediatr (Stockh). 1962;51:293–302. https://doi.org/10.1111/j.1651-2227.1962.tb06544.x

Address for correspondence: Sophie Yacoub, Oxford University Clinical Research Unit, 764 Vo Van Kiet, District 5, Ho Chi Minh City, Vietnam; email: syacoub@oucru.org

Clinical and Laboratory Characteristics and Outcome of Illness Caused by Tick-Borne Encephalitis Virus without Central Nervous System Involvement

Petra Bogovič, Andrej Kastrin, Stanka Lotrič-Furlan, Katarina Ogrinc, Tatjana Avšič Županc, Miša Korva, Nataša Knap, Franc Strle

Medscape ACTIVITY EDUCATION

In support of improving patient care, this activity has been planned and implemented by Medscape, LLC and Emerging Infectious Diseases. Medscape, LLC is jointly accredited by the Accreditation Council for Continuing Medical Education (ACCME), the Accreditation Council for Pharmacy Education (ACPE), and the American Nurses Credentialing Center (ANCC), to provide continuing education for the healthcare team.

Medscape, LLC designates this Journal-based CME activity for a maximum of 1.00 ***AMA PRA Category 1 Credit(s)™***. Physicians should claim only the credit commensurate with the extent of their participation in the activity.

Successful completion of this CME activity, which includes participation in the evaluation component, enables the participant to earn up to 1.0 MOC points in the American Board of Internal Medicine's (ABIM) Maintenance of Certification (MOC) program. Participants will earn MOC points equivalent to the amount of CME credits claimed for the activity. It is the CME activity provider's responsibility to submit participant completion information to ACCME for the purpose of granting ABIM MOC credit.

All other clinicians completing this activity will be issued a certificate of participation. To participate in this journal CME activity: (1) review the learning objectives and author disclosures; (2) study the education content; (3) take the post-test with a 75% minimum passing score and complete the evaluation at http://www.medscape.org/journal/eid; and (4) view/print certificate. For CME questions, see page 498.

Release date: January 21, 2022; Expiration date: January 21, 2023

Learning Objectives

Upon completion of this activity, participants will be able to:

- Distinguish the typical disease course of tick-borne encephalitis virus
- Assess clinical characteristics of patients with tick-borne encephalitis virus
- Analyze trends in laboratory values among patients with tick-borne encephalitis virus
- Identify the rate of central nervous system involvement in the current case series of tick-borne encephalitis virus

CME Editor

Jill Russell, BA, Technical Writer/Editor, Emerging Infectious Diseases. *Disclosure: Jill Russell, BA, has disclosed no relevant financial relationships.*

CME Author

Charles P. Vega, MD, Health Sciences Clinical Professor of Family Medicine, University of California, Irvine School of Medicine, Irvine, California. *Disclosure: Charles P. Vega, MD, has disclosed the following relevant financial relationships: served as an advisor or consultant for Johnson & Johnson.*

Authors

Petra Bogovič, MD, PhD; Andrej Kastrin, PhD; Stanka Lotrič-Furlan, MD, PhD; Katarina Ogrinc, MD, PhD; Tatjana Avšič Županc, PhD; Miša Korva, PhD; Nataša Knap, PhD; and ***Franc Strle, MD, PhD.***

Author affiliations: University Medical Center Ljubljana, Ljubljana, Slovenia (P. Bogovič, S. Lotrič-Furlan, K. Ogrinc, F. Strle); University of Ljubljana, Faculty of Medicine, Ljubljana (A. Kastrin, T. Avšič Županc, M. Korva, N. Knap)

DOI: https://doi.org/10.3201/eid2802.211661

Information on febrile illness caused by tick-borne encephalitis virus (TBEV) without central nervous system involvement is limited. We characterized 98 patients who had TBEV RNA in their blood but no central nervous system involvement at the time of evaluation. Median duration of illness was 7 days; 37 (38%) patients were hospitalized. The most frequent findings were malaise or fatigue (98%), fever (97%), headache (86%), and myalgias (54%); common laboratory findings were leukopenia (88%), thrombocytopenia (59%), and abnormal liver test results (63%). During the illness, blood leukocyte counts tended to improve, whereas thrombocytopenia and liver enzymes tended to deteriorate. At the time of positive PCR findings, 0/98 patients had serum IgG TBEV and 7 serum IgM TBEV; all patients later seroconverted. Viral RNA load was higher in patients with more severe illness but did not differ substantially in relation to several other factors. Illness progressed to tick-borne encephalitis in 84% of patients within 18 days after defervescence.

Tick-borne encephalitis virus (TBEV) is a member of the genus *Flavivirus* in the family *Flaviviridae* and is transmitted to humans predominantly through *Ixodes* spp. tick bites. In addition to 3 well-known subtypes of TBEV (European, Siberian, and Far Eastern) that cause disease in humans, other subtypes, including the currently named Baikalian and Himalayan subtypes, have been reported (*1*,*2*).

Infection with TBEV can be symptomatic or asymptomatic. As is the case for infections with other flaviviruses, most (70%–98%) persons infected with TBEV do not experience symptoms; however, some findings in blood donors suggest that asymptomatic infections might be rare (*3*). Nevertheless, when infection with TBEV is symptomatic, it can manifest as a febrile illness without central nervous system (CNS) involvement (Figure 1, panel A) but often progresses to tick-borne encephalitis (TBE) (i.e., CNS involvement caused by the virus) (Figure 1, panel B). Clinical manifestation differs in some respects according to virus subtype. In 13%–44% of patients, TBE caused by the European subtype manifests with direct CNS involvement (*4*–*15*) (Figure 1, panel C), whereas in most patients, CNS inflammation is preceded by a febrile illness, resulting in a biphasic course (Figure 1, panel B). The initial phase, which corresponds to viremia, manifests as fever, fatigue, malaise, headache, and muscle and joint pain, but in the absence of CNS inflammation; this phase usually lasts <1 week (*8*), and the illness then improves over a few days. The hallmark of the second phase of the disease is CNS involvement. Meningitis is the predominant manifestation in children. In adults, meningitis occurs in ≈50% of patients, meningoencephalitis in ≈40%, and meningoencephalomyelitis in ≈5%–10%. The case-fatality rate of TBE caused by the European subtype of TBEV is 0.5%–2%. In addition, ≈5% of adult patients are affected by permanent pareses, and at least one third suffer from a postencephalitic syndrome (*16*–*19*).

In general, clinical manifestations and laboratory characteristics of symptomatic TBEV infection are well described. However, this statement is valid for cases with neurologic involvement (i.e., for TBE) but less so for the initial phase of TBE, and much less so for TBEV infection manifesting solely as febrile illness without later CNS involvement. That manifestation, also called isolated initial phase of TBE, abortive form of TBE, febrile headache, summer flu, or fever form, is postulated to match clinically and serologically the initial phase of TBE, with the exception that subsequent CNS involvement does not occur. TBEV infection manifesting as febrile illness without later CNS involvement is suggested to be frequent (*20*–*23*), although not in all reports (*5*,*6*,*24*,*25*), and the scientific basis for such a conclusion is unclear. Furthermore, although the outcome of symptomatic TBEV infection without CNS involvement is believed to be favorable, no reliable data on the outcome have been published. Because clinical symptoms and signs of the illness are nonspecific, and because, in parallel to the initial phase of TBE, serum antibodies to TBEV are not yet expected to have developed, the only option for diagnosis at the time of actual illness is demonstrating the presence of TBEV RNA in the blood. However, this approach is not routine and might have a low diagnostic yield owing to several other known or unknown causes of fever, even in a region that is highly endemic for TBE. Therefore, the possibility that a febrile illness is the result of TBEV infection is usually tested for and established only after signs or symptoms of CNS involvement appear, which does not happen in case of the fever form. In that case (and if PCR detection of viral RNA in blood is not available), further clinical and microbiologic (serologic) follow-up after improvement is needed to establish the diagnosis. In this study, we analyzed in detail the clinical and laboratory characteristics of febrile illness after tick bite or exposure to ticks and its outcome in patients in whom infection with TBEV was established by the presence of viral RNA in the blood.

Materials and Methods

Definitions

Febrile illness resulting from infection with TBEV was defined by the presence of fever and constitutional symptoms, demonstration of viral RNA

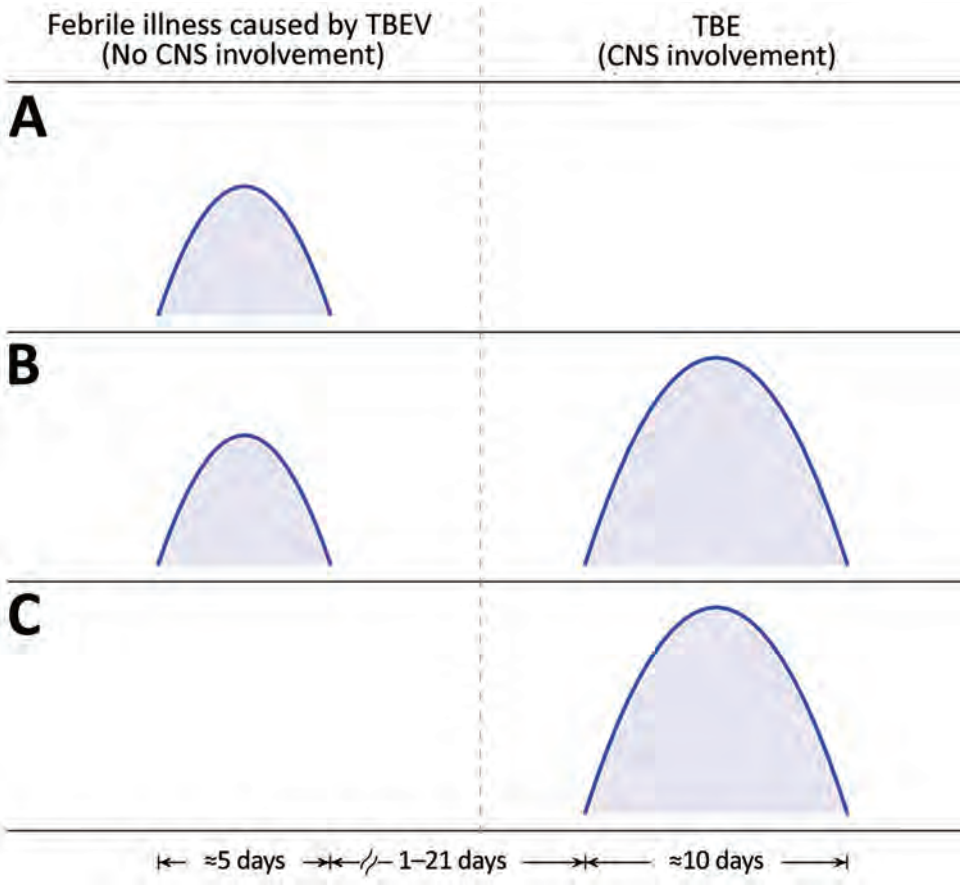

Figure 1. Timelines of clinical manifestations of illness caused by TBEV. A) Febrile headache (fever form); B) biphasic course of TBE; C) monophasic course of TBE. CNS, central nervous system; TBE, tick-borne encephalitis; TBEV, tick-borne encephalitis virus.

in serum specimens, and the absence of signs or symptoms of CNS involvement at the time of illness. In patients with clinical signs potentially suggesting CNS involvement, cerebrospinal fluid (CSF) samples were examined; the threshold for lumbar puncture was low. A CSF leukocyte count $\leq 5 \times 10^6$/L was interpreted as excluding CNS inflammation.

According to the later appearance (or absence) of neurologic involvement, the febrile illness was further subclassified as either the initial phase of TBE (defined as a febrile illness with demonstration of viral RNA in serum samples that, after a clinical improvement, was followed by neurologic involvement within a 2-month follow-up period and fulfilling criteria for TBE) or as febrile illness resulting from infection with TBEV in a narrow sense (fever form, febrile headache) when no signs of CNS involvement were present at the time of actual illness or within a 2-month follow-up period. TBE was defined as the presence of clinical signs or symptoms of meningitis or meningoencephalitis, increased CSF leukocyte counts ($>5 \times 10^6$ cells/L), and demonstration of a recent infection with TBEV indicated by serum IgM and IgG or IgG seroconversion in paired serum samples.

Patients and Samples

Adult patients examined for febrile illness at the Department of Infectious Diseases, University Medical Center Ljubljana (Ljubljana, Slovenia), during 2003–2019, in whom the presence of TBEV RNA was identified by PCR in serum specimens, qualified for the study. Serum samples were obtained either during a prospective study on the etiology of febrile illness after a tick bite or exposure to ticks (62 patients, 63.3%) or represented remnants of samples collected as a part of routine diagnostic testing of patients with febrile illness in whom TBE later occurred (36 patients, 36.7%). Serum specimens were stored at –80°C until further processing. For the 62 patients, we obtained clinical and laboratory information on the etiology of febrile illness occurring after tick bite or tick exposure prospectively. Clinical and laboratory follow-up occurred for these patients for at least 2 months (i.e., at first evaluation and at follow-up visits 1 week, 2 weeks, and 2 months later). For the other 36 patients, we obtained clinical and laboratory information from medical charts.

TBEV Antibodies and RNA Load

We determined the presence of TBEV antibodies in serum samples by using the Enzygnost Anti-TBE/FSME Virus (IgM, IgG) test (Siemens AG, https://www.siemens.com), according to the manufacturer's instructions. We extracted total RNA from serum samples by using the QIAamp Viral RNA Mini Kit (QIAGEN, https://www.qiagen.com), according to the manufacturer's instructions. For the detection of TBEV RNA, we performed quantitative reverse transcription PCR as reported previously (*26*).

Statistical Analysis

We summarized continuous variables as median values and interquartile ranges (IQRs), and discrete variables as counts and percentages with 95% CIs. We based comparisons between groups on Wilcoxon rank-sum tests for continuous variables and Fisher exact tests for discrete variables. We defined statistical significance as a p value of $\leq$0.05.

We examined associations between variables by using linear regression modeling (Figures 2, 3). We used $\log_{10}$-transformed viral RNA loads, and domain experts (P.B. and F.S.) selected included covariates. We modeled continuous covariates that demonstrated a nonlinear relationship by using restricted cubic splines (*27*) and imputed missing values by using multiple imputation on the basis of additive regression, bootstrapping, and predictive mean matching (*28*). We used R software for all statistical analyses (*29*).

Ethics

The study was conducted in accordance with the principles of the Declaration of Helsinki, the Oviedo Convention on Human Rights and Biomedicine, and the Slovene Code of Medical Deontology. The study was approved by the National Medical Ethics Committee of Slovenia (approval nos. 152/06/13, 178/02/13, and 37/12/13). Patients whose specimens were obtained in the study on the etiology of febrile illness after a tick bite or exposure to ticks signed an informed consent form. The Ethics Committee waived the need for written informed consent for patients for whom remnants of routinely collected serum specimens were used.

Results

A total of 98 adult patients examined for febrile illness in whom TBEV RNA was identified by PCR in their serum specimens were enrolled in the study. The median age of the patients was 51 years; 52% were women.

Clinical and Laboratory Characteristics of Febrile Illness Caused by TBEV

Most (88.7%) patients reported a tick bite within 4 weeks of the onset of illness. The median time from the bite to illness onset was 6 days, median duration of illness before evaluation was 5 days, and total duration of the illness was 7 days. A total of 37/98 (37.8%) patients were hospitalized for a median of 3 days. The most frequent symptoms or signs were malaise and fatigue (98%), fever (96.9%), headache (85.7%), and myalgias (54.1%) (Table 1). The most frequent laboratory findings were leukopenia (87.5%), thrombocytopenia (59.4%), and abnormal liver test results (62.5% of patients had $\geq$1 abnormal liver test result, most often elevated aspartate aminotransferase [AST, 55.0%] and alanine aminotransferase [ALT, 26.3%]) (Table 2).

Individual laboratory parameters according to duration of illness before testing demonstrated heterogeneous results. Counts of total peripheral blood leukocytes, neutrophils, lymphocytes, and monocytes were lowest early in the course of illness and tended to increase (improve) with the duration of illness, whereas thrombocytopenia became more pronounced with the duration of illness. Liver tests, including AST, ALT, gamma-glutamyl transferase (GGT), and lactate dehydrogenase, also tended to deteriorate with the duration of illness. These tendencies were noticeably uniform and were significant for total leukocyte and monocyte counts and for AST, ALT, and GGT levels (Figure 2).

None of the 98 patients had serum IgG to TBEV at the time of a positive PCR result (median of 5 days after illness onset) and only 2/98 (2.0%) had TBEV-specific IgM. In these 2 patients, the serologic tests were performed on days 7 and 13 of the illness. An additional 5 patients (5.1%) had borderline specific IgM levels; for most, the duration of illness before testing was somewhat longer (median 6 days, range 3–9 days). Viral RNA load was higher in hospitalized patients with more severe illness than in those who did not need hospitalization but did not differ substantially according to age, sex, duration of illness before testing, or total duration of the actual febrile illness, or for patients with undetectable viral IgM in serum samples when compared with patients in whom antibodies were detectable (Figure 3).

Outcome

Of the 62 patients who received a diagnosis during a prospective study on the etiology of febrile illness after a tick bite or exposure to ticks and in whom TBEV was present in serum samples, 6 (9.7%) did not

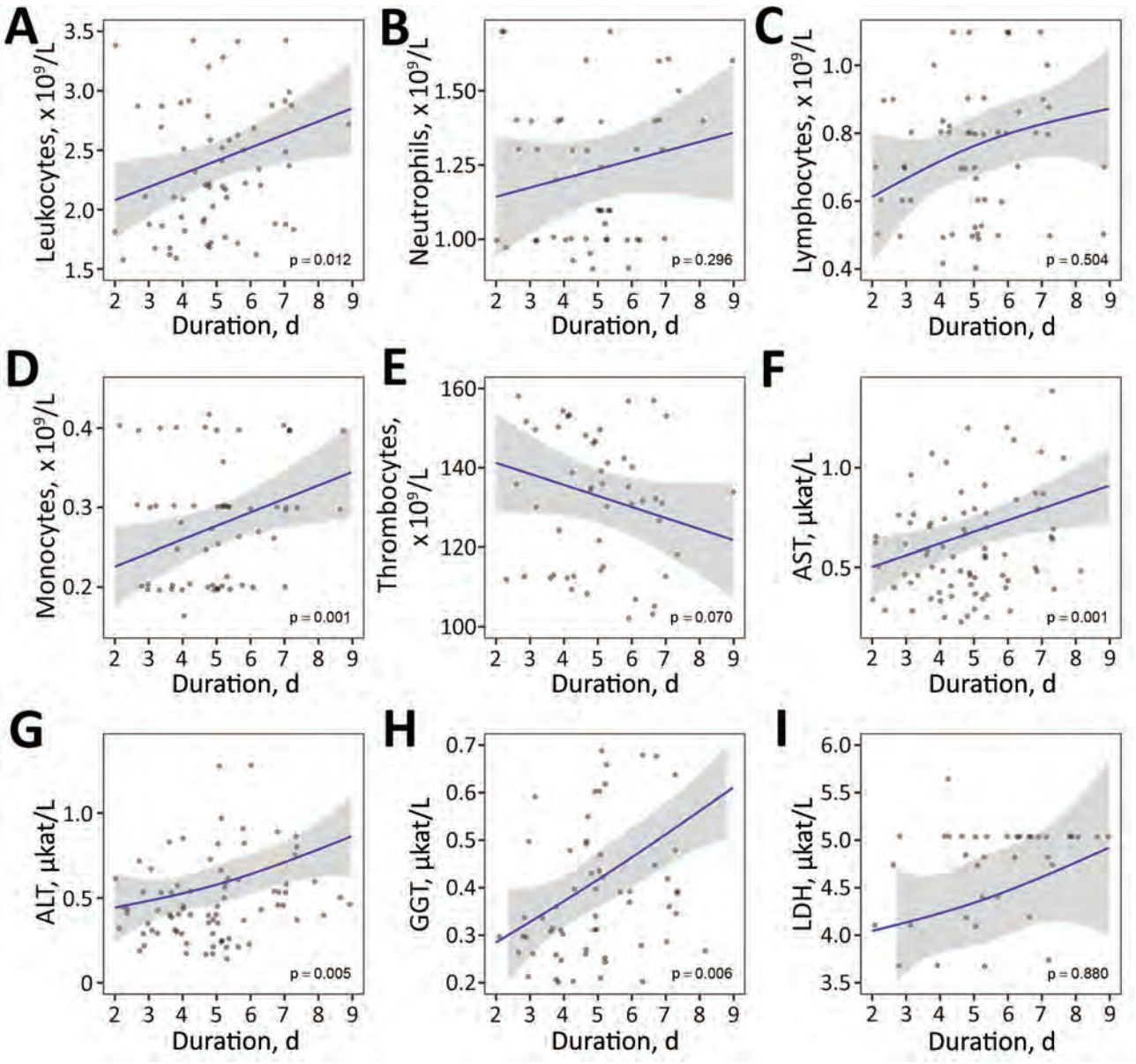

Figure 2. Laboratory findings according to illness duration in cases of febrile illness caused by tick-borne encephalitis virus without central nervous system involvement at the time of evaluations, Slovenia. A) Leukocytes, B) neutrophils, C) lymphocytes, D) monocytes, E) thrombocytes, F) AST, G) ALT, H) GGT, and I) LDH. Blue lines indicate loess regression lines; shaded areas indicate 95% CIs. Relationships between variables in panels C, G, and I were modeled by using restricted cubic splines with 3 knots (*25*). ALT, alanine aminotransferase; AST, aspartate aminotransferase; GGT, gamma-glutamyl transferase; LDH, lactate dehydrogenase.

experience any symptoms or signs during the follow-up period of 2 months. In 4 (4.5%) patients, mild constitutional symptoms not suggesting CNS involvement and without meningeal signs reappeared after a symptom-free interval of up to 12 days. In contrast, the other 52 (83.9%) patients experienced overt signs of meningitis or meningoencephalitis associated with CSF pleocytosis and fulfilled serologic criteria for TBE; in this subgroup, the longest symptom-free interval was 18 days.

The clinical characteristics of the initial phase of TBE and febrile illness without subsequent CNS involvement were not formally compared because the number of patients was too small, but the clinical and laboratory manifestation of the 2 entities appears comparable (Table 3). All patients developed IgM and IgG to the virus during follow-up.

Of the 62 prospectively followed patients, 27 (43.5%) were hospitalized. The likelihood of later CNS involvement in hospitalized patients was similar to that

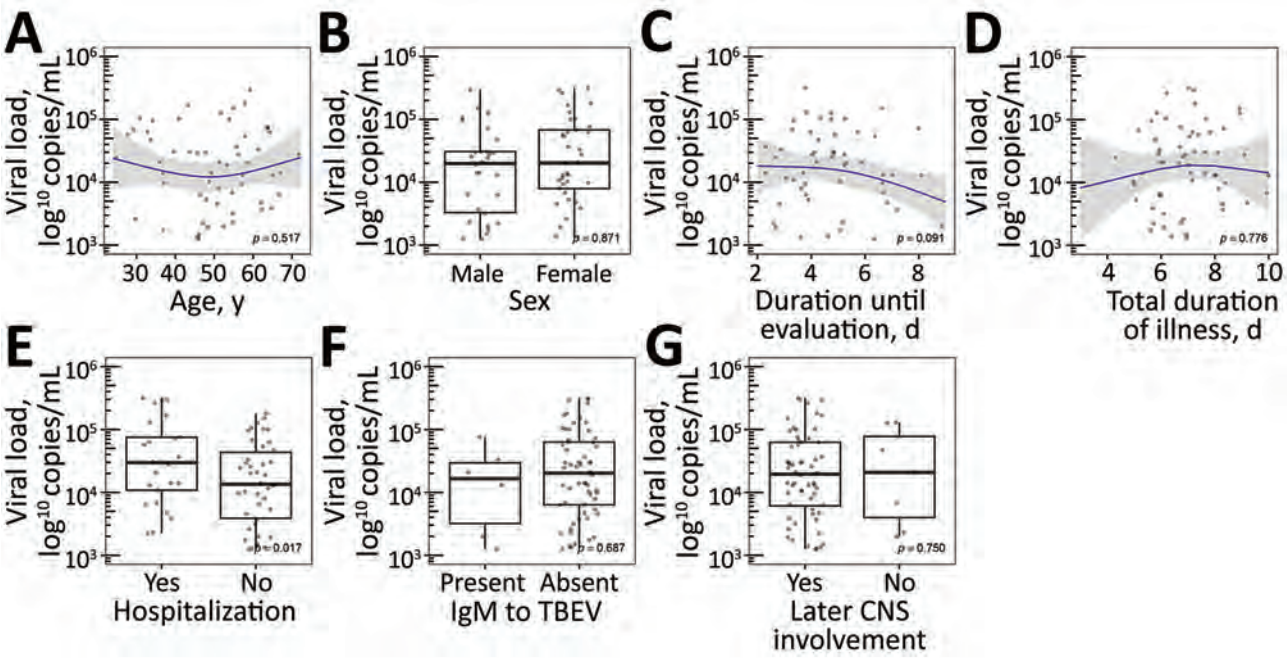

Figure 3. TBEV RNA load according to demographic and clinical characteristics in cases of febrile illness without central nervous system involvement at the time of evaluations, Slovenia. A) Age, B) sex, C) duration of illness until evaluation, D) total duration of illness, E) hospitalization, F) presence of IgM to TBEV, and G) later CNS involvement. Blue lines indicate loess regression lines; shaded areas indicate 95% CIs. Relationships between variables in panels panels A, C, and D are modeled by using restricted cubic splines with 3 knots (*25*). Comparisons between groups in panels B, E, F, and G are based on a Wilcoxon rank-sum test. CNS, central nervous system; TBEV, tick-borne encephalitis virus.

in patients with less severe illness who were treated as outpatients (24/27 [88.9%] vs. 28/35 [80%]; p = 0.49). Furthermore, the level of viral RNA in serum samples in the group in which no CNS involvement occurred was similar to the level in those in whom meningitis or meningoencephalitis later occurred (Figure 3).

Discussion

Symptomatic infection with TBEV can manifest as CNS involvement (TBE) or as a febrile illness with or without subsequent CNS involvement (Figure 1). Although the epidemiology and clinical manifestation of symptomatic TBEV infection is considered well-established, this statement is valid only for neurologic involvement (TBE) and is less well-established for the initial phase of TBE and even less so for TBEV infection manifesting solely as febrile illness without later CNS involvement.

TBE is highly endemic to Slovenia. For as many as 70% of patients in Slovenia who have notified cases of TBE, diagnosis occurs at University Medical Center Ljubljana (*30*,*31*), which provided access to detailed information on a large number of patients with TBE and enabled this study.

The initial phase of TBE consists of fever, headache, myalgias, arthralgias, and fatigue (*5*,*6*,*8*,*9*,*13*,*32*–*34*), but reliable information on the relative frequency of individual symptoms is limited, and results are variable. In this study, which encompasses TBEV febrile illness with and without later CNS involvement (the initial phase of TBE and febrile headache) and is based on a well-defined group of patients with definite proof of TBEV infection (the presence of virus in blood at the time of actual illness and later seroconversion), our findings corroborate previous results on the spectrum of symptom manifestation and add reliable information on their relative frequency. Thus, >85% of patients have malaise or fatigue, fever, and headache; ≈50% of the patients report myalgias, arthralgias, and, rather unexpectedly, gastrointestinal symptoms (abdominal pain, nausea, vomiting, or diarrhea); and the frequency of respiratory symptoms or chills is almost 20%. The finding of chills is somewhat surprising because chills are not common in patients with viral infections and are more characteristic of diseases caused by bacteria. Illness duration in our patients (median 7 days) was somewhat longer than reported in the literature (median 4–6, range 1–19 days) (*5*,*6*,*8*,*9*,*12*,*26*,*32*,*34*). In addition, in some patients, the illness was relatively severe: more than one third of patients were hospitalized. Laboratory findings possibly contributed to decisions to hospitalize

because leukopenia and thrombocytopenia might suggest serious disease in a patient with fever.

The first phase of TBE is known to be accompanied by leukopenia; thrombocytopenia and abnormal liver test results also might be present, although to a lesser extent (*35*,*36*). In contrast, in the second phase of TBE, the blood leukocyte count is elevated or in normal range. Laboratory tests in the patients in our study very often demonstrated abnormalities (leukopenia in 88%, abnormal liver tests in 70%, and thrombocytopenia in 59%) that were more common than previously described (*6*,*13*,*25*,*26*,*35*,*36*). Our study corroborates previous findings that in most patients, the concentration of total leukocytes in the peripheral blood is reduced. In addition, we offer several new findings, such as a reduction in all major subgroups of leukocytes and a tendency for total numbers of leukocytes, neutrophils, lymphocytes, and monocytes to increase (i.e., improve). In contrast, thrombocytopenia, liver tests (including AST, ALT, and GGT), and lactate dehydrogenase tended to deteriorate with duration of illness. Although we do not have an exact explanation for these laboratory abnormalities, they seem biologically plausible. During illness caused by TBEV without CNS involvement (including illness with subsequent CNS involvement), TBEV replicates in various organs and tissues, and this might affect test results. Later, however, when viremia vanishes and CNS damage occurs, the abnormalities are not present (*7*,*8*,*16*–*18*) and obviously are temporally associated with viremia, suggesting a direct or indirect effect of the virus on the bone marrow and liver.

Our results corroborate previous findings (*24*,*26*,*37*) that the appearance of antibodies to TBEV greatly diminishes the likelihood of detecting viral RNA in blood: none of our 98 patients had detectable serum IgG to TBEV at the time of a positive PCR finding, although 7 (7.6%) patients had specific IgM. As expected, in these 7 patients, the duration of illness was longer than for patients who were completely seronegative. We also expected that the viral RNA load would be lower in patients with detectable serum IgM to the virus than in patients in whom the antibodies were undetectable, but we did not confirm this premise. Furthermore, viral RNA load did not differ substantially in relation to age, sex, duration of illness before testing, or total duration of the actual febrile illness; however, viral RNA load was higher

Table 1. Demographic and clinical data on adult patients who had febrile illness caused by tick-borne encephalitis virus without central nervous system involvement at the time of evaluation, Slovenia*

Characteristic	Value
Sex	
F	51 (52.0, 41.7–62.2)
M	47 (48.0, 37.8–58.3)
Median age, y (IQR)	51 (37–60.75)
Underlying illnesses	38 (38.8, 29.1–49.2)
History of tick bite†	86 (88.7, 80.6–94.2)
Median incubation period, d (IQR)‡	6 (4–9.75)
Median duration of illness before first evaluation, d (IQR)	5 (4–6)
Clinical manifestation	
Body temperature ≥37.5°C	95 (96.9, 91.3–99.4)
Median body temperature, °C (IQR)§	38.3 (37.8–38.9)
Chills	19 (19.4, 12.1–28.6)
Headache	84 (85.7, 77.2–92.0)
Myalgia	53 (54.1, 43.7–64.2)
Arthralgia	42 (42.9, 32.9–53.3)
Gastrointestinal symptoms	45 (45.9, 35.8–56.3)
Abdominal pain	2 (2.0, 0.3–7.2)
Nausea, vomiting	37 (37.8, 28.2–48.1)
Diarrhea	16 (16.3, 9.6–25.2)
Malaise and fatigue	96 (98.0, 92.8–99.8)
Respiratory symptoms	18 (18.4, 11.3–27.5)
Sore throat	11 (11.2, 5.7–19.2)
Cough	10 (10.2, 5.0–18.0)
Median duration of illness, initial phase, d (IQR)¶	7 (6–8)
Hospitalization	
No. hospitalized patients	37 (37.8, 28.2–48.1)
Median duration of hospitalization, d (IQR)#	3 (1–5)

*Values are no. (%, 95% CI) except as indicated. IQR, interquartile range.
†Tick bite within 4 weeks before onset of illness. Data available for 97 patients.
‡Time (days) from tick bite to onset of illness calculated only in patients with 1 bite. Data available for 54 patients.
§Highest temperature in the course of the illness.
¶Data available for 82 patients.
#Data available for 33 patients.

Table 2. Laboratory data on adult patients who had febrile illness caused by tick-borne encephalitis virus without central nervous system involvement at the time of evaluation, Slovenia*

Laboratory findings	Value
Median blood leukocyte count, × 10^9/L (IQR)†	2.3 (1.8–3.125)
Blood leukocyte count <4 × 10^9/L	84 (87.5, 79.2–93.4)
Blood leukocyte count >10 × 10^9/L	0 (0, 0–3.8)
Median blood neutrophil count, × 10^9/L (IQR)‡	1.22 (0.9–1.7)
Blood neutrophil count <1.5 × 10^9/L	55 (65.5, 54.3–75.5)
Blood neutrophil count >7.4 × 10^9/L	0 (0, 0–4.3)
Median blood lymphocyte count, × 10^9/L (IQR)‡	0.88 (0.5–1.1)
Blood lymphocyte count <1.1 × 10^9/L	61 (72.6, 61.8–81.8)
Blood lymphocyte count >3.5 × 10^9/L	1 (1.2, 0–6.5)
Median blood monocyte count, × 10^9/L (IQR)‡	0.29 (0.2–0.4)
Blood monocyte count <0.21 × 10^9/L	34 (40.5, 29.9–51.8)
Blood monocyte count >0.92 × 10^9/L	0 (0, 0–4.3)
Median blood platelet count, × 10^9/L (IQR)†	132 (110.5–157)
Blood platelet count <140 × 10^9/L	57 (59.4, 48.9–69.3)
Serum C-reactive protein level >5 mg/L†§	9 (9.4, 4.4–17.1)
Liver test results, μkat/L (IQR)¶	
Median alkaline phosphatase¶	0.93 (0.755–1.06)
Elevated >1.92	0 (0, 0–4.6)
Median aspartate aminotransferase#	0.615 (0.4575–0.8325)
Elevated >0.58	44 (55.0, 43.5–66.2)
Median alanine aminotransferase#	0.53 (0.37–0.805)
Elevated >0.77	21 (26.3, 17.0–37.3)
Median gamma-glutamyl transferase	0.37 (0.265–0.595)
Elevated >0.92	9 (11.4, 5.3–20.5)
Median lactate dehydrogenase**	3.48 (2.92–4.82)
Elevated >4.13	12 (36.4, 20.4–54.9)
No. patients with ≥1 abnormal liver test result††	50 (62.5, 51.0–73.1)

*Values are no. (%, 95% CI) unless otherwise noted. IQR, interquartile range.
†Data available for 96 patients.
‡Data available for 84 patients.
§Median 7, range 6–45.
¶Data available for 79 patients.
#Data available for 80 patients.
**Data available for 33 patients.
††Data available for 80 patients.

in patients with more severe illness (those who were hospitalized compared with those who were not). Information on TBEV RNA load in humans is very limited (*24*,*26*). In our previous report on viral RNA load in patients with biphasic course of TBE, the load was higher in women than in men but was not significantly associated with clinical and laboratory characteristics of the initial phase of illness or with characteristics of the later meningoencephalitic phase of TBE (*26*). However, because several associations tested in this study were not analyzed in our previous study (and vice versa), direct comparison is restricted to matching approaches; within them, the only discordant result was for viral RNA load according to sex, which was significantly higher in women than men in the previous study but not in this study.

Some review articles have stated that febrile illness without later CNS involvement is a frequent clinical manifestation of infection with TBEV, representing approximately two thirds of all clinically manifested infections with TBEV (*20*–*23*). However, a PubMed literature search of titles and abstracts using the search terms "(tick-borne encephalitis) AND (initial phase OR first phase)" and without time limitation (i.e., from 1966 onward) did not reveal any primary source firmly supporting such statements for Western and Central Europe. Nevertheless, febrile illness resulting from TBEV infection without subsequent CNS involvement is usually not recognized, possibly because of the small proportion of such cases (*38*), which is in accordance with some other reports (*5*,*6*,*24*,*25*). Our previous findings, which were based on clinical and serologic analyses of febrile illness after a tick bite, suggested that febrile illness resulting from infection with TBEV occurs as a rule with subsequent CNS involvement (TBE) after an improvement of up to 12 days (*25*,*34*). In this study, which was focused on 62 patients with well-defined TBEV infection, 52 (84%) patients experienced overt symptoms and signs of CNS involvement associated with CSF lymphocytic pleocytosis, 6 (10%) patients remained completely asymptomatic, and 4 (6%) patients in whom CSF was not examined experienced mild symptoms not associated with meningeal signs for a duration of 2–7 days. We expected that patients in whom TBE did not occur would have lower blood levels of virus than those in whom CNS involvement occurred; these speculations were not confirmed.

The main strengths of our study are the sufficiently large number of patients with a well-defined diagnosis of febrile illness resulting from TBEV infection (on the basis of demonstration of viral RNA in serum samples during actual illness and on later seroconversion), together with the comprehensive collection of clinical and laboratory data and assessment of the course and outcome of the illness. We reveal several new clinical and laboratory details of febrile illness caused by TBEV, confirming that in most (at least 84%) of these patients, TBE (i.e., CNS inflammation) later develops. However, because we included only patients referred to us by family physicians, one of the limitations of the study is a potential selection bias: patients with very mild illness probably do not visit primary physicians and, even if they do, the likelihood of referral to us is lower than for patients with more severe disease or unusual laboratory findings, such as leukopenia or thrombocytopenia. Thus, our findings are limited to a subset of patients with more severe disease; consequently, our conclusions might not be valid for milder clinical cases.

In conclusion, febrile illness caused by TBEV infection is characterized clinically by the presence of malaise or fatigue (98%), fever (97%), headache (86%), and myalgias (54%) and in laboratory tests by leukopenia (88%), thrombocytopenia (59%), and abnormal liver test results (63% of patients had ≥1 abnormal liver test, usually elevated AST and ALT) but normal inflammatory markers. The infection proceeded to TBE in ≥5/6 (84%) patients within 18 days after defervescence. Clinical and laboratory findings in patients

Table 3. Basic demographic, clinical, and laboratory characteristics of febrile illness caused by tick-borne encephalitis virus infection with or without subsequent central nervous system involvement*

Characteristic	Febrile illness followed by CNS involvement, n = 52	Febrile illness with possible later CNS involvement, n = 4	Febrile illness without later CNS involvement, n = 6
Sex			
F	26 (50.0, 35.8–64.2)	2 (50.0, 6.8–93.2)	3 (50.0, 11.8–88.2)
M	26 (50.0, 35.8–64.2)	2 (50.0, 6.8–93.2)	3 (50.0, 11.8–88.2)
Median age, y (IQR)	50 (40.75–62)	52 (51.75–55)	45.5 (34.5–55)
Underlying illnesses	22 (42.3, 28.7–56.8)	0 (0, 0–60.2)	3 (50.0, 11.8–88.2)
History of tick bite†	45/51 (88.2, 76.1–95.6)	3/4 (75.0, 19.4–99.4)	5/6 (83.3, 35.9–99.6)
Median incubation period, d (IQR)‡	6 (4.5–9.5)§	9 (9–9)¶	6.5 (3–11)#
Median duration of illness before first evaluation, d (IQR)	5 (3.75–7)	5.5 (5–6.25)	5 (4.25–6.5)
Clinical manifestation			
Body temperature >37.5°C	51/52 (98.1, 89.7–100)	3/4 (75.0, 19.4–99.4)	6 (100, 54.1–100)
Median body temperature, °C (IQR)**	38.5 (38–39)	38.3 (38.05–38.45)	39 (38.625–39)
Chills	10 (19.2, 9.6–32.5)	1 (25.0, 0.6–80.7)	1 (16.7, 0.4–64.1)
Headache	47 (90.4, 79.0–96.8)	2 (50.0, 6.8–93.2)	6 (100, 54.1–100)
Myalgias	27 (51.9, 37.6–66.0)	3 (75.0, 19.4–99.4)	3 (50.0, 11.8–88.2)
Arthralgias	22 (42.3, 28.7–56.8)	3 (75.0, 19.4–99.4)	2 (33.3, 4.3–77.7)
Gastrointestinal symptoms	24 (46.2, 32.2–60.5)	2 (50.0, 6.8–93.2)	3 (50.0, 11.8–88.2)
Abdominal pain	1 (1.9, 0.1–10.3)	1 (25.0, 0.6–80.7)	0 (0, 0–45.9)
Nausea, vomiting	22 (42.3, 28.7–56.8)	2 (25.0, 0.6–80.7)	2 (33.3, 4.3–77.7)
Diarrhea	6 (11.5, 4.4–23.4)	2 (50.0, 6.8–93.2)	1 (16.7, 0.4–64.1)
Malaise or fatigue	52 (100, 93.2–100)	4 (100, 39.8–100)	5 (83.3, 35.9–99.6)
Respiratory symptoms	7 (13.4, 5.6–25.8)	0 (0, 0–60.2)	1 (16.7, 0.4–64.1)
Sore throat	7 (13.4, 5.6–25.8)	0 (0, 0–60.2)	1 (16.7, 0.4–64.1)
Cough	1 (1.9, 0.1–10.3)	0 (0, 0–60.2)	0 (0, 0–45.9)
Median duration of illness, d (IQR)	7 (6–8)††	8 (7–9)‡‡	9 (7.5–9.75)
Hospitalization			
No. hospitalized patients	20 (38.5, 25.3–53.0)	2 (50.0, 6.8–93.2)	3 (50.0, 11.8–88.2)
Median duration, d (IQR)	4 (1–6)§§	4.5 (3.75–5.25)	4 (2.5–5)
Laboratory findings			
Median blood leukocyte count, × 10^9/L (IQR)	2.2 (1.8–2.85)¶¶	1.7 (1.675–1.95)	2.95 (2.5–4.15)
Blood leukocyte count <4 × 10^9/L	50 (100, 92.9–100)	4 (100, 39.8–100)	4 (66.7, 22.3–95.7)
Blood leukocyte count >10 × 10^9/L	0 (0, 0–7.1)	0 (0, 0–60.2)	0 (0, 0–45.9)
Median blood platelet count, × 10^9/L (IQR)	125.5 (108.25–152.75)¶¶	110 (86–134.25)	139 (118.5–162.5)
Blood platelet count <140 × 10^9/L	34 (68.0, 53.3–80.5)	3 (75.0, 19.4–99.4)	3 (50.0, 11.8–88.2)
Serum C-reactive protein elevated, >5 mg/L	3/50 (6.0, 1.3–16.6)##	0 (0, 0–60.2)	1 (16.7, 0.4–64.1)***
Liver tests, μkat/L (IQR)			
Median aspartate aminotransferase	0.605 (0.4575–0.84)†††	1.05 (0.59–3.55)	0.62 (0.5075–0.845)
Elevated >0.58	26 (54.2, 39.2–68.6)	3 (75.0, 19.4–99.4)	4 (66.7, 22.3–95.7)
Median alanine aminotransferase	0.535 (0.4–0.82)†††	1.285 (0.48–3.5225)	0.56 (0.3475–0.78)
Elevated >0.77 μkat/L	13 (27.1, 15.3–41.9)	2 (50.0, 6.8–93.2)	2 (33.3, 4.3–77.7)
No. patients with ≥1 abnormal liver test result	29/48 (60.4, 45.3–74.2)	3 (75.0, 19.4–99.4)	4 (66.7, 22.3–95.7)

*Values are no. (%, 95% CI) except as indicated. CNS, central nervous system; IQR, interquartile range.
†Tick bite within 4 weeks before onset of illness.
‡Time (d) from tick bite to onset of illness calculated only in patients with 1 bite.
§Data available for 27 patients.
¶Data available for 1 patient.
#Data available for 4 patients.
**The highest temperature in the course of the illness.
††Data available for 45 patients.
‡‡Data available for 2 patients.
§§Data available for 17 patients.
¶¶Data available for 50 patients.
##Median 6, range 6–9.
***Value 45.
†††Data available for 48 patients.

with TBEV febrile illness do not distinguish between patients in whom TBE later develops and those in whom it does not.

About the Author

Dr. Bogovič is an infectious diseases specialist in the Department of Infectious Diseases of the University Medical Center Ljubljana, Ljubljana, Slovenia. Her primary research interests are zoonoses, particularly tick-transmitted diseases.

References

1. Demina TV, Dzhioev YP, Verkhozina MM, Kozlova IV, Tkachev SE, Plyusnin A, et al. Genotyping and characterization of the geographical distribution of tick-borne encephalitis virus variants with a set of molecular probes. J Med Virol. 2010;82:965–76. https://doi.org/10.1002/jmv.21765
2. Kozlova IV, Demina TV, Tkachev SE, Doroschenko EK, Lisak OV, Verkhozina MM, et al. Characteristics of the Baikal subtype of tick-borne encephalitis virus circulating in Eastern Siberia. Acta Biomedicia Scientifica. 2018;3:53–60. https://doi.org/10.29413/ABS.2018-3.4.9
3. Marvik Å, Tveten Y, Pedersen AB, Stiasny K, Andreassen ÅK, Grude N. Low prevalence of tick-borne encephalitis virus antibodies in Norwegian blood donors. Infect Dis (Lond). 2021;53:44–51. https://doi.org/10.1080/23744235.2020.1819561
4. Tomažič J, Pikelj F, Schwartz B, Kunze M, Kraigher A, Matjašič M, et al.; Slovenian TBE study group. The clinical features of tick-borne encephalitis in Slovenia. A study of 492 cases in 1994. Antibiot Monitor. 1996;12:115–20.
5. Günther G, Haglund M, Lindquist L, Forsgren M, Sköldenberg B. Tick-bone encephalitis in Sweden in relation to aseptic meningo-encephalitis of other etiology: a prospective study of clinical course and outcome. J Neurol. 1997;244:230–8. https://doi.org/10.1007/s004150050077
6. Kaiser R. The clinical and epidemiological profile of tick-borne encephalitis in southern Germany 1994-98: a prospective study of 656 patients. Brain. 1999;122:2067–78. https://doi.org/10.1093/brain/122.11.2067
7. Kaiser R, Holzmann H. Laboratory findings in tick-borne encephalitis—correlation with clinical outcome. Infection. 2000;28:78–84. https://doi.org/10.1007/s150100050051
8. Mickiene A, Laiskonis A, Günther G, Vene S, Lundkvist A, Lindquist L. Tickborne encephalitis in an area of high endemicity in lithuania: disease severity and long-term prognosis. Clin Infect Dis. 2002;35:650–8. https://doi.org/10.1086/342059
9. Kaiser R. Tick-borne encephalitis (TBE) in Germany and clinical course of the disease. Int J Med Microbiol. 2002;291(Suppl 33):58–61. https://doi.org/10.1016/S1438-4221(02)80012-1
10. Logar M, Bogovic P, Cerar D, Avsic-Zupanc T, Strle F. Tick-borne encephalitis in Slovenia from 2000 to 2004: comparison of the course in adult and elderly patients. Wien Klin Wochenschr. 2006;118:702–7. https://doi.org/10.1007/s00508-006-0699-6
11. Misić Majerus L, Daković Rode O, Ruzić Sabljić E. Post-encephalitic syndrome in patients with tick-borne encephalitis [in Croatian]. Acta Med Croatica. 2009;63:269–78.
12. Radzišauskienė D, Urbonienė J, Kaubrys G, Andruškevičius S, Jatužis D, Matulytė E, et al. The epidemiology, clinical presentation, and predictors of severe tick-borne encephalitis in Lithuania, a highly endemic country: A retrospective study of 1040 patients. PLoS One. 2020;15:e0241587. https://doi.org/10.1371/journal.pone.0241587
13. Barp N, Trentini A, Di Nuzzo M, Mondardini V, Francavilla E, Contini C. Clinical and laboratory findings in tick-borne encephalitis virus infection. Parasite Epidemiol Control. 2020;10:e00160. https://doi.org/10.1016/j.parepi.2020.e00160
14. Bogovič P, Lotrič-Furlan S, Avšič-Županc T, Korva M, Kastrin A, Lusa L, et al. Comparison of clinical, laboratory and immune characteristics of the monophasic and biphasic course of tick-borne encephalitis. Microorganisms. 2021;9:796. https://doi.org/10.3390/microorganisms9040796
15. Kohlmaier B, Schweintzger NA, Sagmeister MG, Švendová V, Kohlfürst DS, Sonnleitner A, et al.; The Eu-Tick-Bo Study Group. Clinical characteristics of patients with tick-borne encephalitis (TBE): a European multicentre study from 2010 to 2017. Microorganisms. 2021;9:1420. https://doi.org/10.3390/microorganisms9071420
16. Mansfield KL, Johnson N, Phipps LP, Stephenson JR, Fooks AR, Solomon T. Tick-borne encephalitis virus—a review of an emerging zoonosis. J Gen Virol. 2009;90:1781–94. https://doi.org/10.1099/vir.0.011437-0
17. Bogovic P, Strle F. Tick-borne encephalitis: a review of epidemiology, clinical characteristics, and management. World J Clin Cases. 2015;3:430–41. https://doi.org/10.12998/wjcc.v3.i5.430
18. Taba P, Schmutzhard E, Forsberg P, Lutsar I, Ljøstad U, Mygland Å, et al. EAN consensus review on prevention, diagnosis and management of tick-borne encephalitis. Eur J Neurol. 2017;24:1214–e61. https://doi.org/10.1111/ene.13356
19. Bogovič P, Stupica D, Rojko T, Lotrič-Furlan S, Avšič-Županc T, Kastrin A, et al. The long-term outcome of tick-borne encephalitis in Central Europe. Ticks Tick Borne Dis. 2018;9:369–78. https://doi.org/10.1016/j.ttbdis.2017.12.001
20. Kunz C. Tick-borne encephalitis in Europe. Acta Leiden. 1992; 60:1–14.
21. Granström M. Tick-borne zoonoses in Europe. Clin Microbiol Infect. 1997;3:156–69. https://doi.org/10.1111/j.1469-0691.1997.tb00592.x
22. Dumpis U, Crook D, Oksi J. Tick-borne encephalitis. Clin Infect Dis. 1999;28:882–90. https://doi.org/10.1086/515195
23. Borde JP, Zajkowska J. TBE in adults. In: Dobler G, Erber W, Bröker M, Schmitt HJ, editors. The TBE Book, 2nd ed. Singapore: Global Health Press; 2019. p. 105–24.
24. Schultze D, Dollenmaier G, Rohner A, Guidi T, Cassinotti P. Benefit of detecting tick-borne encephalitis viremia in the first phase of illness. J Clin Virol. 2007;38:172–5. https://doi.org/10.1016/j.jcv.2006.11.008
25. Lotrič-Furlan S, Avsic-Zupanc T, Strle F. Is an isolated initial phase of a tick-borne encephalitis a common event? Clin Infect Dis. 2000;30:987–8. https://doi.org/10.1086/313838
26. Saksida A, Jakopin N, Jelovšek M, Knap N, Fajs L, Lusa L, et al. Virus RNA load in patients with tick-borne encephalitis, Slovenia. Emerg Infect Dis. 2018;24:1315–23. https://doi.org/10.3201/eid2407.180059
27. van Buuren S. Multiple imputation of discrete and continuous data by fully conditional specification. Stat Methods Med Res. 2007;16:219–42. https://doi.org/10.1177/0962280206074463
28. Perperoglou A, Sauerbrei W, Abrahamowicz M, Schmid M. A review of spline function procedures in R. BMC Med Res Methodol. 2019;19:46. https://doi.org/10.1186/s12874-019-0666-3

29. R Core Team. R: A language and environment for statistical computing. Vienna, Austria: R Foundation for Statistical Computing [cited 2021 May 18]. http://www.r-project.org
30. Lotrič-Furlan S, Bogovič P, Avšič-Županc T, Jelovšek M, Lusa L, Strle F. Tick-borne encephalitis in patients vaccinated against this disease. J Intern Med. 2017;282:142–55. https://doi.org/10.1111/joim.12625
31. Bogovič P, Lotrič-Furlan S, Avšič-Županc T, Lusa L, Strle F. Factors associated with severity of tick-borne encephalitis: a prospective observational study. Travel Med Infect Dis. 2018;26:25–31. https://doi.org/10.1016/j.tmaid.2018.10.003
32. Anić K, Soldo I, Perić L, Karner I, Barac B. Tick-borne encephalitis in eastern Croatia. Scand J Infect Dis. 1998;30:509–12. https://doi.org/10.1080/00365549850161548
33. Lotric-Furlan S, Petrovec M, Avsic-Zupanc T, Strle F. Clinical distinction between human granulocytic ehrlichiosis and the initial phase of tick-borne encephalitis. J Infect. 2000;40:55–8. https://doi.org/10.1053/jinf.1999.0587
34. Lotric-Furlan S, Petrovec M, Avsic-Zupanc T, Logar M, Strle F. Epidemiological, clinical and laboratory distinction between human granulocytic ehrlichiosis and the initial phase of tick-borne encephalitis. Wien Klin Wochenschr. 2002;114:636–40.
35. Lotric-Furlan S, Strle F. Thrombocytopenia, leukopenia and abnormal liver function tests in the initial phase of tick-borne encephalitis. Zentralbl Bakteriol. 1995;282:275–8. https://doi.org/10.1016/S0934-8840(11)80127-1
36. Lotric-Furlan S, Strle F. Thrombocytopenia—a common finding in the initial phase of tick-borne encephalitis. Infection. 1995;23:203–6. https://doi.org/10.1007/BF01781197
37. Saksida A, Duh D, Lotric-Furlan S, Strle F, Petrovec M, Avsic-Zupanc T. The importance of tick-borne encephalitis virus RNA detection for early differential diagnosis of tick-borne encephalitis. J Clin Virol. 2005;33:331–5. https://doi.org/10.1016/j.jcv.2004.07.014
38. Ackermann R, Krüger K, Roggendorf M, Rehse-Küpper B, Mörtter M, Schneider M, et al. Spread of early-summer meningoencephalitis in the Federal Republic of Germany [in German]. Dtsch Med Wochenschr. 1986;111:927–33. https://doi.org/10.1055/s-2008-1068558

Address for correspondence: Petra Bogovič, University Medical Center Ljubljana, Department of Infectious Diseases, Japljeva 2, 1525 Ljubljana, Slovenia; email: petra.bogovic@kclj.si

etymologia

The Color Puce (*Pyüs*)

Clyde Partin

For those with synesthesia, in whom stimulating 1 sensory pathway gives rise to a subjective sensation of a different character, the word plague may chromatically resonate with puce. In pre-revolutionary France, an era of "evocative color nomenclature," Marie Antoinette's reign was precipitating intense criticism. Her countrymen were experiencing severe socioeconomic stress, thus her sartorial self-indulgence was much resented.

After discovering the Queen wearing a new gown, her husband, Louis XVI, the King of France, chided her, describing the dress's unflattering purple–brown hue as "*couleur de puce*" (color of fleas). This admonishment had the unintended consequence of promoting puce as the exclusive color worn by the French court. Puce, the French word for flea, descends from *pulex* (Latin). Flea droppings leave puce colored "bloodstains" on bedsheets. The role of fleas, however, as a vector for bubonic plague was not proven until about 1895.

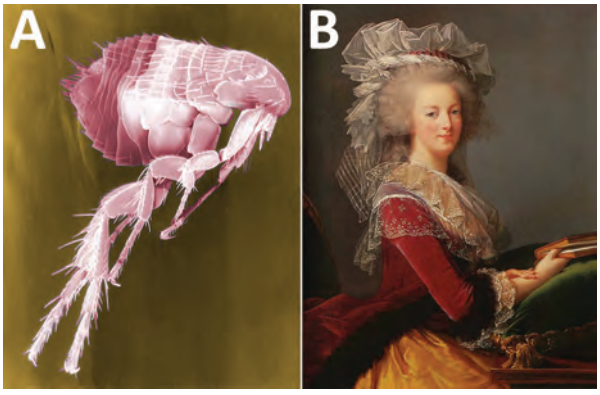

Figure. A) Digitally colored scanning electron microscopic image of a flea. Puce is a particularly difficult color to describe. Numerous shades of puce exist, some of which are associated with different anatomic areas of the flea. Image no. 11436: Janice Haney Carr/CDC. B) Portrait of Marie Antoinette painted in 1785 for the Ministry of Foreign Affairs, by Louise Élisabeth Vigée Le Brun. Private collection, Public domain, https://www.theawl.com/2017/10/the-sexy-gross-story-of-puce. She seemed to have "preferred a shade leaning more toward ash-gray," but is seen here modeling a more standard hue of puce.

Sources

1. Stedman's Medical Dictionary. 23rd ed. Baltimore: The Williams & Wilkins Company; 1976. p. 1392.
2. St. Clair K. The secret lives of color. New York: Penguin Books; 2017. p. 122–3.
3. Zietz BP, Dunkelberg H. The history of the plague and the research on the causative agent *Yersinia pestis*. Int J Hyg Environ Health. 2004;207:165–78. https://doi.org/10.1078/1438-4639-00259
4. Plague bacteria found in Arizona fleas, by Rachael Rettner, August 14, 2017 [cited 2021 Nov 4]. https://www.livescience.com/60130-plague-fleas-arizona.html.)

Author affiliation: Emory University, Atlanta, Georgia, USA

Address for correspondence: Clyde Partin, Department of Internal Medicine, Emory University, 1365 Clifton Rd NE, Atlanta, GA 30322-1007, USA; email: wpart01@emory.edu

DOI: https://doi.org/10.3201/eid2802.212274

Role of *Anopheles* Mosquitoes in Cache Valley Virus Lineage Displacement, New York, USA

Constentin Dieme,[1] Kiet A. Ngo,[1] Shaun Tyler, Joseph G. Maffei, Steven D. Zink, Alan P. Dupuis, Cheri A. Koetzner, Chelsea Shultis, Jessica Stout, Anne F. Payne, P. Bryon Backenson, Lili Kuo, Michael A. Drebot, Alexander T. Ciota, Laura D. Kramer

Cache Valley virus (CVV) is a mosquitoborne virus that infects livestock and humans. We report results of surveillance for CVV in New York, USA, during 2000–2016; full-genome analysis of selected CVV isolates from sheep, horse, humans, and mosquitoes from New York and Canada; and phenotypic characterization of selected strains. We calculated infection rates by using the maximum-likelihood estimation method by year, region, month, and mosquito species. The highest maximum-likelihood estimations were for *Anopheles* spp. mosquitoes. Our phylogenetic analysis identified 2 lineages and found evidence of segment reassortment. Furthermore, our data suggest displacement of CVV lineage 1 by lineage 2 in New York and Canada. Finally, we showed increased vector competence of *An. quadrimaculatus* mosquitoes for lineage 2 strains of CVV compared with lineage 1 strains.

Cache Valley virus (CVV; family *Peribunyaviridae*, genus *Orthobunyavirus*) belongs to the order *Bunyavirales*, which consists of 12 families and 46 genera that are major human, livestock, and plant pathogens (*1*). CVV contains negative-sense, single-stranded RNA organized into 3 separate segments designated large (L), medium (M), and small (S) (*2*). The L RNA segment encodes the RNA-dependent RNA polymerase (L protein); the M segment encodes 2 glycoproteins, Gn and Gc, which are inserted in the viral membrane, plus a nonstructural protein; and the S segment encodes the nucleocapsid protein and a second nonstructural protein (*3*).

CVV isolates fall into 2 lineages. Lineage 1 viruses were isolated in the United States and Canada during 1956–2011, and lineage 2 consists of more recent strains from the northeastern United States (*4*). Lineage 2 was shown to have displaced lineage 1 in Connecticut, USA, during 2010–2014 (*4*). CVV is widespread throughout North and Central America and infects sheep, cattle, white-tailed deer, and humans (*4*). The virus has been isolated from >30 mosquito species in several genera; however, the principal vectors remain unknown (*5*). Accumulating evidence from surveillance suggests that *Anopheles quadrimaculatus* and *An. punctipennis* mosquitoes might be major vectors of CVV (*6*).

We performed surveillance of CVV during 2000–2016 in New York. We also determined vector competence of *An. quadrimaculatus* for representative CVV strains.

Materials and Methods

Mosquito Collection

Mosquitoes were submitted from the following regions in New York: West, Finger Lakes, North, Central, Hudson Valley, and Long Island (Figure 1). Mosquitoes were collected by local health districts by using Centers for Disease Control and Prevention light traps with CO_2 (*7*) or gravid (*8*) traps. We identified mosquitoes to species morphologically (*9*), and pooled females into groups of ≈50 mosquitoes by trap type, date collected, and trap location. Mosquitoes were transported on dry ice to the Arbovirus Laboratories, Wadsworth Center, New York State Department of Health (Slingerlands, NY, USA), for testing and were stored at −80°C until processed.

Author affiliations: New York State Department of Health, Slingerlands, New York, USA (C. Dieme, K.A. Ngo, J.G. Maffei, S.D. Zink, A.P. Dupuis, C.A. Koetzner, C. Shultis, J. Stout, A.F. Payne, L. Kuo, A.T. Ciota, L.D. Kramer); Public Health Agency of Canada, Winnipeg, Manitoba, Canada (S. Tyler, M.A Drebot); New York State Department of Health, Albany, New York, USA (P.B. Backenson); State University of New York at Albany, Albany (A.T. Ciota, L.D. Kramer)

DOI: https://doi.org/10.3201/eid2802.203810

[1]These authors contributed equally to this article.

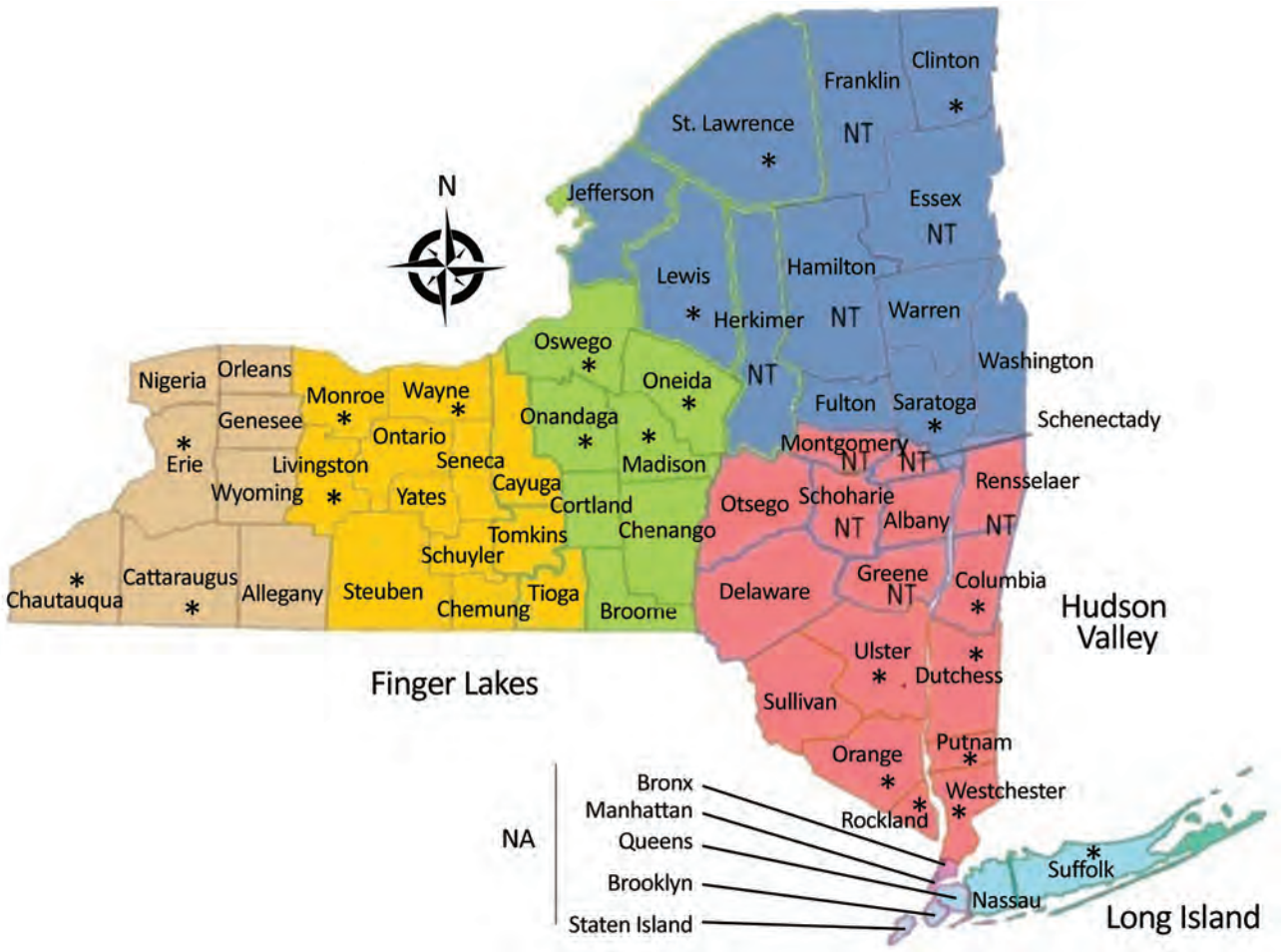

Figure 1. Counties in New York, USA, in which Cache Valley virus was studied during 2000–2016 (https://www.health.ny.gov/statistics/cancer/registry/images/nycounty). Asterisks (*) indicate counties in which samples positive for Cache Valley virus were collected. NA, counties not included in data; NT, counties not tested for Cache Valley virus.

Virus Isolation

We processed mosquito pools as described (*10*,*11*). In brief, we homogenized pools in 1 mL of mosquito diluent containing 20% fetal bovine serum, 50 μg of streptomycin/mL, 50 U of penicillin, and 2.5 μg of amphotericin B/mL in phosphate-buffered saline in a Retsch Mixer Mill (https://www.retsch.com) set to 24 cycles/s for 2 min. We used viral stocks of 2 CVV strains isolated from cerebrospinal fluid of humans (strain Hu-2022) and from brain tissue (strain PA) (*12*,*13*) for RNA extraction. We used RNA extracted from brain tissues of a horse that died from neurologic disease and tested positive for CVV in this analysis. We homogenized placenta tissues from sheep (from a ewe that had given birth to a deformed lamb in a southern Ontario flock during 2011) and used them to infect Vero E6 cells for virus isolation. Cytopathic effect was observed after 6 days, and supernatant was harvested and used for RNA extraction and to generate virus stocks.

RNA Extraction

We used extraction plates (Thermofisher, https://www.thermofisher.com), which were prepared on a Tecan Evo 150 Liquid Handler (Tecan, https://www.tecan.com) and used 50 μL of homogenates or viral stocks to extract RNA on a Magmax 96 Express (Applied Biosystems, https://www.thermofisher.com) and a MagMax Viral Isolation Kit (Thermofisher). A total of 90 μL of homogenized sample RNA was eluted.

Primer Design and Reverse Transcription PCR

We used a standard PCR to identify CVV isolates as described (*14*). Beginning in 2012, we developed a real-time reverse transcription PCR (RT-PCR) by using new primers and probes (CVVF1, CVVR1, and CVV1 probe) to expedite the surveillance process (Table 1). A quantitative RT-PCR was developed according to manufacturer's protocol (Quanta Biosciences, https://www.quantabio.com) with slight modifications.

Table 1. Sequences of primers and probes used for detection of CVV, New York, USA*

Name	Sequence, 5′ → 3′	Primer/probe
CVVF1	ACAGCCAATGGTGTCGAAAAC	Primer
CVVR1	TGCAGGGATGCTAGACAAGATG	Primer
CVV1Probe	6FAM-CTGACGGTATTGAATCAGCAT-MGBNFQ	Probe
CVVF2	GGTGCCACATAAAGAAAACTG	Primer
CVVR2	GCCAAGCAACCAAACTC	Primer
CVV-1-R	TGATGGCCAAACAACCAA AT	Primer
CVV-1-F	GTGCCACATAAAGAGAACTGGATG	Primer
CVV2Probe	56FAM-CACCCCCATCTGCTTGTTCTTTCCTGAGAG-3IBkFQ	Probe

*CVV, Cache Valley virus.

The final volume of the reaction was 15 µL and consisted of 10 µL of master mixture and 5 µL of template. Each reaction contained 0.7 µmol/L of each forward and reverse primers and 0.3 µmol/L of probe. We performed real-time quantitation by using ABI Prism 7500 (Life Technologies, https://www.thermofisher.com). Cycling conditions were as follows: 3 min at 50°C, followed by 10 min at 95°C, then 40 cycles of alternating 95°C for 10 s and 60°C for 30 s. After introduction of CVV lineage 2, we developed new primers and probes (CVVF2, CVVR2, and CVV2 probe) for better detection (Table 1).

Maximum-Likelihood Estimation

We used maximum-likelihood estimation calculations to determine prevalence of CVV in mosquitoes. These calculations were based on a program developed by Brad Biggerstaff (https://www.cdc.gov/westnile/resourcepages/mosqsurvsoft.html).

Sequencing

We chose representative CVV samples by county, year, and species and sent them to the National Microbiology Laboratory (Winnipeg, Manitoba, Canada) for full-genome sequencing. One PCR fragment was developed for the S segment, 3 for the M segment, and 5 for L segment (Table 2), and Sanger sequencing was performed by using BigDye version 3.1 on an ABI 3730X Analyzer L (both Thermofisher). Trace files were compiled by using SeqMan II (DNAStar, https://www.dnastar.com) to get consensus sequence for each segment. Alignments were generated by using ClustalW (https://www.clustal.org) and MEGA4 software (*15*). Phylogenetic trees were generated by using the maximum-likelihood method in Geneious version 11.1.5 (https://www.geneious.com) and PhyML (http://www.atgc-montpellier.fr) with the Jukes–Cantor substitution model. Robustness of the nodes was evaluated by performing 500 bootstrap replicates. Trees were rooted with the Fort Sherman virus S, M, and L segments (GenBank accession nos. KX100130, KX100131, and KX100132). Mean nucleotide distances between and within CVV lineages were calculated by using MEGAX software (https://berkstech.psu.edu).

Mosquito Vector Competence

A colony of unknown generations of *An. quadrimaculatus* mosquitoes (Orlando strain) was obtained from BEI

Table 2. Primers used for Sanger sequencing of CVV, New York, USA*

Primer	Sequence, 5′ → 3′	Target
CVVM	AGTAGTGTGCTACCGATA	M segment
CVVMR5	ACTCCTGCCTGCCAGAGTGC	1–2239 bp
CVVMF4	AATGCATTCCCAGGAACAAC	M segment
CVVMR2	CCTCTAGAGTCTCATGATTA	1984–3725 bp
CVVMF6	ATCCCTGCATTAGGTGGAAT	M segment
CVVM	AGTAGTGTGCTACCGATA	2981–4464 bp
CVVrtL	CTGACCATACCCGAGAGGCTAGTAGTGTACTCCT	L segment
NLR10	CTGTTGCTCTTTTTGTCTTGATGTCTGAAG	1–1717 bp
LF3	GGGGGTATTCTCAGACCAGA	L segment
NLR7	GGATCTAAAACTATAAGCCAAAAATACTT	1482–3221 bp
NLF6	CTAAAGAAAGATGTAAGTTAAATACAGATG	L segment
LR4	CATCAGTGGGTCATTTAATA	2984–4722 bp
NLF8	ATATCAATGCGCCATTATACCTTATATC	L segment
LR2	CTGACATAAATTCGAACTTC	3986–5722 bp
LF11b	ACAAATTCGATGCTCTAAAAACAA	L segment
CVVrtL	CTGACCATACCCGAGAGGCTAGTAGTGTACTCCT	5474–6871 bp
CVVrtALL	CTGACCATACCCGAGAGGCTAGTGTGTACT	S segment
CVVs	AGTAGTGTGCTCCAC	1–922 bp

*CVV, Cache Valley virus; L, large; M, medium; S, small.

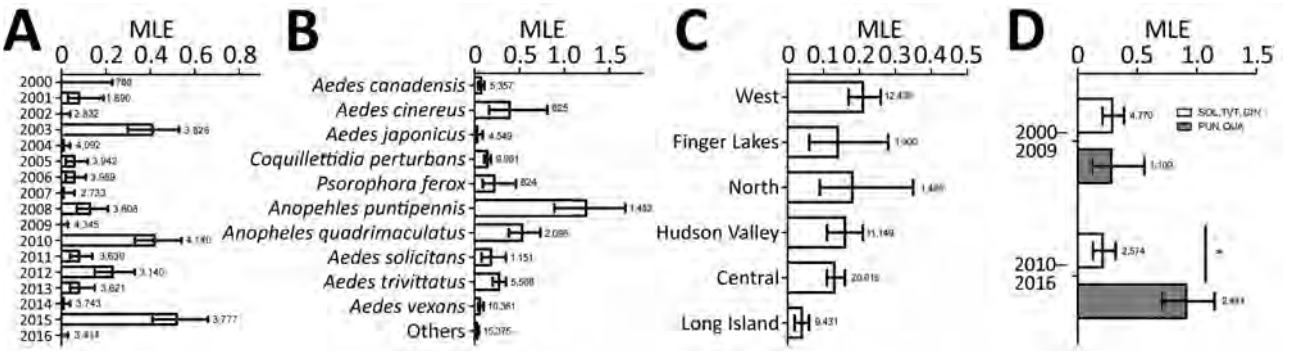

Figure 2. Cache Valley virus infection rate, New York, USA, during 2000–2016, calculated by using MLE, by year (A), mosquito species (B), New York regions (C), and combined mosquito species and years (D). Error bars indicate upper and lower limits of infection rate based on 95% confidence levels. Numbers next to bars indicate number of pools tested. MLEs were calculated by using a Centers for Disease Control and Prevention resource (https://www.cdc.gov/westnile/resourcepages/mosqsurvsoft.html). *p<0.05 by χ^2 test. CIN, *Ae. cinereus*; MLE, maximum-likelihood estimation; PUN, *An. punctipennis*; QUA, *An. quadrimaculatus*; SOL, *Ae. sollictans*; TVT, *Ae. trivittatus*.

Resources (https://www.beiresources.org) (MRA-139) and were maintained at 27°C under standard rearing conditions (27 ± 1°C, 70% relative humidity, 12:12-h light:dark photoperiod) (*16*). Freshly propagated virus supernatant from infected Vero (African green monkey kidney) cultures were harvested at 48 h after infection (multiplicity of infection ≈1.0) and diluted 1:1 with defibrinated sheep blood and 2.5% sucrose mixture without freezing. In addition to undiluted supernatant, 10-fold dilutions from 1:10 to 1:10,000 were made in C6/36 maintenance medium (Eagle minimum essential medium containing 2% fetal bovine serum heat-inactivated with 0.5 g/L of sodium bicarbonate plus 0.1 mmol/L nonessential amino acids plus 100 U/mL penicillin/streptomycin) before being mixed 1:1 with defibrinated sheep blood and a final concentration of 2.5% sucrose. Female mosquitoes (3–5 days old) were deprived of sugar for 1–2 hours and allowed to feed on CVV-defibrinated sheep blood–sucrose mixture for 30 min in a Hemotek membrane feeding system (Discovery Workshops, https://accrington.cylex-uk.co.uk) with a porcine sausage casing membrane at 37°C.

After feeding, females were anesthetized with CO_2 and fully engorged mosquitoes were transferred to 0.6-liter cardboard containers and maintained with 10% sucrose at 27°C, 70% relative humidity, and a 12:12-h light: dark photoperiod. Infection, dissemination, and transmission assays were performed on days 6 and 15 after the infectious blood meal as described (*17*). On day 2 after feeding, because of the early time point, only infection and dissemination assays were performed. Dissemination rate is the proportion of mosquitoes with infected legs among infected mosquitoes; transmission rate is the proportion of mosquitoes with positive saliva among mosquitoes with disseminated infection. We compared infection, dissemination, and transmission rates among strains by using χ^2 analysis, followed by Bonferroni corrections for multiple comparisons in GraphPad Prism version 7.05 (GraphPad Software, https://www.graphpad.com). We used a TaqMan real-time reverse transcription to detect CVV by using primers and probe targeting both lineage 1 and 2 (Table 1).

Results

CVV Surveillance

We sampled 1,842,352 female mosquitoes in 57,321 mosquito pools from 2000–2016, yielding a total of 255 CVV-positive pools. We compared MLE of prevalence by year (Figure 2, panel A), mosquito species (Figure 2, panel B), and regions (Figure 2, panel C). CVV activity fluctuated substantially during the 17-year sampling period. The highest estimates of prevalence were during 2003 (0.41, 95% CI 0.30–0.53), 2010 (0.42, 95% CI 0.33–0.54), and 2015 (0.52, 95% CI 0.41–0.66). No CVV was detected during 2000, 2002, 2009, and 2016. Comparable CVV prevalence was measured in 2001 (0.08, 95% CI 0.03–0.19), 2005 (0.06, 95% CI 0.02–0.12), 2006 (0.06, 95% CI 0.02–0.11), 2008 (0.13, 95% CI 0.07–0.21), 2011 (0.08, 95% CI 0.04–0.14), and 2013 (0.08, 95% CI 0.04–0.08).

In addition, we calculated prevalence for 10 mosquito species that had the highest number of CVV isolations. The 5 mosquito species with the highest MLE were *An. punctipennis* (1.24), *An. quadrimaculatus* (0.53), *Aedes cinereus* (0.39), *Ae. trivittatus* (0.27), and *Ae. sollicitans* (0.18) (Figure 2, panel B). To show which mosquito genus was driving transmission of CVV in New York, we compared the combined top 5 mosquito MLEs of *Aedes* and *Anopheles* species. The prevalence for *Ae. sollicitans*, *Ae. cinereus*, and *Ae. trivittatus*

mosquitoes was 0.29 compared with 0.28 for *An. quadrimaculatus* and *An. punctipennis* mosquitoes during 2000–2009 (Figure 2, panel D). During 2010–2016, the combined prevalence for *An. quadrimaculatus* and *An. punctipennis* mosquitoes increased significantly to 0.91 ($p<0.05$ by χ^2 test), and prevalence for *Ae. sollictans*, *Ae. cinereus*, and *Ae. trivitattus* mosquitoes decreased to 0.21. Similar infection rates were observed throughout New York regions, except Long Island, where the rate was on average lower than those for the rest of the regions (0.04) (Figure 2, panel C).

Phylogenetic Analysis of CVV

We sequenced 48 CVV isolates representing various New York counties, hosts, and isolation dates and 3 isolates from Canada (Table 3). Most of the CVV isolates were from mosquitoes, except 4 that were isolated from 2 humans, 1 sheep, and 1 horse. Phylogenetic analysis of CVV confirmed 2 distinct lineages (lineages 1 and 2) (Figure 3). Lineage 1 contained all CVV strains obtained during 2001–2010, and lineage 2 contained isolates obtained during 2011–2016. Segment reassortment between M and S was observed

Table 3. Characteristics for Cache Valley virus strains, New York, USA, and Ontario, Canada, 2000–2016

Year	Mosquito species	County	Strain	Lineage
2001	*Coquillettidia perturbans*	Saratoga	NY1	Lineage 1
2001	*Cq. perturbans*	Dutchess	NY15	Lineage 1
2001	*Aedes japonicus*	Ulster	NY16	Lineage 1
2001	*Cq. perturbans*	Saratoga	NY17	Lineage 1
2003	*Cq. perturbans*	Onondaga	NY2	Lineage 1
2003	*Cq. perturbans*	Oswego	NY3	Lineage 1
2003	*Ae sollicitans*	Suffolk	NY4	Lineage 1
2003	*Ae. trivittatus*	Orange	NY5	Lineage 1
2003	*Ae. trivittatus*	Westchester	NY6	Lineage 1
2003	*Ae. cinereus*	Westchester	NY7	Lineage 1
2003	*Ae. vexans*	Erie	NY8	Lineage 1
2003	*Ae. trivittatus*	Columbia	NY9	Lineage 1
2003	*Ae. trivittatus*	Dutchess	NY10	Lineage 1
2003	*Ae. vexans*	Orange	NY11	Lineage 1
2003	*Ae. canadensis*	Westchester	NY12	Lineage 1
2003	*Ae. cinereus*	Westchester	NY13	Lineage 1
2003	*Ae. triseriatus*	Orange	NY14	Lineage 1
2003	*Ae. cinereus*	Erie	NY18	Lineage 1
2003	*Ae. canadensis*	Madison	NY19	Lineage 1
2003	*Culex salinarius*	Orange	NY20	Lineage 1
2003	*Anopheles punctipennis*	Dutchess	NY21	Lineage 1
2003	*Ae. sollicitans*	Suffolk	NY22	Lineage 1
2003	*Ae. triseriatus*	Putnam	NY23	Lineage 1
2004	*Ae. vexans*	Orange	NY24	Lineage 1
2005	*Ae. vexans*	Erie	NY25	Lineage 1
2005	*Ae. vexans*	Monroe	NY26	Lineage 1
2005	*Cq. perturbans*	Lewis	NY27	Lineage 1
2006	*Ae. trivittatus*	Chautauqua	6048	Lineage 1
2006	*Ae. trivittatus*	Chautauqua	6065	Lineage 1
2006	*Ae. trivittatus*	Chautauqua	6066	Lineage 1
2006	*Ae. trivittatus*	Chautauqua	6078	Lineage 1
2006	*Ae vexans*	Chautauqua	6194	Lineage 1
2006	*An. punctipennis*	Wayne	58027	Lineage 1
2007	*An. punctipennis*	Madison	26119	Lineage 1
2011	Horse	Cattaraugus	R11–5096	Lineage 1
2011	Human	Unknown	Hu-2011	Lineage 2
2012	Sheep	Ontario	cvv_placenta	Lineage 2
2012	*Ae. trivittatus*	Ontario	OT4651	Lineage 2
2012	*An. punctipennis*	Ontario	OT4688	Lineage 2
2015	*Ae. trivittatus*	Orange	15350152	Lineage 2
2015	*Ae. vexans*	Oswego	15370591	Lineage 2
2015	*Cq. perturbans*	Onondaga	15330577	Lineage 2
2015	*Cq. perturbans*	Oswego	15370479	Lineage 2
2015	*Cq. perturbans*	Oswego	15370500	Lineage 2
2015	*Cq. perturbans*	Oswego	15370522	Lineage 2
2015	*Cq. perturbans*	Oswego	15370514	Lineage 2
2015	*Cq. perturbans*	Oswego	15370550	Lineage 2
2015	*An. punctipennis*	Cattaraugus	15041170	Reassortant
2015	*An. punctipennis*	Chatauqua	15060131	Reassortant
2015	*An. quadrimaculatus*	Cattaraugus	15041084	Reassortant
2016	Human	Allegany	PA	Reassortant

in 4 samples, 3 from mosquito isolates (15041170, 15060131, and 15041084) and 1 from a human isolate (PA). All reassortants contain an lineage 1 L segment and lineage 2 S and M RNA segments. The 3 CVV strains isolated in Canada (1 isolate from a ewe placenta and 2 isolates from mosquito pools, all collected in Ontario during 2012) all grouped within lineage 2. There was no evidence of spatial clustering of clades

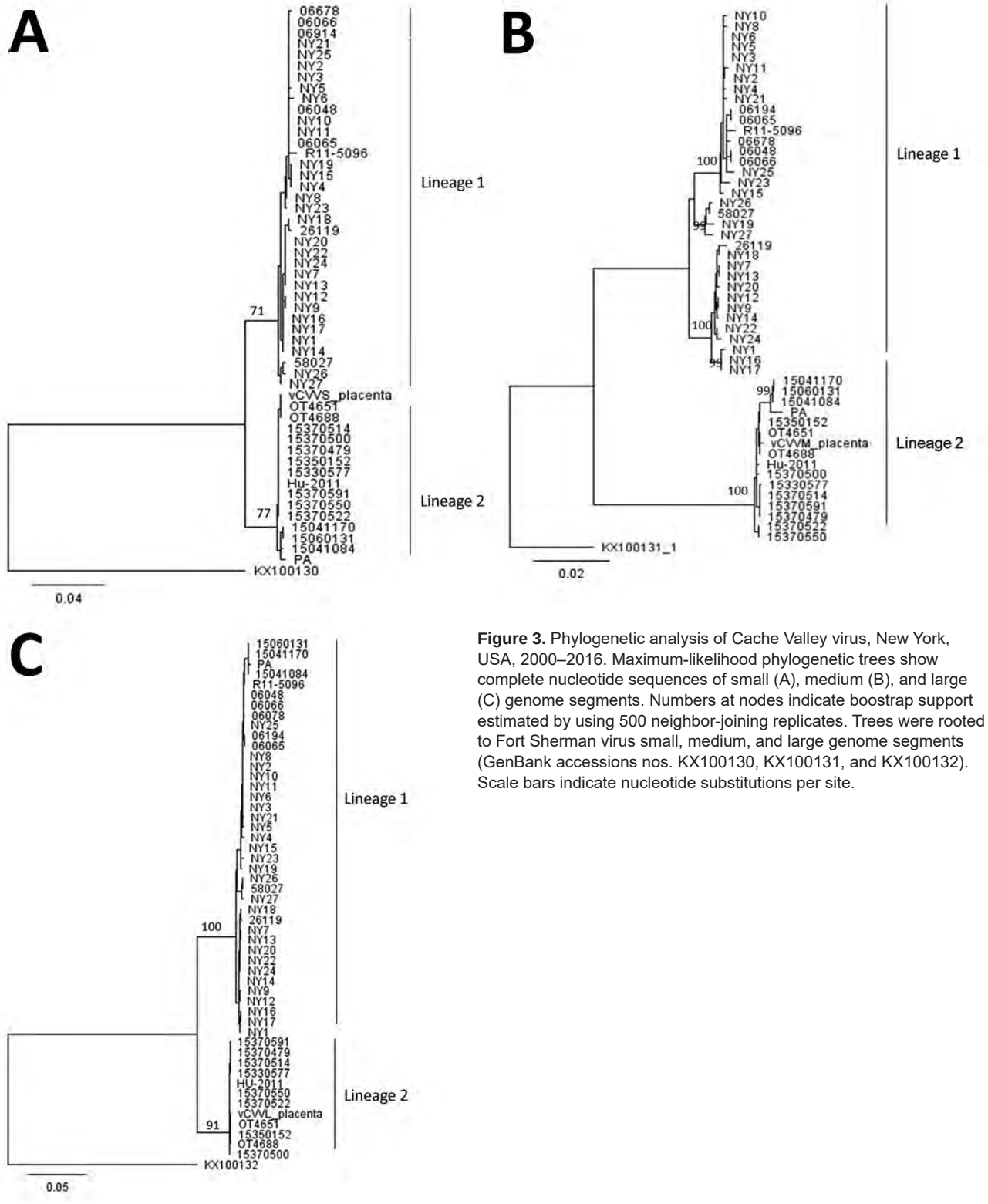

Figure 3. Phylogenetic analysis of Cache Valley virus, New York, USA, 2000–2016. Maximum-likelihood phylogenetic trees show complete nucleotide sequences of small (A), medium (B), and large (C) genome segments. Numbers at nodes indicate boostrap support estimated by using 500 neighbor-joining replicates. Trees were rooted to Fort Sherman virus small, medium, and large genome segments (GenBank accessions nos. KX100130, KX100131, and KX100132). Scale bars indicate nucleotide substitutions per site.

within the S, M, and L segments, except the reassortants, which all came from western New York regions (Cattaraugus, Chautauqua, and Allegany Counties). Mean genetic distance calculated as the number of nucleotide substitutions per site between lineage was 0.040 for the S segment, 0.074 for the M segment, and 0.051 for the L segment (Table 4). On average, there were more nucleotide substitutions for the M segment (0.074) than for the S (0.040) and L (0.051) segments.

Mosquito Vector Competence

We conducted vector competence assays with *An. quadrimaculatus* mosquitoes for 2 lineage 1 (NY10, NY25), 3 lineage 2 (15350152, 15330577, and Hu2011), and 4 reassortant (15041084, PA, 15041170, and 15060131) strains to determine whether there were differences between the lineages or between strains in the same lineage and to address effects of reassortment. We also hoped to determine whether vector competence was a potential mechanism of displacement of lineage 1 (Tables 5, 6). Our results indicate that lineage 1 strains are generally less infectious in *An. quadrimaculatus* mosquitoes because they had a 50% infectious dose ≈0.5–1.0 $\log_{10}$ higher than that for lineage 2 (Table 5).

We also found decreased dissemination and transmission for lineage 1 strains of CVV compared with lineage 2 strains ($p<0.05$ by χ^2 test) (Tables 5, 6). We observed that CVV disseminated efficiently in *An. quadrimaculatus* mosquitoes by 2 days postfeeding. All mosquitoes infected with lineage 2 strains had disseminated virus, and dissemination of lineage 1 strains was more variable (Tables 5, 6). In addition, *An. quadrimaculatus* mosquitoes are a competent vector for the lineage 2 human strain but not for the human reassortant (PA) strain (lineage 1 L RNA segment and lineage 2 S and M RNA segments), which had a low dissemination rate. Except for the PA strain, *An. quadrimaculatus* mosquitoes were able to transmit CVV at day 6 postfeeding on an artificial blood meal with a high viral titer (6.0–7.0 $\log_{10}$ PFU/mL). When mosquitoes were infected with a lower viral titer (4.0 $\log_{10}$ PFU/mL), the infection rate decreased from 95%–100% to 12% for lineage 1, from 100% to 28%–64% for lineage 2, and from 85%–100% to 24%–52% for reassortants (Tables 5, 6).

Discussion

Consistent with the findings of Armstrong et al., who analyzed CVV strains from Connecticut (*4*), we identified substantial variability in CVV activity in New York during 2000–2016. In addition, in both states, CVV could be isolated from different mosquito genera, including *Aedes, Anopheles,* and *Coquillettidia* (*6*). In our study, the prevalence of CVV in *An. punctipennis* and *An. quadrimaculatus* mosquitoes during 2010–2016 (0.91) was higher than that during 2000–2009 (0.21). Although many mosquito species are apparently infected with CVV, our data and previous surveillance data for Connecticut (*6*) all point to *Anopheles* spp. mosquitoes driving virus activity.

At least 51 different viruses have been detected in *Anopheles* spp, including 14 viruses with potential to cause febrile disease if transmitted to humans or other vertebrates, such as o'nyong nyong virus, Venezuelan equine encephalitis virus, Western equine encephalitis virus, Sindbis virus, Semliki Forest virus, Rift Valley fever virus, West Nile virus, Japanese encephalitis virus, Wesselsbron virus, Tataguine virus, Batai virus, CVV, Tahyna virus, and Tensaw virus (*18*). However, only o'nyong nyong virus, which is closely related to chikungunya virus, is known to be consistently transmitted to vertebrates by *Anopheles* mosquitoes (*19*). Other studies supported potential roles of *Anopheles* mosquito species in the transmission of Rift Valley fever virus, Mayaro virus, Eastern equine encephalitis virus, and CVV (*20*–*24*). These data and our results confirmed that *Anopheles* mosquitoes have the potential to sustain transmission cycles of arboviruses. Additional studies are needed to elucidate their role in these cycles.

An. quadrimaculatus and *An. punctipennis* mosquitoes are mainly mammalian feeders in the northeastern United States, and white-tailed deer is the most commonly identified vertebrate host (*25*). Both mosquito species bite outdoors throughout the night and show higher activity at dusk and dawn and resting outdoors (*26*,*27*). In New York, white-tailed deer tested for CVV antibodies showed infection rates of 25.7% (*28*). White-tailed deer have been identified as the principal reservoir and amplification hosts for CVV, and their overabundance and availability for both *Anopheles* mosquitoes species that are frequently infected by the virus in nature (*6*,*27*–*30*) could partially explain the increase of CVV activity in *Anopheles* spp. observed in our study.

Early phylogenetic analysis of CVV strains from United States and Canada showed only a single lineage (*31*,*32*). Armstrong et al. reported emergence of a new lineage of CVV in Connecticut during 2010, displacement of lineage 1 by 2014, and no evidence of genome reassortment (*4*). Our phylogenetic analysis confirmed that the displacement of CVV lineage 1 was widespread in the region and throughout eastern Canada because the CVV lineage 2 was responsible for several outbreaks of fetal malformation disease

Table 4. Mean genetic distances for 3 genomic segments of 2 lineages of Cache Valley virus, New York, USA, 2000–2016

Lineage	Intralineage (interlineage)		
	Small	Medium	Large
1	0.0046 (0.040)	0.0109 (0.074)	0.0062 (0.051)
2	0.0023 (0.040)	0.0033 (0.074)	0.0278 (0.051)

in Ontario and Quebec sheep flocks during 2012 and 2013 (M.A. Drebot, unpub. data). Furthermore, we demonstrated that *An. quadrimaculatus* mosquitoes are a competent vector for both CVV lineages and reassortants. The differential susceptibility between lineage 1 and lineage 2 suggest that *An. quadrimaculatus* mosquitoes might be actively involved in lineage 1 displacement in the northeast United States and can potentially increase the risk for spillover to humans in the region because lineage 2 is more infectious and more readily transmitted.

We isolated 4 reassortant strains that contained lineage 1 L segments and lineage 2 S and M RNA segments, and all came from counties in western New York. Reassortment is an evolutionary mechanism of segmented RNA viruses to exchange genetic information during co-infection of cells, which generates new genotypes and phenotypes (*33*,*34*). During reassortment, entire genes are exchanged among different viral strains or species by the swapping of segments, which confer major fitness advantages or disadvantages to the progeny virus (*34*). In the family *Peribunyaviridae*, reassortment events have occurred between virus lineages. Intraspecies, interlineage reassortment events were reported for Rift Valley fever virus, a phlebovirus and a mosquitoborne zoonotic virus that affects domestic animals and humans (*35*), and also for Crimean-Congo hemorrhagic fever virus (*33*,*36*,*37*), a highly infectious orthonairovirus transmitted by *Hyalomma* spp. ticks. Furthermore, interspecies reassortment also occurs. For example, reassortment among Bunymawera serogroup viruses has been documented with Ngari virus and Potosi virus (*38*–*41*), among others. In addition, although segment reassortment among California serogroup viruses is infrequent (*42*), evidence of reassortment has been documented (*43*,*44*).

Earlier studies had demonstrated that genetic reassortment between members of the family *Peribunyaviridae* can occur in vitro in mosquito and mammal cells and in vivo in mosquitoes during a mixed infection and can produce viable new strains with major phenotypic changes in terms of infectivity and pathogenicity (*38*–*40*,*42*,*45*–*47*). Furthermore, the phenomenon of superinfection resistance might promote opportunities for segment reassortment between more distantly related viruses. However, co-infection by closely related viruses can occur only in cases in which the second virus infects rapidly after the first virus and before superinfection resistance becomes effective (*38*). In our study, 3 CVV reassortants were isolated from mosquitoes and 1 was

Table 5. Relationship between dose and competence of *Anopheles quadrimaculatus* mosquitoes for Cache Valley virus, New York, USA, 2000–2016*

Strain	Day postinfection	Blood meal titer $\log_{10}$ PFU/mL	No. infected/no. tested (%)	No. disseminated/no. tested (%)	No. transmitted.no. tested (%)
L1-NY10	15	5.1	11 /25 (44)	10/11 (90.91)	0/10 (0)
		4.2	3/25 (12)†	2/3 (66.67)	0/2 (0)
		3	0/25 (0)	NT	NT
L1-NY25	15	6.8	24/25 (96)	22/24 (91.67)	1/22 (4.55)
		5.7	13/25 (52)	12/13 (92.31)	1/12 (8.33)
		4.5	3/25 (12)†	0/3 (0)‡	NT
L2–15350152	15	5.1	18/25 (72)	18/18 (100)	0/18 (0)
		4.3	16/25 (64)	16/16 (100)	2/16 (12.50)
		3	7/25 (28)	7/7 (100)	1/7 (14.29)
L2–15330577	15	5.7	19/25 (76)	19/19 (100)	8/19 (42.11)
		5	15/25 (60)	15/15 (100)	7/15 (46.67)
		3.7	7/25 (28)	7/7 (100)	2/7 (28.57)
R-15041084	15	5.3	15/25 (60)	15/15 (100)	1/15 (6.67)
		4.4	13/25 (52)	13/13 (100)	1/13 (7.69)
		3.2	5/25 (20)	3/5 (60)	0/3 (0)
R-PA	15	4.9	10/25 (40)	0/10 (0)	NT
		3.7	6/25 (24)	0/6 (0)	NT
		2.9	0/25 (0)	NT	NT

*L1, lineage 1; L2, lineage 2; NT, not tested; R, reassortant (containing lineage 1 large RNA segment and lineage 2 small and medium RNA segments); NT, not tested.
†$p<0.05$: lineage 1 strain infection rate compared with lineage 2 (15350152) strain when mosquitoes were fed on infectious blood ≈4–4.5 $\log_{10}$ PFU/mL titer.
‡$p<0.05$: lineage 1 strains dissemination rate compared with lineage 2 strains when mosquitoes were fed on infectious blood ≈4–4.5 $\log_{10}$ PFU/mL titer.

Table 6. Infection, dissemination, and transmission rates for *Anopheles quadrimaculatus* mosquitoes for different Cache Valley virus isolates, New York, USA, 2000–2016*

Strain	Blood meal titer, log_{10} PFU/mL	Day postinfection	No. infected/no. tested (%)	No. disseminated/no. tested (%)	No. transmitted/no. tested (%)
L1-NY10	7.1	2	25/25 (100)	18/25 (72)†	NT
		6	42/42 (100)	42/42 (100)	5/42 (11.90)
		15	41/41 (100)	41/41 (100)	5/41 (12.20)
L1-NY25	6.6	2	18/25 (72)‡	3/18 (16.67)†	NT
		6	31/35 (88.57)‡	16/31 (51.61)†	0/16 (0)
		15	32/35 (91.43)‡	23/32 (71.88)†	4/23 (17.39)
L2–15350152	7.2	2	25/25 (100)	25/25 (100)	NT
		6	37/37 (100)	37/37 (100)	11/37 (29.73)
		15	44/44 (100)	44/44 (100)	24/44 (54.54)
L2–15330577	7.1	2	25/25 (100)	25/25 (100)	NT
		6	35/35 (100)	35/35 (100)	7/35 (20)
		15	35/35 (100)	35/35 (100)	10/35 (28.57)
L2-Hu2011	6.3	2	25/25 (100)	25/25 (100)	NT
		6	30/30 (100)	30/30 (100)	8/30 (26.67)
		15	30/30 (100)	30/30 (100)	9/30 (30)
	5.5	2	25/25 (100)	25/25 (100)	NT
		6	30/30 (100)	30/30 (100)	1/30 (3.33)
		15	24/24 (100)	24/24 (100)	5/24 (20.83)
R-15041084	7.1	2	25/25 (100)	25/25 (100)	NT
		6	41/41 (100)	41/41 (100)	6/41 (14.63)
		15	34/34 (100)	34/34 (100)	18/34 (52.94)
R-PA	5	2	10/25 (40)	4/10 (40)	NT
		6	21/35 (60)	3/21 (14.29)	0/3 (0)
		15	30/35 (85.71)	0/30 (0)	NT
R-15041170	7	2	25/25 (100)	25/25 (100)	NT
		6	30/30 (100)	30/30 (100)	1/30 (3.33)
		15	30/30 (100)	30/30 (100)	11/30 (36.67)
	4.7	2	24/25 (96)	11/24 (45.83)	NT
		6	30/30 (100)	29/30 (96.67)	0/29 (0)
		15	25/27 (92.59)	23/25 (92)	1/23 (4.34)
R-15060131	7.4	2	25/25 (100)	25/25 (100)	NT
		6	30/30 (100)	30/30 (100)	2/30 (6.67)
		15	21/21 (100)	21/21 (100)	4/21 (19.05)
	4.1	2	25/25 (100)	17/25 (68)	NT
		6	30/30 (100)	28/30 (93.33)	1/28 (3.57)
		15	29/30 (96.67)	26/29 (89.66)	2/26 (7.69)

*L1, lineage 1; L2, lineage 2; NT, not tested; R, reassortant (containing lineage 1 large RNA segment and lineage 2 small and medium RNA segments); NT, not tested.
†$p<0.05$: lineage 1 strains dissemination rate compared with lineage 2 strains when mosquito fed on infectious blood ≈6.3–7.4 log_{10} PFU/mL titer.
‡$p<0.05$: lineage 1 strain infection rate compared with lineage 2 strains when mosquito fed on infectious blood ≈6.3–7.4 log_{10} PFU/mL titer.

isolated from a human, and all contained the CVV lineage 1 L segment and CVV lineage 2 S and M segments. In addition, reassortant mosquito isolates that contained the L RNA segment with CVV lineage 1 were more infectious for *An. quadrimaculatus* mosquitoes than the lineage 1 strains, suggesting a probable role of the S or M RNA segments of lineage 2 strain in mosquito infectivity.

The vector competence of *Ae. albopictus* mosquitoes for Potosi virus and the susceptibility of *An. gambiae* Giles mosquitoes for Ngari virus has been demonstrated (*48*,*49*). Among the reassortant strains tested in our study, only the human reassortant strain was not transmitted by *An. quadrimaculatus* mosquitoes despite persistent infection. This difference in phenotype was probably not caused by the viral titer in the infectious blood meal because the titer was only ≈0.5 log_{10} lower for the human reassortant strain. We suspect that difference might be caused by other factors involving the virus strain and mosquito species used in our study. Addressing the potential mechanisms involved in differential vector competence phenotypes observed in *An. quadrimaculatus* mosquitoes and evaluating the role of strain variation in host competence and pathogenicity will help to clarify the consequences of genetic variation and displacement of CVV.

Acknowledgments

We thank the New York State Department of Health, the Wadsworth Center Media, and the Tissue Core Facility for providing cells and media for these studies; the New York State Arbovirus Laboratory insectary staff for providing assistance with rearing and experimentation; and Maya Andonova and Kimberly Holloway for providing technical assistance.

This study was supported by cooperative agreement U01CK000509 from the Centers for Disease Control and Prevention.

About the Author

Dr. Dieme is research scientist at the Wadsworth Center, New York State Department of Health, Slingerlands, NY. Her primary research interest is vector–pathogen interactions, especially in mosquito infections.

References

1. Virus Taxonomy. 2018b release EC 50, Washington, DC, July 2018 Email ratification February 2019 (MSL #34) [cited 2021 Oct 16]. https://talk.ictvonline.org/files/master-species-lists/m/msl/8266
2. Elliott RM. Molecular biology of the Bunyaviridae. J Gen Virol. 1990;71:501–22. https://doi.org/10.1099/0022-1317-71-3-501
3. Dunlop JI, Szemiel AM, Navarro A, Wilkie GS, Tong L, Modha S, et al. Development of reverse genetics systems and investigation of host response antagonism and reassortment potential for Cache Valley and Kairi viruses, two emerging orthobunyaviruses of the Americas. PLoS Negl Trop Dis. 2018;12:e0006884. https://doi.org/10.1371/journal.pntd.0006884
4. Armstrong PM, Andreadis TG, Anderson JF. Emergence of a new lineage of Cache Valley virus (Bunyaviridae: Orthobunyavirus) in the northeastern United States. Am J Trop Med Hyg. 2015;93:11–7. https://doi.org/10.4269/ajtmh.15-0132
5. Waddell L, Pachal N, Mascarenhas M, Greig J, Harding S, Young I, et al. Cache Valley virus: a scoping review of the global evidence. Zoonoses Public Health. 2019;66:739–58. https://doi.org/10.1111/zph.12621
6. Andreadis TG, Armstrong PM, Anderson JF, Main AJ. Spatial-temporal analysis of Cache Valley virus (Bunyaviridae: Orthobunyavirus) infection in anopheline and culicine mosquitoes (Diptera: Culicidae) in the northeastern United States, 1997–2012. Vector Borne Zoonotic Dis. 2014;14:763–73. https://doi.org/10.1089/vbz.2014.1669
7. Newhouse VF, Siverly RE. St. Louis encephalitis virus from mosquitoes in southwestern Indiana, 1964. J Med Entomol. 1966;3:340–2. https://doi.org/10.1093/jmedent/3.3-4.340
8. Reiter P. A portable battery-powered trap for collecting gravid *Culex* mosquitoes. Mosquito News. 1983;43:496–8.
9. Means RG. Mosquitoes of New York, Part II: genera of Culicidae other than *Aedes* occuring in New York. New York State Museum, 1987;430B [cited 2021 Oct 16]. http://www.nysm.nysed.gov/staff-publications/mosquitoes-new-york-part-ii-genera-culicidae-other-ae
10. Kauffman EB, Jones SA, Dupuis AP II, Ngo KA, Bernard KA, Kramer LD. Virus detection protocols for West Nile virus in vertebrate and mosquito specimens. J Clin Microbiol. 2003;41:3661–7. https://doi.org/10.1128/JCM.41.8.3661-3667.2003
11. Oliver J, Lukacik G, Kokas J, Campbell SR, Kramer LD, Sherwood JA, et al. Twenty years of surveillance for Eastern equine encephalitis virus in mosquitoes in New York State from 1993 to 2012. Parasit Vectors. 2018;11:362. https://doi.org/10.1186/s13071-018-2950-1
12. Yang Y, Qiu J, Snyder-Keller A, Wu Y, Sun S, Sui H, et al. Fatal Cache Valley virus meningoencephalitis associated with rituximab maintenance therapy. Am J Hematol. 2018;93:590–4. https://doi.org/10.1002/ajh.25024
13. Nguyen NL, Zhao G, Hull R, Shelly MA, Wong SJ, Wu G, et al. Cache valley virus in a patient diagnosed with aseptic meningitis. J Clin Microbiol. 2013;51:1966–9. https://doi.org/10.1128/JCM.00252-13
14. Ngo KA, Maffei JG, Dupuis AP II, Kauffman EB, Backenson PB, Kramer LD. Isolation of Bunyamwera serogroup viruses (Bunyaviridae, Orthobunyavirus) in New York state. J Med Entomol. 2006;43:1004–9.
15. Tamura K, Dudley J, Nei M, Kumar S. MEGA4: Molecular Evolutionary Genetics Analysis (MEGA) software version 4.0. Mol Biol Evol. 2007;24:1596–9. https://doi.org/10.1093/molbev/msm092
16. Ciota AT, Matacchiero AC, Kilpatrick AM, Kramer LD. The effect of temperature on life history traits of *Culex* mosquitoes. J Med Entomol. 2014;51:55–62. https://doi.org/10.1603/ME13003
17. Ciota AT, Bialosuknia SM, Zink SD, Brecher M, Ehrbar DJ, Morrissette MN, et al. Effects of Zika Virus strain and *Aedes* mosquito species on vector competence. Emerg Infect Dis. 2017;23:1110–7. https://doi.org/10.3201/eid2307.161633
18. Nanfack Minkeu F, Vernick KD. A systematic review of the natural virome of *Anopheles* mosquitoes. Viruses. 2018;10:10. https://doi.org/10.3390/v10050222
19. Carissimo G, Pain A, Belda E, Vernick KD. Highly focused transcriptional response of *Anopheles coluzzii* to O'nyong nyong arbovirus during the primary midgut infection. BMC Genomics. 2018;19:526. https://doi.org/10.1186/s12864-018-4918-0
20. Dieme C, Ciota AT, Kramer LD. Transmission potential of Mayaro virus by *Aedes albopictus*, and *Anopheles quadrimaculatus* from the USA. Parasit Vectors. 2020;13:613. https://doi.org/10.1186/s13071-020-04478-4
21. Blackmore CG, Blackmore MS, Grimstad PR. Role of *Anopheles quadrimaculatus* and *Coquillettidia perturbans* (Diptera: Culicidae) in the transmission cycle of Cache Valley virus (Bunyaviridae: Bunyavirus) in the Midwest, USA. J Med Entomol. 1998;35:660–4. https://doi.org/10.1093/jmedent/35.5.660
22. Brustolin M, Pujhari S, Henderson CA, Rasgon JL. *Anopheles* mosquitoes may drive invasion and transmission of Mayaro virus across geographically diverse regions. PLoS Negl Trop Dis. 018;12:e0006895. https://doi.org/10.1371/journal.pntd.0006895
23. Moncayo AC, Edman JD, Turell MJ. Effect of eastern equine encephalomyelitis virus on the survival of *Aedes albopictus, Anopheles quadrimaculatus*, and *Coquillettidia perturbans* (Diptera: Culicidae). J Med Entomol. 2000;37:701–6. https://doi.org/10.1603/0022-2585-37.5.701
24. Nepomichene TN, Raharimalala FN, Andriamandimby SF, Ravalohery J-P, Failloux A-B, Heraud J-M, et al. Vector competence of *Culex antennatus* and *Anopheles coustani* mosquitoes for Rift Valley fever virus in Madagascar. Med Vet Entomol. 2018;32:259–62. https://doi.org/10.1111/mve.12291
25. Molaei G, Farajollahi A, Armstrong PM, Oliver J, Howard JJ, Andreadis TG. Identification of bloodmeals in *Anopheles quadrimaculatus* and *Anopheles punctipennis* from eastern equine encephalitis virus foci in northeastern U.S.A. Med Vet Entomol. 2009;23:350–6. https://doi.org/10.1111/j.1365-2915.2009.00838.x
26. Molaei G, Andreadis TG, Armstrong PM, Diuk-Wasser M. Host-feeding patterns of potential mosquito vectors in Connecticut, U.S.A.: molecular analysis of bloodmeals from 23 species of *Aedes, Anopheles, Culex, Coquillettidia, Psorophora*,

and *Uranotaenia*. J Med Entomol. 2008;45:1143–51. https://doi.org/10.1093/jmedent/45.6.1143
27. McMillan JR, Armstrong PM, Andreadis TG. Patterns of mosquito and arbovirus community composition and ecological indexes of arboviral risk in the northeast United States. PLoS Negl Trop Dis. 2020;14:e0008066. https://doi.org/10.1371/journal.pntd.0008066
28. Dupuis AP, Prusinski MA, Russell A, O'Connor C, Maffei JG, Oliver J, et al. Serologic survey of mosquito-borne viruses in hunter-harvested white-tailed deer (*Odocoileus virginianus*), New York State. Am J Trop Med Hyg. 2020;104:593–603. https://doi.org/10.4269/ajtmh.20-1090
29. Whitney E, Roz AP, Rayner GA, Deibel R. Serologic survey for arbovirus activity in deer sera from nine counties in New York State. Wildl Dis. 1969;5:392–7. https://doi.org/10.7589/0090-3558-5.4.392
30. Seggos B. Deer management in urban and suburban New York : a report to the New York State Senate and Assembly, 2018 [cited 2021 Oct 16]. https://www.dec.ny.gov/docs/wildlife
31. Blitvich BJ, Loroño-Pino MA, Garcia-Rejon JE, Farfan-Ale JA, Dorman KS. Nucleotide sequencing and serologic analysis of Cache Valley virus isolates from the Yucatan Peninsula of Mexico. Virus Genes. 2012;45:176–80. https://doi.org/10.1007/s11262-012-0741-x
32. Pabbaraju K, Ho KC, Wong S, Fox JD, Kaplen B, Tyler S, et al. Surveillance of mosquito-borne viruses in Alberta using reverse transcription polymerase chain reaction with generic primers. J Med Entomol. 2009;46:640–8. https://doi.org/10.1603/033.046.0332
33. Zhou Z, Deng F, Han N, Wang H, Sun S, Zhang Y, et al. Reassortment and migration analysis of Crimean-Congo haemorrhagic fever virus. J Gen Virol. 2013;94:2536–48. https://doi.org/10.1099/vir.0.056374-0
34. McDonald SM, Nelson MI, Turner PE, Patton JT. Reassortment in segmented RNA viruses: mechanisms and outcomes. Nat Rev Microbiol. 2016;14:448–60. https://doi.org/10.1038/nrmicro.2016.46
35. Bird BH, Khristova ML, Rollin PE, Ksiazek TG, Nichol ST. Complete genome analysis of 33 ecologically and biologically diverse Rift Valley fever virus strains reveals widespread virus movement and low genetic diversity due to recent common ancestry. J Virol. 2007;81:2805–16. https://doi.org/10.1128/JVI.02095-06
36. Goedhals D, Bester PA, Paweska JT, Swanepoel R, Burt FJ. Next-generation sequencing of southern African Crimean-Congo haemorrhagic fever virus isolates reveals a high frequency of M segment reassortment. Epidemiol Infect. 2014;142:1952–62. https://doi.org/10.1017/S0950268814000818
37. Hewson R, Gmyl A, Gmyl L, Smirnova SE, Karganova G, Jamil B, et al. Evidence of segment reassortment in Crimean-Congo haemorrhagic fever virus. J Gen Virol. 2004;85:3059–70. https://doi.org/10.1099/vir.0.80121-0
38. Briese T, Calisher CH, Higgs S. Viruses of the family Bunyaviridae: are all available isolates reassortants? Virology. 2013;446:207–16. https://doi.org/10.1016/j.virol.2013.07.030
39. Groseth A, Weisend C, Ebihara H. Complete genome sequencing of mosquito and human isolates of Ngari virus. J Virol. 2012;86:13846–7. https://doi.org/10.1128/JVI.02644-12
40. Dutuze MF, Nzayirambaho M, Mores CN, Christofferson RC. A review of Bunyamwera, Batai, and Ngari viruses: understudied orthobunyaviruses with potential one health implications. Front Vet Sci. 2018;5:69. https://doi.org/10.3389/fvets.2018.00069
41. Briese T, Kapoor V, Lipkin WI. Natural M-segment reassortment in Potosi and Main Drain viruses: implications for the evolution of orthobunyaviruses. Arch Virol. 2007;152:2237–47. https://doi.org/10.1007/s00705-007-1069-z
42. Hughes HR, Lanciotti RS, Blair CD, Lambert AJ. Full genomic characterization of California serogroup viruses, genus Orthobunyavirus, family Peribunyaviridae including phylogenetic relationships. Virology. 2017;512:201–10. https://doi.org/10.1016/j.virol.2017.09.022
43. Urquidi V, Bishop DH. Non-random reassortment between the tripartite RNA genomes of La Crosse and snowshoe hare viruses. J Gen Virol. 1992;73:2255–65. https://doi.org/10.1099/0022-1317-73-9-2255
44. Reese SM, Blitvich BJ, Blair CD, Geske D, Beaty BJ, Black WC IV. Potential for La Crosse virus segment reassortment in nature. Virol J. 2008;5:164. https://doi.org/10.1186/1743-422X-5-164
45. Endres MJ, Griot C, Gonzalez-Scarano F, Nathanson N. Neuroattenuation of an avirulent bunyavirus variant maps to the L RNA segment. J Virol. 1991;65:5465–70. https://doi.org/10.1128/jvi.65.10.5465-5470.1991
46. Gerrard SR, Li L, Barrett AD, Nichol ST. Ngari virus is a Bunyamwera virus reassortant that can be associated with large outbreaks of hemorrhagic fever in Africa. J Virol. 2004;78:8922–6. https://doi.org/10.1128/JVI.78.16.8922-8926.2004
47. Cheng LL, Rodas JD, Schultz KT, Christensen BM, Yuill TM, Israel BA. Potential for evolution of California serogroup bunyaviruses by genome reassortment in *Aedes albopictus*. Am J Trop Med Hyg. 1999;60:430–8. https://doi.org/10.4269/ajtmh.1999.60.430
48. Mitchell CJ, Smith GC, Miller BR. Vector competence of *Aedes albopictus* for a newly recognized Bunyavirus from mosquitoes collected in Potosi, Missouri. J Am Mosq Control Assoc. 1990;6:523–7.
49. Odhiambo C, Venter M, Chepkorir E, Mbaika S, Lutomiah J, Swanepoel R, et al. Vector competence of selected mosquito species in Kenya for Ngari and Bunyamwera viruses. J Med Entomol. 2014;51:1248–53. https://doi.org/10.1603/ME14063

Address for correspondence: Constentin Dieme, New York State Department of Health, 5668 State Farm Rd, Slingerlands, NY 12159, USA; email: constentin.dieme@health.ny.gov

Burden of Tick-Borne Encephalitis, Sweden

Daniel Slunge, Anders Boman, Marie Studahl[1]

In recent decades, the incidence of tick-borne encephalitis (TBE) in Sweden has increased. To calculate the burden of disease over a 17-year period, we analyzed data from the Swedish National Health Data Register for TBE cases diagnosed during 1998–2014. We compared healthcare use and sick leave associated with 2,429 persons with TBE with a referent cohort of 7,287 persons without TBE. Patients with TBE were hospitalized for significantly more days during the first year after disease onset (11.5 vs. 1.1 days), logged more specialist outpatient visits (3.6 vs. 1.2 visits), and logged more sick leave days (66 vs. 10.7 days). These differences generally increased over time. The case-fatality rate for TBE was 1.1%. Our calculated cost of TBE to society provides a baseline for decisions on immunization programs. Analyzing register data, our study adds to clinical studies of smaller cohorts and model-based studies that calculate disease burden.

Tick-borne encephalitis virus (TBEV) is the cause of tick-borne encephalitis (TBE), an infectious disease of growing public health concern (*1*,*2*). In Sweden, the disease is caused by the European subtype (TBEV-Eu), which is transmitted by the vector tick *Ixodes ricinus* (*3*). Over the past 3 decades, the number of cases has dramatically increased, with an average of 391 notified cases annually during the past 5 years (2017–2021), corresponding to an incidence of 3.8 cases/100,000 population (*4*,*5*) (Figure 1). In certain regions of Sweden, however, the incidence among unvaccinated persons has been up to 8.5–12 cases/100,000 population (*6*). In Europe, only Lithuania, Latvia, Estonia, Czechia and Slovenia report higher notification rates, on national levels, than Sweden (*7*). TBEV infection is mainly asymptomatic or associated with mild signs/symptoms (e.g., fever and general malaise) but may also cause neurologic signs/symptoms in persons in all age groups (*8*). Clinical studies show that children account for 10%–16% of TBE cases (*9*). Clinical presentation ranges from mild meningitis to severe manifestations such as meningoencephalomyelitis with a risk for respiratory insufficiency requiring ventilator support in an intensive care unit (ICU) (*10*–*12*). In Europe, ≈95% of case-patients with notified TBE require hospitalization (*13*).

Although the case-fatality rate associated with TBEV-Eu (based on previous case series in Sweden) is estimated at only 0–1.4% (*14*,*15*), neurologic sequelae are common and often long lasting. The rate of incomplete recovery severely affecting quality of life at long-term follow-up is reported to be ≈40%–46% (*15*,*16*). There is no cure for TBE, but 2 inactivated TBEV-Eu vaccines resulting in 95%–100% immunogenicity are available (*17*).

In Europe, only Austria has implemented a national universal TBE vaccination program targeting the entire population, resulting in a pronounced decrease in TBE incidence (*18*,*19*). The growing incidence of TBE has stimulated discussion regarding the need for public vaccination programs in Sweden (*20*,*21*) and other countries in Europe (*22*–*24*), but thorough data concerning the burden of TBE are needed to determine cost-effectiveness.

Our purpose with this study was to provide a baseline concerning the burden of TBE to enable informed decisions on immunization programs and other healthcare interventions. We analyzed the overall burden of TBE in Sweden in terms of hospitalization, specialist outpatient visits, primary care visits, and sick leave, on the basis of register data on TBE case-patients and a matched cohort. For TBE case-patients, we also included the cost of death. The study was approved by the Regional Ethical Review Board in Gothenburg (no. 141-16).

Materials and Methods

Data Sources

We collected data from various sources and periods (Figure 2). We obtained data from the Swedish National Patient Register (provided by the National Board of Health and Welfare, https://www.socialstyrelsen.se) related to the diagnosis code for TBE (A84, International Classification of Diseases

Author affiliations: University of Gothenburg, Gothenburg, Sweden (D. Slunge, A. Boman, M. Studahl); Region Västra Götaland, Sahlgrenska University Hospital, Gothenburg (M. Studahl)

DOI: https://doi.org/10.3201/eid2802.204324

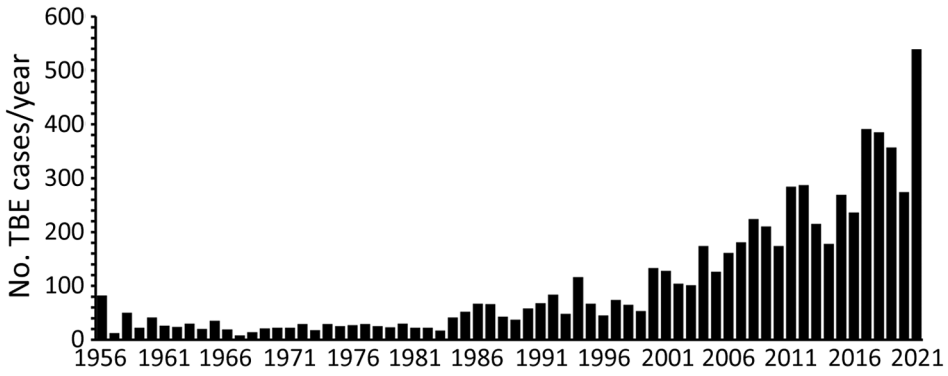

Figure 1. Reported tick-borne encephalitis cases per year, Sweden, 1956–2021. Tick-borne encephalitis became a notifiable disease in Sweden in July 2004; thus, the number of reported cases before 2005 is less certain than the number of cases from 2005 on. Source: Swedish Public Health Agency (https://www.folkhalsomyndigheten.se), 2022.

10th revision [ICD-10]), including date of notification of TBE, among patients who received inpatient care or specialist outpatient care for this diagnosis during 1998–2014. This register includes patients for whom TBE was a primary cause for hospitalization and patients ill with TBE but for whom a different primary diagnosis was the cause for hospitalization. Including both primary and nonprimary diagnoses of TBE in the data ensures that no hospitalized TBE patients are omitted. Statistics Sweden (https://www.scb.se) created a matched referent cohort encompassing 3 referent persons per TBE case-patient, on the basis of sex, age in 2014, and county of residence.

The Swedish Social Insurance Agency (https://www.forsakringskassan.se) provided data concerning numbers of sick leave days and amount of sick leave compensation during the study period for the TBE case-patients and the referent cohort. By law, the Swedish social system covers all residents 16–64 years of age and grants economic security when the ability to work is limited by ≥25% because of sickness, disability, or injury (*25*). Statistics Sweden provided the social security numbers of the referent cohort to the National Board of Health and Welfare, which provided the same information for the referent cohort as for the TBE case-patient group.

We obtained data from the Region Västra Götaland Primary Healthcare Register (https://www.vgregion.se) regarding primary care visits for persons with TBE and those in the matched cohort living in this region (1.7 million of 10 million inhabitants in Sweden). Data encompassed 5 years before through 5 years after TBE diagnosis.

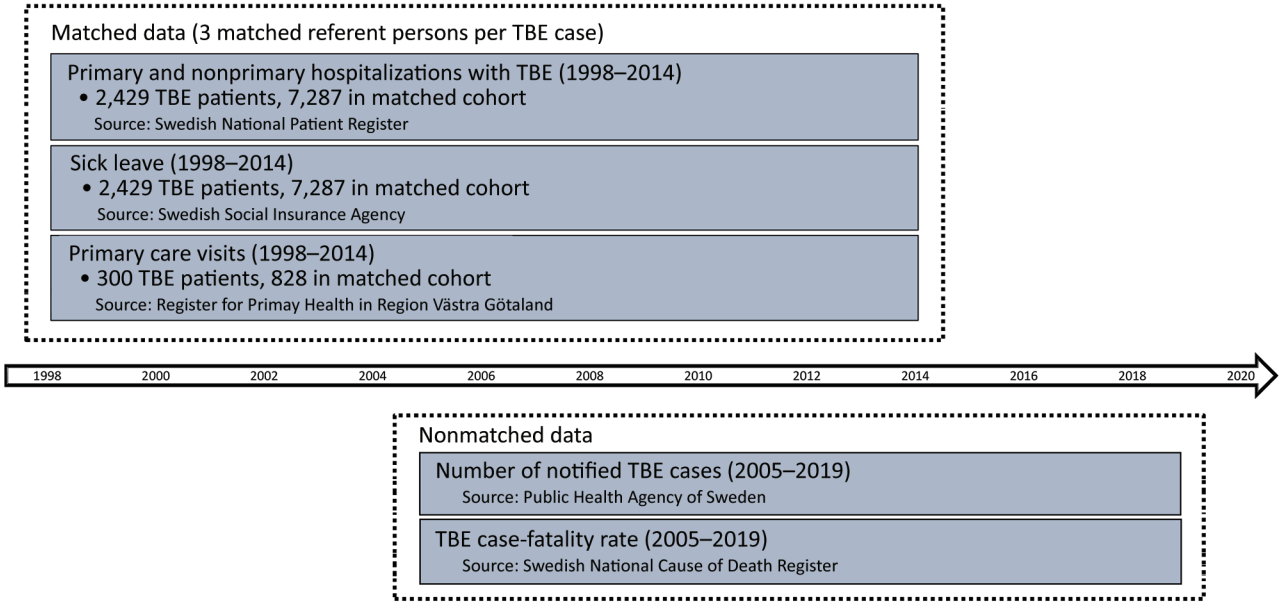

Figure 2. Sources and periods of matched and nonmatched data used in study of tick-borne encephalitis, Sweden. Swedish National Patient Register, https://www.socialstyrelsen.se; Swedish Social Insurance Agency, https://www.forsakringskassan.se; Register for Primary Health in Region Vastra Gotaland, https://www.vgregion.se; Public Health Agency of Sweden, https://www.folkhalsomyndigheten.se; Swedish National Cause of Death Register, https://www.socialstyrelsen.se.

TBE has been a notifiable disease in Sweden since July 1, 2004. The involved microbiology laboratories and the attending physicians are responsible for notifications to authorities. We obtained data on notified cases from the Public Health Agency (https://www.folkhalsomyndigheten.se)) for 2005–2019, including date of reported TBE diagnosis.

Data concerning death caused by TBE (ICD-10 code A84) were obtained from the Swedish National Cause of Death Register (https://www.socialstyrelsen.se), which covers ≈98% of deaths in Sweden. We calculated the case-fatality rate for 2005–2019, after TBE had become a notifiable disease in Sweden, and expressed it as a ratio between the number of deceased persons divided by the number of notified TBE cases in the register maintained by the Public Health Agency of Sweden.

Data Analyses

We calculated TBE-related sick leave and healthcare consumption by analyzing the number of days of sick leave and hospitalization as well as primary care and specialist outpatient visits during years 1, 3, and 5 after TBE diagnosis, after which we compared the data with that from the referent cohort. By comparing these differences with the differences in healthcare use and sick leave days over the 3-year period before date of TBE onset, we segregated the effects exclusively caused by TBE from other potential differences between the TBE case-patients and the referent cohort. We used *t*-tests to determine whether differences between the TBE case-patients and the referent cohort were statistically significant. To account for potential sick leave days and healthcare visits resulting from TBEV infection before diagnosis, we defined the date of TBE onset as occurring 31 days before the TBE diagnosis (ICD-10 code A84) was made. Febrile TBEV-related illness precedes onset of encephalitis in the biphasic course of disease, which occurs in most patients. The duration of this febrile phase is usually ≈5 days (range 2–10 days), which is then followed by a symptom-free interval of ≈7 days (range 1–21 days) before onset of the actual TBE symptoms that prompt contact with either outpatient or inpatient care (*8*). Hence, we chose 31 days to encompass the maximum number of days of illness relating to TBE before diagnosis.

We established the date of diagnosis as the first date when a diagnosis of TBE (ICD-10 code A84) was made in either outpatient specialist or inpatient care. This date was chosen because there may be a delay of weeks to months before the Public Health Agency is notified after hospitalization and because the date on which the TBE diagnosis is entered in the Swedish National Patient Register usually corresponds to the date of hospital discharge.

We calculated the burden of TBE for each outcome from the differences in mean values between TBE case-patients and the referent cohort, while also taking into account differences in the baseline values 3 years before TBE onset.

We calculated the cost of illness for all TBE patients in Sweden by using the following monetary values, based on the burden of disease estimates. The average cost per day of hospital stay during 2014–2018 was calculated to be €1,049, and the cost per specialist outpatient visit was €338, based on the cost per patient database from the Swedish Association of Local Authorities and Regions (*26*). The average cost per primary care visit was calculated to be €164, based on 2019 prices charged for a physician visit in Västra Götaland (*27*). The average cost per day of sick leave was calculated to be €199, based on loss of income and calculated by using the 2018 median monthly wage (€3,090) plus mandatory employer social security contributions in Sweden (36% of the wage), divided by the number of working days in that year (253 days) (*28*,*29*). For the purposes of this study, we counted 2 half days of sick leave as 1 full day. The cost of death caused by TBE was calculated to be €4.05 million, based on the value of a statistical life used by the Swedish Transport Administration (*30*). For all calculations, we used the following exchange rate: €1 equals 10 Swedish krona (SEK) (€1 is approximately equal to US $1.20). Statistical analyses were performed by using STATA version 16 (https://www.stata.com).

Results

TBE Diagnosis in the Swedish National Patient Register

Data obtained from the Swedish National Patient Register identified 2,429 reported patients hospitalized with TBE ICD-10 diagnosis code A84 during 1998–2014. Of these, 1,751 case-patients were entered in the register during 2005–2014. Over that same period, 2,047 TBE case-patients were reported in Sweden, indicating that 296 (14%) such case-patients did not require hospitalization. Of the 2,429 case-patients entered in the register, 995 (41%) were women and 1,434 (59%) men.

Mean age of the 2,429 TBE case-patients entered in the National Patient Register was 47 years (47.8 for women and 46.4 for men). Comparing the age distribution of TBE cases with the general population shows that hospitalization for TBE is skewed to-

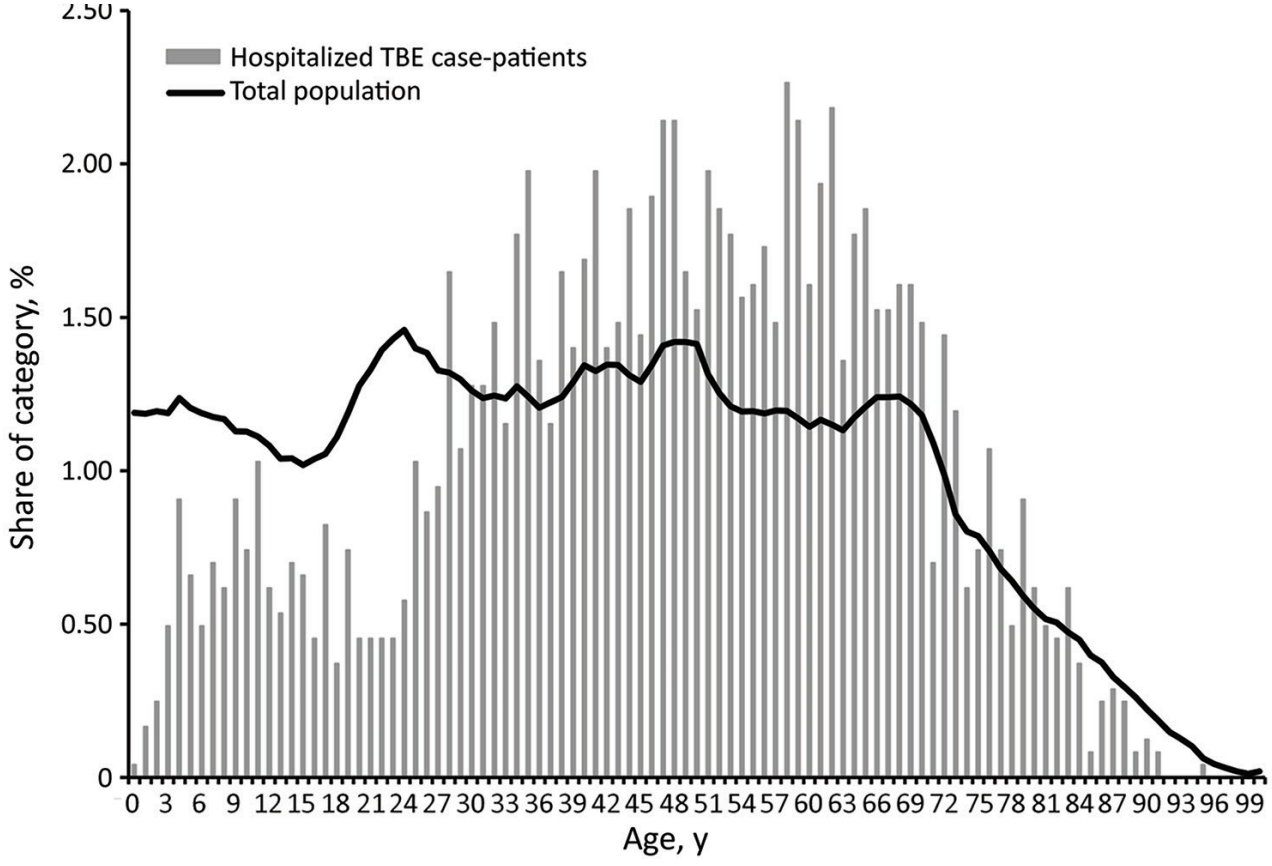

Figure 3. Percentage of hospitalized tick-borne encephalitis case-patients, by age, during 1998–2014 and percentage of population of Sweden in 2014, by age.

ward a higher mean age than the population at large (Figure 3).

Death from TBE

A total of 39 TBE-related deaths were entered in the Swedish National Cause of Death Register during 2005–2019. During the same period, 3,681 TBE cases were reported to the Public Health Agency of Sweden, corresponding to a case-fatality rate of 1.1%. In all, 25 (64%) of the deceased patients were men and 14 (36%) were women; 35 (90%) of deceased patients were ≥60 years of age.

Days of Inpatient Care and Number of Specialist Outpatient Visits

When we compared the burden of TBE in terms of healthcare use between TBE case-patients and the referent cohort at 3 years before and 1, 3 and 5 years after TBE onset date, we found that before TBE onset, differences in the average number of days spent in hospital care were small and statistically insignificant; however, after TBE onset, TBE case-patients spent significantly longer than the referent cohort in hospital care (Table 1). During the first year after TBE onset, case-patients were hospitalized an average of 11.5 days, compared with an average of 1.1 days for the referent cohort. These differences remained largely unchanged in the following years.

Within the 3-year period before date of TBE onset, the average number of specialist outpatient visits was slightly higher among patients with a TBE diagnosis than among the referent cohort (Table 1). By 1 year after date of onset of TBE, these differences became much more pronounced and grew over time; after 5 years, the average difference was almost 4 visits.

Sick Leave Days

Compared with the referent cohort, patients with TBE spent an average of 12 days more on sick leave over the 3-year period before TBE onset (Table 1). One year after TBE onset, this difference increased significantly; those with TBE spent an average of 66 days on sick leave, compared with 11 days for the referent cohort. Three years after TBE onset, this

Table 1. Healthcare use and sick leave days for persons with TBE and the matched referent cohort, Sweden, 1998–2014*

Variable	Within 3 y before TBE	After TBE		
		Within 1 y	Within 3 y	Within 5 y
Days hospitalized				
Case cohort, mean (no.)	1.35 (2,228)	11.50 (2,274)	12.73 (1,863)	14.69 (1,466)
Referent cohort, mean (no.)	2.07 (6,684)	1.12 (6,822)	3.27 (5,589)	5.64 (4,404)
Difference in means	0.28	10.38†	9.46†	9.05†
Specialist outpatient visits				
Case cohort, mean (no.)	3.92 (2,228)	3.65 (2,270)	6.78 (1,863)	9.45 (1,466)
Referent cohort, mean (no.)	3.31 (6,684)	1.22 (6,810)	3.53 (5,583)	5.74 (4,398)
Difference in means	0.62†	2.42†	3.25†	3.71†
Days of sick leave				
Case cohort, mean (no.)	63.3 (1406)	66.0 (1,434)	122.6 (1,169)	144.0 (902)
Referent cohort, mean (no.)	51.4 (2765)	10.7 (2,802)	45.9 (2,286)	78.1 (1,793)
Difference in means	11.82‡	55.32†	76.66†	65.85†
Primary healthcare visits				
Case cohort, mean (no.)	9.19 (280)	6.44 (276)	14.43 (228)	23.29 (175)
Referent cohort, mean (no.)	10.55 (779)	3.90 (763)	11.54 (638)	19.55 (502)
Difference in means	−1.36	2.54†	2.89§	3.74

*TBE, tick-borne encephalitis.
†Significance at the 1% level.
‡Significance at the 5% level.
§Significance at the 10% level.

difference was even greater but decreased again; after 5 years, it returned to the same level as 1 year after the onset of TBE.

Primary Care Visits

The number of primary care visits during the 3 years before TBE onset did not differ significantly between the 2 groups (Table 1). However, in the first year after TBE onset, the number of visits was substantially higher for those with a TBE diagnosis. This difference declined over time, and after 3 years there were no statistically significant differences.

Burden of TBE and Cost of Illness

Calculations of the burden of TBE in terms of healthcare use and sick leave and the associated cost of illness per TBE case 1, 3 and 5 years after TBE onset take into account the differences between the TBE case-patients and referent cohort within the 3-year period before date of TBE onset (Table 2). The average cost of illness for 1 TBE case-patient was ≈€20,504 during the first year after TBE onset. Days spent in hospital accounted for 52% of this cost; days on sick leave, 42%. Specialist and primary care visits accounted for 3% each. The cost grew by ≈€3,600 in years 2 and 3 to a cumulative cost of €24,126 by 3 years after TBE onset. During years 4–5, the per patient cost decreased by about €2,300 to a cumulative cost of €21,834/TBE case 5 years after TBE onset. Over time, the share of costs for inpatient care decreased to 41%, and the costs associated with sick leave increased to 49% at 5 years after TBE onset. The share of costs for specialist visits increased only slightly to 5% and for primary care visits to 4%.

Of the 359 TBE cases registered in Sweden in 2019, a total of 4 case-patients died of this disease, equating to a cost of illness of €7.3 million and a cost of death of €16.2 million, for a total cost of €23.5 million (Table 3). The corresponding average annual cost for 2015–2019 is €24.5 million; the cost of illness accounts for €6.6 million and that of death €17.8 million.

Discussion

The burden of tick-borne encephalitis was higher than previously estimated. This study, based on register data in Sweden, where underreporting of TBE is demonstrably low (*31*), shows that TBE poses a

Table 2. Burden of TBE in terms of healthcare use, sick leave days, and cost of illness per case, Sweden, 1998–2014*

Variable	Within 1 y after TBE onset			Within 3 y after TBE onset			Within 5 y after TBE onset		
	Healthcare use and sick leave, no.	Cost of illness/ case, €	Share of total cost of illness, %	Healthcare use and sick leave, no.	Cost of illness/ case, €	Share of total cost of illness, %	Healthcare use and sick leave, no.	Cost of illness/ case, €	Share of total cost of illness, %
Days hospitalized	10.10	10,599	51.7	9.19	9,638	39.9	8.77	9,203	41.2
Specialist outpatient visits	1.80	610	3.0	2.63	890	3.7	3.09	1,045	4.8
Primary care visits	3.90	639	3.1	4.25	696	2.9	5.10	836	3.8
Days of sick leave	43.50	8,656	42.2	64.80	12,902	53.5	54.00	10,750	49.2
Total	NA	20,504	NA	NA	24,126	NA	NA	21,834	NA

*Calculations account for differences between TBE case-patients and referent cohort during a 3-y period before date of disease onset. NA, not applicable; TBE, tick-borne encephalitis.

Table 3. Cost of illness and death from TBE in Sweden in 2019 and per year 2015–2019*

Variable	2019	2015–2019, average yearly cost
Registered TBE cases, no.	359	1,641
Deaths caused by TBE, no.	4	22
Cost of illness, €	7,279,054†	6,639,317†
Cost of death, €	16,200,000 ††	17,820,000 ††
Total cost of illness and death, €	23,479,054	24,459,317

*TBE, tick-borne encephalitis.
†No. registered TBE cases minus the number of deaths caused by TBE times the cost of illness per TBE case within 1 y after TBE onset (€20,504).
††No. deaths caused by TBE times the value of a statistical life in Sweden (€4.05 million).

substantial burden as measured by use of healthcare and sick leave.

The average of 11.5 days of hospitalization during the first year after TBE onset found in this study is similar to the 12 days found in a register-based study in Latvia, which covered ≈2,000 TBE cases (*32*). Our figures fall between findings of smaller studies from Slovenia (9 days) (*33*) and Germany (18 days) (*10*). By comparison, an earlier study in Sweden found that herpes simplex encephalitis, one of the most severe viral encephalitides, required an average of 55 days of hospitalization (*34*). Not surprisingly, the same pattern was observed in a recent US study quantifying the health economic effects of viral encephalitis, which found that patients with herpes simplex encephalitis were associated with longer cumulative hospital stays than were patients with all other viral encephalitides (*35*). However, comparisons between TBE and other viral encephalitides are complicated by differences in severity and prognosis.

According to our analysis, hospitalization accounted for only about half of the disease burden from TBE but sick leave days accounted for a substantial share. We found a difference in sick leave days taken before the onset of TBE, and those who received a TBE diagnosis took more sick leave days on average. We see no obvious explanation for this difference. Among those with TBE, sick leave days increased sharply over the first 3 years after TBE onset. In the 4–5 years after TBE onset, patients with this illness instead took fewer sick leave days on average than the referent cohort. This finding may be associated with rules regarding the maximum number of sick leave days allowed, but the register data on which this study was based did not permit further analysis.

This pattern of sick leave for TBE differs somewhat from that for another tickborne disease, neuroborreliosis, which was investigated through a register study in Denmark that showed that more days were taken for sick leave during the first year but tapered rapidly thereafter (*36*). In that study, 2 years after diagnosis the number of sick leave days did not differ substantially between neuroborreliosis case-patients and controls. The differences in sick leave pattern between these 2 diseases probably reflect the moderate to severe sequelae of TBE in up to one half of case-patients at long-term follow-up, compared with neuroborreliosis, for which only 12% experienced sequelae that affected their activities of daily living (*15*,*16*,*37*).

The TBE case-fatality rate calculated in this study (1.1%), based on register data from a 15-year period, is considerably higher than that reported for Sweden during the historical period 1956–1989 (0.5%) (*38*) and among the average notified cases from 23 countries in Europe during 2012–2016 (0.5%) (*13*). However, in smaller cohorts from different parts of Europe, fatality rates vary from 0.75% to 3.6% (*16*,*39*). Fatality rates may vary according to several factors, including virus virulence, sensitivities of different surveillance systems, variations in how death is recorded in different countries, demographics (e.g., age), and immunosuppression; the latter 2 factors are known to increase severity and death (*39*–*43*).

As in previous studies (*10*,*16*,*22*), we found that TBE affects more men than women, probably because compared with men, women are more likely to use protective measures, appreciate the risk, and be more knowledgeable about tickborne diseases (*44*–*46*). Moreover, the mortality rate was somewhat higher among men than women.

Translating the societal burden of TBE that arises from increased healthcare use and sick leave into monetary cost of illness is helpful for assessing the cost-effectiveness of immunization programs and other healthcare interventions. The average cost of hospitalization and specialist outpatient visits during the first year after TBE diagnosis, derived from this study, is of the same order of magnitude as earlier estimates used in models to calculate the cost-effectiveness of TBE immunization programs (*21*). However, we found that it is also essential to include the substantial cost of illness related to sick leave when comparing costs and benefits of TBE immunization programs. Excluding sick leave-related costs from such analysis would underestimate the cost of illness, especially after the year of incidence, because the percentage of costs associated with sick leave increases over time.

Using a referent cohort comparison in this study made it possible to identify the net burden of disease through analysis of the differences between the 2 groups before and after TBE onset. Including the costs of healthcare use and sick leave of only the TBE case-patients would overestimate the cost of illness.

The proportion of TBE case-patients requiring intensive care could not be reliably identified from the registers, which poses a study limitation. However, ICU stays are probably associated with a large part of hospitalization costs, as shown in a large US study of >25,000 adult patients with meningitis and encephalitis (*47*). One of few studies to include the need for intensive care over the course of TBE showed that 12% of 656 TBE patients in Germany received treatment in an ICU for an average of 12 days (*10*). Another study of 448 TBE patients in Slovenia showed that 7% received treatment in ICUs (*33*). Assuming that 10% of the TBE patients in our study received treatment in an ICU for an average of 12 days, at an average cost of €6,500 per day (*48*), the estimated cost of hospitalization 1 year after TBE onset would increase by 62% to €17,140 per case and the total cost of illness for the 359 TBE cases in Sweden in 2019 by 32% to €9.6 million.

Another study limitation is that our burden of disease calculations did not take into account less-tangible costs, such as the pain and suffering associated with long-term sequelae commonly associated with TBE or changes in recreational behavior motivated by the increased risk for TBE (*49*). The short time perspective of the study is also a limitation because it only analyzes healthcare use and sick leave for 5 years after TBE onset. Some studies do address long-term effects (*50*), but these need to be complemented by additional studies that take into account the costs associated with the long-term sequelae of TBE.

By analyzing data from the Swedish National Patient Register, our findings add to clinical studies of smaller cohorts (*10*,*15*) and to model-based studies that calculate disease burden (*21*–*23*). Such studies are of value to patient care with regard to detecting cognitive and neurologic impairments, and they provide an estimate of the frequency, nature, and severity of sequelae. Register data relating to healthcare use, sick leave, and death provide a broader base of knowledge concerning the burden of TBE. The calculated cost of illness per TBE case in this study provides a baseline for analyses of cost-effectiveness of immunization programs, which frequently rely on cost data from other diseases to estimate costs for hospitalization and specialist outpatient visits in subsequent years.

Acknowledgments

We are grateful for the funding provided by the Swedish Government under the ALF agreement (grant no. 74050) of Sahlgrenska Academy at the University of Gothenburg and Stiftelsen Längmanska Kulturfonden.

About the Author

Dr. Slunge is a researcher in health and environmental economics at the Environment for Development Initiative at the University of Gothenburg. His research focuses on risk perception and behavior in relation to environmental health threats.

References

1. Pierson TC, Diamond MS. The continued threat of emerging flaviviruses. Nat Microbiol. 2020;5:796–812. https://doi.org/10.1038/s41564-020-0714-0
2. Kunze U. The International Scientific Working Group on Tick-Borne Encephalitis (ISW TBE): review of 17 years of activity and commitment. Ticks Tick Borne Dis. 2016;7:399–404. https://doi.org/10.1016/j.ttbdis.2015.12.018
3. Haglund M, Vene S, Forsgren M, Günther G, Johansson B, Niedrig M, et al. Characterisation of human tick-borne encephalitis virus from Sweden. J Med Virol. 2003;71:610–21. https://doi.org/10.1002/jmv.10497
4. Jaenson TGT, Hjertqvist M, Bergström T, Lundkvist A. Why is tick-borne encephalitis increasing? A review of the key factors causing the increasing incidence of human TBE in Sweden. Parasit Vectors. 2012;5:184. https://doi.org/10.1186/1756-3305-5-184
5. Public Health Agency of Sweden. Tick-borne encephalitis [in Swedish] [cited 2022 Jan 18.] https://www.folkhalsomyndigheten.se/folkhalsorapportering-statistik/statistik-a-o/sjukdomsstatistik/tick-borne-encephalitis-tbe/?t=county
6. Askling HH, Insulander M, Hergens MP, Leval A. Tick borne encephalitis (TBE)-vaccination coverage and analysis of variables associated with vaccination, Sweden. Vaccine. 2015;33:4962–8. https://doi.org/10.1016/j.vaccine.2015.07.030Euro
7. European Centre for Disease Prevention and Control. Tick-borne encephalitis. Annual epidemiological report for 2019. Stockholm: The Centre; 2021.
8. Lindquist L, Vapalahti O. Tick-borne encephalitis. Lancet. 2008;371:1861–71. https://doi.org/10.1016/S0140-6736(08)60800-4
9. Steffen R. Tick-borne encephalitis (TBE) in children in Europe: epidemiology, clinical outcome and comparison of vaccination recommendations. Ticks Tick Borne Dis. 2019;10:100–10. https://doi.org/10.1016/j.ttbdis.2018.08.003
10. Kaiser R. The clinical and epidemiological profile of tick-borne encephalitis in southern Germany 1994-98: a prospective study of 656 patients. Brain. 1999;122:2067–78. https://doi.org/10.1093/brain/122.11.2067
11. Zambito Marsala S, Pistacchi M, Gioulis M, Mel R, Marchini C, Francavilla E. Neurological complications of tick borne encephalitis: the experience of 89 patients studied and literature review. Neurol Sci. 2014;35:15–21. https://doi.org/10.1007/s10072-013-1565-8
12. Bogovič P, Stupica D, Rojko T, Lotrič-Furlan S, Avšič-Županc T, Kastrin A, et al. The long-term outcome

of tick-borne encephalitis in central Europe. Ticks Tick Borne Dis. 2018;9:369–78. https://doi.org/10.1016/j.ttbdis.2017.12.001
13. Beauté J, Spiteri G, Warns-Petit E, Zeller H. Tick-borne encephalitis in Europe, 2012 to 2016. Euro Surveill. 2018;23:1800201. https://doi.org/10.2807/1560-7917.ES.2018.23.45.1800201
14. Haglund M, Forsgren M, Lindh G, Lindquist L. A 10-year follow-up study of tick-borne encephalitis in the Stockholm area and a review of the literature: need for a vaccination strategy. Scand J Infect Dis. 1996;28:217–24. https://doi.org/10.3109/00365549609027160
15. Günther G, Haglund M, Lindquist L, Forsgren M, Sköldenberg B. Tick-bone encephalitis in Sweden in relation to aseptic meningo-encephalitis of other etiology: a prospective study of clinical course and outcome. J Neurol. 1997;244:230–8. https://doi.org/10.1007/s004150050077
16. Mickiene A, Laiskonis A, Günther G, Vene S, Lundkvist A, Lindquist L. Tickborne encephalitis in an area of high endemicity in Lithuania: disease severity and long-term prognosis. Clin Infect Dis. 2002;35:650–8. https://doi.org/10.1086/342059
17. Loew-Baselli A, Konior R, Pavlova BG, Fritsch S, Poellabauer E, Maritsch F, et al.; FSME-IMMUN study group. Safety and immunogenicity of the modified adult tick-borne encephalitis vaccine FSME-IMMUN: results of two large phase 3 clinical studies. Vaccine. 2006;24:5256–63. https://doi.org/10.1016/j.vaccine.2006.03.061
18. Heinz FX, Stiasny K, Holzmann H, Grgic-Vitek M, Kriz B, Essl A, et al. Vaccination and tick-borne encephalitis, central Europe. Emerg Infect Dis. 2013;19:69–76. https://doi.org/10.3201/eid1901.120458
19. Kollaritsch H, Paulke-Korinek M, Holzmann H, Hombach J, Bjorvatn B, Barrett A. Vaccines and vaccination against tick-borne encephalitis. Expert Rev Vaccines. 2012;11:1103–19. https://doi.org/10.1586/erv.12.86
20. Slunge D. The willingness to pay for vaccination against tick-borne encephalitis and implications for public health policy: evidence from Sweden. PLoS One. 2015;10:e0143875. https://doi.org/10.1371/journal.pone.0143875
21. Shedrawy J, Henriksson M, Hergens MP, Askling HH. Estimating costs and health outcomes of publicly funded tick-born encephalitis vaccination: a cost-effectiveness analysis. Vaccine. 2018;36:7659–65. https://doi.org/10.1016/j.vaccine.2018.10.086
22. Fafangel M, Cassini A, Colzani E, Klavs I, Grgič Vitek M, Učakar V, et al. Estimating the annual burden of tick-borne encephalitis to inform vaccination policy, Slovenia, 2009 to 2013. Euro Surveill. 2017;22:30509. https://doi.org/10.2807/1560-7917.ES.2017.22.16.30509
23. Šmit R, Postma MJ. The burden of tick-borne encephalitis in disability-adjusted life years (DALYs) for Slovenia. PLoS One. 2015;10:e0144988. https://doi.org/10.1371/journal.pone.0144988
24. Zavadska D, Anca I, André F, Bakir M, Chlibek R, Cižman M, et al. Recommendations for tick-borne encephalitis vaccination from the Central European Vaccination Awareness Group (CEVAG). Hum Vaccin Immunother. 2013;9:362–74. https://doi.org/10.4161/hv.22766
25. Borg K, Goine H, Söderberg E, Marnetoft SU, Alexanderson K. Comparison of seven measures of sickness absence based on data from three counties in Sweden. Work. 2006;26:421–8.
26. Swedish Association of Local Authorities and Regions. Cost per patient database [in Swedish] [cited 2020 Oct 7]. https://skr.se/skr/halsasjukvard/ekonomiavgifter/kostnadperpatientkpp/kppdatabas.46722.html
27. Region Västra Götaland. List of prices for medical interventions [in Swedish] [cited 2020 Oct 7]. https://alfresco.vgregion.se/alfresco/service/vgr/storage/node/content/workspace/SpacesStore/c057c2eb-8e34-460d-82b4-b947d7615858/Utoml%c3%a4nsprislista%202019%20version%202019-02-20.pdf?a=false&guest=true
28. Statistics Sweden. Median income 2018 [cited 2019 Dec 12]. https://www.scb.se/en/ http://www.statistikdatabasen.scb.se/pxweb/sv/ssd/START__HE__HE0110__HE0110A/NetInk02
29. Swedish Tax Agency. Number of working days 2018 [in Swedish] [cited 2019 Dec 12]. https://www.skatteverket.se/privat/skatter.4.6a66882312593 09ff1f800029074.html
30. The Swedish Transport Administration. Method of analysis and socio-economic values for the transport sector: ASEK 6.1 [in Swedish] [cited 2019 Dec 12]. http://xn--svrdsj-cua2m.se/wp-content/uploads/2018/12/09_trafiksakerhet_a61.pdf
31. Haglund M, Settergren B, Heinz FX, Günther G; ISW-TBE Study Group. Report of the Meningitis Program of the International Scientific Working Group on TBE. Serological screening of patients with viral CNS-infection of unknown etiology in search of undiagnosed TBE cases. Vaccine. 2003;21(Suppl 1):S66–72. https://doi.org/10.1016/S0264-410X(02)00816-2
32. Zavadska D, Odzelevica Z, Karelis G, Liepina L, Litauniece ZA, Bormane A, et al. Tick-borne encephalitis: a 43-year summary of epidemiological and clinical data from Latvia (1973 to 2016). PLoS One. 2018;13:e0204844. https://doi.org/10.1371/journal.pone.0204844
33. Logar M, Bogovič P, Cerar D, Avsic-Zupanc T, Strle F. Tick-borne encephalitis in Slovenia from 2000 to 2004: comparison of the course in adult and elderly patients. Wien Klin Wochenschr. 2006;118:702–7. https://doi.org/10.1007/s00508-006-0699-6
34. Hjalmarsson A, Blomqvist P, Sköldenberg B. Herpes simplex encephalitis in Sweden, 1990-2001: incidence, morbidity, and mortality. Clin Infect Dis. 2007;45:875–80. https://doi.org/10.1086/521262
35. Kiyani M, Liu B, Charalambous LT, Adil SM, Hodges SE, Yang S, et al. The longitudinal health economic impact of viral encephalitis in the United States. J Med Microbiol. 2020;69:270–9. https://doi.org/10.1099/jmm.0.001153
36. Obel N, Dessau RB, Krogfelt KA, Bodilsen J, Andersen NS, Møller JK, et al. Long term survival, health, social functioning, and education in patients with European Lyme neuroborreliosis: nationwide population based cohort study. BMJ. 2018;361:k1998. https://doi.org/10.1136/bmj.k1998
37. Berglund J, Stjernberg L, Ornstein K, Tykesson-Joelsson K, Walter H. 5-y Follow-up study of patients with neuroborreliosis. Scand J Infect Dis. 2002;34:421–5. https://doi.org/10.1080/00365540110080421
38. Holmgren EB, Forsgren M. Epidemiology of tick-borne encephalitis in Sweden 1956-1989: a study of 1116 cases. Scand J Infect Dis. 1990;22:287–95. https://doi.org/10.3109/00365549009027050
39. Lenhard T, Ott D, Jakob NJ, Pham M, Bäumer P, Martinez-Torres F, et al. Predictors, neuroimaging characteristics and long-term outcome of severe European tick-borne encephalitis: a prospective cohort study. PLoS One. 2016;11:e0154143. https://doi.org/10.1371/journal.pone.0154143
40. Aw D, Silva AB, Palmer DB. Immunosenescence: emerging challenges for an ageing population. Immunology. 2007;120:435–46. https://doi.org/10.1111/j.1365-2567.2007.02555.x
41. Czupryna P, Grygorczuk S, Krawczuk K, Pancewicz S, Zajkowska J, Dunaj J, et al. Sequelae of tick-borne

encephalitis in retrospective analysis of 1072 patients. Epidemiol Infect. 2018;146:1663–70. https://doi.org/10.1017/S0950268818002005
42. Knight A, Pauksens K, Nordmark G, Kumlien E. Fatal outcome of tick-borne encephalitis in two patients with rheumatic disease treated with rituximab. Rheumatology (Oxford). 2017;56:855–6. https://doi.org/10.1093/rheumatology/kew495
43. Lipowski D, Popiel M, Perlejewski K, Nakamura S, Bukowska-Osko I, Rzadkiewicz E, et al. A cluster of fatal tick-borne encephalitis virus infection in organ transplant setting. J Infect Dis. 2017;215:896–901. https://doi.org/10.1093/infdis/jix040
44. Slunge D, Boman A. Learning to live with ticks? The role of exposure and risk perceptions in protective behaviour against tick-borne diseases. PLoS One. 2018;13:e0198286. https://doi.org/10.1371/journal.pone.0198286
45. Slunge D, Jore S, Krogfelt KA, Jepsen MT, Boman A. Who is afraid of ticks and tick-borne diseases? Results from a cross-sectional survey in Scandinavia. BMC Public Health. 2019;19:1666. https://doi.org/10.1186/s12889-019-7977-5
46. Jepsen MT, Jokelainen P, Jore S, Boman A, Slunge D, Krogfelt KA. Protective practices against tick bites in Denmark, Norway and Sweden: a questionnaire-based study. BMC Public Health. 2019;19:1344. https://doi.org/10.1186/s12889-019-7613-4
47. Balada-Llasat JM, Rosenthal N, Hasbun R, Zimmer L, Ginocchio CC, Duff S, et al. Cost of managing meningitis and encephalitis among adult patients in the United States of America. Int J Infect Dis. 2018;71:117–21. https://doi.org/10.1016/j.ijid.2018.04.799
48. Swedish Intensive Care Register. Annual report 2018 [in Swedish] [cited 2020 Sep 10]. https://www.icuregswe.org/globalassets/arsrapporter/analyserande_arsrapport_2018.pdf
49. Slunge D, Sterner T, Adamowicz W. Valuation when baselines are changing: tick-borne disease risk and recreational choice. Resour Energy Econ. 2019;58:101119. https://doi.org/10.1016/j.reseneeco.2019.101119
50. Veje M, Nolskog P, Petzold M, Bergström T, Lindén T, Peker Y, et al. Tick-borne encephalitis sequelae at long-term follow-up: a self-reported case-control study. Acta Neurol Scand. 2016;134:434–41. https://doi.org/10.1111/ane.12561

Address for correspondence: Daniel Slunge, Environment for Development Initiative, University of Gothenburg, PO Box 170, 40530 Gothenburg, Sweden; email: daniel.slunge@gu.se

Invasive *Burkholderia cepacia* Complex Infections among Persons Who Inject Drugs, Hong Kong, China, 2016–2019

Kristine Shik Luk, Yat-ming Tsang, Alex Yat-man Ho, Wing-kin To, Ben Kwok-ho Wong, Maureen Mo-lin Wong, Yiu-chung Wong

During March 2016–January 2019, *Burkholderia cepacia* complex (BCC) infection developed in 13 persons who inject drugs (PWID) in Kowloon West Region, Hong Kong, China. Seven cases were infective spondylitis, 2 endocarditis, 2 septic arthritis, 1 intramuscular abscess and bacteremia, and 1 necrotizing fasciitis. Pulsed-field gel electrophoresis revealed that the isolates from 9 patients were clonally related. This clone caused major illness, and 11 of the 13 patients required surgical treatment. Clinicians should be aware of this pathogen and the appropriate broad-spectrum antimicrobial drugs to empirically prescribe for PWID with this life-threatening infection. Close collaboration among public health authorities, outreach social workers, and methadone clinics is essential for timely prevention and control of outbreaks in the PWID population.

Burkholderia cepacia complex (BCC) is a ubiquitous aerobic gram-negative bacillus composed of ≥20 phylogenetically closely related species (*1*). BCC is commonly found in water, soil, and plants and was the cause of onion rot in the 1950s, when it was first described (*2*). It is a rapidly growing bacterium that can survive for a long time in harsh environments. Studies have demonstrated that it is capable of living for >1 year in a 10% iodine solution and can use penicillin as its only energy source (*3*,*4*).

The bacterium's large genome, twice the size of that of *Escherichia coli*, enables its tremendous adaptability and inherent resistance to multiple antimicrobial drugs (*5*). Its outer membrane is 10 times less permeable that that of *E. coli*, resulting in intrinsic resistance to aminoglycosides and colistin (*6*). The arrangement of circular replicons of transposable elements further enables frequent recombination events. BCC resistance to β-lactams has developed by means of an inducible chromosomal β-lactamase and altered penicillin-binding proteins. Antimicrobial efflux pumps can also lead to resistance to trimethoprim, chloramphenicol, and fluoroquinolones (*6*).

BCC virulence is low, and it generally does not cause illness in immunocompetent persons. Although BCC mainly causes opportunistic infection in patients with cystic fibrosis and chronic granulomatous disease, it has been detected in immunocompromised persons and persons who inject drugs (PWID) who have bacteremia, endocarditis, septic arthritis, or infective spondylitis (*7*–*11*). Outbreaks of nosocomial infection resulting from contaminated heparin and povidone iodine solutions have also been reported (*12*,*13*). The pathogen has been isolated from several medical products such as intravenous fluids, dialysis fluids, ultrasonography gels, nebulizers, thermometers, and tap water (*11*,*14*–*17*).

In October 2018, the infection control officer of Caritas Medical Centre, Kowloon West Region, reported to the Centre of Health Protection, Department of Health, Hong Kong, China, that during March 2017–September 2018, invasive infection caused by a clonal strain of BCC was diagnosed for 8 PWID. We describe the clinical features of patients involved with this unusual outbreak, which may have resulted from external contamination of a batch of drugs or drug paraphernalia. The study protocol was approved by the Kowloon West Cluster Clinical Research Ethics Committee, Hospital Authority.

Author affiliations: Princess Margaret Hospital, Hong Kong, China (K.S. Luk, Y.M. Tsang, A.Y.M. Ho, W.K. To); Caritas Medical Centre, Hong Kong (B.K.H. Wong, M.M.L Wong); Yan Chai Hospital, Hong Kong (Y.C. Wong)

DOI: https://doi.org/10.3201/eid2802.210945

Methods

Clinical Setting

Four regional hospitals (total 3,431 beds) serve an estimated population of 1.4 million in Kowloon West Region, accounting for 19% of the Hong Kong population. We used culture records of the regional microbiology laboratory to identify cases of BCC infection from January 1, 2016, through June 30, 2019. We included in our study PWID patients experiencing their first episode of BCC invasive infection.

Clinical data retrieved from medical charts included patient demographics, underlying diseases, type of abused drugs, signs/symptoms and their duration, sources of infection, recent medical procedures, neurologic status classified by the American Spinal Injury Association impairment scale (https://asia-spinalinjury.org), length of hospital stay, antimicrobial therapy, and surgical treatment. Empiric antimicrobial therapies were defined as antimicrobial agents used before the availability of culture and susceptibility results, and definitive therapies were defined as those used after. We also included leukocyte counts, erythrocyte sedimentation rates, C-reactive protein levels, microbiology results (blood culture, pus aspirate, tissue, or wound swab samples), and radiology findings. The main outcome measures were 7- and 30-day mortality as well as clinical responses at 72 hours after the start of definitive antimicrobial therapy, which included resolution of fever, leukocytosis, and signs of infection.

Microbiological Studies and Genotyping

BCC was isolated on horse blood agar and identified by matrix-assisted laser desorption/ionization time-of-flight mass spectrometry (MALDI Biotyper; Bruker Daltonics, https://www.bruker.com). We performed antimicrobial susceptibility testing of ceftazidime, levofloxacin, meropenem, minocycline, and trimethoprim/sulfamethoxazole according to the guidelines set by the Clinical and Laboratory Standards Institute (*18*). Because whole-genome sequencing was not available in our laboratory, we determined the clonal relatedness of BCC by using pulsed-field gel electrophoresis (PFGE) of DNA digested with *SpeI* endonuclease (New England BioLabs, https://www.neb.com) as previously described (*19*). For controls, we used 7 archived outbreak-unrelated BCC isolates. We analyzed digitalized gel images by using BioNumerics version 7.0 (Applied Maths, https://www.bionumerics.com). We set banding matching tolerance at 1%. We performed cluster analysis by using the unweighted pair-group method with arithmetic averages based on Dice coefficients to quantify similarities. For PFGE interpretation, we applied the criteria described by Tenover et al. and considered patterns to be closely related or indistinguishable if similarity was ≥80% (*20*).

Results

We identified 13 PWID who had BCC invasive infection during March 2016–January 2019, of which 12 were admitted to Caritas Medical Centre and 1 was admitted to Yan Chai Hospital, Kowloon West Region. All PWID used heroin, 11 (84.6%) were men, 11 had hepatitis C, and 4 had a history of deep vein thrombosis (Table 1). The duration of signs/symptoms ranged from 1 to 60 days (median 3 days). Three patients had fever (≥38°C), and 7 had spondylodiscitis.

Concerning antimicrobial therapy, most (n = 10) patients were empirically given amoxicillin/clavulanate (Table 2). All BCC isolates were susceptible to ceftazidime, levofloxacin, meropenem, minocycline, and trimethoprim/sulfamethoxazole. For definitive therapy, 6 patients were given trimethoprim/sulfamethoxazole as combination treatment with levofloxacin (n = 3), ceftazidime (n = 2), and meropenem (n = 1). Among patients with spondylodiscitis, 5 had lumbar spine involvement, and all except 1 had undergone surgery. Four patients had polymicrobial infection. All patients showed good response to treatment. One patient had a relapse of BCC spondylodiscitis 5 months after a 6-week course of meropenem and oral trimethoprim/sulfamethoxazole and subsequently underwent spinal fusion. Two patients died, one of hepatocellular carcinoma and the other of an unknown cause (certified dead at the emergency department 1 day after discharge). Neither patient underwent autopsy. Attempts to contact the surviving patients regarding their drug use behaviors were unsuccessful.

PFGE analysis of the isolates showed that 9 of the 13 invasive infections were caused by the same clone (Figure 1); banding patterns were identical for 8 isolates. All patients except 1 lived in the Shum Shui Po District, which has a total area of 9.48 km^2, within the Kowloon West Region. A marked increase of the clonal isolates was noted during 2017–2018 (Figure 2).

Discussion

In 2018, a reported 3,579 persons in Hong Kong injected heroin (*21*). As a result of hematogenous seeding, drug injection is a substantial risk factor for musculoskeletal infections, including septic arthritis and osteomyelitis of the spine and infective endocarditis (*22*). The common responsible organisms are *Staphylococcus aureus*, *Streptococcus* spp., and occasionally

Pseudomonas aeruginosa (*22*). Other outbreaks of life-threatening infections caused by *Clostridium* spp. and *Bacillus anthracis* have also been associated with use of contaminated heroin (*22*,*23*). On the contrary, the literature has rarely reported BCC as the culprit of drug-injection–associated musculoskeletal infections or infective endocarditis (*24*–*27*). Our report of a common-source outbreak of BCC invasive infection among PWID, in a highly localized geographic area of Hong Kong and supported by PFGE, is unusual.

The mechanism of spread of the epidemic strain of BCC among PWID was unclear because neither

Table 1. Clinical features of invasive infections caused by *Burkholderia cepacia* complex in persons who inject drugs, Hong Kong, China, 2016–2019

Patient no.	Age, y/sex	Underlying conditions	Symptoms (duration, d)	Body temperature, °F (°C)	ASIA impairment scale*	Infection type
1	51/F	Diabetes mellitus, hepatitis C	Back pain lower limb numbness and weakness (3)	98.2 (36.8)	D	T11/12 spondylodiscitis with cord compression
2	66/M	Hepatitis C	Back pain (20)	97.9 (36.6)	E	L4/5 spondylodiscitis
3	66/M	Hepatocellular carcinoma, hepatitis C	Right upper limb numbness and weakness (60)	98.8 (37.1)	D	C5/6, C6/7 spondylodiscitis with prevertebral abscess
4	65/M	Deep vein thrombosis, pseudo-aneurysm, right above-knee amputation, hepatitis C	Reduced general condition, dizziness and vomiting (1)	99.3 (37.4)	NA	Endocarditis and septic emboli in lungs
5	60/M	Schizophrenia, deep vein thrombosis, pseudo-aneurysm, hepatitis C	Fever, right leg pain and redness (1)	103.1 (39.5)	NA	Intramuscular abscess and bacteremia†
6	59/M	Gout	Back pain and bilateral foot numbness (7)	98.4 (36.9)	E	L5/S1 spondylodiscitis
7	51/F	Psoas abscess, deep vein thrombosis, fractured right hip with open fixation, hepatitis C	Right hip pain, not able to bear weight (7)	99.0 (37.2)	NA	Right hip prosthetic joint infection and osteomyelitis
8	69/M	Asthma, infective spondylodiscitis	Right knee pain (3)	101.1 (38.4)	NA	Right knee septic arthritis and intramuscular abscess†
9	62/M	Stroke, hepatitis B, hepatitis C	Fever, back pain, right lower limb numbness, and tingling sensation (4)	99.1 (37.3)	E	L3/4, L5/S1 spondylodiscitis
10	64/M	Stroke, deep vein thrombosis, infective cervical spondylitis, hepatitis C	Back pain with radiation to right lateral thigh and weakness (3)	99.3 (37.4)	D	L2/3 spondylodiscitis
11	46/M	Esophageal cancer, hepatitis C	Fever, drowsiness, cough, dyspnea (1)	103.3 (39.6)	NA	Endocarditis and septic emboli in brain†
12	66/M	Infective endocarditis, hepatitis C	Back pain and lower limb weakness (14)	98.2 (36.8)	D	L1/2 spondylodiscitis with cord compression
13	55/M	Hepatitis C	Left knee and thigh pain (2)	96.8 (36)	NA	Left thigh intramuscular abscess and necrotizing fasciitis†

*ASIA impairment scale: A = complete (no motor or sensory function in S4–S5); B = incomplete (sensory function below neurologic level and in S4–S5, no motor function below neurologic level); C = incomplete (motor function is preserved below neurologic level, and more than half of the key muscle groups below neurologic level have a muscle grade <3); D = incomplete (motor function is preserved below neurologic level, and at least half of the key muscle groups below neurologic level have a muscle grade 3); E = normal. ASIA, American Spinal Injury Association; NA, not applicable.
†Polymicrobial infection: *Arcanobacterium haemolyticum* in abscess aspirate of patient 5; *Streptococcus pneumoniae, Streptococcus constellatus*, and *Bacteroides fragilis* in joint fluid from patient 8; *Staphylococcus aureus* and *Enterococcus faecalis* in blood of patient 11; and group G *Streptococcus*, *Peptoniphilus harei*, and *Finegoldia magna* in abscess aspirate from patient 13.

Table 2. Laboratory and microbiological findings, treatments, and outcomes of invasive infections caused by *Burkholderia cepacia* complex in persons who inject drugs, Hong Kong, China, 2016–2019*

Variable	Finding
Median leukocytes, $\times 10^9$ cells/L (range)	9.2 (3.94–24.7)
Median ESR, mm/h (range)	79.5 (43 to >120)
Median CRP, mg/L (range)	68 (21 to >294)
Empirical antimicrobial therapy (no. patients)	Amoxicillin/clavulanate (10); cloxacillin (3); vancomycin (2); ampicillin, cefoperazone/sulbactam, gentamicin, piperacillin/tazobactam (1)
Definitive antimicrobial therapy (no. patients)	Trimethoprim/sulfamethoxazole (6); ceftazidime (5); levofloxacin (5); meropenem (2); minocycline, piperacillin/tazobactam (1)
Median duration of antimicrobial therapy (range), wk	6 (1–12)
Surgery (no. patients)	Vertebral disk excision (3), incision and drainage (1), spinal fusion† (3), joint arthrotomy (2), excisional arthroplasty (1)
Positive culture (no. patients)	Bone (5), blood† (4), intervertebral disk (3), abscess (2), joint fluid (1)
Median length of stay (range), d	43 (11 – 97)
Death (d after first visit)	Patient 3 (124); patient 4 (13)

*CRP, C-reactive protein; ESR, erythrocyte sedimentation rate.
†Patient 2 had a relapse of *Burkholderia cepacia* complex infective spondylitis 5 mo after receiving meropenem and oral trimethoprim/sulfamethoxazole for 6 wk; spinal fusion was performed during the relapse episode.

microbiological investigation regarding the possible contaminated batch of heroin nor environmental sampling of the injection gallery or drug distribution site was conducted by the local public health agency. BCC is commonly found in the environment instead of the commensal flora. In addition, there was a strong association between the outbreak and the place of residence of PWID. The mode of transmission was possibly through the drug, drug adulterants, or drug paraphernalia. Bacterial contaminants, including *P. aeruginosa*, were identified in 40% of seized drug samples (*28*). *P. aeruginosa* contamination of syringes causing an outbreak of infective endocarditis has also been documented (*29*). Most patients in our study had hepatitis C virus infection, and sharing paraphernalia (e.g., needles) was believed to be frequent. Needle sharing could increase transmission of an epidemic strain. A recent polyclonal BCC outbreak in peritoneal dialysis patients in Hong Kong was caused by contaminated aqueous chlorhexidine (*30*); however, PFGE typing of the strains from the patients in our study and the strains isolated in the aqueous chlorhexidine suggested that they were unrelated (K.S. Luk, unpub. data). The preponderance of BCC in the outbreak we report could result from its environmental survival advantage and intrinsic resistance to multiple disinfectants and antimicrobials. The outbreak ended after the Centre of Health Protection issued press releases (*31*), and the health advice to inject only with single-use disposable needles was

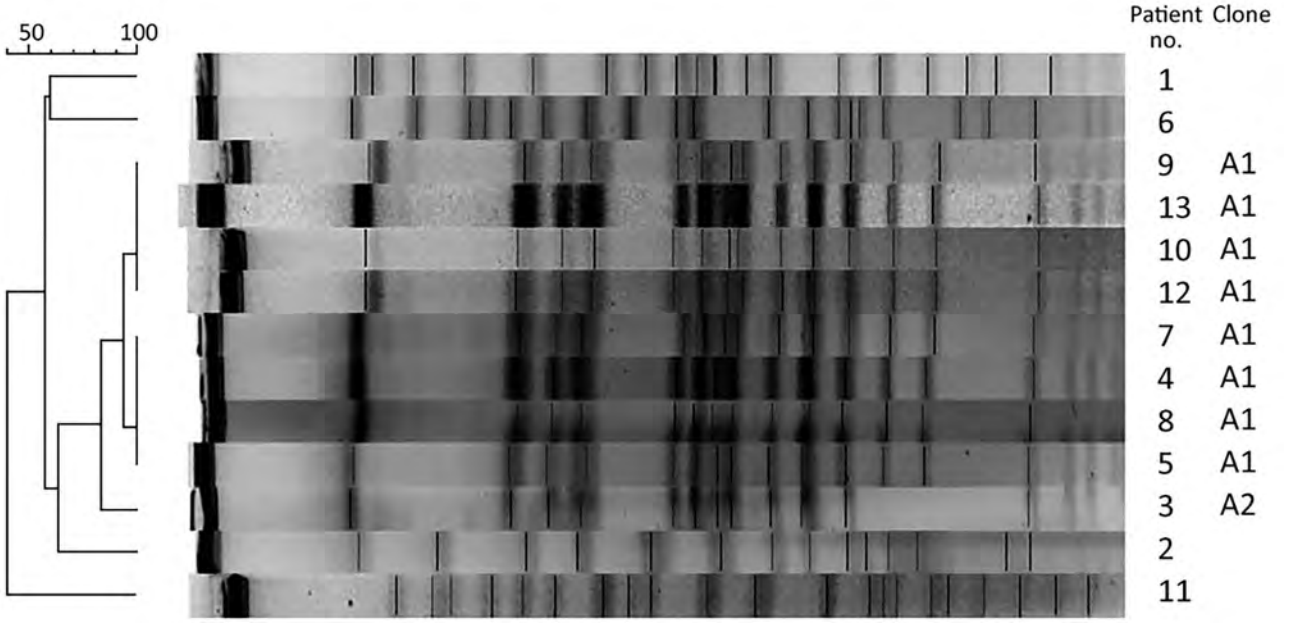

Figure 1. Pulsed-field gel electrophoresis of *Burkholderia cepacia* complex causing invasive infection in 13 persons who inject drugs, Hong Kong, China, 2016–2019.

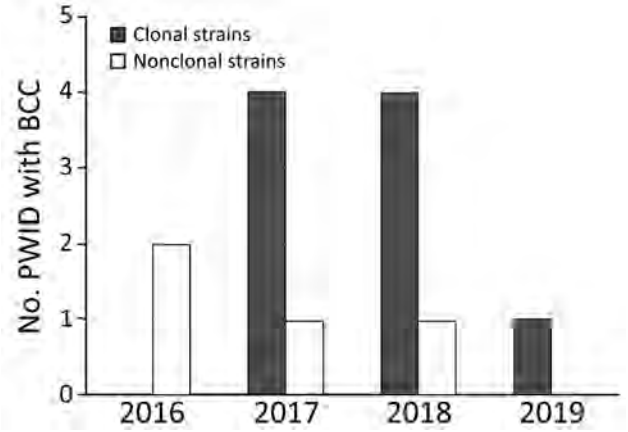

Figure 2. Number of PWID with newly detected BCC invasive infection, by clonal types per year, Hong Kong, China, 2016 through June 30, 2019. PWID, persons who inject drugs; BCC, *Burkholderia cepacia* complex.

strengthened at methadone clinics and by outreach social workers.

Invasive infections caused by BCC are rarely reported and result in considerable illness. The high infection rate may also be increased by contributions from malnutrition, concurrent chronic viral hepatitis, and lymphocyte opiate receptor–mediated natural killer T-lymphocyte inactivation (*22*). The most commonly used antimicrobial option is trimethoprim/sulfamethoxazole. Because of resistance to multiple antimicrobial drugs, successful treatment usually requires combinations of drugs and surgery. Drug combinations that have demonstrated synergy in vitro include trimethoprim/sulfamethoxazole and ceftazidime, ciprofloxacin and carbapenem, and ceftazidime and ciprofloxacin (*32*).

The most frequent invasive infection in our series was spondylodiscitis. Arterial seeding is apt to involve the vascular intervertebral disk and adjoining vertebral end plates. Most frequently involved was the lumbar area (5 patients), followed by the thoracic (1 patient) and cervical (1 patient) areas. BCC spondylodiscitis is a rare entity; the medical literature has reported only 6 cases, 3 of which were in patients with the risk factor of being PWID (*11*,*25*,*26*). Pyogenic osteomyelitis after rhinoplasty has also been described; other affected persons were a healthy elderly farmer and a patient after a fall and intramuscular procedure (*33*–*35*). Similar to the reported cases, patients in our study did not have fever, and symptom onset duration varied from 1 day to 2 months. The subtle exacerbation of axial pain might contribute to delayed diagnosis, as reflected by most (5 of 7) patients for whom abnormal findings were seen on plain vertebral radiographs. All patients had preserved sensory function, and 4 had mild limb weakness. Of note, 5 patients had a normal leukocyte count at the time of admission, and all had elevated inflammatory markers. A history of injection drug use associated with axial pain should alert clinicians to the possibility of spinal infections, despite absence of fever or abnormal leukocyte count, physical examination, or radiographic findings. Further diagnostic workup to exclude spinal infection, including magnetic resonance imaging with and without contrast, should be performed. In addition, empiric prescription of antimicrobial drugs should be withheld to increase the chance of isolating an organism, which is advantageous for a successful outcome. In this case, BCC was resistant to commonly prescribed antimicrobial drugs such as amoxicillin/clavulanate, so BCC was successfully isolated from vertebral tissue (3 patients). intervertebral disk (3 patients), and blood culture (1 patient). Because BCC was positively identified in blood culture, patient 6 did not undergo further biopsy or surgical treatment. He recovered after 6 weeks of treatment with ceftazidime and oral trimethoprim/sulfamethoxazole.

Three patients underwent spinal fusion because of infection relapse (patient 2), cord compression (patient 1), and spinal instability (patient 3). Of 3 patients with early infection, discectomy and oral levofloxacin for 6 months resulted in cure. Of the 13 patients, outcomes were good for 12, but 1 patient (patient 3) died of metastatic hepatocellular carcinoma 4 months after initial visit.

Oral administration of antimicrobial drugs has the advantage of avoiding difficult intravenous access and the need for prolonged hospitalization. Nevertheless, parenteral therapy for <4 weeks is associated with a 25% relapse rate, and use of oral antimicrobial drugs should be reserved only for patients with early disease under close monitoring of clinical response (*36*).

Endocarditis caused by BCC was more commonly reported for patients with prosthetic valves (*37*) and for patients with a history of injection drug use and native valve involvement (*38*). Patient 3 exhibited the clinical features of right-sided endocarditis. The diagnosis was not suspected, and ceftazidime was prescribed for only 8 days. The patient's death shortly after discharge may be associated with the endocarditis, although no autopsy was performed. Patient 11 had polymicrobial infection (BCC, *S. aureus*, and *Enterococcus faecalis*) of the mitral valve and cerebral septic emboli. Treatment with ampicillin, cloxacillin, and meropenem was successful without valve replacement, despite the relatively large size (2.0 × 1.5 cm) of the vegetation. Successful outcome after antimicrobial treatment has been

reported for only a few cases (*39*,*40*). An endovascular source should be investigated for all PWID with bacteremia, and early treatment may substantially improve patient outcomes.

Only 5 previous reports have described BCC isolation from joint fluid culture, affecting the ankle, knee, shoulder, and hip. Predisposing factors included history of intra-articular steroid injection, weakened immunity because of T-cell lymphoma or premature birth, and physical trauma (*10*,*41*–*45*). Patient 7 had a right prosthetic hip joint infection 6 weeks after undergoing screw fixation of the proximal femur; the source of the infection was speculated to be hematologic seeding. The patient had glucose-6-phosphate dehydrogenase deficiency, and trimethoprim/sulfamethoxazole was not given. Infection was well controlled with excisional arthroplasty and administration of ceftazidime for 11 weeks. The implanted device was removed because of severe contracture and dislocation of hip cement spacer.

Patient 8 had an intramuscular abscess of the right thigh and polymicrobial septic arthritis (BCC, *Streptococcus pneumoniae, Streptococcus constellatus, Bacteriodes fragilis*) after having injected drug into the right thigh. The injection site was probably contaminated. Treatment consisted of 4 weeks of oral levofloxacin, minocycline, and metronidazole, as well as multiple operations including incision and drainage of the thigh abscess, arthroscopy, and arthrotomy. The clinical course and inferior outcome were also reported for a patient with polymicrobial septic arthritis after a trauma-induced wound had been contaminated with dirt and soil (*43*).

Two patients had polymicrobial intramuscular abscesses of the thigh after drug injection. For patient 5, BCC was also isolated in blood culture; infection was cured after surgical drainage and debridement and 2 weeks of ceftazidime. Patient 13 experienced septic shock, and an intramuscular abscess (BCC, group G *Streptococcus*, *Peptoniphilus harei*, *Finegoldia magna*) was complicated by early necrotizing fasciitis. The patient required ventilator and vasopressor support and stayed in an intensive care unit for 7 weeks. He responded well after 2 weeks of piperacillin/tazobactam, multiple debridements, left knee arthrotomy (group G *Streptococcus* in joint fluid), and skin grafting. It is worth considering broad-spectrum antimicrobial drugs to cover gram-positive, nonfermentative gram-negative, and anaerobic bacteria for PWID who have severe musculoskeletal infections possibly caused by injection-site contamination.

A limitation of our study is that we failed to contact the surviving patients regarding their drug-use behaviors, and the local health agency did not initiate an investigation including microbiological testing of confiscated heroin or environmental sampling of the injection gallery or drug distribution site. Therefore, we were not certain about the mode of transmission. Also, we did not conduct a prospective epidemiologic study of BCC among PWID, and we may have underestimated the scale of the outbreak because patients with mild infection might not seek hospital care and specimens would not be obtained for culture. The baseline incidence of invasive BCC infection in PWID was <1 case/year, and we believe that the predominance of clonal strains during 2017–2019 represented a significant outbreak. Last, whole-genome sequencing is not readily available in our laboratory, and the resolution of PFGE may not be enough for a large-scale outbreak. Nevertheless, there is no well-established cutoff for the number of single-nucleotide polymorphisms of BCC to be classified as a cluster, and it could be quite variable (*26*). PFGE consists of genomic information that was considered to provide sufficient information for evaluating this focused outbreak (*46*–*49*).

In conclusion, this clonal epidemic of BCC invasive infections among PWID in a Hong Kong region was rare. BCC isolated from sterile sites may be dismissed as sporadic, especially for patients with the risk factor of injection drug use. Molecular typing enables the timely identification of an outbreak and contributes to the investigation and control measures and should be routinely performed for BCC isolated from sterile sites (e.g., blood, pus aspirate, joint fluid, tissue, bone) in special patient groups, such as PWID. The finding of clonal isolates from multiple patients within a geographic area should prompt further investigation by public health agencies.

This outbreak caused severe illness among affected patients. If healthcare providers are alert to invasive infection caused by this unusual, multidrug-resistant organism in PWID, they can empirically prescribe appropriate broad spectrum antimicrobial drugs for PWID with life-threatening infection. At the other end of spectrum, the clinical appearance of patients may be subtle, and further diagnostic workups should be performed so as not to miss any debilitating infection.

About the Author

Dr. Luk works as a consultant microbiologist and infection control officer in the Department of Pathology, Princess Margaret Hospital, Hong Kong, China. Her research interest is molecular epidemiology and control of multidrug-resistant organisms in healthcare settings.

References

1. Bach E, Sant'Anna FH, Magrich Dos Passos JF, Balsanelli E, de Baura VA, Pedrosa FO, et al. Detection of misidentifications of species from the *Burkholderia cepacia* complex and description of a new member, the soil bacterium *Burkholderia catarinensis* sp. nov. Pathog Dis. 2017;75:1–8. https://doi.org/10.1093/femspd/ftx076
2. Burkholder W. Sour skin, a bacterial rot of onion bulbs. Phytopathology. 1950;40:115–8.
3. Anderson RL, Vess RW, Panlilio AL, Favero MS. Prolonged survival of *Pseudomonas cepacia* in commercially manufactured povidone-iodine. Appl Environ Microbiol. 1990;56:3598–600. https://doi.org/10.1128/aem.56.11.3598-3600.1990
4. Beckman W, Lessie TG. Response of *Pseudomonas cepacia* to beta-lactam antibiotics: utilization of penicillin G as the carbon source. J Bacteriol. 1979;140:1126–8. https://doi.org/10.1128/jb.140.3.1126-1128.1979
5. Mahenthiralingam E, Urban TA, Goldberg JB. The multifarious, multireplicon *Burkholderia cepacia* complex. Nat Rev Microbiol. 2005;3:144–56. https://doi.org/10.1038/nrmicro1085
6. Rhodes KA, Schweizer HP. Antibiotic resistance in *Burkholderia* species. Drug Resist Updat. 2016;28:82–90. https://doi.org/10.1016/j.drup.2016.07.003
7. LiPuma JJ. Update on the *Burkholderia cepacia* complex. Curr Opin Pulm Med. 2005;11:528–33. https://doi.org/10.1097/01.mcp.0000181475.85187.ed
8. Lau SM, Yu WL, Wang JH. Cardiac cirrhosis with cellulitis caused by *Burkholderia cepacia* bacteremia. Clin Infect Dis. 1999;29:447–8. https://doi.org/10.1086/520235
9. Williamson DA, McBride SJ. A case of tricuspid valve endocarditis due to *Burkholderia cepacia* complex. N Z Med J. 2011;124:84–6.
10. Miki RA, Rubin LE, Kirk J, Dodds SD. Spontaneous septic arthritis caused by *Burkholderia cepacia.* Iowa Orthop J. 2006;26:147–50.
11. Jaafar D, Rizkallah M, Atallah F, Bachour F, Barakat A, Maalouf G, et al. Lumbar spondylodiscitis caused by *Burkholderia cepacia* in a previously healthy patient. Case Rep Orthop. 2017;2017:1396950. https://doi.org/10.1155/2017/1396950
12. van Laer F, Raes D, Vandamme P, Lammens C, Sion JP, Vrints C, et al. An outbreak of *Burkholderia cepacia* with septicemia on a cardiology ward. Infect Control Hosp Epidemiol. 1998;19:112–3. https://doi.org/10.2307/30142001
13. Panlilio AL, Beck-Sague CM, Siegel JD, Anderson RL, Yetts SY, Clark NC, et al. Infections and pseudoinfections due to povidone-iodine solution contaminated with *Pseudomonas cepacia.* Clin Infect Dis. 1992;14:1078–83. https://doi.org/10.1093/clinids/14.5.1078
14. Martone WJ, Tablan OC, Jarvis WR. The epidemiology of nosocomial epidemic *Pseudomonas cepacia* infections. Eur J Epidemiol. 1987;3:222–32. https://doi.org/10.1007/BF00149728
15. Held MR, Begier EM, Beardsley DS, Browne FA, Martinello RA, Baltimore RS, et al. Life-threatening sepsis caused by *Burkholderia cepacia* from contaminated intravenous flush solutions prepared by a compounding pharmacy in another state. Pediatrics. 2006;118:e212–5. https://doi.org/10.1542/peds.2005-2617
16. Magalhães M, Doherty C, Govan JR, Vandamme P. Polyclonal outbreak of *Burkholderia cepacia* complex bacteraemia in haemodialysis patients. J Hosp Infect. 2003;54:120–3. https://doi.org/10.1016/S0195-6701(03)00118-X
17. Nannini EC, Ponessa A, Muratori R, Marchiaro P, Ballerini V, Flynn L, et al. Polyclonal outbreak of bacteremia caused by *Burkholderia cepacia* complex and the presumptive role of ultrasound gel. Braz J Infect Dis. 2015;19:543–5. https://doi.org/10.1016/j.bjid.2015.06.009
18. Clinical Laboratory Standards Institute. Performance standards for antimicrobial susceptibility testing, 26th information supplement, document M100–S26. Wayne (PA): The Institute; 2016.
19. Heath DG, Hohneker K, Carriker C, Smith K, Routh J, LiPuma JJ, et al. Six-year molecular analysis of *Burkholderia cepacia* complex isolates among cystic fibrosis patients at a referral center for lung transplantation. J Clin Microbiol. 2002;40:1188–93. https://doi.org/10.1128/JCM.40.4.1188-1193.2002
20. Tenover FC, Arbeit RD, Goering RV, Mickelsen PA, Murray BE, Persing DH, et al. Interpreting chromosomal DNA restriction patterns produced by pulsed-field gel electrophoresis: criteria for bacterial strain typing. J Clin Microbiol. 1995;33:2233–9. https://doi.org/10.1128/jcm.33.9.2233-2239.1995
21. Research Office Legislative Council Secretariat. Statistical highlights ISSH28/18–19 [cited 2019 Sep 23]. https://www.legco.gov.hk/research-publications/english/1819issh28-drug-abuse-in-hong-kong-20190531-e.pdf
22. Gordon RJ, Lowy FD. Bacterial infections in drug users. N Engl J Med. 2005;353:1945–54. https://doi.org/10.1056/NEJMra042823
23. Abbara A, Brooks T, Taylor GP, Nolan M, Donaldson H, Manikon M, et al. Lessons for control of heroin-associated anthrax in Europe from 2009–2010 outbreak case studies, London, UK. Emerg Infect Dis. 2014;20:1115–22. https://doi.org/10.3201/eid2007.131764
24. Sapico FL, Montgomerie JZ. Vertebral osteomyelitis in intravenous drug abusers: report of three cases and review of the literature. Rev Infect Dis. 1980;2:196–206. https://doi.org/10.1093/clinids/2.2.196
25. Smith MA, Trowers NRH, Klein RS. Cervical osteomyelitis caused by *Pseudomonas cepacia* in an intravenous-drug abuser. J Clin Microbiol. 1985;21:445–6. https://doi.org/10.1128/jcm.21.3.445-446.1985
26. Li SK, Messer WB. *Burkholderia cepacia complex* cervical osteomyelitis in an intravenous drug user. Case Rep Infect Dis. 2018;2018:7638639. https://doi.org/10.1155/2018/7638639
27. Nnaoma C, Chika-Nwosuh O, Sossou C. A rare culprit of infective endocarditis in an IV drug user: *Burkholderia cepacia.* Case Rep Med. 2019;2019:6403943. https://doi.org/10.1155/2019/6403943
28. Aghababaei R, Javadi I, Nili-Ahmadabadi A, Parsafar S, Ahmadimoghaddam D. Occurrence of bacterial and toxic metals contamination in illegal opioid-like drugs in Iran: a significant health challenge in drug abusers. Daru. 2018;26:77–83. https://doi.org/10.1007/s40199-018-0205-5
29. Shekar R, Rice TW, Zierdt CH, Kallick CA. Outbreak of endocarditis caused by *Pseudomonas aeruginosa* serotype O11 among pentazocine and tripelennamine abusers in Chicago. J Infect Dis. 1985;151:203–8. https://doi.org/10.1093/infdis/151.2.203
30. Wong SCY, Wong SC, Chen JHK, Poon RWS, Hung DLL, Chiu KHY, et al. Polyclonal *Burkholderia cepacia* complex outbreak in peritoneal dialysis patients caused by contaminated aqueous chlorhexidine. Emerg Infect Dis. 2020;26:1987–97. https://doi.org/10.3201/eid2609.191746
31. The Government of the Hong Kong Special Administrative Region. Cluster of invasive *Burkholderia cepacia* infection under DH investigation [cited 2019 Sep 23]. https://www.info.gov.hk/gia/general/201810/10/P2018101000923.htm

32. Huang CH, Jang TN, Liu CY, Fung CP, Yu KW, Wong WW. Characteristics of patients with *Burkholderia cepacia* bacteremia. J Microbiol Immunol Infect. 2001;34:215–9.
33. Weinstein L, Knowlton CA, Smith MA. Cervical osteomyelitis caused by *Burkholderia cepacia* after rhinoplasty. J Infect Dev Ctries. 2008;2:76–7.
34. Hsieh CT, Hsu SK, Chang CJ. Thoracic vertebral osteomyelitis caused by *Burkholderia cepacia* in an immunocompetent adult. Surg Infect (Larchmt). 2013;14:476–9. https://doi.org/10.1089/sur.2012.025
35. Yang BH, Lee MS, Lee JH, Lee HJ. Pyogenic spondylitis in a healthy adult caused by *Burkholderia cepacia.* Infect Chemother. 2008;40:233–6. https://doi.org/10.3947/ic.2008.40.4.233
36. Chuo CY, Fu YC, Lu YM, Chen JC, Shen WJ, Yang CH, et al. Spinal infection in intravenous drug abusers. J Spinal Disord Tech. 2007;20:324–8. https://doi.org/10.1097/BSD.0b013e31802c144a
37. Dellalana LE, Byrge KC, Gandelman JS, Lines T, Aronoff DM, Person AK. A unique case of *Burkholderia cepacia* prosthetic mitral valve endocarditis and literature review. Infect Dis Clin Pract (Baltim Md). 2019;27:123–5. https://doi.org/10.1097/IPC.0000000000000708
38. Noriega ER, Rubinstein E, Simberkoff MS, Rahal JJ Jr. Subacute and acute endocarditis due to *Pseudomonas cepacia* in heroin addicts. Am J Med. 1975;59:29–36. https://doi.org/10.1016/0002-9343(75)90318-6
39. Ki HK, Kim SH, Han SW, Cheong HS. A case of native valve endocarditis caused by *Burkholderia cepacia* without predisposing factors. BMC Infect Dis. 2011;11:114. https://doi.org/10.1186/1471-2334-11-114
40. Saaraswat V, Barzani Y, Saaraswat B, Mishra S, Adler M, Chandra P. Late prosthetic valve endocarditis caused by *Burkholderia cepacia* and *Candida dublienensis* – the first reported case in the medical literature [cited 2019 Sep 24]. https://print.ispub.com/api/0/ispub-article/3838
41. Kothari T, Reyes MP, Brooks N. *Pseudomonas cepacia* septic arthritis due to intra-articular injections of methylprednisolone. Can Med Assoc J. 1977;116:1230, 1232, 1235.
42. Matteson EL, McCune WJ. Septic arthritis caused by treatment resistant *Pseudomonas cepacia.* Ann Rheum Dis. 1990;49:258–9. https://doi.org/10.1136/ard.49.4.258
43. Chiu LQ, Wang W. A case of unusual Gram-negative bacilli septic arthritis in an immunocompetent patient. Singapore Med J. 2013;54:e164–8. https://doi.org/10.11622/smedj.2013162
44. Miki RA, Rubin LE, Kirk J, Dodds SD. Spontaneous septic arthritis caused by *Burkholderia cepacia*. Iowa Orthop J. 2006;26:147–50.
45. Nivedhana S, Sulochana P, Shobana R. Spontaneous septic arthritis due to *Burkholderia cepacia* in a 3-month-old pre-term infant. Indian J Med Microbiol. 2016;34:394–5. https://doi.org/10.4103/0255-0857.188374
46. Woods CW, Bressler AM, LiPuma JJ, Alexander BD, Clements DA, Weber DJ, et al. Virulence associated with outbreak-related strains of *Burkholderia cepacia* complex among a cohort of patients with bacteremia. Clin Infect Dis. 2004;38:1243–50. https://doi.org/10.1086/383313
47. Jenney A, Liolios L, Spelman D, Russo P, Wilson J, Wesselingh S, et al. Use of pulsed-field gel electrophoresis in infection control issues concerning *Burkholderia cepacia*. Infect Control Hosp Epidemiol. 2003;24:624–6. https://doi.org/10.1086/502265
48. Steinbach S, Sun L, Jiang RZ, Flume P, Gilligan P, Egan TM, et al. Transmissibility of *Pseudomonas cepacia* infection in clinic patients and lung-transplant recipients with cystic fibrosis. N Engl J Med. 1994;331:981–7. https://doi.org/10.1056/NEJM199410133311504
49. Du M, Song L, Wang Y, Suo J, Bai Y, Xing Y, et al. Investigation and control of an outbreak of urinary tract infections caused by *Burkholderia cepacia*-contaminated anesthetic gel. Antimicrob Resist Infect Control. 2021;10:1. https://doi.org/10.1186/s13756-020-00855-x

Address for correspondence: Yat-ming Tsang, Room 1224, G12, Block G, Princess Margaret Hospital, 2-11 Princess Margaret Hospital Rd, Lai King, NT, Hong Kong, China; email: tym508@ha.org.hk

Comparative Effectiveness of Coronavirus Vaccine in Preventing Breakthrough Infections among Vaccinated Persons Infected with Delta and Alpha Variants

Irina Kislaya,[1] Eduardo Freire Rodrigues,[1] Vítor Borges, João P. Gomes, Carlos Sousa, José P. Almeida, André Peralta-Santos, Baltazar Nunes, PT-COVID-19 Group[2]

We developed a case–case study to compare mRNA vaccine effectiveness against Delta versus Alpha coronavirus variants. We used data on 2,097 case-patients with PCR-positive severe acute respiratory syndrome coronavirus 2 infections reported in Portugal during May–July 2021. We estimated the odds of vaccine breakthrough infection in Delta-infected versus Alpha-infected patients by using conditional logistic regression adjusted for age group and sex and matched by the week of diagnosis. We compared reverse-transcription PCR cycle threshold values by vaccination status and variant as an indirect measure of viral load. We found significantly higher odds of vaccine breakthrough infection in Delta-infected patients than in Alpha-infected patients (odds ratio 1.96 [95% CI 1.22–3.14]), suggesting lower effectiveness of the mRNA vaccines in preventing infection with the Delta variant. We estimated lower mean cycle threshold values for the Delta cases (mean difference −2.10 [95% CI −2.74 to −1.47]), suggesting higher infectiousness than the Alpha variant.

The severe acute respiratory syndrome coronavirus 2 (SARS-CoV-2) B.1.617.2 lineage, also known as Delta variant of concern (VOC), first sequenced in India in December 2020, was identified in Portugal in late April and quickly became dominant, reaching 90% of all sequenced cases in late June 2021 (epidemiologic week 26), just 2 months after it was first identified (*1*). Available evidence suggests that this VOC is associated with higher transmissibility, higher risk for hospitalization, and reduced antibody neutralization compared with other VOCs (*2*,*3*).

Author affiliations: Instituto Nacional de Saúde Doutor Ricardo Jorge, Lisbon, Portugal (I. Kislaya, V. Borges, J.P. Gomes, B. Nunes); Direção-Geral da Saúde, Lisbon (E.F. Rodrigues, A. Peralta-Santos); Unilabs, Porto, Portugal (C. Sousa, J.P. Almeida)

DOI: https://doi.org/10.3201/eid2802.211789

Vaccination is the primary pharmacologic measure to control the transmission of SARS-CoV-2 and mitigate its effect on hospitalizations and mortality rates. In Portugal, vaccination was initiated in late December 2020 for those at higher risk for severe disease or exposure and since February 2021 has been rolled out by descending age criteria. By week 26 (June 28–July 4), 36% of the population was fully vaccinated, and 56% had started or completed vaccination (Appendix Figure 1, https://wwwnc.cdc.gov/EID/article/28/2/21-1789-App1.pdf), most (75%) with mRNA vaccines (BNT162b2 [Pfizer-BioNTech, https://www.pfizer.com] or mRNA-1273 [Moderna, https://www.modernatx.com]) administrated with a 28-day dose interval (*4*).

Early reports of vaccine effectiveness indicate a high protection for mRNA vaccines against infection and disease (*5*,*6*) and a reduced viral load in the vaccinated case-patients (*7*,*8*). However, reports of vaccine effectiveness against Delta have shown decreased protection of the vaccines compared with the Alpha variant (*2*,*9*). Validating this potential reduction of vaccine effectiveness against the Delta VOC is critical to inform further public health measures, particularly as the variant becomes globally dominant.

We aimed to provide a measure of comparative effectiveness of mRNA vaccines (BNT162b2 and mRNA-1273) against B.1.617.2 (Delta) versus B.1.1.7 (Alpha) VOCs, using a case–case study design. As a secondary objective, we compared reverse-transcription PCR (RT-PCR) cycle threshold (C_t) values between vaccine status for Alpha and Delta variants as an indirect

[1]These first authors contributed equally to this article.

[2]Members of the PT-Covid-19 Group are listed at the end of this article.

measure of viral load and, thus, transmissibility of the vaccine breakthrough cases for both variants.

Methods

Study Design

We developed an observational case–case study (*10*) comparing odds of vaccination (partial or complete) between RT-PCR–positive cases (symptomatic or asymptomatic) classified as infected with Delta versus Alpha VOCs. The study period was May 17–July 4, 2021 (epidemiologic weeks 20–26), to cover the period of VOC replacement in Portugal, from the Alpha (84.8%, week 19) to Delta dominance (96.1%, week 27) (*1*). Our analysis included persons with data on whole-genome sequencing (WGS) or spike (S) gene target failure (SGTF) who were ≥40 years of age and eligible for vaccination during the study period. Persons for whom data on national health registry number, age, sex, or diagnosis date were missing, and those vaccinated with Ad26.COV2-S (Johnson & Johnson/Janssen, https://www.janssen.com) or ChAdOx1 nCoV-19 (AstraZeneca, https://www.astrazeneca.com) vaccines were excluded from the study.

To indirectly infer the level of infectiousness of case-patients according to vaccination status and VOC type, we performed a secondary analysis by comparing the paired means of RT-PCR C_t values for nucleocapsid and open reading frame 1ab genes, by using data from a single large laboratory (Unilabs, https://unilabs.com). Lower C_t values reflect a reduced number of RT-PCR cycles required for amplification of SARS-CoV-2 RNA and, therefore, a higher number of virus copies within the sample. As such, studies have used C_t values to estimate viral load or viral shedding (*8*,*11*).

Data Sources

SARS-CoV-2 Cases

RT-PCR testing for SARS-CoV-2 in Portugal is done by hospitals as well as by public and private laboratories, and is available free of charge to anyone with symptoms consistent with coronavirus disease (COVID-19) (*12*). Laboratory-confirmed cases are reported to the mandatory National Epidemiologic Surveillance Information System (Sistema Nacional de Vigilância Epidemiológica, https://www.spms.min-saude.pt/2020/07/sinave-2). For this study, each notifying laboratory selected a random subset of RT-PCR–positive nasopharyngeal samples collected during the study period to be sent to the National SARS-CoV-2 Genomic Surveillance Network (*1*,*13*) and, thus, to be included in the study. We also included samples from a private molecular biology laboratory (Unilabs) with nationwide coverage that routinely performs analysis on SGTF. We collected RT-PCR C_t values as an indirect measure of viral load (*11*). We removed duplicate records on the basis of national health register numbers, maintaining only the first collected sample.

Variant Classification

We classified SARS-CoV-2 variants by viral WGS or inferred by SGTF data. For nonsequenced samples, we considered S-positive specimens (with amplification of structural gene) as Delta and SGTF samples as Alpha by using the TaqPath COVID-19 CE IVD RT-PCR Kit (Thermo Fisher Scientific, https://www.thermofisher.com) that targets 3 genes (structural, nucleocapsid, and open reading frame 1ab), performed according to the manufacturer's specifications, as described elsewhere (*13*).

Vaccination Status, Demographics, and Data Linkage

We obtained COVID-19 vaccination status through the electronic national vaccination register (https://www.sns.gov.pt/monitorizacao-do-sns/vacinas-covid-19). We classified vaccination exposure as no register of vaccine administration before diagnosis (i.e., unvaccinated); SARS-CoV-2 infection diagnosis <14 days after first dose mRNA vaccination (1 dose [<14 days]); SARS-CoV-2 infection diagnosis ≥14 days after first dose or <14 days after second dose (1 dose [≥14 days] or 2 doses [<14 days]) (i.e., partial vaccination); and ≥14 days after second dose of the mRNA vaccine (2 doses [≥14 days]) (i.e., complete vaccination). Information about age, sex, and date at diagnosis was routinely collected by National Epidemiologic Surveillance Information System. We performed a deterministic record linkage to join all data sources, namely on vaccination status, outcomes (VOC classification), and other covariates (e.g., age group and sex) and to remove duplicate data from the dataset.

Statistical Analysis

We compared characteristics of delta and alpha SARS-CoV-2 case-patients by using the χ^2 test. We considered Delta-infected case-patients as case-patients of interest and Alpha-infected case-patients as the reference group. We used conditional logistic regression matched by the week of diagnosis and adjusted for age group and sex to estimate confounder-adjusted odds of having been infected by SARS-CoV-2 and vaccinated among Delta case-patients compared with Alpha case-patients. These covariates might be associated with the probability of having been vaccinated and being exposed to the virus and type of variant.

In our analysis, odds ratio (OR) = 1 indicates no difference in odds of having been infected by SARS-CoV-2 and vaccinated and, thus, a proxy of no difference between mRNA vaccine effectiveness against the Delta versus Alpha VOC. OR >1 indicates a higher odds of having been infected by SARS-CoV-2 and vaccinated, thus lower vaccine effectiveness against the Delta versus Alpha VOC, whereas OR <1 indicates a lower odds of having been infected by SARS-CoV-2 and vaccinated among Delta case-patients and a higher vaccine effectiveness against the Delta versus Alpha VOC (Appendix).

We stratified mean and SD C_t values for Alpha-infected and Delta-infected case-patients on the basis of vaccination status. We evaluated differences between mean C_t values by vaccination status and VOC by fitting a linear multiple regression model with C_t values as outcome, adjusting for sex, age group, and week of case diagnosis. We included an interaction term between vaccination status and VOC type in the regression model to determine whether the effect of vaccination status on C_t values differed between Delta and Alpha.

Sensitivity Analysis

To assess the change of the sampling strategy for WGS from a monthly to weekly basis, which occurred on week 21, we restricted our analysis to weeks 22–26. In addition, to assess the bias of misclassification error associated with the SGTF method (particularly in the early weeks of the study period, when overall prevalence of the Delta variant was lower and SGTF sensitivity may also have been lower), we analyzed samples identified exclusively through WGS during weeks 22–26. Finally, to address whether having been infected and vaccinated was associated with lower infectiousness in any of the studied VOCs, we restricted analysis to samples with C_t values <25 (*8*).

Ethics Considerations

Genomic surveillance of SARS-CoV-2 in Portugal is regulated by Assistant Secretary of State and Health Executive Order no. 331/2021, issued on January 11, 2021. The research on genomic epidemiology of SARS-COV-2 received the clearance of the Ethics Committee of Instituto Nacional de Saúde Doutor Ricardo Jorge on March 30, 2021.

Results

Main Analysis

A total of 22,784 SARS-CoV-2–positive cases were reported in Portugal during May 17–July 4, 2021, among persons ≥40 years of age. Of 2,097 cases included in the analysis, 966 (46.1%) were variant-classified with WGS and 1,131 (53.9%) with SGTF. During the study period, 94.7% (827/873) of the S-positive sequenced samples were confirmed as Delta and 96.9% (372/384) of SGTF samples were classified as Alpha through WGS, thus indicating that the SGTF-derived VOC classification was robust.

Among Delta case-patients, we observed a higher proportion of persons ≥70 years of age (p<0.001) (Table 1), and a higher proportion of vaccinated persons (p<0.001) than among the Alpha case-patients. We report a statistically significant higher odds of being partially vaccinated (OR 1.70 [95% CI 1.18–2.47]) or completely vaccinated (OR 1.96 [95% CI 1.22–3.14]) among the Delta case-patients than among the Alpha case-patients, suggesting lower mRNA vaccine effectiveness for the Delta variant (Table 2). After adjustment for age group and sex, similar estimated ORs were observed for the complete vaccination scheme (OR 1.96 [95% CI 1.43–2.69]) or for partial vaccination (OR 1.81 [95% CI 1.37–2.39]).

Table 1. Characteristics of patients in the study sample, by severe acute respiratory syndrome coronavirus 2 variant of concern, Portugal, epidemiologic weeks 20–26 (May 17–July 4), 2021

Characteristic	Delta (B.1.617.2), no. (%)	Alpha (B.1.1.7), no. (%)	Total, no. (%)
Overall	1,366 (100)	731 (100)	2,097 (100)
Week of diagnosis			
20	53 (4)	137 (19)	190 (9)
21	64 (5)	154 (21)	218 (10)
22	112 (8)	171 (23)	283 (13)
23	192 (14)	114 (16)	306 (15)
24	249 (18)	73 (10)	322 (15)
25	350 (26)	38 (5)	388 (19)
26	346 (25)	44 (6)	390 (19)
Age group, y			
40–49	760 (56)	378 (52)	1,138 (54)
50–69	474 (35)	313 (43)	787 (38)
≥70	132 (10)	40 (5)	172 (8)
Sex			
F	707 (52)	402 (55)	1,109 (53)
M	659 (48)	329 (45)	988 (47)

Secondary Analysis

We observed statistically significant higher mean C_t values among those with complete vaccination compared with unvaccinated case-patients for Delta (17.7 vs. 16.5) as well as for Alpha (21.8 vs. 18.4) (Table 3; Figure), suggesting lower viral loads in vaccinated compared with unvaccinated case-patients for both VOCs. Although the Alpha variant cases had statistically significant confounder-adjusted C_t values mean difference (MD) of 4.49 (95% CI 2.07–6.91) after complete vaccination, representing an increase of C_t values (lower infectiousness), the Delta variant cases showed only about half of that increase, with a statistically significant confounder-adjusted C_t value mean difference point estimate of 2.24 (95% CI 0.85–3.64) between unvaccinated and fully vaccinated breakthrough case-patients. For partial vaccination, statistically significant differences in mean C_t values were observed for Alpha (MD 1.87 [95% CI 0.2–3.53]) but not for Delta cases (MD −0.15 [95% CI −0.99 to 0.96]), suggesting similar viral load between unvaccinated and partially vaccinated Delta case-patients.

The confounder-adjusted paired-mean difference in C_t values between Delta and Alpha was statistically significant for unvaccinated persons (MD –1.66 [95% CI –2.37 to –0.95]). For partially (MD –1.88 [95% CI –3.77 to 0.003]) and completely vaccinated persons (MD –2.24 [95% CI –4.8 to 0.32]) we did not observed statistically significant mean differences in C_t values between delta and alpha.

Sensitivity Analysis

In a sensitivity analysis (Table 4), restricted to weeks 22–26, confounder-adjusted OR estimates for having been infected and completely vaccinated (OR 1.78 [95% CI 1.01–3.13]) and partially vaccinated (OR 1.91 [95% CI 1.22–3.00]) remained similar and statistically significant. Restricting the analysis to the cases identified through WGS, we observed a drop in the adjusted OR point estimate of complete vaccination (OR 1.48 [95% CI 0.75–2.93]) with a loss of statistical significance, but for partial vaccination, estimates yielded increased significant results (OR 2.5 [95% CI 1.23–5.08]). Restricting to cases with C_t values <25 (n = 1,363), we observed an increase of the OR of infection and vaccination against Delta versus Alpha variants both for partial (OR 2.47 [95% CI 1.48–4.12]) and complete vaccination (OR 2.42 [95% CI 1.06–5.51).

Discussion

We observed statistically significant higher odds of having been infected and vaccinated (vaccine infection breakthrough) among Delta-infected versus Alpha-infected case-patients, suggesting a lower mRNA vaccines effectiveness for SARS-CoV-2 infection with the Delta VOC. The findings were consistent for both complete and partial vaccination. Delta breakthrough case-patients have a higher viral load (lower C_t values) compared with Alpha breakthrough case-patients.

The OR estimates for complete vaccination (vaccine infection breakthrough) (1.96) are in line with findings of test-negative design studies on vaccine effectiveness from Scotland and England (*2*,*9*) based only on SGTF or mixed SGTF and WGS methodology for variant identification. Those studies reported a 5.9 percentage point reduction of BNT162b2 vaccine effectiveness against the Delta VOC compared with 13.0 percentage points for the alpha VOC for complete vaccination (*2*,*9*), with nonoverlapping CIs for vaccine effectiveness estimates.

For partial vaccination, our results indicated statistically significant lower mRNA vaccine effectiveness against the Delta VOC (OR = 1.8), supporting the need to promptly complete vaccination schedules to account for swiftly reduced effectiveness against this variant. This result is not in line with previous research conducted in England (*9*). Several factors may explain the differences between that study (*9*) and our work: the target population is different (persons ≥16 years of age vs. ≥40 years of age); differences exist in the Alpha and Delta relative frequencies during the study period; differences exist in vaccination calendar and time between doses administration, with England having a higher proportion of persons exposed to 2 doses because of an earlier campaign roll out and

Table 2. Crude and adjusted odds ratio of being infected with severe acute respiratory syndrome coronavirus 2 and vaccinated (odds of vaccine infection breakthrough) in Delta-infected versus Alpha-infected patients, Portugal, epidemiologic weeks 20–26 (May 17–July 4), 2021*

Vaccination status	Delta, no. (%)	Alpha, no. (%)	Crude OR (95% CI)	Confounder-adjusted† OR (95% CI)
Unvaccinated	777 (57)	517 (78)	Referent	Referent
1 dose (<14 d)	229 (17)	73 (10)	1.23 (0.83 to 1.82)	1.29 (0.85 to 1.95)
1 dose (≥14 d) or 2 doses (<14 d)‡	198 (14)	49 (7)	1.70 (1.18 to 2.47)	1.81 (1.37 to 2.39)
2 doses (≥14 d)§	162 (12)	38 (5)	1.96 (1.43 to 2.69)	1.96 (1.22 to 3.14)

*OR, odds ratio.
†Adjusted for sex and age group by conditional logistic regression using week of diagnosis result as matching variable.
‡Partial vaccination.
§Complete vaccination.

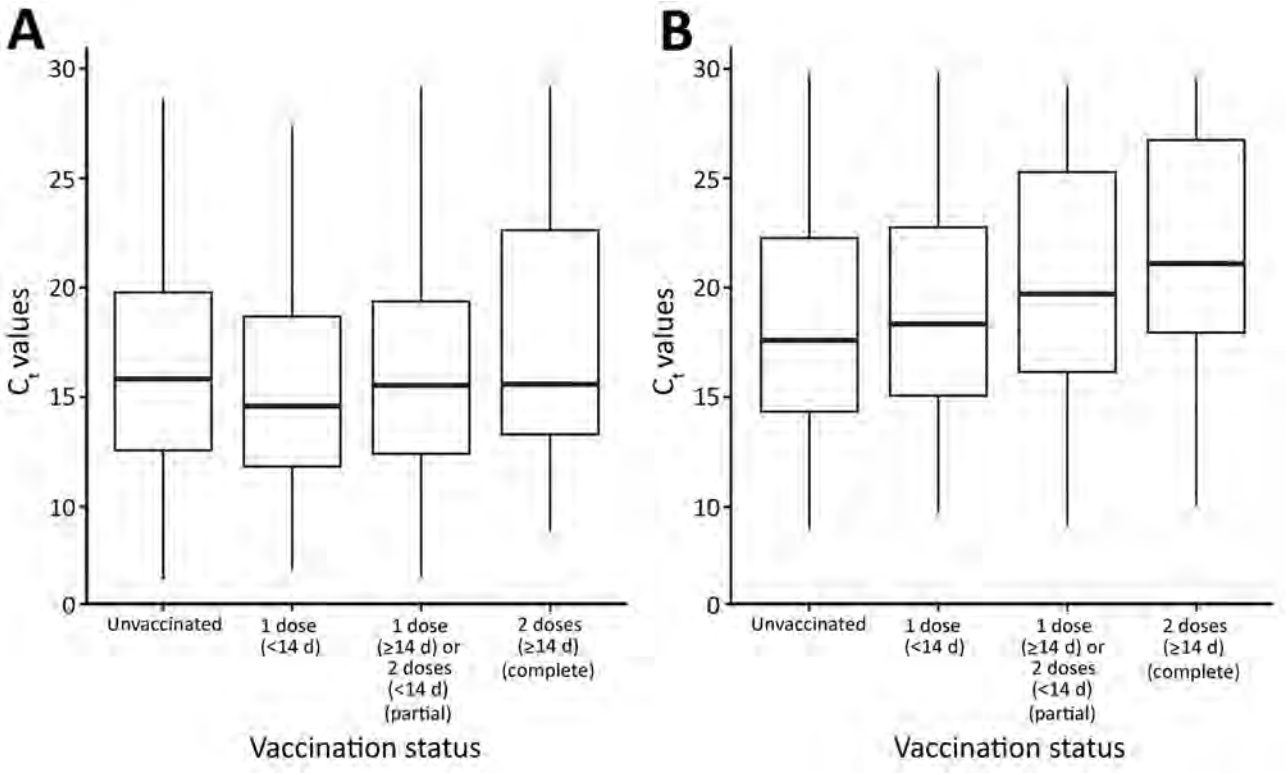

Figure. Distribution of C_t paired mean (reverse-transcription PCR C_t values for nucleocapsid and open reading frame 1ab genes) by coronavirus variant and vaccination status, Portugal, epidemiologic weeks 20–26 (May 17–July 4), 2021. Box top and bottom indicate first and the third quartiles of C_t distribution, horizontal line inside box indicates median, and whiskers indicate minimum and maximum values. C_t, cycle threshold.

Portugal having shorter time of exposure to a single dose; and a sample selection methodology for WGS.

On our secondary analysis, we observed lower C_t values (indicative of higher viral loads) among Delta compared with Alpha case-patients (MD −2.10 [95% CI −2.74 to −1.47]). Furthermore, although complete vaccination increases C_t values (thus reducing estimated viral loads) in Alpha case-patients by 4.49 (95% CI 2.07–6.91), for the Delta variant, complete vaccination had a much lower increase of C_t values (2.24 [95% CI 0.85–3.64]), only half of the difference observed for Alpha case-patients. These findings are consistent with vaccine infection breakthrough cases; Delta variant case-patients have higher infectiousness than alpha variant case-patients. Our findings were similar to results of the studies performed in Israel, when Alpha variant was the dominant variant, that also found a 5.09 (95% CI 2.8–7.4) increase of nucleocapsid gene C_t values (*8*) between completely vaccinated and unvaccinated cases and 1.51 for those partially vaccinated with BNT162b2 (*7*). Those findings are consistent with our results for the Alpha variant.

Our results were robust to variations in the sampling strategy, including changing the weeks of diagnosis included. Restricting analysis to samples with higher viral loads (selected on the basis of low C_t values [C_t <25]), we observed an even higher OR of vaccine infection breakthrough between Delta and Alpha variant cases, which supports the relevance of the Delta relative vaccine effectiveness reduction effect in the transmission of SARS-CoV-2, both for partial (OR 2.47 [95% CI 1.48–4.12]) and complete vaccination (OR 2.42 [95% CI 1.06–5.51]). The restriction to WGS samples only, however, resulted in a loss in a sample size and lack of statistical power to detect differences for complete vaccination.

This study has several limitations; in particular, possible misclassification and selection and confounding bias should be acknowledged. Although we observed a high positive predictive value (94.7%) of non-SGTF data to identify Delta cases within the study sample, a misclassification error may have led to underestimating the reported effect. However, SGTF methodology has previously shown good classification accuracy to identify B.1.1.7 in Portugal (*13*) and has more recently been shown to distinguish between Alpha and Delta VOCs in Scotland and England (*2*,*9*) and may be highly useful when a large-scale testing

Table 3. C_t values based on mean reverse-transcription PCR C_t values for nucleocapsid and open reading frame 1ab genes, stratified by vaccination status and severe acute respiratory syndrome coronavirus 2 variant of concern, and confounder-adjusted mean differences, Portugal, epidemiologic weeks 20–26 (May 17–July 4), 2021

Vaccination status	Delta (B.1.617.2), mean (SD)	Alpha (B.1.1.7), mean (SD)	Mean difference,* Delta vs. Alpha (95% CI)
Overall	16.4 (5.0)	18.7 (5.3)	−2.10 (−2.74 to −1.47)
Unvaccinated	16.5 (4.9)	18.4 (5.2)	−1.66 (−2.37 to −0.95)
1 dose (<14 d)	15.7 (4.9)	19.2 (5.6)	−1.42 (−3.07 to 0.23)
1 dose (≥14 d) or 2 doses (<14 d)†	16.1 (5.0)	20.0 (5.6)	−1.88 (−3.77 to −0.003)
2 doses (≥14 d)‡	17.7 (5.7)	21.8 (5.7)	−2.24 (−4.8 to 0.32)
Mean difference, partial vaccinated vs. unvaccinated*	−0.15 (−0.99 to 0.96)	1.87 (0.2 to 3.53)	
Mean difference, complete vaccinated vs. unvaccinated*	2.24 (0.85 to 3.64)	4.49 (2.07 to 6.91)	

*Mean difference and respective 95% CIs estimated by linear regression model adjusted to sex, age group, and week of diagnosis.
†Partial vaccination.
‡Complete vaccination.

strategy is in place and electronic vaccination registers are used. In addition, information bias caused by misclassification of vaccination status can arise from delays in registering vaccination status and diagnosis. However, data extraction was performed 3 weeks after the end of the study period to minimize bias (e.g., vaccination centers are instructed to register vaccinations up to 24 hours after administration). Our sampling strategy resulted in some selection bias. Overall, 22,784 cases were identified in Portugal during the study period among those ≥40 years of age, and their age distribution was different from the study sample (Appendix Figure 4), skewed toward younger ages in the study sample, possibly because our sample was collected mainly through ambulatory laboratories, whereas older persons (>80 years of age) are expected to be more frequently diagnosed by hospital laboratories. This result could bias our estimates if the reduction of vaccine effectiveness between Delta and Alpha variant is age-dependent. For example, if the vaccine effectiveness reduction is higher among older persons, our results could be underestimated. Moreover, Delta cases occurred more frequently among older participants, and older participants were the first to be vaccinated in Portugal (*4*) and, thus, had a longer exposure time after their second dose. With time, a waning of the vaccine effect can occur, possibly contributing to the observed differences among persons who were completely vaccinated.

After adjusting for confounding, we did not observe a substantial change in OR estimates. Although we cannot exclude residual confounding bias, given that other factors not accounted for might be associated with the probability of exposure to the virus and of being vaccinated (e.g., health and social services worker status, ethnicity, and education). However, we found that other studies (*9*) that adjusted for these potential confounding factors not accounted in our study did not observe a substantial difference between crude and confounder-adjusted estimates. Hence, if any residual confounding occurred, it could have a small effect on the effect estimates.

The results must always be interpreted in context because they do not provide evidence to question the

Table 4. Sensitivity analysis crude and adjusted odds ratio of being infected and vaccinated (odds of vaccine infection breakthrough) in Delta versus Alpha SARS-CoV-2 cases, Portugal, weeks 20–26 (May 17–July 4), 2021*

Vaccination status	Delta (B.1.617.2), no. (%)	Alpha (B.1.1.7), no. (%)	Crude OR (95% CI)	Confounder-adjusted† OR (95% CI)
Restricted to epidemiologic weeks 22–26, n = 1,689				
Unvaccinated	682 (55)	328 (75)	Referent	Referent
1 dose (<14 d)	224 (18)	54 (12)	1.34 (0.94 to 1.91)	1.38 (0.96 to 1.98)
1 dose (≥14 d) or 2 doses (<14 d)‡	190 (15)	32 (7)	1.87 (1.22 to 2.86)	1.91 (1.22 to 3.00)
2 doses (≥14 d)§	153 (12)	26 (6)	1.99 (1.25 to 3.16)	1.78 (1.01 to 3.13)
Restricted to WGS-classified VOC patients, n = 931				
Unvaccinated	406 (59)	189 (77)	Referent	Referent
1 dose (<14 d)	104 (15)	29 (12)	1.21 (0.75 to 1.95)	1.20 (0.73 to 1.96)
1 dose (≥14 d) or 2 doses (<14 d)‡	84 (12)	11 (4)	2.63 (1.34 to 5.20)	2.50 (1.23 to 5.08)
2 doses (≥14 d)§	90 (13)	18 (7)	1.91 (1.09 to 3.34)	1.48 (0.75 to 2.93)
Restricted to patients with C_t values <25, n = 1,363				
Unvaccinated	492 (57)	412 (82)	Referent	Referent
1 dose (<14 d)	161 (19)	48 (10)	1.20 (0.79 to 1.81)	1.30 (0.85 to 1.98)
1 dose (≥14 d) or 2 doses (<14 d)‡	142 (17)	30 (6)	2.14 (1.32 to 3.46)	2.47 (1.48 to 4.12)
2 doses (≥14 d)§	64 (7)	14 (3)	1.92 (0.97 to 3.82)	2.42 (1.06 to 5.51)

*C_t, cycle threshold; OR, odds ratio; WGS, whole-genome sequencing; VOC, variant of concern.
†Adjusted for sex and age group by conditional logistic regression using week of diagnosis result as matching variable.
‡Partial vaccination.
§Complete vaccination.

benefits of the mRNA vaccines to individual health, such as reducing symptoms, disease severity, or the impact on health services capacity. We reported odds of vaccine breakthrough between Delta and Alpha VOCs, which can be interpreted as a measure of the relative vaccine effectiveness. Although a case–case study design does not provide a direct measure of effectiveness against a specific VOC, it may be useful to rapidly detect changes in vaccine effectiveness in the context of novel VOC emergence, providing substantial evidence for further public health measures to control the transmission of SARS-CoV-2.

Overall, we found significantly higher odds of vaccination in Delta case-patients than in Alpha case-patients, suggesting possible lower effectiveness of the mRNA vaccines in preventing infection with the Delta VOC. Case–case design has proven to be helpful to compare vaccine effectiveness for SARS-CoV-2 VOCs because of its quick implementation and valuable insights in the context of frequent and swift VOC emergence. These findings can help decision-makers as they consider applying or lifting of control measures and adjusting vaccine roll-out depending on the predominance of the Delta variant and levels of partial and complete mRNA vaccination coverage.

Members of the PT-COVID-19 Group: Ausenda Machado, Ana Paula Rodrigues, Carlos Matias Dias, Rita Ferreira, Joana Isidro, Miguel Pinto, Sílvia Duarte, Luís Vieira, Pedro Pinto Leite, Joana Moreno, António Maia Gonçalves, and Luís Menezes.

E.F. Rodrigues is a board member and owns stocks at UPHILL, a software company that provides digital training solutions and has customers in the pharmaceutical sector (e.g., Pfizer). No business was conducted between the 2 entities regarding mRNA vaccine products, similar products, or anything pertaining to this study.

About the Author

Ms. Kislaya is a biostatistician in the Department of Epidemiology at the Instituto Nacional de Saúde Doutor Ricardo Jorge, Lisbon, Portugal. Her primary research interests include vaccine effectiveness and population-level impact of public health interventions.

References

1. Instituto Nacional de Saúde Doutor Ricardo Jorge. Genetic diversity of the novel coronavirus SARS-CoV-2 (COVID-19) in Portugal. 2021 [cited 2021 Aug 13]. https://insaflu.insa.pt/covid19
2. Sheikh A, McMenamin J, Taylor B, Robertson C; Public Health Scotland and the EAVE II Collaborators. SARS-CoV-2 delta VOC in Scotland: demographics, risk of hospital admission, and vaccine effectiveness. Lancet. 2021;397:2461–2. https://doi.org/10.1016/S0140-6736(21)01358-1
3. Wall EC, Wu M, Harvey R, Kelly G, Warchal S, Sawyer C, et al. Neutralising antibody activity against SARS-CoV-2 VOCs B.1.617.2 and B.1.351 by BNT162b2 vaccination. Lancet. 2021;397:2331–3. https://doi.org/10.1016/S0140-6736(21)01290-3
4. Direção-Geral da Saúde. Norma circular no. 002/2021. Vaccination campaign against COVID-19 [in Portuguese]. 2021 [cited 2021 Aug 13]. https://covid19.min-saude.pt/wp-content/uploads/2021/10/Norma_002_2021_act_15_10_2021.pdf
5. Haas EJ, Angulo FJ, McLaughlin JM, Anis E, Singer SR, Khan F, et al. Impact and effectiveness of mRNA BNT162b2 vaccine against SARS-CoV-2 infections and COVID-19 cases, hospitalisations, and deaths following a nationwide vaccination campaign in Israel: an observational study using national surveillance data. Lancet. 2021;397:1819–29. https://doi.org/10.1016/S0140-6736(21)00947-8
6. Kissling E, Hooiveld M, Sandonis Martín V, Martínez-Baz I, William N, Vilcu A-M, et al. I-MOVE-COVID-19 primary care study team; I-MOVE-COVID-19 primary care study team. Vaccine effectiveness against symptomatic SARS-CoV-2 infection in adults aged 65 years and older in primary care: I-MOVE-COVID-19 Project, Europe, December 2020 to May 2021. Euro Surveill. 2021;26:2100670. https://doi.org/10.2807/1560-7917.ES.2021.26.29.2100670
7. Levine-Tiefenbrun M, Yelin I, Katz R, Herzel E, Golan Z, Schreiber L, et al. Initial report of decreased SARS-CoV-2 viral load after inoculation with the BNT162b2 vaccine. Nat Med. 2021;27:790–2. https://doi.org/10.1038/s41591-021-01316-7
8. Regev-Yochay G, Amit S, Bergwerk M, Lipsitch M, Leshem E, Kahn R, et al. Decreased infectivity following BNT162b2 vaccination: a prospective cohort study in Israel. Lancet Reg Health Eur. 2021;7:100150. https://doi.org/10.1016/j.lanepe.2021.100150
9. Lopez Bernal J, Andrews N, Gower C, Gallagher E, Simmons R, Thelwall S, et al. Effectiveness of Covid-19 vaccines against the B.1.617.2 (delta) variant. N Engl J Med. 2021;385:585–94. https://doi.org/10.1056/NEJMoa2108891
10. Pogreba-Brown K, Austhof E, Ellingson K. Methodology minute: an overview of the case-case study design and its applications in infection prevention. Am J Infect Control. 2020;48:342–4. https://doi.org/10.1016/j.ajic.2018.11.024
11. Rabaan AA, Tirupathi R, Sule AA, Aldali J, Mutair AA, Alhumaid S, et al. Viral dynamics and real-time RT-PCR C_t values correlation with disease severity in COVID-19. Diagnostics (Basel). 2021;11:1091. https://doi.org/10.3390/diagnostics11061091
12. Direção-Geral de Saúde. Norma circular no. 004/2020. Approach to suspected and confirmed COVID-19 cases [in Portuguese]. 2020 [cited 2021 Aug 13]. https://covid19.min-saude.pt/wp-content/uploads/2021/04/Norma_004_2020_act_19_04_2021.pdf
13. Borges V, Sousa C, Menezes L, Gonçalves AM, Picão M, Almeida JP, et al. Tracking SARS-CoV-2 lineage B.1.1.7 dissemination: insights from nationwide spike gene target failure (SGTF) and spike gene late detection (SGTL) data, Portugal, week 49 2020 to week 3 2021. Euro Surveill. 2021;26:1–6. https://doi.org/10.2807/1560-7917.ES.2021.26.10.2100130

Address for correspondence: Irina Kislaya, Instituto Nacional de Saúde Doutor Ricardo Jorge, Av Padre Cruz, 1649-016 Lisbon, Portugal; email: irina.kislaya@insa.min-saude.pt

Effectiveness of mRNA BNT162b2 Vaccine 6 Months after Vaccination among Patients in Large Health Maintenance Organization, Israel

Jennifer Kertes, Sharon Baruch Gez, Yaki Saciuk, Lia Supino-Rosin, Naama Shamir Stein, Miri Mizrahi-Reuveni, Anat E. Zohar

Israel experienced a new wave of coronavirus disease during June 2021, six months after implementing a national vaccination campaign. We conducted 3 discrete analyses using data from a large health maintenance organization in Israel to determine whether IgG levels of fully vaccinated persons decrease over time, describe the relationship between IgG titer and subsequent PCR-confirmed infection, and compare PCR-confirmed infection rates by period of vaccination. Mean IgG levels steadily decreased over the 6-month period in the total tested population and in all age groups. An inverse relationship was found between IgG titer and subsequent PCR-positive infection. Persons vaccinated during the first 2 months of the campaign were more likely to become infected than those subsequently vaccinated. The vaccinated group ≥60 years of age had lower initial IgG levels and were at greater risk for infection. The findings support the decision to add a booster vaccine for persons ≥60 years of age.

Coronavirus disease (COVID-19) was identified in Israel at the end of February 2019 (*1*). As in other countries, Israel has experienced several infection waves. The third wave, largely attributed to entry of the Alpha virus variant into Israel, began during in September 2020; at its peak, >8,000 new cases were being identified daily (*2*). Israel was among the first countries to introduce a national vaccination campaign using the mRNA BNT162b2 vaccine (Pfizer-BioNTech, https://www.pfizer.com). The BNT162b2 vaccine received emergency approval for use by the US Food and Drug Administration after the vaccine showed 95% efficacy over an average 2-month follow-up period (*3*,*4*). The vaccine was initially approved for any person ≥16 years of age, with a recommended 21-day interval, 2-dose administration.

The vaccine campaign began on December 20, 2020 (concurrent with a 2-month nationwide lockdown), first targeting all healthcare workers and the population ≥60 years of age and quickly extending to all persons ≥16 years of age. Initially, those persons who had a previous infection were not eligible for vaccination, but within 3 months, policy was changed to offer a single dose to all persons who had a previous infection. By April 2021, >50% of persons ≥16 years of age and 88% of persons ≥50 years of age countrywide had been fully vaccinated (*2*). The number of new cases decreased to 140 cases/day by April 2021 (*2*). Initial population-based studies in Israel comparing vaccinated and unvaccinated groups reported vaccine effectiveness rates of 95% (*5*,*6*).

One of the biggest questions regarding the vaccine is the length of protection provided. In publishing third-phase research results, Pfizer-BioNTech reported a 91% efficacy rate over a 6-month follow-up period and an estimated 6% decrease in efficacy every 2 months (*7*). Population-based observational studies in Israel are no longer a feasible method of evaluating long-term effectiveness of the vaccine, given that most persons have now been fully vaccinated. Infection rates in Israel increased again during June–September 2021 (fourth wave), and most (97%) positive cases were infected with the Delta variant (B.1.617.2) (G. Rahib, Israel Ministry of Health Laboratories, pers. comm., 2021 Aug 8). Initial serologic studies of the Delta variant suggest that the BNT162b2 vaccine provides protection against Delta variant infection, but at lower rates than for the Alpha variant (88% vs. 93.7%) (*8*). Given the increase in infection rates, the dilemma arose whether this increase was attributable to

Author affiliation: Maccabi HealthCare Services, Tel Aviv–Jaffa Israel

DOI: https://doi.org/10.3201/eid2802.211834

reduced effectiveness of the vaccine against the Delta variant or a waning of protection provided by the vaccine over time.

The objective of this study was to determine if the BNT162b2 vaccine had become less effective in preventing infection, and if so, in which population groups and to what degree. To meet this objective, we conducted 3 discrete analyses to answer the following questions. First, do antibody levels (IgG) of those fully vaccinated decrease over time and if so, for who and how quickly? Second, what is the relationship between antibody level (IgG) and subsequent PCR-confirmed infection? Third, is there a difference in PCR-confirmed infection incidence rates between persons vaccinated in the initial months of the vaccination campaign and persons vaccinated later?

Methods

We conducted a series of retrospective cohort analyses to meet the study objectives. We extracted all data from the Maccabi Healthcare Services database (https://www.maccabi4u.co.il/1781-he/Maccabi.aspx). Maccabi is the second-largest health maintenance organization (HMO) in Israel and provides healthcare coverage for >2.5 million citizens (27% of the population of Israel). The database includes demographic data (date of birth, sex, socioeconomic status based on census, and national survey classifications applied to home address); laboratory data (all PCR and IgG test results); and health status data (chronic illness registries, such as heart disease, hypertension, chronic kidney disease [CKD], diabetes and immunosuppressive disorder, based on hospital and community-based diagnoses and procedures, and relevant laboratory and test results). The study was approved by the Maccabi Helsinki Committee (#0178-20-MHS). Informed consent was waived because all data extracted from the database were anonymized and aggregated.

Testing Procedures

PCR testing is conducted free of charge for any HMO member who has symptoms or reported exposure to a confirmed case. Testing is conducted by using real-time reverse transcription PCR (Allplex 2019-nCoV Assay; Seegene Inc., https://www.seegene.com). We offered serologic testing to specific target populations, such as employees (19%) and residents and employees of geriatric medical and retirement home facilities owned by the HMO (4%) at discrete points in time, but most (77%) testing was carried out in the general HMO population for whom testing is freely available upon request (patients initiative). We conducted IgG testing by using severe acute respiratory syndrome coronavirus 2 (SARS-CoV-2) spike-specific antibodies and a follow-up chemo-luminescence immunoassay (Quant II IgG anti-Spike CoV2-SARS; Abbott Laboratories, https://www.abbott.com) and reported as arbitrary units per milliliter (AU/mL). Antibody levels are reported numerically, except for outliers (<21 AU/mL and >40,000 AU/mL), which are coded. Coded results were converted to numeric results (<21 to 21 and >40,000 to 40,001).

IgG Levels of Vaccinated Population over Time

All HMO members who had received both vaccine doses and had a subsequent IgG test for SARS-CoV-2 antibodies ≥7 days after the second vaccination were included in this component of the study. The study period extended from January 11, 2021 (when those first vaccinated reached day 7 after the second dose), through July 7, 2021. We mapped IgG results over a 180-day period by using demographic and health characteristics (age group, sex, socioeconomic status, and presence of selected chronic illnesses).

Relationship between IgG Levels and Subsequent SARS-CoV-2 Infection

We included all HMO members who had a PCR test (irrespective of vaccination status) during June 1–July 14, 2021 (peak of fourth wave of infection), and an IgG serologic test 7–120 days before the PCR test in this component of the study. We used the most recent test result for persons who had >1 test. We used the most recent PCR test date if all results were negative and the date of the first positive PCR result for persons who had >1 result. We calculated the proportion of participants who had subsequent positive PCR results by antibody level status.

Comparison of Infection Rates by Vaccination Period

We included all HMO members who as of June 9, 2021, were ≥7 days post–second vaccination dose and had no previous positive PCR result in this component of the study. We excluded from analysis members who received 3 doses or had an appointment to receive the third dose (n = 320) during the follow-up period. (At this time, a recommendation to offer a booster vaccination for persons who had an immune-suppressive disorder had been authorized.) We categorized the study population by using vaccination completion: January–February 2021 and March–May 2021. For both groups, we calculated the proportion who were PCR positive during June 9–July 18, 2021 (yes/no).

Statistical Analyses

We used Mann–Whitney and Kruskal–Wallis tests to compare antibody levels over time between different population groups. We used linear regression to identify those factors associated with serologic levels. Natural logarithm (ln) of serologic levels showed a normal distribution and was selected as the outcome variable. Other variables we entered into a hierarchical model were days from vaccination; age, sex, and socioeconomic status; and selected chronic illnesses.

We used χ^2 analyses to test the association between serologic levels (categorized) and PCR outcomes. We categorized serologic status into ≤300 AU/mL or >300 AU/mL We calculated Kaplan–Meier survival curves to compare time from serologic test to positive PCR result for the serologic categories by using log-rank tests. We defined an event as a positive PCR result. Time to event was the number of days from a serologic test to PCR, with censoring for those who died, left the HMO, or had a follow-up period of <120 days. We used logistic regression analysis to compare PCR-positive outcomes between vaccination periods, while controlling for age group, socioeconomic status, and presence of chronic illness (heart disease, hypertension, diabetes, CKD, and immunosuppressive disorder).We performed statistical analyses by using SPSS Statistics 25 (https://www.ibm.com) and R version 3.6.2 (https://cran.r-project.org).

Results

IgG Levels of Vaccinated Population Over Time

The study population consisted of 8,395 persons (Table 1). Of all HMO members who received both vaccine doses, those subsequently tested for IgG were more likely to be male, younger (18–44 years of age), and in a higher socioeconomic bracket and less likely to have a chronic illness than those not tested for IgG.

We found that serologic levels in the study population decreased over time, from a mean of 14,008 for those tested within a month of being vaccinated to a mean of 1,411 for those tested in the sixth month after vaccination (Table 2). We observed a decrease over time in all subpopulation groups when results were stratified by age group, sex, socioeconomic status, and selected chronic illnesses (Table 2). The largest mean differences between subpopulations were observed in their initial serologic levels (within the first month). Mean serologic levels for participants ≥60 years of age (n = 1,004, mean 9,433) were approximately half of those for participants <60 years of age (n = 1,453, mean 17,169) in the first month, attenuating to a <10% difference 6 months later (Figure 1). Large differences in initial serologic levels were also observed for participants with chronic illness, in particular participants with an immunosuppressive disorder, CKD or heart

Table 1. Demographic and health characteristics of population vaccinated against coronavirus disease, by serologic test status, Maccabi Healthcare Services, Israel, January–July 2021

Characteristic	No. (%) not tested, n = 1,423,257	No. (%) tested, n = 8,395
Sex		
M	683,946 (48.1)	2,774 (33.0)
F	739,311 (51.9)	5,621 (67.0)
Age group, y		
<18	39,123 (2.7)	92 (1.1)
18–44	644,038 (45.3)	2,199 (26.2)
45–59	384,100 (27.0)	3,016 (35.9)
60–74	255,377 (17.9)	2,515 (30.0)
≥75	100,619 (7.1)	573 (6.8)
Socioeconomic status		
Low	481,470 (33.8)	3,202 (38.1)
Middle	232,824 (16.4)	1,281 (15.3)
High	708,963 (49.8)	3,912 (46.6)
Heart disease		
No	1,346,990 (94.6)	7,790 (92.8)
Yes	76,267 (5.4)	605 (7.2)
Diabetes		
No	1,297,140 (91.1)	7,342 (87.5)
Yes	126,117 (8.9)	1,053 (12.5)
Hypertension		
No	1,145,327 (80.5)	5,960 (71.0)
Yes	277,930 (19.5)	2,435 (29.0)
Chronic kidney disease		
No	1,353,406 (95.1)	7,715 (91.9)
Yes	69,851 (4.9)	680 (8.1)
Immunosuppressive disorder		
No	1,396,529 (98.1)	7,411 (88.3)
Yes	26,728 (1.9)	984 (11.7)

Table 2. Mean antibody level by demographic and health variables and time from vaccination against coronavirus disease for population vaccinated against coronavirus disease, Maccabi Healthcare Services, Israel, January–July 2021

Characteristic	Days from vaccination to serologic test						p value
	7–29	30–59	60–89	90–119	120–150	>150	
Total population	2,457	1,845	946	827	500	1,820	
Antibody levels							
Mean	14,008	8,175	4,365	2,706	1,773	1,411	<0.001
SD	12,146	7,742	5,022	3,957	1,934	1,751	
Median	11,322	6,080	2,974	1,683	1,217	1,217	
Sex							
No. male	1,075	676	354	269	105	295	
Mean antibody level	12,278	6,837	3,799	2,633	1,695	1,309	<0.001
No. female	1,382	1,169	592	558	395	1,525	
Mean antibody level	15,354	8,949	4,703	2,740	1,794	1,431	
Age group, y							
No. <18	32	40	14	6	0	0	
Mean antibody level	29,781	15,348	9,971	9,421			<0.001
No. 18–44	677	469	262	201	142	448	
Mean antibody level	18,522	9,866	5,621	3,271	2,006	1,479	
No. 45–59	744	602	288	237	224	921	
Mean antibody level	15,396	8,875	4,279	2,793	1,929	1,419	
No. 60–74	821	599	302	264	99	430	
Mean antibody level	9,999	6,280	3,684	2,670	1,478	1,256	
No. ≥75	183	135	80	119	35	20	
Mean antibody level	6,892	5,468	2,147	1,316	668	912	
Socioeconomic status							
No. low	553	278	143	113	59	135	
Mean antibody level	15,994	10,048	4,481	4,056	2,443	1,625	<0.001
No. middle	1,088	827	414	392	259	932	
Mean antibody level	13,989	8,473	4,739	2,523	1,695	1,468	<0.001
No. H\high	816	740	389	322	182	753	
Mean antibody level	12,687	7,139	3,924	2,454	1,667	1,301	<0.001
Underlying conditions							
Heart disease							
No. patients	206	165	79	75	25	55	
Mean antibody level	7,341	4,307	2,520	2,455	690	1,575	<0.001
Diabetes							
No. patients	377	245	121	123	57	130	
Mean antibody level	8,624	6,647	2,742	2,189	843	1,401	<0.001
Hypertension							
No. patients	803	572	274	290	133	363	
Mean antibody level	9,930	6,624	3,032	2,118	1,341	1,409	<0.001
Chronic kidney disease							
No. patients	248	163	81	88	45	55	
Mean antibody level	6,756	4,331	2,614	2,339	887	1,910	<0.001
Immunosuppressive disorder							
No. patients	307	280	156	126	57	58	
Mean antibody level	6,824	4,371	2,336	1,500	1,033	1,813	<0.001

disease. Initial (first month) serologic levels increased by socioeconomic level.

Of all persons who were vaccinated with both doses, 2.8% also had a positive PCR result. Comparable decreases in serologic means by month were observed in this group, as in others. However, the mean serologic level for those tested in the first 7–30 days was much higher than that for the total study population (22,630 AU/mL; p<0.001).

When demographic and health variables were entered into a linear regression model (Appendix Table 1, https://wwwnc.cdc.gov/EID/article/27/2/21-1834-App1.pdf), all factors remained independently associated with serologic levels; the highest coefficient was observed for participants who had an immunosuppressive disorder. No multicollinearity was observed between the factors in the regression model.

Relationship between IgG Levels and Subsequent SARS-CoV-2 Infection

Demographic and health characteristics of HMO members who had a serologic result and who had subsequently been tested by PCR were similar to those who had no PCR test result (Table 3), with the exception of socioeconomic status and diabetes status. Persons who were tested by PCR were more likely to be in the lower socioeconomic bracket and have diabetes than persons not tested by PCR.

Of persons who had both serologic and PCR tests (n = 5,141), 57% had a serologic test result of ≤150 AU/

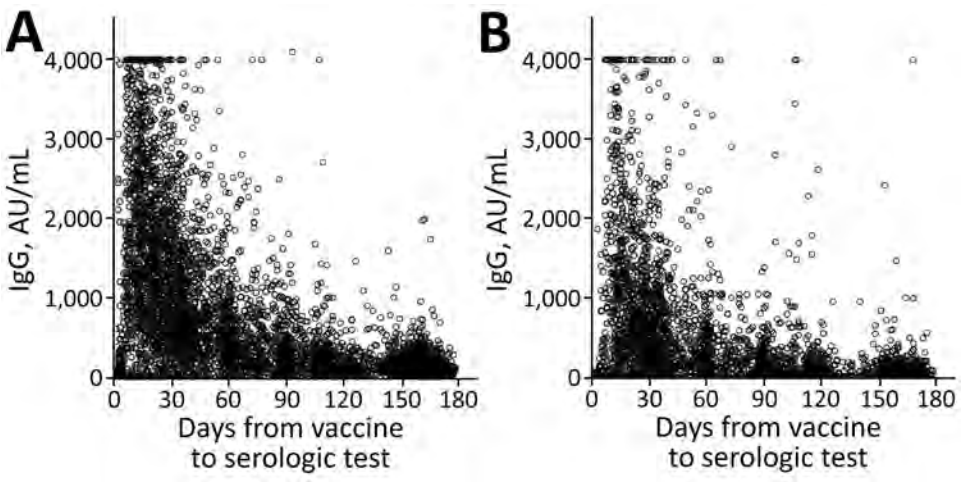

Figure 1. IgG levels for population vaccinated with mRNA BNT162b2 vaccine (Pfizer-BioNTech, https://www.pfizer.com) against coronavirus disease over time, by age group, Maccabi Healthcare Services, Israel, January–June 2021. A) <60 years of age. B) ≥60 years of age.

mL, 6% had a result of 150–299 AU/mL, 10% had a result of 300–799 AU/mL, and 27% had a result >800 AU/mL. The proportion of participants with a positive PCR result were 1.2% for those who had serologic levels ≤150 AU/mL, 1.3% for those who had serologic levels of 150–299 AU/mL, 0.2% for those who had serologic levels of 300–799 AU/mL, and 27% for those who had serologic levels of ≥800 AU/mL (p = 0.004. Mean serologic levels for the 42 study participants who had a positive PCR result were 175 AU/mL (SD ±490 AU/mL) compared a mean serologic level of 2,057 AU/mL (SD ±6,030 AU/mL) for those with a negative result (p<0.001).

Of all the study participants for this component of the study, 365 (7%) had a previous infection (37% of whom received 1 vaccine dose). Those who had a previous infection were less likely to have a serologic level of ≤300 AU/mL than those who did not have a previous infection (40.3% vs. 65.2%; p<0.001). However, irrespective of previous infection (yes/no), the proportion of those with a new PCR positive result was 0.8%. We provide Kaplan–Meier survival curves (over time by serologic status and ±300 AU/mL) (Figure 2). The curves indicate that participants who had lower serologic levels (≤300 AU/mL) had lower

Table 3. Demographic and health characteristics of population vaccinated against coronavirus disease, by PCR test status, Maccabi Healthcare Services, Israel, January–July 2021

Characteristic	No. (%) not tested, n = 79,404	No. (%) tested, n = 5,141
Sex		
M	33,871 (42.7)	2,128 (41.4)
F	45,533 (57.3)	3,013 (58.6)
Age group, y		
<18	21,563 (27.2)	937 (18.2)
18–44	37,470 (47.2)	2,338 (45.5)
45–59	13,553 (17.1)	1,090 (21.2)
60–74	5,672 (7.1)	657 (12.8)
≥75	1,146 (1.4)	119 (2.3)
Socioeconomic status		
Low	10,744 (13.5)	1,339 (26.0)
Middle	36,358 (45.8)	1,234 (24.0)
High	32,302 (40.7)	2,568 (50.0)
Heart disease		
No	78,105 (98.4)	5,021 (97.7)
Yes	1,299 (1.6)	120 (2.3)
Diabetes		
No	76,320 (96.1)	4,903 (95.4)
Yes	3,084 (3.9)	238 (4.6)
Hypertension		
No	73,063 (92.0)	4,524 (88.0)
Yes	6,341 (8.0)	617 (12.0)
Chronic kidney disease		
No	78,058 (98.3)	5,012 (97.5)
Yes	1,346 (1.7)	129 (2.5)
Immunosuppressive disorder		
No	78,193 (98.5)	5,010 (97.5)
Yes	1,211 (1.5)	131 (2.5)

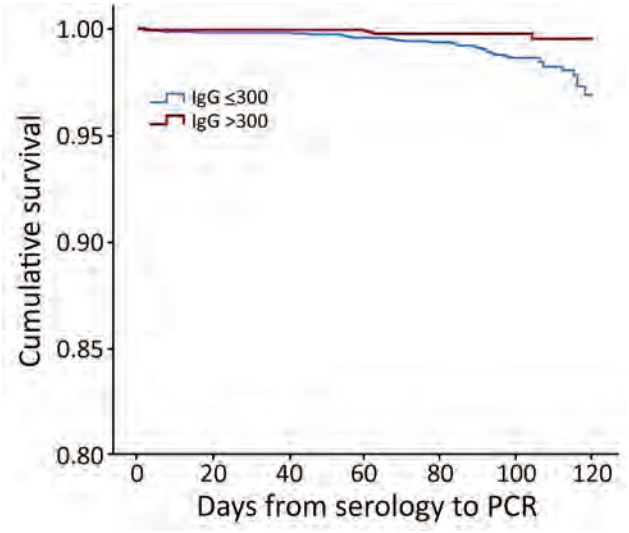

Figure 2. Kaplan-Meier cumulative survival for PCR-positive outcome for population vaccinated with mRNA BNT162b2 vaccine (Pfizer-BioNTech, https://www.pfizer.com) against coronavirus, by antibody (IgG) level, Maccabi Healthcare Services, Israel, June–July 2021.

survival rates than participants who had higher serologic levels (±300 AU/mL; p = 0.03 by log-rank test).

Comparison of Infection Rates by Vaccination Period

At the time of the study, 86% of those eligible for vaccination (≥16 years of age; n = 1,423,098) had received both doses in the HMO (90% of those ≥60 years of age). We compared demographic and health variables between those who were vaccinated in the first 2 months with those vaccinated later (Table 4). Those who were vaccinated in the first 2 months were more likely to be older, in a higher socioeconomic bracket, and have higher rates of chronic illness. We found that 1,518 (0.19%) of those vaccinated during January–February 2021 were PCR positive compared with 644 (0.11%) of those vaccinated during March–May 2021 (p<0.001). Univariate analyses (Appendix Table 2) also showed that age, sex, socioeconomic status and presence of chronic illnesses (health disease, diabetes, hypertension, and CKD) were associated with having a positive PCR result.

Factors associated with subsequent infection (positive PCR result) in a logistic regression model (Table 5) were socioeconomic status, age group, vaccination period, sex, and heart disease. When controlling for all other factors, we found that members vaccinated first were 1.6 times more likely to get infected with COVID-19 than those vaccinated later.

Discussion

In this study, we found that IgG serologic levels for SARS-CoV-2 virus decreased progressively over time for the total vaccinated population and in each subpopulation when stratified by demographic and

Table 4. Demographic and health characteristics of population vaccinated against coronavirus disease, by vaccination period, Maccabi Healthcare Services, Israel, January–July 2021

Characteristic	Jan–Feb, no. (%), n = 821,231	Mar–May, no. (%), n = 601,867
Sex		
M	394,546 (48.0)	285,089 (47.6)
F	426,685 (52.0)	313,482 (52.4)
Age group, y		
<18	21,232 (2.6)	62,793 (10.4)
18–44	211,351 (25.7)	414,514 (68.9)
45–59	289,813 (35.3)	86,013 (14.3)
60–74	219,437 (26.7)	28,620 (4.8)
≥75	79,398 (9.7)	9,927 (1.6)
Socioeconomic status		
Low	102,689 (12.5)	125,924 (20.9)
Middle	398,474 (48.5)	307,724 (51.1)
High	320,068 (39.0)	168,219 (27.9)
Heart disease		
No	755,979 (92.1)	592,608 (98.5)
Yes	65,252 (7.9)	9,259 (1.5)
Diabetes		
No	717,950 (87.4)	581,893 (96.7)
Yes	103,281 (12.6)	19,974 (3.3)
Hypertension		
No	593,368 (72.3)	556,545 (92.5)
Yes	227,863 (27.7)	45,322 (7.5)
Chronic kidney disease		
No	762,717 (92.9)	592,447 (98.4)
Yes	58,514 (7.1)	9,420 (1.6)
Immunosuppressive disorder		
No	808,061 (98.4)	598,499 (99.4)
Yes	13,170 (1.6)	3,368 (0.6)

Table 5. Factors associated with coronavirus disease for population vaccinated against coronavirus disease, by logistic regression model, Maccabi Healthcare Services, Israel, January–July 2021

Variable	No.	Adjusted odds ratio (95% CI)
Vaccination period		
Jan–Feb	821,231	1.61 (1.45–1.79)
Mar–May	601,867	Referent
Sex		
M	681,382	0.11 (1.01–1.20)
F	741,716	Referent
Age group, y		
<18	84,025	Referent
18–44	625,865	1.92 (1.51–2.49)
45–59	375,826	1.88 (1.46–2.45)
60–74	248,057	1.54 (1.17–2.04)
≥75	89,325	1.06 (0.75–1.50)
Socioeconomic status		
Low	228,613	Referent
Moderate	706,198	2.85 (2.34–3.50)
High	488,287	4.40 (3.61–5.41)
Heart disease		
No	1,348,587	Referent
Yes	74,511	1.35 (1.11–1.79)
Diabetes		
No	1,299,843	Referent
Yes	123,255	1.03 (0.87–1.12)
Hypertension		
No	1,149,913	Referent
Yes	273,185	0.98 (0.86–1.22)
Chronic kidney disease		
No	1,355,164	Referent
Yes	67,934	0.82 (0.63–1.05)
Immunosuppressive disorder		
No	1,406,596	Referent
Yes	16,502	0.90 (0.58–1.63)

health variables. We also found an association between serologic levels and subsequent risk for infection, wherein participants who had a serologic level ≤300 AU/mL were more likely to get COVID-19 than those who had a serologic level >300 AU/mL. We established that those vaccinated at the beginning of the national vaccination campaign were more likely to get infected (during the current wave of infection) than those vaccinated later. These findings suggest that effectiveness of the vaccine decreases over time and that the current wave of infection can be attributed, at least in part, to the reduced effectiveness of the vaccine over time.

Initial serologic studies focused on patients found to be PCR positive for COVID-19 reported a decrease over time of antibody presence from time of infection (*9*–*11*). Fewer studies have looked specifically at serologic response of the vaccinated population. Most of the studies based on vaccinated populations reported ≈100% seroconversion rates but had short follow-up periods (*12*,*13*). Serologic levels were much higher among the vaccinated population than those convalescing after infection (*12*) and among those <50 years of age ((*13*). In a case–control study of PCR-positive case-patients divided by previous vaccination status (yes/no), Lopez-Bernal et al. (*8*) found that those vaccinated (2 doses) with the BNT162b2 vaccine and were infected with the Alpha variant achieved 93.7% vaccine effectiveness rate compared with an 88% vaccine effectiveness rate for those infected with the Delta variant.

We did not find published studies that described serologic status over longer follow-up periods for a vaccinated population. Mean levels of IgG decreased progressively over time for all subpopulations in this study. The difference between the groups was mostly evident in initial (first month) starting means; the elderly and those having chronic illness had lower levels, but these levels attenuated to more comparable levels between groups 6 months after vaccination. In a large household study in the United Kingdom (*14*), IgG response measured over the first 3 months after vaccination found higher seroconversion rates for younger age groups (20–40 years of age), female participants, those receiving both doses, vaccination with BNT162b2 vaccine compared with AstraZeneca (https://www.astrazeneca.com) vaccine, and those with evidence of a previous infection. Low responders were older and had higher prevalence of chronic illness/disease, such as patients receiving immune suppressants or who had diabetes. These

same population groups were found in this study to start with lower serologic levels and have lower mean serologic levels 6 months after vaccination.

One of the many unknowns regarding COVID-19 is to what extent IgG is indicative of protection against the virus. The manufacturer's recommended cutoff indicating a positive serologic response (<50 AU/mL) is much lower than the mean serologic levels we found at 6 months after vaccination. Are higher levels indicative of higher protection? Other mechanisms of protection, such as antiviral T and B cell memory, have been suggested as offering protection, even in the absence of seroconversion (*15*). In a meta-analysis, Khoury et al. (*16*) found a strong relationship between mean neutralization levels and reported protection. They further estimated that protection was likely to occur over 250 days, although with still largely preserved protection from severe infection. In the second component of our study, we found an association between serologic level and PCR outcome in which increased serologic level was associated with decreasing infection rates. Using a cutoff value of 300 AU/mL, we found higher rates of infection for those with low serologic levels. However, given that those coming for testing were not randomly selected, repeat studies in a large randomly selected population are required to confirm this cutoff value.

Few data are available to compare vaccine effectiveness over time, and observational follow-up studies are becoming less appropriate, given the potential bias between those electing to vaccinate and those who do not. Pfizer-BioNTech published a recent efficacy study that compared symptomatic infection rates between vaccinated and unvaccinated groups over a period of 6 months (*7*). Vaccine efficacy for infection decreased from 96% within the first 2 months post–second dose to 84% vaccine efficacy 4–6 months post–second dose. Consistent with the findings of Pfizer-BionTech, we found higher rates of COVID-19 infection among those vaccinated in the initial months of the vaccine campaign compared with those vaccinated later. Even after controlling for age (those vaccinated first were more likely to be older), incidence rates were higher in the first vaccinated group. Were most of the fourth wave of infections attributable to the Delta virus, we would have expected consistent incidence rates, irrespective of when the individual was vaccinated. We suggest that the difference found here between time periods indicates a reduction in vaccine effectiveness over time. However, we cannot rule out some contribution of the Delta variant to reduced effectiveness.

One limitation of our study was that test findings were not based on repeated tests in the same population but a description of the results over time of those coming for a serologic test. Those coming for serologic and PCR testing were not randomly selected groups but, rather, persons volunteering in a study or, more commonly, requesting to be tested. Participants requesting a test (serologic and PCR) might have had greater concerns regarding exposure, infection, or perceived infection risk, potentially increasing the proportion of persons who had lower serologic levels or a positive PCR result. We calculated mean serologic levels for each subpopulation, despite the potential for outlier measures to skew results, to enable statistical comparison between subpopulation groups. Numbers were small for some stratified data, particularly for the 120–149 day period, and should be interpreted with caution. Study findings were not adjusted for serologic test accuracy. Conclusions are made on the assumption that most of those infected in the third component of the study (by time of vaccination) were infected with the Delta variant, given its prevalence in Israel.

All data presented are for Maccabi Healthcare Service members. Maccabi members are more likely to come from a higher socioeconomic bracket, and the service has a somewhat larger prevalence of members 35–55 years of age than that for the total population of Israel (*17*). Although these differences would not affect stratified data in our study, these differences might effect mean serologic results for the total population and vaccine effectiveness results. Generalizability of results to Israel and other countries should be made cautiously.

Given these limitations, the different elements of the study were based on large numbers of a vaccinated population who had 6 months of follow-up time to measure COVID-19 infection. We found that serologic levels for all groups decreased over time and that there was an association between serologic levels and subsequent infection. We further observed that persons vaccinated early in the vaccination campaign had higher infection rates. These factors taken together suggest that the BNT162b2 vaccine, as indicated by the manufacturer, offers lower protection against infection over time, independent of SARS-CoV-2 variant type. These results contributed to the decision to offer a third dose of the BNT162b2 vaccine to persons ≥60 years of age. Follow-up of infection and illness rates in this group will enable us to confirm the wisdom of providing a booster dose.

About the Author

Ms. Kertes is a senior researcher in the Division of Data and Digital Health, Maccabi Healthcare Services Tel Aviv–Jaffa, Israel. Her primary research interests are design and implementation of public health studies, public health and health promotion studies (especially regarding smoking), and pharma–therapeutic studies.

References

1. Rosen B, Waitzberg R, Israeli A. Israel's rapid rollout of vaccinations for COVID-19. Isr J Health Policy Res. 2021;10:6. https://doi.org/10.1186/s13584-021-00440-6
2. Leshem E, Wilder-Smith A. COVID-19 vaccine impact in Israel and a way out of the pandemic. Lancet. 2021;397:1783–5. https://doi.org/10.1016/S0140-6736(21)01018-7
3. Vaccines and Related Biological Products Advisory Committee Meeting. December 10, 2020. FDA briefing document—Pfizer BioNTech COVID-19 vaccine 2021 [cited 2021 Nov 16]. https://www.fda.gov/media/144245/download
4. Polack FP, Thomas SJ, Kitchin N, Absalon J, Gurtman A, Lockhart S, et al.; C4591001 Clinical Trial Group. Safety and efficacy of the BNT162b2 mRNA COVID-19 vaccine. N Engl J Med. 2020;383:2603–15. https://doi.org/10.1056/NEJMoa2034577
5. Haas EJ, Angulo FJ, McLaughlin JM, Anis E, Singer SR, Khan F, et al. Impact and effectiveness of mRNA BNT162b2 vaccine against SARS-CoV-2 infections and COVID-19 cases, hospitalisations, and deaths following a nationwide vaccination campaign in Israel: an observational study using national surveillance data. Lancet. 2021;397:1819–29. https://doi.org/10.1016/S0140-6736(21)00947-8
6. Dagan N, Barda N, Kepten E, Miron O, Perchik S, Katz MA, et al. BNT162b2 mRNA COVID-19 vaccine in a nationwide mass vaccination setting. N Engl J Med. 2021;384:1412–23. https://doi.org/10.1056/NEJMoa2101765
7. Thomas SJ, Moreira ED, Kitchin N, Absalon J, Gurtman A, Lockhart S, et al. Six month safety and efficacy of the BNT162b2 mRNA COVID-19 vaccine. N Engl J Med. 2021;385:1761–73.
8. Lopez Bernal J, Andrews N, Gower C, Gallagher E, Simmons R, Thelwall S, et al. Effectiveness of COVID-19 vaccines against the B.1.617.2 (Delta) variant. N Engl J Med. 2021;385:585–94. https://doi.org/10.1056/NEJMoa2108891
9. Zhao J, Yuan Q, Wang H, Liu W, Liao X, Su Y, et al. Antibody responses to SARS-CoV-2 in patients of novel coronavirus disease 2019. Clin Infect Dis. 2020;71:2027–34. https://doi.org/10.1093/cid/ciaa344
10. Zhou W, Xu X, Chang Z, Wang H, Zhong X, Tong X, et al. The dynamic changes of serum IgM and IgG against SARS-CoV-2 in patients with COVID-19. J Med Virol. 2021;93:924–33. https://doi.org/10.1002/jmv.26353
11. Harvey RA, Rassen JA, Kabelac CA, Turenne W, Leonard S, Klesh R, et al. Association of SARS-CoV-2 seropositive antibody test with risk of future infection. JAMA Intern Med. 2021;181:672–9. https://doi.org/10.1001/jamainternmed.2021.0366
12. Jalkanen P, Kolehmainen P, Häkkinen HK, Huttunen M, Tähtinen PA, Lundberg R, et al. COVID-19 mRNA vaccine induced antibody responses against three SARS-CoV-2 variants. Nat Commun. 2021;12:3991. https://doi.org/10.1038/s41467-021-24285-4
13. Grupel D, Gazit S, Schreiber L, Nadler V, Wolf T, Lazar R, et al. Kinetics of SARS-CoV-2 anti-S IgG after BNT162b2 vaccination. Vaccine. 2021;39:5337–40. https://doi.org/10.1016/j.vaccine.2021.08.025
14. Wei J, Stoesser N, Matthews PC, Ayoubkhani D, Studley R, Bell I, et al.; COVID-19 Infection Survey team. Antibody responses to SARS-CoV-2 vaccines in 45,965 adults from the general population of the United Kingdom. Nat Microbiol. 2021;6:1140–9. https://doi.org/10.1038/s41564-021-00947-3
15. Cox RJ, Brokstad KA. Not just antibodies: B cells and T cells mediate immunity to COVID-19. Nat Rev Immunol. 2020;20:581–2. https://doi.org/10.1038/s41577-020-00436-4
16. Khoury DS, Cromer D, Reynaldi A, Schlub TE, Wheatley AK, Juno JA, et al. Neutralizing antibody levels are highly predictive of immune protection from symptomatic SARS-CoV-2 infection. Nat Med. 2021;27:1205–11. https://doi.org/10.1038/s41591-021-01377-8
17. Damari N, Cohen R. Health maintenance organizations 2018–2019. Periodic surveys number 317, October 2020. National Insurance Agency, Israel [cited 2021 Nov 16]. https://www.btl.gov.il/Publications/survey/Documents/seker317/seker_317.pdf

Address for correspondence: Jennifer Kertes, Division of Data and Digital Health, Maccabi Healthcare Services, Rehov HaMered 27, Tel Aviv–Jaffa 16825, Israel, email: dortal_j@mac.org.il

Comparison of Complications after Coronavirus Disease and Seasonal Influenza, South Korea

Hyejin Lee,[1] Ho Kyung Sung,[1] Dokyoung Lee,[1] Yeonmi Choi, Ji Yoon Lee, Jin Yong Lee,[2] Myoung-don Oh[2]

We conducted a retrospective cohort study using claims data to determine the number and types of complications from coronavirus disease (COVID-19) that patients experience and which patients are more vulnerable to those complications compared with complications in patients with influenza. Among the cohort, 19.6% of COVID-19 patients and 28.5% of influenza patients had ≥1 new complication. In most complications, COVID-19 patients had lower or similar relative risk compared with influenza patients; exceptions were hair loss, heart failure, mood disorder, and dementia. Young to middle-aged adult COVID-19 patients and patients in COVID-19 hotspots had a higher risk for complications. Overall, COVID-19 patients had fewer complications than influenza patients, but caution is necessary in high-risk groups. If the fatality rate for COVID-19 is reduced through vaccination, management strategies for this disease could be adapted, similar to those for influenza management, such as easing restrictions on economic activity or requirements for close-contact isolation.

The symptoms, incidence, and risk for complications of coronavirus disease (COVID-19) remain controversial. Several types of long COVID, meaning prolonged symptoms or long-term complications of COVID-19, have been reported (*1*). In addition to fibrosis and decreased pulmonary function from inflammation of the lungs (*2*), other long-term complications have been reported as well (*3*–*7*). In one study, ≥1 symptoms remained in 87.4% of COVID-19 patients at a mean duration of 2 months after infection; fatigue and dyspnea were most common (*3*). Neurologic complications, such as loss of smell or taste, have also been reported (*4*,*5*). Moreover, unlike in severe acute respiratory syndrome (SARS) and Middle East respiratory syndrome (MERS), cerebral vascular disease has been reported to be more common in COVID-19. Ischemic stroke, hemorrhage, and cerebral venous sinus thrombosis have been reported in 2%–6% of hospitalized patients with COVID-19 (*6*), and it has been estimated that cognitive impairment and dementia associated with cerebral vascular disease will increase (*7*).

The National Institute for Health and Care Excellence in the United Kingdom recently defined long COVID as signs and symptoms that develop during or after an infection consistent with COVID-19 that continue for >4 weeks and cannot be explained by an alternative diagnosis (*8*). Long COVID is classified according to duration of signs and symptoms: those lasting 4–12 weeks are classified as ongoing symptomatic COVID-19, and those lasting >12 weeks are defined as post–COVID-19 syndrome.

Many patients report long COVID, and the need for management is high; however, definitive identification of symptoms, characteristics of vulnerable patients, and risk for COVID complications remain elusive. One study compared the illness and death rates of hospitalized patients for COVID-19 and influenza but did not include nonhospitalized COVID-19 or influenza patients with mild illness (*9*). In this study, we aimed to investigate the number and type of COVID-19 complications that occur and which COVID-19 patients are more vulnerable to complications compared with influenza patients. The Institutional Review Board (IRB) of the Health Insurance Review and Assessment Service approved this study (IRB no. 2021087-001).

Author affiliations: Seoul National University Bundang Hospital, Seongnam-si, South Korea (H. Lee); National Medical Center, Seoul, South Korea (H.K. Sung, M. Oh); Health Insurance Review & Assessment Service Research Institute, Wonju-si, South Korea (D. Lee, Y. Choi, J.Y. Lee, J.Y. Lee); Seoul National University Hospital, Seoul (J.Y. Lee); Seoul National University College of Medicine, Seoul (J.Y. Lee, M. Oh)

DOI: https://doi.org/10.3201/eid2802.211848

[1]These first authors contributed equally to this article.

[2]These corresponding authors contributed equally to this article.

Methods

Study Design, Setting, and Population

We conducted a retrospective cohort study using claims data provided by the Health Insurance Review and Assessment Service (HIRA). South Korea has adopted mandatory universal health coverage; therefore, 97% of South Korea residents are National Health Insurance Service (NHIS) beneficiaries and pay NHIS premiums according to their income levels or property values. The remaining 3% are medical-aid (MA) recipients who are unable to pay premiums; their medical costs are covered by the government through taxes (*10*). Therefore, medical use, diagnosis, and treatment history of COVID-19 and influenza patients can all be identified from claim data. The diagnosis code was based on the Korean Standard Classification of Diseases and Causes of Death, 7th edition (KCD-7), which is a modification of the International Classification of Diseases, 10th Revision.

We defined COVID-19 patients as those who received diagnosis of and were treated for COVID-19 (KCD-7 code U07.1); we enrolled a total of 21,615 patients during January 1–September 30, 2020. We defined influenza patients as those who were prescribed the antiviral drugs oseltamivir, zanamivir, or amantadine for an influenza-like illness (*11*) or who had influenza diagnosed (KCD-7 code J09-J11) as determined by a doctor; we enrolled 2,380,696 patients during July 1, 2017–June 30, 2018. We defined complications for COVID-19 and influenza patients as signs or symptoms in patients who had not received a diagnosis of those specific conditions in the last 3 years but who received new diagnoses of complications during the follow-up period after COVID-19 or influenza diagnosis.

We followed influenza patients for up to 1 year after diagnosis (follow-up duration 365 days) and COVID-19 patients from the date of COVID-19 diagnosis to December 31, 2020 (median follow-up duration 209 days; interquartile range 127–297 days) (Figure 1).

Data Collection

We extracted patient sex, age, insurance type, region, Charlson Comorbidity Index (CCI), severity and complications from the claims data. We defined age groups as 0–19 years, 20–44 years, 45–64 years, 65–74 years, and ≥75 years of age. We categorized insurance as NHIS beneficiaries and MA recipients. We classified regions into the Seoul metropolitan area, Daegu and Gyeongsangbuk Province, and other areas, in accordance with the COVID-19 epidemic areas in South Korea. We calculated the CCI, an indicator of underlying conditions, using claims data from 1 year before the diagnosis of COVID-19 or influenza.

We classified severity as ambulatory, hospitalized mild disease, and hospitalized severe disease using the COVID-19 severity scale from the World Health Organization (*12*). The scale indicates the clinical severity of the disease and can be used during any infectious disease epidemic; therefore, influenza patients were classified on the same scale (*13*). The complications we used were gastrointestinal disease, musculoskeletal

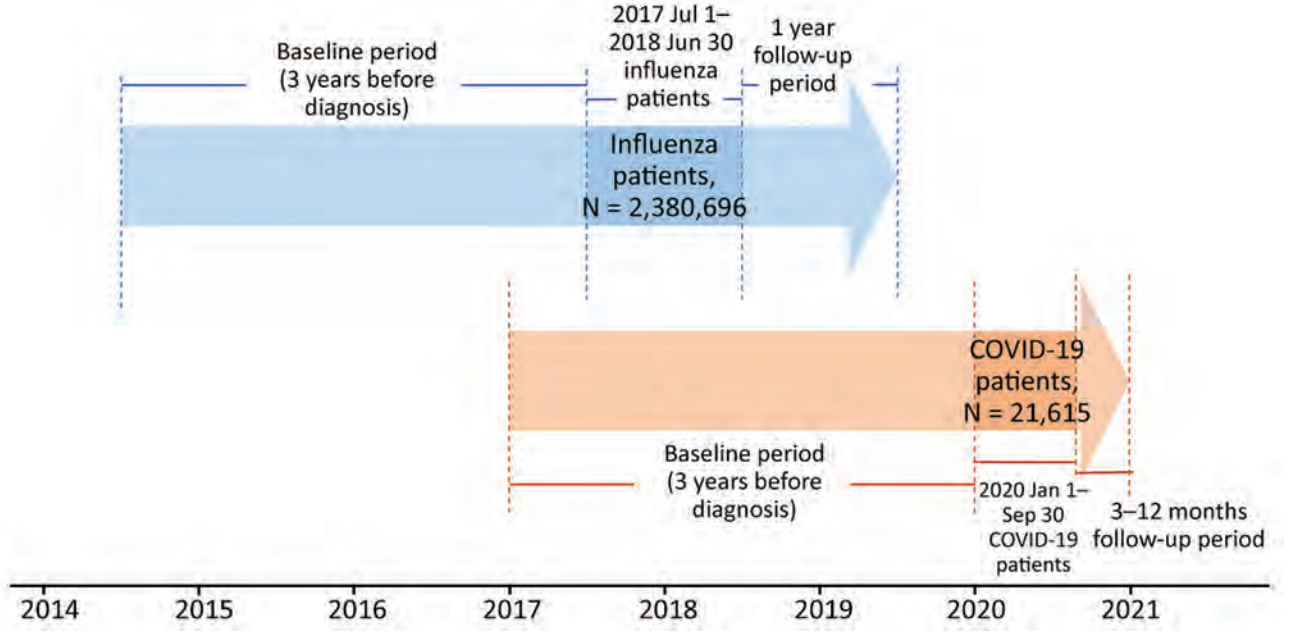

Figure 1. Study design for comparison of complications in coronavirus disease and influenza patients, South Korea. COVID-19, coronavirus disease.

disorder, periodontal disease, dermatitis, hair loss, asthma, chronic obstruction pulmonary disease, pneumonia, cardiovascular disease, heart failure, cerebrovascular disease, autoimmune disease, mood disorder, and dementia. Complications were confirmed with the KCD-7 code (Appendix Table 1, https://wwwnc.cdc.gov/EID/article/28/2/21-1848-App1.pdf).

Statistical Analysis

We analyzed characteristics of the general population, COVID-19 patients, and influenza patients by frequency and percentage. We determined homogeneity by χ^2 test. We determined the number of patients with complications by χ^2 test and calculated the age-standardized incidence rate as the number of patients with complications divided by the sum of the total person-months by age, standardized by the population in 2020. The censoring time of the observation period was at the time when complications occurred or at the time of the last observation (1 year after influenza diagnosis; December 31, 2020, for COVID-19). The incidence of COVID-19 complications compared with influenza complications is a rate ratio. We performed multivariable logistic regression analysis to identify factors related to COVID-19 complication occurrence. We defined significance level as a 2-tailed p-value <0.05. We used SAS Enterprise guide version 7.15 (SAS Institute Inc., https://www.sas.com) for all analyses.

Results

We reviewed a total of 21,615 cases of COVID-19 from January 1–September 30, 2020, and 2,380,696 cases of influenza from July 1, 2017–June 30, 2018. We report results by study characteristic: patient sex, age, insurance type, region, CCI, severity, and complications.

The sex ratio (M:F) was similar to that of the general population in both the COVID-19 and influenza patient groups. In the COVID-19 patient group, the number of patients 0–19 years of age was 1,467 (6.8%), whereas that age group was the largest of the influenza patient groups at 1,180,279 (49.6%). A total of 1,397 (6.5%) of MA recipients were COVID-19 patients, which was higher than for the general population (1,526,030, 2.9%) and for influenza patients (53,051, 2.2%) (p<0.001). A total of 4,963 (23.0%) COVID-19 patients lived in the provinces of Daegu and Gyeongsangbuk, hotspots of the pandemic; there was no regional influenza epidemic of influenza. A CCI score ≥3 was more common in COVID-19 patients (7.7%, 1,664) than in influenza patients (3.9%, 91,847). More COVID-19 patients than influenza patients were hospitalized with mild cases (71.5% vs. 9.4%) and severe cases (4.4% vs. 0.3%) (Table 1).

Among all COVID-19 patients, 4,139 (19.1%) had ≥1 complications after their diagnosis, and 678,845 (28.5%) of influenza patients had ≥1 complications after their diagnosis; thus, significantly more complications occurred in influenza patients (p<0.001). Skin disease (5.4% vs. 11.3%; p<0.001), asthma (0.5% vs. 3.1%; p<0.001) and pneumonia (2.1% vs. 4.4%; p<0.0001) were more prevalent in influenza patients than in COVID-19 patients. When the age-standardized incidence rate was calculated after standardization to the population in 2020, most of the COVID-19 patient group had a lower or similar relative risk (RR) of complications than the influenza group. However, COVID-19 patients had higher RRs for hair loss (RR 1.52, 95% CI 1.18–1.97), heart failure (RR 1.88, 95% CI 1.42–2.50), mood disorder (RR 1.73, 95% CI 1.56–1.93), and dementia (RR 1.96, 95% CI 1.52–2.55)(Table 2).

In COVID-19 patients, when we analyzed the risk for COVID-19 complications by age, the 20–44-year age group had the highest odds ratio (OR) for complications (Table 3). NHIS beneficiaries had a lower risk for complications than MA recipients (OR 0.85, 95% CI 0.75–0.97). Patients in the provinces of Daegu and Gyeongsangbuk had an OR of 1.44 (95% CI 1.31–1.59) higher than those in other areas. Patients hospitalized with mild disease had a higher OR than ambulatory patients (OR 1.19, 95% CI 1.09–1.30). In influenza patients, when we analyzed the risk for influenza complications, OR for female patients was 1.04 (95% CI 1.04–1.05); the OR was lower in patients <19 years of age and 45–64 years of age than in those 20–44 years of age and higher in patients 65–74 years and >75 years of age. NHIS beneficiaries had a lower risk for influenza complications (OR 0.94, 0.95% CI 0.92–0.96) than did MA recipients. Patients whose CCI scores were 1–2 points (OR 1.08, 95% CI 1.08–1.09) or >3 points (OR 1.12, 95% CI 1.10–1.13) had higher risk than those with a CCI score of 0. Patients with hospitalized mild disease (OR 1.22, 95% CI 1.21–1.23) and patients with hospitalized severe disease (OR 1.36, 95% CI 1.29–1.43) had higher ORs than ambulatory patients (Table 3).

Female patients had higher risk than male patients for gastrointestinal disease (OR 1.37, 95% CI 1.19–1.58), musculoskeletal disorder (OR 1.31, 95% CI 1.12–1.52), periodontal disease (OR 1.23, 95% CI 1.06–1.41), and autoimmune disease (OR 2.11, 95% CI 1.40–3.19). Older patients (≥65 years of age) had a higher risk for pneumonia, cardiovascular disease, heart failure, and cerebrovascular disease than young and middle-aged adults. Compared with MA recipients, NHIS beneficiaries had less dermatitis (OR 0.69, 95% CI 0.53–0.90), cardiovascular disease (OR 0.51, 95% CI 0.30–0.90), heart failure (OR 0.49, 95% CI 0.27–0.90), cerebrovascular

Table 1. Baseline characteristics of participants in study comparing complications of COVID-19 and influenza, South Korea*

Characteristic	General population†	COVID-19	Influenza	p value‡
Total no. participants	52,870,968	21,615	2,380,696	
Sex				0.14
M	26,455,169 (50.0)	9,700 (44.9)	1,080,288 (45.4)	
F	26,415,799 (50.0)	11,915 (55.1)	1,300,408 (54.6)	
Age, y				<0.001
0–19	8,822,808 (16.7)	1,467 (6.8)	1,180,279 (49.6)	
20–44	18,223,124 (34.5)	7,665 (35.5)	531,254 (22.3)	
45–64	17,344,828 (32.8)	7,841 (36.3)	462,183 (19.4)	
65–74	4,907,575 (9.3)	2,755 (12.8)	11,5673 (4.9)	
≥75	3,572,633 (6.8)	1,887 (8.7)	9,1307 (3.8)	
Type of insurance				<0.001
Health insurance	51,344,938 (97.1)	20,218 (93.5)	2,327,645 (97.8)	
Medical aid	1,526,030 (2.9)	1,397 (6.5)	53,051 (2.2)	
Region				<0.001
Seoul metropolitan area	26,724,640 (50.5)	12,386 (57.3)	1,070,695 (45.0)	
Daegu and Gyeongsangbuk province	5,111,575 (9.7)	4,963 (23.0)	256,833 (10.8)	
Other areas	21,034,753 (39.8)	4,266 (19.7)	1,053,168 (44.2)	
Charlson Comorbidity Index score				<0.001
0	NA	13,467 (62.3)	1,533,247 (64.4)	
1–2	NA	6,484 (30.0)	755,602 (31.7)	
≥3	NA	1,664 (7.7)	91,847 (3.9)	
Severity	NA			<0.001
Ambulatory state	NA	5,224 (24.2)	2,151,801 (90.4)	
Hospitalized mild disease	NA	15,447 (71.5)	222,572 (9.4)	
Hospitalized severe disease	NA	944 (4.4)	6,323 (0.3)	

*Values are no. (%) patients except as indicated. COVID-19, coronavirus disease; NA, not applicable.
†Data source: 2020 National health insurance statistics.
‡χ^2 tests were performed to assess the difference in proportion between COVID-19 and influenza patients.

disease (OR 0.40, 95% CI 0.22–0.73), autoimmune disease (OR 0.57, 95% CI 0.33–0.93), and dementia (OR 0.32, 95% CI 0.20–0.49). By region, the provinces of Daegu and Gyeongsangbuk had an increased risk of cerebrovascular disease (OR 2.11, 95% CI 1.02–4.37), mood disorder (OR 1.36, 95% CI 1.02–1.82), and dementia (OR 2.11, 95% CI 1.89–3.76). Hospitalized mild or severe patients had a higher risk for hair loss, pneumonia, and cardiovascular disease. The OR for pneumonia was 2.95 (95% CI 2.09–4.17) in patients 65–74 years of age and 4.25 (95% CI 2.96–6.12) in those ≥75 years. Cardiovascular disease risk was also higher for patients 65–74 years (OR 7.22, 95% CI 3.20–16.27) and for those ≥75 years of age (OR 5.15, 95% CI 2.11–12.60) (Appendix Table 2).

COVID-19 complications typically occurred 2–3 months after diagnosis (n = 1,711, 35.4%), and incidence within 1 month was 188 (3.9%). The incidence of influenza complications was high 2 months after diagnosis

Table 2. Frequency and incidence rate of complications among COVID-19 and influenza patients, South Korea*

Complications	Frequency†			Incidence‡		Rate ratio (95% CI)§
	COVID-19	Influenza	p value¶	COVID-19	Influenza	
Total	4,139/21,615 (19.1)	678,845/2,380,696 (28.5)	<0.001	NA	NA	NA
Gastrointestinal disease	856/12,089 (7.1)	138,926/1,487,277 (9.3)	<0.001	11.39	14.57	0.78 (0.73–0.84)
Musculoskeletal disorder	772/9,712 (7.9)	104,663/1,512,773 (6.9)	<0.001	13.24	17.57	0.75 (0.70–0.81)
Periodontal disease	953/7,121 (13.4)	182,738/1,112,593 (16.4)	<0.001	15.61	24.02	0.65 (0.61–0.70)
Skin disease	797/14,638 (5.4)	153,928/1,358,895 (11.3)	<0.001	9.56	10.70	0.89 (0.82–0.98)
Hair loss	67/21,364 (0.3)	5,643/2,358,346 (0.2)	0.02	0.46	0.30	1.52 (1.18–1.97)
Asthma	99/20,372 (0.5)	61,699/1,990,519 (3.1)	<0.001	0.80	2.20	0.36 (0.28–0.47)
COPD	33/21,416 (0.2)	4,048/2,362,939 (0.2)	0.54	0.18	0.23	0.79 (0.54–1.15)
Pneumonia	419/20,189 (2.1)	82,460/1,895,100 (4.4)	<0.001	3.0	2.94	1.02 (0.90–1.16)
Cardiovascular disease	88/20,849 (0.4)	7,930/2,333,972 (0.3)	0.42	0.56	0.54	1.05 (0.83–1.32)
Heart failure	73/21,306 (0.3)	3,602/2,365,516 (0.2)	<0.001	0.34	0.18	1.88 (1.42–2.50)
Cerebrovascular disease	64/21,001 (0.3)	5,020/2,353,824 (0.2)	0.004	0.34	0.28	1.21 (0.91–1.60)
Autoimmune disease	119/20,759 (0.6)	13,813/2,307,629 (0.6)	0.64	0.87	0.84	1.03 (0.86–1.25)
Mood disorder	381/19,916 (1.9)	23,993/2,279,373 (1.1)	<0.001	2.80	1.61	1.73 (1.56–1.93)
Dementia	106/20,921 (0.5)	5,534/2,358,412 (0.2)	<0.001	0.40	0.21	1.96 (1.52–2.55)

*COPD, chronic obstruction pulmonary disease; COVID-19, coronavirus disease; NA, not applicable.
†The numerator is the number of persons who experienced complications in the disease-free population and the denominator is the number of persons who did not have a history of the selected complication within a 3-y period before COVID-19 or influenza infection. The proportion is cumulative incidence.
‡Age-standardized incidence (cases per 1,000 person-months) for COVID-19 was divided by the standardized incidence rate for influenza and standardized to the 2020 population.
§Rate ratios are standardized to the 2020 population.
¶χ^2 tests were performed to assess the difference in proportion between COVID-19 and influenza patients.

Table 3. Factors associated with incidence of complications in study of COVID-19 and influenza patients, South Korea*

Variable	Adjusted odds ratio (95% CI)†	
	COVID-19, n = 21,615	Influenza, n = 2,380,696
Female (referent: male)	1.03 (0.96–1.11)	1.04 (1.04–1.05)
Age, y (referent: 20–44 y)		
0–19	0.69 (0.59–0.80)	0.94 (0.94–0.95)
45–64	0.81 (0.74–0.88)	0.97 (0.96–0.98)
65–74	0.86 (0.76–0.96)	1.07 (1.05–1.08)
≥75	0.86 (0.75–0.99)	1.26 (1.24–1.28)
National Health Insurance Service (referent: Medical Aid)	0.85 (0.75–0.97)	0.94 (0.92–0.96)
Region (referent: other areas)		
Seoul metropolitan area	0.90 (0.82–0.99)	1.03 (1.02–1.03)
Daegu and Gyeongsangbuk province	1.44 (1.31–1.59)	1.02 (1.01–1.03)
Charlson Comorbidity Index score (referent: 0)		
1–2	1.02 (0.94–1.11)	1.08 (1.08–1.09)
≥3	1.01 (0.88–1.16)	1.12 (1.10–1.13)
Severity (referent ambulatory state)		
Hospitalized mild disease	1.19 (1.09–1.30)	1.22 (1.21–1.23)
Hospitalized severe disease	1.11 (0.91–1.34)	1.36 (1.29–1.43)

*COVID-19, coronavirus disease.
†Multivariable logistic regression includes sex, age, type of insurance, region, and Charlson Comorbidity Index.

in 68,608 patients (9.0%), 1 month in 53,332 (7.0%), and 6 months in 373,853 (48.9%) (Figure 2; Appendix Table 3).

Discussion

In our study, COVID-19 typically had complication rates lower than or similar to those for influenza. However, the RRs for hair loss, heart failure, mood disorder, and dementia were marginally higher in the COVID-19 patient group. The incidence of COVID-19 complications was higher for patients 20–44 years of age, patients receiving MA, residents of the provinces of Daegu and Gyeongsangbuk, and patients with high CCI scores. In a subgroup analysis, the risk for hair loss was higher in younger adults, but the risk for mood disorders and dementia was higher in the elderly. Among those who had COVID-19, the elderly and the group with high CCI scores had more occurrences of pneumonia and cardiovascular disease; furthermore, the risk for cerebrovascular disease, mood disorder, and dementia was marginally higher in the provinces of Daegu and Gyeongsangbuk. We found that influenza patients were more likely to be younger than COVID-19 patients. Nevertheless, even after adjusting for age, complications were more common in influenza patients. Complications of COVID-19 that are more common than influenza complications are those that are more common in older adults. Although we adjusted for age, the effect of age may remain, and a stratified analysis by age is needed in future studies.

Various symptoms of COVID-19 persist even after recovery. In previous studies, general symptoms occur after COVID-19 infection, such as fatigue, sweating, and muscle pain; respiratory symptoms such as breathing difficulty and cough; psychosocial symptoms such as depression, anxiety, poor sleep quality, alopecia; and peripheral neuropathy, such as olfactory dysfunction (*14*–*18*). Because the natural course of COVID-19 is unknown, the types of long COVID are likely to increase (*19*,*20*). However, given that many persons are infected with COVID-19 globally or have recovered after being infected, it is necessary to assess the risk for long COVID-19.

In this study, 19.6% of COVID-19 patients had ≥1 complications. In South Korea, asymptomatic COVID-19 patients were discovered and managed, so almost all COVID-19 patients were included in the study. As a result, the complication rate from COVID-19 may be lower than that for other studies (*21*). Complications occurred more frequently in COVID-19 patients than in influenza patients and are consistent with previously known complications of COVID-19. Heart failure was more common in COVID-19 patients than in influenza patients. Both diseases have been reported to be associated with cardiovascular events because they are associated with inflammation. However, COVID-19 is associated with myocardial injury resulting from cytokine storm–related hyperinflammation and high expression of angiotensin-converting enzyme 2 receptors in myocardial tissue (*22*,*23*) that is thought to be followed by cardiomyopathy, arrhythmia, and heart failure (*24*,*25*). COVID-19 has proved to be an unprecedented long pandemic. Long-term social isolation causes loneliness, depression, and substance abuse (*26*,*27*) and alcohol consumption (*28*), and the rate of smoking increases during social isolation because of COVID-19 (*29*). In our study, we observed an increase in mood disorders; from our own and previously reported results, we inferred that the incidence rate may vary depending on the intensity of lockdown in each country. Hair loss is also a commonly reported symptom after COVID-19 infection (*16*,*30*). Although its pathogenesis is unclear, studies show that androgen increases COVID-19 susceptibility

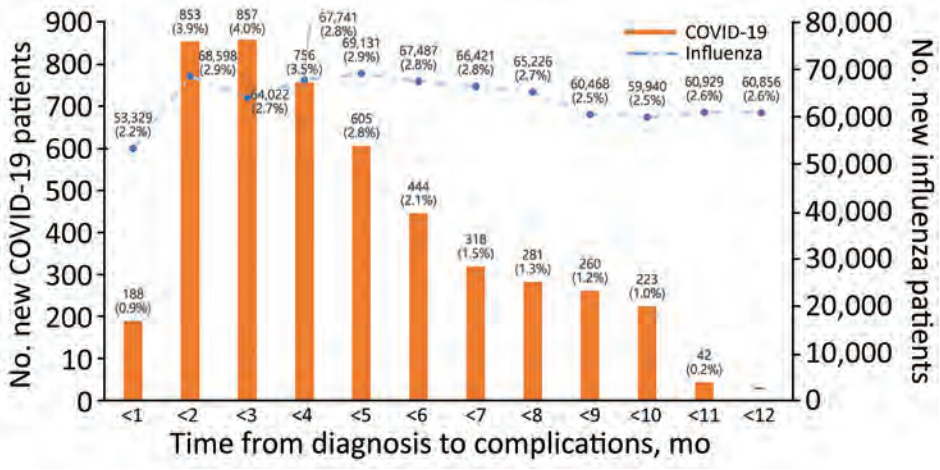

Figure 2. Time from diagnosis of COVID-19 or influenza to complications in study comparing complications in the 2 diseases, South Korea. COVID-19, coronavirus disease.

and enhances inflammation (*31*). Several reports of cerebrovascular disease have been reported after COVID-19 infection (*6*,*18*). The sequelae of cerebrovascular disease may have increased incidence of dementia; trends need to be monitored going forward.

This study has the advantage of confirming complications before and after diagnosis for all patients with COVID-19, influenza-like illness, or influenza who came to the hospital during the study period. South Korea conducted proactive testing for COVID-19, even for persons with no symptoms. Consequently, almost all COVID-19 patients, even those that were asymptomatic, were discovered and managed (*32*,*33*). Thus, the risk for selection bias was considered low. Moreover, because all residents were enrolled in the NHIS or MA, we were able to select patients who did not previously have the condition corresponding to the complication according to insurance data, increasing the accuracy of new complication detection. Influenza co-infection is possible among COVID-19 patients. However, in our study, only 259 (1.2%) patients had both COVID-19 and influenza, so we expected to see no significant effect.

Our study's first limitation is that, because we identified the occurrence of complications from the claims data, the number of occurrences may have not been counted if the patient experienced mild or vague symptoms that did not prompt them to go to the hospital. Second, we recorded diagnoses that occurred after COVID-19 infection; however, we could not confirm a direct association with COVID-19. Third, it was difficult to determine the actual duration of symptoms; therefore, we could not clearly differentiate acute complications and long COVID. However, most symptoms occurred after 1 month; thus, they were considered long COVID. Fourth, only data through December 31, 2020, could be analyzed because of limitations in the claims data collection; therefore, we could not analyze complications caused by more recent SARS-CoV-2 variants, such as B.1.1.7 (Alpha) and B.1.351 (Beta). Further tracking of new complications is required. Monitoring with a prospective cohort that can be traced, including vague symptoms, is necessary.

In conclusion, although COVID is generally associated with fewer complications than influenza, caution is needed in groups with a high risk for hair loss, heart failure, mood disorder, dementia, and in patients with a high risk for complications, such as younger patients 20–44 years of age, and patients in COVID-19 hotspots. The risk for mood disorders and dementia was higher in the elderly. Although the complication rate of COVID-19 is not high, the fatality rate is of grave concern. If the fatality rate for COVID-19 is reduced through vaccination, the country can consider adopting less stringent COVID-19 management strategies, similar to those for influenza. Restrictions on economic activity or cross-border movement could be eased, and requirements for isolation of patients and close contacts could be modified.

About the Author

Dr. Lee is a doctor and a researcher with the Seoul National University Bundang Hospital. Her primary research interest is epidemiology and health policy.

References

1. Del Rio C, Collins LF, Malani P. Long-term health consequences of COVID-19. JAMA. 2020;324:1723–4. https://doi.org/10.1001/jama.2020.19719
2. Fraser E. Long term respiratory complications of COVID-19. BMJ. 2020;370:m3001. https://doi.org/10.1136/bmj.m3001
3. Carfì A, Bernabei R, Landi F; Gemelli against COVID-19 Post-Acute Care Study Group. Persistent symptoms in patients after acute COVID-19. JAMA. 2020;324:603–5. https://doi.org/10.1001/jama.2020.12603

4. Wang F, Kream RM, Stefano GB. Long-term respiratory and neurological sequelae of COVID-19. Med Sci Monit. 2020;26:e928996. https://doi.org/10.12659/MSM.928996
5. Whitcroft KL, Hummel T. Olfactory dysfunction in COVID-19. JAMA. 2020;323:2512–4. https://doi.org/10.1001/jama.2020.8391
6. Ellul MA, Benjamin L, Singh B, Lant S, Michael BD, Easton A, et al. Neurological associations of COVID-19. Lancet Neurol. 2020;19:767–83. https://doi.org/10.1016/S1474-4422(20)30221-0
7. Miners S, Kehoe PG, Love S. Cognitive impact of COVID-19: looking beyond the short term. Alzheimers Res Ther. 2020;12:170. https://doi.org/10.1186/s13195-020-00744-w
8. Sivan M, Taylor S. NICE guideline on long COVID. BMJ. 2020;371:m4938. https://doi.org/10.1136/bmj.m4938
9. Piroth L, Cottenet J, Mariet A-S, Bonniaud P, Blot M, Tubert-Bitter P, et al. Comparison of the characteristics, morbidity, and mortality of COVID-19 and seasonal influenza: a nationwide, population-based retrospective cohort study. Lancet Respir Med. 2021;9:251–9. https://doi.org/10.1016/S2213-2600(20)30527-0
10. National Health Insurance Service. 2018 Medical Aid statistics. 2019. [cited 2021 Dec 20]. https://www.hira.or.kr/bbsDummy.do?pgmid=HIRAA020045010000&brdScnBltNo=4&brdBltNo=2318
11. US Centers for Disease Control and Prevention. Influenza activity—United States, 2012–13 season and composition of the 2013–14 influenza vaccine. MMWR Morb Mortal Wkly Rep. 2013;62:473–9.
12. World Health Organization. R&D blueprint and COVID-19. 2020 [cited 2021 Dec 2]. https://www.who.int/teams/blueprint/covid-19
13. Marshall JC, Murthy S, Diaz J, Adhikari NK, Angus DC, Arabi YM, et al.; WHO Working Group on the Clinical Characterisation and Management of COVID-19 infection. A minimal common outcome measure set for COVID-19 clinical research. Lancet Infect Dis. 2020;20:e192–7. https://doi.org/10.1016/S1473-3099(20)30483-7
14. Xiong Q, Xu M, Li J, Liu Y, Zhang J, Xu Y, et al. Clinical sequelae of COVID-19 survivors in Wuhan, China: a single-centre longitudinal study. Clin Microbiol Infect. 2021;27:89–95. https://doi.org/10.1016/j.cmi.2020.09.023
15. Mandal S, Barnett J, Brill SE, Brown JS, Denneny EK, Hare SS, et al.; ARC Study Group. "Long-COVID": a cross-sectional study of persisting symptoms, biomarker and imaging abnormalities following hospitalization for COVID-19. Thorax. 2021;76:396–8. https://doi.org/10.1136/thoraxjnl-2020-215818
16. Wambier CG, Vaño-Galván S, McCoy J, Gomez-Zubiaur A, Herrera S, Hermosa-Gelbard Á, et al. Androgenetic alopecia present in the majority of patients hospitalized with COVID-19: the "Gabrin sign." J Am Acad Dermatol. 2020;83:680–2. https://doi.org/10.1016/j.jaad.2020.05.079
17. Leung TYM, Chan AYL, Chan EW, Chan VKY, Chui CSL, Cowling BJ, et al. Short- and potential long-term adverse health outcomes of COVID-19: a rapid review. Emerg Microbes Infect. 2020;9:2190–9. https://doi.org/10.1080/22221751.2020.1825914
18. Varatharaj A, Thomas N, Ellul MA, Davies NWS, Pollak TA, Tenorio EL, et al.; CoroNerve Study Group. Neurological and neuropsychiatric complications of COVID-19 in 153 patients: a UK-wide surveillance study. Lancet Psychiatry. 2020;7:875–82. https://doi.org/10.1016/S2215-0366(20)30287-X
19. Gorna R, MacDermott N, Rayner C, O'Hara M, Evans S, Agyen L, et al. Long COVID guidelines need to reflect lived experience. Lancet. 2021;397:455–7. https://doi.org/10.1016/S0140-6736(20)32705-7
20. Yelin D, Wirtheim E, Vetter P, Kalil AC, Bruchfeld J, Runold M, et al. Long-term consequences of COVID-19: research needs. Lancet Infect Dis. 2020;20:1115–7. https://doi.org/10.1016/S1473-3099(20)30701-5
21. Michelen M, Manoharan L, Elkheir N, Cheng V, Dagens A, Hastie C, et al. Characterising long COVID: a living systematic review. BMJ Glob Health. 2021;6:e005427. https://doi.org/10.1136/bmjgh-2021-005427
22. Khan MS, Shahid I, Anker SD, Solomon SD, Vardeny O, Michos ED, et al. Cardiovascular implications of COVID-19 versus influenza infection: a review. BMC Med. 2020;18:403. https://doi.org/10.1186/s12916-020-01816-2
23. Shchendrygina A, Nagel E, Puntmann VO, Valbuena-Lopez S. COVID-19 myocarditis and prospective heart failure burden. Expert Rev Cardiovasc Ther. 2021;19:5–14. https://doi.org/10.1080/14779072.2021.1844005
24. Jiang DH, McCoy RG. Planning for the post-COVID syndrome: how payers can mitigate long-term complications of the pandemic. J Gen Intern Med. 2020;35:3036–9. https://doi.org/10.1007/s11606-020-06042-3
25. Becker RC. Anticipating the long-term cardiovascular effects of COVID-19. J Thromb Thrombolysis. 2020;50:512–24. https://doi.org/10.1007/s11239-020-02266-6
26. Simard J, Volicer L. Loneliness and isolation in long-term care and the COVID-19 pandemic. J Am Med Dir Assoc. 2020;21:966–7. https://doi.org/10.1016/j.jamda.2020.05.006
27. Jackson SE, Garnett C, Shahab L, Oldham M, Brown J. Association of the COVID-19 lockdown with smoking, drinking, and attempts to quit in England: an analysis of 2019–2020 data. Addiction. 2020;116:1233–44. https://doi.org/10.1111/add.15295
28. Jacob L, Smith L, Armstrong NC, Yakkundi A, Barnett Y, Butler L, et al. Alcohol use and mental health during COVID-19 lockdown: a cross-sectional study in a sample of UK adults. Drug Alcohol Depend. 2021;219:108488. https://doi.org/10.1016/j.drugalcdep.2020.108488
29. Vanderbruggen N, Matthys F, Van Laere S, Zeeuws D, Santermans L, Van den Ameele S, et al. Self-reported alcohol, tobacco, and cannabis use during COVID-19 lockdown measures: results from a web-based survey. Eur Addict Res. 2020;26:309–15. https://doi.org/10.1159/000510822
30. Huang C, Huang L, Wang Y, Li X, Ren L, Gu X, et al. 6-month consequences of COVID-19 in patients discharged from hospital: a cohort study. Lancet. 2021;397:220–32. https://doi.org/10.1016/S0140-6736(20)32656-8
31. Moradi F, Enjezab B, Ghadiri-Anari A. The role of androgens in COVID-19. Diabetes Metab Syndr. 2020;14:2003–6. https://doi.org/10.1016/j.dsx.2020.10.014
32. Lee H, Lee JR, Jung H, Lee JY. Power of universal health coverage in the era of COVID-19: a nationwide observational study. Lancet Reg Health West Pac. 2021;7:100088. https://doi.org/10.1016/j.lanwpc.2020.100088
33. Park Y, Huh IS, Lee J, Kang CR, Cho SI, Ham HJ, et al.; Seoul Metropolitan Government COVID-19 Rapid Response (SCoRR) Team. Application of testing-tracing-treatment strategy in response to the COVID-19 outbreak in Seoul, Korea. J Korean Med Sci. 2020;35:e396. https://doi.org/10.3346/jkms.2020.35.e396

Address for correspondence: Jin Yong Lee, Public Healthcare Center, Seoul National University Hospital, 101 Daehak-ro, Jongno-gu, Seoul 03080, South Korea; email: jylee2000@gmail.com. Myoung-don Oh, Department of Internal Medicine, Seoul National University College of Medicine, 101 Daehak-ro, Jongno-gu, Seoul 03080, South Korea; email: mdohmd@snu.ac.kr

Epidemiology of Hospitalized Patients with Babesiosis, United States, 2010–2016

Evan M. Bloch, Jonathan R. Day, Peter J. Krause, Anne Kjemtrup, Sheila F. O'Brien, Aaron A.R. Tobian, Ruchika Goel

Medscape ACTIVITY EDUCATION

In support of improving patient care, this activity has been planned and implemented by Medscape, LLC and Emerging Infectious Diseases. Medscape, LLC is jointly accredited by the Accreditation Council for Continuing Medical Education (ACCME), the Accreditation Council for Pharmacy Education (ACPE), and the American Nurses Credentialing Center (ANCC), to provide continuing education for the healthcare team.

Medscape, LLC designates this Journal-based CME activity for a maximum of 1.00 ***AMA PRA Category 1 Credit(s)™***. Physicians should claim only the credit commensurate with the extent of their participation in the activity.

Successful completion of this CME activity, which includes participation in the evaluation component, enables the participant to earn up to 1.0 MOC points in the American Board of Internal Medicine's (ABIM) Maintenance of Certification (MOC) program. Participants will earn MOC points equivalent to the amount of CME credits claimed for the activity. It is the CME activity provider's responsibility to submit participant completion information to ACCME for the purpose of granting ABIM MOC credit.

All other clinicians completing this activity will be issued a certificate of participation. To participate in this journal CME activity: (1) review the learning objectives and author disclosures; (2) study the education content; (3) take the post-test with a 75% minimum passing score and complete the evaluation at http://www.medscape.org/journal/eid; and (4) view/print certificate. For CME questions, see page 499.

Release date: January 20, 2022; Expiration date: January 20, 2023

Learning Objectives

Upon completion of this activity, participants will be able to:

- Assess the pathology and outcomes of babesiosis
- Distinguish the characteristics of patients with babesiosis
- Analyze the most common season and geographic areas for babesiosis in the US
- Identify the most common complication of babesiosis in the current study

CME Editor

Karen L. Foster, Technical Writer/Editor, Emerging Infectious Diseases. *Disclosure: Karen L. Foster has disclosed no relevant financial relationships.*

CME Author

Charles P. Vega, MD, Health Sciences Clinical Professor of Family Medicine, University of California, Irvine School of Medicine, Irvine, California. *Disclosure: Charles P. Vega, MD, has disclosed the following relevant financial relationships: served as an advisor or consultant for Johnson & Johnson.*

Authors

Evan M. Bloch, MBChB; Jonathan R. Day, MD, PharmD; Peter J. Krause, MD; Anne Kjemtrup, DVM, MPVM, PhD; Sheila F. O'Brien, PhD; Aaron A.R. Tobian, MD, PhD; *and* ***Ruchika Goel, MD, MPH.***

Author affiliations: Johns Hopkins School of Medicine, Baltimore, Maryland, USA (E.M. Bloch, A.A.R. Tobian, R. Goel); University of Iowa Health Care, Iowa City, Iowa, USA (J.R. Day); Simmons Cancer Institute at Southern Illinois University, Springfield, Illinois, USA (J.R. Day, R. Goel); Yale School of Public Health and Yale School of Medicine, New Haven, Connecticut USA (P.J. Krause); California Department of Public Health, Sacramento, California, USA (A. Kjemtrup); Canadian Blood Services, Ottawa, Ontario, Canada (S.F. O'Brien)

DOI: https://doi.org/10.3201/eid2802.210213

Babesia spp. are tickborne parasites that cause the clinical infection babesiosis, which has an increasing incidence in the United States. We performed an analysis of hospitalizations in the United States during 2010–2016 in which babesiosis was listed as a diagnosis. We used the National Inpatient Sample database to characterize the epidemiology of *Babesia*–associated admissions, reflecting severe *Babesia*-related disease. Over a 7-year period, a total of 7,818 hospitalizations listed babesiosis as a primary or secondary admitting diagnosis. Hospitalizations were seasonal (71.2% occurred during June–August) and situated overwhelmingly in the Northeast and Midwest. The patients were predominantly male and of advanced age, which is consistent with the expected epidemiology. Despite a higher severity of illness in more than (58.5%), the mortality rate was low (1.6%). Comparison with state reporting data suggests that the number of hospitalized persons with babesiosis increased modestly during the observation period.

Babesia spp. are tickborne intraerythrocytic apicomplexan parasites responsible for the clinical infection babesiosis. *Babesia microti*, the leading cause of human babesiosis, is endemic in the northeastern and north-midwestern United States (*1*). Although infection in immunocompetent adults may be mild or even subclinical, manifesting as a self-limiting viral-like illness (i.e., fever, headache, myalgia, fatigue), risk for severe disease and complications exists in certain patient populations (i.e., the very young, the elderly, persons with asplenia, and others with immunosuppression). Like *Plasmodium* parasites that cause malaria, *Babesia* spp. infect erythrocytes and induce hemolysis. Clinical complications include severe anemia, renal failure, cardiorespiratory failure, and death (*1*). *Babesia* spp. also are readily transmissible by transfusion of infected erythrocytes. Given that anemia is the major indication for erythrocyte transfusion, coupled with the high proportion of patients at high risk for severe disease in the transfused population, transfusion-transmitted babesiosis has a death rate of ≈20% (*1*,*2*).

Reported cases of babesiosis and other tickborne diseases are increasing (*3*–*5*). Postulated reasons for the increase include expansion of the geographic range of tick vector population, increase in deer (and consequent tick) populations, encroachment of humans into *Babesia* zoonotic habitats, climate change, and other ecologic changes that contribute to a rise in incidence of *Babesia* infection (*6*,*7*). Babesiosis was designated a nationally notifiable disease in the United States in 2011, meaning that states where it was reportable were charged to voluntarily notify the Centers for Disease Control and Prevention (CDC) of cases. As of 2015, babesiosis was reportable in 33 states (*8*,*9*). Although an increase in babesiosis cases has been reported, whether the increase includes primarily outpatients, hospitalized case-patients, or both is uncertain. To test whether hospitalized babesiosis patients are increasing, we analyzed hospitalizations in the United States in which babesiosis was listed as a diagnosis, using the National (Nationwide) Inpatient Sample (NIS) database, which offers a representative sampling of US-based hospitals. This analysis enabled characterization of the epidemiology of admissions, reflecting severe *Babesia*-related disease.

Methods

This study uses 7 years of data (i.e., 2010–2016) from the NIS, the largest publicly available inpatient healthcare database in the United States. The NIS was developed as a federal–state–industry partnership by the Agency for Healthcare Research and Quality for the Healthcare Cost and Utilization Project (HCUP). Data before 2012 used a 20% stratified probability sample of hospitals rather than discharges (*10*). After a redesign in 2012, the NIS adopted a sampling design that uses a stratified probability sample of 20% of all HCUP participating hospital discharges for each calendar year. This sampling scheme is estimated to cover 90%–97% of the US population across the different years (*11*). The unit of analysis is a single hospitalization and not a specific patient; therefore, a single patient may be represented in multiple observations. Observations are self-weighted and calculated by strata, which are defined by census division (categorized as census region before 2012), bed size, location, teaching status, and hospital ownership.

The NIS provides de-identified discharge data without individual patient or hospital-level identifiers. These data include 1 primary or principal diagnosis code, up to 29 secondary diagnosis codes, and up to 15 procedure codes. The principal diagnosis is the primary reason for admission and is coded in the first diagnosis field. The number of diagnoses and associated data elements was increased from 15 to 25 in 2009 and from 25 to 30 beginning in 2014. We have captured this change in our analysis.

Demographic details extracted from the database were age, sex, and race. Hospital-level characteristics were location (urban vs rural), academic designation (teaching vs. nonteaching), and bed size. Hospitals were categorized as small, medium, or large according to the criteria defined by HCUP, which were based on region, urban–rural designation, and teaching status (*12*). Other variables included admission and discharge status, total charges, expected payment

source, length of hospital stay, and hospital characteristics. The NIS database uses All Patient Refined Diagnosis Related Groups (APR-DRGs), a validated inpatient classification system that is widely used in the United States to assess severity of illness and risk for death during hospitalization using multiple variables. The risk for death and severity of illness are ranked on a scale of 1 to 4, corresponding to mild, moderate, major, and extreme.

We used diagnosis and procedure codes from the International Classification of Diseases, Ninth Revision, Clinical Modification (ICD-9-CM), from 2010 through the third quarter of 2015. After the third quarter of 2015, billing codes switched from ICD-9-CM to the International Classification of Diseases, Tenth Revision, Clinical Modification (ICD-10-CM). Babesiosis cases were identified by ICD-9 code 088.82 or ICD-10 code B60.0. Transfusion-transmitted babesiosis infections could not be identified independently because there are no specific ICD-9 or ICD-10 codes for that diagnosis. We described demographic and clinical characteristics as counts, percentages, mean (SD) and median (interquartile range) as appropriate. We stratified results into ICD-9 (2010–2015q3) and ICD-10 (2015q4–2016) data. We analyzed the geographic distribution, demographics. and seasonality of *Babesia*-related hospitalizations and stratified and analyzed hospitalizations by the leading regional divisions. We calculated transfusions and incidence of erythrocyte exchanges during admissions as the binomial proportion of encounters during which ≥1 blood product was issued or erythrocyte exchange was performed. We performed logistic regression to compare the incidence of various clinical co-morbidities and outcomes. All p values were 2-tailed and statistical significance was set at $p<0.05$. We analyzed data using Stata version 15 (StataCorp LLC, https://www.stata.com), using survey analysis commands applying the sampling weights as determined by HCUP.

We also performed a graphical comparison of the number and incidence of babesiosis cases reported to CDC during 2011–2016 to compare the overall trends in reporting. The CDC data that were included were reported by individual state health departments; cases were reported by the state of residence, which might not have been the state of exposure.

To test specificity, we performed a sensitivity analysis that restricted the assessment to hospitalizations in which babesiosis was listed in the top 5 diagnoses. The analysis also excluded admissions associated with a primary diagnosis of Lyme disease.

Given that the NIS is a de-identified, publicly available dataset, this study was deemed exempt from review from the Johns Hopkins Institutional Review Board. This analysis was conducted in accordance with the HCUP data use agreement guidelines.

Results

During a 7-year period, babesiosis was listed as an admitting diagnosis for 7,818 hospitalizations, of which 4,648 (59.5%) listed babesiosis as a primary diagnosis and 3,170 (40.5%) as a secondary diagnosis (Table 1, https://wwwnc.cdc.gov/EID/article/28/2/21-0213-T1.htm). Annual hospitalizations varied by year, from 676 in 2010 to 1415 in 2013 (Figure). For all hospitalizations, the median age of patients was 67 years (interquartile range 55–77 years); 5,001 (64%) of the associated patients were male, and 6,024 (80.1%) were White.

Of all hospitalizations, 2,325 (71.2%) occurred in summer (June–August); 6,616 (92.7%) occurred in the Northeast and Midwest. New England (1,150 [44.1%] hospitalizations) and Mid-Atlantic (1,115 [42.7%] hospitalizations) were the leading regions. The admitting hospitals were predominantly urban (6,529 [91.4%]), and admissions were overwhelmingly nonelective (7,452 [95.4%]).

A greater severity of illness was reported in 4,574 (58.5%) hospitalizations; risk for death was assessed as major or extreme for 1,339 (17.2%) hospitalizations (Table 2). The leading complications included acute renal failure (1,594 [20.4%] hospitalizations), respiratory failure (528 [6.8%]), and cardiac failure (270 [3.5%]) (Table 3). A total of 128 deaths occurred over the 7-year period, representing 1.6% of all babesiosis-associated admissions. Babesiosis was the primary hospital-associated diagnosis for 20 of those deaths and secondary for the other 108 deaths. Similar to the distribution of all hospitalizations, most deaths occurred in the Northeast (89 [69.5%]) and the Midwest (10 [7.8%]).

Babesiosis-related deaths were significantly associated with acute renal failure ($p<0.001$), acute respiratory failure ($p<0.001$), and disseminated intravascular coagulation ($p = 0.001$) when compared with nonfatal hospitalizations. The mean length of stay was 5.8 ± 7.3 days (Table 3). The aggregate national bill for the 7-year period for a principal diagnosis of babesiosis was >$170 million USD ($171,281,170), averaging $24.4 million USD per year, and the mean hospital charge for a *Babesia*-associated admission was $36,850.

At least 1 erythrocyte transfusion was reported in 1,560 (20%) hospital admissions (Table 3). Transfusion of other blood products was comparatively rare. Hospitalizations in which erythrocyte transfusions were

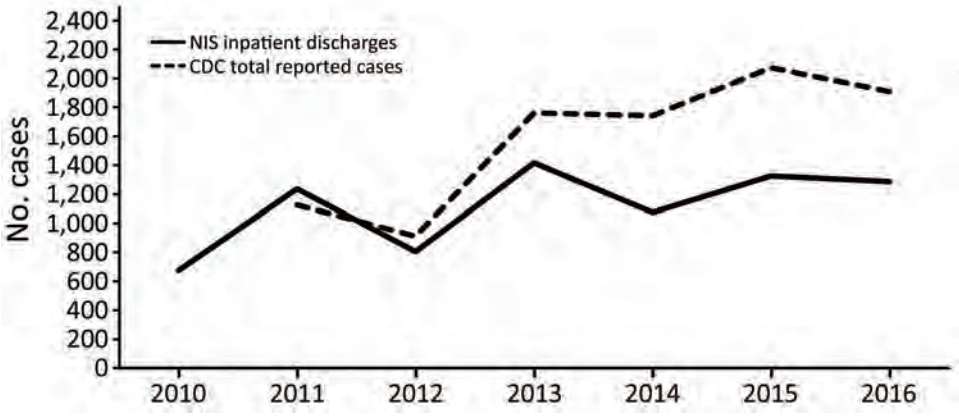

Figure. Cases of babesiosis in the United States, 2010–2016, CDC versus NIS data. CDC, Centers for Disease Control and Prevention; NIS, National Inpatient Sample.

reported were associated with severe illness. Major or extreme severity of illness was reported in ≈80% in the erythrocyte transfusion group, compared with 53% in those for which erythrocyte transfusions were not reported. Furthermore, 59.9% of the cases in the erythrocyte transfusion group were assessed as having a major or extreme risk for death in comparison with 32.3% for those in which no erythrocyte transfusion was reported. A significantly higher rate of death was observed in the transfusion group (3.18% vs. 1.27%; p = 0.02). Erythrocyte exchange (i.e., erythrocytapheresis) was performed in 80 (1%) admissions. Most admissions in which erythrocytapheresis was undertaken were associated with high illness severity. Specifically, 18.3% were associated with moderate, 18.8% with major, and 63% with extreme severity of illness.

A total of 1,953 (25%) babesiosis-related hospitalizations listed Lyme disease as a concurrent diagnosis; 276 (3.5%) listed Lyme disease as a primary diagnosis. Neither disease severity nor mortality differed for those hospitalizations in which only babesiosis was listed, compared with those hospitalizations in which both babesiosis and Lyme disease were listed (p>0.05). Rates of respiratory failure, heart failure, disseminated intravascular coagulation, and mean length of stay did not differ between those with and without a concurrent diagnosis of Lyme disease.

Other notable concurrent diagnoses in babesiosis-associated hospitalizations were anaplasmosis and ehrlichiosis (658 [8.4%]); these 2 entities are combined because it was not possible to distinguish them on the basis of the coding in use. Malaria, a clinical and morphologic diagnostic mimic of babesiosis, was reported in 52 (0.7%) babesiosis-associated hospitalizations. In 560 (7.2%) of babesiosis-associated hospitalizations, the patients were noted to have decreased splenic function or were asplenic.

When we restricted the hospitalizations to those in which babesiosis was listed in the top 5 diagnoses and a primary diagnosis of Lyme disease was excluded, the number of admissions changed from 7,818 to 6,903. However, all analyses remained comparable (Appendix Tables 1–3, https://wwwnc.cdc.gov/EID/article/28/2/21-0213-App1.pdf).

Discussion

Our findings offer a nationally representative estimate of in-hospital babesiosis in the United States. During a 7-year period, most (≈85%) *Babesia*-related hospitalizations occurred in the New England and Mid-Atlantic states, and two thirds occurred in the summer (June–August). More than half of all patients were ≥65 years of age, and almost two thirds were male. A concurrent diagnosis of Lyme disease was reported in one quarter of all babesiosis-related hospitalizations. Reported clinical complications, notably acute renal failure, were common. Consistent with a selection for severe cases that warrant hospital admission, a high proportion of patients experienced major or extreme severity of illness and were deemed to be at high risk for death. Nonetheless, the overall mortality rate was low. Despite an upward trend in annual cases of babesiosis that have been reported to CDC, *Babesia*-related hospitalizations appeared stable or modestly increasing during the study period.

The data on geographic distribution, demographics, and seasonality of *Babesia*-related hospitalizations in this report are consistent with what is known about the parasite's general epidemiology in the United States. Specifically, *B. microti* is widely endemic in the Northeast and upper Midwest. *B. microti* is the most common species causing human babesiosis in the United States and worldwide. Other species (e.g., *B. duncani*) and variants (e.g., *B.* divergens–like/MO-1) have been reported in the United States but are comparatively rare (*13*–*16*). Male predominance may be

attributable to the spectrum of activities that place humans at risk for tick bite. Advanced age is an established risk factor for severe babesiosis because of possible underlying conditions (e.g., cardiorespiratory disease, immunocompromised), immunosenescence, or age-related differential effect of the parasite on the host (*17*–*19*).

Babesia infection is seasonal, as illustrated by the more than two thirds of hospitalizations that occurred in summer. Although few hospitalizations occurred in the spring, one fifth of cases occurred from September through December. This finding could be ascribed to a lag in diagnosis; transmission occurs in late spring and summer (i.e., corresponding to the presence of *Ixodes scapularis* nymphs, the primary tick stage that transmits babesiosis), yet hospitalization follows a period of incubation, symptom onset, and progression. Delayed diagnosis and misdiagnosis further account for hospitalizations in late summer and fall. An additional explanation for delayed presentation may be transmission of *Babesia* spp. attributed to bites from adult ticks, which are active into the fall (*20*). Although *I. scapularis* adults are larger than nymphs, and therefore are often removed before transmission, some bites by adult ticks still go unnoticed.

Our findings provided new insights about the overall health burden of babesiosis in the United States, including the number of cases, the severity of illness, and the financial costs incurred by the disease. The overall rate of severe babesiosis requiring hospital admission is increasing, albeit slowly. These findings complement those of Menis et al. who analyzed US Medicare-related claims pertaining to babesiosis during 2006–2017, thus describing a significant increase, from 4 claims/100,000 beneficiaries in 2006 to 9 claims/100,000 beneficiaries in 2017 (*21*). Since babesiosis was designated as a nationally notifiable disease, the number of states where babesiosis is endemic and where reporting of cases is mandatory has increased (*8*,*9*). However, reporting is still incomplete and is not a requirement across all states. Data from CDC indicate an increase in reported cases, which may reflect both a true increase in the number of cases and an increase in awareness and reporting of the disease. In support of this hypothesis, there was a 94% increase in hospitalized patients with babesiosis from the year before national notification to the year after; there were 1,236 *Babesia*-associated discharges from hospitals in 2011, compared with only 636 in 2010. Given that data from NIS hospitalizations represent only a subset of all *Babesia* infections (the most severe cases), increased physician awareness and reporting may play a larger role than an increase in the number of cases.

Table 2. Disease severity, risk for death, and concurrent conditions in hospitalizations in which babesiosis was listed as an admitting diagnoses, United States, 2010–2016*

Disease severity and conditions	All data, no. (%)	ICD 9 data, 2010–2015q3,† no. (%)	ICD10 data, 2015q4–2016,† no. (%)
APD-RG severity of illness			
Minor	376 (4.8)	316 (5.0)	60 (4.1)
Moderate	2,863 (36.6)	2,318 (36.4)	545 (37.6)
Major	3,660 (46.8)	2,990 (47.0)	670 (46.2)
Extreme	914 (11.7)	744 (11.7)	170 (11.7)
APD-RG risk for death			
Minor	2,004 (25.6)	1,639 (25.7)	365 (25.2)
Moderate	2,852 (36.5)	2,377 (37.3)	475 (32.8)
Major	2,178 (27.9)	1,718 (27.0)	460 (31.7)
Extreme	779 (10.0)	634 (10.0)	145 (10.0)
Concurrent conditions			
Decreased splenic function or asplenia	560 (7.2)	475 (7.1)	85 (5.9)
HIV‡	20 (0.3)	15 (0.2)	‡
Sickle cell disease	30 (0.4)	30 (0.5)	‡
Lyme disease (any diagnosis)	1,953 (25.0)	1,573 (24.7)	380 (26.2)
Lyme disease (primary diagnosis)	276 (3.5)	221 (3.5)	55 (3.8)
Anaplasmosis and ehrlichiosis	658 (8.4)	548 (8.6)	110 (7.6)
Malaria	52 (0.7)	32 (0.5)	20 (1.4)
Rocky Mountain spotted fever/rickettsial illness	25 (0.1)	20 (0.3)	§
Powassan virus disease, other tick-borne viral encephalitis	§	§	§
Relapsing fever	§	§	§

*Data are from the NIS, which offers a representative sampling of US-based hospitals. APR-DRG, All Patient Refined Diagnosis Related Group; HCUP, Healthcare Cost and Utilization Project; ICD-9, International Classification of Diseases, Ninth Revision; ICD-10, International Classification of Diseases, Tenth Revision; NIS, National Inpatient Sample.
†Because of the transition from ICD-9-CM to ICD-10-CM in October 2015, the data represent 2 time periods. ICD-9 data reflect 2010 through the third quarter of 2015 (2015q3), and ICD-10 data represent the fourth quarter of 2015 (2015q4) through 2016.
‡Data from 2011–2014 not available.
§Statistics that are based on estimates with a relative SE (SE/weighted estimate) >0.30 or a total cell count <10 in the NIS are not reliable. These statistics are suppressed per HCUP policies.

Table 3. Clinical outcomes and healthcare use in patients with babesiosis-associated hospitalizations, United States, 2010–2016*

Clinical outcome	All data	ICD-9 data, 2010–2015q3†	ICD-10 data, 2015q4–2016†
Mortality, no. (%)	128 (1.6)	108 (1.7)	20 (1.4)
Length of stay, d			
Mean (SD)	5.8 (7.3)	5.8 (10.3)	5.8 (6.5)
Median (IQR)	4 (3–7)	4 (2–6)	4 (3–7)
Total hospital charges for primary diagnosis of babesiosis‡			
Mean	$36,850.51	$37,236.39	$36,464.62
Aggregate national bill, USD	$171,281,170	$142,911,768	$29,536,342
Mean national bill per year, USD	$24,468,739	$24,854,221	$23,629,074
Transfusion and apheresis use, no. (%)			
Erythrocyte transfusion	1560 (20.0)	1375 (21.6)	185 (12.8)
Platelet transfusion	208 (2.7)	183 (2.9)	25 (1.7)
Plasma transfused	88 (1.1)	78 (1.2)	10 (0.7)
Erythrocyte exchange	80 (1.0)	75 (1.2)	§
Erythrocyte or plasma exchange	90 (1.2)	75 (1.2)	15 (1.0)
Complications, no. (%)			
Acute renal failure	1,594 (20.4)	1,209 (19)	385 (26.6)
Respiratory failure	528 (6.8)	363 (5.7)	165 (11.4)
Acute heart failure	270 (3.5)	200 (3.1)	70 (4.8)
Disseminated intravascular coagulation	149 (1.9)	129 (2.0)	20 (1.4)

*Data are from the NIS, which offers a representative sampling of US-based hospitals. Weighted national estimates are based on data that were collected by individual states and provided to AHRQ. Total number of weighted discharges in the United States based on HCUP NIS: 37,352,013 (2010); 36,962,415 (2011); 36,484,846 (2012); 35,597,792 (2013); 35,358,818 (2014); 35,769,942 (2015); 35,675,421 (2016). Statistics based on estimates with a relative SE (SE/weighted estimate) >0.30 or with SE 0 in the nationwide statistics (NIS, Nationwide Emergency Department Sample, and Kids' Inpatient Database) are not reliable. In 2012, the National Inpatient Sample was redesigned to optimize national estimates. The nationwide statistics in HCUPnet for years before 2012 were regenerated using new trend weights to permit longitudinal analysis. The regenerated data were posted to HCUPnet on July 2, 2014. The statistics for years before 2012 currently on HCUPnet will differ slightly from statistics obtained before July 2, 2014. Information about the NIS redesign and trend weights is available at https://hcupnet.ahrq.gov. For more information about HCUP data, see http://www.hcup-us.ahrq.gov. ICD-9-International Classification of Diseases, Ninth Revision; ICD-10, International Classification of Diseases, Tenth Revision; HCUP, Healthcare Cost and Utilization Project; NIS, National Inpatient Sample.
†Because of the transition from ICD-9-CM to ICD-10-CM in October 2015, the data represent 2 time periods. ICD-9 data reflect 2010 through the third quarter of 2015 (2015q3), and ICD-10 data represent the fourth quarter of 2015 (2015q4) through 2016.
‡Cost data were calculated for primary diagnosis only. ICD-9 charge data were obtained solely from HCUP (http://www.hcup-us.ahrq.gov). The aggregate national bill was determined by calculating the mean total charges per year multiplied by number of cases.
§Statistics that are based on estimates with a relative SE (SE/weighted estimate) >0.30 or a total cell count <10 in the NIS are not reliable. These statistics are suppressed per HCUP policies.

A stable or modest increase in severe babesiosis (i.e., hospitalizations) does not correlate well with the general epidemiology of this infection, whereby an increase in cases of babesiosis has been observed over the past 3 decades (*22*). Several factors may contribute to a general increase, such as increased geographic spread of the disease, allied with increased recognition of the disease. A group of investigators have used tick surveillance to estimate the geographic range and disease burden of babesiosis (*23*–*26*). A close association between *B. microti* in ticks and reported rates of human infection was demonstrated in babesiosis-endemic areas but not in areas of emerging disease, suggesting underreporting outside of established areas of endemicity (*25*). Furthermore, that the overall reported cases (which included the hospitalized patients) were only ≈50% more may suggest that cases are either not reported or not recognized.

We found that clinical complications of babesiosis in our study population were common, but the overall mortality rate (≈1.3%) was low. The observed rates of clinical complications in our study differ from prior reports, which tended to cite pulmonary sequelae (e.g., pulmonary edema, acute respiratory failure, and acute respiratory distress syndrome) as the most common severe complication of babesiosis (prevalence ranging from 6.3% to 43%) (*17*,*27*–*29*). By contrast, acute renal failure was the leading complication in our population (prevalence of 20.4% for acute renal failure, compared with 6.8% for acute respiratory failure). Previously published prevalence estimates for renal failure have ranged from 4.3% to 7%, the latter in immunocompromised patients (*17*,*27*,*28*). These discrepancies could be due to differences in the definition of organ failure and the scope of prior studies. Many of the reports of organ morbidity are based on small numbers of study participants.

Similarly, previously reported death rates for babesiosis in the United States have been highly variable, from 0% to 27% (*29*,*30*). Differences by reporting source could account for the observed variability. Specifically, most studies that have reported death rates are case series, most of which have been constrained by small sample sizes. There are also differences in the populations that have been described; higher rates have been observed in asplenic patients,

immunocompromised persons, and transfusion recipients (*2*,*28*,*30*). Although our study offers a population-based estimate of babesiosis-related death in hospitalized patients, its findings need to be interpreted within the bounds of the acknowledged limitations pertaining to diagnostic coding and clinical imputability. Thus, data are insufficient to conclude whether death rates for babesiosis are improving; rather, the low death rate found in our study may provide a false sense of optimism regarding the disease.

Not surprisingly, erythrocyte transfusion, which was reported in one fifth of hospitalizations, was associated with a significantly higher death rate (≈3%). Erythrocyte transfusions are administered for severe anemia, so they are an index of severe disease, especially for transfusion-transmitted babesiosis, which carries a high death rate (19%) (*2*). Another potential risk factor for severe babesiosis is concurrent Lyme disease; previous studies have found that patients with both babesiosis and Lyme disease have more symptoms that last longer than do those with Lyme disease alone (*31*–*33*). However, the same studies failed to find a difference in the number of symptoms in patients with babesiosis and Lyme disease (i.e., co-infection), compared with patients with babesiosis alone; our data were consistent with those findings. As noted in this analysis, death was a more common outcome in admissions in which babesiosis was listed as a primary rather than as a secondary diagnosis. At least some of the secondary diagnoses are likely to be cases in which the infection was detected incidentally, where parasitemia would likely be low.

The medical care costs of babesiosis also add to the health burden of the disease. The observed charges are comparable to those associated with hospitalizations for Lyme disease; that is, the average hospital charge for a primary diagnosis of Lyme disease was $25,025.53–$31,209.36 during the study period, depending on the reporting period (ICD-9 vs. ICD-10) (data not shown). Although Lyme disease poses a greater health and economic burden, given a greater number of cases and persistence of complications of illness, deaths from Lyme disease, unlike babesiosis, are rarely encountered (*34*).

A limitation of our study is that the analysis is confined to hospitalized case-patients. By design, hospitalizations offer insight into the most severe cases (i.e., there is an inherent selection bias favoring severe infection). Although our findings are informative, quantifying the complete burden of disease given this highly selected sampling is difficult. Furthermore, the sampling approach does not include all hospitalized patients, nor does it include all hospitals; however, it is a validated, robust sampling approach, correlating well with other national survey methods (*35*,*36*). The NIS database is not designed to capture all pediatric patients, although children who are treated in adult hospitals may be captured in these analyses. There are also technical limitations. We cannot determine whether each hospitalization was for a unique patient; a proportion may be readmissions for the same patients, although readmissions are not expected to be common. The analysis also leaves some uncertainty surrounding the relationship between babesiosis and possible concurrent diseases. For example, the observed prevalence of anaplasmosis and ehrlichiosis may reflect infection with *Ehrlichia muris* (also vectored by *I. scapularis* ticks), exposure to similar tick habitats where *I. scapularis* and *Amblyomma* ticks co-exist, or a misdiagnosis. Another limitation is the estimation of hospitalizations for transfusion-transmitted babesiosis. Unfortunately, rates of transfusion-transmitted babesiosis cannot be quantified because causality cannot be established; although one can deduce whether a transfusion was administered, it is not possible to determine whether infection was ascribed to the index transfusion using the database alone. Given the nature of this analysis, we have been cautious not to overinterpret the findings. For example, we cannot be certain whether admissions are increasing in general, whether the demographics of those who are likely to require hospitalization for babesiosis is increasing (i.e., "baby boomers"), or whether babesiosis is simply being recognized in patients because of greater awareness of symptoms.

In conclusion, we found that there has been a modest increase in hospitalized patients with babesiosis in the United States, yet the associated death rate appears to be low. Nonetheless, the overall health burden, particularly for selected patient subsets who are at risk for severe or even fatal disease, remains a concern.

E.M.B. was supported in part by National Heart Lung and Blood Institute (1K23HL151826-01). P.J.K. received support from the The Llura A. Gund Laboratory for Vector-borne Diseases and the Gordon and Llura Gund Foundation.

E.M.B. reports personal fees and nonfinancial support from Terumo BCT, Abbott Laboratories, and Grifols Diagnostics Solutions, outside of the submitted work. R.G. reports personal fees from Terumo BCT, and Alexion pharmaceuticals, outside of the submitted work.

About the Author

Dr. Bloch is an associate professor of pathology at Johns Hopkins University School of Medicine. where he serves as associate director in the Division of Transfusion Medicine. He has a joint appointment in International Health in the Johns Hopkins Bloomberg School of Public Health. His research interests include global blood transfusion safety, particularly in the context of infectious risk and how to respond to emerging and neglected transfusion transmissible infections.

References

1. Vannier E, Krause PJ. Human babesiosis. N Engl J Med. 2012;366:2397–407. https://doi.org/10.1056/NEJMra1202018
2. Herwaldt BL, Linden JV, Bosserman E, Young C, Olkowska D, Wilson M. Transfusion-associated babesiosis in the United States: a description of cases. Ann Intern Med. 2011;155:509–19. https://doi.org/10.7326/0003-4819-155-8-201110180-00362
3. Leiby DA, Gill JE. Transfusion-transmitted tick-borne infections: a cornucopia of threats. Transfus Med Rev. 2004;-18:293–306. https://doi.org/10.1016/j.tmrv.2004.07.001
4. Centers for Disease Control and Prevention. Lyme and other tickborne diseases increasing. April 22, 2019 [cited 2020 Feb 1]. https://www.cdc.gov/ncezid/dvbd/media/lyme-tickborne-diseases-increasing.html
5. Joseph JT, Roy SS, Shams N, Visintainer P, Nadelman RB, Hosur S, et al. Babesiosis in lower Hudson Valley, New York, USA. Emerg Infect Dis. 2011;17:843–7. https://doi.org/10.3201/eid1705.101334
6. Ostfeld RS, Levi T, Keesing F, Oggenfuss K, Canham CD. Tick-borne disease risk in a forest food web. Ecology. 2018;99:1562–73. https://doi.org/10.1002/ecy.2386
7. Hahn MB, Jarnevich CS, Monaghan AJ, Eisen RJ. Modeling the geographic distribution of *Ixodes scapularis* and *Ixodes pacificus* (Acari: Ixodidae) in the contiguous United States. J Med Entomol. 2016;53:1176–91. https://doi.org/10.1093/jme/tjw076
8. Centers for Disease Control and Prevention). Babesiosis surveillance—18 states, 2011. MMWR Morb Mortal Wkly Rep. 2012;61:505–9.
9. Gray EB, Herwaldt BL. Babesiosis surveillance—United States, 2011–2015. MMWR Surveill Summ. 2019;68:1–11. https://doi.org/10.15585/mmwr.ss6806a1
10. Healthcare Cost and Utilization Project. Overview of the HCUP Nationwide Impatient Sample. 2011 [cited 2021 Jan 29]. https://www.hcup-us.ahrq.gov/db/nation/nis/Overview_of_NIS_1998.pdf
11. HCUP National Inpatient Sample (NIS). Healthcare Cost and Utilization Project (HCUP). Overview of the HCUP Nationwide Impatient Sample. 2012. Agency for Healthcare Research and Quality. 2012 [cited 2021 Jan 29]. https://www.hcup-us.ahrq.gov/nisoverview.jsp
12. Healthcare Cost and Utilization Project. HCUP NIS Description of data elements. September 2008 [cited 2021 Jan 29]. https://www.hcup-us.ahrq.gov/db/vars/hosp_bedsize/nisnote.jsp
13. Burgess MJ, Rosenbaum ER, Pritt BS, Haselow DT, Ferren KM, Alzghoul BN, et al. Possible transfusion-transmitted *Babesia divergens*–like/MO-1 infection in an Arkansas patient. Clin Infect Dis. 2017;64:1622–5. https://doi.org/10.1093/cid/cix216
14. Bloch EM, Herwaldt BL, Leiby DA, Shaieb A, Herron RM, Chervenak M, et al. The third described case of transfusion-transmitted *Babesia duncani*. Transfusion. 2012;52:1517–22. https://doi.org/10.1111/j.1537-2995.2011.03467.x
15. Herwaldt BL, Kjemtrup AM, Conrad PA, Barnes RC, Wilson M, McCarthy MG, et al. Transfusion-transmitted babesiosis in Washington state: first reported case caused by a WA1-type parasite. J Infect Dis. 1997;175:1259–62. https://doi.org/10.1086/593812
16. Herc E, Pritt B, Huizenga T, Douce R, Hysell M, Newton D, et al. Probable locally acquired *Babesia divergens*–like infection in woman, Michigan, USA. Emerg Infect Dis. 2018;24:1558–60. https://doi.org/10.3201/eid2408.180309
17. White DJ, Talarico J, Chang H-G, Birkhead GS, Heimberger T, Morse DL. Human babesiosis in New York state: review of 139 hospitalized cases and analysis of prognostic factors. Arch Intern Med. 1998;158:2149–54. https://doi.org/10.1001/archinte.158.19.2149
18. Djokic V, Primus S, Akoolo L, Chakraborti M, Parveen N. Age-related differential stimulation of immune response by *Babesia microti* and *Borrelia burgdorferi* during acute phase of infection affects disease severity. Front Immunol. 2018;9:2891.
19. Shaw AC, Joshi S, Greenwood H, Panda A, Lord JM. Aging of the innate immune system. Curr Opin Immunol. 2010;22:507–13. https://doi.org/10.1016/j.coi.2010.05.003
20. Centers for Disease Control and Prevention. Blacklegged tick (*Ixodes scapularis*) surveillance [cited 2021 Jun 29]. https://www.cdc.gov/ticks/surveillance/BlackleggedTick.html
21. Menis M, Whitaker BI, Wernecke M, Jiao Y, Eder A, Kumar S, et al. Babesiosis occurrence among United States Medicare beneficiaries, ages 65 and older, during 2006–2017: overall and by state and county of residence. Open Forum Infect Dis. 2020;8:a608. https://doi.org/10.1093/ofid/ofaa608
22. Krause PJ, Auwaerter PG, Bannuru RR, Branda JA, Falck-Ytter YT, Lantos PM, et al. Clinical practice guidelines by the Infectious Diseases Society of America (IDSA): 2020 guideline on diagnosis and management of babesiosis. Clin Infect Dis. 2021;72:e49–64. https://doi.org/10.1093/cid/ciaa1216
23. Spielman A. The emergence of Lyme disease and human babesiosis in a changing environment. Ann N Y Acad Sci. 1994;740(1 Disease in Ev):146–56. https://doi.org/10.1111/j.1749-6632.1994.tb19865.x
24. Rodgers SE, Mather TN. Human *Babesia microti* incidence and *Ixodes scapularis* distribution, Rhode Island, 1998–2004. Emerg Infect Dis. 2007;13:633–5. https://doi.org/10.3201/eid1304.061035
25. Diuk-Wasser MA, Liu Y, Steeves TK, Folsom-O'Keefe C, Dardick KR, Lepore T, et al. Monitoring human babesiosis emergence through vector surveillance New England, USA. Emerg Infect Dis. 2014;20:225–31. https://doi.org/10.3201/eid2002.130644
26. Walter KS, Pepin KM, Webb CT, Gaff HD, Krause PJ, Pitzer VE, et al. Invasion of two tick-borne diseases across New England: harnessing human surveillance data to capture underlying ecological invasion processes. Proc Biol Sci. 2016;283:20160834.
27. Hatcher JC, Greenberg PD, Antique J, Jimenez-Lucho VE. Severe babesiosis in Long Island: review of 34 cases and their complications. Clin Infect Dis. 2001;32:1117–25. https://doi.org/10.1086/319742
28. Krause PJ, Gewurz BE, Hill D, Marty FM, Vannier E, Foppa IM, et al. Persistent and relapsing babesiosis in immunocompromised patients. Clin Infect Dis. 2008;46:370–6. https://doi.org/10.1086/525852

29. Mareedu N, Schotthoefer AM, Tompkins J, Hall MC, Fritsche TR, Frost HM. Risk factors for severe infection, hospitalization, and prolonged antimicrobial therapy in patients with babesiosis. Am J Trop Med Hyg. 2017;97:1218–25. https://doi.org/10.4269/ajtmh.17-0146
30. Rosner F, Zarrabi MH, Benach JL, Habicht GS. Babesiosis in splenectomized adults. Review of 22 reported cases. Am J Med. 1984;76:696–701. https://doi.org/10.1016/0002-9343(84)90298-5
31. Krause PJ, Telford SR III, Spielman A, Sikand V, Ryan R, Christianson D, et al. Concurrent Lyme disease and babesiosis. Evidence for increased severity and duration of illness. JAMA. 1996;275:1657–60. https://doi.org/10.1001/jama.1996.03530450047031
32. Krause PJ, McKay K, Thompson CA, Sikand VK, Lentz R, Lepore T, et al.; Deer-associated Infection Study Group. Disease-specific diagnosis of coinfecting tickborne zoonoses: babesiosis, human granulocytic ehrlichiosis, and Lyme disease. Clin Infect Dis. 2002;34:1184–91. https://doi.org/10.1086/339813
33. Steere AC, McHugh G, Suarez C, Hoitt J, Damle N, Sikand VK. Prospective study of coinfection in patients with erythema migrans. Clin Infect Dis. 2003;36:1078–81. https://doi.org/10.1086/368187
34. Kugeler KJ, Griffith KS, Gould LH, Kochanek K, Delorey MJ, Biggerstaff BJ, et al. A review of death certificates listing Lyme disease as a cause of death in the United States. Clin Infect Dis. 2011;52:364–7. https://doi.org/10.1093/cid/ciq157
35. Agency for Healthcare Research and Quality. 1996 HCUP Nationwide Inpatient Sample (NIS) Design Report. 1996 [cited 2021 Jul 26]. https://www.hcup-us.ahrq.gov/db/nation/nis/reports/NIS_1996_Design_Report.jsp
36. Coffey R, Barrett M, Houchens R, Moy E, Ho K, Andrews R, et al. Methods applying AHRQ Quality Indicators to the Cost and Utilization Project (HCUP) data for the Seventh (2009) National Healthcare Disparities Report. Rockville (MD): US Agency for Healthcare Research and Quality; 2009.

Address for correspondence: Evan M. Bloch, Johns Hopkins University School of Medicine, Department of Pathology, 600 N Wolfe St/Carnegie 446D1, Baltimore, MD 21287, USA; email: ebloch2@jhmi.edu

Rapid Spread of Severe Fever with Thrombocytopenia Syndrome Virus by Parthenogenetic Asian Longhorned Ticks

Xing Zhang,[1] Chaoyue Zhao,[1] Chaoyuan Cheng,[1] Guogang Zhang,[1] Tao Yu, Kevin Lawrence, Hongyue Li, Jimin Sun, Zeyu Yang, Ling Ye, Hongliang Chu, Ying Wang, Xiaohu Han, Yongchao Jia, Shuozhang Fan, Hirotaka Kanuka, Tetsuya Tanaka, Cheryl Jenkins, Kristene Gedye, Shona Chandra, Dana C. Price, Qiyong Liu, Young Ki Choi, Xiangjiang Zhan, Zhibin Zhang, Aihua Zheng

Severe fever with thrombocytopenia syndrome virus (SFTSV) is spreading rapidly in Asia. This virus is transmitted by the Asian longhorned tick (*Haemaphysalis longicornis*), which has parthenogenetically and sexually reproducing populations. Parthenogenetic populations were found in ≥15 provinces in China and strongly correlated with the distribution of severe fever with thrombocytopenia syndrome cases. However, distribution of these cases was poorly correlated with the distribution of populations of bisexual ticks. Phylogeographic analysis suggested that the parthenogenetic population spread much faster than bisexual population because colonization is independent of sexual reproduction. A higher proportion of parthenogenetic ticks was collected from migratory birds captured at an SFTSV-endemic area, implicating the contribution to the long-range movement of these ticks in China. The SFTSV susceptibility of parthenogenetic females was similar to that of bisexual females under laboratory conditions. These results suggest that parthenogenetic Asian longhorned ticks, probably transported by migratory birds, play a major role in the rapid spread of SFTSV.

Parthenogenesis is the development of an embryo from an unfertilized egg and is a common reproductive mechanism in invertebrate arthropods, especially insects and mites (*1*). One of the potential advantages of parthenogenesis is that the offspring are all genetically identical, which in relatively stable environments can lead to a rapid expansion in numbers. After dispersal, new populations can be established from 1 female. The Asian longhorned tick (*Haemaphysalis longicornis*) is among a small number of medically relevant tick species that have parthenogenetic and bisexual populations (*2*). The parthenogenetic population of these ticks originated in northern Japan (*3*) and is now common in the Asia–Pacific region. Parthenogenetic and bisexual populations are found in eastern East Asia, but only the parthenogenetic population is found in Oceania (*3*). In China, the parthenogenetic population has only been reported in a few locations (*4*). During 2017, parthenogenetic Asian longhorned ticks were found in New Jersey, USA (*5*),

Author affiliations: State Key Laboratory of Integrated Management of Pest Insects and Rodents, Institute of Zoology, CAS, Beijing (X. Zhang, C. Zhao, C. Cheng, H. Li, X. Zhan, Z. Zhang, A. Zheng); University of Chinese Academy of Sciences, Beijing (X. Zhang, C. Zhao, C. Cheng, H. Li, Z. Zhang, A. Zheng); Yantai Center for Disease Control and Prevention, Yantai, China (T. Yu); Massey University, Palmerston North, New Zealand (K. Lawrence, K. Gedye); Zhejiang Center for Disease Control and Prevention, Zhejiang, China (J. Sun); Research Institute of Forest Ecology, Environment and Protection, Chinese Academy of Forestry, Beijing (Z. Yang, G. Zhang); Daishan Center for Disease Control and Prevention, Zhoushan, China (L. Ye); Jiangsu Center for Disease Control and Prevention, Nanjing, China (H. Chu); Xinyang Center for Disease Control and Prevention, Xinyang, China (Y. Wang); Shenyang Agricultural University, Shenyang, China (X. Han); Guangyuan Center for Disease Control and Prevention, Guangyuan, China (Y. Jia); Hebei University, Baoding, China (S. Fan); Jikei University School of Medicine, Tokyo, Japan (H. Kanuka); Kagoshima University, Kagoshima, Japan (T. Tanaka); Elizabeth Macarthur Agricultural Institute, Menangle, New South Wales, Australia (C. Jenkins); University of Sydney, Camden, New South Wales, Australia (S. Chandra); Rutgers University, New Brunswick, New Jersey, USA (D.C. Price): National Institute for Communicable Disease Control and Prevention, Beijing (Q. Liu); Chungbuk National University, Cheongju City, South Korea (Y.K. Choi)

DOI: https://doi.org/10.3201/eid2802.211532

[1]These authors contributed equally to this article.

and by 2020, they had been found across 12 states, primarily in the eastern United States (*6*).

Severe fever with thrombocytopenia syndrome virus (SFTSV) is a tickborne phlebovirus transmitted by Asian longhorned ticks that was described in China during 2009 at the border of Henan, Anhui, and Hubei Provinces (*7*,*8*). SFTSV is maintained and transmitted by Asian longhorned ticks in the larva, nymph, and adult stages in both transovarial and transstadial modes (*8*–*10*). Human mortality rates for SFTSV infection range from 6% to 30% (*7*,*11*). During 2011–2016, cases of severe fever with thrombocytopenia syndrome (SFTS) were reported in 18 of the 34 provinces in China, and there was a 3-fold increase in case numbers (from 500 cases to 1,500 cases) (*11*). Most cases were in the rural areas of Henan (37%), Shandong (26.6%), Anhui (14%), and Hubei (12.6%) Provinces (*11*). SFTSV has also been reported in South Korea (2012), Japan (2014), Vietnam (2019), and Pakistan (2020) (*12*–*15*). Phylogenetic analysis showed that SFTSV isolates separate into the Chinese clade and the Japanese clade, which is consistent with their geographic distribution (*16*). A close relative of SFTSV, Heartland virus, was reported in the United States during 2012 and is transmitted by *Amblyomma americanum* ticks (*17*,*18*).

The Asian longhorned tick is the dominant tick species in SFTSV-endemic areas. Tick prevalence rates are 88% in Jiangsu Province, China, and 91% in Gangwon Province, South Korea (*19*,*20*). Most of the SFTSV-endemic areas are rural, and 97% of the patients are farmers living in wooded and hilly areas, far from modern transportation and cities (*21*). The rapid spread of SFTSV is unexplained, although Asian longhorned ticks have a broad host range (*18*), enabling several possible modes of dissemination. For example, because livestock and wild mammals are common hosts for Asian longhorned ticks, grazing of cattle or foraging of wild mammals, such as hares, could rapidly distribute ticks in an area with a suitable habitat (*22*). Furthermore, birds range far enough to transport ticks within a district, and long-range dispersal of tickborne pathogens can also be accelerated by tick-infested migratory birds (*23*).

During 2016, SFTSV antibodies were detected in tick-infested migratory greater white-fronted geese in Jiangsu Province, China (*24*). This finding has led to the suggestion that migratory birds might have been involved in the rapid spread of this disease in China. Two areas of China that have high endemic levels of SFTSV are situated on major bird migratory routes (*25*). The Dabie Mountain area region, where SFTSV was originally reported, is in the middle of a major bird migration route from Dongting Lake and Poyang Lake to Siberia, and Penglai City and Dalian City are located on the northern part of the Asia–Pacific migratory route. Dongting Lake and Poyang Lake are 2 of the major overwintering sites for migratory birds in China (*26*,*27*).

The aim of this study was to test the hypothesis that parthenogenetic Asian longhorned ticks, possibly carried by migratory birds, are responsible for the rapid spread of SFTSV in China and Asia. To test this hypothesis, we conducted a series of linked experiments, which included mapping the distribution of bisexual and parthenogenetic Asian longhorned ticks in those provinces in China that had a high prevalence of SFTS. We also estimated the geographic correlation between bisexual and parthenogenetic ticks and SFTS cases for those provinces, surveyed infestation of Asian longhorned ticks in migratory birds in a city that had a high prevalence of SFTS, tested virus acquisition and transstadial passage of Asian longhorned ticks for SFTSV, inferred the phylogeny of Asian longhorned ticks by using ticks collected from other regions, and estimated the correlation between migratory bird routes and bisexual and parthenogenetic tick populations in China.

Materials and Methods

Ethics

We conducted all animal studies in accordance with the recommendations in the Guide for the Care and Use of Laboratory Animals of the Ministry of Science and Technology of the People's Republic of China. Protocols for animal studies were approved by the Committee on the Ethics of Animal Experiments of the Institute of Zoology, Chinese Academy of Sciences (approval no. IOZ-IACUC-2020-062).

Tick Collection in China

We collected Asian longhorned ticks from 73 counties covering 20 provinces in China to which SFTSV is endemic (Figure 1; Appendix Table 1, https://wwwnc.cdc.gov/EID/article/28/02/21-1532-App1.pdf). We collected ticks of all life stages by using flag-dragging and removal directly from animals during April–November 2019. We identified ticks on the basis of morphologic characteristics, visualized through a light microscope, and further confirmed by molecular analysis in the laboratory by sequencing the mitochondrial 16S rRNA gene by using primers 16S-1, 5′-CTGCTCAATGATTTTTTAAATTGCTGTGG-3′, and 16S-2, 5′-CGCTGTTATCCCTAGAGTATT-3′. We removed 1 leg from each tick for molecular analysis to confirm identification. We used a random sample of 5–6 live ticks

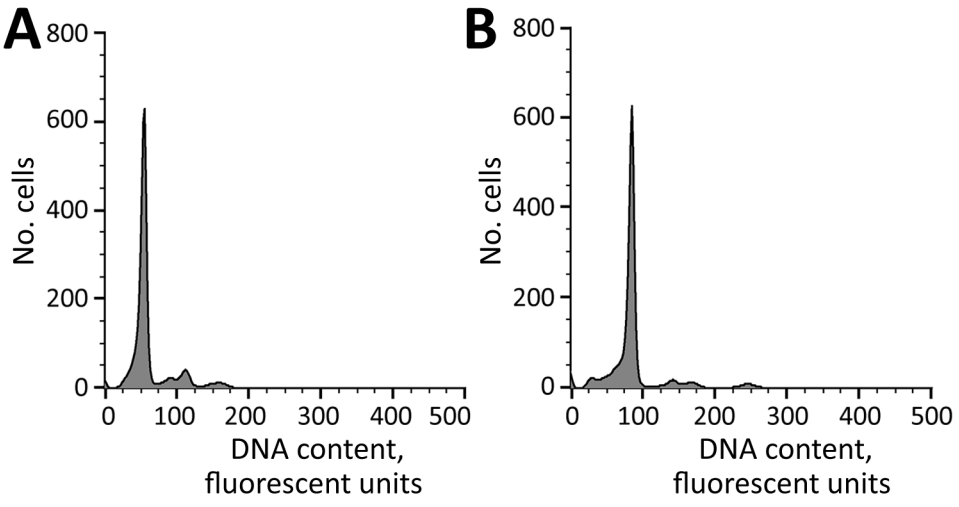

Figure 1. Polyploid analysis of bisexual and parthenogenetic Asian longhorned tick populations in China. Ploidy of ticks was tested by using flow cytometry and measuring fluorescence intensity of cell nuclei stained with 4′,6-diamidino-2-phenylindole. A) Bisexual (2n) sample with a peak at the 66 position. B) Parthenogenetic (3n) sample with a peak at the 99 position.

from each county sampled and stored then at room temperature until ploidy detection; we stored the remaining tick specimens at −80°C.

Tick Collection in Other Regions

We obtained 8 extracted tick DNA samples from overseas collaborators, including those in Japan, South Korea, New Zealand, Australia, and the United States during 2019 (Appendix Table 2). We subjected these ticks to the same molecular analysis as the Asian longhorned ticks collected in China.

Polyploid Analysis of Ticks

Because bisexual and parthenogenetic ticks are difficult to distinguish by using classical taxonomic methods but can be identified by karyotype analysis, we used flow cytometry to test the ploidy of tick chromosomes (*4*). This identification was accomplished by measuring the fluorescence intensity of cell nuclei stained with 4′,6-diamidino-2-phenylindole. We used the Sysmex Partec CyFlow Apparatus Space (Sysmex Partec, https://www.sysmex-partec.com) in this analysis and the Sysmex Partec CyStain DNA 1 Step Kit.

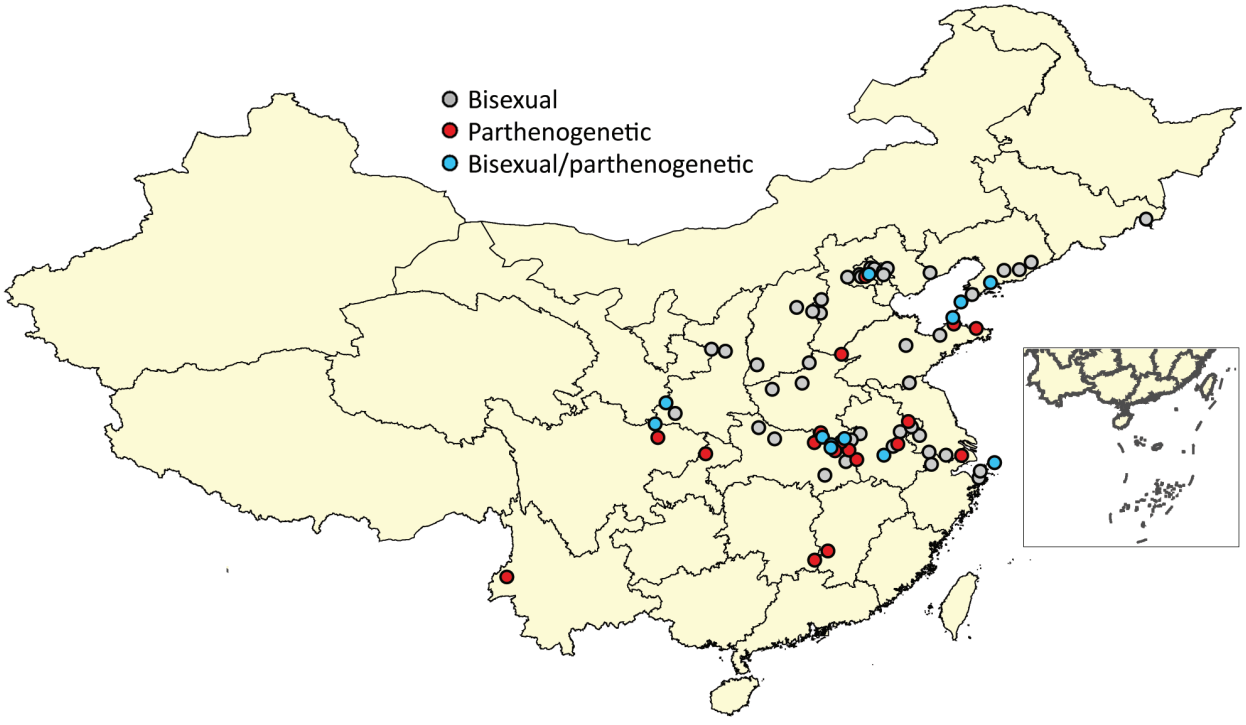

Figure 2. Geographic distribution of bisexual and parthenogenetic Asian longhorned ticks collected in China. Red dots indicate parthenogenetic ticks, gray dots indicate bisexual ticks, and blue dots indicate bisexual and parthenogenetic ticks. Inset shows the islands of Hainan Province.

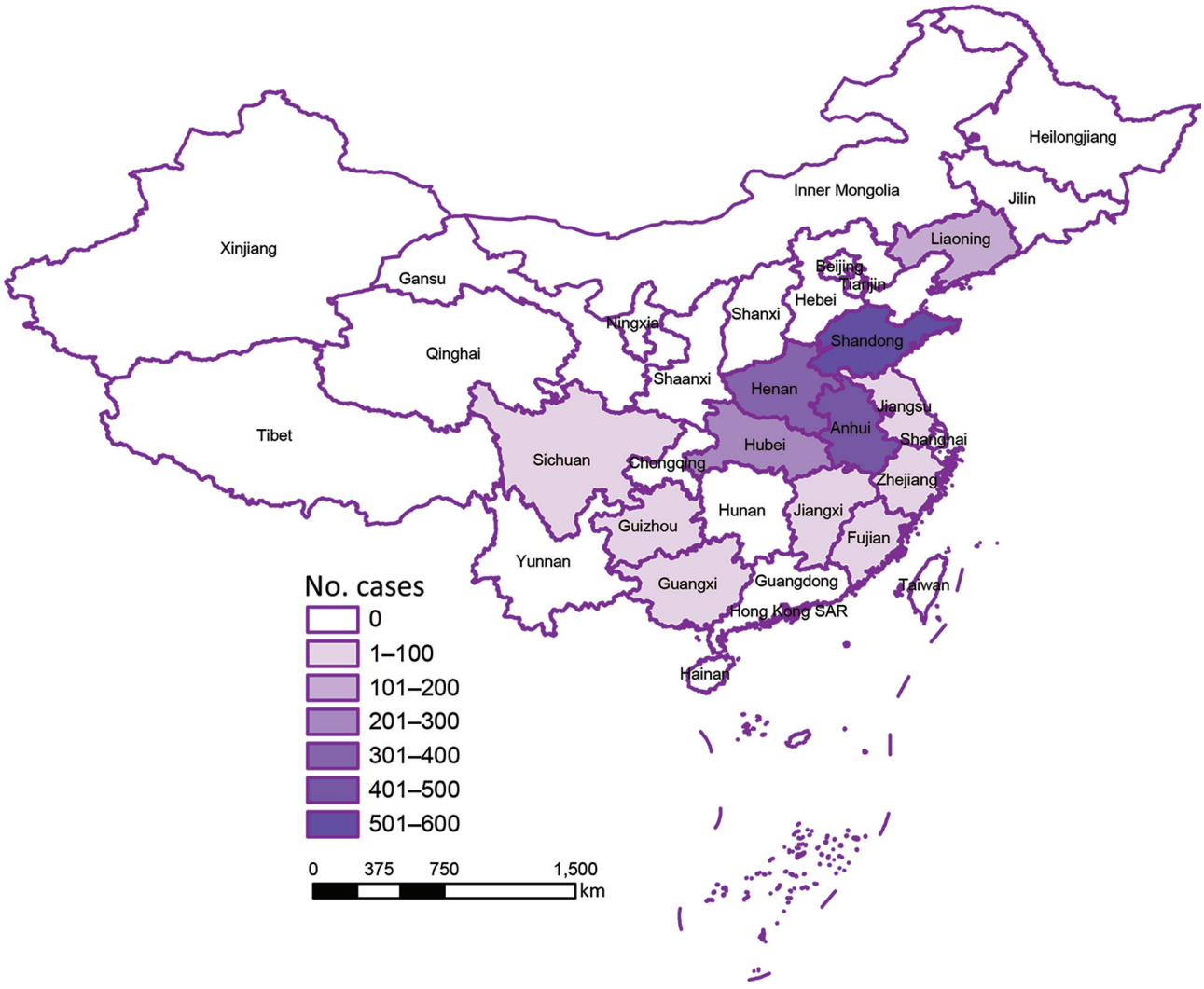

Figure 3. Distribution of severe fever with thrombocytopenia syndrome cases in China during 2019 (Chinese Center for Disease Control and Prevention), showing high correlation with parthenogenetic Asian longhorned tick population (shown in Figure 2).

Correlation between Bisexual and Parthenogenic Ticks and Cases of SFTS

We analyzed the geographic correlation between SFTS cases and the distribution of different populations of Asian longhorned ticks by using linear regression (*28*). We used the total number of recovered ticks, aggregated at the province or municipality level, as the independent variable and the incidence of SFTS cases (cases per million persons) reported in each respective province or municipality as the dependent variable. We obtained data for SFTS cases summarized by province or municipality for 2019 from the Chinese Center for Disease Control and Prevention.

Phylogenetic Tree and Genetic Distance

For each county, we randomly picked 1 bisexual tick sample or 1 parthenogenetic tick sample for whole mitochondrial sequencing. We sequenced whole mitochondrial genomes by using next-generation sequencing (Tsingke Biotech, https://career.tsinghua.edu.cn). We performed phylogenetic analysis by using whole mitochondrial genomes of 46 bisexual and 35 parthenogenetic ticks collected from China, Japan, South Korea, New Zealand, Australia, and the United States. We extracted Tick DNA by using the MightyPrep Reagent for DNA Kit (TaKaRa, https://www.takarabio.com) according to the manufacturer's instructions. We sequenced mitochondrial DNA by using next-generation sequencing (Tsingke Biotech) and deposited sequences in GenBank (accession nos. MW642336–407). We constructed 2 phylogenetic trees by using this data. the first tree by using the maximum-likelihood method MEGA-X (https://www.megasoftware.net) with the bootstrap

value set at 1,000 and the second tree by using the Bayesian interference method with MrBayes version 3.2.7 (http://nbisweden.github.io/MrBayes/index.html) and 1,500,000 generations. We used the genetic distance (GD) to calculate the dispersal index, which was equal to the nucleotide substitution rate.

Nucleotide Diversity

The nucleotide diversity (Pi) in each dataset is estimated by the equation

$$Pi = 2\sum_{i<j} d_{ij}/[n(n-1)],$$

where d_{ij} is an estimate of the number of nucleotide substitutions per site between DNA sequences *i* and *j* and *n* is the number of DNA sequences examined (*29*). We implanted the calculation for *Pi* in DnaSP-V6 (*30*).

Dispersal Index

Because without longitudinal surveillance data, we could not evaluate the spread velocity of ticks directly, we defined a dispersal index to quantify and compare the dispersal ability of bisexual and parthenogenetic ticks. According to the molecular clock theory, because the mutation rate is relatively constant, genetic distance can be used to represent time distance (*31*). The dispersal index (I) was defined as I = D/G, where D represents the sum of the spatial distances between every 2 samples (i.e., pairwise geographic distance) and G represents the genetic distance (nucleotide substitutions) between every 2 samples (i.e., pairwise genetic distance). This index is not the true dispersal velocity itself, but we can infer that the greater the dispersal index value, the greater the dispersal velocity. We performed an independent sample *t*-test to contrast the dispersal rates for bisexual and parthenogenetic ticks. We calculated dispersal index and *t*-test by using customed scripts written in Python version 3.7 (https://www.python.org).

Migratory Bird Capture and Tick Collection

To test our hypothesis that migratory birds are carrying Asian longhorned ticks, we investigated the presence of ticks on northward migratory birds at a high-density stopover site at Penglai City (37°55′13.84″N, 120°43′53.27″E), Yantai City, Shandong Province, during April 2021. Shandong Province is a major location on the Asia–Pacific migratory route. We captured birds by using mist nets (2.5 × 6 m or 2.5 × 12 m, mesh size 3.0 cm) placed in a wooded habitat. Upon capture, we meticulously examined birds for ticks by searching ear canals, backs of heads, mandibular areas, and perimeter of the eyes. We then removed ticks by using fine forceps.

Tick Diversity in Penglai City

Penglai City is 1 of the most SFTS-endemic areas in China and a major location in the Asia–Pacific migratory route. We collected and sequenced parthenogenetic ticks from 9 locations in Penglai City. We used phylogenetic analysis to compare the diversity of ticks from Penglai City with the diversity of ticks from 15 other provinces in China.

Virus Acquisition by and Transstadial Passage of Ticks for SFTSV

We tested the virus susceptibility of parthenogenetic and bisexual populations for transmitting SFTSV by using laboratory-adapted Asian longhorned tick colonies and an IFNAR (interferon α/β receptor knockout) mouse model. We infected nymphal ticks by feeding them on IFNAR$^{-/-}$C57/BL6 mice, which were previously inoculated with 2 × 10^3 focal-forming units of SFTSV (Wuhan strain; GenBank accession nos.: small segment, KU361341.1; medium segment KU361342.1; large segment, KU361343.1). We collected fed nymphs after they were fully engorged and had detached from the mice.

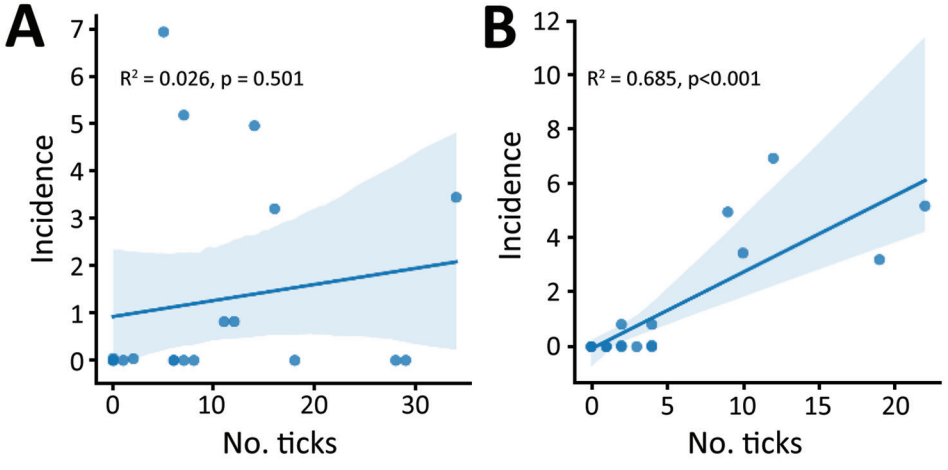

Figure 4. Correlation between incidence of severe fever with thrombocytopenia syndrome virus cases (cases per 1 million persons) and number of bisexual (A) and parthenogenetic (B) Asian longhorned ticks in different provinces, China. Each dot represents the number of cases in a province. Blue shading indicates 95% CI.

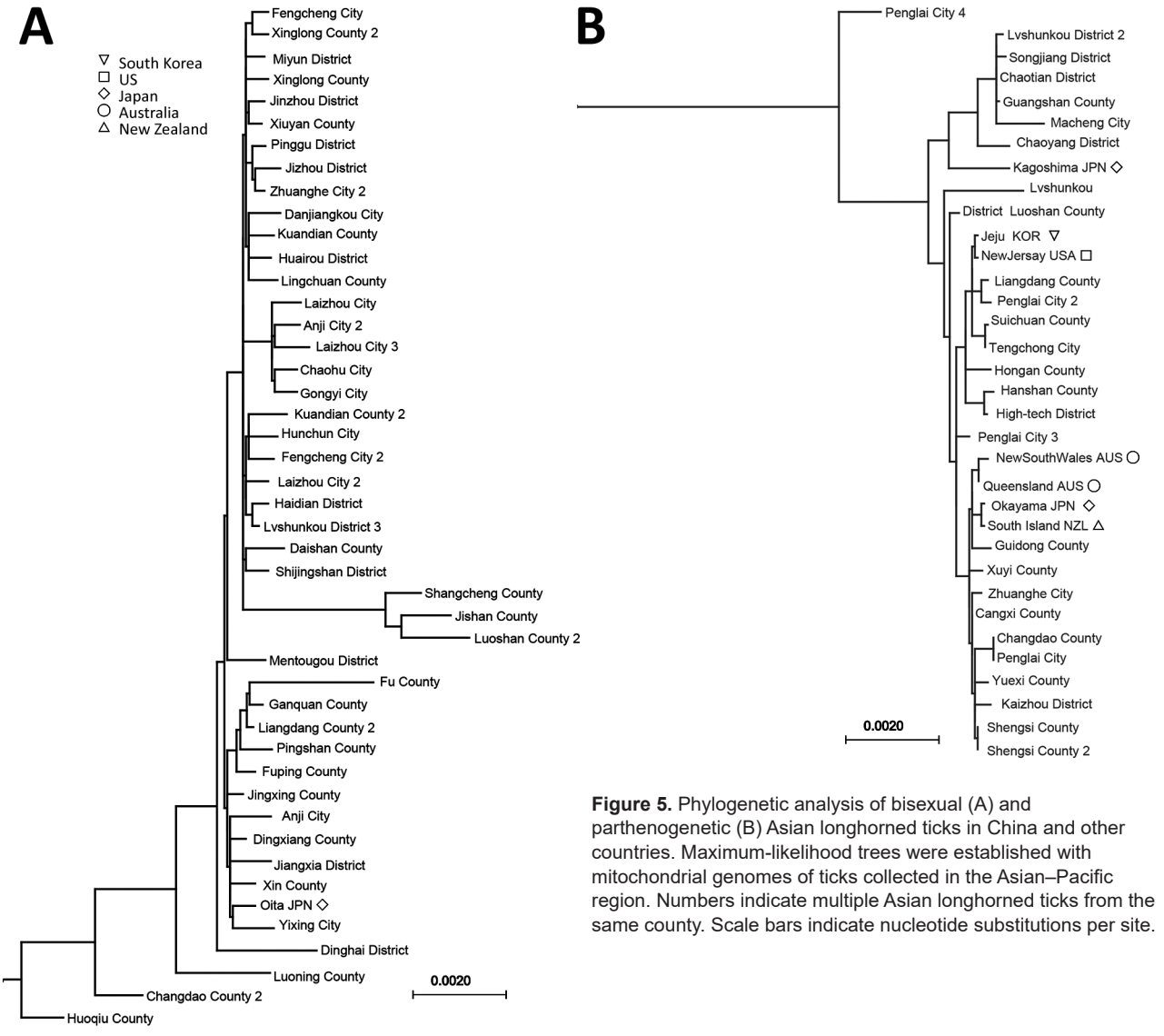

Figure 5. Phylogenetic analysis of bisexual (A) and parthenogenetic (B) Asian longhorned ticks in China and other countries. Maximum-likelihood trees were established with mitochondrial genomes of ticks collected in the Asian–Pacific region. Numbers indicate multiple Asian longhorned ticks from the same county. Scale bars indicate nucleotide substitutions per site.

We analyzed SFTSV RNA levels in the ticks after they molted into adults. We extracted total RNA prepared from homogenates of ticks by using TRIzol reagent (Thermo Fisher Scientific, https://www.thermofisher.com) according to manufacturer's instructions. We analyzed samples by using a One-Step SYBR PrimerScript Reverse Transcription PCR Kit (TaKaRa) on an Applied Biosystems QuantStudio (https://www.thermofisher.com) and measured each sample in triplicate. Primers were designed as previously described (32).

Results

Tick Distribution and Ploidy Analysis

There were 1,328 Asian longhorned ticks confirmed by 16S rRNA sequencing, of which 271 (20.4%) live ticks were further submitted for ploidy analysis by flow cytometry (255 ticks) or by mitochondrial sequencing (16 ticks) (Appendix Table 1). Ploidy testing showed a peak for the bisexual (diploid) population at the 66 position and for the parthenogenetic (triploid) population at the 99 position (Figure 1). Of ticks submitted for ploidy analysis, 186 (69%) of 271 were identified as bisexual and 85 (31%) of 271 as parthenogenetic. Bisexual ticks were detected in 55 (75%) of 73 counties, parthenogenetic ticks were detected in 30 (42%) of 73 of counties, and a mixture of both populations was detected in 12 (16%) of 73 counties (Figure 2; Appendix Table 1). In 18 (25%) of 73 counties, only parthenogenetic ticks were found, and in 43 (59%) of 73 counties, only bisexual ticks were found.

Correlation of SFTSV with Bisexual and Parthenogenic Ticks

SFTS cases showed a strong correlation with the parthenogenetic population (R^2 = 0.685, p<0.001) but almost no correlation with the bisexual population (R^2 = 0.026, p = 0.501) (Figures 3, 4). In the highly endemic Dabie Mountain area (located at the border of Henan, Anhui, and Hubei Provinces in central China), 66% of the collected Asian longhorned ticks were parthenogenetic in 11 of 14 counties (Appendix Table 1). These results suggest that the parthenogenetic populations of Asian longhorned ticks are strongly associated geographically with cases of SFTS.

Phylogenetic Analysis of Bisexual and Parthenogenic Ticks

For each county, 1 bisexual or parthenogenetic Asian longhorned tick was submitted for mitochondrial sequencing. We obtained 81 whole mitochondrial genomes from 73 ticks from China ticks and 8 ticks from outside China (Appendix Table 2). Results clearly show that the parthenogenetic and bisexual populations are divided into 2 distinct lineages that can be discriminated by 1 T deletion at position 8497 in the untranslated region (Figure 5; Appendix Figures 2–5). This finding suggests that the parthenogenetic population might have originated from 1 event without gene exchange. The mean GD between all sequences was 0.0078, as measured by the nucleotide substitution rate. The parthenogenetic strains from New Zealand and Australia were similar to the parthenogenetic strain from Okayama, Japan (mean GD 0.0003). The parthenogenetic strain from Kagoshima, Japan, was a close relative to strains collected from Beijing, Hubei, and Henan, China (Appendix Figure 1), which are geographically separate. The strain from New Jersey, USA, was similar to the strain from Jeju Island, South Korea (GD 0.0001).

Genetic Diversity

Despite the loss of sexual reproduction, high genetic diversity has been reported in the asexual populations of many insect species (32). The Pi values for the 2 populations, as measured by the mitochondrial genome, were 0.00249 for bisexual and 0.00188 for parthenogenetic. These results indicate that the genetic diversity of the bisexual and parthenogenetic populations was similar and that the parthenogenetic population might have diverged from the bisexual population at an early age.

Dispersal Index of Bisexual and Parthenogenic Ticks

When compared with bisexual ticks, we found that parthenogenetic ticks have a wider pairwise geographic distance distribution and a narrower pairwise genetic distance distribution (Figure 6, panel A). The dispersal index for parthenogenetic ticks was significantly higher than that for bisexual ticks (t = 7.67, p<0.001), and the mean dispersal index for parthenogenetic ticks (910,228) was 2.3 times higher than that for bisexual ticks (393,156) (Figure 6, panels B, C). These results indicate that parthenogenetic ticks have a higher dispersal capacity.

Correlation between Migratory Birds and Ticks

We collected and examined migratory birds for Asian longhorned ticks in Penglai City, which is an area to which SFTSV is highly endemic and is located in the Asia–Pacific migratory route (Appendix Figure 1). We netted 95 birds in 17 species. However, 54

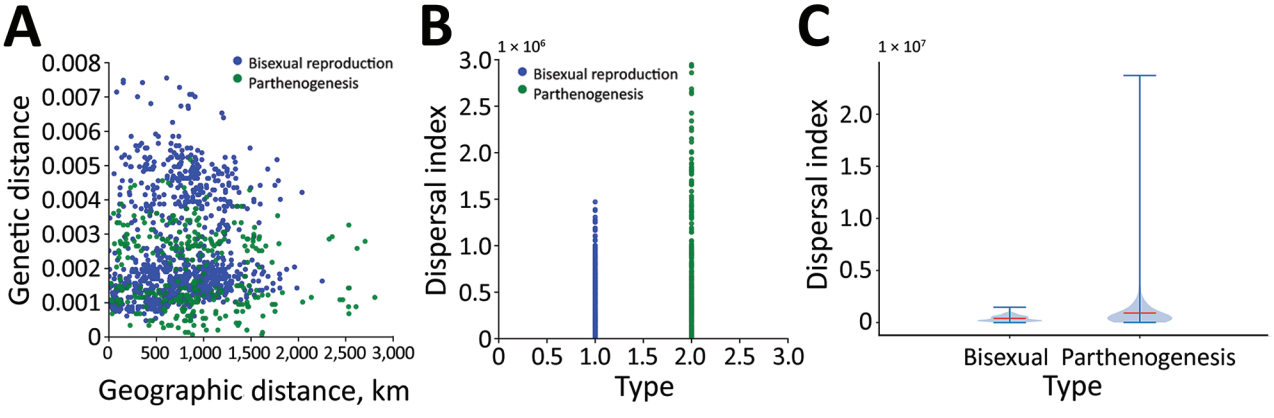

Figure 6. Phylogeographic analysis of bisexual and parthenogenetic Asian longhorned ticks, China. A) Distribution of bisexual and parthenogenetic Asian longhorned ticks in pairwise genetic distance and pairwise geographic distance. B, C) Distribution (B) and difference (C) of dispersal index between bisexual and parthenogenetic Asian longhorned ticks. Horizontal red line in the violin plot indicates the mean dispersal index, shaded blue areas indicate the kernel density estimation, and error bars indicate the maximum (top line) and minimum (bottom line) values.

Table. *Haemaphysalis longicornis* ticks collected from migratory birds and their hosts in Penglai City, China, 2021

Avian host	No. birds examined	No. birds with ticks	No. ticks	No. Asian longhorned ticks	Parthenogenetic,%
Turdus naumanni	45	8	11	3	33
Turdus hortulorum	7	2	8	8	100
Parus major	1	1	5	5	100
Emberiza fucata	1	1	3	3	100

Asian longhorned ticks were found on only 4 species: Naumann's thrush (*Turdus naumanni*), grey-backed thrush (*Turdus hortulorum*), great tit (*Parus major*), and chestnut-eared bunting (*Emberiza fucata*). Only 27 ticks were recovered from these birds, of which 19 (70%) were identified as Asian longhorned ticks; 17 (89%) of 19 Asian longhorned ticks were parthenogenetic (Table). All recovered Asian longhorned ticks were nymphs.

Tick Diversity in Penglai City

Phylogenetic analysis showed that the mitochondrial sequences of the parthenogenetic Asian longhorned ticks collected in Penglai City from vegetation were highly diverse when compared with those from 15 provinces in China (Appendix Figure 6). These data suggest that ticks from many different provinces were present in Penglai City and were probably spread to this region by migratory birds.

Virus Acquisition by Ticks and Transstadial Passage for Spreading SFTSV

We detected a robust viremia in mice inoculated with SFTSV (Figure 7, panel A). After feeding until engorgement and molting, the parthenogenetic and bisexual populations showed average titers of 3 log RNA copies/mg without obvious differences (Figure 7, panel B). The SFTSV-acquisition and transstadial passage efficiency of the parthenogenetic population appeared comparable with that of the bisexual population.

Discussion

We found that the parthenogenetic population of Asian longhorned ticks is more widely distributed in China than previously believed and that the distribution is highly correlated with regions to which SFTSV is endemic. Phylogeographic analysis suggests that the parthenogenetic Asian longhorned tick population has spread more rapidly over a greater distance than the bisexual population, and assessment of virus acquisition and transstadial passage showed that bisexual and parthenogenetic populations were comparable in maintaining local transmission of SFTSV. Although only a small number of ticks were recovered, parthenogenetic Asian longhorned ticks were the dominant variety found in migratory birds collected in an area to which SFTS is endemic. We suggest that these results strongly support the hypothesis that parthenogenetic Asian longhorned tick populations are responsible for the rapid spread of SFTSV within China, most likely through being disseminated by migratory birds.

If, as we suggest, migratory birds have played a major role in the spread of parthenogenetic Asian longhorned ticks, then this role would partially explain the wide distribution of these ticks from

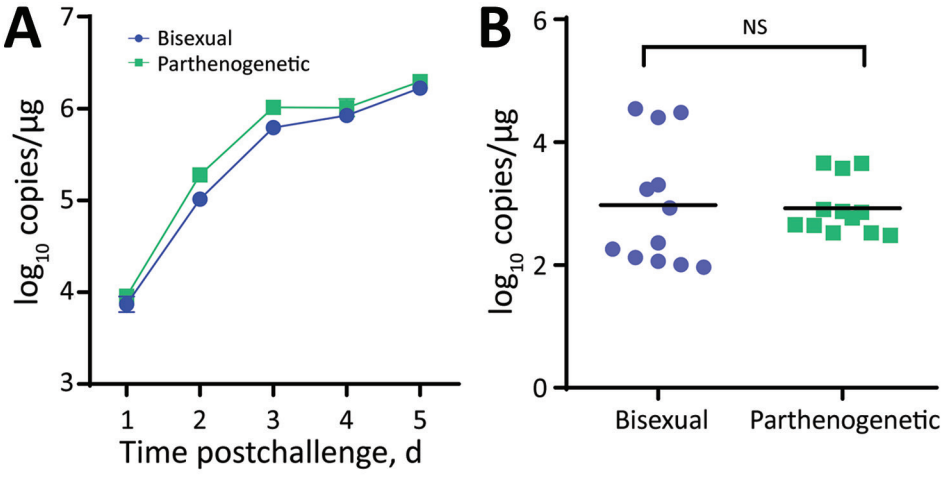

Figure 7. Susceptibility of bisexual and parthenogenetic Asian longhorned ticks to severe fever with thrombocytopenia syndrome virus (SFTSV), China. Groups of bisexual or parthenogenetic nymph Asian longhorned ticks were fed separately on 1 IFNAR$^{-/-}$ (interferon α/β receptor knockout) C57/BL6 mouse that was intraperitoneal inoculated with 2 x 10^3 focus-forming units of SFTSV. A) Viremias of IFNAR$^{-/-}$ C57/BL6 mice were monitored by using real-time PCR during tick feeding. B) SFTSV infection in the Asian longhorned ticks were tested by real-time PCR after molting into adults. Each dot or square indicates 1 tick. Black horizontal bars indicate means. NS, not significant.

the cold, far eastern region of Russia to the tropical areas of Australia and the Fiji Islands. However, the role of livestock, wild mammals, companion animals, and humans in translocation of parthenogenetic Asian longhorned ticks should not be overlooked (*22*).

Migratory birds are known to be carriers of ticks. Penglai City is 1 of the most endemic areas for SFTS and is a key passage in the northern part of East Asian–Australasian Flyway. In this area, 96% of Asian longhorned ticks were parthenogenetic and showed extremely high diversity (Appendix Figure 6). During a spring bird survey in Penglai City during 2021, we found that Asian longhorned ticks were found in 4 bird species (*Turdus naumanni*, *Turdus hortulorum*, *Parus major*, and *Emberiza fucata*), and 89% of them were parthenogenetic. Among the 4 bird species, 3 of them (*Turdus naumanni*, *Turdus hortulorum*, and *Emberiza fucata*) migrate between eastern Asia and Siberia, and are occasionally found in Alaska (https://www.ebird.org). The preferred habitats for these 4 species are grasslands and bushes, which are also the preferred habitats of Asian longhorned ticks. These results suggest that migratory birds have a major role in long-range movement of parthenogenetic ticks within China and potentially even transoceanic spread of SFTSV.

Parthenogenetic Asian longhorned ticks are also implicated in the spread of a pathogenic form of the blood parasite *Theileria orientalis* throughout the Asia–Pacific region (*18*). Asian longhorned ticks are purported to have been introduced to Australia in the 19th century from northern Japan and later disseminated to New Zealand, New Caledonia, and Fiji. This theory is supported by phylogenetic results of this study, which show that the New Zealand and Australia Asian longhorned ticks are alike and closely resemble the parthenogenetic strain from Okayama, Japan (*33*). *T. orientalis* parasites have been present in Australia for >100 years, having been introduced with the vector tick, and until 2006 caused only minor signs in livestock (*34*). During 2006, the pathogenic Ikeda genotype of *T. orientalis* was introduced from eastern Asia into New South Wales, Australia (*35*) and by 2014, had spread to most of the states in Australia (*36*). The recent spread of *T. orientalis* parasites across the Asia–Pacific region and into North America highlights the risk for rapid disease agent transmission into areas in which a competent vector (Asian longhorned tick) is already established. Thus, although SFTSV has not yet been detected in the Western Hemisphere, the presence of Asian longhorned parthenogenetic ticks in several countries within the study region presents a clear risk for future emergence of this virus.

Acknowledgments

We thank Chaodong Zhu for critically reviewing the manuscript and Shu Shen and Jingwen Wang for providing Asian longhorned ticks.

This study was supported by the National Science and Technology Major Project (2018ZX10101004); the State Key Research Development Program of China (2019YFC12005004); National Natural Science Foundation of China, General Program (81871687); and the Open Research Fund Program of the State Key Laboratory of Integrated Pest Management (IPM1603 and IPM1806).

About the Author

Dr. Xing Zhang is an associate professor at the College of Life Sciences, University of Chinese Academy of Sciences, Beijing, China. His primary research interests include vector biology and genetics, vectorborne pathogens, and endosymbionts in ticks.

References

1. Hoffmann AA, Reynolds KT, Nash MA, Weeks AR. A high incidence of parthenogenesis in agricultural pests. Proc Biol Sci. 2008;275:2473–81. https://doi.org/10.1098/rspb.2008.0685
2. Oliver JH Jr. Parthenogenesis in mites and ticks (Arachnida: Acari). Am Zool. 1971;11:283–99. https://doi.org/10.1093/icb/11.2.283
3 Hoogstraal H, Roberts FH, Kohls GM, Tipton VJ. Review of *Haemaphysalis* (*kaiseriana*) *longicornis* Neumann (resurrected) of Australia, New Zealand, New Caledonia, Fiji, Japan, Korea, and Northeastern China and USSR, and its parthenogenetic and bisexual populations (Ixodoidea, Ixodidae). J Parasitol. 1968;54:1197–213. https://doi.org/10.2307/3276992
4. Chen X, Xu S, Yu Z, Guo L, Yang S, Liu L, et al. Multiple lines of evidence on the genetic relatedness of the parthenogenetic and bisexual *Haemaphysalis longicornis* (Acari: Ixodidae). Infect Genet Evol. 2014;21:308–14. https://doi.org/10.1016/j.meegid.2013.12.002
5. Rainey T, Occi JL, Robbins RG, Egizi A. Discovery of *Haemaphysalis longicornis* (Ixodida: Ixodidae) parasitizing a sheep in New Jersey, United States. J Med Entomol. 2018;55:757–9. https://doi.org/10.1093/jme/tjy006
6. Egizi A, Bulaga-Seraphin L, Alt E, Bajwa WI, Bernick J, Bickerton M, et al. First glimpse into the origin and spread of the Asian longhorned tick, *Haemaphysalis longicornis*, in the United States. Zoonoses Public Health. 2020;67:637–50. https://doi.org/10.1111/zph.12743
7. Yu XJ, Liang MF, Zhang SY, Liu Y, Li JD, Sun YL, et al. Fever with thrombocytopenia associated with a novel bunyavirus in China. N Engl J Med. 2011;364:1523–32. https://doi.org/10.1056/NEJMoa1010095
8. Zhuang L, Sun Y, Cui XM, Tang F, Hu JG, Wang LY, et al. Transmission of severe fever with thrombocytopenia syndrome virus by *Haemaphysalis longicornis* ticks, China.

Emerg Infect Dis. 2018;24:868–71. https://doi.org/10.3201/eid2405.151435
9. Yun SM, Song BG, Choi W, Roh JY, Lee YJ, Park WI, et al. First isolation of severe fever with thrombocytopenia syndrome virus from *Haemaphysalis longicornis* ticks collected in severe fever with thrombocytopenia syndrome outbreak areas in the Republic of Korea. Vector Borne Zoonotic Dis. 2016;16:66–70. https://doi.org/10.1089/vbz.2015.1832
10. Luo LM, Zhao L, Wen HL, Zhang ZT, Liu JW, Fang LZ, et al. *Haemaphysalis longicornis* ticks as reservoir and vector of severe fever with thrombocytopenia syndrome virus in China. Emerg Infect Dis. 2015;21:1770–6. https://doi.org/10.3201/eid2110.150126
11. Zhan J, Wang Q, Cheng J, Hu B, Li J, Zhan F, et al. Current status of severe fever with thrombocytopenia syndrome in China. Virol Sin. 2017;32:51–62. https://doi.org/10.1007/s12250-016-3931-1
12. Takahashi T, Maeda K, Suzuki T, Ishido A, Shigeoka T, Tominaga T, et al. The first identification and retrospective study of severe fever with thrombocytopenia syndrome in Japan. J Infect Dis. 2014;209:816–27. https://doi.org/10.1093/infdis/jit603
13. Kim KH, Yi J, Kim G, Choi SJ, Jun KI, Kim NH, et al. Severe fever with thrombocytopenia syndrome, South Korea, 2012. Emerg Infect Dis. 2013;19:1892–4. https://doi.org/10.3201/eid1911.130792
14. Tran XC, Yun Y, Van An L, Kim SH, Thao NT, Man PK, et al. Endemic severe fever with thrombocytopenia syndrome, Vietnam. Emerg Infect Dis. 2019;25:1029–31. https://doi.org/10.3201/eid2505.181463
15. Zohaib A, Zhang J, Saqib M, Athar MA, Hussain MH, Chen J, et al. Serologic evidence of severe fever with thrombocytopenia syndrome virus and related viruses in Pakistan. Emerg Infect Dis. 2020;26:1513–6. https://doi.org/10.3201/eid2607.190611
16. Yoshikawa T, Shimojima M, Fukushi S, Tani H, Fukuma A, Taniguchi S, et al. Phylogenetic and geographic relationships of severe fever with thrombocytopenia syndrome virus in China, South Korea, and Japan. J Infect Dis. 2015;212:889–98. https://doi.org/10.1093/infdis/jiv144
17. McMullan LK, Folk SM, Kelly AJ, MacNeil A, Goldsmith CS, Metcalfe MG, et al. A new phlebovirus associated with severe febrile illness in Missouri. N Engl J Med. 2012;367:834–41. https://doi.org/10.1056/NEJMoa1203378
18. Brault AC, Savage HM, Duggal NK, Eisen RJ, Staples JE. Heartland virus epidemiology, vector association, and disease potential. Viruses. 2018;10:498. https://doi.org/10.3390/v10090498
19. Zhang YZ, Zhou DJ, Qin XC, Tian JH, Xiong Y, Wang JB, et al. The ecology, genetic diversity, and phylogeny of Huaiyangshan virus in China. J Virol. 2012;86:2864–8. https://doi.org/10.1128/JVI.06192-11
20. Park SW, Song BG, Shin EH, Yun SM, Han MG, Park MY, et al. Prevalence of severe fever with thrombocytopenia syndrome virus in *Haemaphysalis longicornis* ticks in South Korea. Ticks Tick Borne Dis. 2014;5:975–7. https://doi.org/10.1016/j.ttbdis.2014.07.020
21. Liu K, Cui N, Fang LQ, Wang BJ, Lu QB, Peng W, et al. Epidemiologic features and environmental risk factors of severe fever with thrombocytopenia syndrome, Xinyang, China. PLoS Negl Trop Dis. 2014;8:e2820. https://doi.org/10.1371/journal.pntd.0002820
22. Heath A. Biology, ecology and distribution of the tick, *Haemaphysalis longicornis* Neumann (Acari: Ixodidae) in New Zealand. N Z Vet J. 2016;64:10–20. https://doi.org/10.1080/00480169.2015.1035769
23. Zhang YZ, Xu J. The emergence and cross species transmission of newly discovered tick-borne bunyavirus in China. Curr Opin Virol. 2016;16:126–31. https://doi.org/10.1016/j.coviro.2016.02.006
24. Li Z, Bao C, Hu J, Liu W, Wang X, Zhang L, et al. Ecology of the tick-borne phlebovirus causing severe fever with thrombocytopenia syndrome in an endemic area of China. PLoS Negl Trop Dis. 2016;10:e0004574. https://doi.org/10.1371/journal.pntd.0004574
25. Yun Y, Heo ST, Kim G, Hewson R, Kim H, Park D, et al. Phylogenetic analysis of severe fever with thrombocytopenia syndrome virus in South Korea and migratory bird routes between China, South Korea, and Japan. Am J Trop Med Hyg. 2015;93:468–74. https://doi.org/10.4269/ajtmh.15-0047
26. Zou YA, Zhang PY, Zhang SQ, Chen XS, Li F, Deng ZM, et al. Crucial sites and environmental variables for wintering migratory waterbird population distributions in the natural wetlands in East Dongting Lake, China. Sci Total Environ. 2019;655:147–57. https://doi.org/10.1016/j.scitotenv.2018.11.185
27. Takekawa JY, Newman SH, Xiao X, Prosser DJ, Spragens KA, Palm EC, et al. Migration of waterfowl in the East Asian flyway and spatial relationship to HPAI H5N1 outbreaks. Avian Dis. 2010;54(Suppl):466–76. https://doi.org/10.1637/8914-043009-Reg.1
28. Altman N, Krzywinski M. Simple linear regression. Nat Methods. 2015;12:999–1000. https://doi.org/10.1038/nmeth.3627
29. Nei M, Miller JC. A simple method for estimating average number of nucleotide substitutions within and between populations from restriction data. Genetics. 1990;125:873–9. https://doi.org/10.1093/genetics/125.4.873
30. Rozas J, Ferrer-Mata A, Sánchez-DelBarrio JC, Guirao-Rico S, Librado P, Ramos-Onsins SE, et al. DnaSP 6: DNA sequence polymorphism analysis of large data sets. Mol Biol Evol. 2017;34:3299–302. https://doi.org/10.1093/molbev/msx248
31. King JL, Jukes TH. Non-Darwinian evolution. Science. 1969;164:788–98. https://doi.org/10.1126/science.164.3881.788
32. Tvedte ES, Logsdon JM Jr, Forbes AA. Sex loss in insects: causes of asexuality and consequences for genomes. Curr Opin Insect Sci. 2019;31:77–83. https://doi.org/10.1016/j.cois.2018.11.007
33. van der Kooi CJ, Matthey-Doret C, Schwander T. Evolution and comparative ecology of parthenogenesis in haplodiploid arthropods. Evol Lett. 2017;1:304–16. https://doi.org/10.1002/evl3.30
34. Izzo MM, Poe I, Horadagoda N, De Vos AJ, House JK. Haemolytic anaemia in cattle in NSW associated with *Theileria* infections. Aust Vet J. 2010;88:45–51. https://doi.org/10.1111/j.1751-0813.2009.00540.x
35. Islam MK, Jabbar A, Campbell BE, Cantacessi C, Gasser RB. Bovine theileriosis: an emerging problem in south-eastern Australia? Infect Genet Evol. 2011;11:2095–7. https://doi.org/10.1016/j.meegid.2011.08.012
36. Hammer JF, Emery D, Bogema DR, Jenkins C. Detection of *Theileria orientalis* genotypes in *Haemaphysalis longicornis* ticks from southern Australia. Parasit Vectors. 2015;8:229. https://doi.org/10.1186/s13071-015-0839-9

Address for correspondence: Aihua Zheng, Zhibin Zhang, or Xiangjiang Zhan, Institute of Zoology, Chinese Academy of Sciences, 1 Beichen Rd, Chaoyang District, Beijing 100101, China; emails: zhengaihua@ioz.ac.cn, zhangzb@ioz.ac.cn, or zhanxj@ioz.ac.cn

Genetic Relatedness of Infectious Hypodermal and Hematopoietic Necrosis Virus Isolates, United States, 2019

Arun K. Dhar, Roberto Cruz-Flores, Janet Warg, Mary L. Killian, Andrew Orry, Jorge Ramos, Michelle Garfias, Gregory Lyons

Infectious hypodermal and hematopoietic necrosis virus (IHHNV) is a nonenveloped, linear, single-stranded DNA virus belonging to the family *Parvoviridae* and is a World Organisation for Animal Health (OIE)–notifiable crustacean pathogen. During screening of *Penaeus vannamei* shrimp from 3 commercial shrimp facilities in the United States for a panel of OIE-listed (n = 7) and nonlisted (n = 2) crustacean diseases, shrimp from these facilities tested positive for IHHNV. Nucleotide sequences of PCR amplicons showed 99%–100% similarity to IHHNV isolates from Latin America and Asia. The whole genome of the isolates also showed high similarity to type 2 infectious forms of IHHNV. Phylogenetic analysis using capsid gene and whole-genome sequences demonstrated that the isolates clustered with an IHHNV isolate from Ecuador. The detection of an OIE-listed crustacean pathogen in the United States highlights the need for biosecurity protocols in hatcheries and grow-out ponds to mitigate losses.

The *Penstylhamaparvovirus* species *Decapod penstylhamaparvovirus 1*, commonly known as infectious hypodermal and hematopoietic necrosis virus (IHHNV), is the smallest of known shrimp viruses belonging to the family *Parvoviridae*, subfamily *Hamaparvovirinae* (*1*,*2*). The virions are icosahedral, nonenveloped, measure 22–23 nm in size, and contain a single-stranded DNA genome ≈4.1 kb in length (*3*,*4*).

IHHNV was first reported in juveniles and subadults of blue shrimp (*Penaeus stylirostris*) in Hawaii in the early 1980s and caused mass deaths (*5*). The virus also caused large-scale deaths in blue shrimp in Mexico (*6*). The virus outbreak in *P. stylirostris* shrimp in Mexico in the early 1980s led to a transition in the captive breeding program from a more susceptible and physically larger shrimp species, *P. stylirostris* (a preferred cultured species in the mid-1980s), to the smaller but more tolerant *P. vannamei* shrimp (*7*). In the black tiger shrimp (*P. monodon*), another economically vital species, IHHNV is reported to cause asymptomatic infection and deformities (*4*,*8*). In a recent study, a farm-level IHHNV infection resulted in reduced growth performance, a higher food-conversion ratio, and a lower survival rate, which led to a production loss of approximately US $67,000 per hectare of farm gate value when ponds were stocked with IHHNV-infected postlarvae having high viral load compared with postlarvae with low viral load (*9*). This finding suggests that IHHNV remains an economically relevant viral pathogen in shrimp aquaculture.

Most of the genetic lines of *P. vannamei* shrimp farmed in Latin America and Asia today are claimed to be tolerant or resistant to the virus, and IHHNV is assumed to have no ill effect on the production parameters in these shrimp lines, although scientific evidence to support this assumption is lacking. Considering these genetic lines can tolerate high levels of IHHNV without displaying clinical manifestations of the disease, transboundary movement of shrimp broodstock and larvae from these lines might lead to widespread distribution of IHHNV unless rigorous biosecurity is practiced in hatcheries. Routine disease surveillance that adheres to the US Department of Agriculture and World Organisation for Animal Health (OIE) guidelines and diagnostics performed by the Aquaculture Pathology Laboratory (APL) and the National Veterinary Services

Author affiliations: The University of Arizona, Tucson, Arizona, USA (A.K. Dhar, R. Cruz-Flores, J. Ramos, M. Garfias, G. Lyons); US Department of Agriculture National Veterinary Services Laboratories, Ames, Iowa, USA (J. Warg, M.L. Killian); Molsoft, Inc., San Diego, California, USA (A. Orry)

DOI: https://doi.org/10.3201/eid2802.211874

Laboratories (NVSL) have helped to mitigate the spread of major pathogens in the United States. This success is reflected by the 26-year absence of the virus from all US-based farms until now.

During June 2019, *P. vannamei* shrimp samples from broodstock and postlarvae originating in commercial shrimp facilities in Texas and Florida were submitted to the APL at the University of Arizona for routine screening for viral, bacterial, and fungal pathogens. IHHNV was the only pathogen identified in shrimp from both facilities. Trace testing resulted in additional IHHNV-positive animals. We further characterized the IHHNV strains detected in the United States by genome sequencing and determined their genetic similarities to other IHHNV strains. Considering the history of economic losses caused by IHHNV over the past 4 decades, the recent detection of IHHNV in commercial facilities in the United States highlights the need to enhance biosecurity to prevent spread and future disease outbreaks caused by IHHNV or other diseases in shrimp aquaculture. The need to further enhance diagnostic testing and biosecurity measures was underscored by the subsequent detection of IHNNV in the United Kingdom and Canada, which was directly linked to commercial shrimp facilities in the United States (*10*,*11*). The objectives of this study were to elucidate the genomic characteristics of the virus to ensure that the IHHNV isolate is an infectious form of the virus and not a genome-integrated form, as well as to determine its genetic relatedness to IHHNV isolates described in the literature.

Materials and Methods

Sample Submission

Samples of *P. vannamei* shrimp were collected from commercial shrimp facilities, 2 in Texas (case nos. 19-428 and 19-644) and 1 in Florida (case no. 19-490) and submitted to the University of Arizona APL. Samples from case no. 19–428 consisted of 6 vials containing shrimp pleopods and postlarvae preserved in ethanol. Case no. 19-644 consisted of 4 bags of frozen whole shrimp. Case no. 19-490 consisted of pleopods in ethanol. We collected representative samples (≈30 mg) for nucleic acid extraction. Samples testing positive for IHHNV at the University of Arizona were submitted to the NVSL (Ames, Iowa, USA) for confirmation and further characterization.

Nucleic Acid Extraction and PCR

We extracted total nucleic acid from pools of pleopods and whole postlarvae (case nos. 19-428 and 19-490). For case no. 19-644, in which whole animals were submitted, we extracted total nucleic acid from tail muscle tissues (for screening systemic pathogens) or hepatopancreas (for screening enteric pathogens) by using the Maxwell 16 Cell LEV DNA and RNA Purification Kits (Promega, https://www.promega.com) or using the Maxwell 16 Instrument configured with LEV Hardware, according to manufacturer instructions.

We used pleopod DNA to screen for IHHNV (*12*), IHHNV–related genome-integrated sequence (*13*), and white spot syndrome virus (*14*). We used hepatopancreas DNA for PCR screening of *Baculovirus penaei* (according to an in-house method), necrotizing hepatopancreatitis bacterium (*15*), *Enterocytozoon hepatopenaei* (*16*), and acute hepatopancreatic necrosis disease (*17*). We evaluated pleopod and tail muscle RNA by using reverse transcription PCR tests for yellow head virus (*18*), Taura syndrome virus (*19*), and infectious myonecrosis virus (*20*). For all reactions, we used 1 μL of nucleic acids at a concentration range of 1–50 ng/μL.

We performed testing for IHHNV first by using the OIE-recommended 389 F/R primer pair, followed by the 309 F/R primer pair to detect the presence of the infectious form of IHHNV (*13*). We visualized PCR products on a 1.5% agarose gel to confirm presence of viral DNA. We used DNA from samples testing positive for IHHNV by PCR screening to amplify the nonstructural (NS1) and capsid protein (CP) genes. We amplified the NS1 gene by using 2 sets of primers to generate 2 amplicons with a 66-bp overlap (Table 1) and the CP gene by using the method of Robles-Sikisaka et al. (*21*), which yields a 1,088-bp amplicon.

Sanger Sequencing and Data Analysis

We column purified PCR amplicons by using the GeneJET PCR Purification Kit (ThermoFisher Scientific, https://www.thermofisher.com) according to manufacturer instructions. Purified PCR products were submitted to the University of Arizona Genetics Core for Sanger sequencing (Table 2). We aligned sequence data in Geneious Prime to generate a consensus sequence (*22*) and compared those sequences with published genomes using BLASTn (*23*).

Whole-Genome Sequencing and Bioinformatics Analyses

We extracted total nucleic acids from tissue homogenates for initial testing by using the MagMAX-Ambion kit 1836 on an automated MagMAX Express magnetic particle processor (ThermoFisher Scientific). We extracted additional DNA from tissue homogenates

Table 1. Primers used for the detection of the IHHNV genome in commercially raised *Penaeus vannamei* shrimp, Texas and Florida, United States, 2019*

Target gene	Primer name	Sequence, 5′ → 3′	Amplicon size, bp	Reference
NS1	389F	CGGAACACAACCCGACTTTA	389	(*13*)
NS1	389R	GGCCAAGACCAAAATACGAA		
NS1	IHHNV-309F	TCCAACACTTAGTCAAAACCAA	309	(*13*)
NS1	IHHNV-309R	TGTCTGCTACGATGATTATCCA		
NS1 (Left)	159_IH_NS1_S	AACTGACGAGTGAAGAGGCT	1295	This study
NS1 (Left)	1446_IH_NS1_AS	GTGTCCGGAGTATGTGATGT		This study
NS1 (Right)	1400_IH_NS1_S	GGACGAACGCCAAACTTCAC	1313	This study
NS1 (Right)	2698_IH_NS1_AS	ATCTGTGTGGGTCTGGTCC		This study
CP	CP1F	GATCACCAGCACGACTTCCT	1088	(*21*)
CP	CP2R	CGGGTATATATTGCACATCGAA		

*CP, capsid protein gene; IHHNV, infectious hypodermal and hematopoietic necrosis virus; NS1, nonstructural gene 1.

treated with Benzonase to reduce host DNA by using the DNeasy Blood and Tissue Kit (QIAGEN, https://www.quiagen.com). We prepared libraries by using the Ion Xpress Plus Fragment Library Kit (ThermoFisher Scientific) according to manufacturer instructions and templates by using the Ion 520 on the Ion Chef System, then sequenced by using an Ion 520 Chip on the Ion S5 System (ThermoFisher Scientific). We performed reference-based mapping (GenBank accession no. NC_002190) by using SeqMan NGen version 14 (DNASTAR, https://www.dnastar.com) with default parameters for automatic read trimming and assembly and verified alignments resulting in the final consensus sequence. The genomes (minus ends because random priming was used) of IHHNV from Texas and Florida were deposited in GenBank (accession nos. MN968717.1 and MN968716.1).

Phylogenetic Analyses

Initially, we inferred the phylogenetic analysis by using the neighbor-joining method (*24*) for the CP gene of IHHNV with 1,000 bootstraps. The tree was drawn to scale; branch lengths were in the same units as those of the evolutionary distances used to infer the phylogenetic tree. We computed the evolutionary distances (base substitutions per site) by using the maximum composite likelihood method (*25*). This analysis involved 32 nt sequences. All ambiguous positions were removed for each sequence pair (pairwise deletion option). A total of 995 positions were represented in the final dataset. We conducted evolutionary analyses in MEGA X (*25*).

We downloaded all available complete genomes from GenBank on November 1, 2019, for phylogenetic analysis. We inferred evolutionary history by using the maximum-likelihood method based on the Tamura-Nei model (*24*). We obtained initial tree(s) for the heuristic search automatically by applying neighbor-joining and BioNJ algorithms to a matrix of pairwise distances estimated by using the maximum-likelihood approach and then by selecting the topology with superior log likelihood value. The tree is drawn to scale; branch lengths are measured in the number of substitutions per site. The analysis involved 28 nt sequences. Codon positions included were 1st+2nd+3rd+Noncoding. We eliminated all

Table 2. Additional primers designed and used for Sanger sequencing of CP and NS1 genes of IHHNV, Texas and Florida, United States, 2019*

Target gene	Primer name	Sequence, 5′ → 3′
NS1	159_IH_NS1_S	AAC TGA CGA GTG AAG AGG CT
NS1	1446_IH_NS1_AS	GTG TCC GGA GTA TGT GAT GT
NS1	482_IHHNV_NS1_S	CCC CAA CAA ATA TCG CTG CG
NS1	511_IHHNV_NS1_S	AGA TCA CAT TCT ACC GTG GTG
NS1	342_IH_NS1_Seq_AS	ACTT GTA CTT ACA TTT GTA T
NS1	1400_IH_NS1_S	GGA CGA ACG CCA AAC TTC AC
NS1	2627_IH_NS1_Seq_S	CAA GCC CAA GGA AAA GAT CC
NS1	2390 CP_S	CTA CTG GGT ACC ACC AGC
NS1	2698 IH_NS1_AS	ATC TGT GTG GGT CTG GTC C
NS1	2540 IH_CP_S	AGG CCT CTT CCA AGA ATA CG
NS1	2682 IHHNV_NS1_AS	ACT TGA TCC TTC GGC GTG TT
NS1	2540 IH_CP_S	AGG CCT CTT CCA AGA ATA CG
NS1	2682 IHHNV_NS1_AS	ACT TGA TCC TTC GGC GTG TT
NS1	IHHNV-1942_F	GTC ACT AAT TAC AAA CCT GCA G
NS1	IHHNV-2020R	GCA TAT TGT CGT AGT CTG GT
CP	IHHNV-CP_S	ATG TGC GCC GAT TCA ACA AG
CP	IH_CP_Seq_S	CAT AAT CAA CTA TCA ACT AA
CP	IH_CP_Seq_AS	TGC CAA TGT TAC GTC GGT TTC C

*CP, capsid protein gene; IHHNV, infectious hypodermal and hematopoietic necrosis virus; NS1, nonstructural gene 1.

positions containing gaps and missing data. A total of 2,368 positions were represented in the final dataset. We conducted evolutionary analyses in MEGA7 (*25*).

Predicted Tertiary Structure of IHHNV CP

We performed all molecular modeling by using ICM-Pro desktop modeling software version 3.8 (MolSoft LLC, https://www.molsoft.com). Homology models of the CP gene of the IHHNV Texas isolate (case no. 19-428) and Florida isolate (case no. 19-490) were built by using the crystal structure of *Decapod penstylhamaparvovirus* 1 CP as a template (PDB code 3N7X) (*26*). First, we built a sequence alignment that demonstrated the amino acid sequences have very high homology (88%). Considering that the Texas isolates (case nos. 19-428 and 19-644) had identical amino acid sequences, we used only 1 for the analysis. The amino acid sequence of the isolates was then threaded onto the backbone of the full biomolecule capsid template structure by using ICM-Pro, and the model was energy minimized.

Results

Detection of IHHNV in Shrimp Hatchery– and Field-Collected Samples from Texas and Florida

We detected IHHNV in samples from Texas (case nos. 19-428 and 19-644) and Florida (case no. 19-490) by using the OIE-recommended conventional PCR-based diagnostic method (*12*) (Figure 1). These results confirmed the first detection of the virus in 2 commercial aquaculture facilities in the United States since 1993 (*27*).

Amplification and Sequencing of CP and NS1 Genes of IHHNV

The complete CP and NS1 genes of the IHHNV isolates from Texas and Florida were successfully amplified in overlapping fragments. The 2 amplicons together represent ≈88% of total length of IHHNV genome. We sequenced the NS1 and CP amplicons of both Texas and Florida IHHNV isolates. BLAST analysis demonstrated that both genes showed highest similarity to homologous genes of the IHHNV Ecuador strain (GenBank accession no. AY362548.1) (Table 3).

Whole-Genome Sequencing of IHHNV Texas and Florida Isolates

For isolate 19-490 from Florida, 22,166 sequences were assembled to generate a consensus sequence 3749 bp in length with a median depth of coverage of 1,036×. For isolates 19-428 and 19-644 from Texas, 118,348 sequences were assembled to generate a consensus sequence of 3,750 bp in length with a median depth of coverage of 5,825×. Consensus sequences represent the complete coding region of the virus. The 2 isolates shared 99.71% sequence identity. Furthermore, the sequences had 99.44% (Texas) and 99.52% (Florida) identity to IHHNV from Ecuador.

Phylogenetic Analysis

Phylogenetic analysis using only the CP gene sequences showed that IHHNV from both Texas and Florida formed a highly supported cluster with the Ecuador strain of IHHNV. This cluster represents the type 2 infectious form of IHHNV (Figure 2). The IHHNV in this cluster infect penaeid species including *P. vannamei*, *P. stylirostris*, and *P. monodon* shrimp. In the neighbor-joining phylogenetic tree, the type 3 clade is represented by IHHNV isolates from India, Tanzania, Madagascar, and Australia. These strains infect *P. monodon* shrimp, are noninfectious, and remain integrated into the *P. monodon* genome. The third genotype, type 1, is represented by isolates from the Philippines and Thailand that infect both *P. monodon* and *P. vannamei* shrimp. Whole-genome phylogeny showed equivalent results (tree not shown).

Predicted Tertiary Structure of CP of Texas and Florida IHHNV Isolates

The IHHNV Texas and Florida viruses detected have ≈88% amino acid sequence identity with the crystal structure of *Penaeus stylirostris densovirus* (*Pst*DNV) capsid (PDB code 3N7X) (Figure 3, panel A). The crystal structure of *Pst*DNV was determined to 2.5-Å resolution by x-ray crystallography and based on 299 out of 329 aa of capsid protein missed 30 N′-terminal aa (*26*) (Figure 3, panel B). Because of the high sequence similarity, the modeled structure showed key β-barrel motifs that are hallmarks of many icosahedral viruses.

Discussion

During routine disease surveillance, 3 Pacific white shrimp (*P. vannamei*) samples from 2 facilities in Texas and 1 facility in Florida tested positive for IHHNV. The samples were initially screened according to the OIE-recommended PCR protocol using the primer pair IHHNV 389 F/R (*13*). The results were further confirmed by using primer pair IHHNV 309 F/R. The amplicons 389 bp and 309 bp from all 3 cases were sequenced by Sanger methods; the nucleotide sequence of these amplicons showed a 99% identity with previously reported IHHNV sequences deposited in GenBank. Confirming the presence of IHHV by

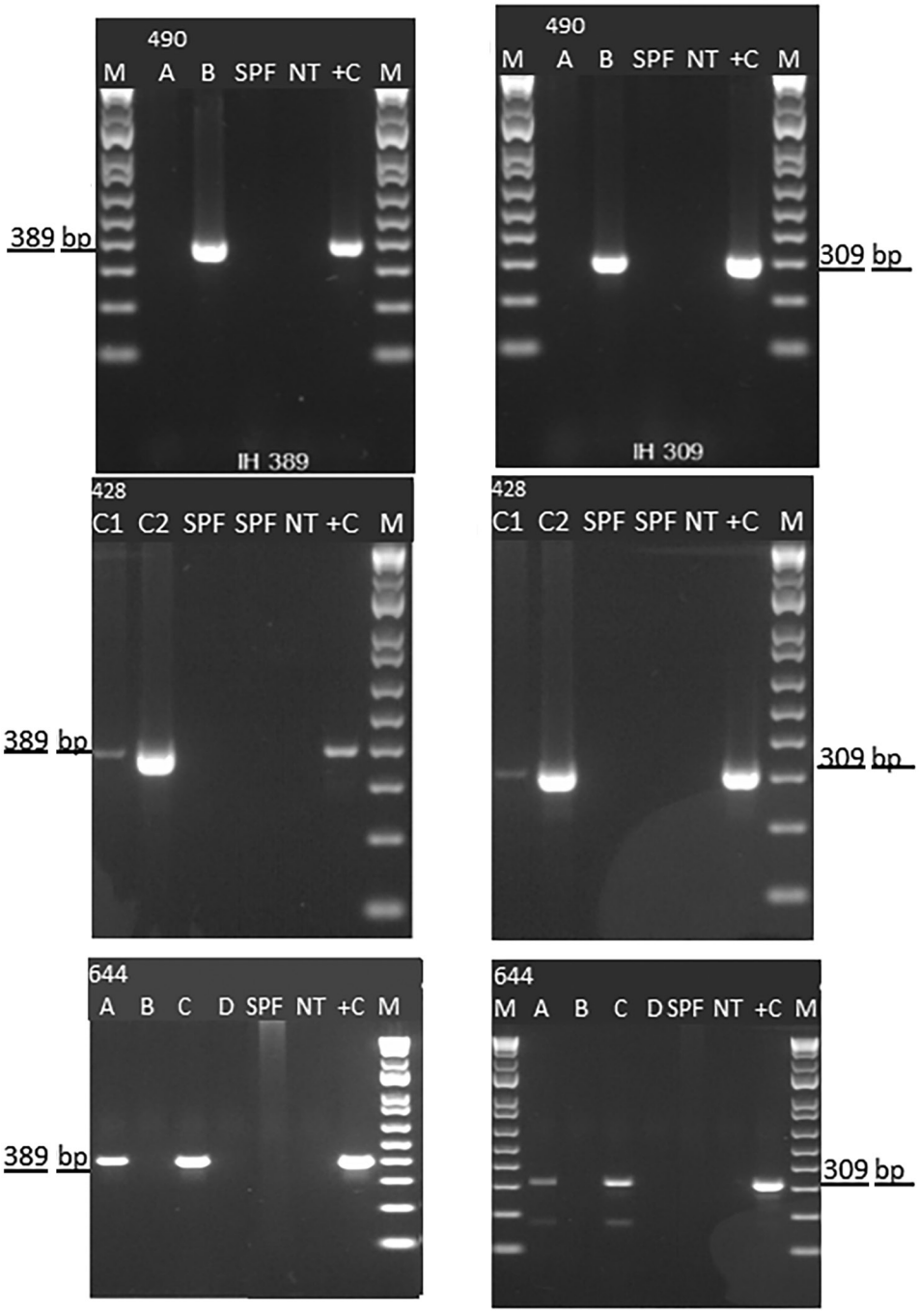

Figure 1. Detection of infectious hypodermal and hematopoietic necrosis virus (IHHNV) in *Penaeus vannamei* shrimp from the United States by conventional PCR, 2019. Agarose gel photographs show 389-bp IHHNV–specific amplicon (left column) and 309-bp IHHNV–specific amplicon (right column). Top row represents case number 19-490, *P. vannamei* broodstock samples originating in Florida (A and B). Middle row represents case number 19-428, *P. vannamei* post-larvae samples originating in Texas (C1 and C2). Bottom row represents case number 19-644, frozen *P. vannamei* shrimp originating from an indoor farm in Texas (A, B, C, and D). Lane M, 100-bp molecular weight marker (New England Biolabs, Inc., https://www.neb.com); lane SPF, specific pathogen-free *P. vannamei* shrimp; lane NT, no template control; lane +C, positive control for PCR.

PCR and genome sequencing is needed for diagnostic certainty, because genome-integrated sequences of IHHNV have been shown to be present in *P. monodon* and *P. vannamei* shrimp (*13*,*28*). Because IHHNV is an OIE-listed disease, once the virus was detected at the APL, an aliquot of all the nucleic acid and tissue samples was sent to the NVSL (Ames, Iowa, USA) for confirmation and further characterization. Under this testing scheme performed by APL and NVSL, IHHNV has been successfully kept at bay from US-based broodstock and hatchery operations for more than 2 decades. This recent detection, however, shows that stringent surveillance is needed to ensure facilities are free of disease before broodstock and larvae are moved across countries and continents.

The IHHNV genome contains 2 overlapping open reading frames encoding the nonstructural proteins NS1 and NS2 and a third open reading frame that

Table 3. Sequence similarity of CP and NS-1 genes of Texas and Florida IHHNV isolates to IHHNV Ecuador strain, 2019*

Case no.	CP identity, %	NS1 identity, %	Strain	GenBank accession no.
19–428-C2	99.36	99.06	Ecuador	AY362548.1
16–490-B	99.72	99.69	Ecuador	AY362548.1
19–644-A	99.36	99.65	Ecuador	AY362548.1
19–644-C	99.36	99.65	Ecuador	AY362548.1

*CP, capsid protein gene; IHHNV, infectious hypodermal and hematopoietic necrosis virus; NS1, nonstructural gene 1.

encodes the viral capsid protein (*3*,*4*,*7*). Together, these 3 gene segments comprise ≈88% of the complete genome. In this study, after IHHNV was detected in the 3 samples, the CP (990 bp) and NS1 (2440 bp) genes were amplified and sequenced. Subsequently, the near full-length genome of 2 isolates originating from 2 shrimp facilities in Texas and Florida were sequenced by using next-generation sequencing, generating contigs of 3,750 bases in length for the Texas isolates and 3,749 bases in length for the Florida isolates. All 3 cases (19-428, 19-490, and 19-644) had high sequence identity (99%) among them, as well as to an IHHNV isolate originating in Ecuador (GenBank accession no. AY362548.1). In 2003, two genotypes of IHHNV were described. At that time, type 1 strains were found in the Americas and East Asia (primarily the Philippines), and type 2 strains were detected in Southeast Asia (*29*). Since then, an additional genotype, type 3, has been described, and the geographic range of type 1 and type 2 viruses has spread worldwide. Phylogenetic analysis using the CP gene and full-length genomes indicate the recently detected IHHNV viruses from the United States form a strongly supported cluster with type 2 strains from the Americas. These strains represent the infectious forms of IHHNV and are clearly distinct from type 1 (infectious) and type 3 (noninfectious). (Figure 2). Since the virus was first described in the early 1980s, <50 complete genomes have been published in GenBank, and many of the genomes have incomplete metadata, including date of isolation or detection, which confounds interpretation of phylogenetic analysis. The lack of these critical pieces of information limits the ability to infer transmission of the virus on the basis of phylogeny alone. Epidemiologic information for the Texas isolates and the phylogenetic analysis suggest a link between the detections of IHHNV in Texas and Florida, supporting their close genetic relationship.

The close similarity at the whole-genome level and the phylogenetic data indicate that all sequences derive from a strain from Ecuador, suggesting a

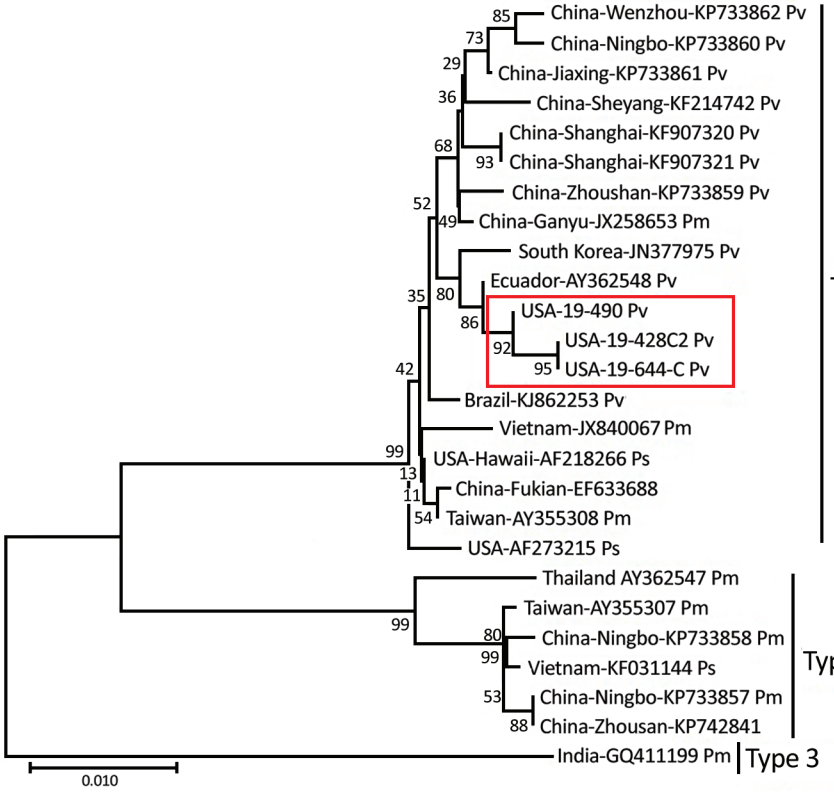

Figure 2. Evolutionary relationships of the infectious hypodermal and hematopoietic necrosis virus (IHHNV) strains (19-428, 19-490, and 19-644) recently detected in the United States and published capsid protein gene sequences. The recent IHHNV strains (red box) fall into the type 2 lineage. The evolutionary history was inferred by using the neighbor-joining method (*24*). The optimal tree with the sum of branch length = 0.20086053 is shown. The percentage of replicate trees in which the associated taxa clustered together in the bootstrap test (1,000 replicates) are shown next to the branches. The tree is drawn to scale, with branch lengths in the same units as those of the evolutionary distances used to infer the phylogenetic tree. The evolutionary distances were computed by using the maximum-likelihood method (*25*). Based upon full-genome phylogenetic analysis, the Texas and Florida IHHNV viruses appear to be related to a strain from Ecuador (GenBank accession no. AY362548.1). Scale bar indicates substitutions per site.

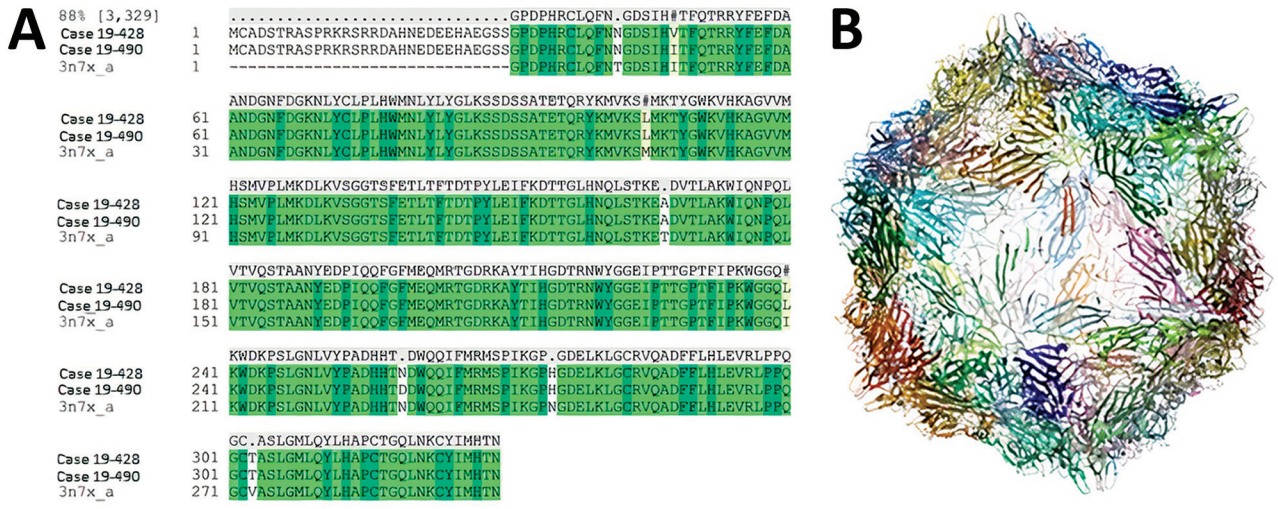

Figure 3. Alignment and structure of infectious hypodermal and hematopoietic necrosis virus (IHHNV) strains recently detected in Texas (19-428) and Florida (19-490), USA. A) Multiple alignment of amino acid sequence based on translation of the capsid protein gene of isolates with *Penaeus stylirostris densovirus* capsid protein sequence (PDB code 3N7X). B) Predicted tertiary structure of the isolates from Texas and Florida.

common origin for both Texas and Florida strains. This occurrence is not uncommon in shrimp aquaculture; other viral pathogens such as Taura syndrome virus and infectious myonecrosis virus have been traced back to their original source (*30*,*31*). The transboundary movement of shrimp has gone hand-in-hand with the expansion of shrimp farming and will not cease anytime soon. Investment in newer, more sensitive diagnostic methodologies based on CRISPR, digital droplet PCR, and next-generation sequencing approaches could help limit the spread of pathogens (*32*,*33*). In addition, rigorous screening of animals for IHHNV and other pathogens is necessary to make moving shrimp safer and thereby make the industry more sustainable and resilient in the long run. This rigorous screening would entail collaborative efforts between shrimp producers, diagnostic and research institutions, and corresponding government entities.

To determine whether the predicted amino acid sequences of the IHHNV capsid protein from Texas and Florida isolates can conform an icosahedral symmetry, homology modeling was performed with a reference tertiary structure of another IHHNV isolate, *Pst*HPV-1, for which a crystal structure is available in the Protein Data Bank (PDB code 3N7X). Although a sequence identity of 88% between the reference strains and US strains might seem low, this identity is because of the absence of 20 aa from the N′-terminal of the reference strain. The analysis of the same sections (excluding the first 20 aa from the N′-terminal of US strains) of the CP of the 3 strains demonstrates a sequence identity of 97.5%. The tertiary structure showed that IHHNV Texas and Florida isolates can conform an icosahedral symmetry, as expected for a parvovirus infectious virion (*26*). Thus, the predicted tertiary structure analysis supports the phylogenetic data that IHHNV Texas and Florida isolates represent an infectious form of the virus and not a type 3 strain.

Although it might seem redundant at first sight to perform protein modeling, we considered it fundamental for the study to confirm the capsid protein coding regions were not endogenous viral elements (EVEs). These EVEs are well characterized in *P. monodon* shrimp, but they have not been reported as frequently in *P. vannamei* shrimp. Furthermore, the EVEs from *P. vannamei* shrimp might contain regions of the IHHNV genome that are different to the regions reported in *P. monodon* shrimp. Because of the lack of frozen shrimp samples, we could not delineate the pathogenicity of the virus in experimental bioassay, and hence could not perform histopathology to assess cellular manifestation of the viral infection; the in silico analysis of IHHNV capsid protein data gave further confidence that these strains represented an infectious form of IHHNV and not an EVE. A combination of protein modeling, whole-genome sequencing, PCR, and phylogenetic analysis are complementary in nature and sufficient to deem the IHHNV strain detected in the United States in 2019 an infectious type 2 strain of the virus.

IHHNV is well known to be endemic in shrimp-producing countries in the Americas, Asia, and Australia (*7*). IHHNV is also well established in wild shrimp populations in the Gulf of Mexico (*21*). In

the United States, however, the virus had not been reported in farmed shrimp since 1993 (*27*). Over the past 4 decades, as shrimp farming evolved from subsistence levels of farming to an intensive culture system worldwide, infectious diseases have emerged and spread regularly. The spread of diseases has been further exacerbated by the movement of broodstock and post-larvae across countries and continents. The movement of infected shrimp has played a critical role in the spread of pathogens like white spot syndrome virus, Taura syndrome virus, and IHHNV (*34*). The origin of the IHHNV isolates described in this study remains unknown, but the data suggest these isolates could have originated in Latin America. This finding highlights the need to keep following strict biosecurity protocols, including disease surveillance in shrimp hatcheries and grow-out ponds, to prevent further introduction of IHHNV or other OIE-listed and nonlisted pathogens in shrimp facilities in the United States and elsewhere.

Acknowledgments

We would like to thank Jasmine Millabas, Tiffany Bledsoe, Gwendolyn Mioduszewska, Angela Cruz, and Kerrie Franzen for their aid in sample processing and molecular procedures.

Funding for this research was provided by the Aquaculture Pathology Laboratory Disease Diagnostic Fund. Partial funding was provided by the College of Agriculture & Life Sciences of The University of Arizona to A.K.D.

About the Author

Dr. Dhar is an associate professor and director of the Aquaculture Pathology Laboratory in the School of Animal and Comparative Biomedical Sciences, University of Arizona, Tucson, Arizona, and an OIE Expert of Crustacean Diseases. His expertise involves developing diagnostics, oral vaccines, and therapies against infectious diseases in shrimp and fin fish.

References

1. Tijssen P, Agbandje-McKenna M, Almendral J, Bergoin M, Flegel T, Hedman K, et al. Parvoviridae. In: Murphy FA, Fauquet C, Bishop D, editors. Virus taxonomy: ninth report of the international committee on taxonomy of viruses. Amsterdam: Elsevier; 2012. p. 405–25.
2. Pénzes JJ, Pham HT, Chipman P, Bhattacharya N, McKenna R, Agbandje-McKenna M, et al. Molecular biology and structure of a novel penaeid shrimp densovirus elucidate convergent parvoviral host capsid evolution. Proc Natl Acad Sci U S A. 2020;117:20211–22. https://doi.org/10.1073/pnas.2008191117
3. Shike H, Dhar AK, Burns JC, Shimizu C, Jousset FX, Klimpel KR, et al. Infectious hypodermal and hematopoietic necrosis virus of shrimp is related to mosquito brevidensoviruses. Virology. 2000;277:167–77. https://doi.org/10.1006/viro.2000.0589
4. Dhar AK, Robles-Sikisaka R, Saksmerprome V, Lakshman DK. Biology, genome organization, and evolution of parvoviruses in marine shrimp. In: Advances in virus research, 1st ed. Amsterdam: Elsevier Inc.; 2014. p. 85–139.
5. Lightner DV, Redman RM, Bell T, Brock J. Detection of IHHN virus in *Penaeys stylirostris* and *P. vannamei* imported into Hawaii. J World Maric Soc. 1983;225:212–25.
6. Bell TA, Lightner DV. IHHN virus: Infectivity and pathogenicity studies in *Penaeus stylirostris* and *Penaeus vannamei*. Aquaculture. 1984;38:185–94. https://doi.org/10.1016/0044-8486(84)90142-X
7. Dhar AK, Cruz-Flores R, Caro LFA, Siewiora HM, Jory D. Diversity of single-stranded DNA containing viruses in shrimp. Virusdisease. 2019;30:43–57. https://doi.org/10.1007/s13337-019-00528-3
8. Flegel TW. Detection of major penaeid shrimp viruses in Asia, a historical perspective with emphasis on Thailand. Aquaculture. 2006;258:1–33. https://doi.org/10.1016/j.aquaculture.2006.05.013
9. Sellars MJ, Cowley JA, Musson D, Rao M, Menzies ML, Coman GJ, et al. Reduced growth performance of black tiger shrimp (*Penaeus monodon*) infected with infectious hypodermal and hematopoietic necrosis virus. Aquaculture. 2019;499:160–6. https://doi.org/10.1016/j.aquaculture.2018.09.032
10. Centre for Environment Fisheries and Aquaculture Science. International database on aquatic animal disease: infectious hypodermal and haematopoietic necrosis, United Kingdom [Immediate notification 20/08/19]. 2019 [cited 2021 Jul 11]. https://www.cefas.co.uk/international-database-on-aquatic-animal-diseases/abstract/?id=1938
11. Government of Canada. Fact sheet—infectious hypodermal and haematopoitic necrosis. 2019 [cited 2021 Jul 11]. https://inspection.canada.ca/animal-health/aquatic-animals/diseases/immediately-notifiable/infectious-hypodermal-and-haematopoitic-necrosis/eng/1562271424092/1562271424389#shr-pg0
12. Tang KFJ, Lightner DV. Infectious hypodermal and hematopoietic necrosis virus (IHHNV)-related sequences in the genome of the black tiger prawn *Penaeus monodon* from Africa and Australia. Virus Res. 2006;118:185–91. https://doi.org/10.1016/j.virusres.2006.01.003
13. Tang KFJ, Navarro SA, Lightner DV. PCR assay for discriminating between infectious hypodermal and hematopoietic necrosis virus (IHHNV) and virus-related sequences in the genome of *Penaeus monodon*. Dis Aquat Organ. 2007;74:165–70. https://doi.org/10.3354/dao074165
14. Durand SV, Lightner DV. Quantitative real time PCR for the measurement of white spot syndrome virus in shrimp. J Fish Dis. 2002;25:381–9. https://doi.org/10.1046/j.1365-2761.2002.00367.x
15. Aranguren LF, Tang KFJ, Lightner DV. Quantification of the bacterial agent of necrotizing hepatopancreatitis (NHP-B) by real-time PCR and comparison of survival and NHP load of two shrimp populations. Aquaculture. 2010;307:187–92. https://doi.org/10.1016/j.aquaculture.2010.07.022
16. Tang KFJ, Pantoja CR, Redman RM, Han JE, Tran LH, Lightner DV. Development of in situ hybridization and PCR assays for the detection of *Enterocytozoon hepatopenaei* (EHP), a microsporidian parasite infecting penaeid shrimp. J Invertebr Pathol. 2015;130:37–41. https://doi.org/10.1016/j.jip.2015.06.009

17. Han JE, Tang KF, Tran LH, Lightner DV. Photorhabdus insect-related (Pir) toxin-like genes in a plasmid of *Vibrio parahaemolyticus*, the causative agent of acute hepatopancreatic necrosis disease (AHPND) of shrimp. Dis Aquat Organ. 2015;113:33–40. https://doi.org/10.3354/dao02830
18. Aranguren LF, Tang KFJ, Lightner DV. Protection from yellow head virus (YHV) infection in *Penaeus vannamei* pre-infected with Taura syndrome virus (TSV). Dis Aquat Organ. 2012;98:185–92. https://doi.org/10.3354/dao02448
19. Tang KFJ, Wang J, Lightner DV. Quantitation of Taura syndrome virus by real-time RT-PCR with a TaqMan assay. J Virol Methods. 2004;115:109–14. https://doi.org/10.1016/j.jviromet.2003.09.021
20. Andrade TPD, Srisuvan T, Tang KFJ, Lightner DV. Real-time reverse transcription polymerase chain reaction assay using TaqMan probe for detection and quantification of infectious myonecrosis virus (IMNV). Aquaculture. 2007;264:9–15. https://doi.org/10.1016/j.aquaculture. 2006.11.030
21. Robles-Sikisaka R, Bohonak AJ, McClenaghan LR Jr, Dhar AK. Genetic signature of rapid IHHNV (infectious hypodermal and hematopoietic necrosis virus) expansion in wild *Penaeus* shrimp populations. PLoS One. 2010;5:e11799. https://doi.org/10.1371/journal.pone.0011799
22. Kearse M, Moir R, Wilson A, Stones-Havas S, Cheung M, Sturrock S, et al. Geneious Basic: an integrated and extendable desktop software platform for the organization and analysis of sequence data. Bioinformatics. 2012;28:1647–9. https://doi.org/10.1093/bioinformatics/bts199
23. Altschul SF, Gish W, Miller W, Myers EW, Lipman DJ. Basic local alignment search tool. J Mol Biol. 1990;215:403–10. https://doi.org/10.1016/S0022-2836(05)80360-2
24. Tamura K, Nei M. Estimation of the number of nucleotide substitutions in the control region of mitochondrial DNA in humans and chimpanzees. Mol Biol Evol. 1993;10:512–26.
25. Kumar S, Stecher G, Tamura K. MEGA7: molecular evolutionary genetics analysis version 7.0 for bigger datasets. Mol Biol Evol. 2016;33:1870–4. https://doi.org/10.1093/molbev/msw054
26. Kaufmann B, Bowman VD, Li Y, Szelei J, Waddell PJ, Tijssen P, et al. Structure of *Penaeus stylirostris densovirus*, a shrimp pathogen. J Virol. 2010;84:11289–96. https://doi.org/10.1128/JVI.01240-10
27. Nunan LM, Poulos BT, Lightner DV. Use of polymerase chain reaction for the detection of infectious hypodermal and hematopoietic necrosis virus in Penaeid shrimp. Mar Biotechnol (NY). 2000;2:319–28. https://doi.org/10.1007/s101260000003
28. Saksmerprome V, Jitrakorn S, Chayaburakul K, Laiphrom S, Boonsua K, Flegel TW. Additional random, single to multiple genome fragments of *Penaeus stylirostris densovirus* in the giant tiger shrimp genome have implications for viral disease diagnosis. Virus Res. 2011;160:180–90. https://doi.org/10.1016/j.virusres. 2011.06.010
29. World Organisation for Animal Health (OIE). Infection with infectious hypodermal and haematopoietic necrosis virus. In: Manual of diagnostic tests for aquatic animals, 4th ed. Paris, France: Office International des Epizooties; 2017. p. 1–18.
30. Senapin S, Phewsaiya K, Briggs M, Flegel TW. Outbreaks of infectious myonecrosis virus (IMNV) in Indonesia confirmed by genome sequencing and use of an alternative RT-PCR detection method. Aquaculture. 2007;266:32–8. https://doi.org/10.1016/j.aquaculture.2007.02.026
31. Dhar AK, Lakshman DK, Amundsen K, Robles-Sikisaka R, Kaizer KN, Roy S, et al. Characterization of a Taura syndrome virus isolate originating from the 2004 Texas epizootic in cultured shrimp. Arch Virol. 2010;155:315–27. https://doi.org/10.1007/s00705-009-0584-5
32. Chaijarasphong T, Thammachai T, Itsathitphaisarn O, Sritunyalucksana K, Suebsing R. Potential application of CRISPR-Cas12a fluorescence assay coupled with rapid nucleic acid amplification for detection of white spot syndrome virus in shrimp. Aquaculture. 2019;512:734340. https://doi.org/10.1016/j.aquaculture.2019.734340
33. Sullivan TJ, Dhar AK, Cruz-Flores R, Bodnar AG. Rapid, CRISPR-based, field-deployable detection of white spot syndrome virus in shrimp. Sci Rep. 2019;9:19702. https://doi.org/10.1038/s41598-019-56170-y
34. Lightner V. Biosecurity in shrimp farming: pathogen exclusion through use of SPF stock and routine surveillance. J World Aquacult Soc. 2005;36:230–48. https://doi.org/10.1111/j.1749-7345.2005.tb00328.x

Address for correspondence: Arun K. Dhar, Aquaculture Pathology Laboratory, School of Animal and Comparative Biomedical Sciences, Bldg 90, The University of Arizona, 1117 E Lowell St, Tucson, AZ 85721, USA; email: adhar@email.arizona.edu

Wild Boars as Reservoir of Highly Virulent Clone of Hybrid Shiga Toxigenic and Enterotoxigenic *Escherichia coli* Responsible for Edema Disease, France

Alexandre Perrat, Priscilla Branchu, Anouk Decors, Silvia Turci, Marie-Hélène Bayon-Auboyer, Geoffrey Petit, Vladimir Grosbois, Hubert Brugère, Frédéric Auvray, Eric Oswald

Edema disease is an often fatal enterotoxemia caused by specific strains of Shiga toxin–producing *Escherichia coli* (STEC) that affect primarily healthy, rapidly growing nursery pigs. Recently, outbreaks of edema disease have also emerged in France in wild boars. Analysis of STEC strains isolated from wild boars during 2013–2019 showed that they belonged to the serotype O139:H1 and were positive for both Stx2e and F18 fimbriae. However, in contrast to classical STEC O139:H1 strains circulating in pigs, they also possessed enterotoxin genes *sta1* and *stb*, typical of enterotoxigenic *E. coli*. In addition, the strains contained a unique accessory genome composition and did not harbor antimicrobial-resistance genes, in contrast to domestic pig isolates. These data thus reveal that the emergence of edema disease in wild boars was caused by atypical hybrid of STEC and enterotoxigenic *E. coli* O139:H1, which so far has been restricted to the wildlife environment.

Author affiliations: Institut de Recherche en Santé Digestive, Université de Toulouse, Institut National de la Santé et de la Recherche Médicale, Institut National de Recherche pour l'Agriculture, l'Alimentation et l'Environnement (INRAE), Ecole Nationale Vétérinaire de Toulouse, Université Paul Sabatier, Toulouse, France (A. Perrat, P. Branchu, H. Brugère, F. Auvray, E. Oswald); Office Français de la Biodiversité, Orléans, France (A. Decors); Labocea, Ploufragan, France (S. Turci, M.-H. Bayon-Auboyer); Université Clermont Auvergne INRAE, VetAgro Sup, Unité Mixte de Recherche (UMR) Epidémiologie des Maladies Animales et Zoonotiques, Saint-Genès-Champanelle, France (G. Petit); UMR Animal-Santé-Territoires-Risques-Ecosystèmes, Centre de Coopération Internationale en Recherche Agronomique pour le Développement, INRAE, Montpellier, France (G. Petit, V. Grosbois); Centre Hospitalier Universitaire de Toulouse, Hôpital Purpan, Toulouse (E. Oswald)

DOI: https://doi.org/10.3201/eid2802.211491

First described in 1938, edema disease (ED) causes edema in various tissues of the domestic pig (*Sus scrofa domesticus*), characterized by neurologic disorders (ataxia, convulsions, incoordination, and lateral decubitus with paddling of limbs); swollen eyelids, forehead, and ears; a peculiar squeal; and sometimes sudden death (all usually without diarrhea or fever) (*1*). More commonly affecting pigs within 2 weeks after weaning, this disease can also occur in older pigs. The disease is the result of infection with a subset of Shiga toxin (Stx)–producing *Escherichia coli* (STEC), expressing plasmid-encoded F18 fimbriae and α-hemolysin (*hly*) and prophage-encoded Stx2e subtype (*2*,*3*). After F18-mediated STEC adhesion to the intestinal mucosa, Stx2e reaches the bloodstream and causes vascular damage in several target organs, commonly the brain and gastrointestinal tract (*4*,*5*). In Europe, ED-causing STEC strains mainly belong to the following serotypes (in order of importance): O139:K82:H1, O141:K85:H4, and O138:K81:NM (*1*,*6*,*7*). Outbreaks of ED caused by the O147 serogroup have also been reported in the United States (*8*).

Neonatal enteric colibacillosis and postweaning diarrhea (PWD) are other crucial factors contributing to death in nursery pigs in global swine production. These diseases are caused by enterotoxigenic *E. coli* (ETEC), which produce heat-stable toxins (STa, STb), heat-labile toxins (LT), or both. These toxins bind to specific receptors of the intestinal epithelial cells and cause secretion of water and electrolytes into the intestinal lumen. ETEC causing neonatal diarrhea typically produce F4, F5, F6, or F41 fimbriae, whereas those causing PWD produce either F4 or F18 fimbriae (*1*,*9*). The F4 receptors are expressed on porcine enterocytes irrespective of age, whereas F18

receptors are not fully expressed in pigs <3 weeks of age (*10*). Most PWD F4-positive ETEC are of the serogroup O149, whereas F18-positive ETEC belong to many serogroups, including O138, O139, O141, O147, and O157, because the F4 or F18 fimbriae gene cluster and enterotoxin genes are encoded on conjugative plasmids that result in their spread (*1*). Most of these strains are also hemolytic because the *hly* operon is frequently associated with fimbriae gene clusters on conjugative plasmids (*11*–*13*). Some F18-positive strains produce both enterotoxins and Stx2e (*1*,*11*) and thus belong to a hybrid STEC–ETEC pathotype.

In 2013, a total of 109 wild boars (*S. scrofa scrofa*) were suspected of being affected by ED in the southeast of France, thus corresponding to the first ED cases reported in wild boars living in natural environmental conditions (*14*). Other ED outbreaks occurred later in 2014 (51 cases), 2015 (26 cases), and 2016 (5 cases), as well as in 2019 (7 cases), in the same region. The boars were mainly 4–6 months old, corresponding to the weaning period in this species (*15*). Given the increase of the wild boar population in Europe in the last decades (*16*), which can lead to more frequent contact with domestic pigs and increasing risk for disease transmission (*17*), we characterized the strains responsible for the emergence of ED in wild boars. To this aim, we sequenced the whole genome of 28 wild boar STEC O139:H1 isolates from the different ED outbreaks and performed a genetic and genomic comparison with STEC O139:H1 and non-O139:H1 strains isolated from domestic pigs and other sources worldwide.

Materials and Methods

Bacterial Strains Analyzed

We analyzed a collection of 28 STEC O139:H1 strains isolated in France from the intestinal content or lymph nodes, after necropsy, of wild boars with clinical signs and lesions consistent with ED, along with 16 STEC O139:H1 and 6 STEC O141:H4 strains isolated in France from pigs affected by ED (Appendix 1 Table 1, https://wwwnc.cdc.gov/EID/article/28/2/21-1491-App1.xlsx). We also included in this study an additional 168 *E. coli* strains isolated from pigs or other sources, whose genome sequences were retrieved from the GenBank (*18*) and Enterobase (*19*) databases (Appendix 1 Table 2).

Whole-Genome Sequencing

For short-read sequencing, we purified genomic DNA from 200 μL of lysogeny broth overnight cultures by using MagNA Pure 96 DNA and Viral NA Small volume Kit (Roche Molecular Systems Inc., https://www.roche.com). We then sequenced genomic DNA and generated 2 × 150 bp paired-end reads by using Illumina NextSeq500 (IntegraGen SA, https://integragen.com) with 80× coverage from libraries we obtained by enzymatic fragmentation by using a 5× whole-genome sequencing fragmentation mix kit (Enzymatics Inc., https://www.enzymatics.com).

We performed long-read sequencing for 3 strains (P13-6, P15-25, and W13-16) by using PacBio RSII system (GenoScreen SAS, https://www.genoscreen.fr) with 50× coverage. We extracted genomic DNA by using Gentra Puregene Yeast/Bact Kit (QIAGEN, https://www.qiagen.com) and prepared the libraries according to the protocol of SMRTbell Express Template Prep Kit 2.0 (PacBio, https://www.pacb.com) with selection of fragment size at 15–20 kb. We conducted an additional paired-end 2 × 100-bp Illumina MiSeq sequencing (GenoScreen SAS) with 50× coverage for these 3 strains by using genomic DNA extracted with Wizard Genomic DNA Purification Kit (Promega Corporation, https://www.promega.com) and libraries we prepared with a Nextera XT DNA Library Preparation Kit (Illumina, https://www.illumina.com).

Genome Assembly and Phylogeny

We trimmed the raw sequencing reads by using TrimGalore 0.6.5 (http://www.bioinformatics.babraham.ac.uk/projects/trim_galore), then assembled them with Unicycler 0.4.8.0 (*20*), excluding contigs <100 bp, with a normal bridging mode. We combined long reads with short reads during assembly. We annotated each assembly by using Prokka 1.14.5 (*21*) with a similarity e-value cutoff of 1^{-6}. We aligned the core genomes by using Roary 3.13.0 (*22*), with a minimum percentage identity of 95% for blastp (https://blast.ncbi.nlm.nih.gov/Blast.cgi?PAGE=Proteins), a minimum percentage of 99% isolates for genes included in the core genome, and Markov clustering inflation value of 1.5. For the O139-specific tree, we mapped the raw reads against the *E. coli* K-12 MG1655 reference strain by using Bowtie2 (*23*) and performed single-nucleotide polymorphism (SNP) calling by using BioNumerics 7.6.3 (bioMérieux, https://www.biomerieux.com), removing positions with ≥1 unreliable or ambiguous base and a minimum absolute coverage of 5. We generated the minimum-spanning tree with BioNumerics 7.6.3 and performed maximum-likelihood phylogenetic trees with IQ-TREE 1.5.5 (*24*). We built the tree of the entire collection by using a generalized time-reversible substitution model with an empirical base frequency and a FreeRate model of site heterogeneity (*25*,*26*) with 10 categories, whereas

construction of the O139-specific tree applied a k3Pu substitution model (*27*), after we used ModelFinder (*28*) to identify the best-fitting model according to the Akaike information criterion. We compared the phylogenetic tree with the resistance factors and analyzed the phylogeography of the strains by using Microreact (*29*) and annotated the O139-specific tree by using FigTree 1.4.4 (https://github.com/rambaut/figtree). We produced chromosomal and plasmid maps by using BIG 0.95 (*30*). We submitted all sequence data generated in this study to the National Center for Biotechnology Information's BioProject database (accession no. PRJNA741404).

Composition of the Accessory Genome, Resistance Genes, and Virulence Genes

We detected virulence genes by using VirulenceFinder 2.0.3 (*31*) with a minimum percentage identity of 90% and resistance genes by using BioNumerics 7.6.3 with a minimum percentage identity of 85%, both with a minimum length of 60%. We subtyped F18 fimbriae by using amino acid sequence analysis of the major FedA subunit, including positions 122 and 123 (glycine and serine for F18ab, proline and alanine for F18ac) (*2*).

We analyzed the relationship between strains on the basis of accessory genome composition by using a t-distributed stochastic neighbor embedding (t-SNE) machine learning algorithm with Panini v1 (https://gitlab.com/cgps/panini/bhtsne), with a gradient accuracy (theta) of 0.5 and an auto perplexity (p). Using the table of genes present or absent in the strains of the entire collection outputted from the Roary pipeline, we conducted pan-GWAS analysis to measure the statistical significance of the association of certain genes with the clade of wild boar strains by using Scoary 1.6.16 (https://github.com/AdmiralenOla/Scoary). We retained the annotated genes with a p value $<2.21 \times 10^{-12}$ by Fisher exact test.

Stx2e Phages, Plasmids, and Pairwise Comparison

We detected phages by using Phaster (*32*). We extracted the sequences corresponding to the Stx2e phage and circular contigs (plasmids) from hybrid assemblies. We retrieved the closest similar plasmid sequence available online from the National Center for Biotechnology Information nucleotide collection (nr/nt) database (accessed April 1, 2020). We then compared Stx2e phage and plasmid sequences by using blastn 2.9.0 (https://blast.ncbi.nlm.nih.gov/Blast.cgi?PROGRAM=blastn&PAGE_TYPE=BlastSearch&LINK_LOC=blasthome) with default parameters, along with GenBank annotated sequences, to create pairwise comparison in EasyFigure 2.2.3 (*33*).

Antimicrobial-Susceptibility Testing

We determined antimicrobial drug susceptibility profiles of the 3 PacBio-sequenced strains (P13-6, P15-25, and W13-16) and 3 other *E. coli* strains (W14-3, W15-17, and W19-4) by using the Vitek 2 system (bioMérieux). We interpreted MIC results for ampicillin, ticarcillin, piperacillin/tazobactam, cefalotin, cefoxitin, cefotaxime, ceftazidime, ertapenem, imipenem, amikacin, gentamicin, tobramycin, nalidixic acid, ciprofloxacin, ofloxacin, nitrofurantoin, trimethoprim/sulfamethoxazole, erythromycin, tetracycline, and chloramphenicol according to the 2020 criteria of the European Committee on Antimicrobial Susceptibility Testing (https://www.eucast.org).

Results

Core Genome–Based Phylogenetic Analysis

We performed short-read whole-genome sequence analysis of 28 STEC O139:H1 strains isolated from wild boars that had clinical signs and lesions consistent with ED during multiple outbreaks that occurred in the southeast of France: in the Ardèche Department in 2013 (n = 5), 2014 (n = 6), 2015 (n = 8), and 2016 (n = 2) and in the Drôme Department in 2019 (n = 7) (Appendix 1 Table 1). These strains were phylogenetically close based on SNP analysis (Figure 1), most of them showing <10 SNP differences considered as the threshold to determine strain relatedness (*34*). The most genetically distant isolates corresponded to an Ardèche isolate from 2016 and 6 Drôme isolates from 2019 (Figure 1), suggesting an increase of genetic variability over time, space, or both. We enlarged the phylogenetic analysis to include 35 *E. coli* O139:H1 isolates from domestic pigs of worldwide origin, including France. The core genome–based maximum-likelihood tree showed that the 28 wild boars STEC O139:H1 strains clustered into a distinct clade (named WB1) (Figure 2). This first level of analysis indicated that the STEC strains isolated from the different ED outbreaks in wild boars corresponded to a single *E. coli* clone of serotype O139:H1.

Genomic Features of Wild Boar *E. coli* O139:H1 Compared to Porcine *E. coli* O139:H1 and O141:H4

We used long-read sequencing for strain W13-16 to provide a closed genome for a representative strain of STEC O139:H1 isolated from wild boars (chromosome and plasmid maps in Appendix 2 Figure, https://wwwnc.cdc.gov/EID/article/28/2/21-1491-App2.pdf). We compared that genome with the long-read sequenced genomes obtained for pig ED

STEC strains P15-25 and P13-6, which belonged to the 2 serotypes most commonly reported in ED cases in France (O139:H1 for P15-25, O141:H4 for P13-6) (*6*). Strain W13-16 contained 2 plasmids of 54.7 and 83.4 kb, whereas P15-25 contained 1 plasmid of 77.5 kb and P13-6 contained 9 plasmids with sizes ranging from 3.1 to 226.4 kb (Table; Appendix 2 Figure).

The chromosome of the STEC W13-16 strain carried an Stx2e prophage (Table; Appendix 2 Figure) whose sequence was highly similar to those of the 2 porcine STEC O139:H1 and O141:H4 strains, except for 2 phage regions that were deleted in both STEC O139:H1 isolates, in contrast to STEC O141:H4 (Figure 3). These 2 regions contained several late genes

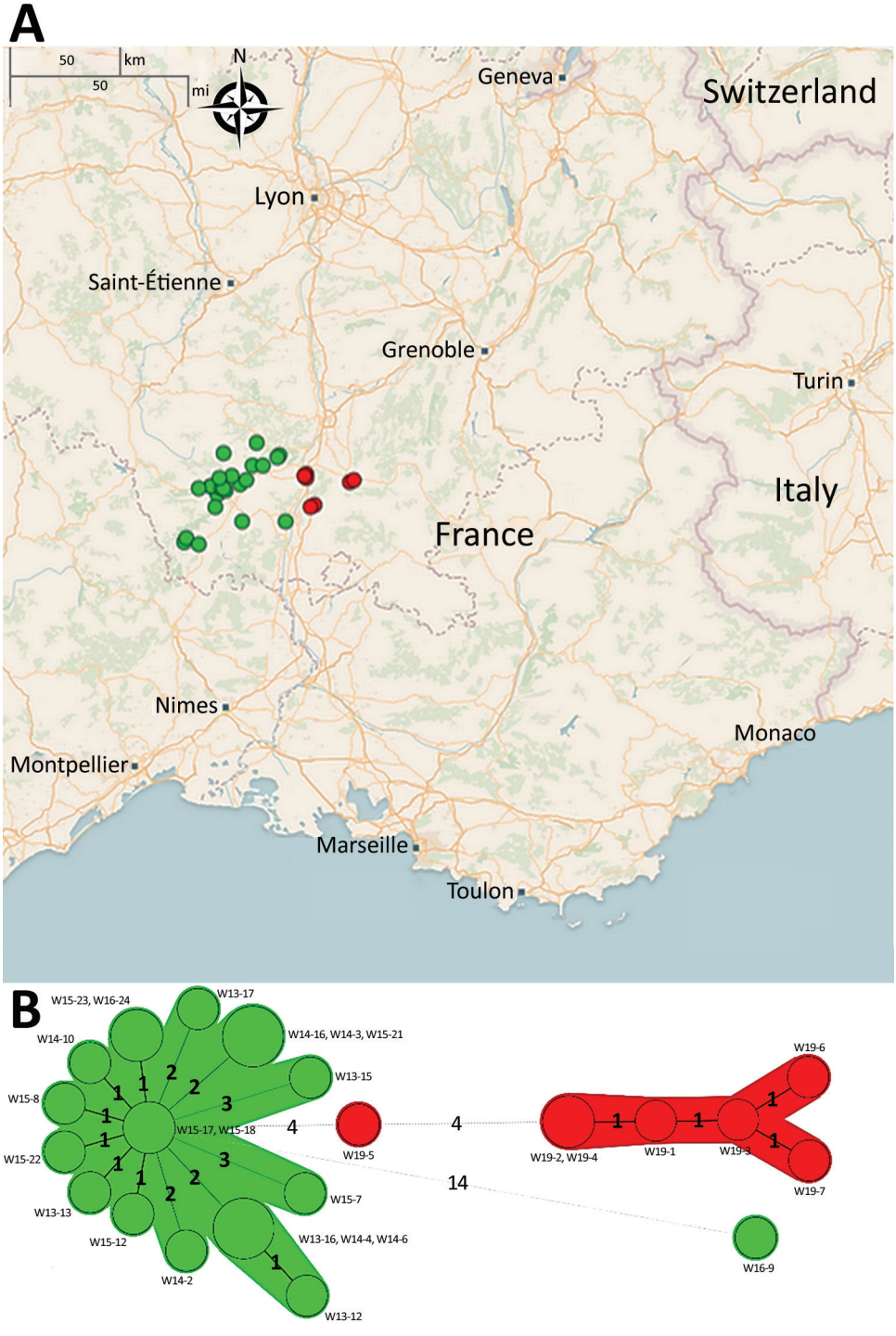

Figure 1. Geographic location of 28 wild boar *Escherichia coli* O139:H1 strains in France (A) and phylogeny represented as a minimum spanning tree (B) using BioNumerics 7.6.3 (bioMérieux, https://www.biomerieux.com). Sizes of the discs represent number of isolates. Colors of the discs represent year of isolation (green, 2013–2016; red, 2019). Numbers of differing single-nucleotide polymorphisms (SNPs) are indicated on connecting lines between the nodes.

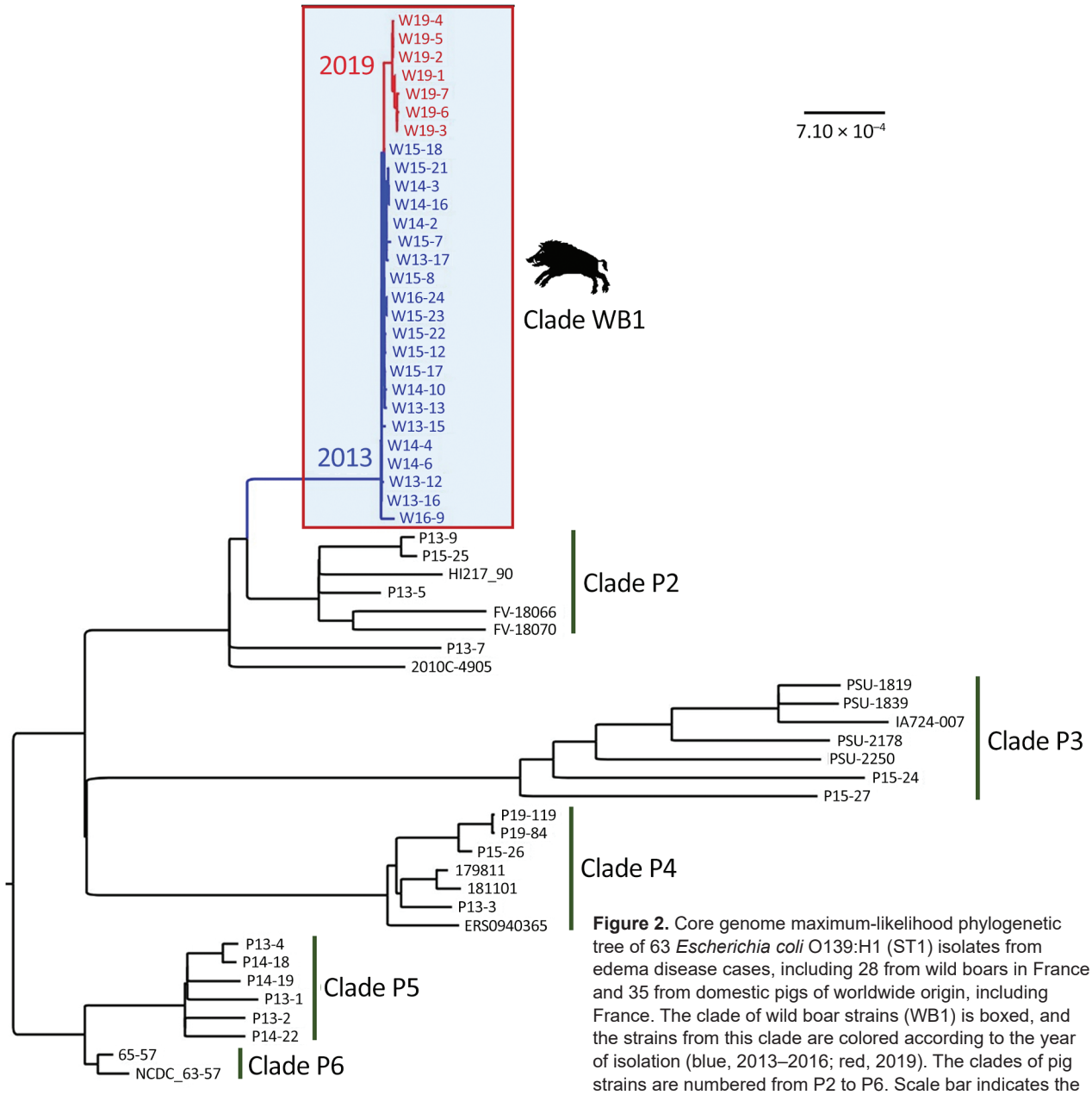

Figure 2. Core genome maximum-likelihood phylogenetic tree of 63 *Escherichia coli* O139:H1 (ST1) isolates from edema disease cases, including 28 from wild boars in France and 35 from domestic pigs of worldwide origin, including France. The clade of wild boar strains (WB1) is boxed, and the strains from this clade are colored according to the year of isolation (blue, 2013–2016; red, 2019). The clades of pig strains are numbered from P2 to P6. Scale bar indicates the number of substitutions per site.

involved in the phage lytic cycle and more precisely in the assembly of the head, collar, fibers, and tail (region 1) and lysis (region 2) (Figure 3). Such deletions thus probably result in deficiency of STEC O139 for the production of Stx2e phage particles, as observed previously for many other *stx2e*-positive *E. coli* strains whose Stx2e phages were shown to lack ≥1 genes and to be not inducible (*35*,*36*).

We identified a plasmid, pW1316-2, classically found in STEC O139:H1 and encoding F18 fimbriae, Hly, and adhesin AidA-1, in strain W13-16 and assigned it to the incompatibility (Inc) group IncFII/IncX1 (Table). Previous reports showed that F18-positive plasmids from porcine STEC or ETEC strains possessed a replicon of the RepFIc/RepFIIa family (*37*) and that IncX1, IncI1, and IncFII plasmids are frequently encountered within F18-positive ETEC (*38*). F18-positive plasmids are also known to contain *hly* and *aidA* genes (*13*,*39*). Plasmid pW1316-2 possessed the F18ab antigenic variant, as previously observed for porcine ED STEC O139, in contrast to PWD ETEC from other serogroups (including O141), which

Table. Genomic characteristics of chromosomes and plasmids of wild boar *Escherichia coli* strain W13–16 and pig *E. coli* strains P15-25 and P13-6, France*

Strain and support	Length, bp	Typing	Resistance inventory	Virulence inventory
W13-16				
Chromosome	5,091,917	O139:H1 ST1	*mdf(A)*	*chuA*, *ehaG*, *eilA*, *kps*, LPF, *omp1* *rhsA stx*, *terC*, T6SS, *vgrG1*
pW1316-1	83,443	IncFII [F10:A-:B-]		*aidA*, *sta1*, *stb*, *sepA*
pW1316-2	54,694	IncFII/IncX1 [F14:A-:B-]		*aidA-I*, α-*hly,* F18
P15-25				
Chromosome	5,029,591	O139:H1 ST1	*mdf(A)*	*chuA*, *eilA*, *kps*, LPF, *ompT*, *rhsA* *stx*, *terC*, T6SS, *vgrG1*
p1525-1	77,484	IncFII/IncX1 [F14:A-:B-]		*aidA*, *aidA-I,* α-*hly,* F18
P13-6				
Chromosome	4,963,420	O141:H4 ST10	*mdf(A)*	*bcs*, ETT2, *iss*, *ompT*, *stx*, *terC*
pP136-1	226,437	IncHI2 DLST:ST4	*mph(B)*, *tetR*	*terC*
pP136-2	103,673	IncI1-I(Alpha) ST26/CC2	*aadA1*, *aadA2*, *cmlA1*, *mef(B)*, *sul3*	*cib*
pP136-3	82,610	IncFII [F10:A-:B-]		*aidA*, *sta1*, *stb*, *sepA*
pP136-4	82,875	IncFII [F108:A-:B-]		F4
pP136-5	86,378	IncFII/IncX1 [F14:A-:B-]		*aidA-I*, α-*hly,* F18
pP136-6	74,646	p0111		
pP136-7	48,077			
pP136-8	5,125			
pP136-9	3,126			

*Serotype and ST are indicated for the chromosomes, whereas incompatibility group, FAB [FII, FIA, FIB] formulas, and ST or CC are indicated for plasmids. CC, clonal complex; ST, sequence type.

produce F18ac (*40*). This plasmid displayed similarity with the IncFII/IncX1 plasmids pP1525 (F18ab-positive) from the pig STEC O139:H1 strain and pP136-5 (F18ac-positive) from the pig STEC O141:H4 strain (Table; Figure 4). However, these 2 plasmids were larger than pW1316-2 and contained additional regions with open reading frames of unknown function (Figure 4). We identified no transfer region in the 3 F18-positive plasmids pW1316-2, pP1525, and pP136-5 (Figure 4), suggesting that they are transfer-deficient. Only 2 closed F18-positive plasmid sequences have been described in the literature, both from non-O139 strains: an IncFIIA plasmid (pUMNF18_87, 87 kb) from a diarrheic pig STEC/ETEC O147 strain, carrying F18ac, *hly, aidA-1* genes and remnants of an F transfer region (*12*); and an IncFII/IncX1 plasmid (p15ODTXV, 119 kb) from a diarrheic pig STEC/ETEC O141:H4 strain, carrying F18ac, *hly,* and *sta*/*stb* genes and a conjugation transfer region (*11*).

Surprisingly, the second plasmid of W13-16 (pW1316-1) (Table) was not classically found in STEC strains of serotype O139:H1. It belonged to the IncFII group and carried *sta1* and *stb* enterotoxin genes as well as the serine protease autotransporter SepA toxin gene and a second *aidA* gene (Table; Figure 5). The *sta1*/*stb* and *sepA* genes were bordered by many

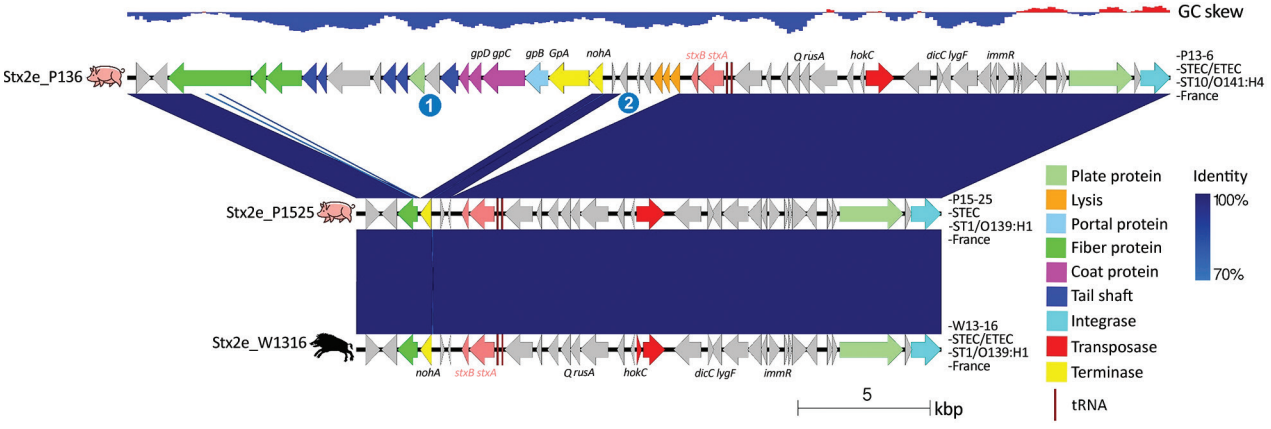

Figure 3. Comparison of the Stx2e prophages of wild boar *Escherichia coli* O139:H1 strain W13-16 and pig *E. coli* O139:H1 P15-25 and O141:H4 P13-6 strains from France. The genes are represented with arrows color coded by function. The 2 regions present in prophage Stx2e_P136 but absent in the 2 other prophages are indicated by numbers 1 and 2. The areas between the genetic maps are shaded in blue, with a color intensity depending on the percentage of identity between each region compared. Strain name, pathotype, sequence type, serotype, and country of isolation are indicated at the right of each map. The GC skew (negative, blue; positive, red) is indicated at the top. ETEC, enterotoxigenic *Escherichia coli;* ST, sequence type; STEC, Shiga toxin–producing *Escherichia coli*.

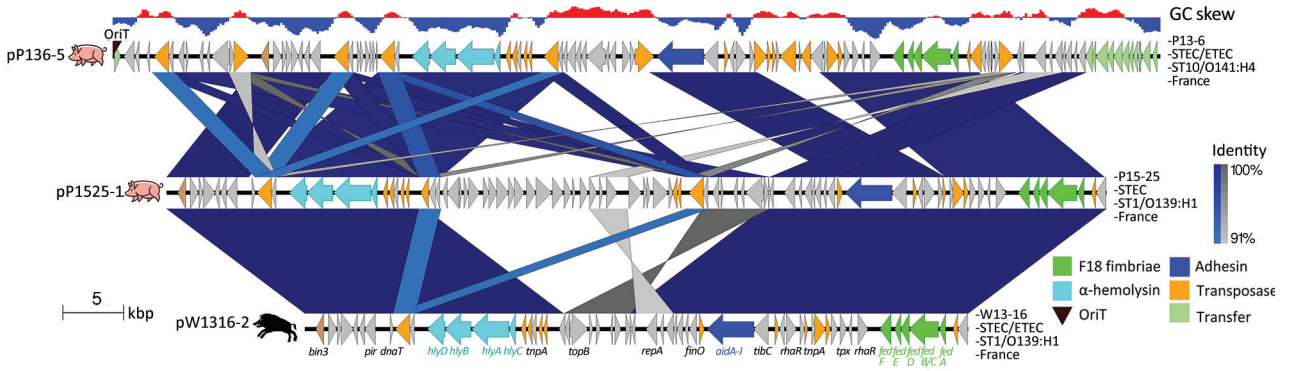

Figure 4. Comparison of plasmids carrying the F18 fimbriae gene cluster of the wild boar *Escherichia coli* O139:H1 strain W13-16 and pig *E. coli* O139:H1 P15-25 and O141:H4 P13-6 strains from France. The genes are represented with arrows color coded by function. The areas between the genetic maps are shaded in blue or gray for regions oriented in the same or opposite direction, respectively, with a color intensity depending on the percentage of similarity between each region compared. Strain name, pathotype, sequence type, serotype, and country of isolation are indicated at the right of each map. The GC skew (negative, blue; positive, red) is indicated at the top. ETEC, enterotoxigenic *Escherichia coli;* OriT, transfer origin; ST, sequence type; STEC, Shiga toxin–producing *Escherichia coli*.

transposase genes and insertion sequence (IS) elements (Figure 5). Plasmid-encoded enterotoxins are a typical feature of porcine PWD ETEC strains, and enterotoxin genes surrounded by IS were also reported elsewhere (*12*,*37*,*41*), suggesting that IS may favor the acquisition of virulence genes. We did not find such a plasmid in the pig STEC O139:H1 strain, in contrast to the pig STEC O141:H4 strain, which carried a similar IncFII plasmid, pP136–3 (Table; Figure 5). A BLAST search (http://blast.ncbi.nlm.nih.gov/Blast.cgi) led to the identification of another similar plasmid (pCV839-15-p1) in a typical diarrheic pig ETEC strain of serotype O9:H21 (GenBank accession no. SAMN0804056) (Figure 5). Sequence comparison of plasmids pW1316-1, pP136-3, and pCV839-15-p1 showed that a highly conserved conjugation region was located downstream of the transfer origin. However, the region spanning the relaxase gene up to the type 4 coupling protein gene was reversed in pW1316-1 (Figure 5), resulting in truncation of the N-terminal part of the relaxase gene and the C-terminal part of the type 4 coupling protein gene, and presumably in conjugation deficiency.

On the basis of this genomic analysis, the wild boar W13-16 isolate should thus be considered as an atypical hybrid STEC–ETEC of the serotype O139:H1.

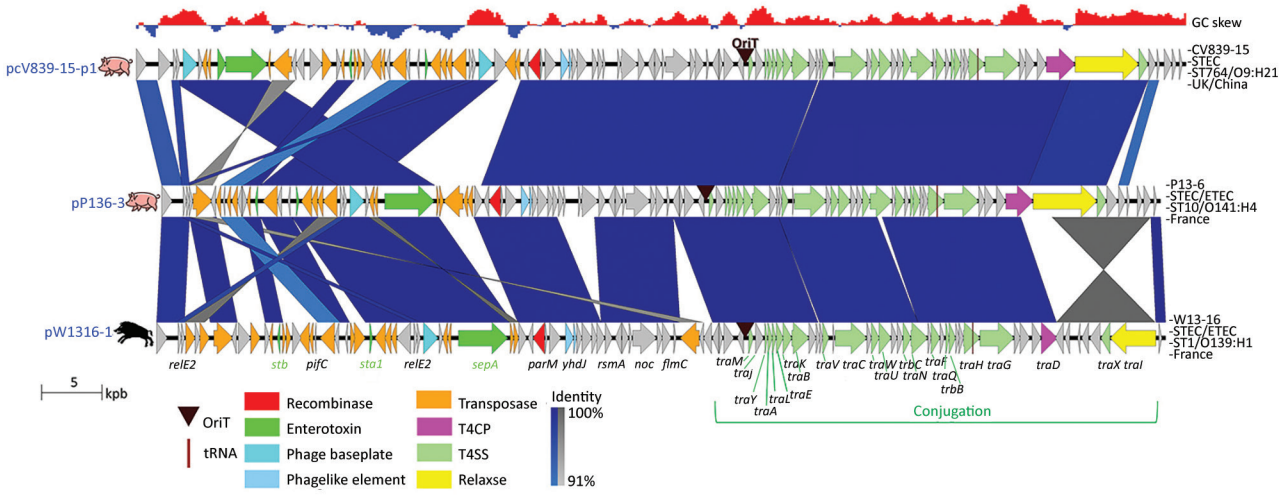

Figure 5. Comparison of plasmids carrying the enterotoxin and *sepA* virulence genes of the wild boar *Escherichia coli* O139:H1 strain W13-16 and pig *E. coli* O141:H4 P13-6 and O9:H21 CV839-15 strains. The genes are represented with arrows color coded by function. The areas between the genetic maps are shaded in blue or gray for regions oriented in the same or opposite direction, respectively, with a color intensity depending on the percentage of similarity between each region compared. Strain name, pathotype, sequence type, serotype, and country of isolation are indicated at the right of each map. The GC skew (negative, blue; positive, red) is indicated at the top. ETEC, enterotoxigenic *Escherichia coli;* ST, sequence type; STEC, Shiga toxin–producing *Escherichia coli*.

We identified the *sta1*, *stb*, and *sepA* genes in all the O139:H1 isolates from clade WB1, except for 1 strain (W15-12), which was lacking these genes (Appendix 1 Table 3), presumably because of the loss of the plasmid carrying these virulence genes. In most O139:H1 isolates from pigs or other sources, the *sta*, *stb*, and *sepA* genes were lacking (Appendix 1 Table 3), indicating that the plasmid pW1316-1 conferring the hybrid STEC–ETEC status to the strains from clade WB1 is absent from O139:H1 strains of non–wild boar origin. By contrast, we frequently encountered the hybrid STEC–ETEC status in other *E. coli* serotypes, such as O138:H14, O141:H4, and O147:H4 (Appendix 1 Table 3).

Comparing Global Composition of Entire Accessory Genome among *E. coli* O139:H1, O141:H4, O147:H4, and O138:H14 Strains

We analyzed the presence of the *E. coli* virulence genes found in the STEC O139:H1 W13-16 strain in the other wild boar O139:H1 strains as well as in 190 additional *E. coli* strains originating in France or worldwide (Appendix 1 Tables 1, 2). These belonged to O139:H1, O141:H4, O147:H4, and O138:H14 serotypes and to various pathotypes (i.e., STEC, ETEC, hybrid STEC–ETEC, or none of these) depending on the presence or absence of *stx* and *sta1*/*stb* virulence genes (Appendix 1 Table 3). By analyzing the global composition of the accessory genome, we found that

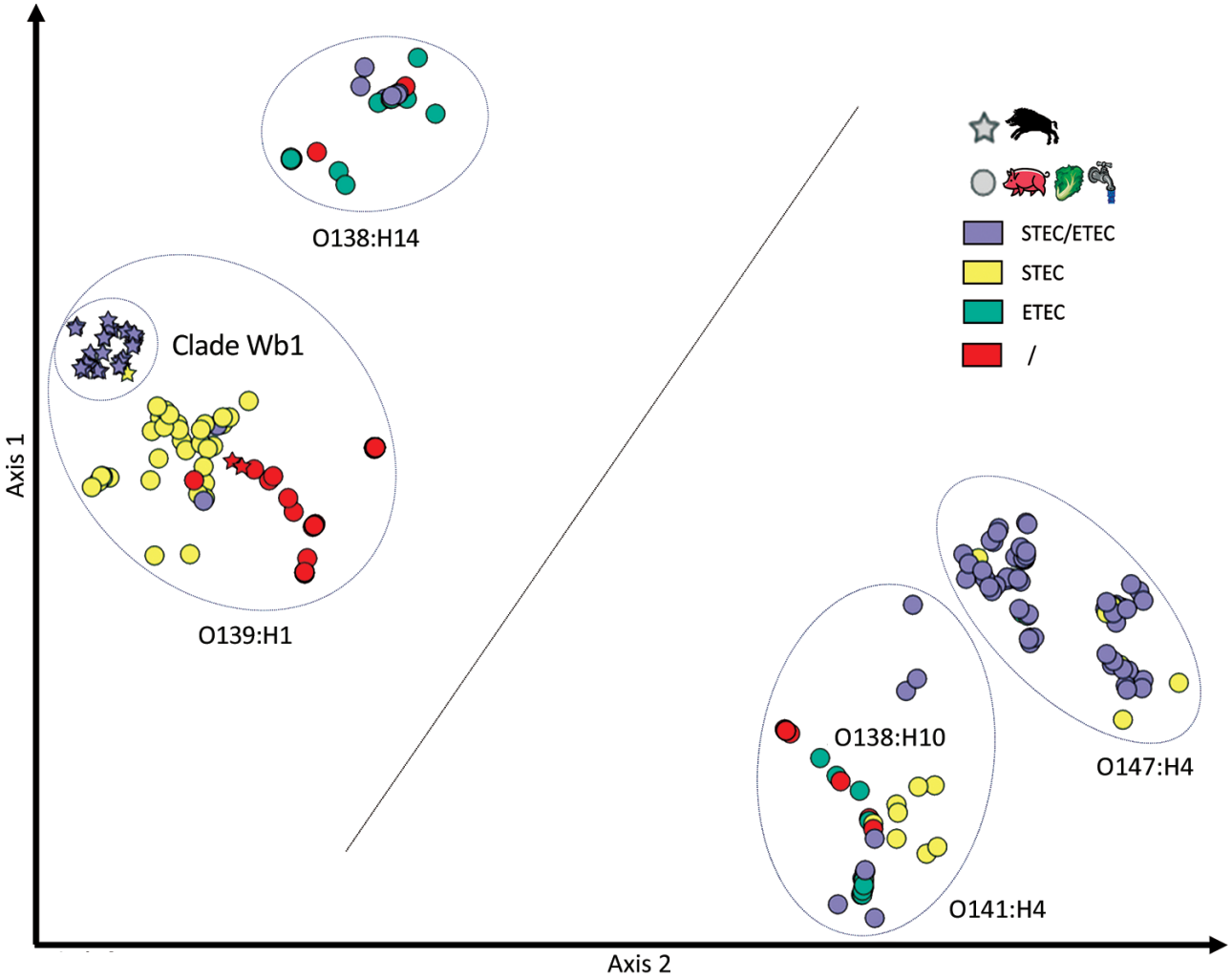

Figure 6. Comparison of the accessory genome composition of wild boar *Escherichia coli* O139:H1 strains in France with that of *E. coli* O139:H1, O141:H4, O147:H4, and O138:H14 of worldwide origin. Each sign represents a strain depending on its origin (star, wild boar; circle, other hosts). The distance between the signs in a 2-dimensional space increases with the decrease in orthologous genes in common between strains represented. The signs are color coded depending on the predicted pathotype. The 28 wild boar O139:H1 strains are represented by gray stars except for 1 strain lacking *sta1*/*stb* genes, represented by a yellow star. Two additional wild boar O139:H1 strains were included in this analysis and are represented by red stars because they lacked the *stx2e* and *sta1*/*stb* genes (Appendix 1 Table 3, https://wwwnc.cdc.gov/EID/article/28/2/21-1491-App1.xlsx); they did not belong to clade WB1 (data not shown). ETEC, enterotoxigenic *Escherichia coli;* STEC, Shiga toxin–producing *Escherichia coli*; /, neither STEC nor ETEC nor hybrid STEC–ETEC.

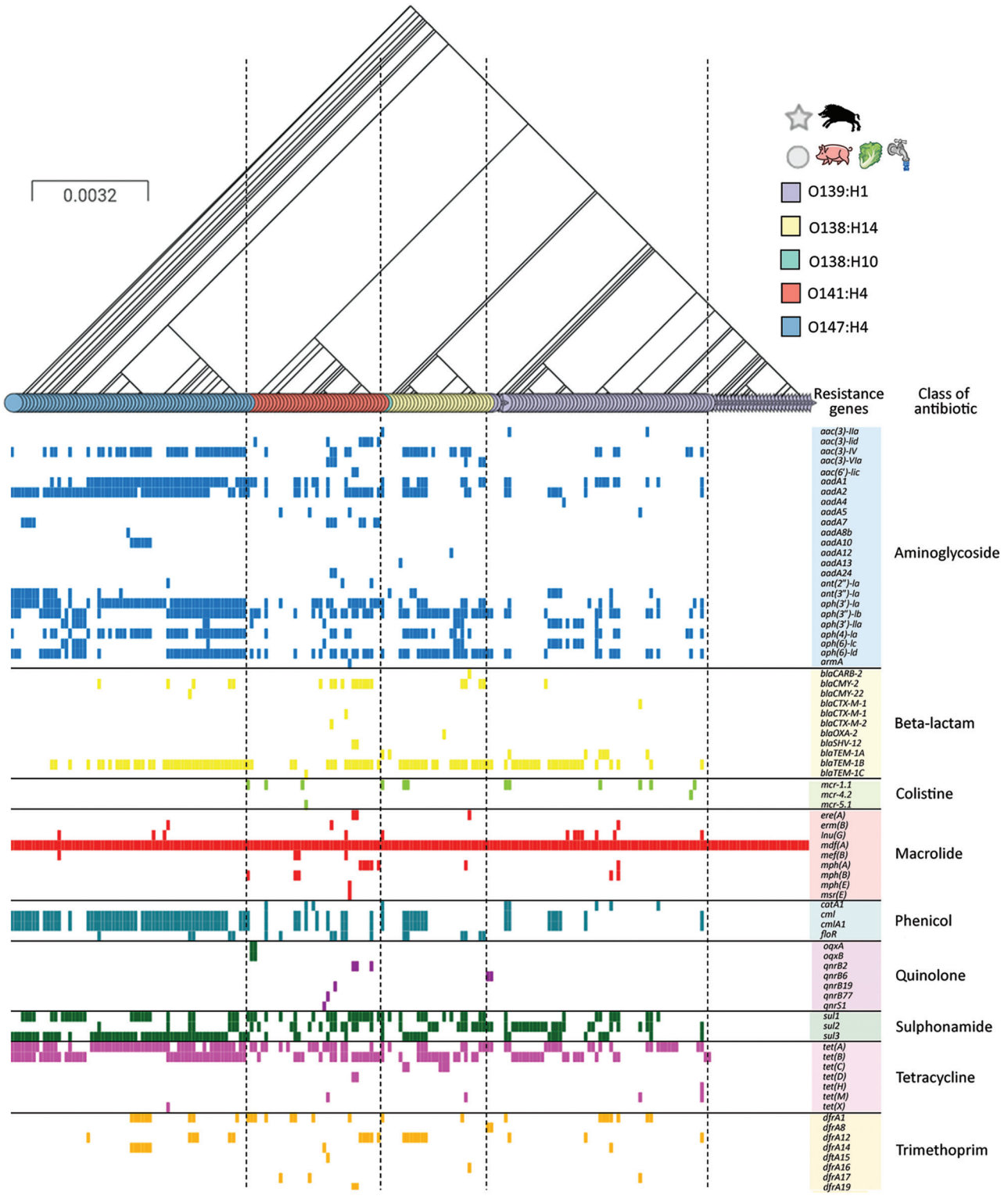

Figure 7. Comparison of antimicrobial-resistance genes with the phylogeny of wild boar *Escherichia coli* O139:H1 strains in France with those of *E. coli* O139:H1, O141:H4, O147:H4, and O138:H14 of worldwide origin. The tree is based on the phylogeny of the strains according to their core genome. The shapes of the leaves in the tree correspond to the origin of the strains (star, wild boars; circle, other hosts), and the colors of the leaves represent their serotype. Antimicrobial-resistance genes are grouped into different categories whose names are indicated at the top, with a color code. Scale bar indicates number of substitutions per site.

all these strains clustered into 4 main groups, consistent with the 4 major serotypes (Figure 6).

Among the accessory genome, certain genes were significantly associated, although not exclusively, with the strains of clade WB1, such as *rhsA*, which encodes an effector of the type 6 secretion system (T6SS) (*42*) and the gene coding for the trimeric autotransporter adhesin EhaG (*43*) (Appendix 1 Table 3). As mentioned previously, the SepA encoding gene was predominant in strains of clade WB1 and quite rare in the other strains of *E. coli* responsible for ED. SepA, originally described in *Shigella flexneri* 2a and enteroaggregative *E. coli*, has been identified only in F4-positive ETEC strains isolated from pigs (*38*,*44*), where it was shown to be also encoded on a large (85 kb) plasmid (*45*). SepA, a serine protease autotransporter of the *Enterobacteriaceae*, could degrade intestinal mucin (*46*).

Antimicrobial-Resistance Genotypes and Phenotypes

The O139:H1 strains of clade WB1 did not carry any gene involved in resistance to classical antibiotics except that of the efflux pump *mdf*(*A*), which can confer resistance to macrolides and is found in most *E. coli* strains (Figure 7). By contrast, the O139:H1 strains from porcine origin carried a high amount of antimicrobial-resistance genes, which was also the case for porcine O138:H14, O141:H4, and O147:H4 strains. Except for a minority of isolates, in most pig strains we identified genes conferring resistance to various classes of antibiotics, including aminoglycosides, β-lactam, colistin, macrolide, phenicol, quinolone, sulphonamide, tetracycline, and trimethoprim (Figure 7).

The antimicrobial-susceptibility testing of 4 wild boar STEC O139:H1 isolates (W13-16, W14-3, W15-17, and W19-4) recovered from different years confirmed the results of the in silico analysis because they were sensitive to all antibiotics tested except for erythromycin.We also tested the 2 pig O139:H1 (P15-25) and O141:H4 (P13-6) strains whose closed genomes we obtained. P15-25 was sensitive to all antibiotics tested except for erythromycin, consistent with the presence of the chromosomal *mdf*(*A*) gene and absence of other antimicrobial-resistance gene on its single plasmid, pP1525. By contrast, P13-6 was resistant to erythromycin, tetracycline, and chloramphenicol, consistent with the presence of plasmid genes *mef(B)* and *tetRACD* (pP136-1) and *cmlA1* (pP136-2), as mentioned previously in our description of plasmids.

Discussion

We show that the STEC O139:H1 strains that caused ED in wild boars in France belong to a specific clade (WB1) of *E. coli* O139:H1 strains that is similar, by virtue of its core genome and F18-encoding plasmid, to clades of pathogenic *E. coli* O139:H1 from domestic pigs but is distinguished from them by the presence of an enterotoxin-encoding plasmid usually found in other *E. coli* serotypes typical of PWD. Indeed, our study rarely found enterotoxin genes in STEC O139, in contrast to non-O139 STEC or ETEC serogroups such as O138 or O141, as reported previously (*10*,*40*). These findings may invite speculation that this enterotoxin-encoding plasmid was acquired by an ancestor of clade WB1 strains from a non-O139 strain, through horizontal gene transfer. In support of this hypothesis, this plasmid displayed similarities with those found in pig strains of serotypes O9:H21 and O141:H4.

Except for the efflux pump *mdf(A)*, the strains from clade WB1 lacked antimicrobial-resistance genes, which contrasted drastically with the situation in pig strains overwhelmingly carrying multiple resistance cassettes (*9*). This finding could indicate that the clade WB1 was under low pressure to select antimicrobial-resistance genes during its recent evolutionary history. This pathogenic clade appears to be endemic to the territory of France and restricted to a wild boar population. From the analysis of the *FUT1* gene regulating the expression of the F18 receptor, the wild boar populations in France were found genetically susceptible to ED (*15*). Production of various virulence factors, including F18 adhesin, Stx2e, and enterotoxins, may be cited to explain the emergence of ED in wild boars because such a combination may confer increased virulence to the strains. In addition to the hybrid STEC–ETEC status, the possession of a specific accessory genome could also be responsible for the adaptation of this clade to wild boar hosts and their environment.

In conclusion, our results argue in favor of a new clade of ED-causing STEC that originated from wildlife and did not result from contacts between wild boars and domestic pigs. ED is thus not restricted to pigs, as usually described, and wild boars are also susceptible hosts. Because the wild boar population is growing and outdoor pig farming is rapidly developing in Europe because of animal welfare considerations, contacts between wild boars and pigs could enable the spread of infectious diseases, if appropriate biosecurity measures are not implemented (*47*). Surveillance of this highly pathogenic clade in the wild boar population and in livestock animals is therefore of the highest importance and is needed to study its spread in the wildlife reservoir and potential transmission to domestic pigs.

Acknowledgments

We thank Laurent Cavalié for his assistance with high throughput DNA extraction and antimicrobial-susceptibility testing.

This work was supported by the National Research Institute for Agriculture, Food, and Environment's GISA metaprogram (https://colloque.inrae.fr/metaprograms-workshops_eng/Metaprograms/GISA) and by funding from the Région Occitanie (grant no. ALDOCT-000610) and Ministry of Agriculture awarded to A.P.

About the Author

Mr. Perrat is a PhD student at the University of Toulouse, France. His main research interests include genomic analysis and molecular epidemiology.

References

1. Fairbrother JM, Nadeau É. Colibacillosis. In: Diseases of swine. 11th edition. Hoboken (NJ): Wiley-Blackwell; 2019. p. 807–34.
2. DebRoy C, Roberts E, Scheuchenzuber W, Kariyawasam S, Jayarao BM. Comparison of genotypes of *Escherichia coli strains* carrying F18ab and F18ac fimbriae from pigs. J Vet Diagn Invest. 2009;21:359–64. https://doi.org/10.1177/104063870902100310
3. Marques LRM, Peiris JSM, Cryz SJ, O'Brien AD. *Escherichia coli strains* isolated from pigs with edema disease produce a variant of Shiga-like toxin II. FEMS Microbiol Lett. 1987;44:33–8. https://doi.org/10.1111/j.1574-6968.1987.tb02237.x
4. Matise I, Sirinarumitr T, Bosworth BT, Moon HW. Vascular ultrastructure and DNA fragmentation in swine infected with Shiga toxin–producing *Escherichia coli*. Vet Pathol. 2000;37:318–27. https://doi.org/10.1354/vp.37-4-318
5. Steil D, Bonse R, Meisen I, Pohlentz G, Vallejo G, Karch H, et al. A topographical atlas of Shiga toxin 2e receptor distribution in the tissues of weaned piglets. Toxins (Basel). 2016;8:357. https://doi.org/10.3390/toxins8120357
6. Jardin A, Leneveu P, Bayon-Auboyer M-H, Morvan H, Moalic P-Y, Le Guennec J, et al. Diagnostic de la maladie de l'oedème chez le porc en France: bilan des connaissances acquises depuis 2014 par la PCR de génotypage des *Escherichia coli*. Journées de la Recherche Porcine en France. 2017;49:177–82 [cited 2021 Jul 2]. http://www.journees-recherche-porcine.com/texte/2017/santeanimale/S01.pdf
7. Broes A, Renault L. Nouvelle classification des souches d'*Escherichia coli* responsables d'infection intestinale chez le porcelet. Bull Acad Vet Fr. 1990;63:181–91. https://doi.org/10.4267/2042/64341
8. Helgerson AF, Sharma V, Dow AM, Schroeder R, Post K, Cornick NA. Edema disease caused by a clone of *Escherichia coli* O147. J Clin Microbiol. 2006;44:3074–7. https://doi.org/10.1128/JCM.00617-06
9. Luppi A. Swine enteric colibacillosis: diagnosis, therapy and antimicrobial resistance. Porcine Health Manag. 2017;3:16. https://doi.org/10.1186/s40813-017-0063-4
10. Fairbrother JM, Nadeau E, Gyles CL. *Escherichia coli* in postweaning diarrhea in pigs: an update on bacterial types, pathogenesis, and prevention strategies. Anim Health Res Rev. 2005;6:17–39. https://doi.org/10.1079/AHR2005105
11. Brilhante M, Perreten V, Donà V. Multidrug resistance and multivirulence plasmids in enterotoxigenic and hybrid Shiga toxin–producing/enterotoxigenic *Escherichia coli* isolated from diarrheic pigs in Switzerland. Vet J. 2019;244:60–8. https://doi.org/10.1016/j.tvjl.2018.12.015
12. Shepard SM, Danzeisen JL, Isaacson RE, Seemann T, Achtman M, Johnson TJ. Genome sequences and phylogenetic analysis of K88- and F18-positive porcine enterotoxigenic *Escherichia coli*. J Bacteriol. 2012;194:395–405. https://doi.org/10.1128/JB.06225-11
13. Wittig W, Prager R, Stamm M, Streckel W, Tschäpe H. Expression and plasmid transfer of genes coding for the fimbrial antigen F107 in porcine *Escherichia coli* strains. Zentralbl Bakteriol. 1994;281:130–9. https://doi.org/10.1016/S0934-8840(11)80563-3
14. Decors A, Richomme C, Morvan H, Botteron C, Nicolier A, Rambaud F, et al. Diagnostiquer un problème de santé dans la faune sauvage: exemple de la maladie de l'oedème chez le sanglier sauvage (*Sus scrofa*) en Ardèche. Bulletin Épidémiologique, Santé Animale et Alimentation. 2015;69:2–7 [cited 2021 Jul 2]. https://be.anses.fr/sites/default/files/BEP-mg-BE69-art1.pdf
15. Petit G, Grosbois V, Chalvet-Monfray K, Ducos A, Desmecht D, Martineau GP, et al. Polymorphism of the alpha-1-fucosyltransferase (FUT1) gene in several wild boar (*Sus scrofa*) populations in France and link to edema disease. Res Vet Sci. 2020;131:78–86. https://doi.org/10.1016/j.rvsc.2020.03.025
16. Massei G, Kindberg J, Licoppe A, Gačić D, Šprem N, Kamler J, et al. Wild boar populations up, numbers of hunters down? A review of trends and implications for Europe. Pest Manag Sci. 2015;71:492–500. https://doi.org/10.1002/ps.3965
17. Miller RS, Sweeney SJ, Slootmaker C, Grear DA, Di Salvo PA, Kiser D, et al. Cross-species transmission potential between wild pigs, livestock, poultry, wildlife, and humans: implications for disease risk management in North America. Sci Rep. 2017;7:7821. https://doi.org/10.1038/s41598-017-07336-z
18. Clark K, Karsch-Mizrachi I, Lipman DJ, Ostell J, Sayers EW. GenBank. Nucleic Acids Res. 2016;44(D1):D67–72. https://doi.org/10.1093/nar/gkv1276
19. Zhou Z, Alikhan NF, Mohamed K, Fan Y, Achtman M; Agama Study Group. The EnteroBase user's guide, with case studies on *Salmonella* transmissions, *Yersinia pestis* phylogeny, and *Escherichia* core genomic diversity. Genome Res. 2020;30:138–52. https://doi.org/10.1101/gr.251678.119
20. Wick RR, Judd LM, Gorrie CL, Holt KE. Unicycler: resolving bacterial genome assemblies from short and long sequencing reads. PLoS Comput Biol. 2017;13:e1005595. https://doi.org/10.1371/journal.pcbi.1005595
21. Seemann T. Prokka: rapid prokaryotic genome annotation. Bioinformatics. 2014;30:2068–9. https://doi.org/10.1093/bioinformatics/btu153
22. Page AJ, Taylor B, Delaney AJ, Soares J, Seemann T, Keane JA, et al. SNP-sites: rapid efficient extraction of SNPs from multi-FASTA alignments. Microb Genom. 2016;2:e000056. https://doi.org/10.1099/mgen.0.000056
23. Langmead B, Salzberg SL. Fast gapped-read alignment with Bowtie 2. Nat Methods. 2012;9:357–9. https://doi.org/10.1038/nmeth.1923
24. Nguyen LT, Schmidt HA, von Haeseler A, Minh BQ. IQ-TREE: a fast and effective stochastic algorithm for estimating maximum-likelihood phylogenies. Mol Biol Evol. 2015;32:268–74. https://doi.org/10.1093/molbev/msu300

25. Soubrier J, Steel M, Lee MS, Der Sarkissian C, Guindon S, Ho SY, et al. The influence of rate heterogeneity among sites on the time dependence of molecular rates. Mol Biol Evol. 2012;29:3345–58. https://doi.org/10.1093/molbev/mss140
26. Yang Z. A space-time process model for the evolution of DNA sequences. Genetics. 1995;139:993–1005. https://doi.org/10.1093/genetics/139.2.993
27. Kimura M. Estimation of evolutionary distances between homologous nucleotide sequences. Proc Natl Acad Sci U S A. 1981;78:454–8. https://doi.org/10.1073/pnas.78.1.454
28. Kalyaanamoorthy S, Minh BQ, Wong TKF, von Haeseler A, Jermiin LS. ModelFinder: fast model selection for accurate phylogenetic estimates. Nat Methods. 2017;14:587–9. https://doi.org/10.1038/nmeth.4285
29. Argimón S, Abudahab K, Goater RJE, Fedosejev A, Bhai J, Glasner C, et al. Microreact: visualizing and sharing data for genomic epidemiology and phylogeography. Microb Genom. 2016;2:e000093. https://doi.org/10.1099/mgen.0.000093
30. Alikhan NF, Petty NK, Ben Zakour NL, Beatson SA. BLAST ring image generator (BRIG): simple prokaryote genome comparisons. BMC Genomics. 2011;12:402. https://doi.org/10.1186/1471-2164-12-402
31. Malberg Tetzschner AM, Johnson JR, Johnston BD, Lund O, Scheutz F. In silico genotyping of *Escherichia coli* isolates for extraintestinal virulence genes by use of whole-genome sequencing data. J Clin Microbiol. 2020;58:e01269-20. https://doi.org/10.1128/JCM.01269-20
32. Arndt D, Grant JR, Marcu A, Sajed T, Pon A, Liang Y, et al. PHASTER: a better, faster version of the PHAST phage search tool. Nucleic Acids Res. 2016;44(W1):W16-21. https://doi.org/10.1093/nar/gkw387
33. Sullivan MJ, Petty NK, Beatson SA. Easyfig: a genome comparison visualizer. Bioinformatics. 2011;27:1009–10. https://doi.org/10.1093/bioinformatics/btr039
34. Schürch AC, Arredondo-Alonso S, Willems RJL, Goering RV. Whole genome sequencing options for bacterial strain typing and epidemiologic analysis based on single nucleotide polymorphism versus gene-by-gene-based approaches. Clin Microbiol Infect. 2018;24:350–4. https://doi.org/10.1016/j.cmi.2017.12.016
35. Beutin L, Krüger U, Krause G, Miko A, Martin A, Strauch E. Evaluation of major types of Shiga toxin 2E–producing *Escherichia coli* bacteria present in food, pigs, and the environment as potential pathogens for humans. Appl Environ Microbiol. 2008;74:4806–16. https://doi.org/10.1128/AEM.00623-08
36. Muniesa M, Recktenwald J, Bielaszewska M, Karch H, Schmidt H. Characterization of a Shiga toxin 2e–converting bacteriophage from an *Escherichia coli* strain of human origin. Infect Immun. 2000;68:4850–5. https://doi.org/10.1128/IAI.68.9.4850-4855.2000
37. Fekete PZ, Gerardin J, Jacquemin E, Mainil JG, Nagy B. Replicon typing of F18 fimbriae encoding plasmids of enterotoxigenic and verotoxigenic *Escherichia coli* strains from porcine postweaning diarrhoea and oedema disease. Vet Microbiol. 2002;85:275–84. https://doi.org/10.1016/S0378-1135(01)00515-6
38. García V, Gambino M, Pedersen K, Haugegaard S, Olsen JE, Herrero-Fresno A. F4- and F18-positive enterotoxigenic *Escherichia coli* isolates from diarrhea of postweaning pigs: genomic characterization. Appl Environ Microbiol. 2020;86:e01913. https://doi.org/10.1128/AEM.01913-20
39. Mainil JG, Jacquemin E, Pohl P, Kaeckenbeeck A, Benz I. DNA sequences coding for the F18 fimbriae and AIDA adhesin are localised on the same plasmid in *Escherichia coli* isolates from piglets. Vet Microbiol. 2002;86:303–11. https://doi.org/10.1016/S0378-1135(02)00019-6
40. Nagy B, Whipp SC, Imberechts H, Bertschinger HU, Dean-Nystrom EA, Casey TA, et al. Biological relationship between F18ab and F18ac fimbriae of enterotoxigenic and verotoxigenic *Escherichia coli* from weaned pigs with oedema disease or diarrhoea. Microb Pathog. 1997;22:1–11. https://doi.org/10.1006/mpat.1996.0085
41. Leonard SR, Mammel MK, Rasko DA, Lacher DW. Hybrid Shiga toxin–producing and enterotoxigenic *Escherichia* sp. cryptic lineage 1 strain 7v harbors a hybrid plasmid. Appl Environ Microbiol. 2016;82:4309–19. https://doi.org/10.1128/AEM.01129-16
42. Whitney JC, Beck CM, Goo YA, Russell AB, Harding BN, De Leon JA, et al. Genetically distinct pathways guide effector export through the type VI secretion system. Mol Microbiol. 2014;92:529–42. https://doi.org/10.1111/mmi.12571
43. Totsika M, Wells TJ, Beloin C, Valle J, Allsopp LP, King NP, et al. Molecular characterization of the EhaG and UpaG trimeric autotransporter proteins from pathogenic *Escherichia coli*. Appl Environ Microbiol. 2012;78:2179–89. https://doi.org/10.1128/AEM.06680-11
44. Boerlin P, Travis R, Gyles CL, Reid-Smith R, Janecko N, Lim H, et al. Antimicrobial resistance and virulence genes of *Escherichia coli* isolates from swine in Ontario. Appl Environ Microbiol. 2005;71:6753–61. https://doi.org/10.1128/AEM.71.11.6753-6761.2005
45. Goswami PS, Gyles CL, Friendship RM, Poppe C, Kozak GK, Boerlin P. Effect of plasmid pTENT2 on severity of porcine post-weaning diarrhoea induced by an O149 enterotoxigenic *Escherichia coli*. Vet Microbiol. 2008;131:400–5. https://doi.org/10.1016/j.vetmic.2008.04.007
46. Kumar P, Luo Q, Vickers TJ, Sheikh A, Lewis WG, Fleckenstein JM. EatA, an immunogenic protective antigen of enterotoxigenic *Escherichia coli*, degrades intestinal mucin. Infect Immun. 2014;82:500–8. https://doi.org/10.1128/IAI.01078-13
47. Jurado C, Martínez-Avilés M, De La Torre A, Štukelj M, de Carvalho Ferreira HC, Cerioli M, et al. Relevant measures to prevent the spread of African swine fever in the European Union domestic pig sector. Front Vet Sci. 2018;5:77. https://doi.org/10.3389/fvets.2018.00077

Address for correspondence: Eric Oswald or Frédéric Auvray, Institut de Recherche en Santé Digestive, INSERM U1220, CHU Purpan, Place du Docteur Baylac, CS60039, 31024 Toulouse CEDEX 3, France; email: eric.oswald@inserm.fr or frederic.auvray@envt.fr

Widespread Detection of Multiple Strains of Crimean-Congo Hemorrhagic Fever Virus in Ticks, Spain

María Paz Sánchez-Seco, María José Sierra, Agustín Estrada-Peña, Félix Valcárcel, Ricardo Molina, Eva Ramírez de Arellano, Angeles Sonia Olmeda, Lucía García San Miguel, Maribel Jiménez, Luis J. Romero, Anabel Negredo; Group for CCHFv Research

Human cases of Crimean-Congo hemorrhagic fever (CCHF) were first detected in Spain in 2016. National human and animal health authorities organized a large, multidisciplinary study focusing on ticks as sentinels to determine the nationwide distribution of ticks with CCHF virus. Ticks were collected from animals and vegetation, samples pooled (12,584 ticks; 4,556 pools), and molecular methods used to look for the virus. We detected the virus in 135 pools from most of the regions studied, indicating that it is widespread in Spain. We found sequences of CCHF virus genotypes I, III, and IV in the tick species collected, most commonly in *Hyalomma lusitanicum*, suggesting this tick has a prominent role in the virus's natural cycle. The red deer (*Cervus elaphus*) was the host that most frequently yielded positive ticks. Our study highlights the need for larger studies in Spain to ascertain the complete risk to public health.

Crimean-Congo hemorrhagic fever (CCHF) is a tickborne zoonotic disease causing severe illness, considered by the World Health Organization to be 1 of the 7 highest-priority epidemic-prone diseases. CCHF is considered the most widespread tickborne viral hemorrhagic disease in the world and poses a great public health risk because of its epidemic potential, high case-fatality rates in humans, and a lack of effective mitigation measures, creating an urgent need for accelerated research (*1*). CCHF is caused by CCHF virus (CCHFV; family *Nairoviridae*, genus *Orthonairovirus*), a negative-sense single-stranded RNA virus. The virus is a spherical virion 80–120 nm diameter and has a lipid envelope. Its genome is divided into 3 segments; the small (S) segment encodes the viral nucleocapsid, the medium (M) segment the membrane glycoprotein precursor, and the large (L) segment the RNA-dependent RNA polymerase protein (*2*). The S segment has been widely used in phylogenetic studies, which have defined 6 of 7 CCHFV lineages, each with a different geographic range (*3*,*4*).

The virus is transmitted to humans mainly by the bite of infected *Hyalomma* spp. ticks, which act as reservoirs and vectors; sexual, transovarial, and transstadial transmissions have been demonstrated in the ticks (*5*). Immature ticks commonly feed on medium-sized mammals and on birds, but adults prefer domestic and wild ungulates, which do not develop clinical signs; reports of the tick on other vertebrates are anecdotal (*6*,*7*). The virus can also be transmitted by direct contact with infected fluids of animals and humans. Groups at risk include farmers and their families, slaughterhouse and healthcare workers, veterinarians, and persons who are otherwise prone to being bitten by ticks (*8*).

CCHFV has been widely reported across the whole of Africa, except for the Sahara Desert, and in Asia and Europe (*9*,*10*), where its range overlaps with that of its main tick vectors. Human CCHF cases in Europe had usually been reported in countries of the former Soviet Union and some Balkan countries before 2 human clinical cases were detected in Spain in 2016 (*11*), raising

Author affiliations: CIBER Enfermedades Infecciosas (CIBERINFEC), Madrid, Spain (M.P. Sánchez-Seco, M.J. Sierra, R. Molina, A. Negredo); Universidad de Zaragoza, Zaragoza, Spain (A. Estrada-Peña); Instituto Nacional de Investigación y Tecnología Agraria y Alimentaria, Madrid (F. Valcárcel); Instituto de Salud Carlos III, Madrid (E. Ramírez de Arellano, M. Jiménez); Universidad Complutense de Madrid, Madrid (A.S. Olmeda); Ministerio de Sanidad, Consumo y Bienestar, Madrid (L. García San Miguel); Ministerio de Agricultura, Alimentación y Pesca, Madrid (L.J. Romero)

DOI: https://doi.org/10.3201/eid2802.211308

awareness of the virus's circulation in western Europe. The index case-patient was bitten by a tick while walking in a field in Ávila province, belonging to the Castile and León (CyL) region (autonomous community) (Figure 1). The second case was a nosocomial infection in a healthcare worker. Since then, 8 additional cases have been described in Spain: 1 in 2013 (documented recently in a retrospective study), 2 in 2018 (1 found retrospectively), 3 in 2020, and 2 in 2021 (*12*–*16*). Epidemiologic tracking of these human cases revealed a wider distribution of the virus than initially expected. The patient in 1 of the 2018 cases was infected in Badajoz province in the Extremadura (EXT) region; all other patients were infected in CyL: 2 in Avila, 1 in León, and 5 in Salamanca provinces (Figure 1). Strikingly, the viral genotypes detected in human cases were highly variable. Genotype III (Africa 3 clade) was found in cases from 2016 and 2020 (*11*,*17*; A. Negredo, pers. comm., email, 2021 Sep 30). Cases detected in 2018 consisted of CCHFV genotype V (Europe 1 clade) (*14*); a reassortment of genotype IV (Africa 4 clade) in the S segment; and genotype III (Africa 3 clade) in the M and L segments (*13*).

In Spain, the virus was first detected in 2010 in *H. lusitanicum* ticks collected while they were feeding on red deer (*Cervus elaphus*) in Cáceres province, EXT region (*18*). Additional surveys detected the virus in the same area over several years, and sequencing revealed that several variants of genotype III (Africa 3 clade) were circulating there (*19*,*20*). Recently, RNA of genotypes IV (Africa 4 clade) and V (Europe 1 clade) have also been detected in ticks collected from red deer and wild boar (*Sus scrofa*) in several regions of southwestern Spain (*21*).

Our study reports the results of an extensive CCHFV surveillance study in Spain, involving more than 12,000 ticks collected while they were questing or feeding. The aim was to provide an up-to-date overview of the current distribution and genetic variability of the CCHFV strains found so far in Spain, with a special focus on future risk assessment.

Materials and Methods

For this study, we considered ticks to be sentinels of CCHFV distribution in Spain. Questing or feeding ticks were collected in 2 different phases from wild and domestic animals across a wide geographic area of Spain during October 2016–2018 (Figure 1). In the first phase, which lasted 6 months (October 2016–March 2017), ticks were collected from livestock flocks in 11 counties in 4 regions, CyL, Madrid (MAD), Castile-La Mancha (CLM), and EXT, where *Hyalomma* ticks were already known to be present (Figure 1). Earlier, smaller surveys had established the presence of CCHFV in both ticks and humans (*11*,*18*,*20*). Adult ticks were collected mainly from wild large game ungulate species such as red deer, wild boar, fallow deer (*Dama dama*), and mouflon (*Ovis orientalis*

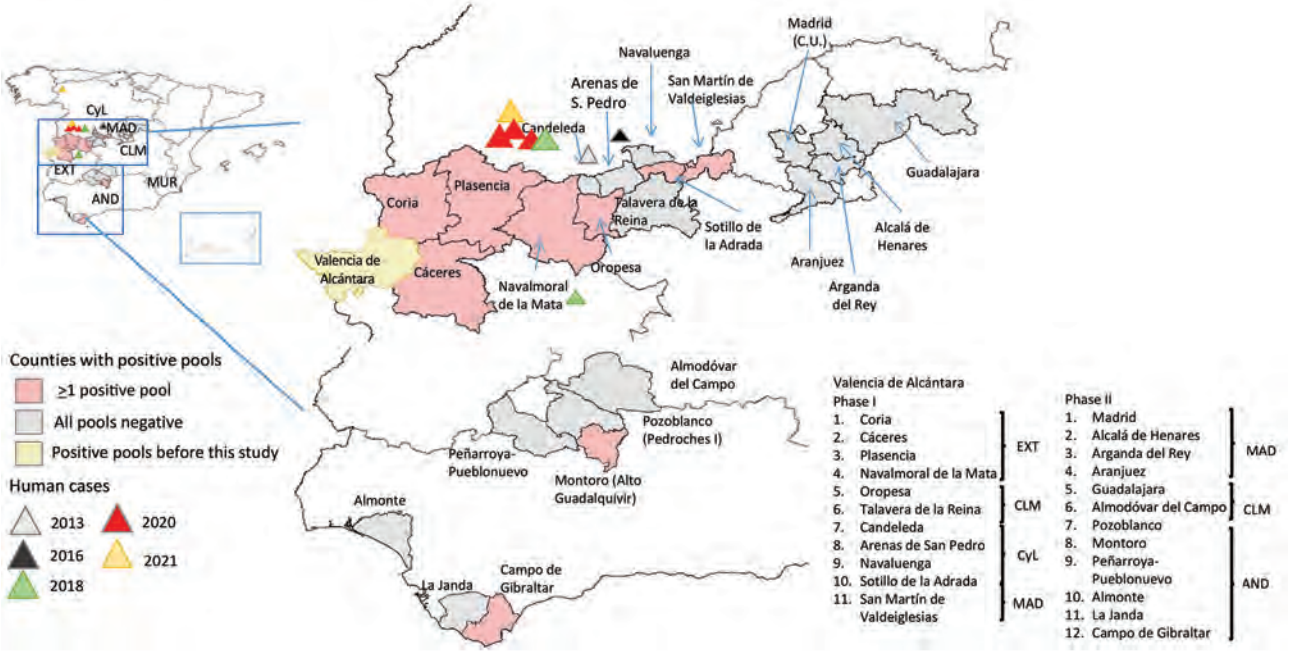

Figure 1. Local distribution of sampling areas in study of Crimean-Congo hemorrhagic fever virus in ticks, Spain. Pink indicates areas where CCHFV was detected in tick pools during this study; triangles indicate human cases. Inset shows locations of sampling areas in Spain. CyL, Castile and León; CLM, Castile-La Mancha; MAD, Madrid; EXT, Extremadura; AND, Andalusia; MUR, Murcia

musimon) and barbary sheep (*Ammotragus lervia*), as well as from grazing livestock cattle (*Bos primigenius taurus*) and goats (*Capra aegagrus hircus*) that had not recently received an ixodicidal treatment and had been grazing on farms for ≥30 days. A maximum of 25 ticks per animal were collected; all ticks were removed from animals on which <10 ticks were found. In small herds of wild ungulates, all of the animals were sampled, but only 10%–15% of the members of larger herds were sampled.

Ticks from the same animal were kept alive in separate, labeled sterile vials and transported at ambient temperature with controlled humidity until they could be frozen at –80°C when possible, then sent to the Spanish National Centre of Microbiology (NCM) for tick identification and viral molecular analysis. Ticks were identified using taxonomic keys (*22*,*23*), and pools were produced with ≤4 fed ticks (depending on size and food status) with specimens collected from the same animal and of the same tick species. Ticks collected in CLM were identified at local laboratories and then sent to NCM. Ticks of the same species collected from different animals were combined in 1 tube.

In the second phase, during May–September 2017 and March–July 2018, ticks were collected from vegetation by standard flagging in 15 counties in 4 regions where the circulation of the virus had not previously been described: MAD, CLM, Murcia (MUR), and Andalusia (AND) (Figure 1). After ticks were collected and transported to the laboratory, they were morphologically identified (*22*,*23*), then samples were frozen and sent to NCM for molecular processing. Pools were produced with 3 ticks obtained from the field.

RNA Extraction

We washed ticks 2× with water and 1× with 70% ethanol, then pooled and crushed them using a plastic homogenizer in a mixture of 560 µL AVL buffer (QIAGEN, https://www.qiagen.com) and 140 µL water. We extracted RNA as described elsewhere (*20*).

Molecular Identification

We performed real-time reverse transcription PCR (RT-PCR) as described elsewhere, but with slight modifications (*14*,*24*), to amplify the 1–122 region of S segments as the screening method. To confirm results, we used a nested RT-PCR that amplifies the 123–764 region in the first amplification and the 450–674 region in the second amplification in the S segment (*11*). We considered a pool positive when both PCRs were positive or when one of the PCR tests gave positive results from 2 different extracts. We sequenced amplicons and performed phylogenetic analysis in a 175 bp fragment of the S gene, as described elsewhere (*20*). We deposited sequences ≥200 nt long obtained with primers CriCon1+ and CriCon1– (*11*) in the European Molecular Biology Laboratory and GenBank databases (accession nos. OK 082060–OK 082067). For Caceres 2140 SPN 2016, we obtained only 1 sequence (CGTCAATGCAAATACAGCAGCCCTAAGCAACAAAGTCCTCTCTGAGTACAAGGTTCCTGGTGAGATTGTGATGTCTGTCAAAGAGATGCTCTCAGACATGATCAGAAGGAGGAATCTGATCCTTAACAGAGGGGGTGATGAGAACCCAAGGGGCCCAGTAGGCAAGGAGCATATA), which was <200 nt long, so we did not deposit it in the database.

Results

A total of 12,584 ticks were collected and pooled, 3,959 pools (10,793 ticks) from animals (Tables 1, 2, 3) and 597 pools (1,791 ticks) from vegetation (Table 4). Adult *H. lusitanicum* were predominant among ticks collected while feeding, but we also recorded *H. excavatum*, *H. marginatum*, *H. rufipes*, *Dermacentor marginatus*, *Ixodes ricinus*, *Haemaphysalis punctata*, *Rhipicephalus annulatus*, *R. bursa*, *R. pusillus*, and *R. sanguineus* sensu lato ticks (Table 1). We identified all but 2 questing ticks as *H. lusitanicum*.

Feeding Ticks

We collected ticks from 1,186 ungulates in CyL, MAD, and EXT: 943 wild and 243 domestic animals (Table 2). Red deer (n = 731) was the most common host species, followed by wild boar (n = 176), fallow deer (n = 19), and mouflon (n = 15) and barbary sheep (n = 2). Among livestock, we surveyed cattle (n = 235) more often than goats (n = 8). No ticks feeding on livestock were positive for CCHFV. Excluding animals from the CLM region, for which data were not available, we found positive ticks on 2.9% (28/943) of all surveyed wild animals.

We found CCHFV-positive feeding ticks in 128 (3.2%) of 3,959 pools (Table 3). We can therefore confirm that feeding ticks carried CCHFV RNA in 7 of 11 counties in 4 provinces in 4 regions: Cáceres (EXT), Madrid (MAD), Toledo (CLM), and Ávila (CyL) (Figure 1). We found marked differences in percentages of positive pools among regions: 1.5% in EXT, 0.3% in CyL, 11.8% in CLM, and 7.7% in MAD (Table 3). Ticks in which we detected CCHFV were mainly *H. lusitanicum*, although the virus was also found in *I. ricinus* (2 pools obtained from red deer), *R. annulatus* (1 pool from a fallow deer), and *D. marginatus* (1 pool from a wild boar) ticks. This finding does not indicate

Table 1. Ticks collected from ungulates and percentages of the different species identified in each region in study of Crimean-Congo hemorrhagic fever virus in ticks, Spain

Tick species	Madrid, %, n = 230	Castile and León, %, n = 829	Extremadura, %, n = 7,917	Castile-La Mancha, %, n = 1,817
Dermacentor marginatus	6.3	12.8	7.1	23.2
Haemaphysalis punctata	0	1.5	0	0.7
Hyalomma excavatum	9.4	0	0	0
H. lusitanicum	81.3	8.3	70.1	55.8
H. marginatum	0	2.3	0.6	1.3
H. rufipes	0	0	0.1	0
Ixodes spp	0	0	0	5.7
I. ricinus	0	24.1	8.0	7.3
Rhipicephalus annulatus	3.1	44.4	14.0	0
R. bursa	0	6.8	0.1	4.4
R. pusillus	0	0	0	0.1
R. sanguineus	0	0	0	0.5

the vectorial characteristics of those tick species, because we collected them while they were feeding, but does indicate the breadth of distribution of the virus. With respect to the genetic variability of S segment sequences, in EXT we found genotypes I (Africa 1 clade), III (Africa 3 clade), and IV (Africa 4 clade) (Table 3; Figure 2); in MAD and CyL, we found genotype IV (Africa 4 clade), and in CLM, we found genotype III (Africa 3 clade).

Questing Ticks

We studied 597 pools (1,791 ticks) collected while questing: 452 pools (1,356 ticks) collected in 2017 and 145 pools (435 ticks) in 2018 (Table 4). The 2 ticks not identified as *H. lusitanicum* were *H. marginatum*. We found CCHFV-positive *H. lusitanicum* ticks in 7 pools, all collected in 2 provinces of AND region, Córdoba and Cádiz (4.2% positive pools in both provinces), of genotypes III (Africa 3 clade) and IV (Africa 4 clade), determined according to their S segment sequences (Table 4; Figures 1, 2).

Discussion

After the diagnosis of the first human cases of CCHF in Spain in 2016 (*11*), a large field study was planned and implemented, with the support of human and animal health authorities, that aimed to estimate the geographic distribution of CCHFV in Spain. The virus is considered a serious human health issue, so risk assessment had to be based on a geographically wide-ranging campaign of viral detection, examining ticks collected while questing or feeding on diverse vertebrates. By testing for CCHFV RNA, we used ticks as sentinels for the presence of the virus. Although the study was not designed to estimate prevalence, our data showed a 2.96% rate of positivity (135 positive pools out of 4,556), close to the values reported from other endemic locations, such as Turkey (3.6%), Albania (3.2%), and Kosovo (3.6%) (*27*–*29*). However, the wide range of methods used to collect ticks and analyze samples make reliable comparisons difficult.

In total, 3,959 pools were processed from 10,793 collected ticks. Tick management with acaricide is routinely practiced with domestic animals so they rarely have ticks; therefore, most of the feeding ticks were collected from wild animals. All of the positive tick pools were obtained from wild ungulates, consistent with the higher CCHFV antibody prevalence found in wildlife (61%) compared with livestock (15%) in the same areas (*30*). Wild ungulates range freely in most of the studied territory, although some are farmed as game, where the animals are confined to large farms. On these farms, game animals can be exposed to immature *Hyalomma* ticks through close contact with prominent hosts, such as rabbits and hares, simultaneously explaining the greater abundance of infected ticks and the higher serologic titers among farmed wild ungulates than among livestock.

The significance of finding CCHFV in feeding ticks is always difficult to interpret, because the virus could have been acquired through the blood meal, which means that determining the ticks' CCHFV status can-

Table 2. Ungulates sampled for tick collection and testing to determine the presence of Crimean-Congo hemorrhagic fever virus in ticks, Spain

Region (province)	Wild ungulates, no. (%)						Domestic ungulates, no. (%)		
	Red deer	Wild boar	Fallow deer	Mouflon	Barbary sheep	Total	Cattle	Goats	Total
Extremadura (Cáceres)	671 (3.2)	161 (1.2)	12 (0)	12 (0)	2 (0)	858 (2.8)	166 (0)	1 (0)	167 (0)
Madrid (Madrid)	16 (6.2)	7 (14.3)	2 (0)	3 (33.3)	0 (0)	28 (10.7)	0 (0)	0 (0)	0 (0)
Castile and León (Toledo)	44 (0)	8 (0)	5 (20.0)	0 (0)	0 (0)	57 (1.7)	69 (0)	7(0)	76 (0)
Total	731 (3.1)	176 (1.7)	19 (5.3)	15 (6.7)	2 (0)	943 (2.9)	235 (0)	8 (0)	243 (0)

*Percentages indicate animals in which Crimean-Congo hemorrhagic fever virus was detected in feeding ticks.

Table 3. Positive pools of ticks and genotypes of CCHFV, according to small segment sequences, detected in ticks collected while they were feeding on ungulates, Spain*

Region (province)	No. pools (no. ticks)	No. (%) positive pools	Tick species found with CCHFV (no. pools)	Animals found with CCHFV-infected ticks (no.)	Genotypes†
Madrid (Madrid)	90 (230)	7 (7.7)	*Hyaloma lusitanicum* (6), *Dermacentor marginatus* (1)‡	Mouflon (1), wild boar (1), red deer (1)	IV
Castile and León (Avila)	338 (829)	1 (0.3)	*Rhipicephalus annulatus* (1)	Fallow deer (1)	IV
Castile-La Mancha (Toledo)	642 (1,817)	76 (11.8)	*H. lusitanicum* (76)	Red deer§	III
Extremadura (Cáceres)	2,889 (7,917)	44 (1.5)	*H. lusitanicum* (42), *Ixodes ricinus* (2)¶	Red deer (22), wild boar (2)	I, III, IV
Total	3,959 (10,793)	128 (3.2)	NA	Red deer (>23), wild boar (3), fallow deer (1), mouflon (1)	I, III, IV

*CCHFV, Crimean-Congo hemorrhagic fever virus; NA, not applicable.
†Genotypes: I, West Africa (Africa 1); II, Central Africa (Africa 2); III, South and West Africa (Africa 3); IV, Middle East/Asia, divided into groups Asia 1 and Asia 2; V, Europe/Turkey (Europe 1); VI, Greece (Europe 2).
‡Collected from wild boar.
§In Castile-La Mancha, ticks of the same species but collected from different animals were mixed in a single tube, so it was not possible to determine the number of animals with positive ticks.
¶Collected from red deer.

not provide an accurate estimate of actual infection rates. We used the feeding ticks as sentinels of the presence of CCHFV and as a means of comparing the prevalence of the virus noted in questing ticks. Although collecting questing ticks is always more expensive and time-consuming, combining data from both sources could help provide a more balanced perspective for large geographic areas such as entire countries.

We found CCHFV from *I. ricinus*, *Rhipicephalus* spp., and *D. marginatus* ticks in 4 pools, but we considered these data to reflect serendipitous detection of viral RNA in feeding ticks. All of our results point toward a predominant role for *H. lusitanicum* in CCHFV circulation. In fact, it is very likely that circulation of the virus is restricted to *H. lusitanicum* ticks, a factor that had been suspected (*20*,*21*) but not confirmed. This finding emerged from the second phase of the study, in which we surveyed questing ticks. We demonstrated that the virus can successfully complete cycles in nature while perpetuating itself in *H. lusitanicum* ticks. This finding adds an extra dimension to our results, because the range of *H. lusitanicum* ticks is rapidly expanding as a consequence of the spread of one of its natural hosts, wild boars. Although the vectorial status of this tick has not been demonstrated, the discovery of viral RNA in molted ticks after a blood meal demonstrates that the virus can at least persist in these ticks (*5*). It is therefore a matter of urgency to establish the vectorial status of the species, as well as its preferences for biting humans, which seems to be a promising field of research. Because this tick is a potential source of CCHFV infection, its ability to be a parasite in humans has clearly been neglected, probably because it has not been reliably identified in the few samples collected from humans.

We identified 5 regions in central and southwest Spain where CCHFV is present. Taken together, findings from our report and an earlier study (*21*) indicate the permanent circulation of CCHFV in these regions, which are characterized by a Mediterranean forest ecosystem rich in wild ungulates that undoubtedly favors the presence of *H. lusitanicum* ticks. The lack of positive detection in MUR, one of the surveyed regions, does not prove that the virus is not present there, but more likely reflects the small number of ticks collected from the region.

Our system of confirmation involved amplification by 2 methods or from 2 extractions amplified using the same method. We confirmed positive amplification by real-time or nested RT-PCR in 118 out of 135 pools. We could not confirm amplification in the other 17 pools and had to repeat extraction and real-time RT-PCR. Given that sensitivity in the 2 PCR methods is similar, these differences in amplification could be because of variability in the target region (*31*). We obtained sequences from 105 of 128 pools of ticks collected from animals and for 3 of 7 pools collected from vegetation, which enabled us to identify genotypes on the basis of their S segment sequences. Viruses belonging to Africa 3 (genotype III) and Europe 1 (genotype V) had previously been detected in ticks; the newly proposed Africa 4 clade should be added to these findings (*18*–*21*) and should be interpreted as arising through the continuous exchange of infected ticks by birds migrating between Africa and southern Europe. This survey also detected the circulation of Africa 1 (genotype I) in Spain. These results confirm the wider-than-expected distribution and broad variability of CCHFV in Spain. These findings were initially unexpected but are compatible with reports of the genetic variability of the virus, because CCHFV is well known to undergo rearrangement to produce diverse combinations of the S, L, and M segments (*32*).

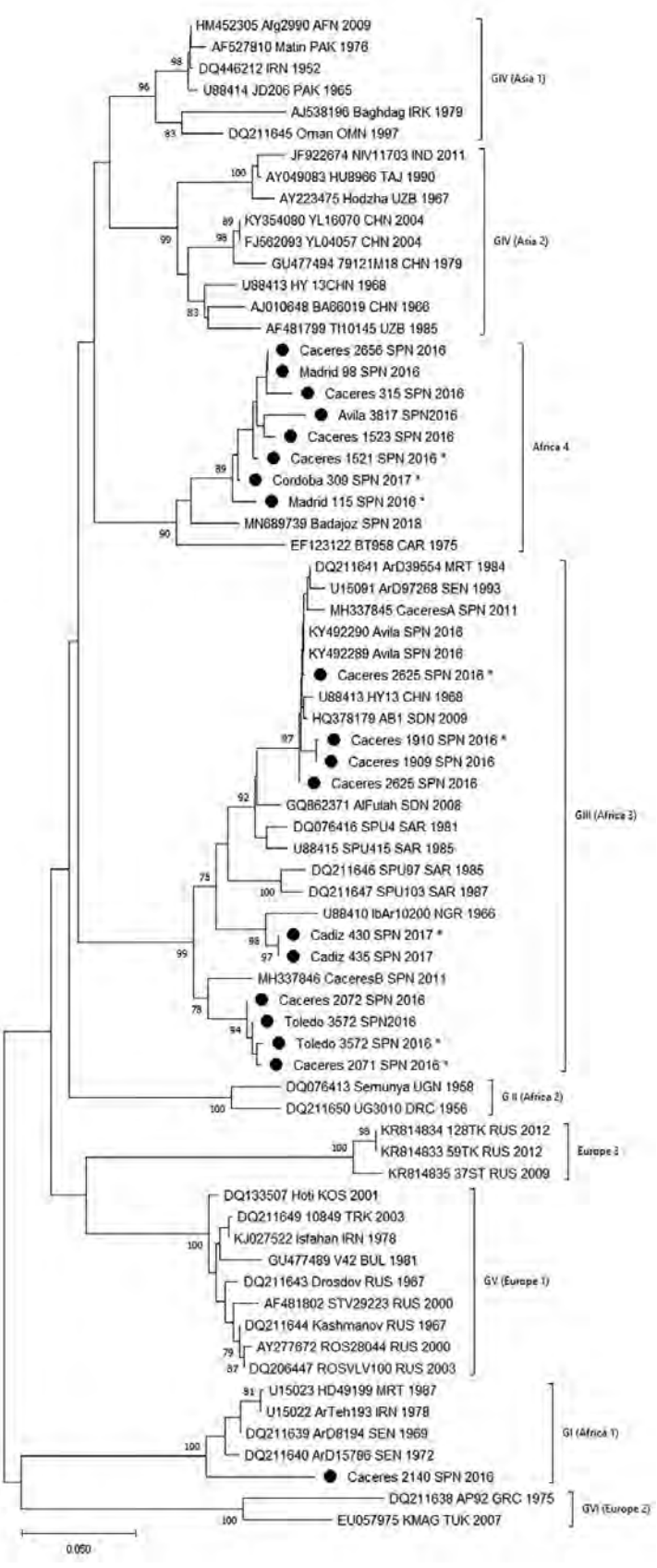

Figure 2. Phylogenetic tree obtained for strains of Crimean-Congo hemorrhagic fever virus detected in Spain (black dots) and other sequences downloaded from GenBank. We built the phylogenetic tree using the neighbor-joining method based on partial (175 nt) sequences of the virus small segment. Numbers in nodes indicate bootstrap values for the groups; values <75 are not shown. Strains detected from Spain are named by geographic origin, locality sampling site, and sampling year; other sequences are named by GenBank accession number, strain, geographic origin, and sampling year. Asterisks indicate sequences from this study that have been submitted to the EMBL (https://www.embl.org) and GenBank databases. Genotypes are indicated by Roman numerals: I, West Africa (Africa 1); II, Central Africa (Africa 2); III, South and West Africa (Africa 3); IV, Middle East/Asia, divided into groups corresponding to groups Asia 1 and Asia 2; V, Europe/Turkey (Europe 1); VI, Greece (Europe 2). Using guidelines published elsewhere (*25*,*26*), we then named and labeled the genotypes with equivalent clade nomenclature indicated in parentheses. Scale bar indicates substitutions/site (evolutionary distance).

Table 4. Genotypes of Crimean-Congo hemorrhagic fever virus, according to small segment sequences, detected in host-seeking adult *Hyalomma lusitanicum* ticks collected from vegetation, Spain*

Region	Province	No. pools (no. ticks)	No. (%) positive pools	Genotype
Andalusia	Huelva	113 (339)	0	NA
	Cádiz	66 (198)	5 (7.6)	III
	Córdoba	103 (309)	2 (1.9)	IV
Castile-La Mancha	Guadalajara	99 (297)	0	NA
	Ciudad Real	37 (111)	0	NA
Madrid	Madrid	146 (438)	0	NA
Murcia	Murcia	33 (99)	0	NA

*NA, not applicable.

The relationship of genotypes III, IV, and V to human cases in Spain has previously been described (Africa 3 in cases from 2016 and Africa 4 and Europe 1 from cases in 2018) (*13*,*14*,*17*). The great variability of genotypes may have resulted from multiple introduction events in Spain, but the complete mechanism of spread is very poorly understood. Published syntheses have reported that immature *H. lusitanicum* ticks feed on small mammals, perhaps mainly leporids, and adults feed on large ungulates (*6*). However, previous studies (*33*–*36*) have documented that when there are huge populations of the tick, large numbers of immature ticks were found on birds, such as the red partridge (*Alectoris rufa*), that spend most of their time on the ground.

Parasitism of birds does not seem to be the rule for *H. lusitanicum* ticks, which have not been found on birds migrating from Africa to Europe. We consider birds to be secondary, or even accidental, hosts for immature *H. lusitanicum* ticks, and therefore that immature *H. marginatum* ticks, which commonly feed on birds, may be the keystone species for transporting and importing CCHFV. We propose that annual migratory journeys from Africa of birds carrying *H. marginatum* ticks may have been the primary source of entry for several viral variants into Spain. Once introduced, the virus could have easily adapted to a cycle of transmission between wild ungulates and *H. lusitanicum* ticks, probably acquiring new mutations or reassortments. This hypothesis will be difficult to prove unless more data about *H. marginatum* ticks transported from Africa become available. Furthermore, the presence of European viral genotypes is difficult to reconcile with our observations and contrasts with data from other countries, such as Turkey and those of the Balkan region, where the virus is endemic. The occurrence of only 1 introduction from Asia to these countries has been proposed, and the strains causing human cases there have remained genetically stable for decades (*37*).

Our findings on the distribution of CCHFV in Spain demonstrate its presence in 5 regions covering the central and southwest part of the country. Our study also drew attention to the importance of *H. lusitanicum* ticks in circulating the virus including several viral genotypes and possible new reassortments. The risk for transmission to humans has not yet been possible to calculate because of the paucity of data. Research is needed to determine the reasons behind the high variability of CCHFV and the actual distribution and origin of circulating strains.

Clinicians, especially general practitioners, as well as laboratory staff, public health workers, stakeholders, and the general public need to be aware of the situation regarding CCHFV in Spain. Because some clinical cases may be mild and etiologically unresolved by practitioners, suitable tools must be made available that can detect the virus in suspected clinical cases in Spain. Diagnosis of CCHF is hampered by the biosafety conditions required to manage a virus of high biologic risk.

Public health activities, including surveillance of zoonoses like CCHF, need to be carried out under the One Health umbrella, as was done in our study. Large-scale seroprevalence studies in animals and humans are currently underway. The huge effort required to coordinate local and national public health representatives and entomologists, virologists, and animal and human health specialists should be an essential step in the control of these pathogens.

CCHFv Research Group: Rufino Álamo, Julio Alejandro Alvarez, Ulises Ameyugo, Enric Durán, Beatriz Fernández, Fernando Fúster, Lourdes Hernández, Laura Herrero, Nicola Lorusso, Francisca Molero, Pilar Peces, Jesús Peinado, Julián Mauro Ramos, Fátima Rodríguez, and Ana Vázquez.

Acknowledgments

We thank the veterinarians and technical staff who provided ticks from the different regions, without which the study would not have been possible, and the department heads who accommodated these efforts. We also thank Ana Sarriá and technicians from the NCM who helped with the molecular detection of ticks. Further, for their support and dedication, we thank Almudena Arribas, Fernando Simón, Ana Junco Bonet, María de la Cruz Pérez, Cristina Escacena Sainz, Andrés Iriso Calle, Eloy Marino Hernando, the staff from Consejería de Medio Ambiente, Olga Mínguez González, Ignacio de la Fuente Cabría, and Felix Gómez-Guillamón.

This study was partially funded by ISCIII, RD16CIII/0003/0003, Red de Enfermedades Tropicales, Subprogram RETICS Plan Estatal de I+D+I 2013-2016, and co-funded by FEDER Una Manera de Hacer Europa. Anabel Negredo, Ricardo Molina, Maribel Jiménez, and María Paz Sánchez-Seco are members of Red de Enfermedades Tropicales. In addition, ISCIII and Autonomous Communities used their own funds to support this work.

About the Author

Dr. Sánchez-Seco is a senior researcher at the Arbovirus and Imported Viral Diseases Laboratory at the National Centre of Microbiology, Madrid, Spain. Her research interests include the detection, characterization, and epidemiology of arboviral, zoonotic, and emerging diseases in Spain.

References

1. World Health Organization. Crimean Congo haemorrhagic fever [cited 2021 Jan 10]. https://www.who.int/health-topics/crimean-congo-haemorrhagic-fever#tab=tab_1
2. Schmaljohn CS, Hooper JW. Bunyaviridae: the viruses and their replication. In: Fields Virology. 4th ed. Philadelphia: Lippincott Williams & Wilkins editors. 2001. p. 1581–602.
3. Deyde VM, Khristova ML, Rollin PE, Ksiazek TG, Nichol ST. Crimean-Congo hemorrhagic fever virus genomics and global diversity. J Virol. 2006;80:8834–42. https://doi.org/10.1128/JVI.00752-06
4. Zehender G, Ebranati E, Shkjezi R, Papa A, Luzzago C, Gabanelli E, et al. Bayesian phylogeography of Crimean-Congo hemorrhagic fever virus in Europe. PLoS One. 2013;8:e79663. https://doi.org/10.1371/journal.pone.0079663
5. Gargili A, Estrada-Peña A, Spengler JR, Lukashev A, Nuttall PA, Bente DA. The role of ticks in the maintenance and transmission of Crimean-Congo hemorrhagic fever virus: a review of published field and laboratory studies. Antiviral Res. 2017;144:93–119. https://doi.org/10.1016/j.antiviral.2017.05.010
6. Apanaskevich DA, Horak IG. The genus *Hyalomma* Koch, 1844: V. Re-evaluation of the taxonomic rank of taxa comprising the *H.* (*Euhyalomma*) *marginatum* Koch complex of species (Acari: Ixodidae) with redescription of all parasitic stages and notes on biology. Int J Acarol. 2008;34:13–42. https://doi.org/10.1080/01647950808683704
7. Estrada-Peña A, Cevidanes A, Sprong H, Millán J. Pitfalls in tick and tick-borne pathogens research, some recommendations and a call for data sharing. Pathogens. 2021;10:712. https://doi.org/10.3390/pathogens10060712
8. Bente DA, Forrester NL, Watts DM, McAuley AJ, Whitehouse CA, Bray M. Crimean-Congo hemorrhagic fever: history, epidemiology, pathogenesis, clinical syndrome and genetic diversity. Antiviral Res. 2013;100:159–89. https://doi.org/10.1016/j.antiviral.2013.07.006
9. Hawman DW, Feldmann H. Recent advances in understanding Crimean-Congo hemorrhagic fever virus. F1000Res. 2018;7:F1000 Faculty Rev-1715. https://doi.org/10.12688/f1000research.16189.1
10. Messina JP, Pigott DM, Golding N, Duda KA, Brownstein JS, Weiss DJ, et al. The global distribution of Crimean-Congo hemorrhagic fever. Trans R Soc Trop Med Hyg. 2015;109:503–13. https://doi.org/10.1093/trstmh/trv050
11. Negredo A, de la Calle-Prieto F, Palencia-Herrejón E, Mora-Rillo M, Astray-Mochales J, Sánchez-Seco MP, et al.; Crimean Congo Hemorrhagic Fever@Madrid Working Group. Autochthonous Crimean-Congo hemorrhagic fever in Spain. N Engl J Med. 2017;377:154–61. https://doi.org/10.1056/NEJMoa1615162
12. Negredo A, Sánchez-Ledesma M, Llorente F, Pérez-Olmeda M, Belhassen-García M, González-Calle D, et al. Retrospective identification of an early autochthonous case of Crimean-Congo hemorrhagic fever in Spain, 2013. Emerg Infect Dis. 2021;27:1754–6. https://doi.org/10.3201/eid2706.204643
13. Negredo A, Sánchez-Arroyo R, Díez-Fuertes F, de Ory F, Budiño MA, Vázquez A, et al. Fatal case of Crimean-Congo hemorrhagic fever caused by reassortant virus, Spain, 2018. Emerg Infect Dis. 2021;27:1211–5. https://doi.org/10.3201/eid2704.203462
14. Monsalve Arteaga L, Muñoz Bellido JL, Negredo AI, García Criado J, Vieira Lista MC, Sánchez Serrano JÁ, et al. New circulation of genotype V of Crimean-Congo haemorrhagic fever virus in humans from Spain. PLoS Negl Trop Dis. 2021;15:e0009197. https://doi.org/10.1371/journal.pntd.0009197
15. Alerts and Health Emergencies Coordination Center. Detection of cases of Crimean-Congo hemorrhagic fever in Salamanca, Madrid, 25 August 2020 [in Spanish] [cited 2021 Sept 10]. https://www.mscbs.gob.es/profesionales/saludPublica/ccayes/alertasActual/Crimea_Congo/docs/20200827_ERR_Crimea_Congo_Salamanca.pdf
16. European Centre for Disease Prevention and Control. Cases of Crimean–Congo haemorrhagic fever in the EU/EEA, 2013–present [cited 2021 Sept 10]. https://www.ecdc.europa.eu/en/crimean-congo-haemorrhagic-fever/surveillance/cases-eu-since-2013
17. Ramírez de Arellano E, Hernández L, Goyanes MJ, Arsuaga M, Cruz AF, Negredo A, et al. Phylogenetic characterization of Crimean-Congo hemorrhagic fever virus, Spain. Emerg Infect Dis. 2017;23:2078–80. https://doi.org/10.3201/eid2312.171002
18. Estrada-Peña A, Palomar AM, Santibáñez P, Sánchez N, Habela MA, Portillo A, et al. Crimean-Congo hemorrhagic fever virus in ticks, Southwestern Europe, 2010. Emerg Infect Dis. 2012;18:179–80. https://doi.org/10.3201/eid1801.111040
19. Cajimat MNB, Rodriguez SE, Schuster IUE, Swetnam DM, Ksiazek TG, Habela MA, et al. Genomic characterization of Crimean-Congo hemorrhagic fever virus in *Hyalomma* tick from Spain, 2014. Vector Borne Zoonotic Dis. 2017;17:714–9. https://doi.org/10.1089/vbz.2017.2190
20. Negredo A, Habela MÁ, Ramírez de Arellano E, Diez F, Lasala F, López P, et al. Survey of Crimean-Congo hemorrhagic fever enzootic focus, Spain, 2011–2015. Emerg Infect Dis. 2019;25:1177–84. https://doi.org/10.3201/eid2506.180877
21. Moraga-Fernández A, Ruiz-Fons F, Habela MA, Royo-Hernández L, Calero-Bernal R, Gortazar C, et al. Detection of new Crimean-Congo haemorrhagic fever virus genotypes in ticks feeding on deer and wild boar, Spain. Transbound Emerg Dis. 2021;68:993–1000. https://doi.org/10.1111/tbed.13756
22. Estrada-Peña A, Bouattour A, Camicas J-L, Guglielmone A, Horak I, Jongejan F, et al. The known distribution and ecological preferences of the tick subgenus *Boophilus* (Acari: Ixodidae) in Africa and Latin America. Exp Appl Acarol. 2006;38:219–35. https://doi.org/10.1007/s10493-006-0003-5
23. Estrada-Peña A, Bouattour A, Camicas JL, Walker AR. Ticks of domestic animals in the Mediterranean region: a guide to identification of species. Zaragoza, Spain: Universidad de Zaragoza; 2004.

24. Atkinson B, Chamberlain J, Logue CH, Cook N, Bruce C, Dowall SD, et al. Development of a real-time RT-PCR assay for the detection of Crimean-Congo hemorrhagic fever virus. Vector Borne Zoonotic Dis. 2012;12:786–93. https://doi.org/10.1089/vbz.2011.0770
25. Carroll SA, Bird BH, Rollin PE, Nichol ST. Ancient common ancestry of Crimean-Congo hemorrhagic fever virus. Mol Phylogenet Evol. 2010;55:1103–10. https://doi.org/10.1016/j.ympev.2010.01.006
26. Chamberlain J, Cook N, Lloyd G, Mioulet V, Tolley H, Hewson R. Co-evolutionary patterns of variation in small and large RNA segments of Crimean-Congo hemorrhagic fever virus. J Gen Virol. 2005;86:3337–41. https://doi.org/10.1099/vir.0.81213-0
27. Orkun Ö, Karaer Z, Çakmak A, Nalbantoğlu S. Crimean-Congo hemorrhagic fever virus in ticks in Turkey: a broad range tick surveillance study. Infect Genet Evol. 2017;52:59–66. https://doi.org/10.1016/j.meegid.2017.04.017
28. Papa A, Velo E, Papadimitriou E, Cahani G, Kota M, Bino S. Ecology of the Crimean-Congo hemorrhagic fever endemic area in Albania. Vector Borne Zoonotic Dis. 2009;9:713–6. https://doi.org/10.1089/vbz.2008.0141
29. Sherifi K, Cadar D, Muji S, Robaj A, Ahmeti S, Jakupi X, et al. Crimean-Congo hemorrhagic fever virus clades V and VI (Europe 1 and 2) in ticks in Kosovo, 2012. PLoS Negl Trop Dis. 2014;8:e3168. https://doi.org/10.1371/journal.pntd.0003168
30. Ministry of Health. Consumption and Social Welfare. Situation report and risk assessment of transmission of Crimean-Congo hemorrhagic fever virus (CCHF) in Spain. July 2019 [in Spanish]. Madrid: Government of Spain; 2019.
31. Gruber CEM, Bartolini B, Castilletti C, Mirazimi A, Hewson R, Christova I, et al. Variability affects CCHFV detection by RT-PCR: a tool for in-silico evaluation of molecular assays. Viruses. 2019;11:953. https://doi.org/10.3390/v11100953
32. Goedhals D, Bester PA, Paweska JT, Swanepoel R, Burt FJ. Next-generation sequencing of southern African Crimean-Congo haemorrhagic fever virus isolates reveals a high frequency of M segment reassortment. Epidemiol Infect. 2014;142:1952–62. https://doi.org/10.1017/S0950268814000818
33. Calvete C, Estrada R, Lucientes J, Estrada A. Ectoparasite ticks and chewing lice of red-legged partridge, Alectoris rufa, in Spain. Med Vet Entomol. 2003;17:33–7. https://doi.org/10.1046/j.1365-2915.2003.00402.x
34. García Fernández P, Hueli LE. Ticks (Acarina, Ixodidae) parasitic on cattle in southern Spain. Identification, geographical and seasonal distribution [in Spanish]. Rev Iber Parasitol. 1984;44:129–38.
35. Guglielmone AA, Robbins RG, Apanaskevich DA, Petney TN, Estrada-Peña A, Horak IG. The hard ticks of the world (Acari: Ixodida: Ixodidae). Dordrecht, Netherlands: Springer Science & Business Media; 2014.
36. Perez-Eid C, Cabrita J. The larva and nymph of Hyalomma (Hyalomma) lusitanicum Koch, 1844 (Acari: Ixodida): morphological description, habitats, hosts [in French]. Acarologia. 2003;43:327–35.
37. Emmerich P, Jakupi X, von Possel R, Berisha L, Halili B, Günther S, et al. Viral metagenomics, genetic and evolutionary characteristics of Crimean-Congo hemorrhagic fever orthonairovirus in humans, Kosovo. Infect Genet Evol. 2018;65:6–11. https://doi.org/10.1016/j.meegid.2018.07.010

Address for correspondence: María Paz Sánchez-Seco, Centro Nacional de Microbiología, ISCIII, Ctra Pozuelo-Majadahonda Km 2, 28220 Madrid, Spain; email: paz.sanchez@isciii.es

West Nile Virus Transmission by Solid Organ Transplantation and Considerations for Organ Donor Screening Practices, United States

Raymond A. Soto, Emily McDonald, Pallavi Annambhotla, Jason O. Velez, Janeen Laven, Amanda J. Panella, Kimberly D. Machesky, Jennifer L. White, Judie Hyun, Emily Freuck, Janice Habel, David Oh, Marilyn Levi, Rick Hasz, Elling Eidbo, J. Erin Staples, Sridhar V. Basavaraju, Carolyn V. Gould

West Nile virus (WNV) is the most common domestic arbovirus in the United States. During 2018, WNV was transmitted through solid organ transplantation to 2 recipients who had neuroinvasive disease develop. Because of increased illness and death in transplant recipients, organ procurement organizations should consider screening during region-specific WNV transmission months.

West Nile virus (WNV) is the leading cause of mosquitoborne disease in the contiguous United States and is spread to humans primarily by *Culex* species mosquitoes (*1*). Transmission through solid organ transplantation (SOT) and blood transfusion was recognized during 2002 (*2,3*). Patients infected by SOT are at increased risk for severe disease and death, probably related to immunosuppression (*2,4–11*). In the United States, WNV screening of deceased organ donors is not mandatory and varies by organ procurement organization (OPO) (*12*). We describe WNV SOT transmission during 2018 and considerations for donor screening practices.

Author affiliations: Centers for Disease Control and Prevention, Fort Collins, Colorado, USA (R.A. Soto, E. McDonald, J.O. Velez, J. Laven, A.J. Panella, J.E. Staples, C.V. Gould); Centers for Disease Control and Prevention, Atlanta, Georgia, USA (P.D. Annambhotla, S.V. Basavaraju); Ohio Department of Health, Columbus, Ohio, USA (K.D. Machesky); New York Department of Health, Albany, New York, USA (J.L. White); Maryland Department of Health, Baltimore, Maryland, USA (J. Hyun); University of Cincinnati, Cincinnati, Ohio, USA (E. Freuck, J. Habel, D. Oh); Health Resources and Services Administration, Rockville, Maryland, USA (M. Levi); Association of Organ Procurement Organizations, Vienna, Virginia, USA (R. Hasz, E. Eidbo)

DOI: https://doi.org/10.3201/eid2802.211697

The Study

A man in his 60s who had diabetes mellitus, end-stage renal disease, and hepatitis C virus infection underwent kidney transplantation during September 2018. Nine days after transplantation, he was hospitalized because of fever and progressive obtundation. Detection of serum WNV IgM prompted suspicion of donor-derived infection. The case was reported to the United Network for Organ Sharing/Organ Procurement and Transplantation Network for investigation by the ad hoc Disease Transmission Advisory Committee and subsequent referral to the Centers for Disease Control and Prevention (CDC). The patient survived with no apparent neurologic deficits.

A recipient of a liver from the same donor was a man in his 30s who had alcoholism, hepatitis C virus infection, and cirrhosis. Sixteen days after transplantation, he became febrile and was hospitalized. He survived but had mild encephalopathy and peripheral neuropathy ≈1 month after transplantation.

The organ donor was a woman in her 20s who had a history of intravenous drug use and was found at home during September in cardiopulmonary arrest attributed to drug overdose. She was resuscitated but later declared brain dead. The left kidney and liver were recovered for transplantation. Interviews of family members yielded discrepant reports about preceding symptoms. In organ donor's state of residence, WNV human and equine disease cases, viremic blood donors, and mosquito infection rates were increased during 2018 compared with previous years.

Organ donor and recipient specimens were tested by state public health and commercial laboratories

for WNV RNA by using reverse transcription PCR (RT-PCR) and for WNV IgM and IgG by using enzyme immunoassay. Additional WNV testing was performed at CDC by using RT-PCR, microsphere immunoassay for IgM, and plaque reduction neutralization testing, as described (*13*,*14*).

We detected WNV IgM and IgG in cerebrospinal fluid from the kidney recipient, and WNV RNA in serum, blood, and urine collected 18 days after transplantation. Whole blood collected 24 days after transplantation still had detectable viremia. Pretransplant specimens were not tested. Serum collected from the liver recipient 18 days after transplantation had WNV IgM and neutralizing antibodies, but no detectable WNV RNA; WNV IgM was also detected in cerebrospinal fluid. No WNV RNA, IgM, or neutralizing antibodies were detected in pretransplant serum from the liver recipient. Donor plasma and serum collected on hospital day 3 had WNV RNA and no detectable IgM or neutralizing antibodies (Table 1).

To determine whether WNV was transmitted to the donor through blood products, the blood collection organization initiated a trace-back investigation. Remaining co-components from index donations were retrieved and quarantined, and blood donors were contacted to provide follow-up serum specimens. The organ donor received 7 blood products from 19 donors during the terminal hospitalization: 3 units of pooled cryoprecipitate (each from 5 donors), 3 units of fresh frozen plasma, and 1 unit of packed erythrocytes. All donations were screened for WNV by using minipool-nucleic acid testing (MP-NAT) before transfusion. All units of cryoprecipitate and plasma were transfused before WNV RNA-positive specimens were collected. Of 19 blood donors, 5 (26%) had no follow-up samples or co-components tested. Fourteen (74%) donors provided follow-up serum samples, including 2 who had plasma co-components from the same unit of pooled cryoprecipitate available for retrieval. All follow-up serum samples and co-components were negative for WNV IgM and neutralizing antibodies. RT-PCR was not performed for co-components because no WNV neutralizing antibodies were detected in follow-up serum samples.

Conclusions

Less than 1% of the general population have neuroinvasive disease develop after being bitten by an infected mosquito. In contrast, we found that patients infected by SOT have high rates of severe disease and death. In previous reports with available data, 14 (67%) infected recipients had neuroinvasive disease develop and 6 (29%) died (Table 2). Both patients in our study had neuroinvasive disease develop but survived.

Because blood transfusion has been implicated in organ donor infection (*2*,*5*), we conducted an extensive blood trace-back investigation. Although WNV-breakthrough transfusion transmission has been rare since routine blood donation screening was implemented in 2003, most cases have been associated with MP-NAT screening, which is less sensitive than individual donation-NAT; MP-NAT was used to test blood donations in this investigation (*15*). Although we could not definitively rule out blood transfusion as the source, the organ donor was probably infected through mosquitoes because widespread WNV transmission was occurring in the area of residence of the donor.

The organ donor did not undergo WNV screening but was found to have WNV viremia on testing of preprocurement specimens. Of 10 reports of SOT transmission, 8 occurred with no WNV donor screening (5 with RNA detected in archived serum samples), 1 occurred despite negative results for donor NAT screening (RNA also not detected in archived

Table 1. West Nile virus test results for organ donor and recipients, United States*

Person	Specimen	DRT	RNA	IgM	Neutralizing antibodies (titer)†	IgG
Organ donor	Plasma	−2	Detected			
	Serum	−2	Detected	ND	ND	
Liver recipient	Serum	0	ND	ND	ND	
	Serum	18	ND	Detected	Detected (1;2,560)	
	CSF	22		Detected		
	Serum	35	ND	Detected		
Kidney recipient	Serum	15		Detected		ND
	CSF	18		Detected		Detected
	Serum	18	Detected	Detected		
	Whole blood	18	Detected			
	Urine	18	Detected			
	Serum	25	ND	Detected		
	Whole blood	25	Detected			

*Blank cells indicate testing not performed. CSF, cerebrospinal fluid; DRT, day relative to transplantation; ND, not detected.
†90% plaque reduction neutralization test result <10 is considered negative.

Table 2. Reported WNV solid organ transplant transmission events, United States, 2002–2013*

		Organ donor				Organ recipient outcomes			
			Archived serum sample test result						
Date	Location	WNV screening	RNA	IgM/IgG	Likely/proven source of infection	No. infected/ total	No. NID/no. infected	No. deaths reported	Ref
2002 Aug	Georgia	No	Detected	ND/NR	Blood transfusion	4/4	3/4	1	(*2*)
2005 Aug	New York, Pennsylvania	No	ND	Detected/ detected	Mosquito	3/4	2/3	2	(*4*)
2008 Sep	Louisiana	No	ND	ND/ND	Blood transfusion	1/1	1/1	0	(*5*)
2009 Sep	Italy	No	Detected	NR	Mosquito	1/1	0/1	0	(*8*)
	California	No	Detected	ND/ND	Mosquito	1/1	1/1	0	(*10*)
	Texas	No	Detected	Detected/ equivocal	Mosquito	1/3	1/1	0	CDC, unpub. data
2010 Oct	California	No	Detected	ND/detected	Mosquito	2/3	1/2	1	(*9*)
2011 Aug	Italy	NAT negative	ND	Detected/ detected	Mosquito	4/5	2/4	0	(*7*)
2011, early fall	California	No	ND (detected in spleen and lymph node)	Detected/ detected (neutralizing antibodies also detected, titer 1:160)	Mosquito	4/4	3/4	2	(*11*)
2013	NR	NR	NR	NR	NR	NR/3	NR	0	(*6*)

*CDC, Centers for Disease Control and Prevention; ND, not detected; NAT, nucleic acid test; NID, neuroinvasive disease; NR, testing not reported; ref, reference; WNV, West Nile virus.

serum samples), and 1 did not report screening (Table 2). RNA might not be detected in infected donors because of hemodilution from transfusions and resuscitation efforts, undetectable viremia early or late in infection, assay detection limitations, or viral persistence in organs after resolution of viremia (*11*).

OPOs conduct extensive testing for infectious diseases, with direction and guidance from boards, medical advisory committees, and medical directors. For living donors, protocols are required for identifying and testing donors at risk for transmissible seasonal or regional endemic diseases, such as WNV disease. In contrast, there is no national policy requiring WNV screening of deceased organ donors. Limitations of screening include costs and logistical challenges of timely testing, false-negative screening results (*7*,*12*), and false-positive results that could lead to organ wasting and delays in lifesaving organ transplantation. A survey during 2008 found that 11 (19%) of 58 US OPOs performed WNV NAT screening of deceased potential organ donors (*12*). A follow-up survey conducted during 2019–2020 found that 16 (35%) of 46 OPOs performed WNV NAT screening, 5 in combination with IgM assays. Most OPOs performed year-round screening, and only 1 conducted seasonal screening (*15*).

During 2009–2018, a total of 89% of WNV disease cases reported nationally had illness onset during July–September (*1*). Furthermore, all WNV SOT transmission events, including the ones we report here, occurred during August–October (Table 2). Therefore, seasonal screening is likely to capture most cases and be more cost-effective than year-round testing. Seasonal screening could also improve the positive predictive value of screening results, reducing the risk for false-positive results. Although spatiotemporal variability in WNV disease incidence is high, OPOs in regions that have consistently high rates of WNV disease might have a more favorable cost-benefit ratio with screening (https://www.cdc.gov/westnile/statsmaps/cumMapsData.html). A triggering strategy using local blood donation screening and working with local or state health departments to determine times of increased virus circulation could also be considered. For a screening strategy to be successful, OPOs would need systems in place for timely test results to prevent allocation of organs from WNV-positive donors.

Given the high risk for severe WNV disease in SOT recipients, OPOs should consider the feasibility of WNV screening in organ donors, at least during months associated with regional WNV transmission. Transplant programs should also continue to inform organ recipients and their families about the possibility of infectious diseases being transmitted by organ transplantation.

Acknowledgments

We thank the Maryland Department of Health Laboratory and New York State Department of Health Wadsworth Center Laboratory for performing WNV diagnostic testing as part of this investigation. In addition, we thank the involved local health departments for their work in the investigation.

About the Author

Dr. Soto is an Epidemic Intelligence Service Officer in the Arboviral Diseases Branch, Division of Vector-Borne Diseases, National Center for Emerging and Zoonotic Infectious Diseases, Centers for Disease Control and Prevention, Fort Collins, CO. His research interests include arboviral epidemiology and prevention.

References

1. McDonald E, Mathis S, Martin SW, Staples JE, Fischer M, Lindsey NP. Surveillance for West Nile virus disease—United States, 2009–2018. MMWR Surveill Summ. 2021 ;70:1–15. https://doi.org/10.15585/mmwr.ss7001a1
2. Iwamoto M, Jernigan DB, Guasch A, Trepka MJ, Blackmore CG, Hellinger WC, et al.; West Nile Virus in Transplant Recipients Investigation Team. Transmission of West Nile virus from an organ donor to four transplant recipients. N Engl J Med. 2003;348:2196–203. https://doi.org/10.1056/NEJMoa022987
3. Pealer LN, Marfin AA, Petersen LR, Lanciotti RS, Page PL, Stramer SL, et al.; West Nile Virus Transmission Investigation Team. Transmission of West Nile virus through blood transfusion in the United States in 2002. N Engl J Med. 2003;349:1236–45. https://doi.org/10.1056/NEJMoa030969
4. Centers for Disease Control and Prevention (CDC). West Nile virus infections in organ transplant recipients—New York and Pennsylvania, August–September, 2005. MMWR Morb Mortal Wkly Rep. 2005;54:1021–3.
5. Centers for Disease Control and Prevention (CDC). West Nile virus transmission via organ transplantation and blood transfusion—Louisiana, 2008. MMWR Morb Mortal Wkly Rep. 2009;58:1263–7.
6. Green M, Covington S, Taranto S, Wolfe C, Bell W, Biggins SW, et al. Donor-derived transmission events in 2013: a report of the Organ Procurement Transplant Network Ad Hoc Disease Transmission Advisory Committee. Transplantation. 2015;99:282–7. https://doi.org/10.1097/TP.0000000000000584
7. Inojosa WO, Scotton PG, Fuser R, Giobbia M, Paolin A, Maresca MC, et al. West Nile virus transmission through organ transplantation in north-eastern Italy: a case report and implications for pre-procurement screening. Infection. 2012;40:557–62. https://doi.org/10.1007/s15010-012-0263-4
8. Morelli MC, Sambri V, Grazi GL, Gaibani P, Pierro A, Cescon M, et al. Absence of neuroinvasive disease in a liver transplant recipient who acquired West Nile virus (WNV) infection from the organ donor and who received WNV antibodies prophylactically. Clin Infect Dis. 2010;51:e34–7. https://doi.org/10.1086/655146
9. Rabe IB, Schwartz BS, Farnon EC, Josephson SA, Webber AB, Roberts JP, et al.; WNV Transplant Investigation Team. Fatal transplant-associated West Nile virus encephalitis and public health investigation-California, 2010. Transplantation. 2013;96:463–8. https://doi.org/10.1097/TP.0b013e31829b4142
10. Rhee C, Eaton EF, Concepcion W, Blackburn BG. West Nile virus encephalitis acquired via liver transplantation and clinical response to intravenous immunoglobulin: case report and review of the literature. Transpl Infect Dis. 2011;13:312–7. https://doi.org/10.1111/j.1399-3062.2010.00595.x
11. Winston DJ, Vikram HR, Rabe IB, Dhillon G, Mulligan D, Hong JC, et al.; West Nile Virus Transplant-Associated Transmission Investigation Team. Donor-derived West Nile virus infection in solid organ transplant recipients: report of four additional cases and review of clinical, diagnostic, and therapeutic features. Transplantation. 2014;97:881–9. https://doi.org/10.1097/TP.0000000000000024
12. Nett RJ, Kuehnert MJ, Ison MG, Orlowski JP, Fischer M, Staples JE. Current practices and evaluation of screening solid organ donors for West Nile virus. Transpl Infect Dis. 2012;14:268–77. https://doi.org/10.1111/j.1399-3062.2012.00743.x
13. Johnson AJ, Noga AJ, Kosoy O, Lanciotti RS, Johnson AA, Biggerstaff BJ. Duplex microsphere-based immunoassay for detection of anti-West Nile virus and anti-St. Louis encephalitis virus immunoglobulin M antibodies. Clin Diagn Lab Immunol. 2005;12:566–74.
14. Lanciotti RS, Kerst AJ, Nasci RS, Godsey MS, Mitchell CJ, Savage HM, et al. Rapid detection of West Nile virus from human clinical specimens, field-collected mosquitoes, and avian samples by a TaqMan reverse transcriptase-PCR assay. J Clin Microbiol. 2000;38:4066–71. https://doi.org/10.1128/JCM.38.11.4066-4071.2000
15. Theodoropoulos NM, Greenwald MA, Chin-Hong P, Ison MG. Testing deceased organ donors for infections: an organ procurement organization survey. Am J Transplant. 2021;21:1924–30. https://doi.org/10.1111/ajt.16552

Address for correspondence: Raymond A. Soto, Centers for Disease Control and Prevention, 3156 Rampart Rd, Fort Collins, CO 80521, USA: email:qdt7@cdc.gov

Serial Interval and Transmission Dynamics during SARS-CoV-2 Delta Variant Predominance, South Korea

Sukhyun Ryu,[1] Dasom Kim,[1] Jun-Sik Lim,[1] Sheikh Taslim Ali, Benjamin J. Cowling

We estimated mean serial interval and superspreading potential for the Delta variant of severe acute respiratory syndrome coronavirus 2 in South Korea. Intervals were similar for the first (3.7 days) and second (3.5 days) study periods. Risk for superspreading events was also similar; 23% and 25% of cases, respectively, seeded 80% of transmissions.

As of August 2021, South Korea is in the middle of a fourth community epidemic of severe acute respiratory syndrome coronavirus 2 (SARS-CoV-2) transmission, which is now predominated by the B.1.617.2 lineage (Delta variant) (*1*,*2*). The epidemic size largely depends on such epidemiologic characteristics as serial interval distribution and transmissibility (*3*,*4*). For the Delta variant of SARS-CoV-2, however, empirical evidence produced using country-level data are limited. We estimated serial interval distribution, reproductive numbers, and superspreading potential of SARS-CoV-2 during the Delta variant predominance in South Korea.

The Study

We obtained line-list data on coronavirus disease (COVID-19) cases reported by South Korea local public health authorities during July 11, 2021–September 1, 2021. Because the detection rate of the Delta variant accounted for >50% of local cases after July 25, 2021, and to avoid right-censoring bias, we divided the study duration into 2 periods (period 1, July 11, 2021–July 24, 2021; period 2, July 25, 2021–August 15, 2021). Overall, 82,671 local cases were obtained during the whole study period; 19,635 cases were identified in period 1, and 34,569 cases were identified in period 2. The data included information on contact tracing with other reported cases of COVID-19 (i.e., the case number of infector or infectee) and dates of symptom onset. The serial interval represents the time between symptom onset for both the infector and the infectee in a transmission chain (*3*). On the basis of line-list information, we reconstructed the transmission pairs by identifying the infector and infectee. We identified 3,728 transmission pairs (1,344 pairs in period 1 and 2,384 pairs in period 2) having the date of symptom onset for both infector and infectee. The overall mean of the serial interval estimate was 3.6 days (95% credible interval [CrI] 3.5–3.6 days) and the SD of the serial interval estimate was 4.9 days (95% CrI 4.9–5.0 days). The mean serial interval estimate were 3.7 (95% CrI 3.5–3.8) days with an SD of 4.8 (95% CrI 4.8–4.9) days during period 1, and 3.5 (95% CrI 3.4–3.6) days with an SD of 5.0 (95% CrI 4.9–5.0) days during period 2 (Figure 1, panel A). We used Welch's 2-sample t-test to compare the mean serial intervals for period 1 and period 2 and found no significant difference (p value = 0.40).

To identify the potential changes in SARS-CoV-2 transmissibility, we estimated the time-varying effective reproductive number (R_t), which defines the mean number of secondary infectious cases generated from a typical primary infectious case at time *t*. The epidemic becomes under control if R_t falls below 1 sustainably. We estimated R_t by using the EpiEstim package in R (*5*). In South Korea, nonpharmaceutical interventions including a nationwide mask mandate have been implemented since 2020. Because a large number of COVID-19 cases were identified by mid-July 2021, a 4-person limit for gatherings was implemented beginning July 19, 2021, nationwide (*6*) (Figure 1, panels B and C). However, we identified that

Author affiliations: Konyang University College of Medicine, Daejeon, South Korea (S. Ryu, D. Kim, J.-S. Lim); Seoul National University, Seoul, South Korea (J.-S. Lim); The University of Hong Kong, Hong Kong, China (S.T. Ali, B.J. Cowling); The Laboratory of Data Discovery for Health, Hong Kong Science and Technology Park, Hong Kong (S.T. Ali, B.J. Cowling)

DOI: https://doi.org/10.3201/eid2802.211774

[1]These authors contributed equally to this article.

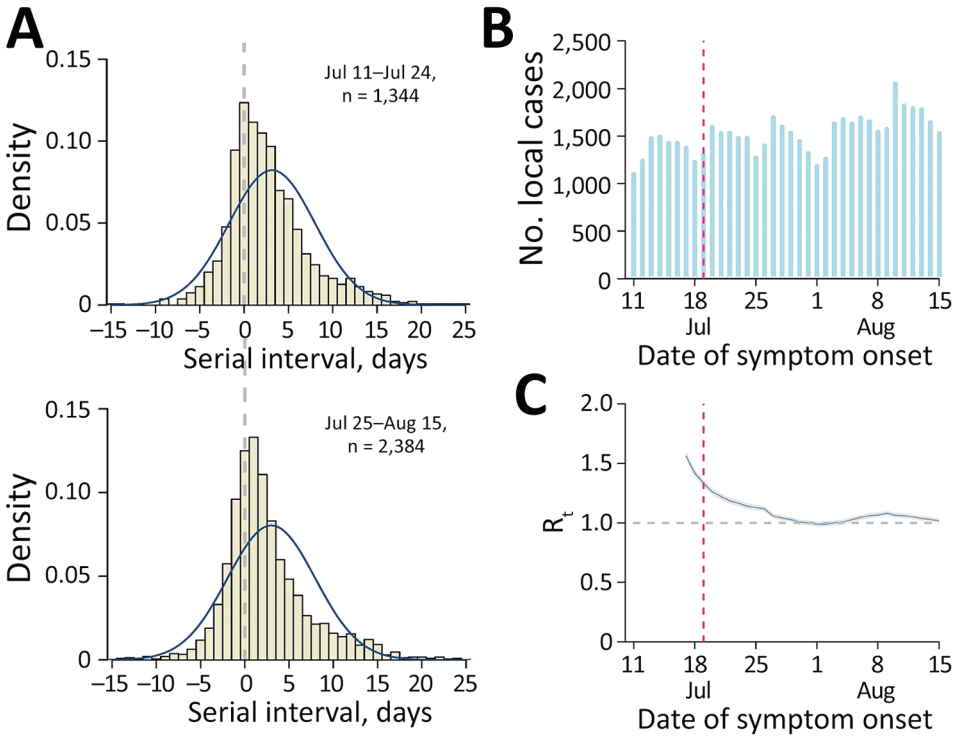

Figure 1. Estimated serial interval distribution, incidence of coronavirus disease, and transmissibility during predominance of the Delta variant of severe acute respiratory syndrome coronavirus 2 in South Korea. A) Estimated serial interval distribution for 3,728 infector-infectee pairs. Solid blue line indicates fitted normal distribution; vertical bars indicate the distribution of empirical serial intervals. B) Reported number of confirmed coronavirus disease cases by date of symptom onset. Red vertical dashed line indicates the date of implementation of an enhanced social distancing, including limiting gathering sizes to 4 persons nationwide on July 19, 2021. C) Estimated daily R_t of severe acute respiratory syndrome coronavirus 2 (blue line) with 95% credible intervals (gray shade). Gray horizontal dashed line indicates the critical threshold of R_t = 1. Red vertical dashed line indicates the date of implementation of an enhanced social distancing. R_t, effective reproductive number.

the estimated R_t was sustained at >1 during the study period (Figure 1, panel C).

To analyze superspreading potential, we identified 5,778 transmission pairs that included the COVID-19 cases for which no date of symptom onset was provided for either infector or infectee (2,169 pairs for period 1 and 3,609 pairs for period 2). We calculated the number of secondary cases for each person from the transmission pairs and fitted the data into a negative binomial distribution (*7*) (Appendix, https://wwwnc.cdc.gov/EID/article/28/2/21-1774-App1.pdf). The 2 parameters of the distribution represent the reproduction number (R_0) and overdispersion parameter (k). The estimated k for period 1 was 0.64 (95% CrI 0.57–0.72) and for period 2 was 0.85 (95% CrI 0.75–0.98), which corresponded to an expected percentage of cases responsible for 80% of secondary cases of 23% (95% CrI 22%–24%) for period 1 and 25% (95% CrI 24%–26%) for period 2 (Figure 2).

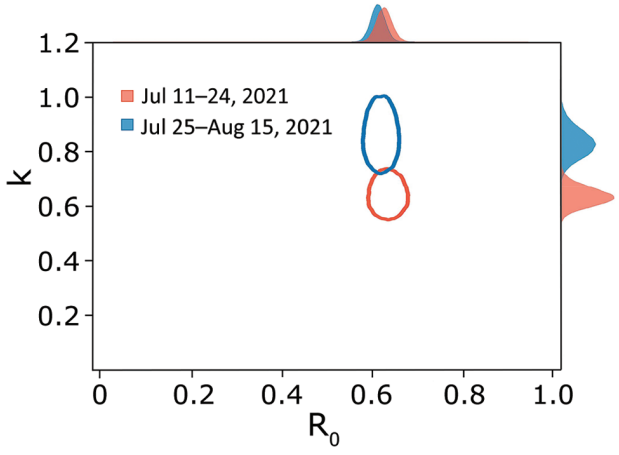

Figure 2. Risk for superspreading events for coronavirus disease during the Delta variant of severe acute respiratory syndrome coronavirus 2 predominance in South Korea. Joint estimates of k and R_0 of coronavirus disease were calculated by using 5,778 pairs (2,169 for period 1 and 3,609 for period 2). The red and blue ovals indicate the bivariate 95% credible region of the estimated k and R_0 for period 1 and period 2. The posterior marginal distributions were plotted in red and blue shaded regions. Period 1, July 11, 2021–July 24, 2021; period 2, July 25, 2021–August 15, 2021. k, overdispersion parameter; R_0, basic reproduction number.

Conclusions

We estimated the serial interval distributions of SARS-CoV-2 for early and later periods of the Delta variant predominance in South Korea and identified that mean serial intervals were similar across 2 different periods. This similarity is consistent with a recent study suggesting no substantial differences in the serial intervals between patients infected with the Delta variant and wild-type virus (*8*). In contrast, however, our findings suggested that the mean serial interval was 1 day longer than the estimates reported in a study describing the faster spread of the Delta

variant in China (mean serial interval of 2.3 days) compared with the wild type (*9*). Changes to public health measures, such as active contact tracing and rapid isolation of COVID-19 patients, would have shortened the serial interval and reduced transmissibility and superspreading potential (*3*,*4*). Since June 10, 2020, however, the South Korean public health authority has consistently implemented strategies for active case finding and immediately isolating laboratory-confirmed COVID-19 patients and exposed persons by using digital QR codes (*10*). Therefore, the effect of enhanced case isolation against the serial interval of SARS-CoV-2 is likely limited in our study. Furthermore, restricting large gatherings had likely reduced the superspreading potential. However, because the R_t was >1 during most of the study period, the nonpharmaceutical interventions implemented were likely insufficient to control the transmission of SARS-CoV-2 in South Korea.

Our study's first limitation is that we did not consider the effect of COVID-19 vaccinations in our analysis. About 14% of transmission pairs used in this study were linked with older adults (≥60 years of age), who might have received COVID-19 vaccinations. However, the vaccination program was not implemented in members of the public <55 years of age in early August 2021. Second, we did not consider changes in nonpharmaceutical interventions on the local level and possible increased travel during the study period, because it included summer holidays. Enhanced social distancing, however, including limiting gatherings to 4 persons, was in place nationwide during the study period. Third, we retrieved online case reports, which could contain some inaccuracies. However, the daily number of laboratory-confirmed local cases was similar between the collected line list and official daily reports (Appendix). Last, because individual genotype information was not included in the line-list data, the proportion of the Delta variant was evaluated from alternative data retrieved from the Korea Disease Control and Prevention Agency.

A previous study from South Korea, which examined the early transmissibility of SARS-CoV-2 in February–March 2020, estimated the mean R_0 as 1.5 for the wild type (*11*), and the early epidemic of COVID-19 was successfully controlled with nonlockdown social distancing (*12*). Our findings suggest that the introduction of the Delta variant is likely to have increased the difficulty of controlling SARS-CoV-2 transmission in South Korea. The large number of COVID-19 cases in South Korea during the study period could be explained by the increased secondary attack rate generated by cases of the Delta variant (*13*,*14*), which is in line with a previous study (*8*). Encouraging COVID-19 vaccination and further strengthening nonpharmaceutical interventions are warranted to mitigate spread of the Delta variant.

This article was preprinted at https://www.medrxiv.org/content/10.1101/2021.08.18.21262166v1.

This work was supported by the Basic Science Research Program through the National Research Foundation of Korea, funded by the Korean Ministry of Education (NRF-2020R1I1A3066471).

About the Author

Dr. Ryu is an assistant professor of preventive medicine at Konyang University College of Medicine, Daejeon, South Korea. His research interests include infectious disease epidemiology with a focus on transmission dynamic and public health interventions.

References

1. Cha S. South Korea reports record daily infections as Delta variant drives surge. Reuters. 2021 Jul 21 [cited 2021 Aug 6]. https://www.reuters.com/world/asia-pacific/south-korea-reports-new-daily-record-1784-covid-19-cases-kdca-2021-07-21/
2. Korea Disease Control and Prevention Agency. COVID-19 update as of 3 August 2021. 2021 Aug 3 [cited 2021 Aug 6]. https://www.korea.kr/news/policyBriefingView.do?newsId=156464695#sitemap-layer
3. Ali ST, Wang L, Lau EHY, Xu XK, Du Z, Wu Y, et al. Serial interval of SARS-CoV-2 was shortened over time by nonpharmaceutical interventions. Science. 2020;369:1106–9. https://doi.org/10.1126/science.abc9004
4. Lim JS, Noh E, Shim E, Ryu S. Temporal changes in the risk of superspreading events of coronavirus disease 2019. Open Forum Infect Dis. 2021;8:ofab350.
5. Thompson RN, Stockwin JE, van Gaalen RD, Polonsky JA, Kamvar ZN, Demarsh PA, et al. Improved inference of time-varying reproduction numbers during infectious disease outbreaks. Epidemics. 2019;29:100356. https://doi.org/10.1016/j.epidem.2019.100356
6. Central Disaster and Safety Countermeasures Headquarters. Private gatherings are possible for up to 4 people. 2021 [cited 2021 Aug 17]. http://ncov.mohw.go.kr/tcmBoardView.do?brdId=&brdGubun=&dataGubun=&ncvContSeq=366501&contSeq=366501&board_id=&gubun=ALL
7. Lloyd-Smith JO, Schreiber SJ, Kopp PE, Getz WM. Superspreading and the effect of individual variation on disease emergence. Nature. 2005;438:355–9. https://doi.org/10.1038/nature04153
8. Pung R, Mak TM, Kucharski AJ, Lee VJ; CMMID COVID-19 working group. Serial intervals in SARS-CoV-2 B.1.617.2 variant cases. Lancet. 2021;398:837–8. https://doi.org/10.1016/S0140-6736(21)01697-4
9. Zhang M, Xiao J, Deng A, Zhang Y, Zhuang Y, Hu T, et al. Transmission dynamics of an outbreak of the COVID-19 Delta variant B.1.617.2—Guangdong Province, China, May–June 2021. China CDC Wkly. 2021;3:584–6. https://doi.org/10.46234/ccdcw2021.148

10. S. Korea to test QR codes at nightclubs, eateries, cinemas to contain virus. Yonhap New Agency. 2020 Jun 1 [cited 2021 Aug 6]. https://en.yna.co.kr/view/AEN20200601003000315
11. Shim E, Tariq A, Choi W, Lee Y, Chowell G. Transmission potential and severity of COVID-19 in South Korea. Int J Infect Dis. 2020;93:339–44. https://doi.org/10.1016/j.ijid.2020.03.031
12. Chen YH, Fang CT, Huang YL. Effect of non-lockdown social distancing and testing—contact tracing during a COVID-19 outbreak in Daegu, South Korea, February to April 2020: a modeling study. Int J Infect Dis. 2021;110:213–21. https://doi.org/10.1016/j.ijid.2021.07.058
13. Dougherty K, Mannell M, Naqvi O, Matson D, Stone J. SARS-CoV-2 B.1.617.2 (Delta) variant COVID-19 outbreak associated with a gymnastics facility—Oklahoma, April–May 2021. MMWR Morb Mortal Wkly Rep. 2021;70:1004–7. https://doi.org/10.15585/mmwr.mm7028e2
14. Hwang H, Lim JS, Song SA, Achangwa C, Sim W, Kim G, et al. Transmission dynamics of the Delta variant of SARS-CoV-2 infections in South Korea. J Infect Dis. 2021 Dec 2 [Epub ahead of print].

Address for correspondence: Sukhyun Ryu, Department of Preventive Medicine, Konyang University College of Medicine, R707, Myungok-Euihak Gwan, 158, Gwanjeodong-ro, Seogu, Daejeon, 35365, South Korea; email: gentryu@onehealth.or.kr

Postvaccination Multisystem Inflammatory Syndrome in Adult with No Evidence of Prior SARS-CoV-2 Infection

Young Kyun Choi, Jae Young Moon, Jungok Kim, In Seol Yoo, Geun-Yong Kwon, Heuisoon Bae, Min Seob Song, Sungmin Kym

Ten days after receiving the first dose of coronavirus disease vaccine, a 22-year-old woman in South Korea experienced myocarditis, myopathy, pericarditis, and gastroenteritis; rash subsequently developed. There was no evidence of prior infection with severe acute respiratory syndrome coronavirus 2. The diagnosis was multisystem inflammatory syndrome resulting from coronavirus disease vaccination.

Multisystem inflammatory syndrome (MIS) is a serious complication of severe acute respiratory syndrome coronavirus 2 (SARS-CoV-2) infection that affects multiple body systems (cardiovascular, gastrointestinal, skin). It occurs predominantly in children (MIS-C) (*1*) and only rarely in adults (MIS-A) (*2*). The Brighton Collaboration Network (https://brightoncollaboration.us) includes MIS-C and MIS-A as possible coronavirus disease (COVID-19) vaccination–related adverse events (*3*). Most MIS cases occur in persons previously or concurrently infected with SARS-CoV-2 (*4*–*6*). We report a case of MIS-A that occurred after vaccination of a patient with no evidence of prior SARS-CoV-2 infection.

The Case

In April 2021, a previously healthy 22-year-old female healthcare worker visited the emergency department of Chungnam National University Sejong Hospital (Sejong, South Korea) with a 2-day history of fever, myalgia, sore throat, diarrhea, and vomiting and a 1-day history of continuous chest pain. She had received her first dose of the ChAdOx1 COVID-19 vaccine (AstraZeneca, https://www.astrazeneca.com) 10 days earlier and had undergone wisdom tooth extraction 8 days earlier. She had no other notable medical history and had not experienced COVID-19 symptoms in the previous 12 weeks. She tested negative for SARS-CoV-2 by real-time reverse transcription PCR. Antipyretics were ineffective.

At initial examination, the patient appeared acutely ill and had an elevated temperature (37.8°C), tachycardia (122 beats/min), mild pharyngeal injection, muscle tenderness, and limb weakness; she exhibited no signs of dental infection. Laboratory tests revealed increased levels of inflammatory markers (Table, https://wwwnc.cdc.gov/EID/article/28/2/21-1938-T1.htm). Chest radiographs and computed tomography (CT) images showed no signs of lung infiltration; abdominal CT images showed enterocolitis of the small and large intestines. Chest angiography and CT of the lower legs showed no evidence of pulmonary embolism or deep vein thrombosis.

Approximately 6 hours after arrival, the patient's blood pressure dropped to 70/45 mm Hg. After she received norepinephrine, her blood pressure normalized, and she was transferred to the intensive care unit, where we diagnosed myocarditis and pericarditis. Additional findings were elevated cardiac enzymes, ST segment elevation on electrocardiogram, and a small pericardial effusion on echocardiogram. Cardiac magnetic resonance imaging and biopsy sampling were not performed because of the patient's hemodynamic instability. PCR results were negative for adenovirus, metapneumovirus, rhinovirus, bocavirus, parainfluenza virus, respiratory syncytial

Author affiliations: Chungnam National University College of Medicine, Sejong, South Korea (Y.K. Choi, J.Y. Moon, J. Kim, I.S. Yoo, S. Kym); Sejong Public Health Center, Sejong (G.Y. Kwon); Sejong City Center for Infectious Diseases Control and Prevention, Sejong (H. Bae); Inje University College of Medicine, Busan, South Korea (M.S. Song)

DOI: https://doi.org/10.3201/eid2802.211938

virus, influenza virus, enterovirus, norovirus, rotavirus, astrovirus, and sapovirus, as were results for other tests for viruses causing viral myocarditis. Test results for C-rheumatoid factors and antineutrophil cytoplasmic, P-antineutrophil cytoplasmic, and antinuclear antibodies were also negative.

On hospital day 4, atrial fibrillation with a rapid ventricular response accompanied by hypotension (80/50 mm Hg) developed. After 2 treatments with cardioversion, the patient's cardiac rhythm reverted to sinus tachycardia, and her blood pressure normalized.

On day 7, a generalized macular rash developed and was treated with dexamethasone (5 mg/d for 3 d, followed by 2.5 mg/d for 4 d), after which methylprednisolone was administered for a possible antimicrobial drug–induced eruption. The patient's fever, rash, and inflammatory marker levels fluctuated according to steroid dose (Figure 1, panel B). Echocardiography images (day 12) showed an increased 1-cm deep pericardial effusion during diastole through the heart circumference without evidence of endocarditis.

On day 15, SARS-CoV-2 serologic testing with a chemiluminescence immunoassay (Liaison SARS-CoV-2 TrimericS IgG assay; DiaSorin, https://ww.diasorin.com) was performed. Antibody level was 21.88, which is high compared with the average value of 5.56 after first vaccination among healthcare workers without prior SARS-CoV-2 infection but low compared with the average value of 46.34 among those with prior infection (*7*). Antibody analysis using an in-house colloidal gold qualitative immunoassay was positive for anti–spike protein receptor-binding antibodies and negative for antinucleocapsid antibodies (Figure 2).

We empirically administered multiple regimens of antimicrobial drugs during the first 21 days of hospitalization. Bacterial cultures were negative, and no focal signs of infection were found. MIS-A was diagnosed on day 21 after the possibility of infection was excluded, and empiric administration of antimicrobial drugs was discontinued.

On days 28 and 29, human immunoglobulin therapy (1 g/kg) was administered because after 2 weeks of steroid therapy, the patient's rash had subsided but her body temperature and C-reactive protein (CRP) level remained high. Muscle weakness, especially hip flexion, had worsened, and the patient was unable to stand without assistance. At that time, the steroid dose was increased, but the disease was not controlled. The immunoglobulin therapy also produced no therapeutic response. The patient's fever spiked to 40°C, and her CRP level increased. On day 34, steroid pulse therapy (methylprednisolone 1 g/d for 3 d) was initiated, resulting in defervescence and decreased CRP levels. When the steroid dose was tapered, her body temperature and CRP level increased, and steroid pulse therapy was extended for another week.

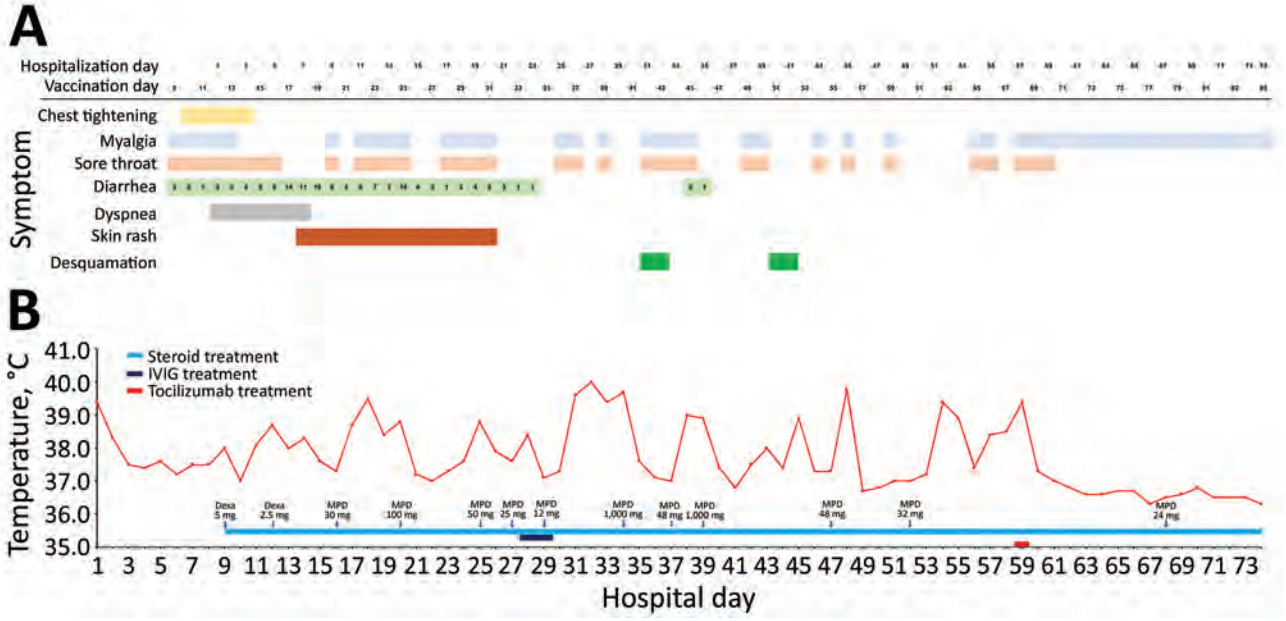

Figure 1. Clinical course of illness in adult with postvaccination multisystem inflammatory syndrome and no evidence of prior SARS-CoV-2 infection, South Korea. A) Signs/symptoms according to the day of hospitalization and the days since vaccination. B) Patient's maximum body temperature and anti-inflammatory therapy according to the day of hospitalization. Dexa, dexamethasone; IVIG, intravenous immunoglobulin; MPD, methylprednisolone.

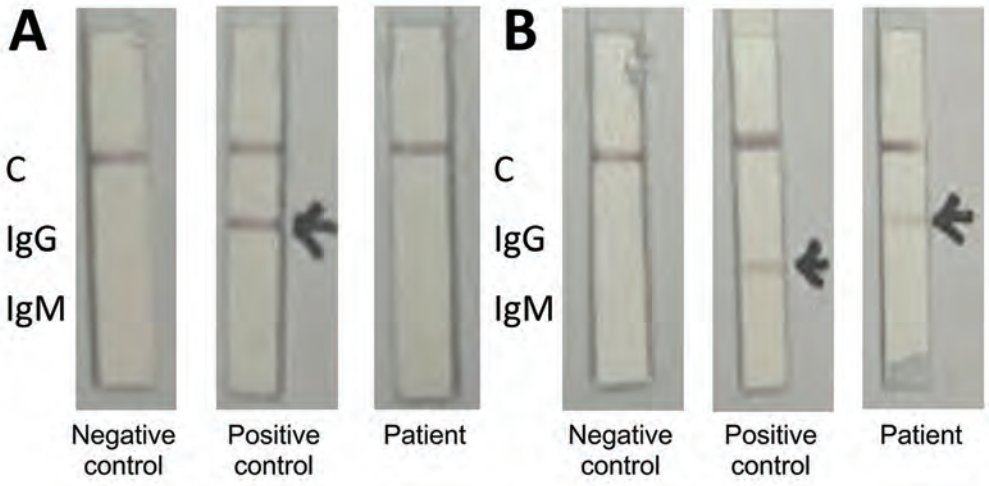

Figure 2. Colloidal gold qualitative immunoassay for antibodies against severe acute respiratory syndrome coronavirus 2, South Korea. A) Nucleocapsid protein conjugate; B) spike receptor-binding domain conjugate. The positive control serum contains antinucleocapsid IgG and anti–spike protein receptor-binding IgM. C, control.

After steroid therapy was discontinued, the patient's body temperature and CRP levels again increased. She experienced desquamation of the skin on her fingers on day 30 and of her toes on day 40.

On day 30, a nerve conduction velocity test and electromyogram showed signs of myopathy. Interventional angiography (day 43) showed no abnormality of her coronary arteries. Positron emission tomography (day 59) showed increased contrast medium uptake by soft tissues resulting from inflammation but no focal signs of infection.

On day 60, tocilizumab (8 mg/kg) was administered, after which the patient remained afebrile and the muscle pain in her extremities decreased (Figure 1). She was discharged on day 74 despite residual muscle weakness requiring rehabilitation therapy.

Conclusions

Most vaccine-related MIS cases have been associated with past or concurrent SARS-CoV-2 infection; recently, MIS cases occurring after mRNA vaccine administration in children and adults in the absence of SARS-CoV-2 infection have also been reported (*8*,*9*). To our knowledge, this case of MIS in an adult was induced by a viral-vector vaccine. This case meets the Brighton Collaboration Criteria for definite MIS-A on the basis of patient age, fever (>3 days), multiorgan involvement, elevated inflammatory markers, elevated N-terminal–pro B-type natriuretic peptide, neutrophilia, lymphopenia, pericardial effusion, and electrocardiographic changes consistent with myopericarditis (*3*).

Antinucleocapsid antibodies typically appear ≥2 weeks after onset of SARS-CoV-2 infection (*10*), although in some patients they do not appear (*11*). For the patient reported here, at the time she visited the hospital, the cumulative incidence of COVID-19 in her community was 333 cases/100,000 population and the average daily number of cases in the 12 weeks before her visit remained low (n = 1.95). The medical institution where she worked did not treat COVID-19 patients. Given that she had not had COVID-19 signs/symptoms within the previous 12 weeks, the likelihood of prior infection is low.

The clinical features of Kawasaki disease, including desquamation, are similar to those reported for this patient. Desquamation has reportedly occurred in COVID-19 patients, MIS patients, and COVID-19 vaccine recipients (*11*–*13*). Kawasaki disease primarily affects children; gastrointestinal involvement is uncommon, and coronary artery dilatation is the main cardiac problem observed. MIS almost universally involves the gastrointestinal and cardiac systems; incidence of shock and myocarditis/pericarditis is high (*3*). We ruled out adult-onset Still's disease on the basis of absence of arthritis, liver enzyme levels within reference range, and an inconsistent skin rash (*14*). Features of toxic shock syndrome are also similar to those reported for this patient, including fever, rash, desquamation, hypotension, gastrointestinal symptoms, myalgia, and mucosal inflammation. However, we found no evidence of staphylococcal or streptococcal infection, and the patient had not used tampons. Although we cannot rule out other infections, autoimmune causes, or malignancies, the most reasonable diagnosis for this patient is MIS-A.

MIS mainly occurs after SARS-CoV-2 infection in children. The reason for this age predilection is unknown, but if it is associated with the SARS-CoV-2 spike protein or antibodies induced by the spike protein (the target of SARS-CoV-2 vaccines), vaccine-associated MIS-C may become more common as more children receive SARS-CoV-2 vaccination.

About the Author

Prof. Choi is an infectious disease physician at the Division of Infectious Diseases and the Department of Intensive Care at the Chungnam National University Sejong Hospital. He is actively engaged in COVID-19 treatment. His primary research interests include intensive care unit infection control and sepsis.

References

1. Godfred-Cato S, Bryant B, Leung J, Oster ME, Conklin L, Abrams J, et al.; California MIS-C Response Team. COVID-19–associated multisystem inflammatory syndrome in children—United States, March–July 2020. MMWR Morb Mortal Wkly Rep. 2020;69:1074–80. https://doi.org/10.15585/mmwr.mm6932e2
2. Morris SB, Schwartz NG, Patel P, Abbo L, Beauchamps L, Balan S, et al. Case series of multisystem inflammatory syndrome in adults associated with SARS-CoV-2 infection—United Kingdom and United States, March–August 2020. MMWR Morb Mortal Wkly Rep. 2020;69:1450–6. https://doi.org/10.15585/mmwr.mm6940e1
3. Vogel TP, Top KA, Karatzios C, Hilmers DC, Tapia LI, Moceri P, et al. Multisystem inflammatory syndrome in children and adults (MIS-C/A): case definition & guidelines for data collection, analysis, and presentation of immunization safety data. Vaccine. 2021;39:3037–49. https://doi.org/10.1016/j.vaccine.2021.01.054
4. Salzman MB, Huang CW, O'Brien CM, Castillo RD. Multisystem inflammatory syndrome after SARS-CoV-2 infection and COVID-19 vaccination. Emerg Infect Dis. 2021;27:1944–8. https://doi.org/10.3201/eid2707.210594
5. Uwaydah AK, Hassan NMM, Abu Ghoush MS, Shahin KMM. Adult multisystem inflammatory syndrome in a patient who recovered from COVID-19 postvaccination. BMJ Case Rep. 2021;14:e242060. https://doi.org/10.1136/bcr-2021-242060
6. Grome HN, Threlkeld M, Threlkeld S, Newman C, Martines RB, Reagan-Steiner S, et al. Fatal multisystem inflammatory syndrome in adult after SARS-CoV-2 natural infection and COVID-19 vaccination. Emerg Infect Dis. 2021;27:2914–8. https://doi.org/10.3201/eid2711.211612
7. Lim SY, Kim JY, Lee JA, Kwon JS, Park JY, Cha HH, et al. Immune responses and reactogenicity after ChAdOx1 in individuals with past SARS-CoV-2 infection and those without. 2021 Jul 28. J Infect. 2021:S0163-4453(21)00375-3. Online ahead of print. PubMed https://doi.org/10.1016/j.jinf.2021.07.032
8. European Medicines Agency. Meeting highlights from the Pharmacovigilance Risk Assessment Committee (PRAC) 30 August–2 September 2021 [cited 2021 Oct 19]. https://www.ema.europa.eu/en/news/meeting-highlights-pharmacovigilance-risk-assessment-committee-prac-30-august-2-september-2021
9. Nune A, Iyengar KP, Goddard C, Ahmed AE. Multisystem inflammatory syndrome in an adult following the SARS-CoV-2 vaccine (MIS-V). BMJ Case Rep. 2021;14:e243888. https://doi.org/10.1136/bcr-2021-243888
10. Brochot E, Demey B, Touzé A, Belouzard S, Dubuisson J, Schmit JL, et al. Anti-spike, anti-nucleocapsid and neutralizing antibodies in SARS-CoV-2 inpatients and asymptomatic individuals. Front Microbiol. 2020;11:584251. https://doi.org/10.3389/fmicb.2020.584251
11. Irvine NJ, Wiles BL. Petechiae and desquamation of fingers following immunization with BNT162b2 messenger RNA (mRNA) COVID-19 vaccine. Cureus. 2021;13:e16858.
12. Marraha F, Al Faker I, Gallouj S. A review of the dermatological manifestations of coronavirus disease 2019 (COVID-19). Dermatol Res Pract. 2020;2020:9360476. https://doi.org/10.1155/2020/9360476
13. Young TK, Shaw KS, Shah JK, Noor A, Alperin RA, Ratner AJ, et al. Mucocutaneous manifestations of multisystem inflammatory syndrome in children during the COVID-19 pandemic. JAMA Dermatol. 2021;157:202–12. https://doi.org/10.1001/jamadermatol.2020.4779
14. Gerfaud-Valentin M, Jamilloux Y, Iwaz J, Sève P. Adult-onset Still's disease. Autoimmun Rev. 2014;13:708–22. https://doi.org/10.1016/j.autrev.2014.01.058

Address for correspondence: Sungmin Kym, Division of Infectious Disease, Department of Internal Medicine, Chungnam National University Sejong Hospital, Chungnam National University College of Medicine, 30099 Sejong, South Korea; email: smkimkor@gmail.com

SARS-CoV-2 B.1.619 and B.1.620 Lineages, South Korea, 2021

Ae Kyung Park, Il-Hwan Kim, Heui Man Kim, Hyeokjin Lee, Nam-Joo Lee, Jeong-Ah Kim, SangHee Woo, Chae young Lee, Jaehee Lee, Sae Jin Oh, JeeEun Rhee, Cheon-Kwon Yoo, Eun-Jin Kim

We report the rapid emergence of severe acute respiratory syndrome coronavirus 2 lineages B.1.619 and B.1.620 in South Korea. The surge in frequency in a relatively short time emphasizes the need for ongoing monitoring for new lineages to track potential increases in transmissibility and disease severity and reductions in vaccine efficacy.

Since the emergence of coronavirus disease (COVID-19) in December 2019, ≈2 million genomes of SARS-CoV-2 have been sequenced worldwide, revealing that the virus is continuously mutating (*1*). The mutations of SARS-CoV-2 spike protein must be monitored because of its vital role in attaching to the host cell-surface receptor, angiotensin-converting enzyme 2 (ACE2) (*2*), which increases its infectivity (*3*).

As of May 31, 2021, the World Health Organization (WHO) reported the appearance of several variants of concern (VOCs) whose characteristics have serious implications on public health: Alpha (B.1.1.7), Beta (B.1.351), Gamma (P.1), and Delta (B.1.617.2) (*4*). These variants arose from changes in the spike protein, especially in the receptor-binding domain (RBD). The RBD plays an important role in direct interaction with human ACE2; the 4 variants contain >1 of the specific substitutions (K417N, L452R, T478K, E484K, and N501Y) that affect viral fitness and transmissibility. These variants possess substantially higher transmissibility, evade immunity, increase disease severity, reduce vaccine efficacy, and escape diagnostic detection (*5*). WHO designated Lambda (C.37) as a variant of interest (VOI) on June 14, 2021, and Mu (B.1.621) as a VOI on August 30, 2021. These variants were considered likely to become highly transmissible and evade vaccine protection, thus threatening South America, where they were first identified (Acevedo et al., unpub. data, https://doi.org/10.1101/2021.06.28.21259673) (*6*).

Author affiliation: Korea Disease Control and Prevention Agency, Cheongju, South Korea

DOI: https://doi.org/10.3201/eid2802.211653

Genomic surveillance and open data sharing of viral genome sequences have enhanced near–real-time detection, comparison, and tracking of SARS-CoV-2 variants (*1*). The Korea Disease Control and Prevention Agency (KDCA) has been conducting whole-genome sequencing (WGS) of SARS-CoV-2 in South Korea since the beginning of the pandemic; targeted sequencing of the spike protein is being implemented to strengthen new variant monitoring. Lineage distribution analysis in South Korea indicated that, from its discovery in March 2020 until January 2021, the B.1.497 lineage was predominant in domestic cases (*7*,*8*). B.1.497 formed 1 of 4 major clusters in South Korea but was the only one that had expanded and predominantly circulated in the country (*9*). Sequence analysis indicated that it was originally clustered with North American viruses; additional genetic mutations in this cluster are H1113Y, T2408N, P4223S, and A5770S in open reading frame 1ab (ORF1ab) and Q52H, A222V, E556K, T716I, and A1070V in the spike protein. However, changes have been observed in lineage distribution since March 2021; increases in B.1.619 and B.1.620 are of note. We report the sudden emergence of these 2 lineages harboring the E484K mutation in the spike protein, which rapidly outcompeted the existing variants in South Korea.

The Study

We collected nasopharyngeal and oropharyngeal swab samples from patients with SARS-CoV-2 cases confirmed by real-time reverse transcription PCR (rRT-PCR). We prepared WGS libraries using QIAseq SARS-CoV-2 Primer Panel and QIAseq FX DNA Library UDI Kit (QIAGEN, https://www.qiagen.com) and sequenced them on MiSeq (Illumina, https://www.illumina.com) with 2 × 150 bp using MiSeq reagent kit version 2 (Illumina). For phylogenetic tree analysis, we aligned whole genomic sequences using MAFFT version 7 (https://mafft.cbrc.jp/alignment/

server), inferred maximum-likelihood phylogenetic trees with FastTree version 2.1.9 (http://www.microbesonline.org/fasttree), and visualized using Interactive Tree of Life version 5 (https://itol.embl.de). The sequences have been uploaded to the GISAID EpiCoV database (https://www.gisaid.org).

We obtained WGS of 9,554 SARS-CoV-2 as of July 21, 2021, representing >5% of the total reported positive cases during this period. Specifically, we obtained WGS for 6.2% of the total positive cases during April–July, when the number of infections by B.1.619 and B.1.620 increased sharply. Of those, 7,585 were domestic cases.

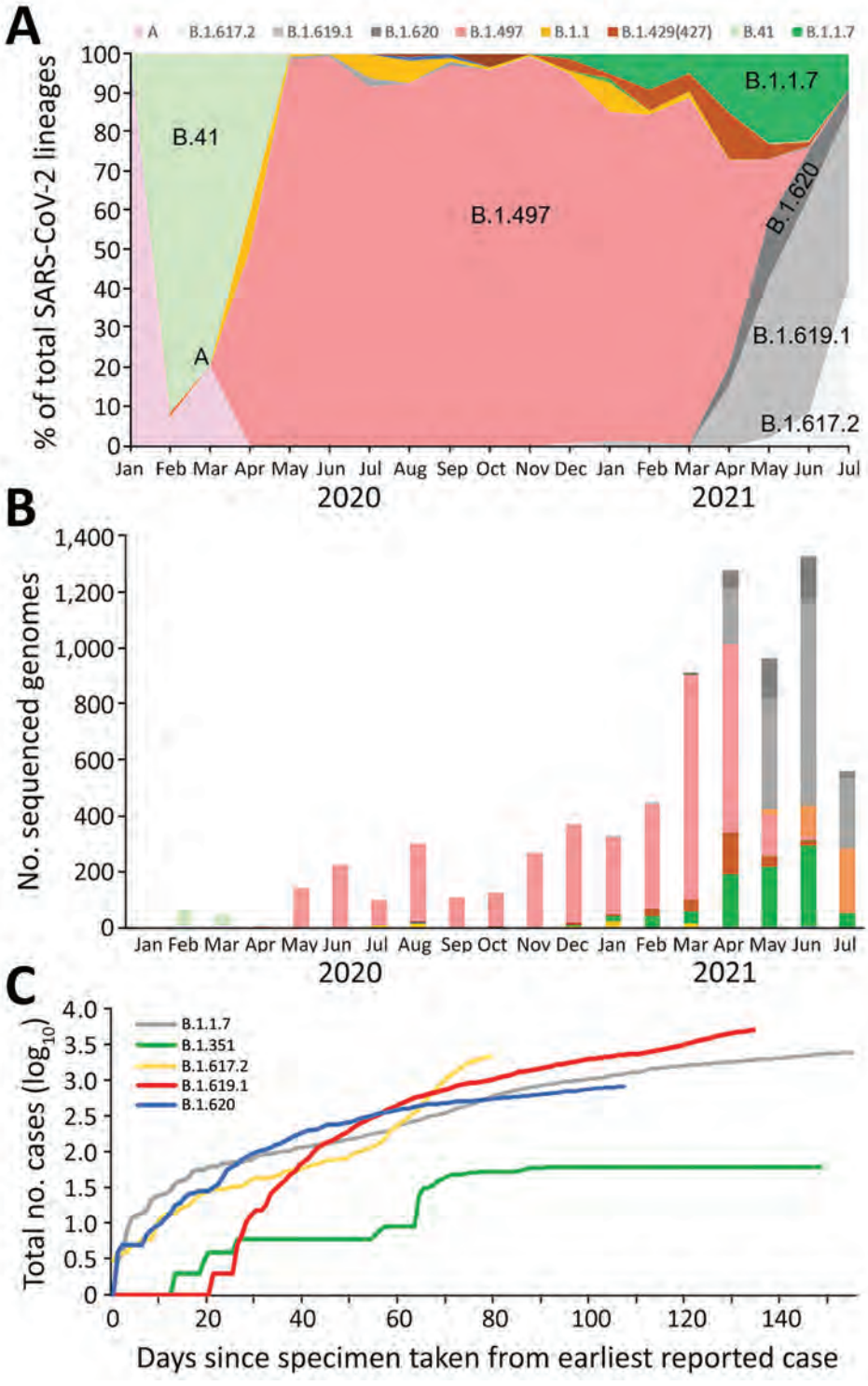

Figure 1. Investigation of SARS-CoV-2 B.1.619 and B.1.620 lineages, South Korea, 2021. A) Distribution of 7 SARS-CoV-2 lineages in domestic cases over time. Data are shown for lineages A, B.41, B.1.497, B.1.1.7 (Alpha variant), B.1.617.2 (Delta variant), B.1.619.1, and B.1.620. B) Number of sequenced genomes over time, by lineage. C) Logarithmic graph of cumulative cases of variants indexed by days since the first reported case as of July 21, 2021. SARS-CoV-2, severe acute respiratory syndrome coronavirus 2.

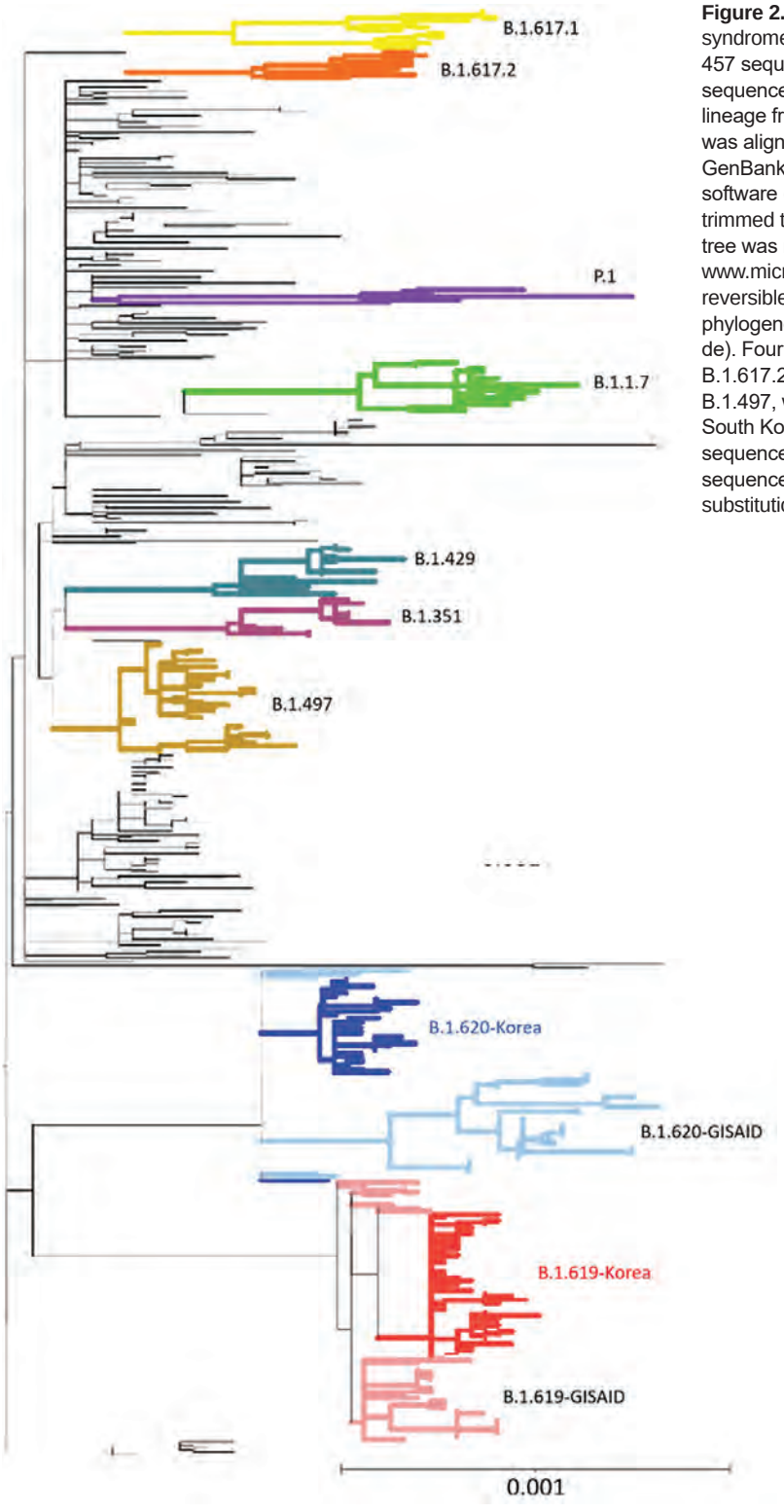

Figure 2. Phylogenetic analysis of severe acute respiratory syndrome coronavirus 2 sequences, South Korea. A total of 457 sequences were used to construct the tree, including 37 sequences of B.1.619 lineage and 36 sequences of B.1.620 lineage from GISAID (https://www.gisaid.org). Each sequence was aligned to the reference sequence (Wuhan-Hu-1, GenBank accession no. NC_045512) using Geneious Prime software (https://www.geneious.com) and then manually trimmed to equal lengths. A maximum-likelihood phylogenetic tree was reconstructed using FastTree version 2.1.9 (http://www.microbesonline.org/fasttree), under the general time reversible plus gamma nucleotide substitution model; the phylogenetic tree was visualized using iTOL (https://itol.embl.de). Four variants of concern (B.1.1.7, B.1.351, P.1, and B.1.617.2), 2 variants of interest (B.1.429 and B.1.617.1), and B.1.497, which were the major lineages of the GH clade in South Korea, are shown. Red indicates South Korea B.1.619 sequences and blue, B.1.620; pink indicates Europe B.1.619 sequences and light blue, B.1.620. Scale bar indicates substitutions per site.

As described previously (*7*), the A and B.41 lineages were the most prevalent at the beginning of the pandemic in South Korea. However, B.1.497 (formerly known as B.1.3.1) gained predominance in South Korea after its emergence in March 2020 (*8*,*9*). The lineage distribution has been changing since January 2021 as VOCs have emerged. The earliest recorded Alpha variant in South Korea was identified on December 22,

Table 1. Amino acid substitutions in severe acute respiratory syndrome coronavirus 2 B.1.619 and B.1.620 lineages, South Korea*

Gene	B.1.497	B.1.619	B.1.620
ORF1a	T265I, P3884L	A2123V, E2607K, del3675/3677, M3752I	T403I, V1991I, del3675/3677
ORF1b	P314L, Q2403L	P314L	P314L, A1215S
S	D614G	I210T, N440K, E484K, D614G, D936N, S939F, T1027I	P26S, del69/70, V126A, del144/145, S477N, E484K, D614G, P681H, T1027I, D1118H
ORF3a	Q57H	None	None
M	None	I82T	None
ORF7a	None	E22D	None
ORF7b	None	None	del14/15
N	None	P13L, S201I, T205I	A220V

*M, membrane glycoprotein; N, nucleocapsid; ORF, open reading frame; S, spike.

2020; its prevalence increased to 22.0% as of June 2021 (Figure 1). Simultaneously, prevalence rates of B.1.619 and B.1.620 increased rapidly; prevalence was 55.4% in March 2021 and 11.5% in June 2021. The increase in the prevalence of these 2 lineages was rapid; it reached 67% in June, but decreased slightly when the Delta variant emerged in July. The prevalence of B.1.497 decreased from 94.3% to 0.9% in June 2021.

B.1.619 and B.1.620 were identified in imported cases in South Korea in 2021; B.1.619 in a case-patient from Cameroon in February and B.1.620 in cases from Kenya and Malawi in March. The phylogenetic analysis of SARS-CoV-2 sequences isolated in South Korea showed that B.1.619 and B.1.620 were distinct from those in countries in Europe (Figure 2); this finding indicates 1 or very few introduction events for B.1.619 and B.1.620 strains into South Korea, from which strains then spread rapidly. South Korea B.1.619 has been reclassified as B.1.619.1, which has an additional mutation in ORF1ab (K3929R) (*10*).

B.1.620 was prevalent in central Africa and later spread to Europe and the United States through travelers (*10*). We were unable to find previous research on B.1.619 in the literature; however, we assumed that B.1.619 was a prevalent strain in central Africa and later spread to Europe because it has been identified in central Africa, according to information from GISAID.

The B.1.619 and B.1.620 lineages have several characteristic spike protein mutations (Table 1); the E484K mutation, which is present in both Beta and Gamma variants and has been identified as an escape mutation (*11*), is the only shared mutation in both lineages. The mutations in the spike protein, specifically in the RBD, have a strong influence on SARS-CoV-2 pathogenesis; B.1.619 has additional N440K mutations in the RBD and B.1.620 has S447N substitutions. The S477N mutation may evade antibody-mediated immunity (*12*) and increase RBD affinity for ACE2 (*13*). In addition, the N440K mutation might confer resistance to monoclonal antibodies and enhance binding affinity to the ACE2 receptor (*13*,*14*). We observed no other specific mutation in the spike protein in B.1.619. In contrast, B.1.620 carries several mutations and deletions, previously observed individually in VOCs and VOIs (Table 1). The HV69/70Δ, Y144Δ, P681H, and D1118H mutations in the spike protein have been found in the Alpha variant, whereas the LAL242/243/244Δ mutation has been found in the Beta variant. Previously, we found that B.1.619 and 620 have no inhibitory effect on the neutralizing activity in vaccinated or convalescent persons (S.J. Oh et al., unpub. data). However, the combined effect of these mutations on viral pathogenicity and transmissibility needs to be elucidated.

Table 2. Results from neutralization testing of serum from persons who were infected with and vaccinated against severe acute respiratory syndrome coronavirus 2, South Korea*

Serum type	$PRNT_{50}$ GMT (95% CI)		
	G (D614G)	B.1.619	B.1.620
Convalescent, n = 7	79 (35–179)	340 (138–830)	546 (248–1,205)
Vaccinated, n = 7	32 (16–62)	76 (37–155)	584 (303–1,125)

*Test results against G clade (D614G) and B.1.619 and B.1.620 lineages. GMT, geometric mean titer; $PRNT_{50}$, 50% plaque reduction neutralization test.

Conclusions

Continuous monitoring of mutations is essential to track potential vaccine efficacy reduction, increased transmissibility, and disease severity. The transmissibility of B.1.619 and B.1.620 and their likelihood to cause more severe infections are not yet confirmed. Preliminary data show that patients who recovered from non-VOC/VOI and vaccinated persons have sufficient neutralizing capacity against these lineages (Table 2). The transmissibility and immune escape of these strains must be investigated further. Continuous genomic surveillance supporting public health response is required to overcome the COVID-19 pandemic.

Acknowledgments

We thank the authors of the originating laboratories and the submitting laboratories who have deposited and shared genome data on GISAID's EpiCoV (https://www.gisaid.org) database.

This work was supported by a grant from the Korea Disease Control and Prevention Agency (grant no. 4800-4837-301).

About the Author

Dr. Ae Kyung Park is a staff scientist at the Korea Disease Control and Prevention Agency. Her research interests include molecular epidemiology of pathogens, and next-generation sequencing.

References

1. Shu Y, McCauley J. GISAID: Global initiative on sharing all influenza data—from vision to reality. Euro Surv. 2017;22:30494.
2. Letko M, Marzi A, Munster V. Functional assessment of cell entry and receptor usage for SARS-CoV-2 and other lineage B betacoronaviruses. Nat Microbiol. 2020;5:562–9. https://doi.org/10.1038/s41564-020-0688-y
3. Zhang L, Jackson CB, Mou H, Ojha A, Peng H, Quinlan BD, et al. SARS-CoV-2 spike-protein D614G mutation increases virion spike density and infectivity. Nat Commun. 2020;11:6013. https://doi.org/10.1038/s41467-020-19808-4
4. World Health Organization. Weekly epidemiological update on COVID-19—1 June 2021. Edition 42. 2021 [cited 2021 Dec 14]. https://www.who.int/publications/m/item/weekly-epidemiological-update-on-covid-19---1-june-2021
5. European Centre for Disease Prevention and Control. SARS-CoV-2 variants of concern as of 3 June 2021. 2021 [cited 2021 Dec 21]. https://ecdc.europa.eu/en/covid-19/variants-concern.
6. Laiton-Donato K, Franco-Munoz C, Alvarez-Diaz DA, Ruiz-Moreno HA, Usme-Ciro JA, Prada DA, et al. Characterization of the emerging B.1.621 variant of interest of SARS-CoV-2. Infect Genet Evol. 2021;95:105038.
7. Park AK, Kim IH, Kim J, Kim JM, Kim HM, Lee CY, et al. Genomic surveillance of SARS-CoV-2: distribution of clades in South Korea in 2020. Osong Public Health Res Perspect. 2021;12:37–43. https://doi.org/10.24171/j.phrp.2021.12.1.06
8. Rambaut A, Holmes EC, Hill V, O'Toole Á, McCrone JT, Ruis C, et al. A dynamic nomenclature proposal for SARS-CoV-2 to assist genomic epidemiology. Nat Microbiol. 2020;5:1403–7. https://doi.org/10.1038/s41564-020-0770-5
9. Kwon J-H, Kim J-M, Lee D-H, Park AK, Kim I-H, Kim D-W, et al. Genomic epidemiology reveals the reduction of the introduction and spread of SARS-CoV-2 after implementing control strategies in Republic of Korea, 2020. Virus Evol. 2021;7:veab077. https://doi.org/10.1093/ve/veab077
10. Latif AA, Mullen JL, Alkuzweny M, Tsueng G, Cano M, Haag E, et al.; Center for Viral Systems Biology. B.1.619.1 lineage report. 2021 [cited 2021 Dec 14]. https://outbreak.info/situation-reports?pango=B.1.619.1
11. Harvey WT, Carabelli AM, Jackson B, Gupta RK, Thomson EC, Harrison EM, et al.; COVID-19 Genomics UK (COG-UK) Consortium. SARS-CoV-2 variants, spike mutations and immune escape. Nat Rev Microbiol. 2021;19:409–24. https://doi.org/10.1038/s41579-021-00573-0
12. Liu Z, VanBlargan LA, Bloyet LM, Rothlauf PW, Chen RE, Stumpf S, et al. Identification of SARS-CoV-2 spike mutations that attenuate monoclonal and serum antibody neutralization. Cell Host Microbe. 2021;29:477–488.e4. https://doi.org/10.1016/j.chom.2021.01.014
13. Starr TN, Greaney AJ, Hilton SK, Ellis D, Crawford KHD, Dingens AS, et al. Deep mutational scanning of SARS-CoV-2 receptor binding domain reveals constraints on folding and ACE2 binding. Cell. 2020;182:1295–1310.e20. https://doi.org/10.1016/j.cell.2020.08.012
14. Weisblum Y, Schmidt F, Zhang F, DaSilva J, Poston D, Lorenzi JC, et al. Escape from neutralizing antibodies by SARS-CoV-2 spike protein variants. eLife. 2020;9:e61312. https://doi.org/10.7554/eLife.61312

Address for correspondence: Eun-Jin Kim, Ph.D. Division of Emerging Infectious Diseases, Bureau of Infectious Diseases Diagnosis Control, Korea Disease Control and Prevention Agency (KDCA), 187 Osongsaengmyeong 2-ro, Osong-eup, Heungdeok-gu, Cheongju-si, Chungcheongbuk-do 28159, South Korea; e-mail: ekim@korea.kr

Postmortem Surveillance for Ebola Virus Using OraQuick Ebola Rapid Diagnostic Tests, Eastern Democratic Republic of the Congo, 2019–2020

Daniel Mukadi-Bamuleka,[1] Yibayiri Osee Sanogo,[1] Junior Bulabula-Penge,[1] Maria E. Morales-Betoulle, Patrice Fillon, Patrick Woodruff, Mary J. Choi, Amy Whitesell, Alison M. Todres, Anja De Weggheleire, Anaïs Legand, Jean-Jacques Muyembe-Tamfum,[2] Pierre Formenty, John D. Klena,[2] Joel M. Montgomery,[2] Steve Ahuka-Mundeke,[2] RDT Working Group[3]

After a pilot study, we tested 443 cadavers using OraQuick Ebola rapid diagnostic tests during surveillance after the 10th Ebola outbreak in the Democratic Republic of the Congo. No false negative and 2% false-positive results were reported. Quickly returning results and engaging the community enabled timely public health actions.

The 10th outbreak of Ebola virus (EBOV) disease (EVD) in North Kivu, Democratic Republic of the Congo (DRC), was the longest (August 1, 2018–July 25, 2020) and largest EVD outbreak in DRC; 2,287 persons died and 1,171 survived. A case of EVD recrudescence (recorded June 15, 2019) resulted in 91 additional infections in 6 health zones (*1*–*3*).

Challenges in controlling this EVD outbreak included security threats, widespread community mistrust in response activities, and low acceptance of systematic safe and dignified burials (SDBs). The difficulty with SDBs was in part because of long turnaround times (4 h to 72 h) of required quantitative reverse transcription PCR (RT-PCR) results for burial to bereaved families.

During the postepidemic period, enhanced surveillance of EVD is critical for controlling outbreaks because of potential flare-ups from undetected transmission chains or recrudescence in survivors (*4*–*7*). The objective of this study was to strengthen laboratory surveillance by quickly returning test results to families for timely public health interventions and to improve community engagement and acceptance of SDBs. After a pilot study conducted during active EVD transmission, we used OraQuick Ebola rapid diagnostic tests (RDTs; OraSure Technologies, Inc., https://www.orasure.com) to screen for EBOV infection in decedents within the community and in healthcare facilities during the postepidemic enhanced surveillance period using real-time field data reporting and molecular confirmation.

The Study

OraQuick Ebola is the first RDT licensed by the US Food and Drug Administration for EVD screening using blood or cadaver fluid samples (*8*). The US Centers for Disease Control and Prevention and the World

Author affiliations: Institut National de Recherche Biomédicale, Kinshasa, Democratic Republic of the Congo (D. Mukadi-Bamuleka, J. Bulabula-Penge, J. Muyembe-Tamfum, S. Ahuka-Mundekea); Kinshasa Teaching School of Medicine, University of Kinshasa, Kinshasa (D. Mukadi-Bamuleka, J. Bulabula-Penge, J. Muyembe-Tamfum, S. Ahuka-Mundekea); US Centers for Disease Control and Prevention, Atlanta, Georgia, USA (Y.O. Sanogo, Maria E. Morales-Betoulle, M.J. Choi, A. Whitesell, A.M. Todres, J.D. Klena, J.M. Montgomery); iMMAP, Geneva, Switzerland (P. Fillon); Family Health International 360 (FHI360), Crisis Response DRC, Democratic Republic of the Congo (P. Woodruff); Institute of Tropical Medicine, Antwerp, Belgium (A. De Weggheleire); World Health Organization Health Emergencies Programme, Geneva, Switzerland (A. Legand, P. Formenty)

DOI: https://doi.org/10.3201/eid2802.210981

[1]These authors contributed equally to this article.

[2]Senior co-authors.

[3]Members of the group who contributed data are listed at the end of this article.

Health Organization have recommended its use for testing cadaver fluids of suspected EVD patients (*9*). Ethics approval and participant consent were not deemed necessary because specimens were collected for outbreak response and data were de-identified before analysis. A consortium of laboratory, epidemiology, communication, and community engagement professionals, led by the DRC Ministry of Health, formed an RDT technical working group to coordinate field implementation, including SDBs, community engagement, and data collection. A steering committee composed of senior leaders from the Institut National de Recherche Biomédicale (INRB) and international partners advised the RDT Working Group.

The pilot study was conducted during active EBOV transmission (October 31–December 31, 2019) in Mambasa, Mandima, and Beni health zones. Trained healthcare workers conducted RDTs in communities and healthcare facilities. Data were collected manually. Samples were shipped to the INRB lab for confirmation by RT-PCR. SDBs were systematically performed on all cadavers regardless of RDT results. Some community reticence was encountered during the pilot study; violence led to change of location from Mambasa to Beni.

Table 1. Summary results of RDT pilot study performed on cadaver oral fluid in Mambasa, Mandima, and Beni health zones during active transmission of Ebola virus, DRC, 2019–2020*

RDT results	PCR results		Total
	Confirmed	Not confirmed	
Reactive	8	4	12
Nonreactive	0	182	182
Invalid	0	2	2
Total	8	188	196

*DRC, Democratic Republic of the Congo; RDT, rapid diagnostic test (OraQuick, OraSure Technologies, Inc., https://www.orasure.com).

Of 196 cadavers tested by RDTs during the pilot study, 12 (6%) were reactive, of which 4 were negative by RT-PCR (2% false positive) (Table 1). Positive predictive value was 66% and negative predictive value 100% (no false negatives). Among confirmed cases, EBOV gene cycle thresholds ranged from 15.8 to 27.7 for nucleoprotein and 12.3 to 31.4 for glycoprotein. Lessons learned from the pilot study included the need for better community engagement, improved data collection and reporting, and more in-depth healthcare worker training.

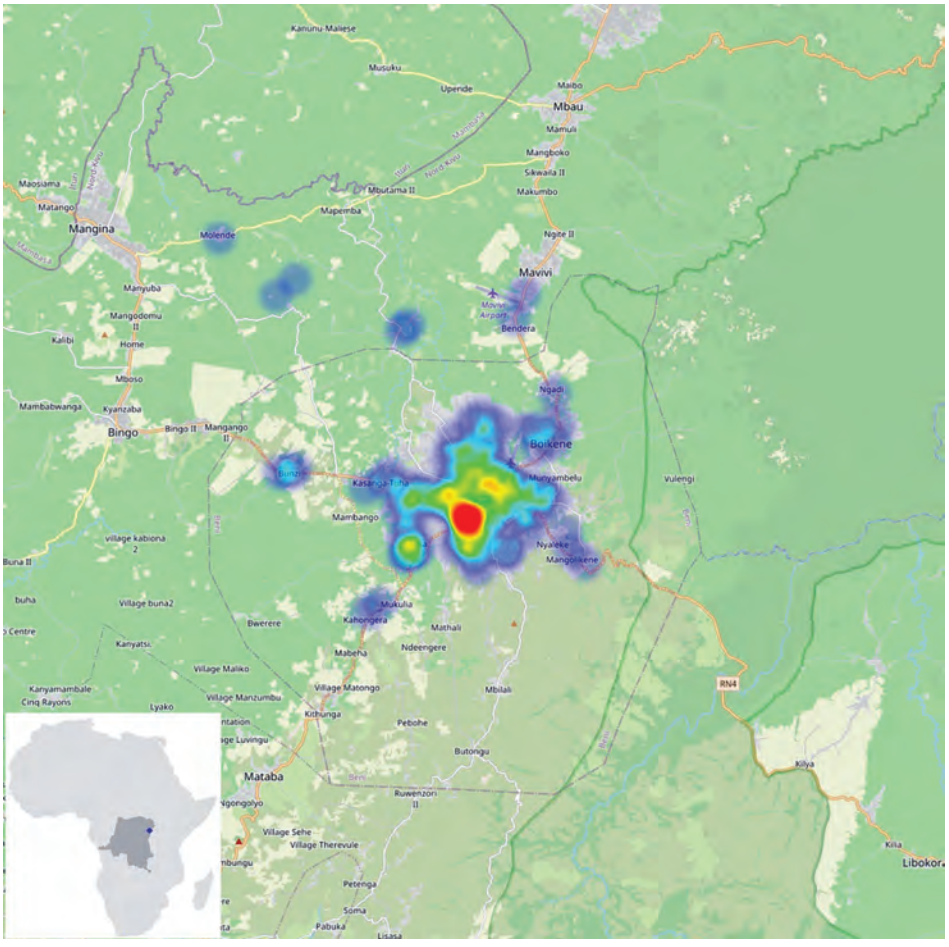

Figure 1. Beni Health zone with sites of Ebola virus disease sample collection for study on postmortem surveillance for Ebola virus using OraQuick (OraSure Technologies, Inc., https://www.orasure.com) Ebola rapid diagnostic tests, eastern Democratic Republic of the Congo, 2019–2020. The numbers and the geolocation rapid diagnostic testing are provided in heatmaps from blue (fewer cases) to red (most cases). Most of the cases were from the health care facilities in Beni township. Inset shows location of the Beni Health zone in the Democratic Republic of the Congo and in Africa.

After the pilot study, RDT postepidemic (August 1–October 31, 2020) surveillance was conducted on cadavers in 19 health areas of the Beni health zone (Figure 1), the last health zone affected during the outbreak. RDTs were administered by 32 teams of locally trained healthcare workers, each composed of a laboratorian or nurse, a hygienist, a community engagement specialist, and a supervisor. The laboratorian/nurse collected 1 swab sample with the pad of the OraQuick device for the RDT and stored another swab sample in viral transport medium for quantitative RT-PCR confirmation. The hygienist oversaw biosafety practices and ensured that biologic waste (used RDT kits and personal protective equipment) was properly incinerated. A community engagement specialist communicated with the family, provided psychosocial support, and engaged the community using media and interactions with local leaders. The supervisor assumed responsibility for RDT quality control. Field teams were provided with the testing algorithm (Figure 2), a field training manual, and communication materials to assist with community engagement. SDB teams were on standby for safe burials as requested by families or if a sample was reactive/invalid.

Data were collected using tablets outfitted with a free, open-source, Kobo–based mobile data collection tool (https://www.humanitarian response.info/fr/applications/kobotoolbox), developed for this purpose using a set of 75 questions in French. The data collection tool operated offline. RDT data, collection site geolocations, and photographs of RDT results were transmitted daily to the Kobo server when inter-

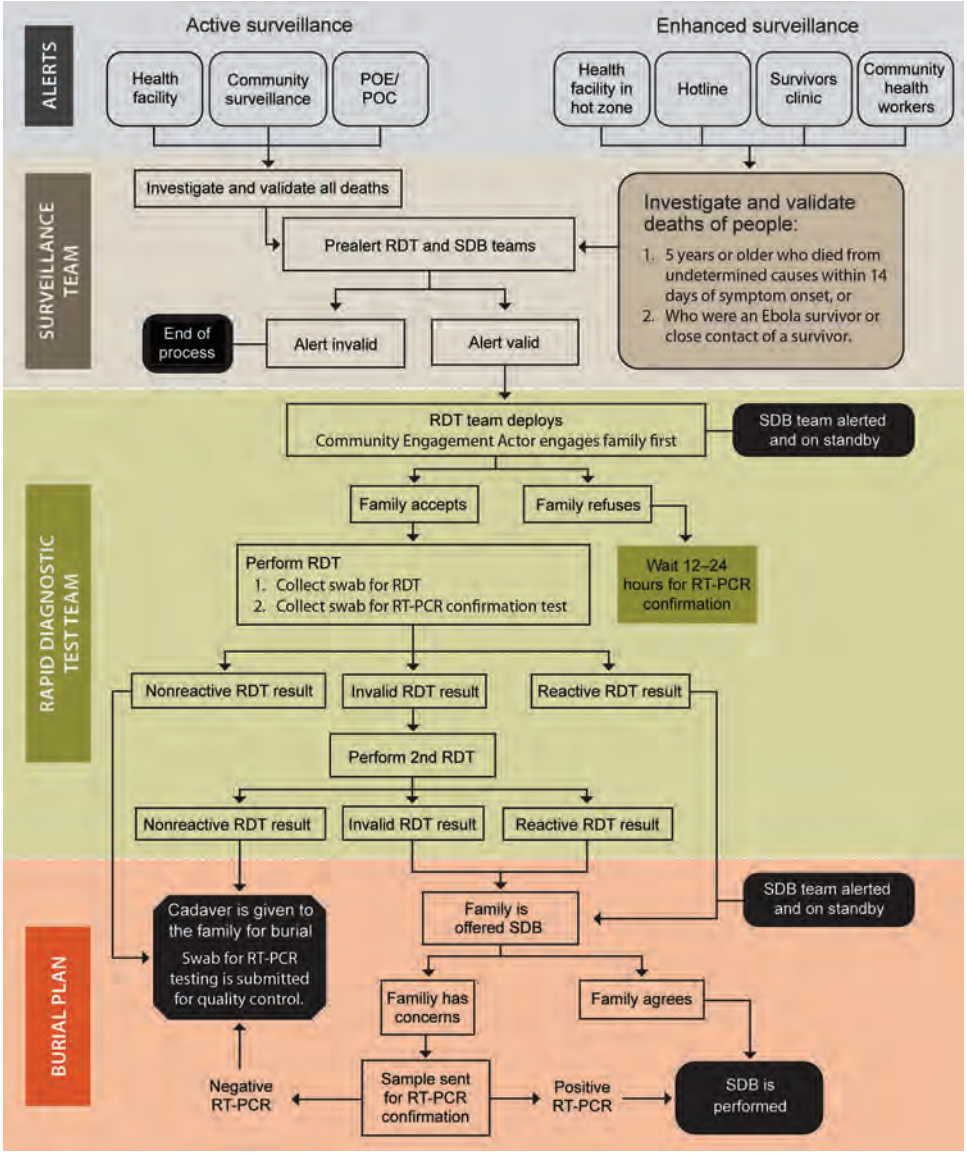

Figure 2. Algorithm of Ebola virus disease RDT implementation in North Kivu in the Beni health zone during active transmission (active surveillance) and postepidemic enhanced surveillance (enhanced surveillance), Democratic Republic of the Congo, 2019–2020. This information was used to inform burial planning and SDBs when indicated. EVD, Ebola virus disease; RDT, rapid diagnostic test (OraQuick, OraSure Technologies, Inc., https://www.orasure.com); RT-PCR, reverse transcription PCR; SDBs, safe and dignified burials.

net connection was available. A dashboard displaying key indicators was updated automatically twice a day. We used R software (*10*) to assess the diagnostic accuracy of the RDTs, using quantitative RT-PCR results as the standard.

After receiving permission from decedents' families, the laboratorian/nurse hygienist performed the test following instructions in the manual (S2). Results were read, interpreted, and photographed at 30 minutes, according to the manufacturer's instructions. If the RDT was nonreactive, families could proceed with traditional burial. If the RDT was reactive or invalid, the sample in viral transport medium, packaged in cooler boxes with ice packs, was transported immediately to an INRB lab for confirmation by GeneXpert Ebola quantitative RT-PCR (Cepheid, https://www.cepheid.com), with result turnaround time under 24 hours. An RDT was considered invalid when, after 1 repeat, no line appeared in the C area of the test, a purple background obscured the results, or a partial line appeared in the C or T area after 30 minutes.

During postepidemic surveillance, 443 cadavers were tested (3 cadavers were removed by families before RDTs were performed): 235 (53%) were from mortuaries, 111 (25%) from the community, and 97 (22%) from hospitals. Swab specimens were collected from 272 (61%) male and 171 (39%) female cadavers; 27% were children <5 years. Of the 443 samples, 425 (96%) had nonreactive RDTs, 11 (2%) were invalid, and 7 (2%) were reactive. Reactive, invalid and nonreactive samples tested by quantitative RT-PCR (363) were all negative, yielding 6 false-positive and no false-negative results (Table 2). One reactive RDT was not confirmed by quantitative RT-PCR. Although no EVD cases were confirmed among decedents, 32 SDBs were requested by families.

Table 2. Summary results of RDTs performed on cadaver oral fluids in the Beni health zone during the 90-day enhanced surveillance period after 10th EVD outbreak in DRC, 2019–2020*

	PCR results			
RDT results	Positive	Negative	Not done	RDT totals
Reactive	0	6	1	7
Nonreactive	0	348	77	425
Invalid	0	9	2	11
PCR total	0	363	80	443

*Fifteen RDTs performed to retest invalid and nonreactive initial RDTs are not included. DRC, Democratic Republic of the Congo; EVD, Ebola virus disease; RDT, rapid diagnostic test (OraQuick, OraSure Technologies, Inc., https://www.orasure.com).

Conclusions

Trained local healthcare workers successfully used OraQuick Ebola RDTs for enhanced postmortem surveillance after the 10th EVD outbreak in DRC. Molecular testing revealed no false-negative RDT results, suggesting that quick public health actions can be based on RDT results alone. The low cycle thresholds observed in positive samples during the pilot study (Appendix Table, https://wwwnc.cdc.gov/EID/article/28/2/21-0981-App1.pdf) support using RDTs in cadavers, in which viral loads are expected to be high (*11*–*13*). Our study shows that RDTs can detect EVD-related deaths and reduce the risk for community transmission. The utility of this tool in EVD surveillance is supported by recent observations that SDBs were not conducted during early stages of recent EVD resurgences in North Kivu and Guinea (CDC 2021 Ebola Response, unpub. data).

In conclusion, postmortem OraQuick Ebola RDTs effectively complemented outbreak-response efforts, improved community trust, and decreased the number of SDBs. However, the reported 2% false-positive tests required further confirmation and were not immediately actionable. SDBs requested by families despite nonreactive RDT further highlight the need for further community engagement.

Members of the RDT Working Group who contributed data: Gnakub Norbert Soke, Peter N. Fonjungo, John Neatherlin, Michael Beach, Athalia Christie, Amanda MacGurn, Stuart T. Nichol, Trevor Shoemaker (Atlanta, GA, USA); Silga Eloi (Ouagadougou, Burkina Faso); Michel Kasereka-Tosalisana, Jean-Paul Kapitula, Nelson Kambale-Sivihwa, Joseph Kambale-Makundi (Beni, DRC); John Kombe, Mathias Mossoko, Fabrice Mambu-Mbika, Antoine Nkuba-Ndaye, Francois Edidi-Atani (Kinshasa, DRC); Jean-Marie Ntampera, Raymond Pallawo, Abou Salam Gueye (Brazzaville, Republic of the Congo); Hubert Dedegbe, Emmanuel Saint Juste (Goma, DRC); Germain Bukassa-Kazadi (Alpharetta, GA, USA).

Acknowledgments

We thank the DRC Ministry of Health and the Ebola Response Coordination for their support with this project. Many thanks to Jon Carver, Mehtab Khan, Héritier Bhayo, Gédéon Banswe, Bilal Al Omari, and Ayat Al-Qarala for support during the development of the iMMAP Kobo data collection tool. We thank the country office of the Centers for Disease Control and Prevention and its staff for logistical support and access to training materials, and Jamie Dawson, Mary Reynolds, and Reinhard Kaiser for their valuable feedback on the manuscript. We thank Mark Perkins for initial work on the RDT protocol and John Lee for his help with acquiring the RDTs. Our thanks also to Victoria Carter for help with developing the training materials, and to Jim Gathany for photography. We thank Tatyana Klimova for professionally editing the manuscript.

About the Authors

Dr. Sanogo is a microbiologist and epidemiologist in the Emergency Response and Recovery Branch (Global Rapid Response Team), Division of Global Health Protection, Center for Global Health, Centers for Disease Control and Prevention. His research interests encompass laboratory diagnostics of emerging pathogens, including vectorborne diseases, hemorrhagic fever viruses, next-generation sequencing, and strengthening laboratory capacity in resource-limited countries. Dr. Mukadi is a physician and medical virologist at the Institut National de Recherche Biomédicale in Kinshasa, DRC. His expertise includes setup and coordination of field laboratories in response to Ebola outbreaks and evaluation of rapid diagnostic tests.

References

1. Christie A, Neatherlin JC, Nichol ST, Beach M, Redfield RR. Ebola response priorities in the time of covid-19. N Engl J Med. 2020;383:1202–4. https://doi.org/10.1056/NEJMp2025512
2. World Health Organization. Ebola virus disease—Democratic Republic of the Congo: disease outbreak news: update 23 January 2020 [cited 2021 Apr 4]. https://wwwwhoint/csr/don/23-january-2020-ebola-drc
3. Mbala-Kingebeni P, Pratt C, Mutafali-Ruffin M, Pauthner MG Bile F, Nkuba-Ndaye A, et al. Ebola virus transmission initiated by relapse of systemic Ebola virus disease. N Engl J Med. 2021;384:1240–7. https://doi.org/10.1056/NEJMoa2024670
4. Den Boon S, Marston BJ, Nyenswah TG, Jambai A, Barry M, Keita S, et al. Ebola virus infection associated with transmission from survivors. Emerg Infect Dis. 2019;25:249–55. https://doi.org/10.3201/eid2502.181011
5. Vetter P, Fischer WA II, Schibler M, Jacobs M, Bausch DG, Kaiser L. Ebola virus shedding and transmission: review of current evidence. J Infect Dis. 2016;214(suppl 3):S177–84. https://doi.org/10.1093/infdis/jiw254
6. Sissoko D, Keïta M, Diallo B, Aliabadi N, Fitter DL, Dahl BA, et al. Ebola virus persistence in breast milk after no reported illness: a likely source of virus transmission from mother to child. Clin Infect Dis. 2017;64:513–6.
7. Diallo B, Sissoko D, Loman NJ, Bah HA, Bah H, Worrell MC, et al. Resurgence of Ebola virus disease in guinea linked to a survivor with virus persistence in seminal fluid for more than 500 days. Clin Infect Dis. 2016;63:1353–6. https://doi.org/10.1093/cid/ciw601
8. Food and Drug Administration. FDA allows marketing of first rapid diagnostic test for detecting Ebola virus antigens [cited 2021 Apr 4]. https://wwwfdagov/news-events/press-announcements/fda-allows-marketing-first-rapid-diagnostic-test-detecting-ebola-virus-antigens
9. Centers for Disease Control and Prevention . Guidance for using rapid diagnostic tests for Ebola in the United States. CDC Health Alert Network [cited 2021 Apr 4]. https://emergencycdcgov/han/han00423asp?deliveryName=USCDC_511-DM15631
10. R Core Team. R: a language and environment for statistical computing. R Foundation for Statistical Computing, Vienna, Austria [cited 2021 Apr 4]. https://www.R-project.org
11. Jean Louis F, Huang JY, Nebie YK, Koivogui L, Jayaraman G, Abiola N, et al. Implementation of broad screening with Ebola rapid diagnostic tests in Forécariah, Guinea. Afr J Lab Med. 2017;6:484. https://doi.org/10.4102/ajlm.v6i1.484
12. VanSteelandt A, Aho J, Franklin K, Likofata J, Kamgang JB, Keita S, et al. Operational evaluation of rapid diagnostic testing for Ebola virus disease in Guinean laboratories. PLoS One. 2017;12:e0188047. https://doi.org/10.1371/journal.pone.0188047
13. Coarsey CT, Esiobu N, Narayanan R, Pavlovic M, Shafiee H, Asghar W. Strategies in Ebola virus disease (EVD) diagnostics at the point of care. Crit Rev Microbiol. 2017;43:779–98. https://doi.org/10.1080/1040841X.2017.1313814

Address for correspondence: Yibayiri Osee Sanogo, Centers for Disease Control and Prevention, 1600 Clifton Rd NE, Mailstop H24-3, Atlanta, GA 30329-4027, USA; email: nkw2@cdc.gov; Daniel Mukadi-Bamuleka, Institut National de Recherche Biomédicale, 5345 Avenue de la Démocratie (Ex Des Huileries), Kinshasa-Gombe, Democratic Republic of the Congo; email: drmukadi@gmail.com

Public Acceptance of and Willingness to Pay for Mosquito Control, Texas, USA

Katherine L. Dickinson, Natalie Banacos, Ester Carbajal, Nina Dacko, Chris Fredregill, Steven Hinojosa, Jose G. Juarez, Caroline Weldon, Gabriel L. Hamer

Mosquito control is essential to reduce vectorborne disease risk. We surveyed residents in Harris, Tarrant, and Hidalgo Counties, Texas, USA, to estimate willingness-to-pay for mosquito control and acceptance of control methods. Results show an unmet demand for expanded mosquito control that could be funded through local taxes or fees.

Public health responses are not purely technical undertakings; these responses happen within and are affected by their social and economic contexts. Whether or not these efforts succeed depends on public acceptance and response and on financial viability (*1*). To fully assess which vectorborne disease control methods will be sustainable and effective, public health practitioners and researchers must understand public perceptions and acceptance of different approaches.

Vector control is a particularly salient public health topic in Texas. The state had one of the highest rates of West Nile virus (WNV) in 2002–2019 (*2*); Texas and Florida are the 2 US states with periodic local transmission of *Aedes* spp. mosquito–borne viruses such as dengue virus (DENV), Zika virus (ZIKV), and chikungunya virus (CHIKV) (*3*). Although Texas shares a border with Mexico, which has had outbreaks of these 3 viruses, and despite the substantial impact of mosquitoborne disease on public health across the state, very few of its cities or counties have organized vector control programs. Those that do focus primarily on nuisance mosquitoes, and disease-carrying mosquitoes are usually targeted in response to cases rather than preventively (*4*). State law requires a petition and a vote to create a new mosquito control district, but establishing such districts requires raising taxes, which is rarely popular among the Texas electorate (*5*).

The objective of this study was to determine public attitudes toward and willingness to pay for mosquito control in Harris, Tarrant, and Hidalgo Counties, regions with varying risk for mosquitoborne pathogens, socioeconomic conditions, and current mosquito control practices (Appendix 1 Figure 1, https://wwwnc.cdc.gov/EID/article/28/2/21-0501-App1.pdf). Participants provided written consent to take the survey. The Colorado Multiple Institutional Review Board (COMIRB) approved the study on March 2, 2018 (protocol no. 18-0348), and the Texas A&M University Institutional Review Board approved the study on July 2, 2018, after determining the proposed activity was not research involving human subjects (protocol no. 2018-0774).

The Study

We conducted a public survey (Appendix 2, https://wwwnc.cdc.gov/EID/article/28/2/21-0501-App2.pdf) to answer 2 research questions: 1) How much are residents willing to pay for increased mosquito control, and how does willingness to pay vary across counties and with individual characteristics?; 2) To what extent do residents support or oppose different methods for controlling mosquitoes, and how does level of support vary across counties and with individual characteristics?

Author affiliations: University of Colorado Anschutz, Aurora, Colorado, USA (K.L. Dickinson); Boston University School of Public Health, Boston, Massachusetts, USA (N. Banacos); Texas A&M University, College Station, Texas, USA (E. Carbajal, J.G. Juarez, G.L. Hamer); Tarrant County Health Department, Fort Worth, Texas, USA (N. Dacko); Harris County Public Health, Houston, Texas, USA (C. Fredregill); Hidalgo County Health and Human Services, Edinburg, Texas, USA (S. Hinojosa); University of Texas Medical Branch, Galveston, Texas, USA (C. Weldon)

DOI: https://doi.org/10.3201/eid2801.210501

To measure willingness to pay, we used a triple-bounded dichotomous choice contingent valuation question design (*6*). We presented participants with background information about current mosquito control methods in their county, including the annual budget per person. We then asked whether they would support a proposal to expand mosquito control efforts in their county at different annual fees; their answers enabled us to estimate a WTP range for each respondent.

We then presented participants with fact sheets on 6 mosquito control methods: adulticides, larvicides, traps, and mass releases of genetically modified mosquitoes, sterile male mosquitoes, or mosquitoes artificially infected with *Wolbachia* bacteria. After viewing information about the control methods, participants were asked to indicate their level of support or opposition to the use of each method as part of an expanded mosquito control program in their area; responses were strongly oppose, oppose, neutral/no opinion, support, strongly support.

In total, 1,831 Texas residents participated in this survey: 610 from Harris County, 609 from Tarrant County, and 612 from Hidalgo County (Appendix 1 Table 1). Participants were willing to pay $53.15 (95% CI $50.09–$56.21) per year on average to expand mosquito control in their area. Harris County residents expressed the highest WTP values at an average of $56.74 (95% CI $50.91–$62.57), followed by Hidalgo County residents at $51.87 (95% CI $46.60–$57.14) and Tarrant County residents at $51.74 (95% CI $46.72–$56.76). Differences in WTP values across counties were not statistically significant ($\chi^2 = 1.22$; $p = 0.54$).

Women were willing to pay $9 less for vector control than men (Figure 1). Persons with graduate degrees were willing to pay $25 more than those with a high school or lower education level, and participants were willing to pay more with increasing income (controlling for education). Participants who identified as politically liberal were willing to pay about $12 more than those who identified as moderate. On average, persons who reported knowing someone who had had WNV, DENV, or ZIKV were willing to pay $21 more than those who did not, and persons who noticed many mosquitoes outdoors at the time of the survey were willing to pay $12 more than those who did not (Figure 1).

Levels of support for the 6 different control methods were similar across counties (Figure 2). Lethal traps were the most favorable mosquito control method. Releasing genetically modified (GM) mosquitoes was the least favorable approach, although most participants still supported it. Support for different control methods varied with individual characteristics (Appendix 1 Figure 2). Women were less supportive of the 3 modified mosquito control methods (GM mosquitoes, sterile males, and *Wolbachia* infected) than men. Compared with White respondents,

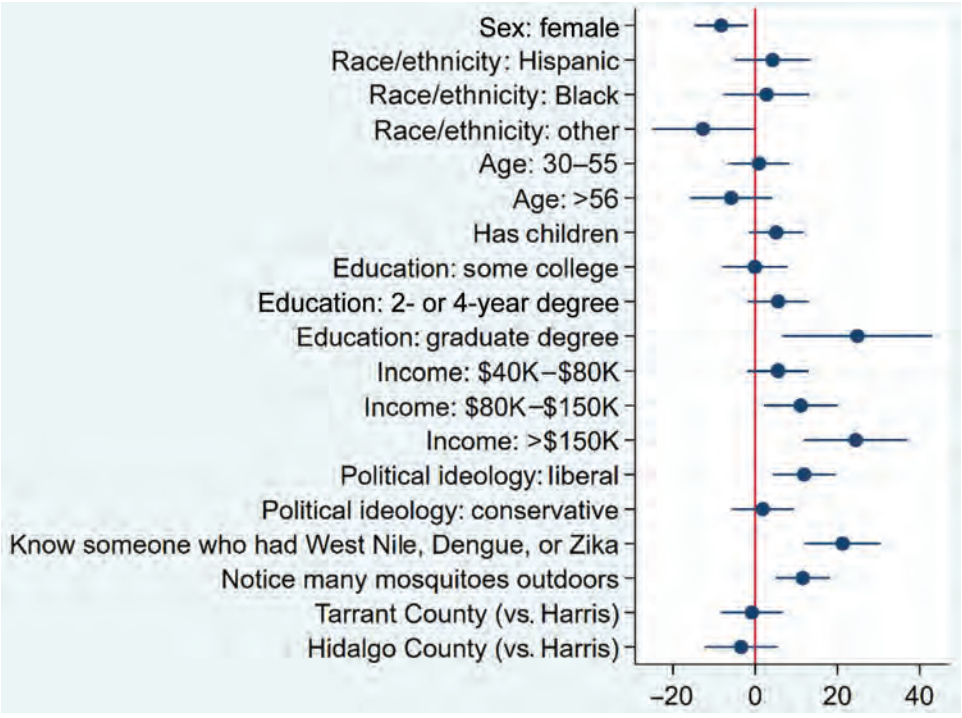

Figure 1. Interval censored regression results showing variation in public willingness to pay for vector control as a function of individual characteristics and county, Harris, Tarrant, and Hidalgo Counties, Texas, USA. Dots represent point estimates and bars 95% CIs. Red line represents the reference category (e.g., male sex, non-Hispanic White race/ethnicity, respondents <30 years of age, respondents without children) (Appendix 1 Table 1, https://wwwnc.cdc.gov/EID/article/28/2/21-0501-App1.pdf).

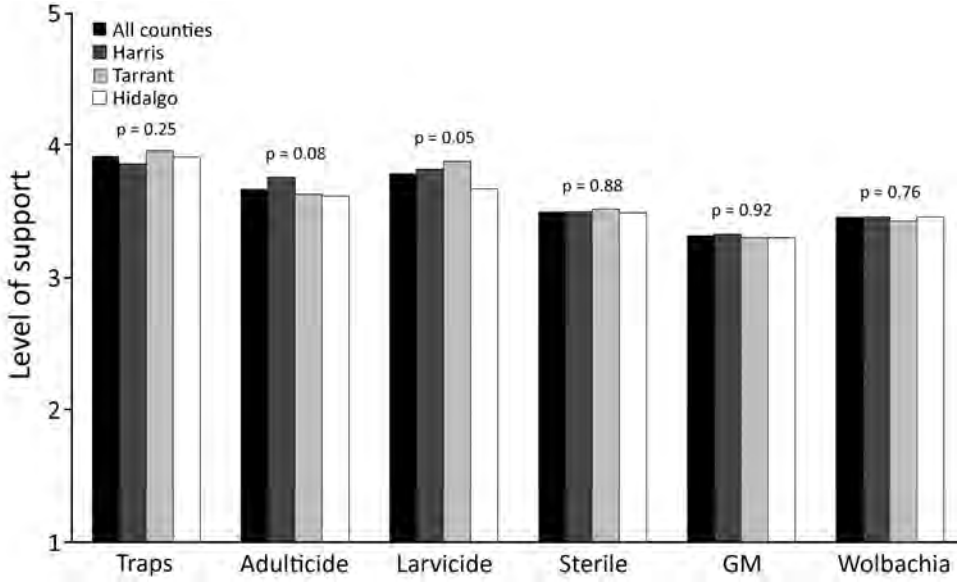

Figure 2. Average (mean) level of public support for mosquito control methods by county, Harris, Tarrant, and Hidalgo Counties, Texas, USA. Level 1, strongly oppose; 2, oppose; 3, neutral; 4, support; 5, strongly support. Kruskal-Wallis test used for differences in level of support across counties. GM, genetic modification.

Black respondents were less supportive of the sterile-male method. Respondents >30 years of age tended to be more supportive of several control methods than younger respondents. Higher education was somewhat predictive of support for adulticides, larvicides, and the sterile male method; respondents in the highest income group were more supportive of traps, adulticides, and larvicides. Respondents who identified as politically conservative were more supportive of adulticides compared with the politically moderate, whereas liberal respondents were somewhat more supportive of GM mosquitoes. Support for adulticides and the *Wolbachia* and GM approaches was also higher among respondents who knew someone who had had WNV, DENV, or ZIKV; respondents who reported noticing many mosquitoes outdoors were more supportive of adulticides and larvicides. Compared with Harris County respondents, Tarrant County participants were more supportive of traps and less supportive of adulticides.

When asked an open-ended question about why they supported or opposed different control methods, many participants said they were in favor of anything that would eliminate mosquitoes, to get rid of the nuisance or protect their families and communities from disease. Others emphasized that they would prefer a control method that was proven safe for humans and other animals. Whereas some expressed skepticism about the safety of GM mosquito options, others simply did not want more mosquitoes released in their area. "Oppose anything with genetically modified anything," wrote one participant. "That's how *Jurassic Park* began." In contrast, a participant who was in favor of the GM methods responded, "… I love the idea of using mosquitoes to fight mosquitoes."

Conclusions

Measuring public demand and support for mosquito control is crucial to successful vectorborne disease prevention strategy. Our results show a demand for expanded mosquito control that could be met through programs funded with local taxes or fees. Follow-up work should assess the feasibility of establishing such programs, examining policies that could enable or prevent local programs from emerging. Community engagement can promote mutual understanding and guide sustainable public health strategies to address the threat of vectorborne disease.

Acknowledgments

We thank the persons who were interviewed to help develop the survey and the persons who helped revise the survey questionnaire. We thank the Texas Department of State Health Services for their assistance with the interviews and questionnaire and the Centers for Disease Control and Prevention for reviewing the questionnaire and manuscript. We thank Scott Weaver for reviewing a draft of this manuscript.

This work was supported by the US Centers for Disease Control and Prevention (cooperative agreement no. U01CK000512). Its contents are solely the responsibility of the authors and do not necessarily represent the official views of the Centers for Disease Control and Prevention or the Department of Health and Human Services.

About the Author

Dr. Dickinson is an assistant professor of environmental and occupational health in the Colorado School of Public Health. Her research focuses on risk perceptions and responses; policy impacts on environmental, health, and social outcomes; and environmental justice issues.

References

1. Spiegel J, Bennett S, Hattersley L, Hayden MH, Kittayapong P, Nalim S, et al. Barriers and bridges to prevention and control of dengue: the need for a social–ecological approach. EcoHealth. 2005;2:273–90. https://doi.org/10.1007/s10393-005-8388-x
2. Centers for Disease Control. Final cumulative maps and data for 1999–2019. 2020 [cited 2021 January 14]. https://www.cdc.gov/westnile/statsmaps/cumMapsData.html
3. Martin E, Medeiros MCI, Carbajal E, Valdez E, Juarez JG, Garcia-Luna S, et al. Surveillance of *Aedes aegypti* indoors and outdoors using Autocidal Gravid Ovitraps in South Texas during local transmission of Zika virus, 2016 to 2018. Acta Trop. 2019;192:129–37. https://doi.org/10.1016/j.actatropica.2019.02.006
4. Ward HM, Qualls WA. Integrating vector and nuisance mosquito control for severe weather response. J Am Mosq Control Assoc. 2020;36(2s):41–8. https://doi.org/10.2987/19-6879.1
5. State of Texas. State of Texas health and safety code, title 5: sanitation and environmental quality, subtitle A: sanitation. Sec 344. 1989 [cited 2021 Dec 27]. https://statutes.capitol.texas.gov/Docs/HS/htm/HS.344.htm
6. Langford IH, Bateman IJ, Langford HD. A multilevel modelling approach to triple-bounded dichotomous choice contingent valuation. Environ Resource Econ. 1996;7:197–211. https://doi.org/10.1007/BF00782145

Address for correspondence: Katherine Dickinson, Colorado School of Public Health—Environmental and Occupational Health, 13001 E 17th Pl, Aurora, CO 80045, USA; email: katherine.dickinson@cuanschutz.edu

SARS-CoV-2 Seroprevalence before Delta Variant Surge, Chattogram, Bangladesh, March–June 2021

Taufiqur Rahman Bhuiyan,[1] Juan Dent Hulse,[1] Sonia T. Hegde,[1] Marjahan Akhtar, Taufiqul Islam, Zahid Hasan Khan, Ishtiakul Islam Khan, Shakeel Ahmed, Mamunur Rashid, Rumana Rashid, Emily S. Gurley, Tahmina Shirin, Ashraful Islam Khan, Andrew S. Azman,[2] Firdausi Qadri[2]

A March–June 2021 representative serosurvey among Sitakunda subdistrict (Chattogram, Bangladesh) residents found an adjusted prevalence of severe acute respiratory syndrome coronavirus 2 antibodies of 64.1% (95% credible interval 60.0%–68.1%). Before the Delta variant surge, most residents had been infected, although cumulative confirmed coronavirus disease incidence was low.

Through November 9, 2021, Bangladesh had reported >1.57 million COVID-19 cases and 27,904 deaths (*1*), with incidence and mortality rates substantially lower than in many other countries. Without performing population-based seroprevalence estimates, it is difficult to know whether differences in rates of illness and death result from undercounts because of limited surveillance and healthcare seeking or reflect actual differences in incidence resulting from interventions or different biological responses to infection. In early March 2021, cases across Bangladesh began to rise at the same time as the Delta variant was detected in neighboring India. Publicly available sequencing data (*2*) indicate that the SARS-CoV-2 Delta variant was first detected in the Chattogram region of Bangladesh in mid-May 2021, and 99% (98/99) of the viral genomes submitted during July 1–October 1, 2021 have been of the Delta variant, similar to national trends.

Author affiliations: icddr,b, Dhaka, Bangladesh (T.R. Bhuiyan, M. Akhtar, T. Islam, Z.H. Khan, I.I. Khan, A.I. Khan, F. Qadri); Johns Hopkins Bloomberg School of Public Health, Baltimore, Maryland, USA (J. Dent Hulse, S.T. Hegde, E.S. Gurley, A.S. Azman); Bangladesh Institute of Tropical and Infectious Diseases, Chattogram, Bangladesh (S. Ahmed, M. Rashid, R. Rashid); Institute of Epidemiology, Disease Control and Research, Dhaka (T. Shirin); Institute of Global Health, University of Geneva, Geneva, Switzerland (A.S. Azman)

DOI: https://doi.org/10.3201/eid2802.211689

The Study

We conducted a representative serosurvey to understand the prevalence of total SARS-CoV-2 antibodies in residents of the Sitakunda subdistrict (Chattogram district) of Bangladesh, a region with an urban-to-rural gradient that includes Chattogram, Bangladesh's second largest city. We conducted the survey over 2 periods, March 27–April 13 and May 23–June 13, because of a national COVID-19 lockdown (April 14–May 30). We used 2-stage sampling based on digitized satellite imagery by first dividing the Sitakunda subdistrict into 1 km^2 grid-cells (or clusters) and randomly selecting grid-cells proportional to the estimated number of households in each, with replacement. We then randomly selected structures weighted by whether they were multistory or single-story. We attempted to enroll all persons ≥1 year of age in each household.

We tested participant serum for total antibodies (IgA, IgM, and IgG) against the receptor-binding domain of SARS-CoV-2 using the SARS-CoV-2 Ab ELISA (Wantai BioPharm, https://www.ystwt.cn), following manufacturer instructions. We corrected seroprevalence estimates for imperfect test performance, household clustering, and individual-level covariates (e.g., age) using a Bayesian modeling approach documented elsewhere and stratified results to match the target population (*3*). Our study was approved by the icddr,b research and ethics review committee and the Johns Hopkins Bloomberg School of Public Health institutional review board.

Given limited data on the immunoassay's performance in south Asia and performance months after infection, we conducted a validation study to estimate its sensitivity and specificity by testing samples from 214

[1]These first authors contributed equally to this article.

[2]These senior authors contributed equally to this article.

healthy participants from a 2014 cholera vaccine study and 81 from 52 symptomatic PCR-confirmed SARS-CoV-2–infected patients; none of the positive controls had been hospitalized or vaccinated for COVID-19. We collected samples 3–275 days after symptom onset. We estimated specificity at 99.1% (95% CI 96.7%–99.9%, n = 212/214) and sensitivity at 87.7% (95% CI 78.5%–93.9%, n = 71/81) for detecting previous infection with little evidence of sensitivity decreasing over time after infection (Appendix Table 4, https://wwwnc.cdc.gov/EID/article/28/2/21-1689-App1.pdf).

We enrolled 580 households and 2,307 participants who provided a blood sample. Most participants (54%, n = 1,235/2,307) were female and the median age was 28 (interquartile ratio 16–45) years; most reported working at home (37%), going to school (29%), or conducting business outside of their home (20%) as their main occupation in the month before enrollment. Among all participants, 22 (0.95%) reported ever having a COVID-19 test; 3/22 had positive results (all 3 were also seropositive in the study). Of 2,307 participants, 125 (5.4%) reported being vaccinated (15–144 days before interview) with ≥1 dose of SARS-CoV-2 vaccines, including 117 with a CoviShield ChAdOx1 (Serum Institute of India, https://www.seruminstitute.com) vaccination card and 1 with a Pfizer/BioNTech BNT162n2 (https://www.pfizer.com) vaccination card. As of June 19, 2021, 6 days after the end of the survey, 6.0% of the entire Chattogram district population was reported to have received ≥1 dose of any vaccine; 4.6% had received 2 doses (4).

There were 1,443 (63%) seropositive participants. Nearly all (98%) who reported having been partially (47/49) or completely vaccinated (75/76) were seropositive. In 85% of enrolled households, ≥1 participant was seropositive and an average of 62% of participants in each household were seropositive. We estimated that 31% of the total variability in seropositivity in the community was attributable to variation in seropositivity between households (intraclass correlation coefficient 0.31, 95% CI 0.27–0.36). We found evidence of a gradient in seropositivity associated with population density. Participants living in higher population density areas were significantly more likely to be seropositive: 69% of participants living in the most population-dense areas were seropositive compared with 52% of participants living in the least population-dense areas (p<0.0001; Appendix Table 1). We found similar results using alternative metrics related to urbanicity (Appendix Table 1). Among seropositive participants, 57% (815/1,442) reported having had ≥1 COVID-consistent symptom since April 2020 and 58% (474/812) of these participants reported seeking healthcare.

Adjusting for age, sex, household clustering, and test performance, we estimated the seroprevalence of SARS-CoV-2 in Sitakunda to be 64.1% (95% credible interval [CrI] 60.0%–68.1%) among all participants and 63.4% (95% CrI 59.2%–67.6%) when considering only unvaccinated participants (Table; Appendix Table 3). We estimated a 7% (95% CrI 1%–13%) higher risk of being seropositive in men compared with women. Risk generally increased with age, with those <10 years of age having the lowest risk, including a ≥34% lower risk of being seropositive compared with those 25–34 years of age (Table; Appendix Table 3). We found similar adjusted seroprevalences in the population recruited before the lockdown (63.1%, 95% CrI 56.2%–69.8%; n = 665) and after the lockdown (65.3%, 95% CrI 60.6%–69.9%; n = 1,643). In between the 2 survey rounds, during the

Table. Overview of SARS-CoV-2 seropositivity, seroprevalence and relative risk seropositivity in Sitakunda subdistrict, Chattogram district, Bangladesh*

Variable	Observations, no.	Positive, no. (%)	Negative, no. (%)	Adjusted seroprevalence, % (95% CrI)	Adjusted relative risk, % (95% CrI)
Age, y					
1–4	90	37 (41.1)	53 (58.9)	47.1 (37.0–57.3)	0.66 (0.51–0.81)
5–9	174	71 (40.8)	103 (59.2)	45.0 (37.1–52.9)	0.63 (0.51–0.74)
10–14	258	140 (54.3)	118 (45.7)	58.8 (52.0–65.3)	0.83 (0.73–0.94)
15–24	482	305 (63.3)	177 (36.7)	67.2 (61.7–72.6)	0.96 (0.88–1.05)
25–34	381	258 (67.7)	123 (32.3)	69.7 (64.5–75.0)	Referent
35–44	325	225 (69.2)	100 (30.8)	74.0 (68.3–79.5)	1.07 (0.97–1.17)
45–54	250	180 (72.0)	70 (28.0)	73.8 (67.2–80.3)	1.06 (0.96–1.17)
55–64	208	132 (63.5)	76 (36.5)	69.0 (62.1–75.8)	0.99 (0.88–1.10)
≥65	139	95 (68.3)	44 (31.7)	73.6 (65.8–81.1)	1.06 (0.94–1.19)
Sex					
M	1,072	690 (64.4)	382 (35.6)	66.7 (62.2–71.3)	1.07 (1.02–1.13)
F	1,235	753 (61.0)	482 (39.0)	61.3 (56.9–65.6)	Referent
Overall	2,307	1,443 (62.5)	864 (37.5)	64.1 (60.0–68.1)	NA

*Adjusted estimates account for sex, age, household clustering, and test performance among all vaccinated and unvaccinated participants. CrI, credible interval; NA, not applicable.

lockdown, the number of clinical cases district-wide decreased and, likely as a result of the Delta variant, began to increase during the end of the second round of data collection (*4*).

In the catchment area of this serosurvey, only 1 healthcare facility (Bangladesh Institute of Tropical and Infectious Diseases) provided SARS-CoV-2 PCR testing. Among the 2,400 participants who had a reverse transcription PCR test during April 2020–May 31, 2021, a total of 705 (29%) tested positive. By crudely extrapolating our serologic estimates by multiplying the estimated population size by the adjusted seroprevalence among those who were unvaccinated, we estimated that >200,000 infections occurred during the same period in Sitakunda. Assuming all positive cases were from Sitakunda and not neighboring areas, this corresponds to a minimum of 300 infections per medically confirmed case, a much higher proportion than has been documented in most settings across the world (*5*,*6*).

Conclusions

These results illustrate that prior to the June 2021 surge in COVID-19 cases in Bangladesh fueled by the Delta variant, most of the population in Sitakunda had already been infected despite a relatively low incidence of reported virologically confirmed SARS-CoV-2 infections. Key limitations to these results include the relatively small geographic area covered by the survey and that we only assessed circulating antibodies to a single SARS-CoV-2 epitope, which does not fully capture the immune profile of participants.

In Bangladesh, where cases captured by surveillance are limited by healthcare seeking, even in population-dense settings, representative seroprevalence surveys can help with continuing to track the evolution of this pandemic. In addition to providing important validation data on a widely used immunoassay, our results help lay the foundation for understanding the role of variant strains on key epidemiologic parameters, including our understanding of reinfection, and help set expectations for SARS-CoV-2 control in the months to come, in the study area and beyond.

This article was preprinted at https://doi.org/10.1101/2021.07.16.21260611.

Acknowledgements

The authors thank the Ministry of Health and Family Welfare (MOHFW) of Bangladesh. The authors also express their sincere thanks to the staff of icddr,b for their dedicated work in the field and laboratory during this pandemic situation. icddr,b is thankful to and supported by the governments of Bangladesh, Canada, Sweden, and the United Kingdom.

This work was supported by the Bill and Melinda Gates Foundation (grant number INV-021879). Code and data to reproduce analyses are available at https://github.com/HopkinsIDD/sitakunda-sarscov2-round1.

About the Author

Dr. Bhuiyan is a scientist at icddr,b. His research interests include immunology, vaccinology, and enteric infections.

References

1. World Health Organization. WHO coronavirus (COVID-19) dashboard: Bangladesh [cited 2021 Nov 09] https://covid19.who.int/region/searo/country/bd
2. GISAID. COVID-19 lineages and variants [cited 2021 Sep 22]. http://www.gisaid.org
3. Stringhini S, Wisniak A, Piumatti G, Azman AS, Lauer SA, Baysson H, et al. Seroprevalence of anti-SARS-CoV-2 IgG antibodies in Geneva, Switzerland (SEROCoV-POP): a population-based study. Lancet. 2020;396:313–9. https://doi.org/10.1016/S0140-6736(20)31304-0
4. Bangladesh Directorate General of Health Services. Ministry of Health and Family Welfare. COVID-19 vaccination dashboard for Bangladesh [cited 2021 Jul 28]. http://103.247.238.92/webportal/pages/covid19-vaccination-update.php
5. Banglapedia: national encyclopedia of Bangladesh. Sitakunda Upazila [cited 2021 Jun 26]. https://en.banglapedia.org/index.php/Sitakunda_Upazila
6. Chen X, Chen Z, Azman AS, Deng X, Sun R, Zhao Z, et al. Serological evidence of human infection with SARS-CoV-2: a systematic review and meta-analysis. Lancet Glob Health. 2021;9:e598–609. https://doi.org/10.1016/S2214-109X(21)00026-7

Address for correspondence: Andrew S. Azman, Johns Hopkins Bloomberg School of Public Health, 615 N. Wolfe St, Baltimore, MD 21205, USA; email: azman@jhu.edu

Neisseria gonorrhoeae FC428 Subclone, Vietnam, 2019–2020

Trang Minh Trinh,[1] Tam Thi Nguyen,[1] Thanh Viet Le, Trang Thu Nguyen, Dan Thi Ninh, Bao Hac Duong, Minh Van Nguyen, Thomas Kesteman, Lan Thi Pham, H. Rogier van Doorn

Among 114 clinical *Neisseria gonorrhoeae* isolates collected in Vietnam during 2019–2020, we detected 15 of subclone sequence type 13871 of the FC428 clonal complex. Fourteen sequence type 13871 isolates with mosaic *penA* allele 60.001 were ceftriaxone or cefixime nonsusceptible, and 3/14 were azithromycin nonsusceptible. Emergence of this subclone threatens treatment effectiveness.

Gonorrhea is a sexually transmitted infection caused by *Neisseria gonorrhoeae*; global incidence is ≈80 million cases/year (*1*,*2*). To treat uncomplicated gonorrhea, the World Health Organization recommends dual therapy with a single-dose extended-spectrum cephalosporin (ESC) (intramuscular ceftriaxone or oral cefixime) and oral azithromycin (*3*). However, *N. gonorrhoeae* resistance to ESCs and azithromycin was recently reported (*4*).

A ceftriaxone-resistant strain (FC428) harboring mutations of mosaic *penA* allele 60.001 (*penA*-60.001) and belonging to sequence type (ST) 1903 was detected in Japan in 2015 (*5*) and has now been reported on all continents (*6*). A subclone of FC428, which also carried a mosaic *penA*-60.001 gene but belonged to ST13871, was detected in Singapore in 2018 (isolate 18DG342) and in France in 2019 (isolate F91) (*7*,*8*). Genomic surveillance of *N. gonorrhoeae* in Vietnam during 2011 and 2015–2016 showed 1%–5% resistance to ceftriaxone that was not associated with *penA*-60.001 (*9*). In 2019–2020, we detected 15 ST13871 isolates related to the FC428 clone in Vietnam.

Author affiliations: National Hospital of Dermatology and Venereology, Hanoi, Vietnam (T.M. Trinh, L.T. Pham); Hanoi Medical University, Hanoi (T.M. Trinh, L.T. Pham); Oxford University Clinical Research Unit, Hanoi (T. Thi Nguyen, T. Thu Nguyen, T. Kesteman, H.R. van Doorn); Quadram Institute Bioscience, Norfolk, UK (T.V. Le); Hospital of Dermatology and Venereology, Ho Chi Minh City, Vietnam (B.H. Duong); Hospital of Dermatology and Venereology, Da Nang City, Vietnam (M.V. Nguyen); University of Oxford, Oxford, UK (T. Kesteman, H.R. van Doorn)

DOI: https://doi.org/10.3201/eid2802.211788

The Study

During June 2019–December 2020, a total of 1,116 *N. gonorrhoeae* isolates were isolated from 6,090 urethral and endocervical swab samples at 3 dermatology and venereology hospitals in Hanoi, Danang, and Ho Chi Minh City, Vietnam. Of these, 427 isolates were sent to a reference laboratory (National Hospital for Tropical Diseases, Hanoi) for antimicrobial susceptibility testing and sequencing. We used disk diffusion (Oxoid, http://www.oxoid.com/uk) to determine susceptibility to penicillin, tetracycline, spectinomycin, ciprofloxacin and an Etest (bioMérieux, https://www.biomerieux.com) for ceftriaxone, cefixime, and azithromycin. We interpreted inhibition zones and MICs according to 2020 Clinical and Laboratory Standards Institute guidelines (*10*). For whole-genome sequencing, we selected 114 isolates (28/104 from Hanoi, 16/56 from Danang, and 70/267 from Ho Chi Minh City) according to reduced susceptibility to ESC/azithromycin (51/114) or epidemiologic features (travel, men having sex with men, contact with sex worker, multiple partners). This study was approved by the Institutional Ethical Review Board of Hanoi Medical University, Hanoi, Vietnam (518/GCN-HDDDNCYSH-DHYHN, 2021 May 17). All participants gave written informed consent.

After extracting DNA with a DNeasy Blood & Tissue kit (QIAGEN, https://www.qiagen.com), we prepared DNA libraries by using Nextera XT library preparation and index kits (Illumina, https://www.illumina.com). We performed sequencing on a MiSeq platform with reagent kit 600 V3 (Illumina). We used fastp version 0.20.0 (GitHub, https://github.com) to filter out low-quality bases with Phred score <30 and to trim off the adapters. We used ARIBA 2.14.6 (GitHub) with a custom database for screening to

[1]These first authors contributed equally to this article.

detect antimicrobial resistance genes. We identified multilocus sequence typing (MLST) records from the *Neisseria* typing scheme PubMLST (https://pubmlst.org). We performed de novo assembly on the processed reads by using Shovill version 1.1.0 with SPades version 3.14 (GitHub) as the assembler. We used MOB-suite version 3.0.0 (GitHub) to reconstruct chromosome and plasmids from the assemblies. We identified *N. gonorrhoeae* multi-antigen sequence type (NG-MAST) by using NGMaster version 0.5.5, and we used *N. gonorrhoeae* Sequence Typing for Antimicrobial Resistance (NG-STAR) with pyngSTar (GitHub). We used the closest complete genome of *N. gonorrhoeae* searched by ReferenceSeeker (GitHub) as reference in Snippy 4.6.0 (GitHub) for variant calling. We created the core-genome alignment by using snippy-core with a provided mask of repeated regions and mobile elements. We used Gubbin version 2.3.4 (GitHub) to filter out the recombination in the alignment and fed it into IQTREE2 (GitHub) to reconstruct a maximum-likelihood phylogenetic tree. We used BEAST version 10.4 and TreeAnnotator (https://beast.community) to estimate the time to the most recent common ancestor (tMRCA), and ggtree version 3.0.2 (GitHub) in R (https://www.r-project.org) for visualization. Sequencing data are available from the European Nucleotide Archive (https://www.ebi.ac.uk/ena; project no. PRJEB45627).

Of 114 *N. gonorrhoeae* isolates, 15 were typed by MLST as ST13871 (Table). All patients recovered clinically after receiving 1 dose of intramuscular ceftriaxone (1 g) and oral azithromycin (1 g), although microbiological clearance of *N. gonorrhoeae* was unknown. However, because neither test-of-cure nor pharyngeal testing was performed, persistent asymptomatic infection may have been missed.

Among the 15 ST13871 isolates, NG-MAST based on 2 antigen genes identified 7 as ST7237 and 1 as ST1086; 7 were of unidentified sequence type (*porB* new, *tbpB* 21). In the NG-STAR system, based on 7 resistance genes, we found that 6 isolates were ST233, 1 was ST345, 1 was ST1133; sequence types were unknown for 7 (Appendix, https://wwwnc.cdc.gov/EID/article/28/02/21-1788-App1.pdf). For 1 isolate from Vietnam, the MLST, NG-MAST, and NG-STAR typing was identical to that of the 2 strains reported from Singapore and France/Cambodia (Appendix).

All ST13871 isolates were resistant to ciprofloxacin, nonsusceptible to penicillin and tetracycline, but susceptible to spectinomycin. For 14 isolates, susceptibility to ESCs was reduced (MIC ranges: cefixime 0.5–1.5 mg/L, ceftriaxone 0.38–0.75 mg/L) and 3 were nonsusceptible to azithromycin (MIC 1.5 mg/L), thus presenting an extensively drug-resistant (XDR) pattern (*11*) (Appendix).

Table. Epidemiologic and clinical characteristics of patients infected with multidrug-resistant *Neisseria gonorrhoeae* ST13871, Vietnam, 2019–2020*

Variable	No. (%)
Patient sex	
M	13 (87)
F	2 (13)
Place of consultation, year	
Ho Chi Minh City, 2019	3 (20)
Ho Chi Minh City, 2020	9 (60)
Danang, 2020	3 (20)
Hanoi	0
Clinical history	
Previous STIs	0
Co-infection with other STIs	
Syphilis	0
Chlamydia trachomatis	0
Sexual history	
Sex partners during past 3 mo	
1	10 (67)
≥2	5 (33)
Sexual contact with commercial sex worker	5 (33)
Unprotected sex during most recent intercourse	12 (80)
Men who have sex with men	0
Current treatment with antibiotic	15 (100)
Ceftriaxone, 1g intramuscularly	15 (100)
Azithromycin, 1g orally	10 (67)

*Patient age range (median) 19–56 (31) y. ST, sequence type; STIs, sexually transmitted infections.

Most ST13871 isolates harbored resistance genes, including *ponA*:L421P, the plasmid-mediated *bla-TEM* 135, the *mtrR* promoter −35Adel mutation causing overexpression of the MtrCDE efflux pump, *rpsJ*:V57M associated with tetracycline resistance, or changes in *penB* (G120K, A121D) associated with decreased influx of porin channel PorB1b. The mosaic *penA*-60.001, associated with resistance to ESCs (*5*), was found in 14 of 15 isolates, all nonsusceptible to ≥1 ESC (Appendix). One ST13871 isolate carrying *penA*-43.002 gene was susceptible to ESCs.

In all 15 isolates, we found mutations in *gyrA* and *parC* genes, conferring resistance to ciprofloxacin, including *gyrA*: S91F/G95A and *parC*: S87R, and 2 mutations (*parC*: V596I, L479F) not previously reported. We found no plasmidborne *tetM* causing resistance to tetracycline and no other gene except for *mtrR* promoter −35Adel conferring resistance to azithromycin.

According to time-scaled Bayesian phylogeny of 17 ST13871 sequences from Vietnam (n = 15), France (n = 1), and Singapore (n = 1) (Figure), samples clustered into 3 distinct clades. Clade 1a contained the 2 previously reported ST13871 isolates from Singapore and France/Cambodia, as well as 3 isolates from this study, including the one sharing the same typing as the international isolates. Median tMRCA of this clade was calculated as March 2017 (95% highest

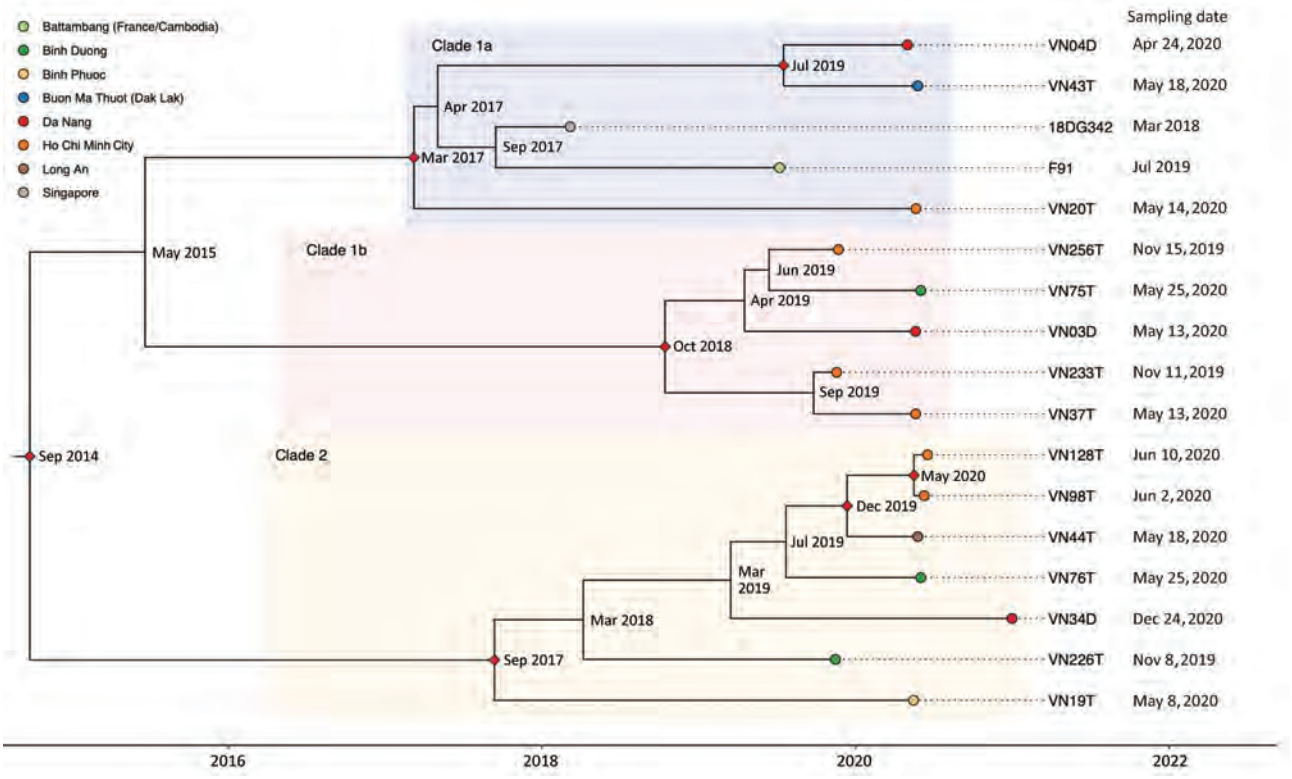

Figure. Time-scaled Bayesian maximum clade credibility phylogenetic tree of *Neisseria gonorrhoeae* ST13871 (17 isolates) with date of collection and location of collected isolates, Vietnam, 2019–2020. Red diamonds show posterior probability >90%; internal node labels show estimated time to most recent common ancestor.

posterior density [HPD] April 2014–February 2018), of clade 1b as October 2018 (95% HPD August 2016–September 2019), and of clade 2 as September 2017 (95% HPD April 2013–May 2019). Estimated median tMRCA for the 17 ST13871 isolates was September 2014. One clade 1b isolate came from a patient who reported having had sexual contact in Laos 1 week before diagnosis. Two of the XDR isolates belonged to clade 2 but were not closely related.

Conclusions

We detected the globally disseminated FC428-related resistant *N. gonorrhoeae* clone in Vietnam in 2019–2020. Among 114 *N. gonorrhoeae* isolates collected, 15 were ST13871 and 14 were related to the FC428 clone by harboring the mosaic *penA*–60.001 gene conferring resistance to ESCs. The ceftriaxone MICs for these 14 isolates were similar to those for globally reported FC428 isolates, but cefixime MICs were lower (*6*,*12*). We found 3 XDR ST13871 isolates, nonsusceptible to azithromycin and ESCs but susceptible to spectinomycin. Resistance determinants to other antimicrobial drugs in all isolates from Vietnam were similar to those of the FC428 clone (*5*,*7*,*8*,*13*,*14*).

Our phylogenetic analysis showed that all 17 ST13871 isolates arose from the rooted FC428 strain and were distributed into 3 clades with a common ancestor estimated in 2014, consistent with estimates of other FC428-like isolates (*13*). These results suggest that ST13871 has been circulating in Southeast Asia for several years.

Emergence of multidrug-resistant FC428 subclone (ST13871) in Vietnam possibly threatens effectiveness of the current presumptive treatment. Therefore, regular monitoring of antimicrobial drug susceptibility of *N. gonorrhoeae* is necessary. Controlling the spread of resistant *N. gonorrhoeae* may be enhanced by follow-up visits, postrecovery culturing, and partner counseling.

Acknowledgments

We thank the laboratory technicians at the Department of Microbiology, National Hospital of Dermatology and Venereology; Ho Chi Minh Hospital of Dermatology and Venereology; and Danang Hospital of Dermatology and Venereology for collecting swab samples and isolating *N. gonorrhoeae*. We acknowledge the laboratory staff at Oxford University Clinical Research Unit, Hanoi, for their support with sample processing and whole-genome sequencing.

This work was conducted with funding from Wellcome (106680), the Fleming Fund pilot grant Vietnam (Department of Health and Social Care, UK), and the Vietnam Fleming Fund Country Grant (Department of Health and Social Care, UK), managed by Mott MacDonald and awarded to FHI360 (FHI360 FF15/184) with a subcontract to OUCRU/University of Oxford (PO20001070), although the views expressed in this publication do not necessarily reflect those of FHI360 or Mott MacDonald. The funders had no role in study design, data collection and analysis, or the decision to publish.

About the Author

Dr. Trinh is a medical doctor at National Hospital of Dermatology and Venereology, Hanoi, Vietnam, and a member of the project of technical assistance and capacity building for identification and antimicrobial susceptibility testing for *N. gonorrhoeae* in the Dermatology and Venereology system in Vietnam. Her research interests are surveillance and molecular mechanisms of antimicrobial resistance of *N. gonorrhoeae* in Vietnam.

References

1. Newman L, Rowley J, Vander Hoorn S, Wijesooriya NS, Unemo M, Low N, et al. Global estimates of the prevalence and incidence of four curable sexually transmitted infections in 2012 based on systematic review and global reporting. PLoS One. 2015;10:e0143304. https://doi.org/10.1371/journal.pone.0143304
2. Rowley J, Vander Hoorn S, Korenromp E, Low N, Unemo M, Abu-Raddad LJ, et al. Chlamydia, gonorrhoea, trichomoniasis and syphilis: global prevalence and incidence estimates, 2016. Bull World Health Organ. 2019;97:548–562P. https://doi.org/10.2471/BLT.18.228486
3. World Health Organization. WHO guidelines for the treatment of *Neisseria gonorrhoeae*. 2016 [cited 2021 Apr 3]. https://www.who.int/reproductivehealth/publications/rtis/gonorrhoea-treatment-guidelines/en/
4. Unemo M, Shafer WM. Antimicrobial resistance in *Neisseria gonorrhoeae* in the 21st century: past, evolution, and future. Clin Microbiol Rev. 2014;27:587–613. https://doi.org/10.1128/CMR.00010-14
5. Nakayama S, Shimuta K, Furubayashi K, Kawahata T, Unemo M, Ohnishi M. New ceftriaxone-and multidrug-resistant *Neisseria gonorrhoeae* strain with a novel mosaic *penA* gene isolated in Japan. Antimicrob Agents Chemother. 2016;60:4339–41. https://doi.org/10.1128/AAC.00504-16
6. Chen S-C, Yuan L-F, Zhu X-Y, van der Veen S, Yin Y-P. Sustained transmission of the ceftriaxone-resistant *Neisseria gonorrhoeae* FC428 clone in China. J Antimicrob Chemother. 2020;75:2499–502. https://doi.org/10.1093/jac/dkaa196
7. Poncin T, Merimeche M, Braille A, Mainardis M, Bebear C, Jacquier H, et al. Two cases of multidrug-resistant *Neisseria gonorrhoeae* related to travel in south-eastern Asia, France, June 2019. Euro Surveill. 2019;24:1900528. https://doi.org/10.2807/1560-7917.ES.2019.24.36.1900528
8. Ko K, Chio M, Goh S, Tan A, Koh T, Rahman N. First case of ceftriaxone-resistant multidrug-resistant *Neisseria gonorrhoeae* in Singapore. Antimicrob Agents Chemother. 2019;63:e02624-18.
9. Lan PT, Golparian D, Ringlander J, Van Hung L, Van Thuong N, Unemo M. Genomic analysis and antimicrobial resistance of *Neisseria gonorrhoeae* isolates from Vietnam in 2011 and 2015–16. J Antimicrob Chemother. 2020;75:1432–8. https://doi.org/10.1093/jac/dkaa040
10. Clinical and Laboratory Standard Institute. Performance standards for antimicrobial susceptibility testing, 30th edition (M100). Wayne (PA): The Institute; 2020.
11. Magiorakos AP, Srinivasan A, Carey RB, Carmeli Y, Falagas ME, Giske CG, et al. Multidrug-resistant, extensively drug-resistant and pandrug-resistant bacteria: an international expert proposal for interim standard definitions for acquired resistance. Clin Microbiol Infect. 2012;18:268–81. https://doi.org/10.1111/j.1469-0691.2011.03570.x
12. Yan J, Chen Y, Yang F, Ling X, Jiang S, Zhao F, et al. High percentage of the ceftriaxone-resistant *Neisseria gonorrhoeae* FC428 clone among isolates from a single hospital in Hangzhou, China. J Antimicrob Chemother. 2021;76:936–9. https://doi.org/10.1093/jac/dkaa526
13. Eyre DW, Town K, Street T, Barker L, Sanderson N, Cole MJ, et al. Detection in the United Kingdom of the *Neisseria gonorrhoeae* FC428 clone, with ceftriaxone resistance and intermediate resistance to azithromycin, October to December 2018. Euro Surveill. 2019;24:1900147. https://doi.org/10.2807/1560-7917.ES.2019.24.10.1900147
14. Lahra MM, Martin I, Demczuk W, Jennison AV, Lee K-I, Nakayama S-I, et al. Cooperative recognition of internationally disseminated ceftriaxone-resistant *Neisseria gonorrhoeae* strain. Emerg Infect Dis. 2018;24:735–40. https://doi.org/10.3201/eid2404.171873

Address for correspondence: Tam T. Nguyen, Oxford University Clinical Research Unit, National Hospital for Tropical Diseases, No.78 Giai Phong St, Dong Da District, Hanoi, Vietnam; email: tamnt@oucru.org

Zoonotic Infection with Oz Virus, a Novel Thogotovirus

Ngo T.B. Tran, Hiroshi Shimoda, Keita Ishijima, Kenzo Yonemitsu, Shohei Minami, Supriyono, Yudai Kuroda, Kango Tatemoto, Milagros V. Mendoza, Ryusei Kuwata, Ai Takano, Masahiko Muto, Kyoko Sawabe, Haruhiko Isawa, Daisuke Hayasaka, Ken Maeda

Oz virus is a novel thogotovirus isolated from ticks that causes lethal infection in mice. We conducted serosurveillance of Oz virus infection among humans and wild mammals in Japan using virus-neutralization tests and ELISAs. Results showed that Oz virus may be naturally infecting humans and other mammalian hosts.

The genus *Thogotovirus*, family *Orthomyxoviridae*, comprises viruses that are most frequently transmitted by a variety of hard and soft tick species (*1*). Although most thogotoviruses are associated with tick species, there are several exceptions, such as Sinu virus, which was isolated from mosquitoes (*2*); Dielmo orthomyxovirus, isolated from *Culicoides* midges (*3*); and Araguari virus, isolated only from vertebrates (*4*). Thogoto, Dhori, and Bourbon viruses have been associated with human disease. Thogoto and Dhori viruses have been reported to cause encephalitis, febrile illness, and death in humans (*5*,*6*), and Bourbon virus to cause febrile illness and death in humans (*7*). In addition, Thogoto virus has been reported to cause abortions in sheep (*8*), and many wild animals are positive for Bourbon virus antibodies (*9*).

Oz virus, a new member of the genus *Thogotovirus*, was first isolated from a pool of 3 *Amblyomma testudinarium* tick nymphs collected in Ehime prefecture, Japan (*10*). Phylogenetic analyses revealed that Oz virus is more closely related to Dhori, Batken, and Bourbon viruses than to other thogotoviruses (*10*). In addition, Oz virus has been shown to cause lethal infection in experimentally challenged suckling mice. To determine the potential of Oz virus as a zoonotic pathogen, we performed serosurveillance of Oz virus infection among mammals, including humans, in Japan.

Author affiliations: Yamaguchi University, Yoshida, Japan (N.T.B. Tran, H. Shimoda, S. Minami, Supriyono, A. Takano, D. Hayasaka, K. Maeda); National Institute of Infectious Diseases, Toyama, Tokyo, Japan (K. Ishijima, K. Yonemitsu, Y. Kuroda, K. Tatemoto, M.V. Mendoza, K. Sawabe, H. Isawa, K. Maeda); Okayama University of Science, Imabari, Japan (R. Kuwata); Yamaguchi Prefectural Grand Medical Center, Hofu, Japan (M. Muto)

DOI: https://doi.org/10.3201/eid2802.211270

The Study

To examine whether mammals are naturally infected with Oz virus, we collected serum samples from 24 hunters and 240 wild animals (40 Japanese macaques [*Macaca fuscata*], 124 wild boars [*Sus scrofa*], and 76 sika deer [*Cervus nippon*]) captured in Yamaguchi prefecture, Japan, during 2013–2019. Because Yamaguchi prefecture is close to Ehime prefecture and the environment in Yamaguchi is very similar to that in Ehime, we used stocked samples in Yamaguchi prefecture for the first surveillance of Oz virus infection. To test for the presence of Oz virus antibodies in the serum samples, we performed a $PRNT_{80}$ (80% plaque-reduction neutralizing test) using Oz virus (Table 1). Among humans, 8.3% of the serum samples had Oz virus neutralization (VN) antibodies; VN titers were 1:40 and 1:80. In wild animals, serum from 47.5% of macaques, 60.5% of wild boars, and 73.7% of sika deer in Yamaguchi had Oz virus VN antibodies (Table 1).

We applied ELISA protocol used for serosurveillance of many infectious diseases (*11*–*13*) to detect Oz virus antibodies in the serum samples from wild animals. We extracted proteins from Oz virus or mock-infected Vero cells and used the extracts as ELISA antigens. To prepare the primary antibody, we diluted serum samples 1:100 in phosphate-buffered saline containing 0.05% Tween 20 and 0.4% Block Ace. We used peroxidase conjugated recombinant protein A/G (Thermo Fisher Scientific, https://www.thermofisher.com) as the secondary antibody and KPL ABTS peroxidase substrate (SeraCare Life Sciences, https://www.seracare.com) as the detection reagent. We measured absorbance using a spectrophotometer

Table 1. Serosurveillance of Oz virus infection by virus-neutralization test among mammals in Yamaguchi prefecture, Japan

Species	Genus and species	Years	Virus-neutralization titer						
			<1:10	1:10	1:20	1:40	1:80	1:160	>1:160
Human	*Homo sapiens*	2015	22	0	0	1	1	0	0
Macaque	*Macaca fuscata*	2018–2019	21	0	2	3	3	6	5
Wild boar	*Sus scrofa leucomystax*	2013–2014	49	2	12	10	15	20	16
Sika deer	*Cervus nippon*	2014–2015	20	5	8	11	12	13	7

(Bio-Rad Laboratories, https://www.bio-rad.com) with a 405 nm filter and subtracted the value of the corresponding control mock-infected cells from all values.

To determine ELISA cutoff values, we tested serum samples from the 40 macaques, 124 wild boars, and 76 sika deer captured in Yamaguchi prefecture. We compared the optical density values of the ELISA to the results of the VN test by 2-graph receiver-operating characteristic (ROC) curve analysis as described elsewhere (*14*). In macaques, the correlation coefficient between the ELISA and VN test was 0.9163, and an ELISA cutoff value of 0.2245 produced 100% sensitivity and specificity. In wild boars, the correlation coefficient was 0.8807, with 88.0% sensitivity and 89.8% specificity at an ELISA cutoff value of 0.1965. In sika deer, the correlation coefficient was 0.7569, sensitivity 78.6%, and specificity 80.0% at an ELISA cutoff value of 0.3165 (Figure 1).

Next, we surveyed Oz virus infection among macaques, wild boars, and sika deer in many prefectures in Japan using the established ELISA (Table 2; Figure 2). Among 197 macaques captured during 2007–2019, seropositivity rates were 47.5% in Yamaguchi, 33.3% in Wakayama, and 6.3% in Mie prefectures. Among 879 wild boars captured during 2007–2014, seropositivity rates were 10.3% in Oita, 55.8% in Yamaguchi, 34.8% in Wakayama, 10.5% in Gifu, and 0% in both Toyama and Tochigi prefectures. Among 450 sika deer, seropositivity rates were 37.8% in Yamaguchi, 11.1% in Wakayama, 8.3% in Gifu, and 30% in Chiba prefectures.

First, we applied $PRNT_{80}$ to detect Oz virus antibodies in humans and wild animals in Yamaguchi prefecture. The results showed that 60.5% of wild boars, a major host of *A. testudinarium*, and 73.7% of sika deer in Yamaguchi prefecture during 2013 and 2015 had Oz virus VN antibodies, indicating that the virus was infecting wild animals in the western part of Japan. Next, we examined wild macaques for Oz virus infection; 48% were infected, and the antibody titers were high. In addition, 2 persons who hunted wild boars and sika deer in Yamaguchi prefecture had Oz virus antibodies. These results indicate that humans and macaques are also exposed to Oz virus.

We compared results from an ELISA, established for this study, using an Oz virus–infected cell extract for the surveillance of Oz virus infection among many mammalians, with those from the VN test to determine correlation between the 2 tests. The correlation coefficient was 0.9163 for macaques, 0.8807 for wild boars, and 0.7569 for sika deer, suggesting that the ELISA is effective for serosurveillance of Oz virus infection in samples from many animal species. However, because its sensitivity and specificity differed among animal species and values were lower for sika deer, in particular, cutoff values should be determined for each animal species. In addition, VN testing should be performed to confirm the presence of Oz virus antibodies.

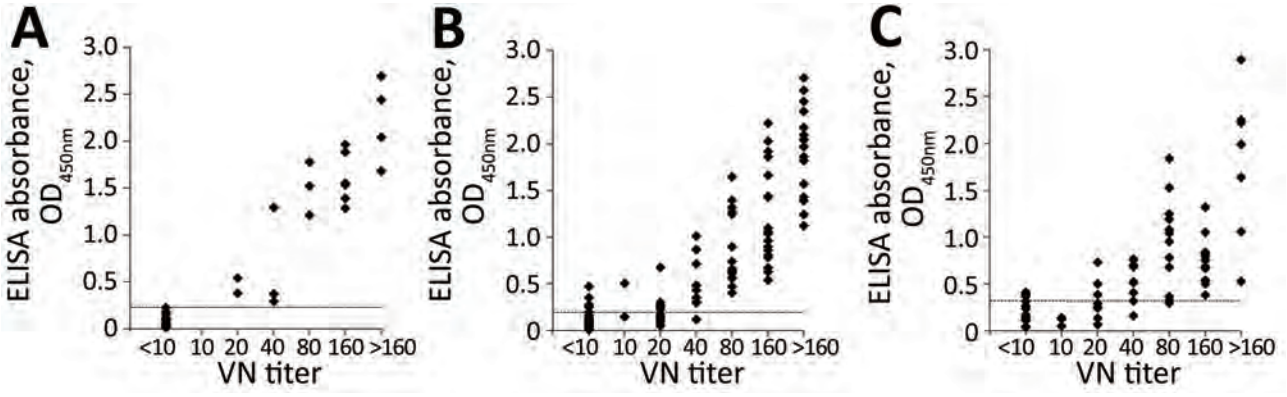

Figure 1. Dot plot comparison between VN test and ELISA against Oz virus in serum samples from wild animals in Yamguchi prefecture, Japan. A) Macaques (n = 40); B) wild boar (n = 124); C) sika deer (n = 76). The correlation coefficient between VN test and ELISA from macaques was 0.9163, from wild boars was 0.8807, and from sika deer was 0.7569. The optimal cutoff value of ELISA was calculated by 2-graph receiver-operating characteristic curve. The optimal cutoff values were set at 0.225 for macaques, 0.197 for wild boar, and 0.317 for sika deer serum samples and are indicated by dotted lines.

Table 2. Serosurveillance of Oz virus infection by ELISA among wild animals, Japan

Species	Prefecture	Years	Cutoff	No. serum samples examined	No. (%) positive serum samples
Macaque	Yamaguchi	2018–2019	0.225	40	19 (47.5)
	Wakayama	2012–2013		15	5 (33.3)
	Mie	2007		142	9 (6.3)
Wild boar	Oita	2012	0.197	58	6 (10.3)
	Yamaguchi	2010–2014		344	192 (55.8)
	Wakayama	2007–2013		89	31 (34.8)
	Gifu	2014		19	2 (10.5)
	Toyama	2014		20	0
	Tochigi	2010–2012		349	0
Sika deer	Yamaguchi	2010–2015	0.317	407	154 (37.8)
	Wakayama	2010–2014		9	1 (11.1)
	Gifu	2014		24	2 (8.3)
	Chiba	2014		10	3 (30.0)

Our nationwide surveillance of Oz virus infection in Japan indicated that many wild animals were positive for Oz virus antibodies. However, wild boars in Toyama and Tochigi prefectures did not have Oz virus antibodies, suggesting that the virus might not be distributed in the northern and eastern parts of Japan. *A. testudinarium* is the major tick species that infests humans in the southern and western parts of Japan (*15*), and because we found Oz virus mainly in those areas, it appears that the distribution of Oz virus–infected animals correlates with the habitat of the tick. In addition, because 2 hunters in Yamaguchi prefecture tested positive for Oz virus antibodies, further investigation is needed to determine whether Oz virus might be a zoonotic pathogen, especially because intracerebral inoculation of the virus in suckling mice causes lethal disease (*10*).

Figure 2. Collection sites of serum samples from macaques, wild boars, and sika deer for study of Oz virus seroprevalence in Japan. Gray shading indicates prefectures in which samples were collected; black shading indicates Ehime prefecture, where Oz virus was first isolated.

Acknowledgments

We thank Mr. Hashimura and Mr. Matsuzaki for the collection of macaque serum samples, Akiko Nakamura and Kishiko Matsumoto for the collection of human serum samples, Tsutomu Takeda for the collection of wild boar serum samples in Tochigi, Kazuo Suzuki for the collection of serum samples from wild animals, and Toshiya Kimura and Hiroto Shinomiya for advice on Oz virus infection in Ehime. We also acknowledge all of the hunters who provided support and cooperated with the collection of serum samples.

This study was supported by grants from AMED (Japan Agency for Medical Research and Development) (JP20wm0225009, JP21fk0108613, JP19fk0108097, JP20fk0108067 and JP16fk0108117). N.T.B.T. received a scholarship from the Government of Vietnam Ministry of Agriculture and Rural Development.

All animal samples used in this study were collected with the appropriate hunting permits issued by the respective local government. This article does not contain any studies with live animals. Human serum samples were collected from 24 hunters in Yamaguchi with the approval of the institutional review board of Yamaguchi University (number H26–116).

About the Author

Mrs. Tran is a PhD student in the Joint Faculty of Veterinary Medicine, Yamaguchi University, Yamaguchi, Japan. Her research interest is zoonoses.

References

1. Hubálek Z, Rudolf I, Nowotny N. Arboviruses pathogenic for domestic and wild animals. Adv Virus Res. 2014;89:201–75. https://doi.org/10.1016/B978-0-12-800172-1.00005-7
2. Contreras-Gutiérrez MA, Nunes MRT, Guzman H, Uribe S, Suaza Vasco JD, Cardoso JF, et al. Sinu virus, a novel and divergent orthomyxovirus related to members of the genus Thogotovirus isolated from mosquitoes in Colombia. Virology. 2017;501:166–75. [Erratum in: Virology. 2017;503:114.] https://doi.org/10.1016/j.virol.2016.11.014
3. Temmam S, Monteil-Bouchard S, Robert C, Baudoin JP, Sambou M, Aubadie-Ladrix M, et al. Characterization of viral communities of biting midges and identification of novel *Thogotovirus* species and *Rhabdovirus* genus. Viruses. 2016;8:77. https://doi.org/10.3390/v8030077
4. Da Silva EV, Da Rosa AP, Nunes MR, Diniz JA, Tesh RB, Cruz AC, et al. Araguari virus, a new member of the family Orthomyxoviridae: serologic, ultrastructural, and molecular characterization. Am J Trop Med Hyg. 2005;73:1050–8. https://doi.org/10.4269/ajtmh.2005.73.1050
5. Moore DL, Causey OR, Carey DE, Reddy S, Cooke AR, Akinkugbe FM, et al. Arthropod-borne viral infections of man in Nigeria, 1964-1970. Ann Trop Med Parasitol. 1975;69:49–64. https://doi.org/10.1080/00034983.1975.11686983
6. Butenko AM, Leshchinskaia EV, Semashko IV, Donets MA, Mart'ianova LI. Dhori virus—a causative agent of human disease. Five cases of laboratory infection [in Russian]. Vopr Virusol. 1987;32:724–9.
7. Kosoy OI, Lambert AJ, Hawkinson DJ, Pastula DM, Goldsmith CS, Hunt DC, et al. Novel thogotovirus associated with febrile illness and death, United States, 2014. Emerg Infect Dis. 2015;21:760–4. https://doi.org/10.3201/eid2105.150150
8. Davies FG, Soi RK, Wariru BN. Abortion in sheep caused by Thogoto virus. Vet Rec. 1984;115:654. https://doi.org/10.1136/vr.115.25-26.654
9. Jackson KC, Gidlewski T, Root JJ, Bosco-Lauth AM, Lash RR, Harmon JR, et al. Bourbon virus in wild and domestic animals, Missouri, USA, 2012–2013. Emerg Infect Dis. 2019;25:1752–3. https://doi.org/10.3201/eid2509.181902
10. Ejiri H, Lim CK, Isawa H, Fujita R, Murota K, Sato T, et al. Characterization of a novel thogotovirus isolated from *Amblyomma testudinarium* ticks in Ehime, Japan: A significant phylogenetic relationship to Bourbon virus. Virus Res. 2018;249:57–65. https://doi.org/10.1016/j.virusres.2018.03.004
11. Shimoda H, Inthong N, Noguchi K, Terada Y, Nagao Y, Shimojima M, et al. Development and application of an indirect enzyme-linked immunosorbent assay for serological survey of Japanese encephalitis virus infection in dogs. J Virol Methods. 2013;187:85–9. https://doi.org/10.1016/j.jviromet.2012.09.022
12. Suzuki J, Nishio Y, Kameo Y, Terada Y, Kuwata R, Shimoda H, et al. Canine distemper virus infection among wildlife before and after the epidemic. J Vet Med Sci. 2015;77:1457–63. https://doi.org/10.1292/jvms.15-0237
13. Yonemitsu K, Minami S, Noguchi K, Kuwata R, Shimoda H, Maeda K. Detection of anti-viral antibodies from meat juice of wild boars. J Vet Med Sci. 2019;81:155–9. https://doi.org/10.1292/jvms.18-0576
14. Ikawa-Yoshida A, Yoshii K, Kuwahara K, Obara M, Kariwa H, Takashima I. Development of an ELISA system for tick-borne encephalitis virus infection in rodents. Microbiol Immunol. 2011;55:100–7. https://doi.org/10.1111/j.1348-0421.2010.00296.x
15. Okino T, Ushirogawa H, Matoba K, Hatsushika R. A bibliographical study of human cases of hard tick (Acarina: Ixodidae) bites received abroad and found in Japan. Kawasaki Med J. 2007;33:189–94.

Address for correspondence: Ken Maeda, Department of Veterinary Science, National Institute of Infectious Diseases, 1-23-1 Toyama, Shinjuku-ku, Tokyo 162-8640, Japan; email: kmaeda@nih.go.jp

SARS-CoV-2 Cross-Reactivity in Prepandemic Serum from Rural Malaria-Infected Persons, Cambodia

Jessica Manning, Irfan Zaidi, Chanthap Lon, Luz Angela Rosas, Jae-Keun Park, Aiyana Ponce, Jennifer Bohl, Sophana Chea, Maria Karkanitsa, Sokunthea Sreng, Huy Rekol, Char Meng Chour, Dominic Esposito, Jeffery K. Taubenberger, Matthew J. Memoli, Kaitlyn Sadtler, Patrick E. Duffy, Fabiano Oliveira

Inhabitants of the Greater Mekong Subregion in Cambodia are exposed to pathogens that might influence serologic cross-reactivity with severe acute respiratory syndrome coronavirus 2. A prepandemic serosurvey of 528 malaria-infected persons demonstrated higher-than-expected positivity of nonneutralizing IgG to spike and receptor-binding domain antigens. These findings could affect interpretation of large-scale serosurveys.

Serosurveys for severe acute respiratory syndrome coronavirus 2 (SARS-CoV-2) in the Greater Mekong Subregion (GMS) of Cambodia have been limited to those screening healthcare workers in 2 urban hospital-based settings (*1*,*2*). These antibody-based studies are necessary to determine at-risk populations and direct disease containment measures; however, before informing public health decisions, serologic assays require careful, country-specific calibration because several regions report fluctuating results or high background reactivity in different populations (*3*–*5*). This variability might be attributable to myriad serologic assays, the hypothesized cross-reactivity from common cold–type respiratory coronaviruses (*6*), previous *Plasmodium* infections (*7*,*8*; S. Lapidus et al., unpub. data, https://www.medrxiv.org/content/10.1101/2021.05.10.21256855v1), or previously uncharacterized betacoronaviruses in wildlife populations in the rural GMS (*9*–*11*). Although many serologic SARS-CoV-2 investigations are in progress, considering how pathogen diversity in the GMS might influence estimations of SARS-CoV-2 seroprevalence is prudent.

Author affiliations: National Institute of Allergy and Infectious Diseases, Bethesda, Maryland, USA (J. Manning, I. Zaidi, C. Lon, L.A. Rosas, J.-K. Park, A. Ponce, J. Bohl, J.K. Taubenberger, M.J. Memoli, P.E. Duffy, F. Oliveira); National Center for Parasitology, Entomology and Malaria Control, Phnom Penh, Cambodia (S. Chea, S. Sreng, H. Rekol, C.M. Chour); Frederick National Institute of Biomedical Imaging and Bioengineering, Bethesda (M. Karkanitsa, K. Sadtler); Frederick National Laboratory for Cancer Research, Frederick, Maryland, USA (D. Esposito)

DOI: https://doi.org/10.3201/eid2802.211725

The Study

We tested serum or plasma samples collected from 528 malaria-infected persons in Cambodia during 2005–2011 (before SARS-CoV-2 emerged in 2019) for IgG reactive to SARS-CoV-2 spike and receptor-binding domain (RBD) proteins by using ELISA (*12*,*13*). We used de-identified, anonymized serum or plasma samples biobanked after malaria research studies (NCT00341003, NCT00663546, and NCT01350856, approved by the National Institute of Allergy and Infectious Diseases and the National Ethics Committee on Human Research in Cambodia) for this retrospective study.

Because 6 other coronaviruses (OC43, HKU1, 229E, NL63, severe acute respiratory syndrome coronavirus 1 [SARS-CoV-1], and Middle East respiratory syndrome coronavirus) possess structural proteins capable of infecting humans, we selected highly specific ELISAs for the SARS-CoV-2 structural proteins (*12*,*13*). Compared with other coronaviruses, SARS-CoV-2 shows varying levels of spike protein sequence homology; levels are highest for SARS-CoV-1 (76% identity, 87% similarity) and lowest for the common cold coronavirus HKU1 (29% identity, 40% similarity) (*12*). Reactivity to both spike and RBD antigens above cutoff values is required for a positive test with reported sensitivity of 100% (95% CI 92.9%–100%) and specificity of 100% (95% CI 98.8%–100%) (*12*,*13*). Prepandemic samples had levels above the set cutoffs for SARS-CoV-2 spike and RBD antigens (Figure 1) varying from 4.4% to 13.8% positivity to both SARS-CoV-2 spike and RBD depending on which cutoff

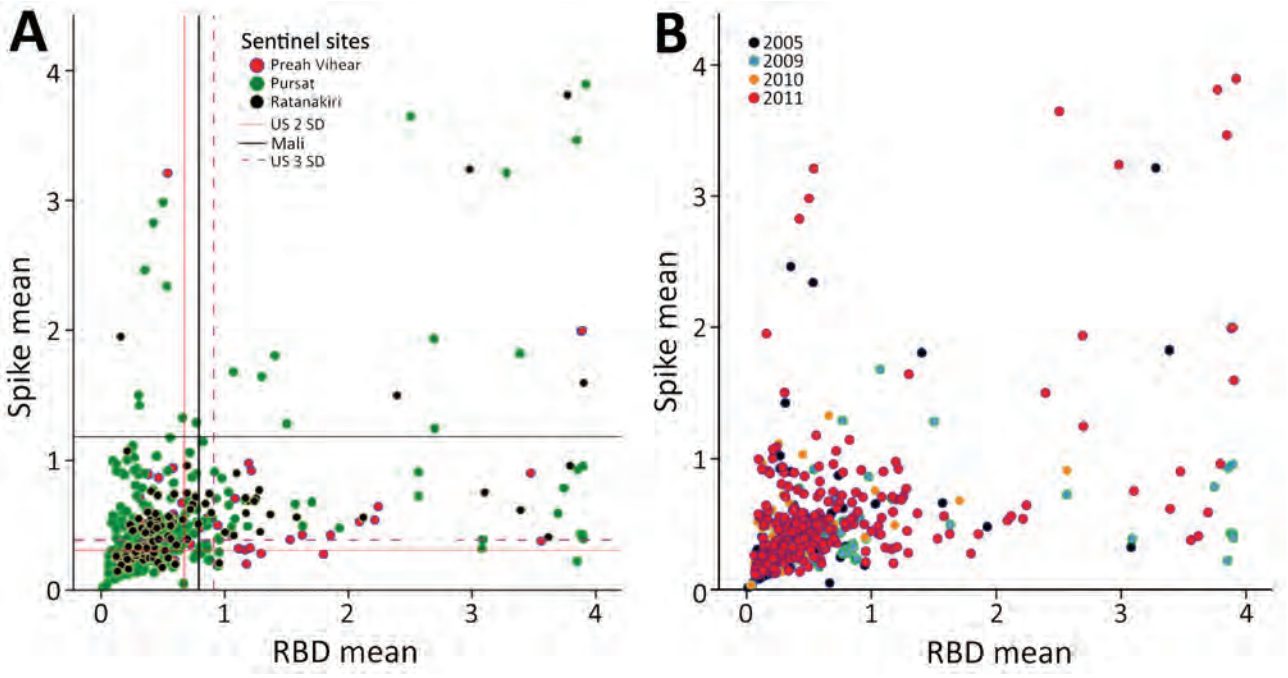

Figure 1. Mean antibody intensity in arbitrary ELISA units to spike and RBD in serum samples from prepandemic, malaria-positive rural persons in Cambodia, 2005–2011. A) Provinces indicated by color: Preah Vihear (pink), Pursat (green), Ratanakiri (black). B) Years indicated by color: 2005 (purple), 2009 (turquoise), 2010 (orange), and 2011 (pink). RBD, receptor binding domain.

values (calibrated for the Mali or US populations) were used for this assay (*4*,*12*,*13*) (Table; Figure 1; Appendix Table 1, https://wwwnc.cdc.gov/EID/article/28/2/21-1725-App1.pdf).

To test whether the higher-than-expected positivity was an artifact of our in-house ELISA, we tested a subset of samples with a commercially validated SARS-CoV-2 Spike S1-RBD IgG ELISA Detection Kit (Genscript, https://www.genscript.com). Of the 24 persons who were seronegative by in-house assay and 11 who were seropositive by in-house assay, 18 tested negative and 9 tested positive by the commercial test, yielding an overall concordance of 77.1% between assays (Appendix Table 2). This inconsistency might be explained by the stringency of the in-house assay that tests both spike and RBD versus the commercial kit that tests for RBD only; nevertheless, higher-than-expected positivity was observed in both assays. Because common cold coronaviruses do circulate in Cambodia, but no cases of SARS-CoV-1 or Middle East respiratory syndrome have been documented, we tested a subset of the cohort for IgG to HKU1 and OC43. Reactivity between subjects was comparable despite SARS-CoV-2 serostatus (Figure 2, panel A).

We further tested 289 samples to assess whether a relationship existed between antibodies to *Plasmodium* spp. and SARS-CoV-2 proteins by using 2 known malarial antigens: *Plasmodium falciparum* apical membrane antigen 1 (AMA-1), which is highly immunogenic and an indicator of parasite exposure, and *P. falciparum* Pfs25 protein (Pfs25), which is poorly immunogenic and expressed only during

Table. SARS-CoV-2 ELISA results by cutoff values in prepandemic serum samples from rural malaria-infected persons in 3 Cambodia provinces, 2005–2011*

Province	Year	Total	No. positive by 2 SDs	No. positive by 3 SDs	No. positive, Mali
Preah Vihear	2011	81	12 (15)	6 (7)	5 (6)
Pursat	2005	80	8 (10)	4 (5)	3 (4)
	2009	76	12 (16)	6 (8)	3 (0.9)
	2010	81	5 (6)	3 (4)	1 (0.3)
	2011	110	17 (15.5)	12 (11)	6 (5.4)
	Subtotal	347	42 (12)	25 (7)	13 (3.7)
Ratanakiri	2011	100	19 (19)	6 (6)	5 (5)
Total	All	528	73 (13.8)	37 (7)	23 (4.4)

*Values are no. (%) except as indicated. Using United States arbitrary ELISA unit cutoffs of 2 SDs for spike (0.674) and receptor binding domain (RBD) (0.306); United States 3 SDs for spike (0.910) and RBD (0.387); and Mali cutoff for spike (0.791) and RBD (1.183). SARS-CoV-2, severe acute respiratory syndrome coronavirus 2.

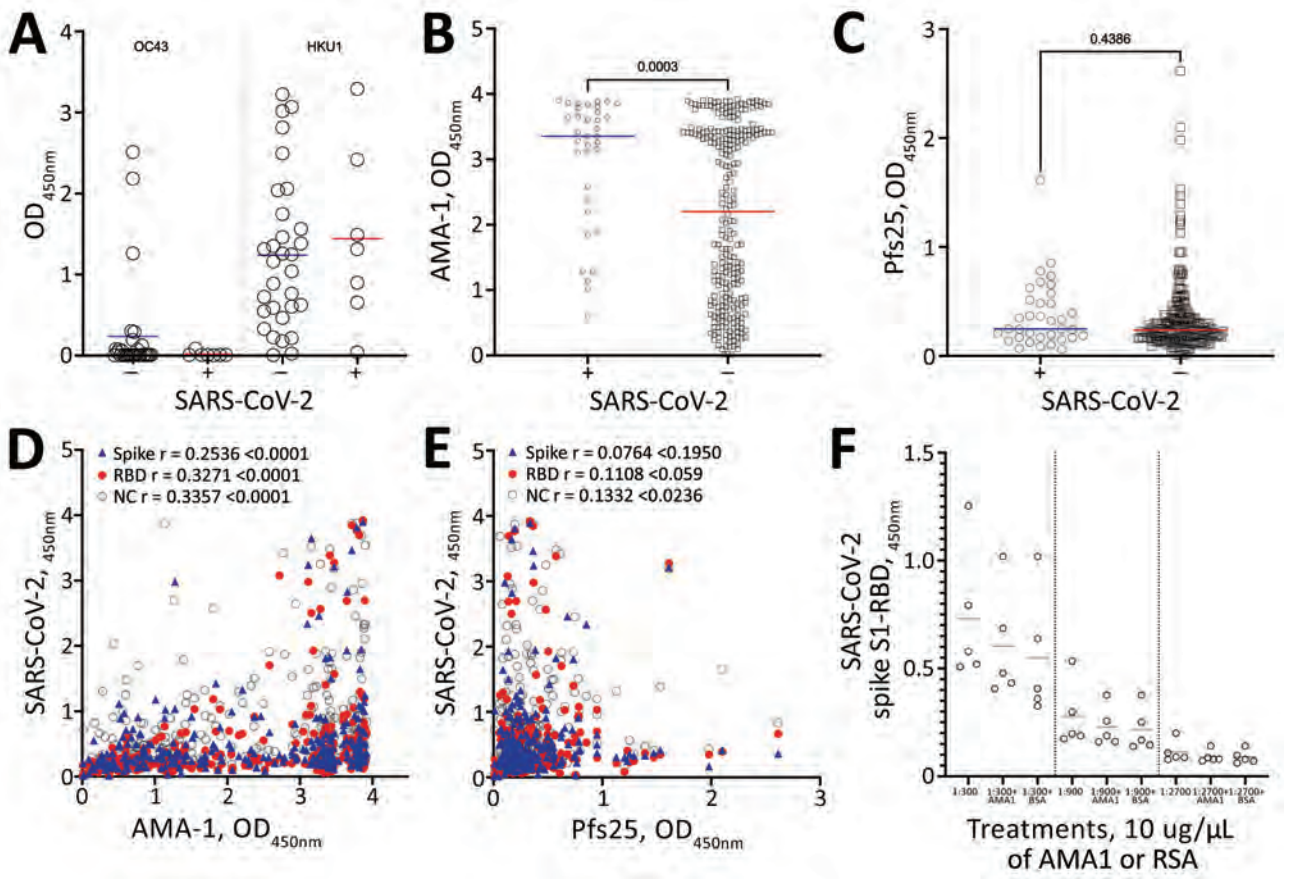

Figure 2. Mean antibody levels in prepandemic serum samples from malaria-positive rural persons in Cambodia, 2005–2011, to A) common cold OC43 and HKU1 viruses, B) *Plasmodium falciparum* AMA-1 and C) *P. falciparum* Pfs25 protein by SARS-CoV-2 serosurvey statuses. D–E) Correlation of mean IgG levels of AMA-1 and Pfs25 against Spike (blue triangles), RBD (red circles) and NC (open circles) IgG levels in prepandemic serum samples from malaria-positive rural persons in Cambodia. F) OD levels of RBD protein after preincubation of serum samples with 10mg/mL of AMA-1 or BSA. AMA-1, apical membrane antigen 1; BSA, bovine serum albumin; NC, nucleocapsid; OD, optical density; RBD, receptor binding domain; SARS-CoV-2, severe acute respiratory syndrome coronavirus 2.

the mosquito stages of parasite development (*4*) (Figure 2, panels B–E). Of note, when we grouped samples by SARS-CoV-2 serostatus, we detected significantly higher levels of AMA-1 antibodies in SARS-CoV-2–seropositive persons than seronegative persons (mean AMA-1 antibody level 3.0 vs. 2.1; p = 0.0003) (Figure 2, panel B). As expected, no difference was seen in antibody levels to Pfs25 with regard to SARS-CoV-2 seropositivity (Figure 2, panel C). A weak but statistically significant positive correlation was detected between spike and RBD with AMA-1 IgG (Figure 2, panel D). This finding corroborates recent observations that higher SARS-CoV-2 seroreactivity by ELISA or rapid tests is detected in persons from malaria-endemic areas, expanding previous observations to include Southeast Asia (*7*,*8*; S. Lapidus et al., unpub. data). We also evaluated samples for seroreactivity against the nucleocapsid protein that also positively correlated with the AMA-1 IgG. Only nucleocapsid antibodies were weakly correlated with Pfs25 antibodies, which reinforces the argument for nonspecific nucleocapsid reactivity (Figure 2, panel E). Preincubation with 10 mg/mL of AMA-1 or bovine serum albumin had no notable effect on reactivity to SARS-CoV-2 spike S1-RBD (Figure 2, panel F). Therefore, *Plasmodium* spp. exposure might contribute to SARS-CoV-2 malaria-related background reactivity. This reactivity could be attributed to immune responses to other *Plasmodium* spp. proteins, polyclonal B cell activation during infection, or interaction with the sialic acid moiety on N-linked glycans of the SARS-CoV-2 spike protein (*7*; S. Lapidus et al., unpub. data). Of note, SARS-CoV-2 spike proteins used in the assays were produced in HEK293 mammalian cells and likely have comparable glycosylation patterns. Elsewhere, malaria-induced cross-reactivity in prepandemic samples from malaria-experienced persons from

Africa was mitigated by the modification of 2 commercial assays to add a urea wash (S. Lapidus et al., unpub. data).

To elucidate the functionality of the detected antibodies, we took a subset (n = 21) of the samples with the highest reactivity to SARS-CoV-2 total IgG and performed neutralization assays (Appendix Figure). No neutralizing activity was identified despite high levels of antibodies reacting to both spike and RBD proteins. Identical results were obtained by using a surrogate virus neutralization test targeting RBD interaction with the host cell receptor ACE2 (Genscript) (Appendix Table 3) (*14*). Both SARS-CoV-2 infection and vaccination can trigger high levels of nonneutralizing antibodies, whereas neutralizing antibodies aimed primarily at the RBD seem to wane faster and remain at low titers (*14*). Plausibly, the cross-reactive nonfunctional antibodies to SARS-CoV-2 were raised during an infection by *Plasmodium* spp. (S. Lapidus et al., unpub. data), but we cannot discard the hypothesis that nonneutralizing SARS-CoV-2–reactive antibodies in prepandemic serum samples might be linked to the ability of betacoronaviruses to evade immune recognition because of their complex surfaces (*14*,*15*). A limitation in understanding the assays' specificity is the lack of prepandemic samples from non–malaria-endemic areas and from present-day confirmed SARS-CoV-2 convalescent samples in Cambodia.

Conclusions

We found in a widely used, highly specific, and validated ELISA that ≈4%–14% of prepandemic serum samples from malaria-infected persons in Cambodia were positive for nonneutralizing antibodies to SARS-CoV-2 spike and RBD antigens by using various standardized optical density cutoff values (*4*,*12*,*13*). We noted a relationship between increased SARS-CoV-2 seroreactivity and antimalarial humoral immunity, which was also recently shown in Africa (S. Lapidus et al., unpub. data). The plausibility of regular spillover events, or simply increased exposure to uncharacterized betacoronaviruses, as a reason for SARS-CoV-2 cross-reactivity is also increased in settings at high risk for zoonotic disease transmission because of agricultural and dietary practices such as bat guano collection and consumption of wild meats (*9*–*11*). Given that 50%–80% of GMS residents are classified as rural, careful calibration of serologic assays targeting SARS-CoV-2 will be necessary in national and subnational serosurveys. Although neutralization assays with live virus are often considered the standard because of their specificity, they are cost-prohibitive for large-scale serosurveys. The use of competition ELISA assays such as surrogate virus neutralization tests targeting the RBD-ACE2 blockade might be an attractive option for populations at high risk for zoonotic exposures in resource-scarce settings without Biosafety Level 3 facilities.

Acknowledgments

We thank the participants of the studies in Pursat, Ratanakiri, and Preah Vihear provinces and the original study protocol staff.

This research was supported by the Intramural Research Program of the NIH, National Institute of Allergy and Infectious Diseases.

About the Author

Dr. Manning is an infectious diseases physician-scientist focused on vector-borne disease epidemiology. She is currently based in Phnom Penh as an Assistant Clinical Investigator for the National Institute of Allergy and I nfectious Diseases and its International Center of Excellence in Research Cambodia.

References

1. Song LH, Hoan NX, Bang MH, Kremsner PG, Velavan TP. Viral and serological testing of SARS-CoV-2 among health care workers and patients in Vietnam. Lancet Reg Health West Pac. 2021;8:100113. https://doi.org/10.1016/j.lanwpc.2021.100113
2. Nopsopon T, Pongpirul K, Chotirosniramit K, Jakaew W, Kaewwijit C, Kanchana S, et al. Seroprevalence of hospital staff in a province with zero COVID-19 cases. PLoS One. 2021;16:e0238088. https://doi.org/10.1371/journal.pone.0238088
3. Uyoga S, Adetifa IMO, Karanja HK, Nyagwange J, Tuju J, Wanjiku P, et al. Seroprevalence of anti-SARS-CoV-2 IgG antibodies in Kenyan blood donors. Science. 2021;371:79–82. https://doi.org/10.1126/science.abe1916
4. Sagara I, Woodford J, Dicko A, Zeguime A, Doucoure M, Kwan J, et al. Rapidly increasing SARS-CoV-2 seroprevalence and limited clinical disease in 3 Malian communities: a prospective cohort study. Clin Infect Dis. 2021 Jun 29 [Epub ahead of print]. https://doi.org/10.1093/cid/ciab589
5. Murhekar MV, Bhatnagar T, Selvaraju S, Saravanakumar V, Thangaraj JWV, Shah N, et al.; ICMR Serosurveillance Group. SARS-CoV-2 antibody seroprevalence in India, August-September, 2020: findings from the second nationwide household serosurvey. Lancet Glob Health. 2021;9:e257–66. https://doi.org/10.1016/S2214-109X(20)30544-1
6. Ng KW, Faulkner N, Cornish GH, Rosa A, Harvey R, Hussain S, et al. Preexisting and de novo humoral immunity to SARS-CoV-2 in humans. Science. 2020;370:1339–43. https://doi.org/10.1126/science.abe1107
7. Steinhardt LC, Ige F, Iriemenam NC, Greby SM, Hamada Y, Uwandu M, et al. Cross-reactivity of two SARS-CoV-2 serological assays in a setting where malaria is endemic. J Clin Microbiol. 2021;59:e0051421. https://doi.org/10.1128/JCM.00514-21

8. Vanroye F, Bossche DVD, Brosius I, Tack B, Esbroeck MV, Jacobs J. COVID-19 antibody detecting rapid diagnostic tests show high cross-reactivity when challenged with pre-pandemic malaria, schistosomiasis and Dengue samples. Diagnostics (Basel). 2021;11:1163. https://doi.org/10.3390/diagnostics11071163
9. Delaune D, Hul V, Karlsson EA, Hassanin A, Ou TP, Baidaliuk A, et al. A novel SARS-CoV-2 related coronavirus in bats from Cambodia. Nat Commun. 2021;12:6563. https://doi.org/10.1038/s41467-021-26809-4
10. Wacharapluesadee S, Tan CW, Maneeorn P, Duengkae P, Zhu F, Joyjinda Y, et al. Evidence for SARS-CoV-2 related coronaviruses circulating in bats and pangolins in Southeast Asia. [Erratum in: Nat Commun. 2021;12:1430]. Nat Commun. 2021;12:972. https://doi.org/10.1038/s41467-021-21240-1
11. Huong NQ, Nga NTT, Long NV, Luu BD, Latinne A, Pruvot M, et al. Coronavirus testing indicates transmission risk increases along wildlife supply chains for human consumption in Viet Nam, 2013-2014. PLoS One. 2020;15:e0237129. https://doi.org/10.1371/journal.pone.0237129
12. Klumpp-Thomas C, Kalish H, Drew M, Hunsberger S, Snead K, Fay MP, et al. Standardization of ELISA protocols for serosurveys of the SARS-CoV-2 pandemic using clinical and at-home blood sampling. Nat Commun. 2021;12:113. https://doi.org/10.1038/s41467-020-20383-x
13. Hicks J, Klumpp-Thomas C, Kalish H, Shunmugavel A, Mehalko J, Denson J-P, et al. Serologic cross-reactivity of SARS-CoV-2 with endemic and seasonal betacoronaviruses. J Clin Immunol. 2021;41:906–13. https://doi.org/10.1007/s10875-021-00997-6
14. Tan CW, Chia WN, Qin X, Liu P, Chen MI-C, Tiu C, et al. A SARS-CoV-2 surrogate virus neutralization test based on antibody-mediated blockage of ACE2-spike protein-protein interaction. Nat Biotechnol. 2020;38:1073–8. https://doi.org/10.1038/s41587-020-0631-z
15. Bachmann MF, Mohsen MO, Zha L, Vogel M, Speiser DE. SARS-CoV-2 structural features may explain limited neutralizing-antibody responses. NPJ Vaccines. 2021;6:2. https://doi.org/10.1038/s41541-020-00264-6

Address for correspondence: Fabiano Oliveira, National Institute of Allergy and Infectious Diseases, 12735 Twinbrook Pkwy, Rockville, MD 20852, USA; email: loliveira@niaid.nih.gov

Tonate Virus and Fetal Abnormalities, French Guiana, 2019

Veronique Lambert, Antoine Enfissi, Mathilde Lefebvre, Leo Pomar, Sobhi Kedous, Fabien Guimiot, Gabriel Carles, Anne Lavergne, Dominique Rousset, Najeh Hcini

We report a case of vertical transmission of Tonate virus in a pregnant woman from French Guiana. The fetus showed severe necrotic and hemorrhagic lesions of the brain and spinal cord. Clinicians should be made aware of possible adverse fetal outcomes in pregnant women infected with Tonate virus.

Venezuelan equine encephalomyelitis (VEE) complex viruses consist of antigenically related arboviruses widely distributed throughout the Americas (*1*). Only subtype I varieties AB and C cause severe equine epizootics and human outbreaks marked by the occurrence of encephalitis and fetal damage (*2*). The other subtypes are endemic in small areas of South America (*3*). In 1973, subtype III-B, the Tonate virus (TONV), was isolated in birds from French Guiana (*4*). It has since been found in neighboring countries and in South Dakota and Colorado in the United States (*5*,*6*). The wild cycle of TONV is still poorly understood. Transmission by Culicidae insects has been observed during the rainy season (*4*). Birds and bats are the only identified vertebrate hosts (*7*). In humans in French Guiana, TONV seroprevalence suggests endemic transmission, particularly along the coast of the Bas Maroni region (*8*). However, clinical descriptions remain scarce, and no adverse pregnancy outcomes or vertical transmission have been reported (*9*,*10*). We report a case of vertical transmission of TONV from a pregnant woman to her fetus and describe ultrasonographic and fetopathological findings.

Author affiliations: West French Guiana Hospital Center, Saint-Laurent-du-Maroni, French Guiana (V. Lambert, L. Pomar, S. Kedous, G. Carles, N. Hcini); Institut Pasteur Arbovirus National Reference Center, Cayenne, French Guiana (A. Enfissi, A. Lavergne, D. Rousset); Centre Hospitalo-Universitaire Robert Debre, Paris, France (M. Lefebvre, F. Guimiot); University of French Guiana, Cayenne, French Guiana (N. Hcini)

DOI: https://doi.org/10.3201/eid2802.210884

The Study

During the 2019 rainy season, a 33-year-old woman living in the Bas Maroni region of French Guiana was referred to the prenatal diagnosis unit at West French Guiana Hospital Center (Saint-Laurent-du-Maroni, French Guiana) for fetal anomalies. This healthy G8P7 woman had no history of genetic disorders or birth defects from previous pregnancies. She was asymptomatic during the first trimester of pregnancy and tested negative for syphilis, toxoplasmosis, rubella, cytomegalovirus, chikungunya, and Zika. An ultrasound screening performed at 20 weeks of gestation showed a hydropic fetus with microcephaly. The atrophic cerebral mantle exhibited calcifications and moderate ventriculomegaly. The corpus callosum, the cerebellum, and the brain stem were dysplastic. The fetus manifested limb malformations and an absence of swallowing at the time of the serially performed sonograms (Appendix Figure, https://wwwnc.cdc.gov/EID/article/28/2/21-0884-App1.pdf). Therefore, we performed amniocentesis for etiological investigation. Because of the poor prognosis, the mother elected to terminate the pregnancy. After approval by the multidisciplinary center for prenatal diagnosis, the pregnancy was terminated without complication. The patient gave written informed consent for the publication of her case.

Karyotype and array comparative genomic hybridization were normal. Results of screening for metabolic diseases were negative. All PCR and reverse transcription PCR (RT-PCR) for toxoplasmosis, rubella, cytomegalovirus, herpes simplex virus, and common arboviruses from the Amazon were negative. However, we reproducibly detected the presence of a VEE complex virus in the amniotic fluid with a real-time RT-PCR test yielding cycle threshold values of 30. Furthermore, although maternal serum samples collected 2 months before pregnancy were negative for TONV IgM, the test was positive at the time of pregnancy termination.

To detect serum TONV IgM, the Arbovirus National Reference Center in French Guiana used an in-house IgM capture ELISA test that used whole virus–based antigens obtained from the brains of newborn mice and hyperimmune ascitic fluids. We calculated the ratio of the optical density obtained from the patient's serum to the TONV antigen divided by the optical density of the same serum on a TONV-negative antigen. We set a ratio of >3 to define the presence of TONV IgM. Evolution of the test ratio from 1.1 (negative) to 19 (strongly positive) between the 2 samples with a threshold of positivity defined by a ratio >3 suggested maternal seroconversion during early pregnancy. We obtained additional molecular amplifications from amniotic fluid using primers targeting different regions of the TONV genome (Appendix Table) and sequenced the amplicons, which yielded partial genome sequences of 256 bp corresponding to the 5′NC/nonstructural protein 1 genomic region, 176 bp to the nonstructural protein 1 region, and 374 bp to the E3/E2. We compared phylogenetic analysis results of the sequences against available VEE complex sequences in GenBank, which showed that the virus was very closely related to TONV (accession no. AF075254); the considered genome sequences shared 96.8%–98.9% nt sequence identity and 98.7%–100% aa sequence identity with TONV (Figure 1; Appendix). The rarity of molecular detection of TONV and its divergence from the only strain previously available at our laboratory ruled out contamination as a possible cause of these results.

Fetal autopsy identified a male fetus, small for 22 weeks of gestation, with dysmorphism and fetal akinesia deformation sequence (Figure 2, panel A). Neuropathologic examination discovered a notable meningeal hemorrhage and confirmed mild hydrocephaly (Figure 2, panel B). Histologic examination found neuronal migration disorders (overmigration and nodular heterotopia), microglial reaction, and subarachnoidal hemorrhage (Figure 2, panel D). The spinal cord was depleted of motor neurons (Figure 2, panel C). We detected multiple calcifications in the grey matter of the brain, cerebellum, upper cervical spine, and mesencephalon (Figure 2, panel B). The retina was dysplastic. In addition, the viscera revealed stigmata of ingestion of inflammatory fluid, rich in polynuclear cells. We found calcification in the liver. Because of the unavailability of a commercial probe and a positive control slide, reading the immunostaining TONV antibody test results was difficult. The high level of background suggested that the positivity of the anti-TONV signal in the cortical mantle should be interpreted with caution (Figure 2, panel E).

We report a detailed description of fetal anomalies, mainly neurological, associated with vertical transmission of TONV in the first half of an asymptomatic pregnancy. Despite a wide prevalence in the Guianese population (52.9% in the Bas Maroni region

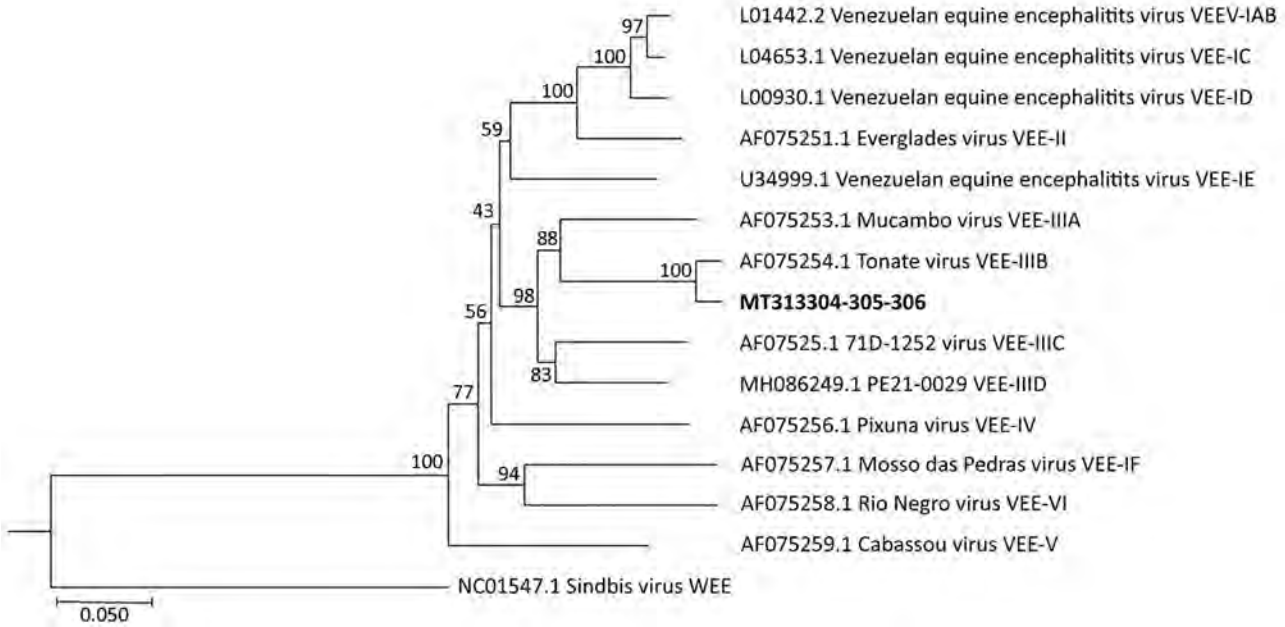

Figure 1. Phylogenetic tree of VEE complex viruses showing close relationship between a virus from the amniotic liquid of a pregnant woman in French Guiana (bold) and a reference Tonate virus sequence. Tree was generated from concatenated sequences (891 bp) using a neighbor-joining algorithm. GenBank accession numbers and VEE complex subtypes are provided for reference sequences. Scale bar represents 5% nucleotide sequence divergence. VEE, Venezuelan equine encephalomyelitis.

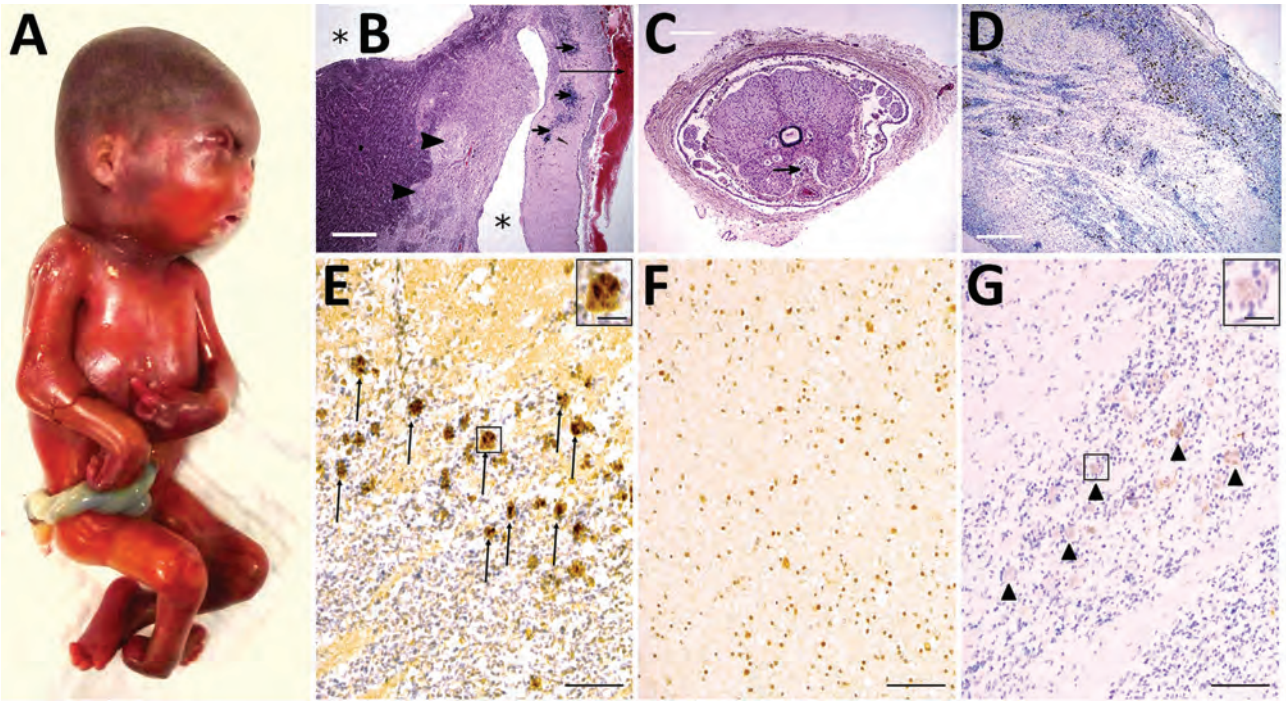

Figure 2. Pathologic findings including results of external examination, histological features of central nervous system, and immunohistochemical staining in a fetus from a woman in French Guiana who was found to be infected with Tonate virus. A) External examination of the body showing subcutaneous edema, microcephaly, craniofacial malformations (short forehead, flat midface), and severe arthrogryposis with upper and lower limb malformations with joint contractures. B) Histologic view of brain section stained in hematoxylin and eosin, displaying lateral ventricle enlargement (asterisk), meningeal hemorrhage (long arrow), diffuse calcifications (short arrows), and nodular heterotopia (arrowheads). Scale bar = 3 mm. C) Spinal cord section showing an abnormally shaped and atrophic spinal cord with the presence of siderophages (sign of premortem meningeal hemorrhage, arrow). Scale bar = 1 mm. D) CD68 immunohistochemistry demonstrating microglial activation and small clusters of microglia and macrophages in the brain (hematoxylin counterstain). Scale bar = 1 mm. E–G) Immunohistochemistry, using anti-TONV mouse serum, of patient (E), control (F), and negative control (G) brains. Note the strong staining of many positive cells in the patient (arrows and inset in panel E), compared to the control brain, where a moderately diffuse background signal is shown but without strong positive cells such as in the patient. In the negative control (without anti-TONV mouse serum antibody), there is a very slight staining (arrowheads and inset in panel G) in the same cells compared with those in the patient, indicating the background signal (color trapping) in these cells. Scale bars = 300 μm; insets in panels E and G = 20 μm.

in 2001), human infections with TONV remain poorly documented, unsurprising given the scarcity of diagnostic tools in French Guiana. TONV often involves signs and symptoms described as dengue fever–like and in rare cases, encephalitis, which attest to the neurotropism of the virus (*9*,*10*). The present diagnosis became possible only through the recent implementation of real-time RT-PCR for VEE detection at the Arbovirus National Reference Center.

The evidence of vertical transmission of TONV we present could be an exception or could be more common, its occurrence having gone undetected mainly because of a lack of testing facilities. Documenting the possibility of vertical transmission of TONV by partially sequencing the viral genome in the amniotic fluid is a substantial finding indicating that the virus should be considered for public health monitoring (*11*,*12*) even though no previous cases of fetal abnormalities related to this virus have been reported. The presence of TONV in the amniotic fluid of a pregnant woman with a fetus with severe anomalies raises questions about a possible causal link that require special attention.

First, the co-occurrence of several histological features (presence of polynuclear cells in the digestive tract, intense glial reactions observed in the nervous system, and cellular calcifications) indicates a potential fetal infection with immunological reaction and cellular deaths. Viral encephalitis is a major cause of microglial activation and microglial nodules. Second, the spectrum of fetal lesions, particularly those observed in the central and peripheral nervous systems, has been observed with other neuroteratogenic viruses (*11*–*14*). Thus, microcephaly, which received broad public attention during the Zika epidemic, appears to be the common outcome of first-trimester infections with a wide range of neuroteratogens (*12*). In our observation, although the hypothesis of a genetic

cause cannot be eliminated, the fact that the patient had a normal karyotype, plus results from an array of comparative genomic hybridization and 3-generation pedigree, suggest low risk that the condition resulted from a genetic disorder. Moreover, a study providing a historical description of 8 fetuses during a 1962 VEE virus outbreak observed a hemorrhagic component in VEE virus–related fetal brain damage (*2*), in line with observations of the fetus in our study, indicating stigmata of hemorrhages, both old and recent, supporting the hypothesis of an infectious origin. On the basis of findings from a series of autopsies, the VEE virus study describes a case of a first-trimester maternal infection in which the fetus manifested the same spectrum of lesions, including microcephaly, arthrogryposis, and ocular anomalies (*2*). However, although immunostaining did not yield any strong evidence for the presence of TONV in the brain, we believe that these anomalies associated with confirmed maternal seroconversion should be reported. As experienced during the 2015–2016 Zika epidemic, any delay in identifying teratogens can have serious consequences (*13*).

In conclusion, our findings illustrate the possibility of vertical transmissibility of TONV and strongly suggest its neuroteratogenic effects, even in asymptomatic women. The virus's potential ability to spread beyond current endemic areas makes it critical that diagnostic tools become widely available to strengthen epidemiological surveillance and to provide more data about the potential danger of TONV for pregnant women.

Acknowledgments

We are grateful to our patient for granting us permission to share her case. We also thank Mathieu Nacher for his writing assistance, Jean-François Carod for the logistic support of his laboratory, and XpertScientific Editing and Consulting Services for language editing and correction.

About the Author

Dr. Lambert specializes in fetal medicine at the West French Guiana Hospital Center, French Guiana, France. Her work focuses on prenatal diagnoses in tropical environments with special interest in infections during pregnancy.

References

1. Forrester NL, Wertheim JO, Dugan VG, Auguste AJ, Lin D, Adams AP, et al. Evolution and spread of Venezuelan equine encephalitis complex alphavirus in the Americas. PLoS Negl Trop Dis. 2017;11:e0005693. https://doi.org/10.1371/journal.pntd.0005693
2. Wenger F. Venezuelan equine encephalitis. Teratology. 1977;16:359–62. https://doi.org/10.1002/tera.1420160317
3. Aguilar PV, Estrada-Franco JG, Navarro-Lopez R, Ferro C, Haddow AD, Weaver SC. Endemic Venezuelan equine encephalitis in the Americas: hidden under the dengue umbrella. Future Virol. 2011;6:721–40. https://doi.org/10.2217/fvl.11.50
4. Degallier N, Digoutte JP, Pajot FX. Epidemiology of 2 Venezuelan equine encephalitis complex arboviruses in French Guyana 1st data on virus vector relations [in French]. Serie Entomologie Medicale et Parasitologie. 1978;16:209–22.
5. Panday RS, Digoutte JP. Tonate and Guama-group viruses isolated from mosquitoes in both a savannah and coastal area in Surinam. Trop Geogr Med. 1979;31:275–82.
6. Monath TP, Lazuick JS, Cropp CB, Rush WA, Calisher CH, Kinney RM, et al. Recovery of Tonate virus ("Bijou Bridge" strain), a member of the Venezuelan equine encephalomyelitis virus complex, from Cliff Swallow nest bugs (*Oeciacus vicarius*) and nestling birds in North America. Am J Trop Med Hyg. 1980;29:969–83. https://doi.org/10.4269/ajtmh.1980.29.969
7. Fischer C, Pontier D, Filippi-Codaccioni O, Pons J-B, Postigo-Hidalgo I, Duhayer J, et al. Venezuelan equine encephalitis complex alphavirus in bats, French Guiana. Emerg Infect Dis. 2021;27:1141–5. https://doi.org/10.3201/eid2704.202676
8. Talarmin A, Trochu J, Gardon J, Laventure S, Hommel D, Lelarge J, et al. Tonate virus infection in French Guiana: clinical aspects and seroepidemiologic study. Am J Trop Med Hyg. 2001;64:274–9. https://doi.org/10.4269/ajtmh.2001.64.274
9. Hommel D, Heraud JM, Hulin A, Talarmin A. Association of Tonate virus (subtype IIIB of the Venezuelan equine encephalitis complex) with encephalitis in a human. Clin Infect Dis. 2000;30:188–90. https://doi.org/10.1086/313611
10. Mutricy R, Djossou F, Matheus S, Lorenzi-Martinez E, De Laval F, Demar M, et al. Discriminating Tonate virus from dengue virus infection: a matched case-control study in French Guiana, 2003–2016. Am J Trop Med Hyg. 2020;102:195–201. https://doi.org/10.4269/ajtmh.19-0156
11. Kim K, Shresta S. Neuroteratogenic viruses and lessons for Zika virus models. Trends Microbiol. 2016;24:622–36. https://doi.org/10.1016/j.tim.2016.06.002
12. Mlakar J, Korva M, Tul N, Popović M, Poljšak-Prijatelj M, Mraz J, et al. Zika virus associated with microcephaly. N Engl J Med. 2016;374:951–8. https://doi.org/10.1056/NEJMoa1600651
13. de Araújo TVB, Rodrigues LC, de Alencar Ximenes RA, de Barros Miranda-Filho D, Montarroyos UR, de Melo APL, et al.; investigators from the Microcephaly Epidemic Research Group; Brazilian Ministry of Health; Pan American Health Organization; Instituto de Medicina Integral Professor Fernando Figueira; State Health Department of Pernambuco. Association between Zika virus infection and microcephaly in Brazil, January to May, 2016: preliminary report of a case-control study. Lancet Infect Dis. 2016;16:1356–63. https://doi.org/10.1016/S1473-3099(16) 30318-8
14. Chimelli L, Melo ASO, Avvad-Portari E, Wiley CA, Camacho AHS, Lopes VS, et al. The spectrum of neuropathological changes associated with congenital Zika virus infection. Acta Neuropathol. 2017;133:983–99. https://doi.org/10.1007/s00401-017-1699-5

Address for correspondence: Veronique Lambert, West French Guiana Hospital Center, 1465, Boulevard de la Liberte-B.P 245, 97393 Saint-Laurent du Maroni, French Guiana email: v.lambert@ch-ouestguyane.fr

Babesia crassa–Like Human Infection Indicating Need for Adapted PCR Diagnosis of Babesiosis, France

Cécile Doderer-Lang, Denis Filisetti, Julie Badin, Charles Delale, Victoria Clavier, Julie Brunet, Chloé Gommenginger, Ahmed Abou-Bacar, Alexander W. Pfaff

Human babesiosis in Europe is caused by multiple zoonotic species. We describe a case in a splenectomized patient, in which a routine *Babesia divergens* PCR result was negative. A universal *Babesia* spp. PCR yielded a positive result and enabled classification of the parasite into the less-described *Babesia crassa*–like complex.

Babesiosis is a widely distributed, tickborne, zoonotic, parasitic disease caused by different species of the apicomplexan genus *Babesia* and occasionally involving human infections (*1*). In its vertebrate host, the parasite undergoes repeated erythrocytic cycles. Clinical manifestations in humans vary widely, ranging from asymptomatic infections to rapidly evolving and sometimes fatal infections. In Europe, symptomatic human cases are infrequently observed and occur mostly in asplenic patients, where infections can rapidly become life-threatening. The most known species in Europe are *Babesia divergens* and *B. venatorum*, which are naturally found in cattle and deer (*2*). In contrast, infections in the United States are predominantly attributed to the rodent parasite species *B. microti* in the Northeast and Midwest and to *B. duncani* on the Pacific Coast and are more frequently described in human cases (*3*). These cases are normally mild to moderate in immunocompetent persons but can be fatal in asplenic patients.

Author affiliations: Université de Strasbourg UR 7292, France (C. Doderer-Lang, D. Filisetti, J. Brunet, A. Abou-Bacar, A.W. Pfaff); Hôpitaux Universitaires de Strasbourg, Strasbourg (D. Filisetti, J. Brunet, C. Gommenginger, A. Abou-Bacar, A.W. Pfaff); Centre Hospitalier de Blois, Blois, France (J. Badin, C. Delale, V. Clavier)

DOI: https://doi.org/10.3201/eid2802.211596

Reports of *B. microti* in ticks (*4*) and humans in Germany and Poland (*5*,*6*) and *B. divergens* in the United States (*7*) cast doubt on the reliability of these clear-cut geographic patterns. In addition, numerous zoonotic species exist and are occasionally described in human cases (*8*). Given the life-threatening potential of *Babesia* infections, rapid and reliable diagnostic methods are needed. Results of serologic testing are often negative during the acute phase. Moreover, sensitivity and specificity are, especially for nonclassical species, not yet well described. Direct parasite detection is therefore preferable. PCR tests are performed in some specialized laboratories. However, they are usually designed to detect the major species, notably *B. divergens* and *B. microti*. We present a case study that demonstrates the need to develop a consensus for a general molecular means of detecting *Babesia*.

The Case Report

This case report was approved by the Ethics Committee of Medical Faculty and University Hospital of Strasbourg, France. A 61-year-old man from western France visited the emergency department of a general hospital for elevated fever, dyspnea, and jaundice. The patient had undergone gastric cancer–related gastrectomy and splenectomy 30 years before. He lived in an isolated woodland environment and raised goats. At initial examination, the only clinical abnormality was oliguria with dark urine. A blood test revealed acute renal failure (creatinine 5.6 mg/dL [reference range 0.7–1.3 mg/dL]), anemia (Hb 112 g/L [reference range 130–170 g/L]), and thrombocytopenia (18,000 platelets/μL [reference range 150,000–450,000 platelets/μL]) with hyperbilirubinemia (bilirubin 10.9 mg/dL [reference range <1.2 mg/dL]).

That night, the patient experienced septic shock and was transferred to an intensive-care unit (ICU). Upon arrival, the patient received fluid challenge associated with vasopressor treatment and broad-spectrum antibiotics (ceftriaxone, metronidazole, and amikacin) for a suspected urinary or biliary infection. A new cellular and biochemical blood examination gave no result because of hemolysis. Twelve hours after ICU admission, the blood sample was again hemolyzed. Microscopic analysis of a blood smear showed intracellular and extracellular parasites suggestive of *Babesia*, demonstrating parasitemia of 14%. A combination treatment with quinine (8 mg/kg/8 h) and dalacine (600 mg/8 h) was started. Antibiotic therapy by ceftriaxone was continued for confirmed urinary sepsis with *Escherichia coli* bacteremia.

On day 2 after admission, the patient was anuric, and renal replacement therapy was started. On day 4, the patient was put on mechanical ventilation because of septic cardiac failure–induced respiratory failure. That day, a tick was found on the patient. The species remained unknown because the tick was not sent to a laboratory. Lyme serologic testing was requested and returned positive results, so ceftriaxone was administered for 3 weeks and quinine/dalacine for 10 days, yielding a negative parasitemia at the end of treatment. The patient slowly recovered; mechanical ventilation and catecholamines were stopped on day 7, dialysis on day 25. He left the ICU on day 34 and left the hospital on day 70 after regaining normal renal function; he returned home after readaptation on day 117.

Microscopic examination (Figure 1; Appendix Figure, https://wwwnc.cdc.gov/EID/article/28/2/21-1596-App1.pdf) showed characteristics typically described for *Babesia* trophozoites, including extracellular parasites, abundant binary fission, and absence of schizonts. The observed forms were highly pleomorphic. We observed piriform parasites, resembling *B. divergens*, as well as more round forms, as shown in the original description of *B. crassa* (*9*), but the round forms were not as abundant as usually described. We also observed voluminous forms resembling band-form trophozoites of *Plasmodium malariae.* Although 4 parasites in 1 erythrocyte were frequently observed, the tetrad (Maltese Cross) form, typical for *B. divergens*, was never seen.

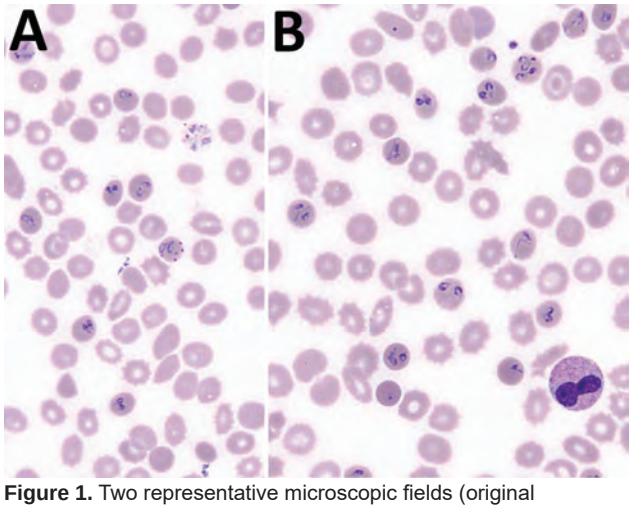

Figure 1. Two representative microscopic fields (original magnification ×1,000) of a May–Grünwald–Giemsa stained blood smear, showing different forms of *Babesia* trophozoites, from a 61-year-old man from western France.

We performed our routine PCR tests for *B. divergens* and *B microti*, using LightCycler FastStart DNA Master HybProbe (Roche, https://www.roche.fr) (Appendix). Unexpectedly, both PCRs came back negative. We then applied a universal *Babesia* spp. PCR, targeting a consensus sequence of the internal transcribed spacer 1 gene of the 18S RNA, as previously reported (*10*) (Appendix). Visual inspection of the agarose gel showed a PCR fragment of ≈480 bp. The PCR product was purified and sequenced on both strands by Eurofins Genomics (https://www.eurofins.com). We identified the consensus sequence (GenBank accession no. MW504968) as *Babesia* spp. by using BLAST (http://blast.ncbi.nlm.nih.gov/Blast.cgi). We conducted phylogenetic and molecular evolutionary analyses by using MEGA X 10.1.8 (https://www.megasoftware.net) (*11*). We constructed a phylogenetic tree with corresponding sequences of the *Babesia* genus obtained from GenBank by using the neighbor-joining method with Kimura 2-parameter distances and using *Theileria* spp. as the outgroup (Figure 2). Our sequence aligned with the *B. crassa* complex and specifically with a *B. crassa*–like sequence from Slovenia (GenBank accession no. MK240324) with 99.11% identity.

Conclusions

Recent serologic and clinical studies suggest that human babesiosis infections are more frequent than expected, especially in Europe, but symptoms are often not recognized as babesiosis (*12*). Microscopic identification of *Babesia* is easily possible in a case-patient with high parasitemia, as in the case we describe. However, in the early phase of infection or in immunocompetent patients, parasitemia often is too low to be detected by routine examination, especially outside specialized laboratories. Therefore, PCR is crucial for reliable diagnosis. The negative result we obtained using our routine PCRs, despite substantial parasitemia, demonstrates once more that unexpected species can be found in human samples and underscores the need to use universal *Babesia* prim-

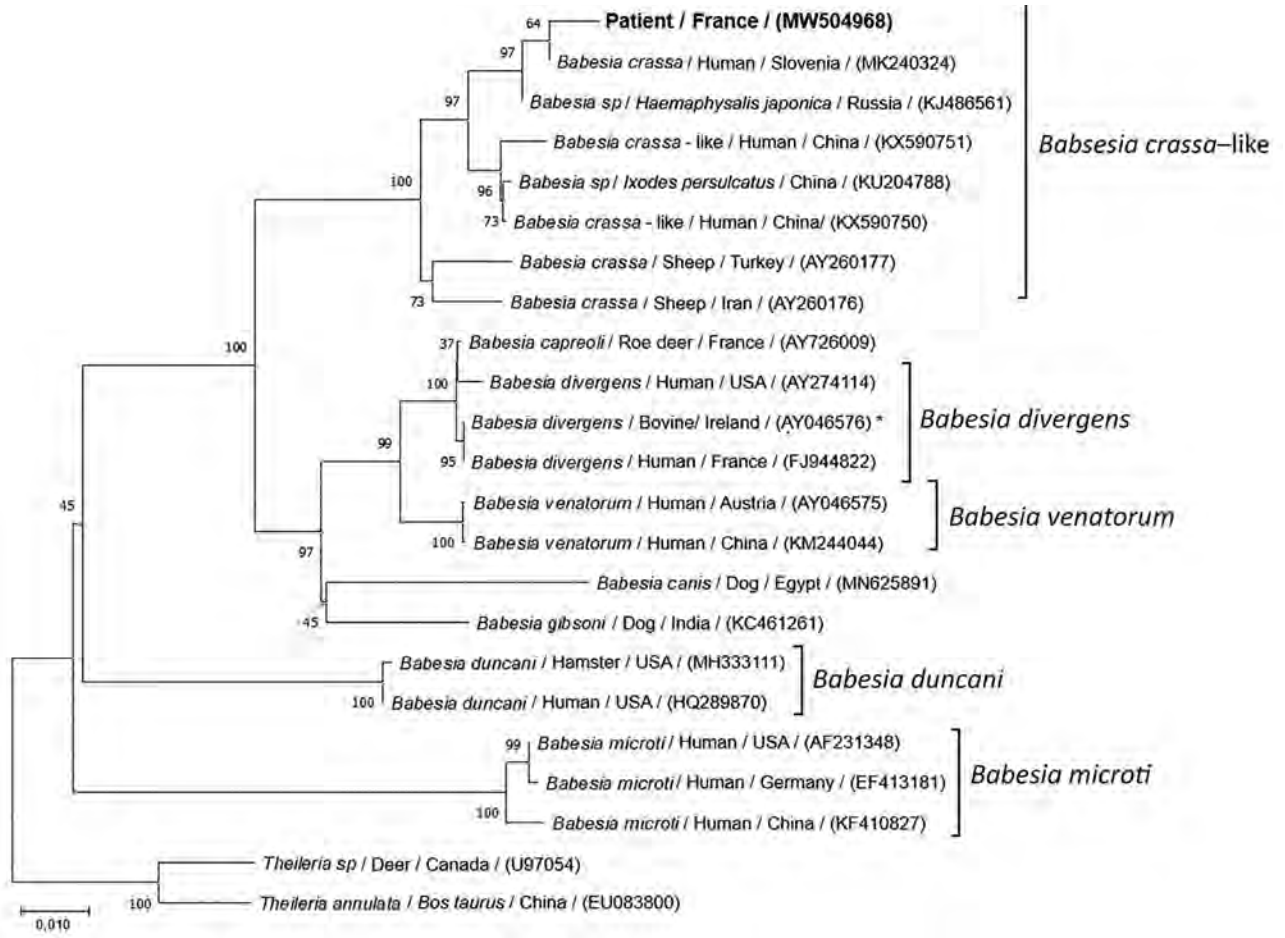

Figure 2. Evolutionary analysis of 18S RNA sequences of *Babesia* from a 61-year-old man from western France and reference sequences. Neighbor-joining tree of 1,000 bootstrap pseudoreplicates with Kimura 2-parameter distances of internal transcribed spacer 1 gene from 18S RNA sequences of the Babesia genus (MEGA X 10.1.8, https://www.megasoftware.net). Bootstrap proportions >50% are indicated. This phylogenetic tree illustrates the relationship between the species infecting this patient (GenBank accession no. MW504968) and the 20 different species of *Babesia* obtained from GenBank. Species, host, origin, and accession number are indicated. *Theileria* spp. was used as outgroup. Scale bar represents 1% of divergence. Asterisk indicates in vitro culture.

ers and sequencing of amplicons in positive samples, such as the PCR we used to successfully detect the parasites (*10*). Sequencing identified the isolate as being close to *B. crassa*, which was originally described in sheep in Iran (*9*) and was later phylogenetically characterized (*13*). Human infections with *B. crassa*–like parasites, all with mild to moderate clinical symptoms, have been described in China, along with numerous isolations from ticks and sheep (*14*), and from an asplenic patient in Slovenia (*15*), demonstrating the wide geographic distribution of these parasites. Our case proves its presence in France, again in a splenectomized patient, which is probably just the visible part of a wider unnoticed presence in Europe. Detailed microscopic and genetic analysis of more isolates would be useful to better characterize this poorly described complex. Cases of *B. crassa*–like infection can be expected in wildlife throughout the palearctic region and sporadically in humans, especially immunocompromised persons.

In summary, we demonstrate that *Babesia* infections in Europe and elsewhere might implicate species not yet been described in humans, which could lead to false-negative PCR results and delayed treatment of patients at high risk. All facilities performing *Babesia* diagnostic tests should be aware of this possibility and make sure that PCRs are adapted accordingly.

About the Author

Ms. Doderer-Lang is a scientist at the Institute of Parasitology and Tropical Pathology in Strasbourg, France. She works on the epidemiology and design of novel diagnostic tools for malaria, toxoplasmosis, and emerging parasitoses, such as babesiosis and intestinal parasitoses.

References

1. Vannier E, Krause PJ. Human babesiosis. N Engl J Med. 2012;366:2397–407. https://doi.org/10.1056/NEJMra1202018
2. Krause PJ. Human babesiosis. Int J Parasitol. 2019;49:165–74. https://doi.org/10.1016/j.ijpara.2018.11.007
3. Gray EB, Herwaldt BL. Babesiosis surveillance—United States, 2011–2015. MMWR Surveill Summ. 2019;68:1–11. https://doi.org/10.15585/mmwr.ss6806a1
4. Eshoo MW, Crowder CD, Carolan HE, Rounds MA, Ecker DJ, Haag H, et al. Broad-range survey of tick-borne pathogens in southern Germany reveals a high prevalence of *Babesia microti* and a diversity of other tick-borne pathogens. Vector Borne Zoonotic Dis. 2014;14:584–91. https://doi.org/10.1089/vbz.2013.1498
5. Hildebrandt A, Hunfeld K-P, Baier M, Krumbholz A, Sachse S, Lorenzen T, et al. First confirmed autochthonous case of human *Babesia microti* infection in Europe. Eur J Clin Microbiol Infect Dis. 2007;26:595–601. https://doi.org/10.1007/s10096-007-0333-1
6. Moniuszko-Malinowska A, Swiecicka I, Dunaj J, Zajkowska J, Czupryna P, Zambrowski G, et al. Infection with *Babesia microti* in humans with non-specific symptoms in north east Poland. Infect Dis (Lond). 2016;48:537–43. https://doi.org/10.3109/23744235.2016.1164339
7. Beattie JF, Michelson ML, Holman PJ. Acute babesiosis caused by *Babesia divergens* in a resident of Kentucky. N Engl J Med. 2002;347:697–8. https://doi.org/10.1056/NEJM200208293470921
8. Schnittger L, Rodriguez AE, Florin-Christensen M, Morrison DA. *Babesia*: a world emerging. Infect Genet Evol. 2012;12:1788–809. https://doi.org/10.1016/j.meegid.2012.07.004
9. Hashemi-Fesharki R, Uilenberg G. Babesia crassa n. sp. (Sporozoa, Babesiidae) of domestic sheep in Iran. Vet Q. 1981;3:1–8. https://doi.org/10.1080/01652176.1981.9693787
10. Casati S, Sager H, Gern L, Piffaretti J-C. Presence of potentially pathogenic *Babesia* sp. for human in *Ixodes ricinus* in Switzerland. Ann Agric Environ Med. 2006;13:65–70.
11. Kumar S, Stecher G, Li M, Knyaz C, Tamura K. MEGA X: Molecular Evolutionary Genetics Analysis across computing platforms. Mol Biol Evol. 2018;35:1547–9. https://doi.org/10.1093/molbev/msy096
12. Paleau A, Candolfi E, Souply L, De Briel D, Delarbre JM, Lipsker D, et al. Human babesiosis in Alsace. Med Mal Infect. 2020;50:486–91. https://doi.org/10.1016/j.medmal.2019.08.007
13. Schnittger L, Yin H, Gubbels MJ, Beyer D, Niemann S, Jongejan F, et al. Phylogeny of sheep and goat *Theileria* and *Babesia* parasites. Parasitol Res. 2003;91:398–406. https://doi.org/10.1007/s00436-003-0979-2
14. Jia N, Zheng Y-C, Jiang J-F, Jiang R-R, Jiang B-G, Wei R, et al. Human babesiosis caused by a *Babesia crassa*–like pathogen: a case series. Clin Infect Dis. 2018;67:1110–9. https://doi.org/10.1093/cid/ciy212
15. Strasek-Smrdel K, Korva M, Pal E, Rajter M, Skvarc M, Avsic-Zupanc T. Case of *Babesia crassa*–like infection, Slovenia, 2014. Emerg Infect Dis. 2020;26:1038–40. https://doi.org/10.3201/eid2605.191201

Address for correspondence: Alexander Pfaff, Institut de Parasitologie et de Pathologie Tropicale, Université de Strasbourg, 3 rue Koeberlé, 67000 Strasbourg, France; email: pfaff@unistra.fr

Clinical Features and Neurodevelopmental Outcomes for Infants with Perinatal Vertical Transmission of Zika Virus, Colombia

Luis A. Pérez-Vera, Valentina Herrera-García, María C. Pérez-Matos, Luis A. Díaz-Martínez, Luis A. Villar-Centeno, Luz S. Pinilla-García, Mario A. Rojas

Transplacental transmission of Zika virus has been reported during all trimesters of pregnancy and might lead to central nervous system anomalies, including microcephaly. We report 3 cases of perinatal Zika infection identified during the epidemic in Colombia and provide detailed descriptions of clinical features, diagnosis, and neurodevelopmental outcome at 18 months of age (corrected).

The emergence of Zika virus (ZIKV) in the Americas has coincided with an abnormal increase in prenatal and neonatal documented cases of microcephaly and other anomalies of the central nervous system (*1*) These alterations of the brain, along with animal models of vertical transmission of ZIKV, a single-stranded RNA flavivirus, are evidence of the neurotropic nature of the virus (*2*–*4*).

Vertical transmission and infection of the fetus during all 3 trimesters of pregnancy with ZIKV has been extensively reported, but little is known about perinatal transmission; only a few cases have been reported (*5*–*8*). We report 3 cases of perinatal ZIKV infection during the epidemic of Zika in Colombia and data on the neurodevelopmental outcome at 18 months of age (corrected).

The Study

The Institutional Review Board and Ethics Committee of the Universidad Industrial de Santander approved this study. Formal written consent was obtained from participating women.

Case-patient 1 was a 26-year-old pregnant woman in labor who was admitted to the Hospital Universitario de Santander on August 7, 2015, after she reported fever, exanthema (maculopapular rash on the torso), and osteoid–muscular pains (Figure). Her initial hemogram showed mild thrombocytopenia (112,000 platelets/μL; reference range 150,000–400,000 platelets/μL). Test results for syphilis, toxoplasmosis, rubella, cytomegalovirus, herpes simplex virus, varicella zoster virus, and parvovirus B19 during hospitalization were negative, as was a test result for dengue virus (DENV) IgM.

A boy was born vaginally at 37 weeks of gestation. Apgar scores were normal. Anthropometric measurements yielded a birthweight of 3.03 kg (32nd percentile), a head circumference (HC) of 32 cm (6th percentile), and a length of 54 cm (99th percentile). Results of a physical examination were unremarkable. The infant was admitted for observation, and cord blood samples were sent to the Instituto Nacional de Salud (INS) for additional testing by reverse transcription PCR (RT-PCR) for DENV and chikungunya virus. On the second day of life, the infant had a distal macular-papular rash with hyperalgesia and mild edema of the hands and feet; a test result for DENV IgM was negative. Hyperthermia developed on the sixth day, and generalized exanthema developed on the seventh day.

Because of persistent fever, we initiated a sepsis work-up. Results for initial complete blood count/differential count, erythrocyte sedimentation rate, blood culture, urine culture, and C-reactive protein were within reference ranges. Fever and exanthema

Author affiliations: Hospital Universitario de Santander, Bucaramanga, Colombia (L.A. Pérez-Vera); Universidad Industrial de Santander, Bucaramanga (L.A. Pérez-Vera, V. Herrera-García, L.A. Díaz-Martínez, L.A. Villar-Centeno, L.S. Pinilla-García, M.A. Rojas); Harvard School of Public Health, Boston, Massachusetts, USA (M.C. Pérez-Matos)

DOI: https://doi.org/10.3201/eid2802.204551

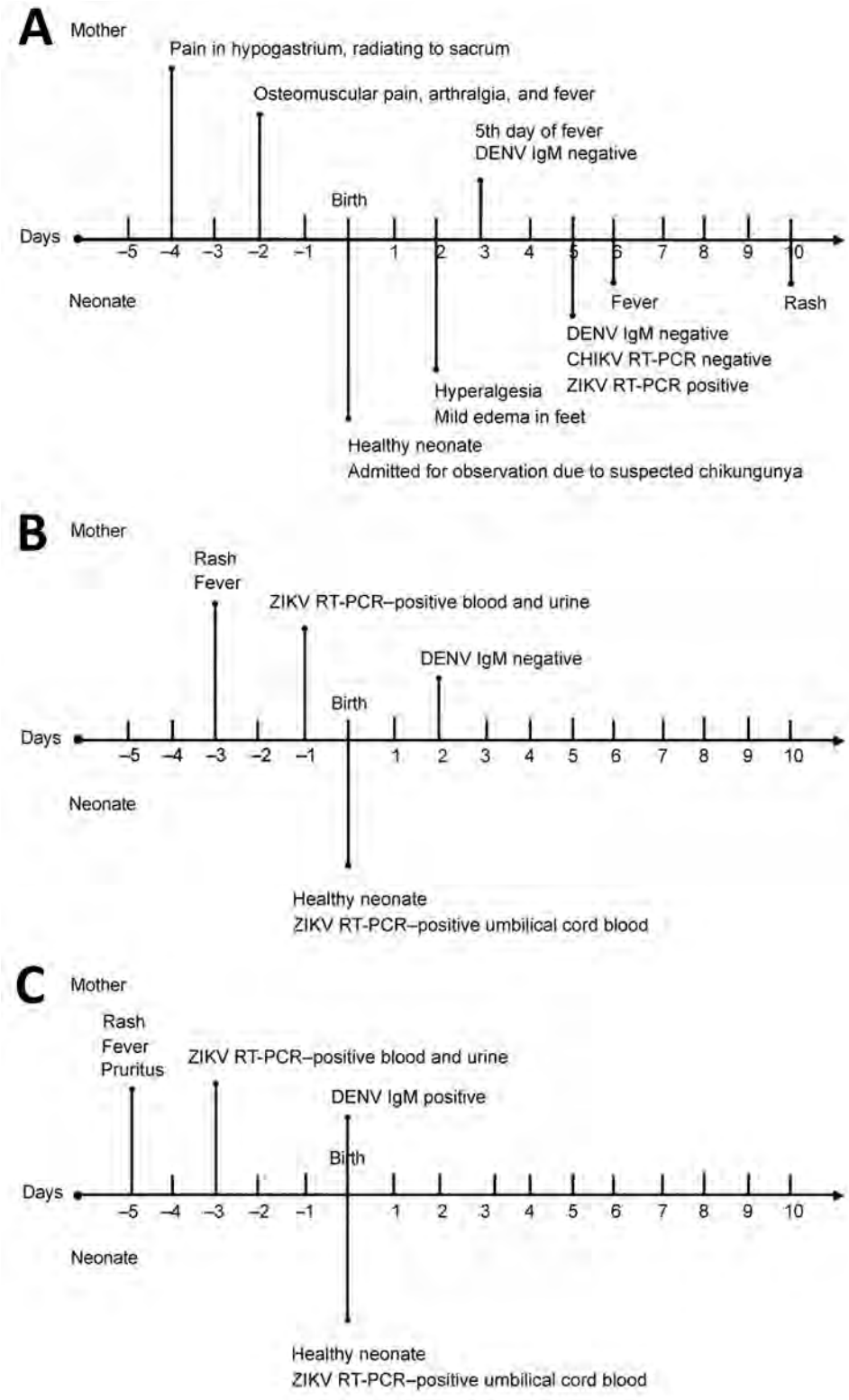

Figure. Timelines for 3 case-patients who had perinatal Zika virus infection during a Zika epidemic, Colombia, 2015. A) Case-patient 1; B) case-patient 2; C) case-patient 3. DENV, dengue virus; CHIKV, chikungunya virus; RT-PCR, reverse transcription PCR; ZIKV, Zika virus.

were present for 4 additional days; a follow-up C-reactive protein level was abnormal (21 mg/dL). Findings for analyses of cerebrospinal fluid and culture were unremarkable. After symptoms improved, the infant was discharged; an RT-PCR result from the INS was negative for chikungunya virus.

Because of the Zika epidemic in Brazil, the INS initiated RT-PCR testing for ZIKV and randomly

retested samples from epidemiologic surveillance of DENV and chikungunya virus (*9*). On January 20, 2016, the INS reported that the RT-PCR result for ZIKV for the infant was positive. Neuroimaging was not indicated. On April 3, 2017, a follow-up was conducted when the child was 19.3 months of age (corrected). Anthropometric measurements showed a weight of 10.6 kg (21st percentile), a height of 85 cm (85th percentile), and an HC of 46 cm (35th percentile). Results of audiology and ophthalmologic evaluations were unremarkable. At 21.4 months of age (corrected), we conducted a neurodevelopmental evaluation by using the Bayley Scale for Infant and Toddler Development (*10*); both gross and fine motor scored at the 50th percentile, cognition at the 75th percentile, and expressive and receptive language at the 18th percentile (Table).

Case-patient 2 was a 30-year-old pregnant woman who was admitted to the Hospital Universitario de Santander at 38 weeks of gestation with a history of unspecified discomfort, musculoskeletal pain, and fever (temperature 38°C) 2 days before admission. She had a history of thrombocytopenia during gestation. Her admission platelet count was 80,000/μL. Results for *Toxoplasma gondii* IgG and IgM, HIV, hepatitis B surface antigen, and venereal disease research laboratory testing were negative. Test results of blood and urine samples by RT-PCR for ZIKV were positive. On the fifth day of maternal symptoms, a test result for DENV IgM was positive, suggesting co-infection with both types of arbovirus. Misoprostol was then administered.

The following day, a boy was delivered vaginally. He had good Apgar scores and was sent to the nursery for observation. He had a birthweight of 3.08 kg and an HC of 35 cm, and his physical examination was uneventful. An umbilical cord blood sample was positive by for RT-PCR for ZIKV. The neonate remained asymptomatic, and both hearing and ophthalmologic evaluations were normal. Neurodevelopmental evaluation with the Bayley Scale for Infant and Toddler Development (*10*) at 7.2, 13.0, and 36.5 months of age for CA was considered within the normal range for age (Table). Neuroimaging was not indicated.

Case-patient 3 was a 25-year-old pregnant woman who was admitted to the Hospital Universitario de Santander hospital on April 5, 2016, at 34 weeks of gestation, with a history of eye irritation, rash, and fever. Test results for syphilis, toxoplasmosis, varicella zoster virus, parvovirus B19, rubella, cytomegalovirus, and herpes simplex virus were negative, but blood and urine RT-PCR results for ZIKV positive. Betamethasone was administered for lung maturation.

On the third day of admission, a boy was delivered vaginally. He had normal Apgar scores and a birthweight of 2.24 kg, an HC of 31 cm, and a length of 42 cm. An umbilical cord blood sample tested by RT-PCR for ZIKV was positive. The infant showed signs of respiratory distress syndrome at birth, requiring supplemental oxygen, ventilatory support with continuous positive airway pressure, and surfactant administration. Symptoms improved after 24 hours and he was subsequently discharged.

We conducted neurodevelopmental follow-up at 6, 12, 24, and 36 months of age by using the Bayley Scale for Infant and Toddler Development (*10*). All evaluations were considered within the normal range for age (corrected). Ophthalmologic and hearing assessments were normal; neuroimaging was not indicated.

Conclusions

The symptoms and diagnostic tests for the 3 pregnant women strongly support maternal infection 5 days before delivery. Vertical transmission is shown by suggestive early neonatal symptoms and a positive

Table. Neurodevelopmental evaluation with the Bayley Scale for Infant and Toddler Development at each visit for 3 case-patients who had perinatal Zika virus infection, Colombia*

Case-patient	Infant age, mo	Cephalic perimeter Z score	Scale domain								
			Motor			Language			Cognitive		
			Score†	Z score	Percentile	Score†	Z score	Percentile	Score†	Z score	Percentile
1	20.1	−0.50	94	−0.40	34	94	−0.40	34	90	−0.67	25
	24.9	−1.70	107	0.47	68	83	−1.13	13	100	0.00	50
	40.3	−0.51	88	−0.80	21	89	−0.73	23	95	−0.33	37
2	7.2	0.86	100	0.00	50	NT	NT	NT	NT	NT	NT
	13.0	0.64	97	−0.20	42	97	−0.20	42	85	−1.00	16
	36.5	0.21	110	0.67	75	91	−0.60	27	90	−0.67	25
3	8.4	0.72	115	1.00	84	NT	NT	NT	NT	NT	NT
	14.5	0.89	112	0.80	79	94	−0.40	34	110	0.67	75
	21.6	0.52	100	0.00	50	89	−0.73	23	110	0,67	75

*NT, not tested.
†Standardized.

RT-PCR result for ZIKV for case-patient 1 and RT-PCR Zika virus–positive cord blood for the other 2 case-patients (Figure). Case-patient 2 had a positive RT-PCR result for ZIKV in blood and urine and a positive result for DENV IgM, suggesting co-infection.

Although cross-reactivity in an RT-PCR for ZIKV and other arbovirus infections is possible (*11*), co-infection with 2 different types of arbovirus is also possible because of the endemic nature of dengue in Colombia where the patients were identified (*12*). Vertical transmission of DENV is considered a rare event, and there have been no reports of congenital dengue infection in neonates born to mothers infected early during pregnancy (*13*). Case-patient 3 had a positive result by RT-PCR for ZIKV in blood and urine, and her infant was positive for ZIKV in cord blood, which enabled us to confirm vertical transmission. However, because testing for DENV or chikungunya virus was not available, we cannot speculate on this issue.

Adverse fetal central nervous system anomalies with maternal ZIKV infection have been reported during the third trimester of pregnancy (*14*,*15*). Neurodevelopmental follow-up results were uneventful for the 3 case-patients we describe who had perinatal vertical transmission. Two previous cases of perinatal transmission reported showed no evidence of neurodevelopmental impairment, thus supporting our findings (*8*). In summary, our findings indicate that perinatal infection within the time frame described for these case-patients does not appear to affect neurodevelopmental outcomes of the newborns.

This study was supported by the Colombian Ministry of Science and Innovation (COLCIENCAS code 110277757376), the Hospital Universitario de Santander, the Universidad Industrial de Santander (grant 758-2017), and the Colombian Association of Neonatology.

About the Author

Dr. Pérez-Vera is a pediatrician/neonatologist at the Hospital Universitario de Santander, Bucaramanga, Colombia and professor of pediatrics at the Universidad Industrial de Santander. His primary research interests are neonatal respiratory and infectious diseases.

References

1. Mlakar J, Korva M, Tul N, Popović M, Poljšak-Prijatelj M, Mraz J, et al. Zika virus associated with microcephaly. N Engl J Med. 2016;374:951–8. https://doi.org/10.1056/NEJMoa1600651
2. Tang H, Hammack C, Ogden SC, Wen Z, Qian X, Li Y, et al. Zika virus infects human cortical neural progenitors and attenuates their growth. Cell Stem Cell. 2016;18:587–90. https://doi.org/10.1016/j.stem.2016.02.016
3. Cugola FR, Fernandes IR, Russo FB, Freitas BC, Dias JL, Guimarães KP, et al. The Brazilian Zika virus strain causes birth defects in experimental models. Nature. 2016;534:267–71. https://doi.org/10.1038/nature18296
4. Driggers RW, Ho CY, Korhonen EM, Kuivanen S, Jääskeläinen AJ, Smura T, et al. Zika virus infection with prolonged maternal viremia and fetal brain abnormalities. N Engl J Med. 2016;374:2142–51. https://doi.org/10.1056/NEJMoa1601824
5. Jurado KA, Simoni MK, Tang Z, Uraki R, Hwang J, Householder S, et al. Zika virus productively infects primary human placenta-specific macrophages. JCI Insight. 2016;1:e88461. https://doi.org/10.1172/jci.insight.88461
6. Runge-Ranzinger S, Morrison AC, Manrique-Saide P, Horstick O. Zika transmission patterns: a meta-review. Trop Med Int Health. 2019;24:523–9. https://doi.org/10.1111/tmi.13216
7. Besnard M, Lastère S, Teissier A, Cao-Lormeau V, Musso D. Evidence of perinatal transmission of Zika virus, French Polynesia, December 2013 and February 2014. Euro Surveill. 2014;19:8–11. https://doi.org/10.2807/1560-7917.ES2014.19.13.20751
8. Besnard M, Dub T, Gérardin P. Outcomes for 2 children after peripartum acquisition of zika virus infection, French Polynesia, 2013–2014. Emerg Infect Dis. 2017;23:1421–3. https://doi.org/10.3201/eid2308.170198
9. Tolosa N. Surveillance protocols in public health: Zika virus diseases [in Spanish]. 2nd ed. Bogotá (Colombia): Instituto Nacional de Salud; 2016.
10. Bayley N. Bayley scales of infant and toddler development. 3rd ed. San Antonio (TX): Harcourt Assessment Inc.; 2006.
11. Zaidi MB, Cedillo-Barron L, González Y Almeida ME, Garcia-Cordero J, Campos FD, Namorado-Tonix K, et al. Serological tests reveal significant cross-reactive human antibody responses to Zika and dengue viruses in the Mexican population. Acta Trop. 2020;201:105201. https://doi.org/10.1016/j.actatropica.2019.105201
12. Estofolete CF, Terzian AC, Colombo TE, de Freitas Guimarães G, Ferraz HC Junior, da Silva RA, et al. Co-infection between Zika and different dengue serotypes during DENV outbreak in Brazil. J Infect Public Health. 2019;12:178–81. https://doi.org/10.1016/j.jiph.2018.09.007
13. Yin X, Zhong X, Pan S. Vertical transmission of dengue infection: the first putative case reported in China. Rev Inst Med Trop São Paulo. 2016;58:90. https://doi.org/10.1590/s1678-9946201658090
14. Brasil P, Pereira JP Jr, Moreira ME, Ribeiro Nogueira RM, Damasceno L, Wakimoto M, et al. Zika virus infection in pregnant women in Rio de Janeiro. N Engl J Med. 2016;375:2321–34. https://doi.org/10.1056/NEJMoa1602412
15. Ades AE, Soriano-Arandes A, Alarcon A, Bonfante F, Thorne C, Peckham CS, et al. Vertical transmission of Zika virus and its outcomes: a Bayesian synthesis of prospective studies. Lancet Infect Dis. 2021;21:537–45. https://doi.org/10.1016/S1473-3099(20)30432-1

Address for correspondence: Luis A. Pérez Vera, Health Faculty, Universidad Industrial de Santander, Carrera 32 # 29-31, Administrative Bldg, Rm 421, Bucaramanga, Colombia; email: iniciativa.zen@uis.edu.co

SARS-CoV-2 Circulation, Guinea, March 2020–July 2021

Solène Grayo,[1] Cécile Troupin,[1,2] Moussa Moïse Diagne, Houlou Sagno, Isabelle Ellis, Bakary Doukouré, Amadou Diallo, Jean-Mathieu Bart, Mohamed Lamine Kaba, Benoit Henry, Billy Sivahera Muyisa, Mamadou Saliou Sow, Ndongo Dia, Ousmane Faye, Sakoba Keita, Noël Tordo

Author affiliations: Institut Pasteur de Guinée, Conakry, Guinea (S. Grayo, C. Troupin, H. Sagno, I. Ellis, B. Doukouré, N. Tordo); Institut Pasteur de Dakar, Dakar, Senegal (M.M. Diagne, A. Diallo, N. Dia, O. Faye); Institut de Recherche pour le Développement-Programme National de Lutte contre la Trypanosomiase Humaine Africaine, Montpellier, France (J.-M. Bart); Camp Militaire Alpha Yaya, Conakry (M.L. Kaba); Centre Médico-Social de l'Ambassade de France, Conakry (B. Henry); Centre Hospitalier de Donka (M.S. Sow); Alliance for International Medical Action, Guinea (B.S. Muyisa), Agence Nationale de Sécurité Sanitaire, Conakry (S. Keita)

DOI: https://doi.org/10.3201/eid2802.212182

This overview of severe acute respiratory syndrome coronavirus 2 circulation over 1.5 years in Guinea demonstrates that virus clades and variants of interest and concern were progressively introduced, mostly by travellers through Conakry, before spreading through the country. Sequencing is key to following virus evolution and establishing efficient control strategies.

In Guinea, the index coronavirus disease (COVID-19) case-patient identified on March 12, 2020, was an expatriate traveling back from Europe. Immediately, a COVID-19 task force was established by the Agence Nationale de Sécurité Sanitaire; 6 national laboratories were involved in the diagnosis of severe acute respiratory syndrome coronavirus 2 (SARS-CoV-2) infections. As of July 16, 2021, a total of 24,668 confirmed cases (23,571 recovered persons and 188 deaths) have been reported (https://www.anss-guinee.org). The Institut Pasteur de Guinée has contributed to the testing of >25,000 human nasopharyngeal swab samples. Most samples originated in the Conakry area from the Donka University Hospital and the Alpha Yaya Military Hospital, which serve the general population, and from the Health Center of the French Embassy, which serves mostly expatriates or travelers. We selected a panel of 252 (12.26%) SARS-CoV-2–positive samples taken during March 12, 2020–July 16, 2021, for whole-genome sequencing, which was performed at the World Health Organization Collaborative Centre of the Institut Pasteur de Dakar, to examine the evolution of SARS-CoV-2 in Guinea.

From these 252 samples, 226 sequences were generated; we excluded 90 sequences showing >10% missing nucleotides. We analyzed the remaining 136 (54%) sequences by using Nextclade (https://clades.nextstrain.org) and Pangolin software (https://cov-lineages.org). The Guinea sequences are distributed into 7 clades (Appendix Figure, https://wwwnc.cdc.gov/EID/article/28/2/21-2182-App1.pdf): 20A clade (n = 55, 40.44%), 20B clade (n = 31, 22.80%), 20C clade (n = 1, 0.74%), 20D clade (n = 8, 5.88%), 20I clade (20I/B.1.1.7/Alpha; n = 19, 13.97%), 21A clade (21A/B.1.617.2/Delta; n = 16, 11.76%), and 21D clade (21D/B.1.525/Eta; n = 6, 4.41%) (Figure, panel A). The 7 clades are subdivided into subclades. None of these subclades gather sequences from specific prefectures in Guinea, suggesting that SARS-CoV-2 viruses circulating inside the country are related to Conakry cases. At the time of this writing, ≥21 sublineages of SARS-CoV-2 viruses were circulating in Guinea (Table).

During March–August 2020, the sequences were exclusively distributed into 2 clades, 20A and 20B, globally circulating in West and Central Africa (Table; Figure, panel B) (*1*–*3*). Their ancestral position in the maximum-likelihood tree outlines their introduction in Guinea, most likely from Europe as illustrated by the index case. Their circulation has persisted in a nonexclusive manner up to May–July 2021. The 20D clade, sparsely detected in Africa (Table), was observed in Guinea through ≥2 introductions in September and October 2020, according to the topology of the maximum-likelihood tree (Figure, panel B). Moreover, a single case of 20C clade originating from North America was detected in January 2021 in a person traveling from Haiti (Table; Figure, panel B).

In 2021, new SARS-CoV-2 variants of concern (VOC) and variants of interest, reputed to be more transmissible, emerged in Guinea (*4*). The VOC 20I/B.1.1.7/Alpha variant, which originally emerged in the United Kingdom, was first identified in Guinea in January 2021, increased in incidence up to March 2021, and then decreased from April to June 2021, corresponding to the dynamic described in Africa (Figure, panel B) (*1*–*3*,*5*; E.A. Ozer et al., unpub. data, https://www.medrxiv.org/content/10.1101/2021.04.09.21255206v3). The variant of interest 21D/B.1.525/Eta was identified in Guinea and other countries in Central and West Africa in February–May 2021 (Table) (*5*; E.A.

[1]These authors contributed equally to this article.

[2]Current affiliation: Institut Pasteur du Cambodge, Phnom Penh, Cambodia.

Ozer et al., unpub. data). The topology of the Guinea maximum-likelihood tree with only one subclade of this variant suggests a unique introduction in this study. Finally, the 21A/B.1.617.2/Delta VOC was first detected in May 2021 in Guinea (Figure, panel B). By July, it had become dominant; >90% of the sequenced

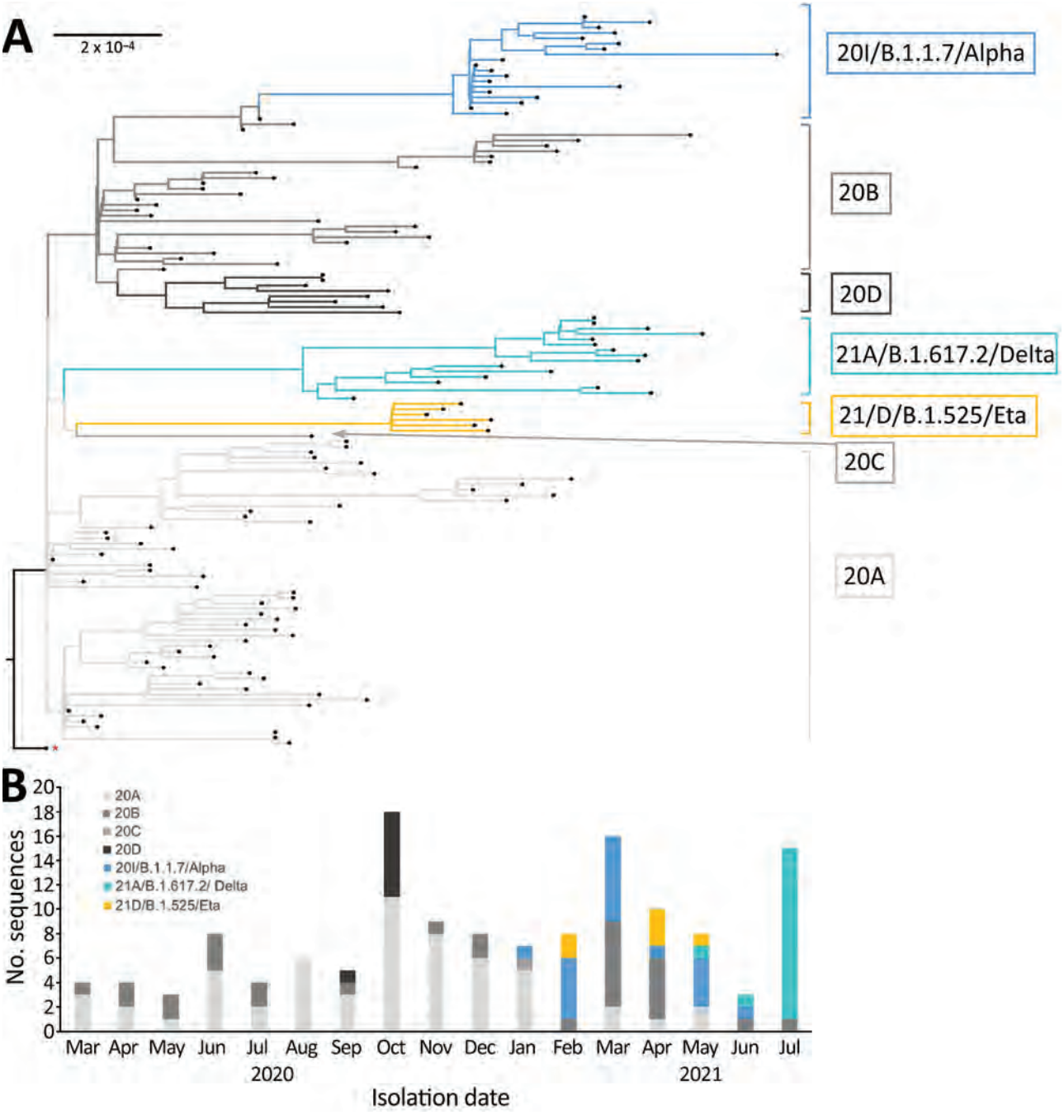

Figure. Phylogenetic and temporal descriptions of severe acute respiratory syndrome coronavirus 2 (SARS-CoV-2) sequences from Institut Pasteur de Guinée from samples collected in Guinea during March 12, 2020–July 16, 2021. A) Maximum-likelihood phylogenetic tree of 136 SARS-CoV-2 genomic sequences. The tree was constructed with IQ-tree software by using multiple-genome sequence alignment and Wuhan-Hu-1 strain (GenBank accession no. NC 045512) as outgroup reference sequence, indicated by the red asterisk. Branches and the sequence names are colored according to Nextclade assigned clades: 20A, light gray; 20B, medium gray; 20C, dark gray; 20D, black; 20I/B.1.1.7/Alpha, blue; 21A/B.1.617.2/Delta, azure; 21D/B.1.525/Eta, yellow. Each sequence is highlighted by a black tip. Scale bar indicates the distance corresponding to substitution per site. B) Chronologic distribution of SARS-CoV-2 genomic variants over 17 months in Guinea. The 136 selected sequences are assigned by Nextclade and classified according to sampling date from March 31, 2020, to July 16, 2021. Clades are colored as in panel A.

Table. Characteristics of clades and lineages identified among the Institut Pasteur de Guinée SARS-CoV-2 sequences from samples taken in Guinea during March 12, 2020–July 16, 2021*

	Worldwide			Africa			Guinea†	
Clade and lineage	1st described	Location	No. sequences	1st described	Location	No. sequences	1st described	No. sequences
20A								
B.1	2020 Jan	UK	83,632	2020 Mar	RDC	2,816	2020 Mar	43
B.1.36.10	2020 Mar	United States	824	2020 Apr	South Africa	17	2021 Jan	1
B.1.210	2020 Mar	India	403	No	No	0	2020 Oct	1
B.1.243	2020 Mar	United States	13,091	2020 Jun	Kenya	6	2020 Jun	1
B.1.298	2020 Mar	United States	397	No	No	0	2020 Oct	1
B.1.540	2020 Feb	India	2,186	2020 Mar	Gambia, Kenya	134	2020 Jun	2
B.1.622	2021 Jan	Réunion	76	No	No	0	2020 Sep	1
B.1.629	2021 Jan	Belgium	84	Unknown	Guinea	14	2021 Mar	5
20B								
B.1.1	2020 Jan	UK	48,119	2020 Feb	Nigeria	1,361	2020 Mar	16
B.1.1.39	2020 Mar	Switzerland	1,861	No	No	0	2021 Jan	1
B.1.1.142	2020 Mar	Australia	51	No	No	0	2021 Apr	1
B.1.1.236	2020 Feb	UK	1,404	2020 Mar	South Africa	36	2020 Mar	1
B.1.1.316.1‡	2020 Jan	Sierra Leone	10,444	2020 Jan	Sierra Leone	35	2020 Dec	4
B.1.1.317	2020 Feb	Russia	2,435	2020 Jun	Zimbabwe	4	2020 Aug	1
B.1.1.318	2021 Jan	UK	3,350	2021 Jan	Nigeria	360	2021 Feb	6
B.1.1.372	2020 Mar	UK	1,381	2020 May	South Africa	16	2020 Jul	1
20C								
B.1.575	2020 Oct	United States	3,026	2020 Dec	Senegal	12	2021 Jan	1
20D								
B.1.1.1	2020 Mar	UK	3,078	2020 Mar	RDC	169	2020 Sep	8
20I								
B.1.1.7 (Alpha)	2020 Sep	UK	1,045,206	2020 Dec	Ghana	2,047	2021 Jan	19
21A								
B.1.617.2 (Delta)	2020 Nov	India	261,339	2021 Mar	South Africa	1,662	2021 May	16
21D								
B.1.525 (Eta)	2020 Dec	UK, Nigeria	7,752	2020 Dec	Nigeria	581	2021 Jan	6

*Clades and lineages are respectively assigned according to Nextclade definition (https://github.com/nextstrain/ncov/blob/master/docs/src/reference/naming_clades.md) and PANGO lineages list (https://github.com/cov-lineages/pangolin) at the same assignment date (August 14, 2021). The Guinea sequences are distributed in 21 lineages clustered into 7 clades: 20A clade (n = 55, 40.44%) with 8 lineages (B.1, B.1.36.10, B.1.210, B.1.243, B.1.298, B.1.540, B.1.622, and B.1.629), 20B clade (n = 31, 22.80%) with 8 lineages (B.1.1, B.1.1.39, B.1.1.142, B.1.1.236, B.1.1.316.1, B.1.1.317, B.1.1.318, and B.1.1.372), 20C clade (n = 1, 0.74%) with 1 lineage (B.1.575), 20D clade (n = 8, 5.88%) with 1 lineage (B.1.1.1), 20I clade (n = 19, 13.97%) with 1 lineage (B.1.1.7 [Alpha]), 21A clade (n = 16, 11.76%) with 1 lineage (B.1.617.2 [Delta]) and 21D clade (n = 6, 4.41%) with 1 lineage (B.1.525 [Eta]). For each lineage, the first worldwide and African descriptions are provided (date and location), as well as the number of deposited sequences in GISAID (August 16, 2021). RDC, Democratic Republic of the Congo; SARS-CoV-2, severe acute respiratory syndrome coronavirus 2; UK, United Kingdom.
†First description and number of sequences in this study.
‡B.1.1.316.1 lineage alias R.1.

viruses by Institut Pasteur de Guinée demonstrated the same dynamics observed during May–August 2021 in Africa (*6*). The maximum-likelihood tree suggests ≥2 main introductions of this variant in Guinea.

In summary, although only 20A and 20B clades circulated in Guinea for the first 6 months of the pandemic (March–August 2020), the reopening of borders and commercial flights have progressively enabled the introduction of variants from surrounding parts of Africa (21D/B.1.525/Eta) and globally (20I/B.1.1.7/Alpha and 21A/B.1.617.2/Delta) several months after their original detection (Table). Although the 20I/B.1.1.7/Alpha and 21A/B.1.617.2/Delta variants have spread successfully in the population, the 21D/B.1.525/Eta variant has only occasionally been detected. We did not detect other variants previously found in Africa, such as the 20H/B.1.351/Beta variant (which populated 50% of sequences in Africa during January–May 2021) and variants from the sublineage A, including the A.23.1 lineage from East Africa and the A.27 lineage of uncertain origin, in this study (*1*–*3*,*5*; E.A. Anoh et al., unpub. data, https://www.medrxiv.org/content/10.1101/2021.05.06.21256282v1).

This overview of the circulation of SARS-CoV-2 viruses in Guinea furthers the examination of infectious diseases control strategies in Africa, which faces vaccination implementation delay (*7*). Beside classical quantitative reverse transcription PCR diagnostic testing, strengthening of the sequencing capacity is the cornerstone of tracking and fighting the emergence of SARS-CoV-2 variants in real time (*8*). Making countries autonomous in sequencing is the next challenge in fighting COVID-19, as well as other emerging zoonoses, in Africa.

Acknowledgments

We are thankful to the members of the SARS-CoV-2 surveillance system network in Guinea for their fruitful contributions in field activities.

This study was funded by the French Ministry for Europe and Foreign Affairs (MEAE) through the project "REPAIR Covid-19-Africa," coordinated by the Pasteur Network association, and by the European Union through the EBO-SURSY project (EU-FOOD/2016/379-660). We are also grateful to the Africa Pathogen Genomics Initiative (Africa PGI) at the Africa Centres for Disease Control and Prevention supported by the Bill and Melinda Gates Foundation.

About the Author

Dr. Grayo is a virologist at Institute Pasteur de Guinée. Her research interests are emerging viral infectious diseases and zoonoses, with a current focus on viral hemorrhagic fevers in West Africa.

References

1. GISAID/Institut Pasteur de Dakar. Phylodynamics of pandemic coronavirus in west Africa. 2021 [cited 2021 Apr 5]. https://www.gisaid.org/phylodynamics/west-africa
2. Wilkinson E, Giovanetti M, Tegally H, San JE, Lessells R, Cuadros D, et al. A year of genomic surveillance reveals how the SARS-CoV-2 pandemic unfolded in Africa. Science. 2021;374:423–31. https://doi.org/10.1126/science.abj4336
3. Wruck W, Adjaye J. Detailed phylogenetic analysis tracks transmission of distinct SARS-COV-2 variants from China and Europe to West Africa. Sci Rep. 2021;11:21108. https://doi.org/10.1038/s41598-021-00267-w
4. Harvey WT, Carabelli AM, Jackson B, Gupta RK, Thomson EC, Harrison EM, et al.; COVID-19 Genomics UK (COG-UK) Consortium. SARS-CoV-2 variants, spike mutations and immune escape. Nat Rev Microbiol. 2021;19:409–24. https://doi.org/10.1038/s41579-021-00573-0
5. Sander AL, Yadouleton A, De Oliveira Filho EF, Tchibozo C, Hounkanrin G, Badou Y, et al. Mutations associated with SARS-CoV-2 variants of concern, Benin, early 2021. Emerg Infect Dis. 2021;27:2889–903. https://doi.org/10.3201/eid2711.211353
6. World Health Organization. COVID-19 situation update for the WHO African Region, 26 August 2020 [cited 2020 Dec 26]. https://apps.who.int/iris/bitstream/handle/10665/334003/SITREP_COVID-19_WHOAFRO_20200826-eng.pdf
7. Ariyo OE, Oladipo EK, Osasona OG, Obe O, Olomojobi F. COVID-19 vaccines and vaccination: how prepared is Africa? Pan Afr Med J. 2021;39:107. https://doi.org/10.11604/pamj.2021.39.107.27912
8. Tsanni A. Covid-19: Africa scrambles to increase genomic testing capacity as variants spread. BMJ. 2021;373:n1122. https://doi.org/10.1136/bmj.n1122

Address for correspondance: Solène Grayo, Virology Unit, Institut Pasteur de Guinée, Route de Donka, BP 4416, Conakry, Guinée; email: solene.grayo.ext@pasteur.fr

Probable Transmission of SARS-CoV-2 Omicron Variant in Quarantine Hotel, Hong Kong, China, November 2021

Haogao Gu, Pavithra Krishnan, Daisy Y.M. Ng, Lydia D.J Chang, Gigi Y.Z. Liu, Samuel S.M. Cheng, Mani M.Y. Hui, Mathew C.Y. Fan, Jacob H.L. Wan, Leo H.K. Lau, Benjamin J. Cowling, Malik Peiris, Leo L.M. Poon

Author affiliation: The University of Hong Kong, Hong Kong, China

DOI: https://doi.org/10.3201/eid2802.212422

We report detection of severe acute respiratory syndrome coronavirus 2 Omicron variant (B.1.1.529) in an asymptomatic, fully vaccinated traveler in a quarantine hotel in Hong Kong, China. The Omicron variant was also detected in a fully vaccinated traveler staying in a room across the corridor from the index patient, suggesting transmission despite strict quarantine precautions.

A new variant of severe acute respiratory syndrome coronavirus 2 (SARS-CoV-2), B.1.1.529, was identified in Botswana and South Africa in early November 2021 and was designated as variant of concern (VOC) Omicron by the World Health Organization on November 26, 2021 (*1*). As of December 1, 2021, ≈220 sequences were available on GISAID (https://www.gisaid.org), and this variant has been detected in countries in Africa and beyond since mid-November (*2*,*3*). This variant contains >30 spike protein amino acid mutations that might be associated with increased transmissibility, severity, and capacity for immune escape. With supporting evidence of epidemiologic and molecular epidemiologic findings, we report the probable transmission of Omicron in a quarantine hotel in Hong Kong, China. We also compare its mutational profile with other VOCs and variants of interest.

Two cases of infection with VOC Omicron (cases A and B) were detected in Hong Kong. Case-patient A arrived in Hong Kong from South Africa on November 11, 2021, and case-patient B arrived in Hong Kong from Canada on November 10, 2021. Both case-patients had previously received 2 vaccine doses (Pfizer-BioNTech, https://www.pfizer.com); the second dose was given on June 4, 2021, for case-patient A and on May 25, 2021, for case-patient B. Both case-patients tested negative by reverse transcription PCR (RT-PCR) for SARS-CoV-2 within 72 hours before arrival. On arrival at the Hong Kong

airport, both case-patients stayed in the same quarantine hotel and had rooms across the corridor from each other on the same floor.

Case-patient A showed a positive result for SARS-CoV-2 without symptoms on November 13, 2021 (cycle threshold [C_t] value 18). He was hospitalized and isolated the next day. Case-patient B had mild symptoms develop on November 17, 2021. He showed a positive result for SARS-CoV-2 (C_t value 19) on November 18, 2021, and was hospitalized on the same day. The 2 C_t values indicate high viral loads. None of the 12 persons staying in nearby rooms on the same floor during the study or related hotel staff have tested positive in repeated tests for SARS-CoV-2 (*4*).

Viral genomes deduced from these 2 SARS-CoV-2–positive cases differed only by 1 nt. Retrospective investigation, including closed-circuit television camera footage, confirmed that neither case-patient left their room during the quarantine period. No items were shared between rooms, and other persons did not enter either room. The only time the 2 quarantined persons opened their respective doors was to collect of food that was placed immediately outside each room door. The only other time they might have opened their doors would be for RT-PCRs, which were conducted in 3-day intervals. However, because these 2 case-patients arrived 1 day apart, it is unlikely that they would be tested on the same day. Airborne transmission across the corridor is the most probable mode of transmission.

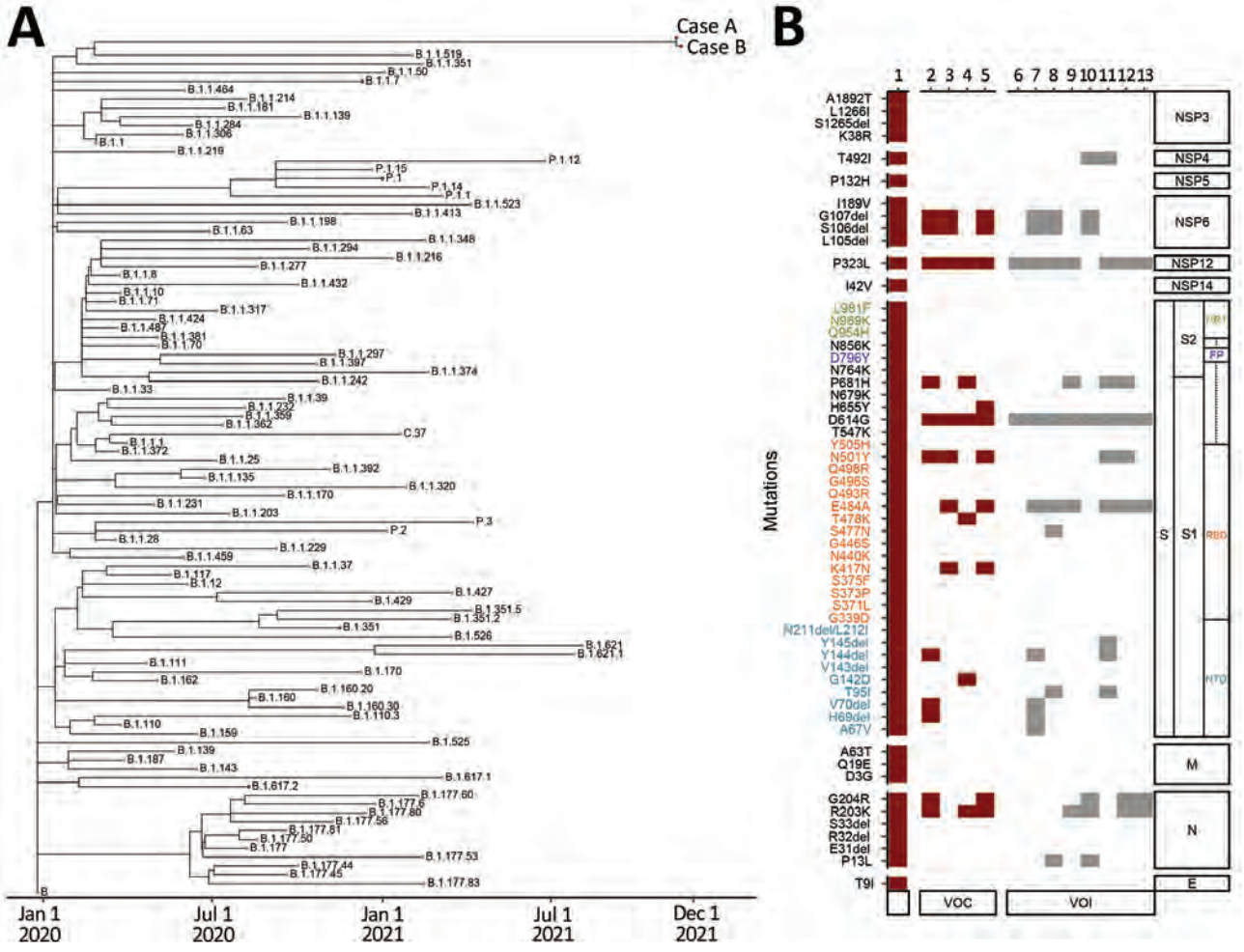

Figure. Detection of severe acute respiratory syndrome coronavirus 2 Omicron variant in 2 patients (cases A and B) in Hong Kong, China, November 2021. A) Phylogenetic time tree of Omicron nucleotide sequences using an early severe acute respiratory syndrome coronavirus sequence as a reference sequence (Wuhan-Hu-1/2019; GenBank accession no. MN908947.3). B) Comparison of Omicron variant mutations in case A to other variants; red indicates VOC and gray VOI (Appendix, https://wwwnc.cdc.gov/EID/article/28/2/21-2422-App1.pdf). Text colors indicate mutations found in NTD (blue), RBD (orange), FP (purple), and HR1 (green). Lane 1, case A; 2, Alpha (B.1.1.7); 3, Beta (B.1351); 4, Delta (B.1.617.2); 5, Gamma (P1); 6, Epsilon (B.1.427/429); 7, Eta (B.1.525); 8, Iota (B.1.526); 9, Kappa (B.1.617.1); 10, Lambda (C.37); 11, Mu (B.1.1.621); 12, Theta (P.3); 13, Zeta (P.2). E, envelope; FP, fusion peptide; HR1, heptad repeat 1; M, matrix; NSP, nonstructural protein; NTD, N-terminal domain; RBD, receptor-binding domain; S, spike; VOC, variant of concern; VOI, variant of interest.

We sequenced complete SARS-CoV-2 genomes from case-patients A and B (Appendix, https://wwwnc.cdc.gov/EID/article/28/2/21-2422-App1.pdf) and confirmed that these genomes were VOC Omicron (Pango lineage B.1.1.529) (Figure, panel A). Viral sequences from these 2 case-patients differed by only 1 nt. Viral sequence from case-patient A was highly similar to those of the first few reported Omicron cases identified in South Africa and Botswana (Appendix Table 1). Because many countries have just reported detection of this VOC (https://www.gisaid.org/hcov19-variants), the actual genetic diversity of this virus lineage requires further investigations.

The long branch of Omicron clade in the phylogenetic tree is attributed to the large number of mutations (Figure, panel A). Nonsynonymous mutations were identified in the spike (S)–encoding (n = 35) and other viral protein–encoding (n = 22) regions (Figure, panel B). Among the nonsynonymous mutations in the S protein, 43% (n = 15) were also identified in other VOCs/variants of interest, and 31% (n = 11) were found only in VOCs (Alpha, n = 6; Beta, n = 4; Gamma, n = 5; Delta, n = 4). Some of the point mutations and deletions found in other regions are not novel and can also be found in other variants at different frequencies (Appendix Table 2). Among these non-S mutations, NSP4-T492I, NSP6-S106del, NSP6-G107del, NSP12-P323L, N-P13L, N-R203K, and N-G204R are commonly found in SARS-CoV-2 variants.

The laboratory and epidemiologic features of the Omicron variant are yet to be fully characterized and cannot be determined on the basis of sequence features alone. Nonetheless, compared with other VOCs, the number of mutations found in the spike of the Omicron variant is unprecedented. This finding results in false-negative results in some diagnostic RT-PCRs specific for the S gene (*3*). Many of the mutations found in the S protein are known to alter SARS-CoV-2 antigenicity and transmissibility (*5*). The R203K and G204R mutations in the nucleocapsid protein are also associated with enhanced virus replication (*6*).

It is not known whether these detected mutations might have affected the effectiveness of existing vaccines and virus transmissibility. However, detection of Omicron variant transmission between 2 fully vaccinated persons across the corridor of a quarantine hotel has highlighted this potential concern. Further experimental characterizations and epidemiologic investigations of this newly found VOC are urgently needed. Increased precautions or additional measures might be warranted while awaiting more data.

Acknowledgments

We thank the staffs from the originating laboratories responsible for obtaining specimens; the submitting laboratories in which genome data were generated and shared via GISAID (Appendix Table 3); colleagues from the Centre for PanorOmic Sciences of the University of Hong Kong for providing technical support; and the Centre for Health Protection of the Department of Health for providing epidemiologic data.

This study was supported by grants from the National Institute of Allergy and Infectious Diseases (U01AI151810, 75N93021C00016), the Health and Medical Research Fund (COVID190205), and the Collaborative Research Fund, Research Grants Council (C7123-20G).

About the Author

Dr. Gu is a postdoctoral fellow at The University of Hong Kong, Hong Kong, China. His primary research interests are bioinformatics and virus evolution.

References

1. World Health Organization. Tracking SARS-CoV-2 variants, 2021 [cited 2021 Nov 27]. https://www.who.int/en/activities/tracking-SARS-CoV-2-variants
2. Callaway E. Heavily mutated coronavirus variant puts scientists on alert. Nature. 2021;600:21 [cited 2021 Dec 2]. https://www.nature.com/articles/d41586-021-03552-w
3. World Health Organization. Classification of Omicron (B.1.1.529): SARS-CoV-2 variant of concern, 2021 [cited 2021 Nov27]. https://www.who.int/news/item/26-11-2021-classification-of-omicron-(b.1.1.529)-sars-cov-2-variant-of-concern
4. Hong-Kong-Government. CHP provides update on latest investigations on COVID-19 imported cases 12388 and 12404, 2021 [cited 2021 Nov 26]. https://www.info.gov.hk/gia/general/202111/22/P2021112200897.htm
5. Tao K, Tzou PL, Nouhin J, Gupta RK, de Oliveira T, Kosakovsky Pond SL, et al. The biological and clinical significance of emerging SARS-CoV-2 variants. Nat Rev Genet. 2021;22:757–73. https://doi.org/10.1038/s41576-021-00408-x
6. Wu H, Xing N, Meng K, Fu B, Xue W, Dong P, et al. Nucleocapsid mutations R203K/G204R increase the infectivity, fitness, and virulence of SARS-CoV-2. Cell Host Microbe. 2021;S1931-3128(21)00511-4.

Address for correspondence: Leo L.M. Poon, School of Public Health, The University of Hong Kong, Hong Kong, China; email: llmpoon@hku.hk

Seroprevalence of SARS-Cov-2 Antibodies in Adults, Arkhangelsk, Russia

Ekaterina Krieger, Alexander Kudryavtsev, Ekaterina Sharashova, Vitaly Postoev, Natalia Belova, Leonid Shagrov, Julia Zvedina, Oxana Drapkina, Anna Kontsevaya, Svetlana Shalnova, Tormod Brenn, Vladimir M. Shkolnikov, Rosalind M. Eggo, David A. Leon

Author affiliations: UiT The Arctic University of Norway, Tromso, Norway (E. Krieger, A. Kudryavtsev, E. Sharashova, T. Brenn, D.A. Leon); Northern State Medical University of the Ministry of Health of the Russian Federation, Arkhangelsk, Russia (E. Krieger, A. Kudryavtsev, V. Postoev, N. Belova, L. Shagrov, J. Zvedina); National Medical Research Centre for Therapy and Preventive Medicine, Moscow, Russia (O. Drapkina, A. Kontsev, S. Shalnova); Max-Planck-Institute for Demographic Research, Mecklenburg, Germany (V.M. Shkolnikov); National Research University Higher School of Economics, Moscow (V.M. Shkolnikov, D.A. Leon); London School of Hygiene & Tropical Medicine, London, UK (R.M. Eggo, D.A. Leon)

DOI: https://doi.org/10.3201/eid2802.211640

Population-based data on coronavirus disease in Russia and on the immunogenicity of the Sputnik V vaccine are sparse. In a survey of 1,080 residents of Arkhangelsk 40–75 years of age, 65% were seropositive for IgG. Fifteen percent of participants had been vaccinated; of those, 97% were seropositive.

Russia is one of the few countries to have produced a coronavirus (COVID-19) vaccine (*1*). It has also experienced substantial excess deaths during the pandemic (*2*). Few published estimates of antibody seroprevalence for severe acute respiratory syndrome coronavirus 2 (SARS-CoV-2) in Russia exist. A St. Petersburg survey in June 2020 used random-digit dialing to contact 66,250 residents; of those, 1,038 provided a blood sample, and the samples had 9%–10% seropositivity (*3*). A study conducted in Chelyabinsk (September 28–December 30, 2020) recruited 1,091 high-risk workers (healthcare workers, education staff, and supermarket employees) ≥18 years of age. Of the 882 screened, 25% were seropositive for IgG (*4*). We are not aware of any seroprevalence estimates from Russia based on samples collected in 2021 that have appeared in the scientific literature.

We interviewed and obtained blood samples from 1,080 adults 40–75 years of age who were residents of the city of Arkhangelsk in northwest Russia during February 24–May 28, 2021. We obtained participants for this study from 2,258 invitations sent to persons who had taken part in the Know Your Heart study (*5*) (2015–2018), which was based on a random sample of the city population (Appendix, https://wwwnc.cdc.gov/EID/article/28/2/21-1640-App1.pdf). The ethics committee of the Northern State Medical University approved our study proposal and protocol on February 17, 2021.

We used a Vector Best ELISA assay (D-5501 SARS-CoV-2-IgG-EIA-BEST; https://vector-best.ru) to analyze qualitatively detected IgG directed against SARS-CoV-2 in human blood serum samples. Data are limited on the performance of this immunoassay, in particular, on its sensitivity for infections that occurred >3 weeks previously. According to the manufacturer, the assay has a sensitivity of 72% when performed 6–12 days after infection and ≈100% at 13–20 days (*6*). An independent assessment of the Vector Best ELISA assay found a sensitivity of 89% and a specificity of 100%, derived from comparisons of test results in prepandemic samples (negative controls) and PCR positive samples for SARS-CoV-2 (*7*). We estimated seroprevalence adjusted for test performance (89% sensitivity, 100% specificity) using the equation (crude prevalence + test specificity – 1)/(sensitivity + specificity – 1) (*8*). We calculated 95% CIs for the adjusted estimates of seroprevalence using the R package bootComb (https://www.r-project.org).

Of the 1,080 samples (634 women, mean age 55 years), we excluded 13 who had an equivocal test result from analysis. Of the 1,067 remaining samples, 690 (65%) were seropositive for IgG (Table 1). Seroprevalence adjusted for test characteristics was 72.6% (95% CI 64.2%–83.1%).

Seroprevalence did not substantively differ by sex or by educational level. Of the 162 participants (15%) who reported having been vaccinated. 150 (93%) were seropositive. Among the 31 who received 1 dose, 20 (65%) were seropositive; of the 131 who had received 2 doses, 130 (99%) were seropositive. Of the 905 participants who said they had not been vaccinated, 256 said that they had previously been ill with COVID-19; of those, 248 (97%) were seropositive. Of those who stated they had not been vaccinated and did not report having previously been ill with COVID-19, 292 (45%) were seropositive, suggesting an appreciable level of unrecognized infection. Our overall estimates of seroprevalence (crude 65%, adjusted 72.6%) is appreciably higher than found in St Petersburg in

Table. Seroprevalence of severe acute respiratory syndrome coronavirus 2 in adults, Arkhangelsk, Russia

Characteristic	Unvaccinated		Vaccinated*		Total	
	No. seropositive/ total (%)	Adjusted seroprevalence, % (95% CI)†	No. seropositive/ total (%)	Adjusted seroprevalence, % (95% CI)†	No. seropositive/ total (%)	Adjusted seroprevalence, % (95% CI)†
Sex						
F	332/553 (60)	67.4 (58.4–77.9)	72/81 (89)	99.7 (87.1–99.9)	404/634 (64)	71.5 (62.6–82.3)
M	208/352 (59)	66.3 (56.5–77.3)	78/81 (96)	100 (93.2–100)	286/433 (66)	74.1 (64.5–85.6)
Age, y						
40–54	291/461 (63)	70.8 (61.4;81.8)	35/38 (92)	100 (84.8–100)	326/499 (65)	73.3 (64.0–84.6)
55–64	181/317 (57)	64.1 (54.1–75.0)	38/43 (88)	99.1 (82.6–100)	219/360 (61)	68.3 (58.4–79.4)
≥65	68/127 (54)	60.1 (46.9–73.1)	77/81 (95)	100 (92.4–100)	145/208 (70)	78.2 (67.0–91.2)
Education						
Secondary and lower	26/47 (55)	62.1 (42.7–81.0)	9/9 (100)	100 (66.7–100)	35/56 (63)	70.1 (52.5–88.1)
Specialized secondary	253/433 (58)	65.6 (56.1–76.0)	81/87 (93)	100 (91.2–100)	334/520 (64)	72.1 (62.9–83.2)
Higher	261/425 (61)	68.9 (59.3–79.8)	60/66 (91)	100 (88.0–100)	321/491 (65)	73.3 (64.0–84.6)
Week of test						
7–14	395/651 (61)	68.1 (59.3–78,4)	49/58 (84)	94.8 (81.0–100)	444/709 (63)	70.3 (61.6–80.8)
15–21	145/254 (57)	64.0 (53.4–75.3)	101/104 (97)	100 (94.8–100)	246/358 (69)	77.1 (67.1–89.1)
Self-reported prior symptoms of infection						
No	172/477 (36)	40.5 (31.7–47.8)	133/143 (93)	100 (92.9–100)	305/620 (49)	55.2 (46.6–64.0)
Yes	248/256 (97)	100 (96.9–100)	8/9 (89)	99.7 (56.8–100)	256/265 (97)	100 (96.7–100)
Do not know	120/172 (70)	78.3 (66.5–91.6)	9/10 (90)	100 (60.4–100)	129/182 (71)	79.5 (68.1–92.8)
Total	540/905 (60)	66.9 (58.6–76.9)	150/162 (93)	100 (92.9–100)	690/1067 (65)	72.6 (64.2–83.1)

*Received ≥1 dose.
†Values >100% were rounded to 100%.
‡Weeks 7–14 are February 24–April 11 and weeks 15–21 are April 12–May 28, 2021.

June 2020 (*3*) (10%) or in Chelyabinsk (25%) in September–December 2020 (*4*). This result is consistent with the second wave of the pandemic in Russia (peak November–December 2020) being larger than the first (peak May–June 2020); our study started during the vaccination period.

Deployment of COVID-19 vaccine, mostly Sputnik V, in the Arkhangelsk region started in mid-January 2021; 11% of the population received ≥1 dose by May 30, 2021 (*9*). Our study covered an urban sample from the city of Arkhangelsk, the capital of the region. Our estimate of 15% coverage of the study population may be higher because the regional estimates included data from more dispersed communities in. Nevertheless, our vaccination rates were low compared with rates in most European Union and European Economic Area countries as reported in June 2021 by the European Centre for Disease Prevention and Control (*10*). Given the vaccination rate in the sample was 15% but the antibodies were present in 65% of participants, we suspect that most of the seropositive results were the result of acquired infection.

Russia is geographically the largest country in the world; its regions vary considerably in terms of socioeconomic level, climate, and healthcare provision. Our study results are restricted to an adult population and cannot be generalized to the total population of Arkhangelsk region or to Russia. The high levels of seroprevalence among vaccinated participants confirms the immunogenicity of the Sputnik vaccine and suggests that it can protect the population if the proportion vaccinated is increased substantially. We recommend further population-based seroprevalence studies, using World Health Organization–approved tests, for public health efforts in the COVID-19 pandemic.

The seroprevalence survey was funded by the Russian Ministry of Health as part of the ESSE-RF3 health survey. The Know Your Heart study is a component of International Project on Cardiovascular Disease in Russia, funded by a Wellcome Trust Strategic Award (award no. 100217), the Arctic University of Norway, the Norwegian Institute of Public Health, and the Norwegian Ministry of Health and Social Affairs.

About the Author

Dr. Krieger is a PhD student in UiT The Arctic University of Norway, Tromso, Norway. Her primary research interest is epidemiology, infectious diseases, and vaccination.

References

1. Logunov DY, Dolzhikova IV, Zubkova OV, Tukhvatulin AI, Shcheblyakov DV, Dzharullaeva AS, et al. Safety and immunogenicity of an rAd26 and rAd5 vector-based heterologous prime-boost COVID-19 vaccine in two formulations: two open, non-randomised phase 1/2 studies from Russia. Lancet. 2020;396:887–97. https://doi.org/10.1016/S0140-6736(20)31866-3

2. Karlinsky A, Kobak D. Tracking excess mortality across countries during the COVID-19 pandemic with the World Mortality Dataset. eLife. 2021;10:10. https://doi.org/10.7554/eLife.69336
3. Barchuk A, Skougarevskiy D, Titaev K, Shirokov D, Raskina Y, Novkunkskaya A, et al. Seroprevalence of SARS-CoV-2 antibodies in Saint Petersburg, Russia: a population-based study. Sci Rep. 2021;11:12930. https://doi.org/10.1038/s41598-021-92206-y
4. Zurochka A, Dobrinina M, Zurochka V, Hu D, Solovyev A, Ryabova L, et al. Seroprevalence of SARS-CoV-2 antibodies in symptomatic individuals is higher than in persons who are at increased risk exposure: the results of the single-center, prospective, cross-sectional study. Vaccines (Basel). 2021;9:627. https://doi.org/10.3390/vaccines9060627
5. Cook S, Malyutina S, Kudryavtsev A, et al. Know Your Heart: rationale, design and conduct of a cross-sectional study of cardiovascular structure, function, and risk factors in 4,500 men and women aged 35–69 years from two Russian cities, 2015–18. Wellcome Open Research 2018;3:67. https://doi.org/10.12688/wellcomeopenres.14619.3
6. Kuvshinova IN, Nekrasov BG, Livitskaya NI, Molodykh SV, Rukavishnikov M. Sensitivity and specificity of reagent kits of JSC "Vector-Best" for the detection of immunoglobulins of different classes to SARS-CoV-2 [in Russian]. Spravochnik Zaveduyushchego KDL. 2021;10:27–32.
7. Barchuk A, Shirokov D, Sergeeva M, Tursunzade R, Dudkina O, Tychkova V, et al. Evaluation of the performance of SARS-CoV-2 antibody assays for a longitudinal population-based study of COVID-19 spread in St. Petersburg, Russia. J Med Virol. 2021;93:5846–52. https://doi.org/10.1002/jmv.27126
8. Sempos CT, Tian L. Adjusting coronavirus prevalence estimates for laboratory test kit error. Am J Epidemiol. 2021;190:109–15. https://doi.org/10.1093/aje/kwaa174
9. Government of Russia. The number of people vaccinated against coronavirus in Arkhangelsk [in Russian]. 2021 [cited 2021 Sep 20]. https://gogov.ru/covid-v-stats/arkhangelsk
10. European Centre for Disease Prevention and Control. Overview of the implementation of COVID-19 vaccination strategies and deployment plans in the EU/EEA, 14 June 2021. 2021 [cited 2021 Sep 20]. https://www.ecdc.europa.eu/en/publications-data/overview-implementation-covid-19-vaccination-strategies-and-deployment-plans

Address for correspondence: David Leon, London School of Hygiene & Tropical Medicine, Keppel St, London, WC1E 7HT, UK; email: david.leon@lshtm.ac.uk

Ulceroglandular Infection and Bacteremia Caused by *Francisella salimarina* in Immunocompromised Patient, France

Aurélie Hennebique,[1] Yvan Caspar,[1] Max Maurin, Sandrine Boisset, Isabelle Pelloux, Maria Pilar Gallego-Hernanz, Christophe Burucoa, France Cazenave-Roblot, Chloé Plouzeau, Blandine Rammaert

Author affiliations: Université Grenoble Alpes, Grenoble (A. Hennebique, Y. Caspar, M. Maurin, S. Boisset); CHU Grenoble Alpes, Grenoble, France (A. Hennebique, Y. Caspar, M. Maurin, S. Boisset, I. Pelloux); CHU de Poitiers, Poitiers, France (M.P. Gallego-Hernanz, C. Burucoa, F. Cazenave-Roblot, C. Plouzeau, B. Rammaert); Université de Poitiers, Poitiers (C. Burucoa, F. Cazenave-Roblot, B. Rammaert)

DOI: https://doi.org/10.3201/eid2802.211380

Although *Francisella tularensis* is a well-known, highly virulent bacterium that causes tularemia in humans, other *Francisella* species have been associated with sporadic human infections. We describe a human cutaneous infection with bacteremia caused by *F. salimarina*, a *Francisella* species recently identified from seawater and fishes, in an immunocompromised patient in France.

Although the taxonomy of the genus *Francisella* includes a wide diversity of species, only *F. tularensis* subspecies *tularensis* and *F. tularensis* subsp. *holarctica* cause the potentially life-threatening disease tularemia (*1*). Several *Francisella* spp., including *F. philomiragia*, *F. novicida*, *F. opportunistica*, and *F. hispaniensis*, are occasional opportunistic human pathogens; the other *Francisella* spp. are not associated with human infections (*1*). We describe a human infection caused by *F. salimarina*, recently identified from aquatic environments and fishes.

In June 2017, a 76-year-old man received a diagnosis of acute myelomonocytic leukemia and was admitted to Poitiers University Hospital (Poitiers, France). The patient lived in a small town 30 km from the Atlantic Ocean, had not travelled abroad recently, and had no pets. The day after admission, first-line chemotherapy of subcutaneous azacitidine was started for 7 days. After 3 days of chemotherapy, piperacillin/tazobactam was introduced for 5 days because of febrile aplasia. The patient was then discharged with

[1]These authors contributed equally to this article.

an antibiotic prophylaxis (sulfamethoxazole/trimethoprim at 800 mg/160 mg 3×/wk). On July 26, the second azacitidine treatment was not administered because the patient again experienced febrile aplasia. Physical examination revealed skin lesions on 2 left-hand fingers that had appeared 3 weeks earlier. These lesions were erythematous and crusty but not purulent (Figure, panel A). They were associated with a left axillary lymphadenopathy. Antibiotic treatment with piperacillin/tazobactam and teicoplanin was started but was changed to imipenem/cilastatin and daptomycin after 5 days because of poor clinical response. Aerobic blood cultures performed at admission tested positive on July 31 and Gram stain showed a small gram-negative coccobacillus (Figure, panel B). Antibiotic treatment was changed to cefepime, administered for 3 days. No identification could be obtained by MALDI-TOF (matrix-assisted laser desorption/ionization time-of-flight) mass spectrometry (Vitek MS; bioMérieux, https://www.biomerieux.com). The strain was identified as a *Francisella* spp. by 16s rDNA amplification and sequencing. A cutaneous biopsy was performed because of persistent fever and worsening skin lesions in the patient; the same *Francisella* spp. strain was isolated. Doxycycline (100 mg 2×/d) was administered for 8 days, followed by sulfamethoxazole/trimethoprim, which led to apyrexia.

The *Francisella* spp. strain (referred to as CHUGA-F75) was sent to the French National Reference Centre for *Francisella* for further characterization. The strain was strictly aerobic and grew well on chocolate agar supplemented with IsoVitaleX (bioMérieux), blood agar, and tryptic soy agar, yielding gray mucoid colonies after 24 h of incubation at 35°C in 5% CO_2, but not on Drigalski agar (Figure, panels C, D). Biochemical testing revealed a positive oxidase, a weakly positive catalase, and a negative urease test. The strain was also halotolerant; it could grow in modified Mueller-Hinton broth with up to 8% NaCl. ISFtu2, Tul4, and type B real-time PCR tests, which detected most *Francisella* spp., *F. tularensis*, and *F. tularensis* subsp. *holarctica*, were all negative for DNA extracted from this strain (*2*,*3*). Species identification could not be obtained by using MALDI-TOF mass spectrometry, either with the routine database (MBT IVD Library DB-7171), the Biotox database (MBT SR Library; both from Bruker, https://www.bruker.com), or the French National Reference Centre for *Francisella* database containing *F. tularensis*, *F. novicida*, and *F. philomiragia* (*4*). Therefore, we performed whole-genome sequencing by using second and third next-generation sequencing platforms MiSeq (Illumina, https://www.illumina.com) and MinION (Oxford Nanopore Technologies, https://nanoporetech.com). Hybrid assembly of the sequencing data using Unicycler software on the Galaxy web platform (https://usegalaxy.org) enabled circularization of a 1,940,863 bp bacterial chromosome (Genbank accession no. CP076680). Whole-genome–based identification of the strain was assessed by using the Type Strain Genome Server (https://tygs.dsmz.de) (*5*). The CHUGA-F75 strain clustered in the same branch as the *F. salimarin*a SYSU SYW-1, the *F. marina* E95-16, and the *F. salina* TX07-7308 strains (Appendix Figure, https://wwwnc.cdc.gov/EID/article/28/2/21-1380-App1.pdf), probably representing the same species because of high genetic homology, although different species names have been published (*6*–*8*). Digital DNA-DNA hybridization >70%, average nucleotide identity >95%, and difference in percent guanine-cytosine content <1 percent between the CHUGA-F75 strain and the 3 *F. salimarina*, *F. marina*, and *F. salina* strains confirmed the CHUGA-F75 isolate belonged to the same species. Because the only validly published species name according to the International Code of Nomenclature of prokaryotes is *F. salimarina*, we identified CHUGA-F75 as *F. salimarina.* Using the broth microdilution method in cation-adjusted Mueller-Hinton broth as recommended by the Clinical and Laboratory Standards

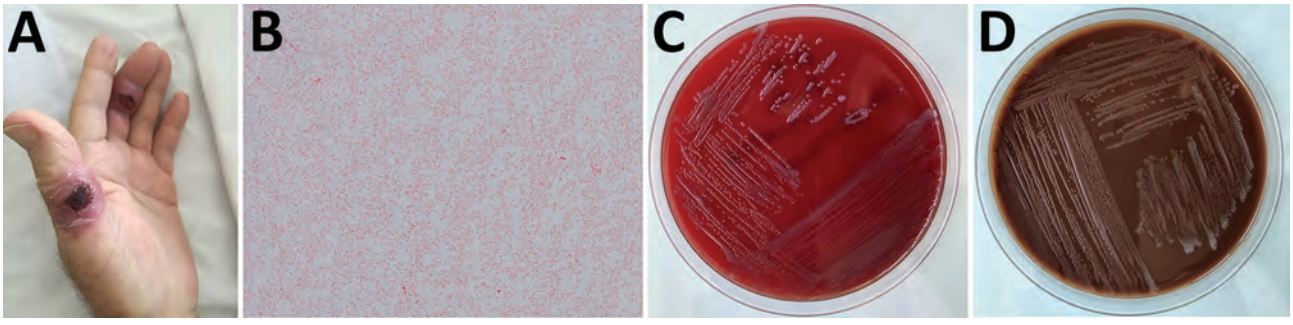

Figure. Skin ulcers and bacteremia caused by *Francisella salimarina* in an immunocompromised patient and isolated bacteria morphology, France. A) Skin lesion on 2 left-hand fingers. B) Small gram-negative coccobacillus isolated from blood and skin lesions (original magnification ×1,000). C) Growth on blood agar after 2 days of incubation at 35°C in 5% CO_2. D) Growth on chocolate agar after 2 days of incubation at 35°C in 5% CO_2.

Institute, we found that the CHUGA-F75 strain was sensitive to gentamicin (MIC = 0.125 mg/L), doxycycline (MIC = 1 mg/L), and ciprofloxacin (MIC = 0.016 mg/L) and resistant to sulfamethoxazole/trimethoprim (MIC = 32 mg/L).

F. marina was described as responsible for systemic disease in fishes (*Lutjanus guttatus*, the cultured spotted rose snapper) in Central America, whereas 4 *F. salimarina* strains have been isolated from costal seawater in Guangdong Province, China, and 1 strain of *F. salina* has been grown from brackish seawater and seaweed off the coast of Galveston, Texas, USA (*6*–*8*). To our knowledge, these *Francisella* spp. were not responsible for human infection so far. This report, like previous descriptions of human infections caused by emergent *Francisella* spp., highlights that environmental or fish-related *Francisella* spp. could be responsible for opportunistic human infections resembling tularemia.

The Direction Générale de l'Armement of France funded this research (ANR-17-ASTR-0024).

About the Author

Dr. Hennebique is a clinical microbiologist in the bacteriology laboratory of Grenoble University Hospital, Grenoble, France, which also hosts the French National Reference Center for *Francisella tularensis*. Her primary research interests are the tularemia agent, with an emphasis on its mechanisms of environmental survival in water, susceptibility to antibiotics, and virulence.

References

1. Hennebique A, Boisset S, Maurin M. Tularemia as a waterborne disease: a review. Emerg Microbes Infect. 2019; 8:1027–42. https://doi.org/10.1080/22221751.2019.1638734
2. Versage JL, Severin DDM, Chu MC, Petersen JM. Development of a multitarget real-time TaqMan PCR assay for enhanced detection of *Francisella tularensis* in complex specimens. J Clin Microbiol. 2003;41:5492–9. https://doi.org/10.1128/JCM.41.12.5492-5499.2003
3. Kugeler KJ, Pappert R, Zhou Y, Petersen JM. Real-time PCR for *Francisella tularensis* types A and B. Emerg Infect Dis. 2006;12:1799–801. https://doi.org/10.3201/eid1211.060629
4. Regoui S, Hennebique A, Girard T, Boisset S, Caspar Y, Maurin M. Optimized MALDI TOF mass spectrometry identification of *Francisella tularensis* subsp. *holarctica*. Microorganisms. 2020;8:E1143. https://doi.org/10.3390/microorganisms8081143
5. Meier-Kolthoff JP, Göker M. TYGS is an automated high-throughput platform for state-of-the-art genome-based taxonomy. Nat Commun. 2019;10:2182. https://doi.org/10.1038/s41467-019-10210-3
6. Challacombe JF, Petersen JM, Gallegos-Graves LV, Hodge D, Pillai S, Kuske CR. Whole-genome relationships among *Francisella* bacteria of diverse origins define new species and provide specific regions for detection. Appl Environ Microbiol. 2017;83:e02589-16.
7. Li L-H, Luo H-M, Feng J-H, Ming Y-Z, Zheng M-L, Deng G-Y, et al. *Francisella salimarina* sp. nov., isolated from coastal seawater. Int J Syst Evol Microbiol. 2020;70:3264–72. https://doi.org/10.1099/ijsem.0.004164
8. Soto E, Griffin MJ, Morales JA, Calvo EB, de Alexandre Sebastião F, Porras AL, et al. *Francisella marina* sp. nov., etiologic agent of systemic disease in cultured Spotted Rose Snapper (Lutjanus guttatus) in Central America. Appl Environ Microbiol. 2018;84:e00144-18. https://doi.org/10.1128/AEM.00144-18

Address for correspondence: Aurélie Hennebique, Service de Bactériologie-Hygiène Hospitalière, Institut de Biologie et de Pathologie, Centre Hospitalier Universitaire Grenoble Alpes, CS10217, 38043 Grenoble CEDEX 9, France; email: ahennebique@chu-grenoble.fr

Surveillance of Rodent Pests for SARS-CoV-2 and Other Coronaviruses, Hong Kong

Elliott F. Miot,[1] Brian M. Worthington,[1] Kar Hon Ng,[1] Lucy de Guilhem de Lataillade,[1] Mac P. Pierce, Yunshi Liao, Ronald Ko, Marcus H. Shum, William Y. Cheung, Edward C. Holmes, Kathy S. Leung, Huachen Zhu, Leo L. Poon, J.S. Malik Peiris, Yi Guan, Gabriel M. Leung, Joseph T. Wu, Tommy T. Lam

DOI: https://doi.org/10.3201/eid2802.211586

Author affiliations: University of Hong Kong State Key Laboratory of Emerging Infectious Diseases, Hong Kong, China (E.F. Miot, B.M. Worthington, K.H. Ng, L. de Guilhem de Lataillade, M.P. Pierce, Y. Liao, M.H. Shum, W.Y. Cheung, H. Zhu, Y. Guan, T.T. Lam); University of Hong Kong School of Public Health, Hong Kong (E.F. Miot, B.M. Worthington, K.H. Ng, L. de Guilhem de Lataillade, M.P. Pierce, Y. Liao, R. Ko, M.H. Shum, W.Y. Cheung, H. Zhu, L.L. Poon, M.J. Peiris, Y. Guan, G.M. Leung, J.T. Wu, T.T. Lam); University of Hong Kong HKU-Pasteur Research Pole, Hong Kong (E.F. Miot, L. de Guilhem de Lataillade, L.L. Poon, J.S.M. Peiris); Centre for Immunology & Infection Limited, Hong Kong (E.F. Miot, L. de Guilhem de Lataillade, L.L. Poon,

[1]These coauthors contributed equally to this article.

M.J. Peiris, T.T. Lam); Shantou University/University of Hong Kong Guangdong-Hongkong Joint Laboratory of Emerging Infectious Diseases, Shantou, Guangdong, China. (B.M. Worthington, W.Y. Cheung, H. Zhu, Y. Guan, T.T. Lam); EKIH (Gewuzhikang) Pathogen Research Institute, Shenzhen City, Guangdong, China. (B.M. Worthington, W.Y. Cheung, H. Zhu, Y. Guan, T.T. Lam); Laboratory of Data Discovery for Health Limited, Hong Kong, China (W.Y. Cheung, E.C. Holmes, K.S. Leung, H. Zhu, Y. Guan, G.M. Leung, J.T. Wu, T.T. Lam); Marie Bashir Institute for Infectious Diseases and Biosecurity, University of Sydney School of Biological Sciences, and Sydney Medical School, Sydney, New South Wales, Australia (E.C. Holmes)

DOI: https://doi.org/10.3201/eid2802.211586

We report surveillance conducted in 217 pestiferous rodents in Hong Kong for severe acute respiratory syndrome coronavirus 2 (SARS-CoV-2). We did not detect SARS-CoV-2 RNA but identified 1 seropositive rodent, suggesting exposure to a virus antigenically similar to SARS-CoV-2. Potential exposure of urban rodents to SARS-CoV-2 cannot be ruled out.

Severe acute respiratory syndrome coronavirus 2 (SARS-CoV-2) was first identified in Wuhan, China, in late 2019 (*1*) and soon spread globally. Although its zoonotic origin remains unclear, animal species potentially susceptible to reverse-zoonotic transmission from humans have been identified (e.g., cats, dogs, minks, deer), some of which (e.g., mink) might maintain the virus and pose a risk of future spillback to humans (*2*,*3*). Domestic animals and urban wildlife are of particular concern (*4*) because of their potential exposure to viruses shed within urban environments. Analysis of the angiotensin-converting enzyme 2 (ACE2) receptor across diverse vertebrates suggests a potentially wide breadth of SARS-CoV-2–susceptible mammal host species (*5*).

The rapid transmission and adaptation of SARS-CoV-2 in humans has been characterized by the evolution of variants of concern (VOCs). Several VOCs, particularly the Alpha (B.1.1.7), Beta (B.1.351), and Gamma (P.1) variants, have convergently evolved an amino acid residue change in the receptor binding domain of the spike protein (N501Y) that was also observed following serial passage of SARS-CoV-2 in BALB/c mice (*6*). Recent in vitro and in vivo experiments have demonstrated that these VOCs are capable of infecting laboratory rats and mice (*7*; Montagutelli X et al., unpub. data, https://doi.org/10.1101/2021.03.18.436013). Such evolutionary processes indicate a possible risk for reverse-zoonotic transmission of VOCs into urban rodents.

We hypothesized that locations with positive SARS-CoV-2 detection in sewage could also serve as key surveillance targets for potential exposure of pestiferous urban rodents to SARS-CoV-2 shed into the environment. We conducted sewage surveillance in Hong Kong to identify hidden infections and localized outbreaks of SARS-CoV-2 (*8*) during the fourth wave of COVID-19 in Hong Kong (Appendix, https://wwwnc.cdc.gov/EID/article/28/2/21-1586-App1.pdf).

During February 3–May 12, 2021, we sampled 217 rodents (*Rattus* spp.), 193 live-trapped rodents and 24 found dead near collection sites (Appendix Table 1). We collected 189 *R. norvegicus* and 28 *R. tanezumi* rats from 8 districts, the majority (n = 186) from Sham Shui Po, Yau Tsim Mong, and Kowloon City (Figure), where SARS-CoV-2 positive sewage has been reported.

We found samples from 1,702 swabs and tissues from 217 rats negative for SARS-CoV-2 by real-time quantitative PCR and 15 from 9 rats positive for murine alphacoronaviruses and betacoronaviruses using PCR and phylogenetic analysis (Appendix Table 2, Figure 1). Using ELISA, we identified 1 of 213 rodent serum samples from an *R. norvegicus* rat collected in Yau Ma Tei seropositive for SARS-CoV-2 (Table; Appendix Figure 2) and 11 samples inconclusive; only 1 of 2 replicates from 8 samples gave a positive absorbance result, and 1 or both replicates from 3 samples gave a borderline absorbance (Table; Appendix Figure 2). The unambiguously positive sample, from rat no. 213, was confirmed positive in surrogate virus neutralization testing (sVNT; 31.7% inhibition), but negative by plaque-reduction neutralization test ($PRNT_{90}$; <10 titers for 90% reduction). All 11 inconclusive samples were negative (<20% inhibition) by sVNT. As a pre–COVID-19 biological control to test for cross-sensitivity, 50 rodent serum samples collected in 2008 were examined by ELISA; none exhibited an unambiguously positive result.

Our rodent surveillance in Hong Kong revealed potential exposure to SARS-CoV-2, and although viral RNA was not detected, this could be a limitation of sample size if prevalence of active infection was low. One serum sample showed positive ELISA and sVNT results but negative $PRNT_{90}$ results. Previous research demonstrated that the sVNT used in our study has >98.8% specificity and sensitivity without cross-reaction to alphacoronaviruses and murine betacoronavirus (*9*). Some sVNT-positive COVID-19–confirmed patients did not meet the threshold for positivity by $PRNT_{90}$ (*9*). This finding suggests that the seropositive result for SARS-CoV-2 or a closely related virus in the brown rat was unlikely to be attributable to past exposure to murine alphacorona-

viruses or betacoronaviruses.

During our study period, SARS-CoV-2 infection was reported in several imported and local human cases in multiple locations and in multiple sewage results. Before December 2020, SARS-CoV-2 locally circulating in Hong Kong predominantly carried 501N with presumably lower rodent infectivity; however, during our study period, Hong Kong reported many imported cases of SARS-CoV-2 variants, including B.1.1.7 and B.1.351, carrying 501Y, which has been demonstrated in mouse experiments to be a critical genetic adaptation (*6*). These imported cases might disseminate virus into the environment near quarantine hotels, presenting an increased risk of spillover into urban rodent populations and requiring enhanced biosecurity to

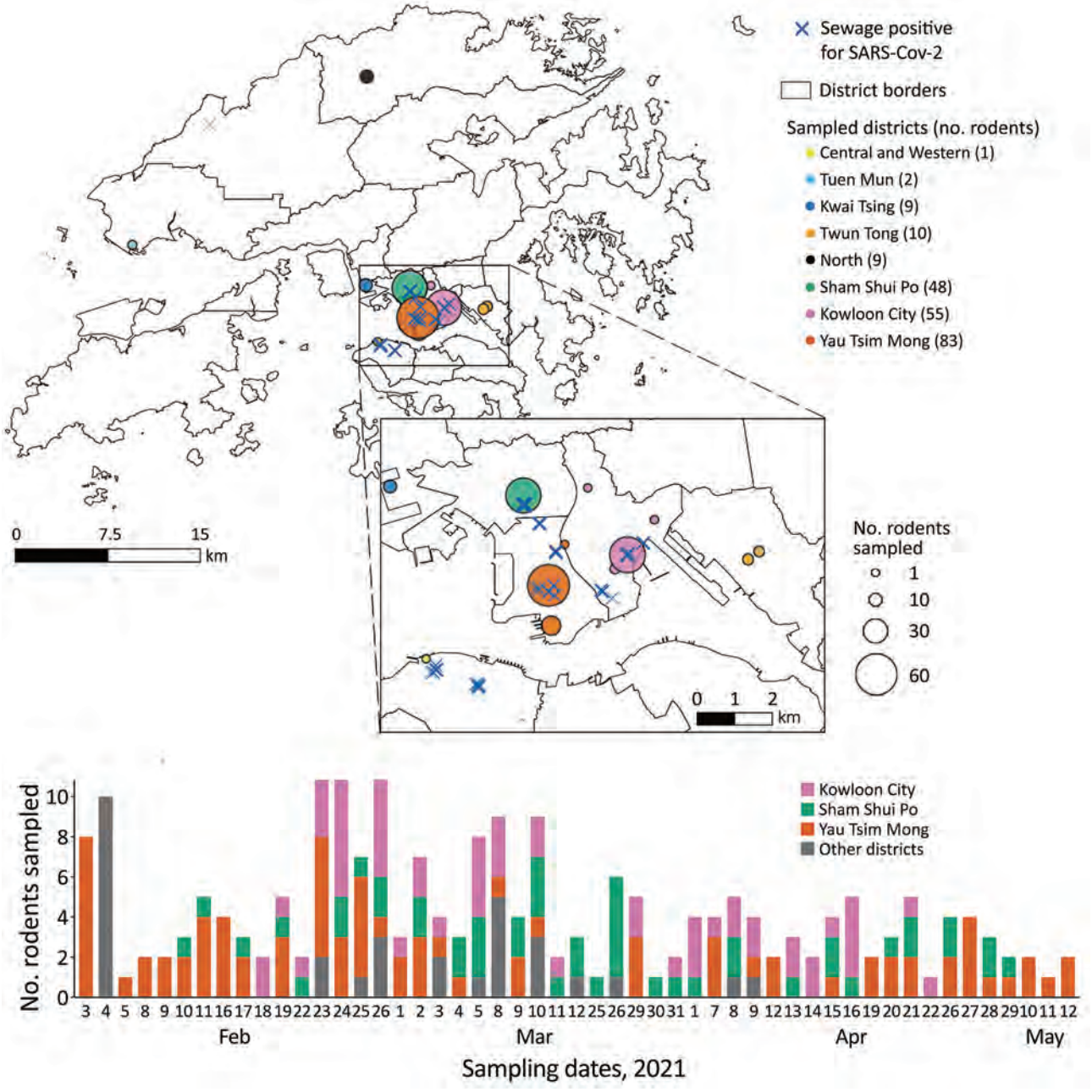

Figure. Surveillance of rodents for SARS-COV-2 conducted February–May 2021 in Hong Kong. A) Sampling sites, with number of rodents sampled and sewage testing positive for SARS-COV-2. Each circle represents a sampling location, color-coded by district and sized proportional to the number of captured rodents. Blue crosses represent locations where sewage was reported positive for SARS-COV-2during January 19–March 30, 2021. B) Number of sampled rodents, by collection dates and district. SARS-COV-2, severe acute respiratory syndrome coronavirus 2

Table. Information on rodents with unambiguous (n = 1) or inconclusive (n = 11) positive serum samples in ELISA testing in study of surveillance of rodent pests for severe acute respiratory syndrome coronavirus 2 and other coronaviruses, Hong Kong*

Animal code	*Rattus* species	Collection date	District	ELISA A/CO		sVNT, inhibition, %
				1st replicate	2nd replicate	
Rat-027	*R. tanezumi*	Feb 11	Sham Shui Po	0.019	0.855	1.281
Rat-069	*R. norvegicus*	Feb 24	Kowloon City	0.837	0.964	0.991
Rat-070	*R. norvegicus*	Feb 24	Kowloon City	1.199	0.472	–2.128
Rat-073	*R. tanezumi*	Feb 25	Yau Tsim Mong	1.445	0.033	2.224
Rat-076	*R. norvegicus*	Feb 25	Sham Shui Po	1.644	0.027	1.136
Rat-089	*R. norvegicus*	Mar 1	Yau Tsim Mong	1.324	–0.041	1.209
Rat-090	*R. norvegicus*	Mar 1	Yau Tsim Mong	1.636	–0.027	–0.532
Rat-096	*R. norvegicus*	Mar 2	Yau Tsim Mong	0.934	–0.007	3.748
Rat-097	*R. norvegicus*	Mar 2	Yau Tsim Mong	1.592	0.013	–4.666
Rat-098	*R. tanezumi*	Mar 2	Sham Shui Po	1.920	–0.724	–2.466
Rat-102	*R. norvegicus*	Mar 3	Kwai Tsing	0.992	–0.499	0.145
Rat-213†	*R. norvegicus*	May 10	Yau Tsim Mong	13.643	14.497	31.7

*A/CO was interpreted as negative if <0.9, borderline if 0.9–1.1, and seropositive if >1.1, according to manufacturer instructions. Serum was considered unambiguously positive if both replicates were seropositive. Positive cutoff for sVNT was 20% inhibition, as described elsewhere (*9*).
A/CO, absorbance cutoff; sVNT, surrogate virus neutralization test.
†Positive in both ELISA and sVNT.

limit potential exposure to urban rodents or other susceptible animals. Our finding of potential SARS-CoV-2 exposure in a pestiferous rat highlights the need for sustained monitoring of rodent populations to rapidly detect spillover events and subsequently put in place timely interventions (e.g., disinfestation using trapping and pesticide) to prevent potential establishment of new reservoirs.

Acknowledgments

We gratefully thank M.W. Lee, S.K. Hung, S.T. Lui, P.H. Yuen, and other staff from the Food and Environmental Hygiene Department who provided assistance with trapping and euthanizing rodents.

This work was supported by National Science Foundation of China Excellent Young Scientists Fund (Hong Kong and Macau) (31922087), Guangdong-Hong Kong-Macau Joint Laboratory Program (2019B121205009), National Key R&D Program of China (2017YFE0190800), and US National Institute of Allergy and Infectious Diseases (U01AI151810).

About the Author

Dr. Miot is a postdoctoral researcher at the Centre for Immunology and Infection, HKU-Pasteur Research Pole, State Key Laboratory of Emerging Infectious Diseases, and University of Hong Kong School of Public Health. His research interest is vectorborne diseases.

References

1. Wu F, Zhao S, Yu B, Chen YM, Wang W, Song ZG, et al. A new coronavirus associated with human respiratory disease in China. [Correction in Nature. 2020;580:E7]. Nature. 2020;579:265–9. https://doi.org/10.1038/s41586-020-2008-3
2. Chandler JC, Bevins SN, Ellis JW, Linder TJ, Tell RM, Jenkins-Moore M, et al. SARS-CoV-2 exposure in wild white-tailed deer (*Odocoileus virginianus*). Proc Natl Acad Sci U S A. 2021;118:e2114828118. https://doi.org/10.1073/pnas.2114828118
3. Oude Munnink BB, Sikkema RS, Nieuwenhuijse DF, Molenaar RJ, Munger E, Molenkamp R, et al. Transmission of SARS-CoV-2 on mink farms between humans and mink and back to humans. Science. 2021;371:172–7. https://doi.org/10.1126/science.abe5901
4. Bosco-Lauth AM, Root JJ, Porter SM, Walker AE, Guilbert L, Hawvermale D, et al. Peridomestic mammal susceptibility to severe acute respiratory syndrome coronavirus 2 infection. Emerg Infect Dis. 2021;27:2073–80. https://doi.org/10.3201/eid2708.210180
5. Damas J, Hughes GM, Keough KC, Painter CA, Persky NS, Corbo M, et al. Broad host range of SARS-CoV-2 predicted by comparative and structural analysis of ACE2 in vertebrates. Proc Natl Acad Sci U S A. 2020;117:22311–22. https://doi.org/10.1073/pnas.2010146117
6. Gu H, Chen Q, Yang G, He L, Fan H, Deng YQ, et al. Adaptation of SARS-CoV-2 in BALB/c mice for testing vaccine efficacy. Science. 2020;369:1603–7. https://doi.org/10.1126/science.abc4730
7. Shuai H, Chan JF, Yuen TT, Yoon C, Hu JC, Wen L, et al. Emerging SARS-CoV-2 variants expand species tropism to murines. EBioMedicine. 2021;73:103643. https://doi.org/10.1016/j.ebiom.2021.103643
8. Xu X, Zheng X, Li S, Lam NS, Wang Y, Chu DKW, et al. The first case study of wastewater-based epidemiology of COVID-19 in Hong Kong. Sci Total Environ. 2021;790:148000. https://doi.org/10.1016/j.scitotenv.2021.148000
9. Perera RAPM, Ko R, Tsang OTY, Hui DSC, Kwan MYM, Brackman CJ, et al. Evaluation of a SARS-CoV-2 surrogate virus neutralization test for detection of antibody in human, canine, cat, and hamster sera. J Clin Microbiol. 2021;59:e02504–20. https://doi.org/10.1128/JCM.02504-20

Address for correspondence: Joseph Tsz-Kei Wu, School of Public Health, University of Hong Kong, 7 Sassoon Road, Pokfulam, Hong Kong, China; email: joewu@hku.hk;
Tommy Tsan-Yuk Lam, State Key Laboratory of Emerging Infectious Diseases, School of Public Health, University of Hong Kong, 21 Sassoon Road, Pokfulam, Hong Kong, China;

email: ttylam@hku.hk

Spillover of Canine Parvovirus Type 2 to Pigs, South Dakota, USA, 2020

Gun Temeeyasen, Tamer A. Sharafeldin, Chun-Ming Lin, Ben M. Hause

Author affiliation: South Dakota State University, Brookings, South Dakota, USA

In 1978, canine parvovirus type 2 originated from spillover of a feline panleukopenia–like virus, causing a worldwide pandemic of enteritis and myocarditis among canids. In 2020, the virus was identified in pigs in South Dakota, USA, by PCR, sequencing, in situ hybridization, and serology. Genetic analysis suggests spillover from wildlife.

DOI: https://doi.org/10.3201/eid2802.211681

Canine parvovirus type 2 (CPV-2) is a variant of the species *Carnivore protoparvovirus 1*, which can cause severe disease in carnivores of many species (*1*–*3*). Besides CPV-2, which causes enteritis in dogs of all ages and myocarditis in puppies, the virus species includes feline panleukopenia virus, which causes severe enteritis and leukopenia in cats of all ages (*4*). In 1978, CPV-2 emerged and caused a worldwide pandemic after spillover from a feline panleukopenia virus–like virus in wildlife. Subsequent adaptation to canine hosts led to genetic and antigenic diversification into subtypes 2a, 2b, and 2c (*5*). Continued CPV host switching has been documented; spillover to wildlife (including skunks, raccoons, coyotes) has resulted in clinical disease and asymptomatic infection (*2*).

In October 2020, a dead pig was submitted to South Dakota State University (Brookings, SD, USA) for diagnostic testing. Histopathologic examination revealed mild to moderate enteritis, hepatitis, and visceral edema. Hemolytic *Escherichia coli* was isolated. No significant lung lesions were noted. Approximately 8 months later, we performed viral metagenomic sequencing on archived lung tissue for an unrelated research project and unexpectedly identified CPV-2. Using a 5′-nuclease PCR (Integrated DNA Technologies, https://www.idtdna.com), we confirmed that the sample was CPV-2 positive; cycle threshold (C_t) was 24.4. Sanger sequencing of overlapping amplicons confirmed the CPV-2 genome sequence determined by metagenomic sequencing. We submitted the strain SDS21601 sequence to GenBank (accession no. MZ666397).

We used a 5′-nuclease PCR to test 90 archived porcine lung samples submitted for respiratory disease diagnostic testing for CPV-2. Of the 90 samples, 9 (10%) were positive for CPV-2, including those with strain SDS21601, and C_t values were 22.4–36.3. The samples were collected September–November 2020 from swine farms within 150 miles of Brookings. We sequenced the genome from a second strongly positive sample (C_t 22.4) and submitted strain SDS21608 to GenBank (accession no. MZ666398). An amplicon from 4 of the remaining 7 samples positive by PCR was generated by PCR and confirmed as CPV-2 by Sanger sequencing. The 3 samples that failed to yield a CPV-2–specific amplicon had C_t values >32. Sequence comparison showed 99.9% nt identity between SDS21601 and SDS21608. blastp (https://blast.ncbi.nlm.nih.gov) analysis of SDS21601 virus capsid protein (VP) 2 found 100% identity to CPV-2 from a coyote sampled in Montana in 2012. Analysis of the VP2 amino acid sequences identified an F212I mutation previously identified only from US wildlife, mainly coyotes.

We performed in situ hybridization on archived formalin-fixed paraffin-embedded tissues from SDS21608 by using a commercially available CPV-2 probe. CPV-2 nucleic acids were hybridized sporadically as intracytoplasmic punctate signals in few monocyte–macrophage lineage cells in the medullary and subcapsular sinuses of a bronchial lymph node (Figure). However, the primary anatomic site of CPV-2 infection and replication was not determined. In other examined tissues, we observed neither typical

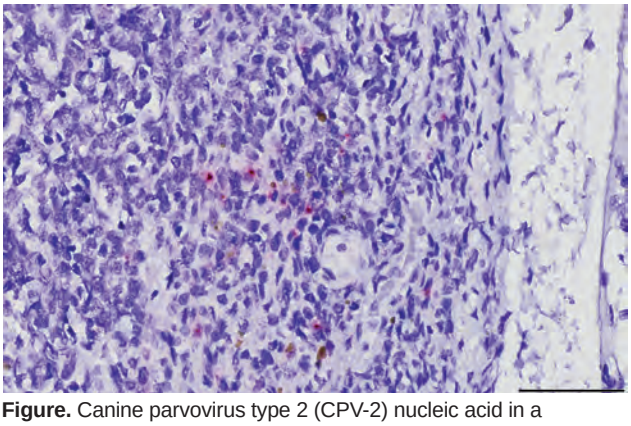

Figure. Canine parvovirus type 2 (CPV-2) nucleic acid in a bronchial lymph node obtained from a commercial pig, South Dakota, USA, 2020. Virus was detected by in situ hybridization with a commercially available CPV-2 probe (Advanced Cell Diagnostics, https://acdbio.com). Signals of CPV-2 nucleic acid were hybridized as intracytoplasmic red pinpoints in a few cells morphologically resembling monocyte–macrophage lineage cells in the medullary sinus. Golden-brown pigments are suggestive of hemosiderin accumulated in the cytoplasm of macrophages. The slide was counter-stained with hematoxylin. Scale bar indicates 50 μm.

Table. Antibody titers for CPV-2 and PPV-1 in serum collected from multiparous sows at origin farm of CPV-2 strain SDS21601 ≈8 months after collection of CPV-2–positive lungs, South Dakota, USA, 2020

Sow no.	CPV-2 titer	PPV-1 titer
3818	20	16
8985	10	256
3407	20	1024
4344	0	256
4345	10	512
3406	0	2048
3410	0	4096
37681	10	4096
38679	20	4096
39692	0	1024
4347	20	64
37683	20	2048
37673	40	2048
8980	0	256
445	10	512
8952	10	512
8953	0	2048
8981	20	1024
3817	20	0
10040	0	128

*Determined by hemagglutination inhibition. CPV-2, canine parvovirus type 2; HI, hemagglutination inhibition; PPV-1, porcine parvovirus type 1.

virus-associated microscopic lesions as seen in carnivores nor obvious CPV-2 hybridization signals.

To further investigate the extent of CPV-2 circulation among swine, 8 months after collection of the CPV-2–positive lung tissue, we collected 20 serum samples from multiparous sows on the farm where strain SDS21601 originated. Of the 20 samples, 13 (65%) were positive for CPV-2–specific antibodies by hemagglutination inhibition (HI) assay; titers were 10–40 (Table). Nearly all serum samples (19 of 20) had antibody titers to porcine parvovirus 1 (PPV-1), ranging from 16 to 4,096. This result was expected given that pigs on the farm received commercial PPV-1 vaccine before farrowing. There was no correlation between CPV-2 and PPV-1 HI titers, indicating a lack of cross-reactivity between CPV-2 and PPV-1 antibodies in the HI assay.

To further investigate seroprevalence of CPV-2 in South Dakota, we randomly selected 25 sow serum samples from unrelated submissions collected at 5 farms (5 samples/farm) and analyzed them by HI for CPV-2. Of the 25 samples, 23 (92%) were positive for CPV-2; titers were 10–80. Together with the 10% positivity detected by quantitative PCR, these results suggest widespread CPV-2 infection of swine in South Dakota.

Members of *Carnivore protoparvovirus 1* display >98% identity. Amino acid residue 300 of VP2 has been shown to be a critical determinant for the cross-species transfer of CPV-2 between carnivores of different species (*6*). Glycine 300 and tyrosine 305, observed in the VP2 of both swine CPV-2 strains (SDS21601 and SDS21608), are diagnostic of CPV-2 isolates from canids (*7*). The F212I mutation present in both swine CPV-2 strains, which was previously found only in wildlife, suggests a sylvatic origin. Of the species in which F212I has been identified, only coyotes are common in the agricultural areas of the upper US Midwest and are peridomestic. We hypothesize that the source of swine CPV-2 infection is CPV-2–positive coyote feces.

Our results demonstrate spillover of CPV-2 to swine. CPV-2 has been associated with severe enteritis in insectivorous Taiwanese pangolin (*Manis pentadactyla pentadactyla*), further demonstrating the propensity of CPV-2 to overcome host barriers (*8*). The ability of CPV-2 to cause disease in swine remains unknown; further surveillance is warranted because this spillover may threaten the health of swine herds.

Acknowledgments

We thank Martha Ohnstad and Craig Long for assistance with metagenomic sequencing.

This project was in part funded by start-up funds provided to B.H. by the South Dakota State University Agricultural Experiment Station Hatch and Animal Health funds in addition to the South Dakota State University Center for Biologics Research and Commercialization.

About the Author

Dr. Temeeyasen is a research associate at the Animal Disease Research and Diagnostic Laboratory, South Dakota State University, in Brookings. His primary research interest is pathogenic porcine and bovine viruses.

References

1. Cotmore SF, Agbandje-McKenna M, Chiorini JA, Mukha DV, Pintel DJ, Qiu J, et al. The family *Parvoviridae*. Arch Virol. 2014;159:1239–47. https://doi.org/10.1007/s00705-013-1914-1
2. Allison AB, Kohler DJ, Fox KA, Brown JD, Gerhold RW, Shearn-Bochsler VI, et al. Frequent cross-species transmission of parvoviruses among diverse carnivore hosts. J Virol. 2013;87:2342–7. https://doi.org/10.1128/JVI.02428-12
3. Steinel A, Parrish CR, Bloom ME, Truyen U. Parvovirus infections in wild carnivores. J Wildl Dis. 2001;37:594–607. https://doi.org/10.7589/0090-3558-37.3.594
4. Parrish CR. Pathogenesis of feline panleukopenia virus and canine parvovirus. Baillieres Clin Haematol. 1995;8:57–71. https://doi.org/10.1016/S0950-3536(05)80232-X
5. Wasik BR, de Wit E, Munster V, Lloyd-Smith JO, Martinez-Sobrido L, Parrish CR. Onward transmission of viruses: how do viruses emerge to cause epidemics after spillover? Philos Trans R Soc Lond B Biol Sci. 2019;374:20190017.

6. Allison AB, Organtini LJ, Zhang S, Hafenstein SL, Holmes EC, Parrish CR. Single mutations in the VP2 300 loop region of the three-fold spike of the carnivore parvovirus capsid can determine host range. J Virol. 2015;90:753–67. https://doi.org/10.1128/JVI.02636-15
7. Allison AB, Kohler DJ, Ortega A, Hoover EA, Grove DM, Holmes EC, et al. Host-specific parvovirus evolution in nature is recapitulated by in vitro adaptation to different carnivore species. PLoS Pathog. 2014;10:e1004475. https://doi.org/10.1371/journal.ppat.1004475
8. Chang YC, Lin ZY, Lin YX, Lin KH, Chan FT, Hsiao ST, et al. Canine parvovirus infections in Taiwanese pangolins (*Manis pentadactyla pentadactyla*). Vet Pathol. 2021;58:743–50. https://doi.org/10.1177/03009858211002198

Address for correspondence: Ben M. Hause, Department of Veterinary and Biomedical Sciences, South Dakota State University, Box 2175, 1155 North Campus Dr, Brookings, SD 57007, USA; email: benjamin.hause@sdstate.edu

Antenatal Seroprevalence of Zika and Chikungunya Viruses, Kingston Metropolitan Area, Jamaica, 2017–2019

Joshua J. Anzinger, Chadwic D. Mears, A.E. Ades, Keisha Francis, Yakima Phillips, Ynolde E. Leys, Moira J. Spyer, David Brown, Ana M. Bispo de Filippis, Eleni Nastouli, Thomas Byrne, Heather Bailey, Paulette Palmer, Lenroy Bryan, Karen Webster-Kerr, Carlo Giaquinto, Claire Thorne, Celia D.C. Christie, on behalf of the ZIKAction Consortium[1,2]

Author affiliations: The Global Virus Network Jamaica Affiliate, Kingston, Jamaica (J.J. Anzinger); The University of the West Indies, Kingston (J.J. Anzinger, C.D. Mears, K. Francis, Y. Phillips, Y.E. Leys, P. Palmer, L. Bryan, C.D.C. Christie); University of Bristol, Bristol, UK (A.E. Ades); University College London, London, UK (M.J. Spyer, E. Nastouli, T. Byrne, H. Bailey, C. Thorne); Instituto Oswaldo Cruz, Rio De Janeiro, Brazil (D. Brown, A.M.B. de Filippis); University College London Hospitals NHS Trust, London (E. Nastouli); Ministry of Health, Kingston (K. Webster-Kerr); University of Padova, Padua, Italy (C. Giaquinto)

To determine the extent of exposure to Zika virus (ZIKV) and chikungunya virus (CHIKV) in Jamaica, we collected serum from 584 pregnant women during 2017–2019. We found that 15.6% had antibodies against ZIKV and 83.6% against CHIKV. These results indicate potential recirculation of ZIKV but not CHIKV in the near future.

DOI: https://doi.org/10.3201/eid2802.211849

The recent introductions of chikungunya virus (CHIKV) and Zika virus (ZIKV) in the Americas led to widespread epidemics with substantial health and economic effects. Small island developing states in the Caribbean are particularly affected by emerging mosquitoborne disease, primarily because of year-round climatic conditions favorable for mosquito breeding, high levels of poverty, and extensive migration.

In Jamaica, introductions of CHIKV in 2014 and ZIKV in 2016 led to epidemics that overwhelmed the healthcare system (*1*,*2*). Despite the Caribbean being greatly affected by the CHIKV and ZIKV epidemics, information regarding the extent of population exposure is limited; most previous studies examined high-resource Caribbean islands. Studies performed after the introduction of CHIKV into the Caribbean showed CHIKV seroprevalence to be Guadeloupe 48.1% (*3*), Haiti 78.7% (*4*), Martinique 41.9% (*3*), Puerto Rico 23.5% (*5*), and Saint Martin 16.9% (*6*). A serosurvey of participants in rural and urban areas in Suriname in 2017 showed a ZIKV seroprevalence of 35.1% overall and 24.5% in a remote village (*7*); in Martinique in 2016, seroprevalence of blood donors was 42.2% (*8*).

To determine seroprevalence in the greater Kingston, St. Andrew, and St. Catherine metropolitan region in Jamaica, we performed a CHIKV IgG and ZIKV IgG serosurvey of 584 pregnant women attending 5 public antenatal clinics in the Kingston Metropolitan Area (KMA) from June 28, 2017, through April 15, 2019. Pregnant women ≥16 years of age attending 1 of the 5 antenatal clinics and planning to deliver at 1 of the 3 KMA public maternity hospitals were eligible for enrollment. The South East Regional Health Authority report of 20,817 total live births at the 3 KMA public maternity hospitals from July 2017 through April 2019 indicates that our study represents ≈3% of

[1]Preliminary results from this study were presented at the 2nd International Conference on Zika Virus and *Aedes* Related Infections; June 14–17, 2018; Tallinn, Estonia.

[2]Members of the ZIKAction Consortium are listed at the end of this article.

pregnant women delivering at a KMA public maternity hospital.

To detect antibodies for each virus, we used the Euroimmun chikungunya virus IgG ELISA (https://www.euroimmun.com) and BLACKBOX Zika virus ELISA (Bernhard-Nocht-Institut für Tropenmedizin, https://www.bnitm.de). Because serologic cross-reactivity with related flaviviruses can be problematic for accurately identifying past ZIKV infections, it is imperative that ZIKV serologic assays account for cross-reactive antibodies. The BLACKBOX Zika virus ELISA is a ZIKV immune complex–binding IgG ELISA that is highly specific and does not show cross-reactivity with dengue virus (DENV) (*9*). For prevalence estimates, we calculated Clopper-Pearson CIs. This study was approved by the University of the West Indies Ethics (ECP 100 18/19) and Ministry of Health Ethics Committees (2017/06).

Among women attending all antenatal clinics, 83.6% (95% CI 80.0%–86.5%, range 72.2%–88.1%) were positive for CHIKV IgG (Table), and 15.6% (95% CI 12.7%–18.8%, range 12.6%–22.4%) of samples tested were positive for ZIKV (Table). Of the 91 ZIKV IgG–positive women, 72 were also positive for CHIKV IgG, indicating a highly significant odds ratio for the association (21.9, 95% CI 13.8–36.7), probably resulting at least in part from the 2 viruses being transmitted primarily by *Aedes aegypti* mosquitoes.

To ensure that the seroprevalence results were not inflated by false positives, we also examined 89 archived serum samples from pregnant women who had attended 1 of the 5 clinics examined (clinic D) during June–December 2013. This period predates CHIKV and ZIKV introductions into Jamaica and was a period of low DENV circulation, similar to 2017–2019 (Ministry of Health Epidemiology Bulletin, https://www.moh.gov). All 89 samples were negative for CHIKV IgG and ZIKV IgG (no results were equivocal), indicating that false-positive results were unlikely to affect the reported CHIKV and ZIKV seroprevalence for 2017–2019.

Our study indicates a high level of past CHIKV infections and a low level of ZIKV exposure among pregnant women in Jamaica receiving antenatal care during 2017–2019. We offer several possible explanations for the higher seroprevalence of CHIKV compared with ZIKV. CHIKV infections result in substantially greater viremia, which could lead to increased transmission rates for CHIKV. In addition to the lower viremia associated with ZIKV, preexisting antibodies to DENV can be cross-protective against ZIKV infection (*10*), which may have limited transmission in Jamaica. During the 2016 ZIKV epidemic in Jamaica, wide circulation of DENV (Appendix Figure, https://wwwnc.cdc.gov/EID/article/28/2/21-1849-App1.pdf) could have limited ZIKV transmission because of cross-reactive antibodies generated during DENV infection or competition between the 2 viruses during cocirculation.

Cases of CHIKV and ZIKV infection in Jamaica have been extremely limited since their initial epidemic years. Only 21 CHIKV cases were reported in Jamaica during 2015–June 2020, and only 1 ZIKV case was reported during 2017–June 2020. CHIKV cases will probably remain limited in Jamaica until a more substantial portion of the population lacks immunity. In contrast, ZIKV could possibly circulate again in Jamaica in the near future because of low population immunity and waning cross-reactive DENV antibodies.

Table. Chikungunya and Zika virus results for 584 pregnant women attending 5 public antenatal clinics, Kingston Metropolitan Area, Jamaica, June 28, 2017–April 15, 2019

Virus, clinic	Tested, no.	Result		
		Negative, no.	Equivocal, no.	Positive, no. (%)
Chikungunya*				
A	54	11	4	39 (72.2)
B	159	19	0	140 (88.1)
C	76	8	2	66 (86.8)
D	197	34	5	158 (80.2)
E	98	9	4	85 (86.7)
Total	584	81	15	488 (83.6)
Zika†				
A	54	44	0	10 (18.5)
B	159	138	1	20 (12.6)
C	76	64	1	11 (14.5)
D	197	166	3	28 (14.2)
E	98	75	1	22 (22.4)
Total	584	487	6	91 (15.6)

*Euroimmun CHIKV IgG ELISA (https://www.euroimmun.com).
†BLACKBOX ZIKV IgG ELISA (https://www.bnitm.de).

Members of the ZIKAction Consortium: A.E. Ades, Joshua J. Anzinger, Heather Bailey, Brittiana Brown, David Brown, Thomas Byrne, Leroy Campbell, C.D.C. Christie, Ana M. Bispo de Filippis, Carla Giaquinto, Georgiana Gordon-Strachan, Marlyn Grindley, Donna Kamicka, Clayton Kelly, John Lindo, Paul Mitchell, Orville Morgan, Eleni Nastouli, Alexander Onyonyor, Paulette Palmer, Russell Pierre, Amanda Rousseau, Sofier Scott, Claire Thorne, and Karen Webster-Kerr.

Acknowledgments

We thank the women who participated in this study, research nurses, pediatricians, medical technologists, and the ZIKAction Project Management team (Francesca Viero and Giorgia Dalla Valle).

As Global Infectious Diseases Scholars, C.M. and Y.L. received mentored research training in the development of this manuscript. This training was supported in part by the University of Buffalo Clinical and Translational Science Institute award UL1TR001412 and the Global Infectious Diseases Research Training Program award D43TW010919.

This project was funded from the Horizon 2020: EU Programme for Research and Innovation under grant agreement no. 734857.

About the Author

Dr. Anzinger is a senior lecturer and director of the Global Virus Network Jamaica Affiliate at the University of the West Indies and is a consultant virologist and head of the virology laboratory at the University Hospital of the West Indies. His research primarily focuses on comorbid disease during chronic HIV infection and emerging mosquitoborne viruses.

References

1. Duncan J, Gordon-Johnson KA, Tulloch-Reid MK, Cunningham-Myrie C, Ernst K, McMorris N, et al. Chikungunya: important lessons from the Jamaican experience. Rev Panam Salud Publica. 2017;41:e60. https://doi.org/10.26633/RPSP.2017.60
2. Webster-Kerr KR, Christie C, Grant A, Chin D, Burrowes H, Clarke K, et al. Emergence of Zika virus epidemic and the national response in Jamaica. West Indian Med J. 2016; 65:243–9.
3. Gallian P, Leparc-Goffart I, Richard P, Maire F, Flusin O, Djoudi R, et al. Epidemiology of chikungunya virus outbreaks in Guadeloupe and Martinique, 2014: an observational study in volunteer blood donors. PLoS Negl Trop Dis. 2017;11:e0005254. https://doi.org/10.1371/journal.pntd.0005254
4. Poirier MJ, Moss DM, Feeser KR, Streit TG, Chang G-JJ, Whitney M, et al. Measuring Haitian children's exposure to chikungunya, dengue and malaria. Bull World Health Organ. 2016;94:817–825A.
5. Simmons G, Brès V, Lu K, Liss NM, Brambilla DJ, Ryff KR, et al. High incidence of chikungunya virus and frequency of viremic blood donations during epidemic, Puerto Rico, USA, 2014. Emerg Infect Dis. 2016;22:1221–8. https://doi.org/10.3201/eid2207.160116
6. Gay N, Rousset D, Huc P, Matheus S, Ledrans M, Rosine J, et al. Seroprevalence of Asian lineage chikungunyua virus infection on Saint Martin Island, 7 months after the 2013 emergence. Am J Trop Med Hyg. 2016;94:393–6. https://doi.org/10.4269/ajtmh.15-0308
7. Langerak T, Brinkman T, Mumtaz N, Arron G, Hermelijn S, Baldewsingh G, et al. Zika virus seroprevalence in urban and rural areas of Suriname, 2017. J Infect Dis. 2019;220:28–31. https://doi.org/10.1093/infdis/jiz063
8. Gallian P, Cabié A, Richard P, Paturel L, Charrel RN, Pastorino B, et al. Zika virus in asymptomatic blood donors in Martinique. Blood. 2017;129:263–6. https://doi.org/10.1182/blood-2016-09-737981
9. Ehmen C, Medialdea-Carrera R, Brown D, Bispo de Filippis AM, de Sequeira PC, Nogueira RMR, et al. Accurate detection of Zika virus IgG using a novel immune complex binding ELISA. Trop Med Int Health. 2020.
10. Rodriguez-Barraquer I, Costa F, Nascimento EJM, Nery N, Castanha PMS, Sacramento GA, et al. Impact of preexisting dengue immunity on Zika virus emergence in a dengue endemic region. Science. 2019;363:607–10. https://doi.org/10.1126/science.aav6618

Address for correspondence: Joshua J. Anzinger, Department of Microbiology, The University of the West Indies, Kingston, Jamaica; email: joshua.anzinger@uwimona.edu.jm

Group IV Getah Virus in *Culex* Mosquitoes, Malaysia

Sing-Sin Sam, Noor-Adila Mohamed-Romai-Noor, Boon-Teong Teoh, Zur-Raiha Hamim, Hoi-Ying Ng, Juraina Abd-Jamil, Chee-Sieng Khor, Sharifah-Syed Hassan, Hamdan Ahmad, Sazaly AbuBakar

Author affiliations: Universiti Malaya, Kuala Lumpur, Malaysia (S.-S. Sam, N.-A. Mohamed-Romai-Noor, B.-T. Teoh, Z.-R. Hamim, H.-Y. Ng, J. Abd-Jamil, C.-S. Khor, S. AbuBakar); Monash University Malaysia, Selangor, Malaysia (S.-S. Hassan); Universiti Sains Malaysia, Pulau Pinang, Malaysia (H. Ahmad)

DOI: https://doi.org/10.3201/eid2802.204887

A new Getah virus (GETV) strain, B254, was isolated from *Culex fuscocephalus* mosquitoes captured at Mount Ophir, Malaysia, in 2012. Phylogenetic analyses revealed that GETV B254 is distinct from the old Malaysia GETV MM2021 strain but closely related to group IV GETV from Russia (LEIV16275Mag), China (YN12031), and Thailand (GETV/SW/Thailand/2017).

Getah virus (GETV) is an emerging mosquitoborne alphavirus of the family *Togaviridae*. The virus was first reported in 1955 from *Culex gelidus* mosquitoes collected near Kuala Lumpur, Malaysia (*1*). Serologic evidence of GETV infection was found in various large domestic mammals (*2*) and humans (*3*). GETV infections in these populations, however, were mostly inapparent. In other regions, reproductive failures in pregnant sows, death in piglets, and hind limb edema in racehorses, as well as neurologic symptoms and death in blue foxes, have been reported (*4*–*7*).

We conducted mosquito surveillance in the forests of 4 different states in Peninsular Malaysia, Perak, Pahang, Selangor, and Johor, during 2011–2014. We captured a total of 4,160 mosquitoes from the study sites by BG-Sentinel CO_2 trap (Biogents AG, https://eu.biogents.com) with the addition of UV light and sorted them into 208 pools according to their species, determined by morphologic keys, and collection sites. We homogenized the pooled mosquitoes, inoculated them into C6/36 mosquito cells, and blind passaged for 5 passages. We obtained cytopathic effects from 1 of the pools on day 4 postinfection during the last passage. The pool comprised *Cx. fuscocephalus* mosquitoes collected from the forested area at Mount Ophir (Malay: Gunung Ledang) in Johor in 2012. We screened the culture supernatants by reverse transcription PCR (RT-PCR) using the in-house developed alphavirus generic primers targeting the nsP4 gene and flavivirus primers targeting the nonstructural 5–3′ untranslated region junction. A similar sample pool that showed cytopathic effects was found positive for the presence of alphaviruses, as indicated by a 683 bp amplicon. Sanger sequencing of the amplicon revealed high sequence similarity to GETV. We obtained the complete coding sequence of the GETV isolate, designated as B254, using 10 pairs of RT-PCR amplification primers and genome sequencing. We deposited the genome in GenBank (accession no. LR990838).

We constructed a maximum clade credibility tree using the Bayesian Markov chain Monte Carlo analysis based on the complete coding regions of GETV B254 and other GETV isolates available in GenBank (Figure). The GETV phylogeny revealed 4 major groups of viruses: group I (GI), GII, GIII, and GIV (*8*). GI and GII consisted of early identified GETV isolates; GI contained the Malaysia MM2021 isolate (1955), and GII, Japan Sagiyama (1956). The GIII and GIV comprised the

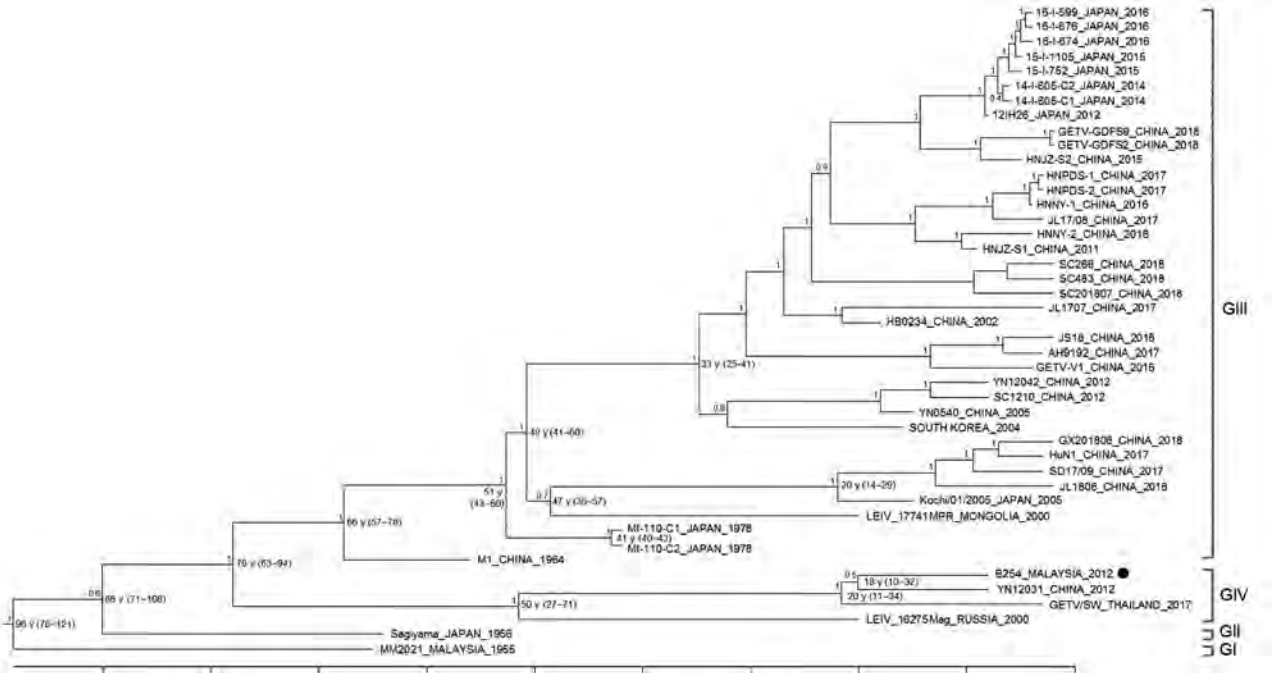

Figure. Maximum-clade credibility tree of complete coding sequences of Getah virus (GETV) strain B254 from Malaysia (black dot) and reference strains. Horizontal branches are drawn to a scale of estimated year of divergence. Times to the most recent common ancestor with 95% highest posterior density values (ranges in parentheses) are shown at nodes. Posterior probability values ≥0.6 of key nodes are shown. G, group.

most recent circulating virus strains. The newly isolated Malaysia GETV B254 is phylogenetically distinct from the ancestral Malaysia MM2021. It clustered within the GIV clade, which included the strains recovered in Russia (LEIV16275Mag, 2007), China (YN12031, 2012) and Thailand (GETV/SW/Thailand/2017). The B254 strain showed the highest nucleotide sequence homology with YN12031 (98.8%), isolated from the *Armigeres subalbatus* mosquito, and GETV/SW/Thailand/2017 (98.6%), isolated from pig serum.

Currently, only the GIII GETV lineage is associated with epidemic outbreaks. The GIV GETV, however, consisted of only a few virus strains. We calculated the mean evolutionary rate of GIV GETV at 4.10×10^{-4} substitutions/site/year and the rate for GIII at 2.98×10^{-4} substitutions/site/year. These results suggest that the GIV viruses may be under a different selection pressure, potentially involving a different host. It is also possible that GIV viruses are maintained in a yet-to-be-identified enzootic transmission cycle involving mosquitoes and asymptomatic hosts.

The *Culex* mosquitoes, particularly *Cx. gelidus* and *Cx. tritaeniorhynchus*, have been identified as the most predominant vector host for GETV in Malaysia (*1*,*2*). *Cx. fuscocephalus* mosquitoes, however, are not an uncommon vector; they have been known to carry the virus in China and Sri Lanka (*9*,*10*). *Cx. fuscocephalus* mosquitoes could be an emerging vector for GETV transmission in Malaysia along with the other *Culex* mosquitoes.

The high similarity of genome sequences of GIV GETV strains recovered thousands of kilometers apart raised the possibility that the virus may share a common dispersal route. One possible route linking the virus is the East Asian–Australasian flyway of migratory birds. GIV GETV could have been introduced to the regions through the migratory birds along the flyway, which included Malaysia as one of the stopover sites; the abundantly available *Culex* mosquitoes at the roosting sites could have maintained the transmission.

In summary, we identified a new GETV strain, B254, in Malaysia that is phylogenetically distinct from the old Malaysia MM2021 strain. The virus strain shares high similarities to the widely distributed GIV GETV. Although further surveillance studies are needed for confirmation, this finding suggests that GIV GETV strains could share a common dispersal origin, possibly through the bird transmigratory flyways.

Acknowledgments

We thank World Refence Center for Emerging Viruses and Arboviruses, The University of Texas Medical Branch, Galveston, USA, for kindly providing us with the Malaysia GETV strain MM2021.

This study was supported in parts by the Ministry of Education Malaysia for niche area research under the Higher Institution Centre of Excellence (HICoE) program (project MO002–2019), the Fundamental Research Grant Scheme (FRGS FP014-2019A), and the Long Term Research Grant Scheme (LRGS/2011A/UM/Penyakit-Berjangkit).

About the Author

Dr. Sam is a researcher at Tropical Infectious Diseases Research and Education Centre, Universiti Malaya. Her primary research interest is emerging mosquitoborne viral diseases.

References

1. Simpson DI, Way HJ, Platt GS, Bowen ET, Hill MN, Kamath S, et al. Arbovirus infections in Sarawak, October 1968–February 1970: GETAH virus isolations from mosquitoes. Trans R Soc Trop Med Hyg. 1975;69:35–8. https://doi.org/10.1016/0035-9203(75)90008-5
2. Marchette NJ, Rudnick A, Garcia R, MacVean DW. Alphaviruses in peninusular Malaysia: I. virus isolations and animal serology. Southeast Asian J Trop Med Public Health. 1978;9:317–29.
3. Marchette NJ, Rudnick A, Garcia R. Alphaviruses in peninsular Malaysia: II. serological evidence of human infection. Southeast Asian J Trop Med Public Health. 1980;11:14–23.
4. Brown CM, Timoney PJ. Getah virus infection of Indian horses. Trop Anim Health Prod. 1998;30:241–52. https://doi.org/10.1023/A:1005079229232
5. Nemoto M, Bannai H, Tsujimura K, Kobayashi M, Kikuchi T, Yamanaka T, et al. Getah virus infection among racehorses, Japan, 2014. Emerg Infect Dis. 2015;21:883–5. https://doi.org/10.3201/eid2105.141975
6. Yang T, Li R, Hu Y, Yang L, Zhao D, Du L, et al. An outbreak of Getah virus infection among pigs in China, 2017. Transbound Emerg Dis. 2018;65:632–7. https://doi.org/10.1111/tbed.12867
7. Shi N, Li LX, Lu RG, Yan XJ, Liu H. Highly pathogenic swine Getah virus in blue foxes, eastern China, 2017. Emerg Infect Dis. 2019;25:1252–4. https://doi.org/10.3201/eid2506.181983
8. Li YY, Liu H, Fu SH, Li XL, Guo XF, Li MH, et al. From discovery to spread: the evolution and phylogeny of Getah virus. Infect Genet Evol. 2017;55:48–55. https://doi.org/10.1016/j.meegid.2017.08.016
9. Peiris JS, Amerasinghe PH, Amerasinghe FP, Calisher CH, Perera LP, Arunagiri CK, et al. Viruses isolated from mosquitoes collected in Sri Lanka. Am J Trop Med Hyg. 1994;51:154–61. https://doi.org/10.4269/ajtmh.1994.51.154
10. Zhang HL, Zhang YZ, Yang WH, Feng Y, Nasci RS, Yang J, et al. Mosquitoes of Western Yunnan Province, China: seasonal abundance, diversity, and arbovirus associations. PLoS One. 2013;8:e77017. https://doi.org/10.1371/journal.pone.0077017

Address for correspondence: Sazaly AbuBakar, Tropical Infectious Diseases Research and Education Centre and Department of Medical Microbiology, Faculty of Medicine, Universiti Malaya, 50603 Kuala Lumpur, Malaysia; email: sazaly@um.edu.my

Rickettsiosis Caused by *Rickettsia parkeri*, Mexico

Gaspar Peniche-Lara,[1] Victor Lara-Perera[1]

Author affiliations: Universidad Autónoma de Yucatán Facultad de Medicina, Merida, Mexico (G. Peniche-Lara); Hospital General Agustin O'Horan, Secretaria de Salud de Yucatán, Merida (V. Lara-Perera)

DOI: https://doi.org/10.3201/eid2802.210454

We report a human case of rickettsiosis caused by *Rickettsia parkeri* strain Atlantic Rainforest in Mexico in an adult woman from a small town in the north of Yucatan, Mexico. We confirmed diagnosis using conventional PCR and sequence analysis. Health providers should be aware of clinical manifestations of rickettsioses in this region.

Rickettsiosis caused by *Rickettsia felis*, *R. rickettsii*, and *R. typhi* is commonly reported in Mexico, mostly in the states of Sonora, Sinaloa, and Baja California (*R. rickettsii*) and Yucatan (*R. felis*, *R. rickettsii*, and *R. typhi*) (*1*). Rickettsiosis caused by *R. parkeri* (*R. parketri*) is a recently discovered disease. The first human case was reported in United States in 2004, and the bacterium was subsequently found in South America (*2*–*5*). *R. parkeri* infection is less virulent than infection with *R. rickettsii*, the agent of Rocky Mountain spotted fever. Signs and symptoms of *R. parkeri* infection are fever, rash, myalgia, and headache. Presence of eschar lesions at the inoculation site are common (*5*). In Mexico, *R. parkeri* strain Atlantic Rainforest has been identified in *Amblyomma ovale* ticks in Veracruz, *R. parkeri* sensu stricto in *A. maculatum* ticks collected from dogs in Sonora, and *R. parkeri* strain Black Gap in *Dermacentor parumapertus* ticks in Sonora and Chihuahua (*6*). These tick species are well distributed in Mexico; *A. ovale* ticks have been identified in northern, central, and southern areas and *A. maculatum* and *D. parumapertus* ticks in northern and central Mexico (*7*), suggesting that *R. parkeri* could be present in the entire country. We document a human case of *R. parkeri* rickettsiosis in the state of Yucatan.

In January 2020, a 48-year-old woman from the municipality of Dzemul in northeastern Yucatan, where no previous cases of rickettsioses had been reported, went to a local health center because of fever (38°C) persisting for 2 days, myalgia, arthralgia in both legs, and abdominal pain. She had removed 2 ticks from her right upper back 2 days before seeking treatment (Figure). The patient stated that she had not traveled to other states or countries or to other regions within the Yucatan in the previous 2 months. Medics prescribed acyclovir and ibuprofen, but signs and symptoms persisted. The patient was therefore admitted to Hospital General Agustin O'Horan in Merida, the capital city of Yucatan. At the time of admission, the patient had fever (38°C), abdominal pain, diffuse arthralgias without rash, and left axillary lymphadenopathy. No palpable adenomegaly or hepatosplenomegaly were reported. We observed 2 skin lesions (12 × 15 mm and 11 × 16 mm, with erythematous haloes) at the bite site. The patient also reported itching and slight pain at the site of the tick bites (Figure).

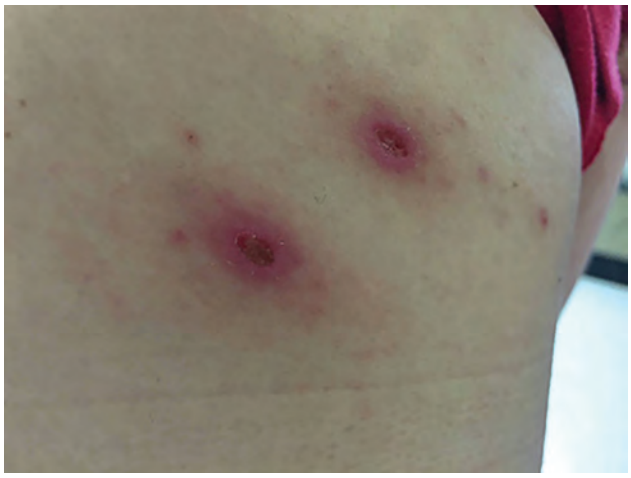

Figure. Tick bite sites identified on the right upper back of a 48-year-old woman from the municipality of Dzemul in northeastern Yucatan, Mexico. The woman received a diagnosis of rickettsiosis caused by *Rickettsia parkeri* strain Atlantic Rainforest.

Based on the tick bite and mild infection, the medic suspected rickettsiosis caused by *R. felis*. For conventional PCR diagnosis, we obtained a 3-mL whole blood sample and sent it to our laboratory. In regions where rickettsiosis caused by *R. parkeri* are common, medics usually take samples from eschar lesions (*5*,*8*,*9*). We obtained a skin biopsy from the eschar lesion 2 days after treatment was initiated. However, conventional PCR analysis returned negative results.

We purified DNA from the blood sample following the instructions from a Quick-gDNA MiniPrep Kit (Zymo Research, https://www.zymoresearch.com) and used conventional PCR to amplify 2 gene fragments (*gltA* and *ompB*) for identifying *Rickettsia* spp. Primer sequences and amplification conditions are described by the Latinamerican Guidelines of RIICER for Diagnosis of Tick-Borne Rickettsiosis (*10*). For the *gltA* gene, we amplified a 380-bp fragment and for the *ompB* gene, a 420-bp fragment. We used sterile water as the nega-

[1]These authors contributed equally to this article.

tive control and *R. typhi* DNA as the positive control. We purified and sequenced products from the PCR. We analyzed DNA sequences using blastn (https://blast.ncbi.nlm.nih.gov/Blast.cgi) and found the amplified products (GenBank accession nos. MW653956 and MW653957) 100% homologous to *R. parkeri* strain Atlantic Rainforest from human cases in Brazil (GenBank accession no. MN027564.1) (*8*) and Colombia (GenBank accession no. MK860201.1) (*5*), as well as to a recently identified *R. parkeri* isolate (GenBank accession no. MK814825.1) from *A. ovale* in Veracruz, Mexico. After diagnosing the *Rickettsia* spp. infection, we treated the patient with doxycycline (100 mg 2×/d for 10 d). After day 2, fever and other symptoms ceased.

Our study documents a case of human rickettsiosis caused by *R. parkeri* strain Atlantic Rainforest in Yucatan, Mexico. This finding represents the fifth *Rickettsia* species identified as infecting humans in southeastern Mexico, but in a municipality, Dzemul, with no previous *Rickettsia* spp. infections reported among humans or identified in vectors or reservoir hosts. Because this rickettsiosis causes mild to moderate febrile illness with initial symptoms such as fever, headache, muscle pain, nausea, vomiting, rash (*2*), it might masquerade as dengue fever in our region and other areas where dengue is common.

Our report emphasizes the importance of continuing to characterize clinical manifestations of rickettsioses in Mexico. Health providers in this region should include this recently discovered rickettsiosis in differential diagnoses of febrile illnesses.

Acknowledgments

Dedicated to the late Víctor Manuel Lara-Perera for his clinical and critical medical eye for the identification of rickettsial diseases and great commitment in teaching and medical practice. We will miss you forever.

About the Author

Dr. Peniche-Lara works at Facultad de Medicina at Universidad Autonoma de Yucatán, Mexico. His research focuses on the epidemiology of pathogens transmitted by ticks in southeastern Mexico.

References

1. Sánchez-Montes S, Colunga-Salas P, Lozano-Sardaneta YN, Zazueta-Islas HM, Ballados-González GG, Salceda-Sánchez B, et al. The genus *Rickettsia* in Mexico: current knowledge and perspectives. Ticks Tick Borne Dis. 2021;12:101633. https://doi.org/10.1016/j.ttbdis.2020.101633
2. Paddock CD, Sumner JW, Comer JA, Zaki SR, Goldsmith CS, Goddard J, et al. *Rickettsia parkeri*: a newly recognized cause of spotted fever rickettsiosis in the United States. Clin Infect Dis. 2004;38:805–11. https://doi.org/10.1086/381894
3. Pacheco RC, Venzal JM, Richtzenhain LJ, Labruna MB. *Rickettsia parkeri* in Uruguay. Emerg Infect Dis. 2006;12:1804–5. https://doi.org/10.3201/eid1211.060577
4. Silveira I, Pacheco RC, Szabó MP, Ramos HG, Labruna MB. *Rickettsia parkeri* in Brazil. Emerg Infect Dis. 2007;13:1111–3. https://doi.org/10.3201/eid1307.061397
5. Arboleda M, Acevedo-Gutiérrez LY, Ávila A, Ospina D, Díaz FJ, Walker DH, et al. Human rickettsiosis caused by *Rickettsia parkeri* strain Atlantic Rainforest, Urabá, Colombia. Emerg Infect Dis. 2020;26:3048–50. https://doi.org/10.3201/eid2612.200388
6. Sánchez-Montes S, Ballados-González GG, Hernández-Velasco A, Zazueta-Islas HM, Solis-Cortés M, Miranda-Ortiz H, et al. Molecular confirmation of *Rickettsia parkeri* in *Amblyomma ovale* ticks, Veracruz, Mexico. Emerg Infect Dis. 2019;25:2315–7. https://doi.org/10.3201/eid2512.190964
7. Guzmán Cornejo C, Robbins RG, Guglielmone AA, Montiel-Parra G, Pérez TM. The *Amblyomma* (Acari: Ixodida: Ixodidae) of Mexico: identification keys, distribution and hosts. Zootaxa. 2011;2998:16–38.
8. da Paixão Sevá A, Martins TF, Muñoz-Leal S, Rodrigues AC, Pinter A, Luz HR, et al. A human case of spotted fever caused by *Rickettsia parkeri* strain Atlantic rainforest and its association to the tick *Amblyomma ovale*. Parasit Vectors. 2019;12:471. https://doi.org/10.1186/s13071-019-3730-2
9. Silva-Ramos CR, Hidalgo M, Faccini-Martínez ÁA. Clinical, epidemiological, and laboratory features of *Rickettsia parkeri* rickettsiosis: A systematic review. Ticks Tick Borne Dis. 2021;12:101734. https://doi.org/10.1016/j.ttbdis.2021.101734
10. Oteo JA, Nava S, Sousa R, Mattar S, Venzal JM, Abarca K, et al.; RIICER. [Latinamerican guidelines of RIICER for diagnosis of tick-borne rickettsioses] [in Spanish]. Rev Chilena Infectol. 2014;31:54–65. https://doi.org/10.4067/S0716-10182014000100009

Address for correspondence: Gaspar Fernando Peniche Lara. Laboratorio de Enfermedades Infecciosas y Parasitarias I. Facultad de Medicina. Universidad Autónoma de Yucatán. Mexico. Avenida Itzaes Num 498 entre 59 y 59A. Centro. Mérida, Yucatan, CP 97000, Mexico; email: gaspar.peniche@correo.uady.mx

Novel Anaplasmataceae agents *Candidatus* Ehrlichia hydrochoerus and *Anaplasma* spp. Infecting Capybaras, Brazil

Thállitha S.W.J. Vieira, Flávia C.M. Collere, Larissa D.R. Ferrari, Rafael A. Baggio, Rogério R. Lange, Marcos V. Ferrari, Juan C.M. Duque, Gustavo S. Sanches, Nathália A. Pereira, Daniel M. Aguiar, Marcelo B. Labruna, Rafael F.C. Vieira

Author affiliations: Universidade Federal do Paraná, Curitiba, Brazil (T.S.W.J. Vieira, F.C.M. Collere, L.D.R. Ferrari, R.R. Lange, M.V. Ferrari, J.C.M. Duque, R.F.C. Vieira); Universidade Federal de Minas Gerais, Belo Horizonte, Brazil (R.A. Baggio); Pontifícia Universidade Católica do Paraná, Curitiba (G.S. Sanches); Universidade Federal do Mato Grosso, Cuiabá, Brazil (N.A. Pereira, D.M. Aguiar); Universidade de São Paulo, São Paulo, Brazil (M.B. Labruna); Global One Health initiative, The Ohio State University, Columbus, Ohio, USA (R.F.C. Vieira)

DOI: https://doi.org/10.3201/eid2802.210705

We amplified *Ehrlichia* and *Anaplasma* DNA from *Amblyomma dubitatum* tick–infested capybaras (*Hydrochoerus hydrochaeris*) in southern Brazil. Sequencing of 16S rRNA, *sodB*, and *groEL* indicated a novel *Ehrlichia* species, and sequencing of 16S rRNA from 2 capybaras indicated a novel *Anaplasma* species. The tick vectors remain unknown.

Ehrlichia and *Anaplasma* species are tickborne bacteria that infect animals and humans worldwide. To date, 6 *Ehrlichia* species have been described (*E. canis*, *E. chaffeensis*, *E. ewingii*, *E. muris*, *E. ruminantium*, and *E. minasensis*), and 8 *Anaplasma* species have been described (*A. bovis*, *A. capra*, *A. centrale*, *A. marginale*, *A. odocoilei*, *A. ovis*, *A. platys*, and *A. phagocytophilum*). In addition, other native *Ehrlichia* species have been described in wild animals from Brazil (*1*).

Although capybaras (*Hydrochoerus hydrochaeris*), the largest living rodents in the world, have been implicated as a major amplifying host of *Rickettsia rickettsii* (the etiologic agent of Brazilian spotted fever) for *Amblyomma sculptum* ticks, studies focusing on other tickborne diseases agents are lacking in this rodent. Accordingly, we conducted a comprehensive survey for the detection of *Ehrlichia* and *Anaplasma* species in a population of capybaras from Pinhais Municipality, Paraná State, southern Brazil.

We retrieved blood samples from 17 capybaras and salivary glands from 11 *Amblyomma dubitatum* ticks from these capybaras that were collected for a previous study conducted in southern Brazil (*2*). We screened blood samples by using PCR targeting of the 16S rRNA gene of *Ehrlichia* and *Anaplasma* (*3*,*4*). We then tested samples positive by PCR by using PCR that targeted a fragment of the *dsb* and *sodB* genes of *Ehrlichia* species (*1*,*5*) and the *groEL* gene of *Ehrlichia* and *Anaplasma* species (*6*). We used blood samples from dogs positive for *E. canis* as positive controls and nuclease-free water samples as negative controls.

The *Ehrlichia* 16S rRNA PCR assay yielded amplicons in 16/17 (94.12% [95% CI 73.02%–98.95%]) capybaras, from which we generated amplicons by the *sodB* PCR (300 bp) and *groEL* PCR (1,100 bp) assays. No sample yielded amplicon by the *dsb* PCR assay. We sequenced amplicons obtained from 4 16S rRNA, 5 *sodB*, and 4 *groEL* PCR-positive samples in both directions by using the Sanger method. We submitted all nucleotide sequences obtained to GenBank (Appendix, https://wwwnc.cdc.gov/EID/article/28/2/21-0705-App1.pdf).

We observed infestations by *A. dubitatum* ticks in all capybaras, from which we collected 26 males, 16 females, and 122 nymphs. Among salivary glands from 11 adult ticks, 1 (9.09%) tested positive for *Ehrlichia* species by the 16S rRNA PCR. However, multiple attempts to sequence the 16S rRNA gene detected in tick salivary glands were unsuccessful because of the faint bands.

We observed neither abnormalities nor inclusion-like bodies of *Ehrlichia* or *Anaplasma* during the evaluation of Giemsa-stained thin blood smears of the capybaras. We tested *Ehrlichia* antibodies in capybara serum samples with an indirect immunofluorescent assay using *E. canis* (São Paulo and Cuiabá strains) as antigens; serum samples were positive if reacting at a dilution ≥1:40 (*7*). A total of 6/17 (35.29% [95% CI 17.31%–58.70%]) capybaras showed antibodies against ≥1 of the *E. canis* antigens. When we used the Cuiabá strain of *E. canis* as antigen, 4/17 (23.53% [95% CI 9.56%–47.26%]) capybaras were seropositive, whereas 6/17 (35.29%) were positive when we used the São Paulo strain. Four capybaras were seropositive for both *E. canis* strains. Antibody endpoint titers ranged from 40 to 640 for both *E. canis* antigens.

According to serologic testing, PCR amplification, and DNA sequencing results, *A. dubitatum* tick–infested capybaras in southern Brazil may be infected with a novel *Ehrlichia* agent and a novel *Anaplasma* species. Serologic screening showed

exposure to *Ehrlichia* species in 35% of the capybaras. A previous study failed to detect *Ehrlichia* DNA in spleen tissue of capybaras from southeastern Brazil (*8*), and we know of no previous study of *Anaplasma* species that has been performed in this rodent species.

Partial sequences of 16S rRNA and 2 protein-coding genes (*sodB* and *groEL*) obtained from capybaras indicate a novel *Ehrlichia* species. Partial 16S rRNA gene sequences from capybara no. II showed that the detected *Ehrlichia* agent shared 95.67% identity with *A. phagocytophilum*, whereas sequences from capybara no. III showed that the detected *Ehrlichia* agent shared 94.28% identity with *E. chaffeensis*. Partial *sodB* genes showed 82.23%–85.07% identity with *E. chaffeensis* or *E. ruminantium*, whereas partial *groEL* genes showed identity with 76.52% with *A. phagocytophilum*. A previous study stated that different bacterial isolates showing <97% similarity in the 16S rRNA gene belong to different species (*9*). In addition, protein-coding genes should be used in addition to the 16S rRNA gene for identification of novel species (*10*). Our genetic findings support the infection of capybaras in Brazil with a novel *Ehrlichia* species, herein named *Candidatus* Ehrlichia hydrochoerus (Figure).

Partial sequences of 16S rRNA gene obtained from capybaras VI and VII demonstrated a novel *Anaplasma* species. Partial 16S rRNA gene sequences showed identity of 96.76% with *Anaplasma* sp. detected in dogs from the Philippines and 97.93% with *A. phagocytophilum*, with 100% query coverage. Bayesian inference showed that the capybara *Anaplasma* species detected was related to *A. odocoilei* from North America, which indicates a novel *Anaplasma* species infecting capybaras in Brazil.

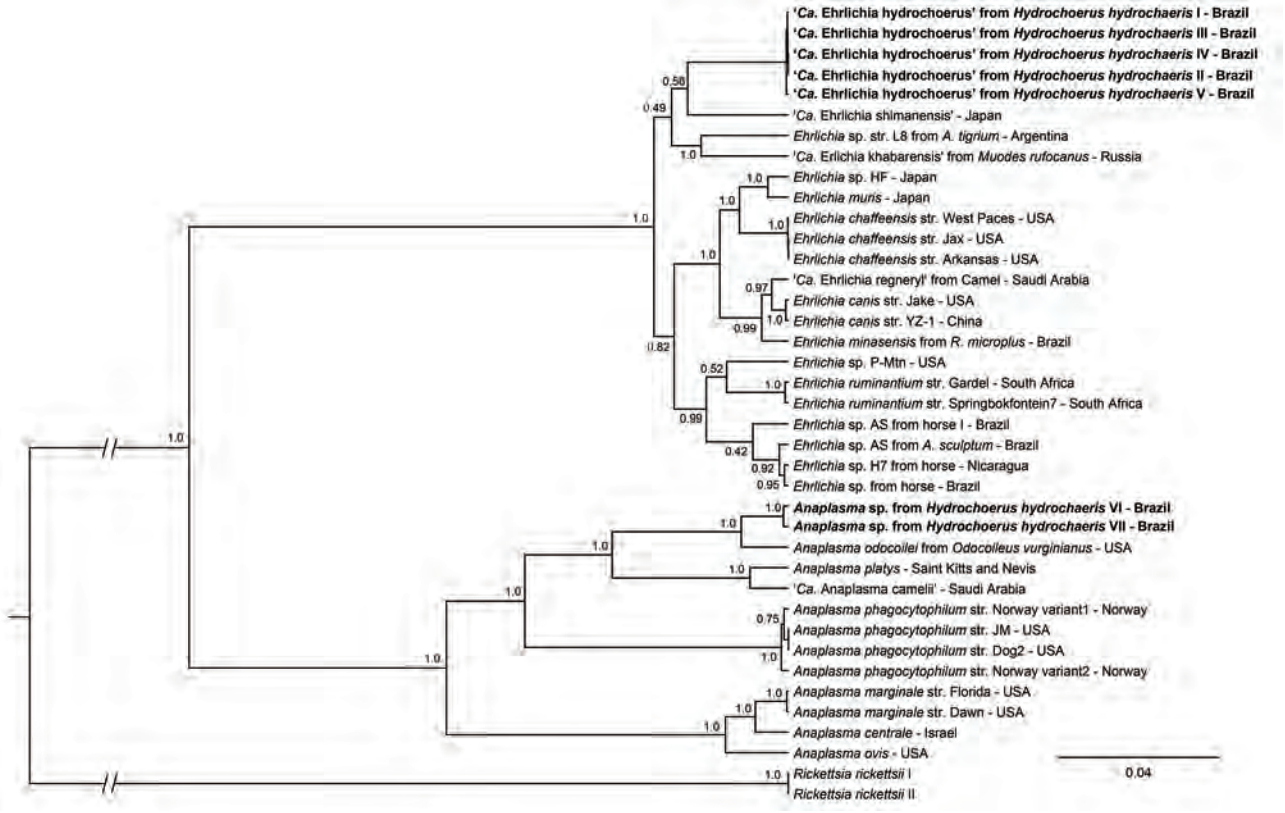

Figure. Phylogenetic analysis of 16S rRNA, *sodB*, and *groEL* partial sequences of *Candidatus* Ehrlichia hydrochoerus and *Anaplasma* spp. obtained from capybaras (*Hydrochoerus hydrochaeris*), southern Brazil. These sequences (in bold) and those of other *Ehrlichia* and *Anaplasma* species were aligned using MAFFT 7.110 (https://mafft.cbrc.jp/alignment/server). Phylogenetic analyses of each gene were based on Bayesian inference using Beast version 1.8.4 (https://beast.community/index.html). We performed 3 independent runs of 100 million generations of Monte Carlo Markov chain with 1 sampling/10,000 generations and a 10% burn-in. We estimated substitution models as generalized time reversible plus gamma for *16S rRNA* (A), Hasegawa–Kishino–Yano plus gamma for *sodB* (B), and Tamura–Nei plus gamma for *groEL* (C) genes on the basis of Akaike information criterion by using jModeltest version 2.1.10 (https://github.com/ddarriba/jmodeltest2/releases/tag/v2.1.10r20160303). The tree was rooted with *Rickettsia rickettsii* (GenBank accession nos. CP000766.3 and CP018913.1). Complete GenBank accession numbers are listed in the Appendix (https://wwwnc.cdc.gov/EID/article/28/2/21-0705-App1.pdf). Scale bar indicates number of substitutions per site. *Ca*., *Candidatus.*

Acknowledgments

We thank Hubert D. Fanien for providing O'TOM/Tick Twister.

The Fundação Araucária (grant no. 09/2016) and the Brazilian National Council of Scientific and Technological Development (grant no. 425597/2018-0) provided financial aid and support to carry out this research. The Brazilian National Council of Scientific and Technological Development also provided research fellowships to D.M.A. (grant no. 303677/2018-0), M.B.L. (grant no. 301641/2019-6), and R.F.C.V. (grant no. 313161/2020-8). F.C.M.C. was sponsored by a fellowship from the Coordenação de Aperfeiçoamento de Pessoal de Nível Superior at the time of this study.

About the Author

Dr. Vieira is a research associate at the Vector-borne Diseases Laboratory, Universidade do Paraná, Curitiba, Brazil, and specializes in tickborne diseases. Her research is focused on molecular characterization of Anaplasmatacae in Brazil.

References

1. Almeida AP, Souza TD, Marcili A, Labruna MB. Novel *Ehrlichia* and *Hepatozoon* agents infecting the crab-eating fox (*Cerdocyon thous*) in southeastern Brazil. J Med Entomol. 2013;50:640–6. https://doi.org/10.1603/ME12272
2. Vieira RFC, Santos NJR, Valente JDM, Santos LP, Lange RR, Duque JCM, et al. '*Candidatus* Mycoplasma haematohydrochoerus', a novel hemoplasma species in capybaras (*Hydrochoerus hydrochaeris*) from Brazil. Infect Genet Evol. 2021;93:104988. https://doi.org/10.1016/j.meegid.2021.104988
3. Parola P, Roux V, Camicas JL, Baradji I, Brouqui P, Raoult D. Detection of *Ehrlichiae* in African ticks by polymerase chain reaction. Trans R Soc Trop Med Hyg. 2000;94:707–8. https://doi.org/10.1016/S0035-9203(00)90243-8
4. Ruiz-Fons F, Fernández-de-Mera IG, Acevedo P, Gortázar C, de la Fuente J. Factors driving the abundance of *Ixodes ricinus* ticks and the prevalence of zoonotic *I. ricinus*–borne pathogens in natural foci. Appl Environ Microbiol. 2012;78:2669–76. https://doi.org/10.1128/AEM.06564-11
5. Qurollo BA, Davenport AC, Sherbert BM, Grindem CB, Birkenheuer AJ, Breitschwerdt EB. Infection with Panola Mountain *Ehrlichia* sp. in a dog with atypical lymphocytes and clonal T-cell expansion. J Vet Intern Med. 2013;27:1251–5. https://doi.org/10.1111/jvim.12148
6. Barber RM, Li Q, Diniz PP, Porter BF, Breitschwerdt EB, Claiborne MK, et al. Evaluation of brain tissue or cerebrospinal fluid with broadly reactive polymerase chain reaction for *Ehrlichia, Anaplasma*, spotted fever group *Rickettsia*, *Bartonella*, and *Borrelia* species in canine neurological diseases (109 cases). J Vet Intern Med. 2010;24:372–8. https://doi.org/10.1111/j.1939-1676.2009.0466.x
7. Aguiar DM, Cavalcante GT, Pinter A, Gennari SM, Camargo LM, Labruna MB. Prevalence of *Ehrlichia canis* (Rickettsiales: Anaplasmataceae) in dogs and *Rhipicephalus sanguineus* (Acari: Ixodidae) ticks from Brazil. J Med Entomol. 2007;44:126–32. https://doi.org/10.1093/jmedent/41.5.126
8. Labruna MB, McBride JW, Camargo LM, Aguiar DM, Yabsley MJ, Davidson WR, et al. A preliminary investigation of *Ehrlichia* species in ticks, humans, dogs, and capybaras from Brazil. Vet Parasitol. 2007;143:189–95. https://doi.org/10.1016/j.vetpar.2006.08.005
9. Drancourt M, Raoult D. Sequence-based identification of new bacteria: a proposition for creation of an orphan bacterium repository. J Clin Microbiol. 2005;43:4311–5. https://doi.org/10.1128/JCM.43.9.4311-4315.2005
10. Fournier PE, Dumler JS, Greub G, Zhang J, Wu Y, Raoult D. Gene sequence-based criteria for identification of new rickettsia isolates and description of *Rickettsia heilongjiangensis* sp. nov. J Clin Microbiol. 2003;41:5456–65. https://doi.org/10.1128/JCM.41.12.5456-5465.2003

Address for correspondence: Thállitha S.W.J. Vieira, Departamento de Medicina Veterinária, Campus Agrárias, Universidade Federal do Paraná. R. dos Funcionários, 1540, Juvevê, Curitiba, PR, 80035-050, Brazil; email: thallitha.vieira@ufpr.br

Dirofilaria immitis Pulmonary Dirofilariasis, Slovakia

Martina Miterpáková, Daniela Antolová, Jana Rampalová, Miroslava Undesser, Tomáš Krajčovič, Bronislava Víchová

Author affiliations: Institute of Parasitology of Slovak Academy of Sciences, Košice, Slovakia (M. Miterpáková, D. Antolová, B. Víchová); Unilabs Slovakia Ltd., Diagnostic Center of Pathology, Bratislava, Slovakia (J. Rampalová, T. Krajčovič); Ambulance of Pneumology and Phthisiology, Dunajská Streda, Slovakia (M. Undesser)

DOI: https://doi.org/10.3201/eid2802.211963

Dirofilaria immitis is a parasite related to pulmonary dirofilariasis in humans, its accidental hosts. We detected an autochthonous case of *D. immitis* infection in a woman from Slovakia. The emergence and spread of this parasite in Europe indicates a critical need for proper diagnosis of infection.

Dirofilaria immitis is a filarioid nematode that infects numerous mammalian species. Dogs are the main reservoir and various mosquito species (e.g., genera *Culex*, *Anopheles*, *Aedes*, and *Ochlerotatus*) the infection vectors. The parasite is related to the pulmonary form of dirofilariasis, manifested by the formation of coin lesions or nodules in lung parenchyma in humans, an accidental parasite host (*1*).

In Europe, the species *D. repens* causes most reported cases of human dirofilariasis. Just over 30 cases of human *D. immitis* infection have been unambiguously diagnosed, compared with >4,000 from *D. repens* (*2*).

In Slovakia, human autochthonous dirofilariasis has occurred since 2007. Meanwhile, 24 cases have been confirmed, all caused by *D. repens* nematodes (*3*,*4*; M. Miterpáková, unpub. data).

In January 2020, a 66-year-old woman from southwestern Slovakia was admitted to the Ambulance of Pneumology and Phthisiology reporting chest pain, cough, and asphyxia. The patient, who had a long-term history of smoking, had been treated for bronchial asthma and chronic obstructive pulmonary disease since 2012. She had not been abroad for >5 years. Results of hematologic and biochemical examinations were within the physiologic ranges; pulmonary function tests revealed moderate obstructive pulmonary disorder: a decrease of vital capacity to 77% (reference range >80%) and forced expiratory volume during the first second to 63% (reference range ≥80%). A chest radiograph showed bilaterally hyperlucent lungs with coarse bronchovascular markings; therefore, emphysema was suspected. Subsequent computed tomography confirmed bilateral paraseptal emphysema and numerous nonspecific lesions, ≈5 mm in diameter, in the S2 segment of the right lung and solitary nodules in the S8/9 segment of the left lung. Because of suspected malignancy, the patient was regularly monitored. After 12 months, the cancer markers had elevated. A control computed tomography examination showed a subpleural focal lesion in the S10 segment of the right lung; positron emission tomography/computed tomography confirmed hypermetabolic activity of the lesion. Biopsy was recommended because of a suspected tumor.

In May 2021, a wedge surgical resection of the nodule was performed. Histologic examination of resected tissue revealed a well-circumscribed necrotic nodule containing small irregularly shaped tubular formations affected by massive degenerative changes. The edge of the nodule consisted of nonspecific fibrotic and inflammatory granulations (Figure). The final pathology report suggested the

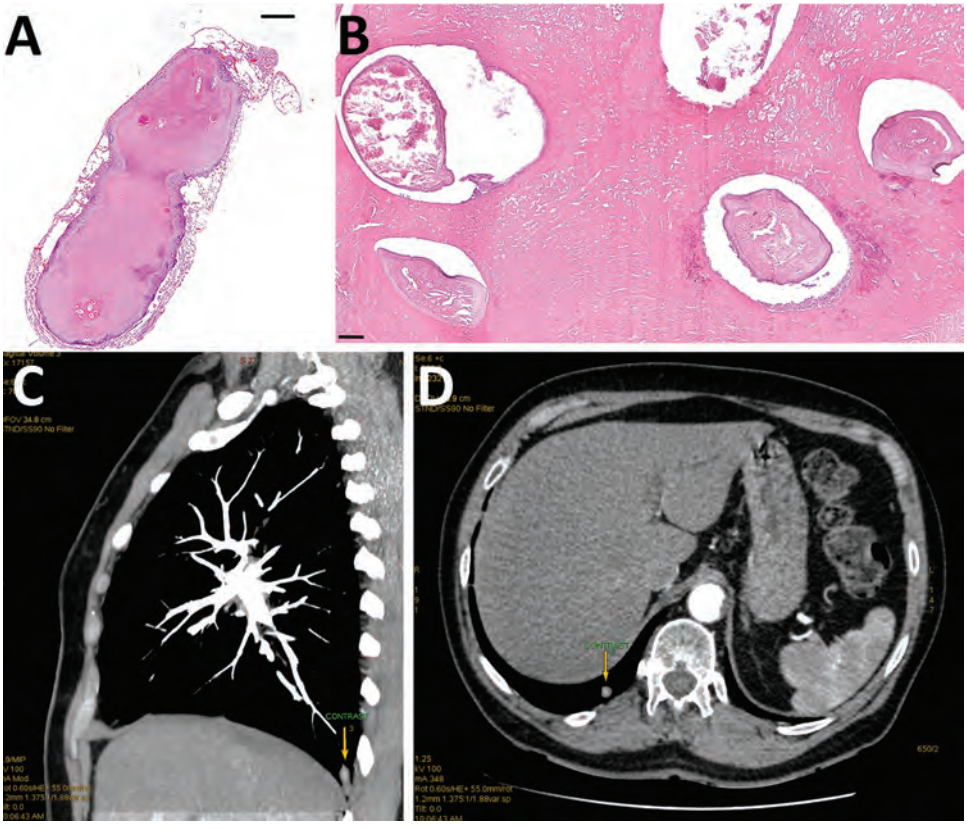

Figure. Histologic examination of resected tissue from a 66-year-old woman from southwestern Slovakia. A, B) Cross section showing *Dirofilaria immitis* nematodes embedded in necrotic material obtained from well-defined pulmonary nodule. Hematoxylin and eosin staining; original magnification ×20 for panel A, ×100 for panel. C, D) Chest computed tomography scan showing a subpleural focal lesion in the S10 segment of the right lung (arrows).

presence of massively degenerated fragments of a nonvital parasite, with *Dirofilaria* spp. suspected.

We amplified the mitochondrial *cox1* gene fragments of *D. repens* (209 bp) and *D. immitis* (203 bp), in accordance with Rishniw et al. (*5*). The analyzed tissue was positive for *D. immitis* and subsequent sequencing and BLAST analysis of the sequence (GenBank accession no. MZ438680) revealed 100% identity within the region overlapping other homologous *D. immitis* sequences from GenBank (e.g., accession nos. KC985239, NC005305).

Pulmonary dirofilariasis is still very rare in Europe, and many cases are evaluated as imported. Even cases published as autochthonous are still under discussion, and no final decision has been reached. For instance, Pampiglione et al. (*6*) published an analysis of 28 human cases diagnosed in Europe and attributed to *D. immitis* parasites or a species other than *D. repens*. In this analysis the researchers excluded *D. immitis* parasites as a causative agent in all the reviewed cases (*6*). A nonspecific localization of *D. repens* infection in lung tissue was recently reported in several patients from Russia, and 1 case was diagnosed in Slovakia (*3*,*7*). Recent data from several European countries, including Slovakia, indicate dramatic increase of *D. immitis* infections in the canine population (*4*,*8*,*9*), which may cause a rise in human cases in the near future.

Human pulmonary dirofilariasis is characterized by the formation of typical nodules (coin lesions) around immature adult worms located mainly on the lung periphery (*6*). Differential diagnosis of the nodules is important because >20 other pathologic conditions manifests by coin lesions, including tumors, cysts, and inflammatory granulomas. Coin lesions observed in patients with pulmonary dirofilariasis are spherical, not pyramidal as embolic infarct, and generally range from 1 cm to 4.5 cm in diameter (*10*). Few patients with pulmonary dirofilariasis show clinical symptoms. When symptoms are present, they are nonspecific and include thoracic pain, cough, and purulent sputum. These symptoms imitate pneumonitis, and patients are often treated incorrectly with antimicrobial drugs (*1*).

Long-term experience from dirofilariasis-endemic areas confirms that diagnosis is key and still a great challenge in the successful encompassment of human pulmonary dirofilariasis. Given the lack of specific and sensitive serologic tests, the only way for correct presurgical diagnosis appears to be the use of medical imaging. According to the European Society of Dirofilariosis and Angiostrongylosis (*2*), the combination of ultrasound and color Doppler charting, which offers findings of well-defined characteristics of *D. immitis* nodules (e.g., regular oval shape, hypoechoic inner content, no signs of polar vascularity) enable attribution to helminthic origin.

The study was supported by the Science Grant Agency, VEGA project no. 2/0014/21 and by the Slovak Research and Development Agency under the contract no. APVV-15-0114.

The patient agreed with all examinations and publication of case report and signed the informed content. No identifying data are presented in the paper. The study was performed in accordance with the ethical standards as laid down in the Declaration of Helsinki of 1975, as revised 2013.

About the Author

Dr. Miterpáková is a senior researcher and deputy director at the Institute of Parasitology of the Slovak Academy of Sciences in Košice, Slovakia. Her primary research interests include epidemiology, ecology and diagnosis of parasitic diseases; zoonoses; and vectorborne diseases.

References

1. Simón F, Siles-Lucas M, Morchón R, González-Miguel J, Mellado I, Carretón E, et al. Human and animal dirofilariasis: the emergence of a zoonotic mosaic. Clin Microbiol Rev. 2012;25:507–44. https://doi.org/10.1128/CMR.00012-12
2. European Society of Dirofilariosis and Angiostrongylosis. Guidelines for clinical management of human *Dirofilaria* infections. 2017 [cited 2021 Jul 28]. https://www.esda.vet/wp-content/uploads/2017/11/Guidelines-For-Clinical-Management-Of-Human-Dirofilaria-Infections.pdf
3. Miterpáková M, Antolová D, Ondriska F, Gál V. Human *Dirofilaria repens* infections diagnosed in Slovakia in the last 10 years (2007–2017). Wien Klin Wochenschr. 2017;129:634–41. https://doi.org/10.1007/s00508-017-1233-8
4. Fuehrer HP, Morelli S, Unterköfler MS, Bajer A, Bakran-Lebl K, Dwużnik-Szarek D, et al. *Dirofilaria* spp. and *Angiostrongylus vasorum*: current risk of spreading in Central and Northern Europe. Pathogens. 2021;10:1268. https://doi.org/10.3390/pathogens10101268
5. Rishniw M, Barr SC, Simpson KW, Frongillo MF, Franz M, Dominguez Alpizar JL. Discrimination between six species of canine microfilariae by a single polymerase chain reaction. Vet Parasitol. 2006;135:303–14. https://doi.org/10.1016/j.vetpar.2005.10.013
6. Pampiglione S, Rivasi F, Gustinelli A. Dirofilarial human cases in the Old World, attributed to *Dirofilaria immitis*: a critical analysis. Histopathology. 2009;54:192–204. https://doi.org/10.1111/j.1365-2559.2008.03197_a.x
7. Moskvina T, Ermolenko AV. Dirofilariasis in Russian Federation: a big problem with large distribution. Russian Open Medical Journal. 2018;7:e0102. https://doi.org/10.15275/rusomj.2018.0102

8. Széll Z, Bacsadi Á, Szeredi L, Nemes C, Fézer B, Bakcsa E, et al. Rapid spread and emergence of heartworm resulting from climate and climate-driven ecological changes in Hungary. Vet Parasitol. 2020;280:109067. https://doi.org/10.1016/j.vetpar.2020.109067
9. Miterpáková M, Hurníková Z, Valentová D, Borková L. Different epidemiological pattern of canine dirofilariosis in two neighboring countries in Central Europe—the Czech Republic and Slovakia. Parasitol Res. 2021;120:547–52. https://doi.org/10.1007/s00436-020-06995-8
10. Seybold WD. Solitary or "coin" lesions of the lung. Postgrad Med. 1964;36:424–30. https://doi.org/10.1080/00325481.1964.11695320

Address for correspondence: Daniela Antolová, Institute of Parasitology SAS, Hlinkova 3, 040 01 Košice, Slovakia; email: antolova@saske.sk

Fatal Case of Mediterranean Spotted Fever Associated with Septic Shock, Iran

Saber Esmaeili, Mina Latifian, Mohammad Khalili, Mehrdad Farrokhnia, John Stenos, Mehdi Shafiei, Ehsan Mostafavi

Author affiliations: Pasteur Institute of Iran, Tehran, Iran (S. Esmaeili, M. Latifian, E. Mostafavi); Pasteur Institute of Iran, Akanlu, Iran (S. Esmaeili, M. Latifian, E. Mostafavi); Shahid Bahonar University of Kerman, Kerman, Iran (M. Khalili); Kerman University of Medical Sciences, Kerman (M. Farrokhni, M. Shafiei); University Hospital Geelong, Geelong, Victoria, Australia (J. Stenos)

A fatal case of Mediterranean spotted fever associated with septic shock was reported in a 61-year-old man living in a village in southeastern Iran. The patient had a history of tick bite a few days before symptom onset. Phylogenetic analysis confirmed infection by *Rickettsia conorii* subspecies *israelensis*.

DOI: https://doi.org/10.3201/eid2802.211023

Mediterranean spotted fever (MSF) is a zoonotic disease caused by *Rickettsia conorii*. The main vector of this bacterium is the *Rhipicephalus sanguineus* tick (*1*); the main hosts of these ticks are domestic dogs, and humans are incidental hosts (*2*). MSF is endemic to the Mediterranean, Europe, Africa, western Asia, and India. The case-fatality rate is 3%–7% in hospitalized patients (*3*,*4*).

In 2017, human cases of MSF were reported in Kerman province in southeastern Iran (*5*). No data are available on the epidemiology of MSF in Iran; we report a fatal case of MSF associated with septic shock.

The patient was a 61-year-old man with a 10-year history of hypertension and rheumatoid arthritis who lived in a village in proximity to Bam County, Kerman province, Iran. He was a farmer, had no history of domestic animal-keeping, and reported contact with livestock and a tick bite a few days before symptom onset. The initial clinical signs of the disease appeared on September 6, 2019, and the patient was admitted to a hospital in Bam on September 9; symptoms were fever, nausea, vomiting, myalgia, urinary retention, and flank pain. The patient had scleral icterus, and a black skin eschar at the tick bite site and skin rash were visible on his left leg.

When the patient's condition deteriorated, he was transferred to a hospital in Kerman on September 15. At admission, symptoms were septic shock, tachycardia, tachypnea, fever, and hypotension (85/50 mm Hg); he immediately began treatment with ceftriaxone, metronidazole, and parenteral hydration. Maculopapular skin rash was visible on the left leg. The patient had thrombocytopenia, and an increase was observed in leukocyte counts, renal factor levels (urea and creatinine), liver enzyme levels (aspartate aminotransferase, alanine transferase, and alkaline phosphatase), partial thromboplastin time of coagulation, and bilirubin levels (Table). Hemoglobin and hematocrit levels decreased, and the patient experienced hematuria and proteinuria; calcium oxalate and amorphous urate crystals were further reported in microscopic examinations. Treatment of prednisolone, heparin, doxycycline, and vancomycin was initiated.

On September 16, the patient was transferred to Afzalipour Hospital in Kerman (Referral Center for Infectious Diseases, Kerman Province). At the time of admission, the patient was conscious, his condition was stable, and his temperature was 37.6°C. No abnormalities were observed in clinical examinations of the heart, chest, and abdomen, but we noted bilateral lower extremity edema and left leg skin lesions (rash and eschar). The results of laboratory tests of blood and urine samples were

Table. Laboratory findings in a patient with Mediterranean spotted fever associated with septic shock, Iran*

Value	2019 Sep 16, 12 AM	2019 Sep 17, 1 AM	2019 Sep 17, 1 AM
Leukocyte, $\times 10^9$/L	18,900	12,700	ND
Hemoglobin, g/dL	12.9	14.1	ND
Platelets, $\times 10^9$/L	56,000	42,000	ND
Hematocrit, %	35.3	43.0	ND
Prothrombin time, s	14.4	13.5	14
Partial thromboplastin time, s	56	39	33
Aspartate aminotransferase, U/L	83	101	ND
Alanine aminotransferase, U/L	71	49	ND
Alkaline phosphatase, U/L	328	510	ND
Bilirubin total, mg/dL	2.7	4.8	ND
Bilirubin direct, mg/dL	2.3	2.8	ND
Blood urea, mg/dL	95	145	161
Blood creatinine, mg/dL	3.6	4.8	5.5
Blood calcium, mEq/L	8.5	ND	ND
Blood sodium, mEq/L	140	135	136
Blood potassium, mEq/L	4.0	4.9	3.5
Proteinuria	+	–	+
Hematuria	+	–	+

*ND, not done; +, positive; –, negative.

abnormal (Table). The patient underwent emergency dialysis and continued to take prednisolone, heparin, doxycycline, and vancomycin. On September 17, the patient lost consciousness; he was subsequently intubated and admitted to the intensive care unit. A few hours later, he experienced septic shock and cardiac arrest and died.

The differential diagnosis for this patient included MSF and Crimean-Congo hemorrhagic fever; on September 17, samples required for these differential diagnoses were prepared. Serum and blood samples were sent to the Pasteur Institute of Iran on September 25 (8 days after the patient's death). Serologic and molecular test results for Crimean-Congo hemorrhagic fever were negative. Testing for *R. conorii* IgM by ELISA was borderline, and titer of *R. conorii* IgM by immunofluorescence assay was 1:48. Serum samples were positive for *Rickettsia* spp. (16S rRNA gene) by real-time reverse transcription PCR (*6*). On the basis of the amplification and sequencing of specific genes of *Rickettsia* spp. (*gltA*, GenBank accession no. MZ545594.1; *17KD*, GenBank accession no. MZ545592.1; *ompA*, GenBank accession no. MZ545593.1), we confirmed infection by *R. conorii* subspecies *israelensis* (Figure).

The patient died as a result of late diagnosis of a rickettsial infection and subsequent septic shock, despite initiation of appropriate treatment. MSF is usually considered to be a mild disease, but severe and fatal cases do occasionally occur (*7*). One of the causes of death from MSF is multiorgan failure, including acute kidney injury, pneumonitis, and encephalitis. When severe, MSF can manifest as septic shock, and acute kidney injury might occur. Thrombocytopenia and elevated liver enzymes are frequent laboratory abnormalities (*4*,*7*).

Phylogenetic trees showed that the infection in this patient was caused by *R. conorii* subsp. *israelensis*. *R. conorii* has 4 subspecies, *caspia*, *israelensis*, *conorii*, and *indica*, each of which cause diseases that have specific clinical features and occur in different geographic regions. *R. conorii* subsp. *israelensis* seems to have the highest death rate of the subspecies (*8*,*9*), reported to be ≈30% (*10*).

MSF appears to be circulating in southern Iran but is a neglected disease that requires more attention from the healthcare system. Because of the nonspecific clinical symptoms of MSF, diagnosing the disease is challenging. Diagnosing and treating MSF early is critical to prevent progression to more severe illness (*6*). Further studies, particularly on elucidating potential reservoirs and vectors, will result in a better understanding of the epidemiology of this disease in Iran. In the meantime, MSF should be included in the differential diagnosis for patients in Iran who are experiencing fever and rash.

The work presented in this publication was supported by the Pasteur Institute of Iran and the Center for Communicable Diseases Control in the Ministry of Health (grant no. 810).

About the Author

Dr. Esmaeili is an assistant professor and researcher in medical microbiology at Pasteur Institute of Iran. His primary research interest is emerging and reemerging bacterial pathogens, including *Coxiella burnetii*, *Bartonella*, *Francisella*, *Rickettsia*, and *Yersinia pestis*.

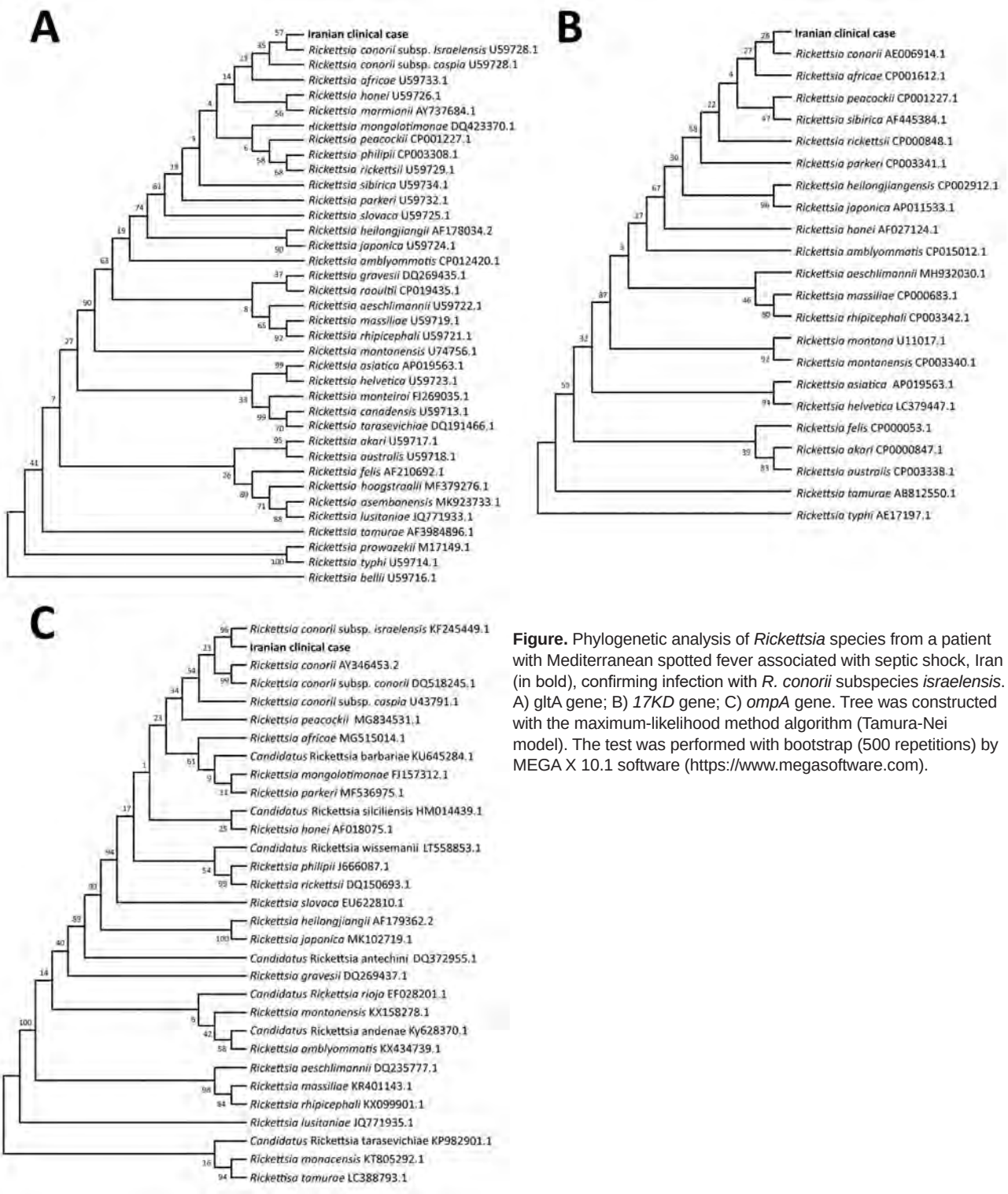

Figure. Phylogenetic analysis of *Rickettsia* species from a patient with Mediterranean spotted fever associated with septic shock, Iran (in bold), confirming infection with *R. conorii* subspecies *israelensis*. A) gltA gene; B) *17KD* gene; C) *ompA* gene. Tree was constructed with the maximum-likelihood method algorithm (Tamura-Nei model). The test was performed with bootstrap (500 repetitions) by MEGA X 10.1 software (https://www.megasoftware.com).

References

1. Rovery C, Brouqui P, Raoult D. Questions on Mediterranean spotted fever a century after its discovery. Emerg Infect Dis. 2008;14:1360–7. https://doi.org/10.3201/eid1409.071133
2. Nafi O, Tarawnah Y, Tarawnah A. Epidemiological evaluation of Mediterranean spotted fever in children of the Karak province in south Jordan. J Infect Dev Ctries. 2017;11:242–6. https://doi.org/10.3855/jidc.8154
3. Parola P, Paddock CD, Raoult D. Tick-borne rickettsioses around the world: emerging diseases challenging old concepts. Clin Microbiol Rev. 2005;18:719–56. https://doi.org/10.1128/CMR.18.4.719-756.2005

4. Baymakova M, Pekova L, Plochev K, Parousheva P. Severe clinical forms of Mediterranean spotted fever: a case series from an endemic area in Bulgaria. Int J Infect Dis. 2016;53:150–1. https://doi.org/10.1016/j.ijid.2016.11.369
5. Farrokhnia M, Ghalejoogh ZY, Rohani M, Ghasemi A, Esmaeili S, Mostafavi E. Cases of Mediterranean spotted fever in southeast of Iran. Iran J Microbiol. 2020;12:256–60. https://doi.org/10.18502/ijm.v12i3.3244
6. Abdeljelil M, Sakly H, Kooli I, Marrakchi W, Aouam A, Loussaief C, et al. Mediterranean spotted fever as a cause of septic shock. IDCases. 2019;15:e00528. https://doi.org/10.1016/j.idcr.2019.e00528
7. Walker DH, Herrero-Herrero JI, Ruiz-Beltrán R, Bullón-Sopelana A, Ramos-Hidalgo A. The pathology of fatal Mediterranean spotted fever. Am J Clin Pathol. 1987;87:669–72. https://doi.org/10.1093/ajcp/87.5.669
8. Parola P, Paddock CD, Socolovschi C, Labruna MB, Mediannikov O, Kernif T, et al. Update on tick-borne rickettsioses around the world: a geographic approach. Clin Microbiol Rev. 2013;26:657–702. https://doi.org/10.1128/CMR.00032-13
9. Cohen R, Babushkin F, Shapiro M, Uda M, Atiya-Nasagi Y, Klein D, et al. Two cases of Israeli spotted fever with Purpura fulminans, Sharon District, Israel. Emerg Infect Dis. 2018;24:835–40. https://doi.org/10.3201/eid2405.171992
10. Sousa R, França A, Dória Nòbrega S, Belo A, Amaro M, Abreu T, et al. Host- and microbe-related risk factors for and pathophysiology of fatal *Rickettsia conorii* infection in Portuguese patients. J Infect Dis. 2008;198:576–85. https://doi.org/10.1086/590211

Address for correspondence: Saber Esmaeili, No. 69, Pasteur Ave, Department of Epidemiology and Biostatistics, Pasteur Institute of Iran, Postal Code 1316943551, Tehran, Iran; email: dr.saberesmaeili@gmail.com, s-esmaeili@pasteur.ac.ir

Genetic Diversity of *Bartonella* spp. in Cave-Dwelling Bats and Bat Flies, Costa Rica, 2018

Miranda M. Mitchell,[1] Amanda Vicente-Santos,[1] Bernal Rodríguez-Herrera, Eugenia Corrales-Aguilar, Thomas R. Gillespie

Author affiliations: Emory University, Atlanta, Georgia, USA (M.M. Mitchell, A. Vicente-Santos, T.R. Gillespie); University of Costa Rica, San José, Costa Rica (B. Rodríguez-Herrera, E. Corrales-Aguilar)

DOI: https://doi.org/10.3201/eid2802.211686

[1]These authors contributed equally to this article.

To determine *Bartonella* spp. dynamics, we sampled bats and bat flies across 15 roosts in Costa Rica. PCR indicated prevalence of 10.7% in bats and 29.0% in ectoparasite pools. Phylogenetic analysis of 8 sequences from bats and 5 from bat fly pools revealed 11 distinct genetic variants, including 2 potentially new genotypes.

Bartonella, the causative agent of bartonellosis, is a genus of gram-negative bacteria. Bartonellosis causes a range of symptoms from severe to life-threatening (e.g., endocarditis and meningitis). Clinical syndromes from *Bartonella* infections include trench fever (*B. quintana*), cat scratch disease (*B. henselae*), and Carrion's disease (*B. bacilliformis*) (*1*). Bats (Order Chiroptera) and their blood-

Table. Prevalence of *Bartonella* spp. in bats and bat flies sampled from roost sites, Costa Rica, 2018

Species	No. positive/no. sampled
Bats	
Artibeus jamaicensis	0/1
Balantiopteryx plicata	0/4
Carollia perspicillata	19/79
Desmodus rotundus	1/25
Diphylla ecaudata	0/1
Glossophaga commisarisi	0/12
Glossophaga soricina	0/10
Lonchophylla robusta	1/25
Lonchorhina aurita	0/13
Macrophyllum macrophyllum	1/1
Phyllostomus hastatus	0/4
Pteronotus gymnonotus	3/11
Pteronotus mesoamericanus	2/56
Pteropteryx kappleri	0/1
Tonatia saurophilia	0/1
Trachops cirrhosis	0/8
Total	27/252
Bat flies	
Aspidoptera phyllostomasis	0/1
Exastinion clovisi	2/2
Megistopoda aranea	1/4
Speiseria ambigua	0/1
Strebla carolliae	0/1
Strebla diaemi	0/1
Strebla galindoi†	1/2
Strebla guajiro	0/1
Strebla hertigi†	1/1
Strebla mirabilis	0/1
Strebla vespertilionis†	2/2
Trichobius cecus	0/3
Trichobius dugesiodes	0/2
Trichobius dunni	0/1
Trichobius furmani	0/1
Trichobius galei	0/3
Trichobius johnsonae	1/3
Trichobius keenani	0/1
Trichobius pallidus†	7/22
Trichobius perspicillata	0/1
Trichobius sparsus†	2/3
Trichobius uniformis†	1/2
Trichobius yunkeri	0/3
Total	18/62

*For bat flies, no. sampled indicates no. sampled pools.
†Newly described species with *Bartonella*.

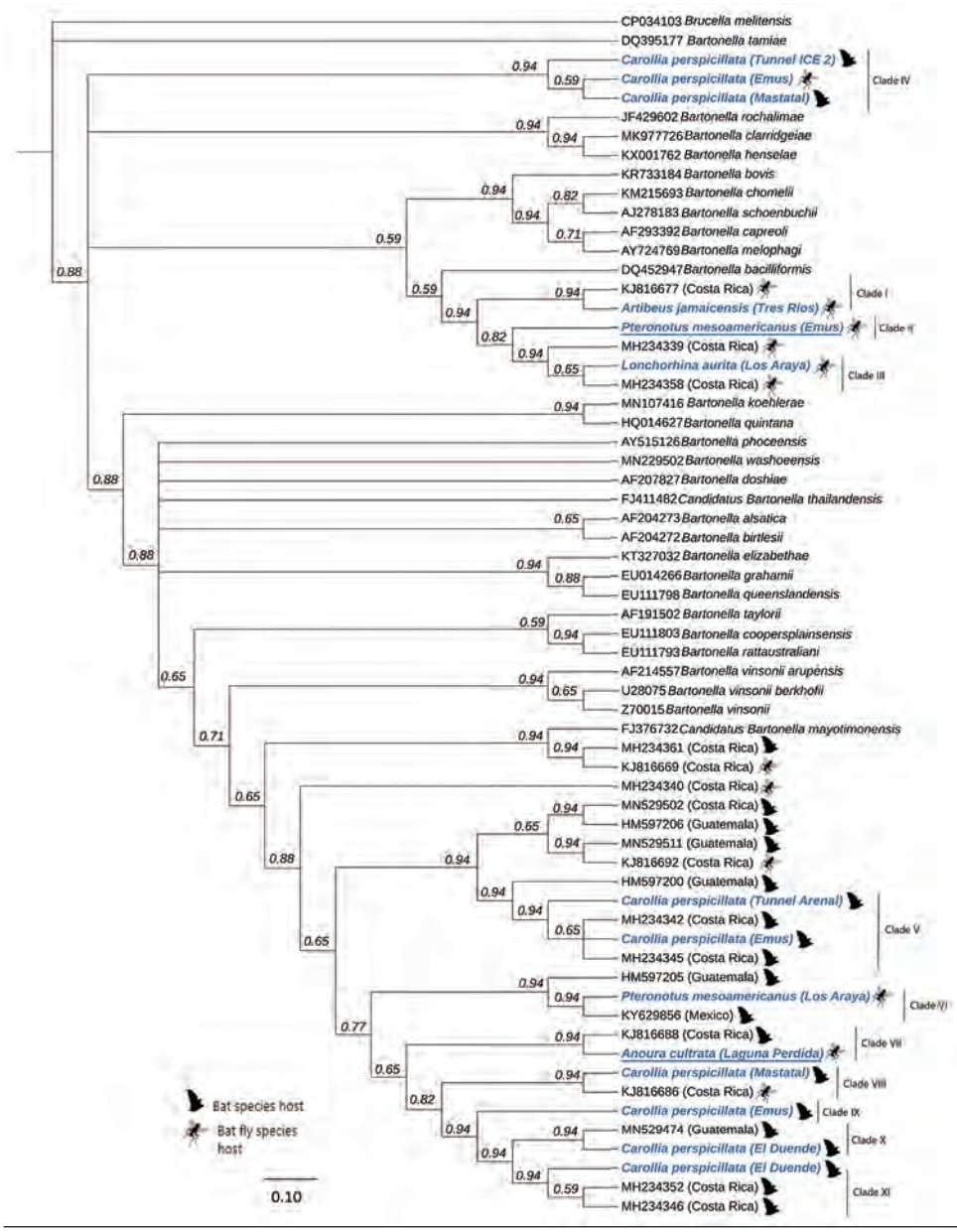

Figure. Phylogenetic tree of 768 bp partial *gltA* gene of *Bartonella* variants found in study of *Bartonella* spp. in bats and bat flies sampled from roost sites, Costa Rica, 2018 (blue), compared with globally named species and other variants found in bats and bat flies in Central America and Mexico. Each sequence is labeled with its GenBank accession number, the organism on which it was detected, and the country of origin. For species in this study, we included the specific site (accession numbers in Appendix Table, https://wwwnc.cdc.gov/EID/article/28/2/21-1686-App1.pdf). Underlining indicates the potential newly described genotypes. We constructed the global phylogenetic tree by using Bayesian Markov chain Monte Carlo (MrBayes 2.2.4, https://www.geneious.com), with 1 million generations and a burn-in fraction of 25%. We determined the parameters for the nucleotide changes by using MEGA X (https://mafft.cbrc.jp/alignment/software). Inner node labels identify consensus support. Scale bar indicates nucleotide substitutions/site (%).

feeding ectoparasitic bat flies (Superfamily Hippoboscoidea) host a diversity of *Bartonella* species, awakening interest in their potential role as natural reservoirs for this pathogen (*2*,*3*). To learn more about this interplay, we examined the genetic diversity and geographic sharing of *Bartonella* spp. in diverse assemblages of bats and bat flies across Costa Rica.

In 2018, we nonlethally sampled 321 bats (18 species) by using hand nets, mist nets, and harp traps across 15 roosts throughout Costa Rica (Appendix Figure, https://wwwnc.cdc.gov/EID/article/28/2/21-1686-App1.pdf). We took blood samples from 252 bats (16 species) and collected 114 ectoparasites from 48 bats, following Emory University Institutional Animal Care and Use Committee protocol (DAR-4000049-ENTRPR-N) and with the approval of the National System of Conservation Areas (SINAC-Costa Rica) (research permit nos. R-SINAC-PNI-ACAHN-016–2018, M-P-SINAC-PNI-ACAT-035–2018, SINAC-ACC-PI-R-068–2018, R-SINAC-ACG-PI-030–2018, R-SINAC-PNI-ACLAC-044–2018, SINAC-ACO-PAC-D-RES-063–2018, INV-ACOSA-046–18, ACT-OR-DR-066–18). We taxonomically identified the bats and bat flies (*4*–*6*), pooled the bat flies (1–8 bat flies/pool) by individual bat host and bat fly species (62 pools) and extracted DNA from bat blood

and ectoparasite pooled samples. We screened extracted DNA for *Bartonella* spp. by amplifying a 770-bp portion of the partial citrate synthase gene (*gltA*) (*7*) and using *B. doshiae* as a positive control (provided by M. Kosoy, M. Rosales Rizzo, Centers for Disease Control and Prevention). Samples positive by PCR were sequenced for confirmation.

To create global phylogenies, we trimmed obtained consensus sequences to 768 bp and aligned them to 45 genetic sequences: 28 from known *Bartonella* species, 12 *Bartonella* sequences from bats and bat flies in Costa Rica (*8*), 4 sequences from bats in Guatemala (*9*), and 1 sequence from Mexico (*3*). We used *B. tamiae* and *Brucella melitensis* as outgroups to root the tree. We created the alignment by using the multiple alignment program MAFFT (https://mafft.cbrc.jp/alignment/software), manually checked in MEGA X (https://www.megasoftware.net), and further refined with alignment refinement tool Gblocks version 0.91b (http://molevol.cmima.csic.es/castresana/Gblocks/Gblocks_documentation.html). We constructed the global phylogenetic tree by using Bayesian Markov chain Monte Carlo analyses (MrBayes 2.2.4, https://www.geneious.com) with 1 million generations and a burn-in fraction of 25% and determined the parameters for the nucleotide changes (MEGA X).

Bartonella prevalence from all samples, determined by PCR, was 14.3% (45/314), 10.7% (27/252) for bats and 29.0% (18/62) for ectoparasite pools (Table). *Bartonella* seems to be widespread and diverse in bats and bat flies in Costa Rica, where 6 of the 16 bat species and 9 of the 23 bat fly species were positive for the bacterium. Because of sequence quality, we included only 8 *Bartonella* sequences from bats and 6 from bat fly pools in phylogenetic analyses, which revealed 11 genetic variants, including 2 potentially new genotypes (93.2% similarity value; Figure; Appendix Table). These 11 genetic variants clustered into 9 clades of 96.0%–99.2% similarity.

Our results suggest that within Costa Rica variants are shared between bats and their flies in different parts of the country and in different years. For example, *Bartonella* sequences from Emus Cave (GenBank accession no. MW115627) and Túnel Arenal (GenBank accession no. MW115628) at opposite ends of the country (clade V; Appendix Figure) clustered together with sequences from a study conducted in Costa Rica in 2015 (*8*). In addition, *Bartonella* sequences from our study clustered with previously identified sequences from bats and bat flies from Guatemala (*9*) and Mexico (*3*), suggesting wide geographic distribution.

We also found a high level of diversity of *Bartonella* variants within caves and species (Figure). For example, *Bartonella* sequences from different bats (of same and different species) in Emus Cave clustered in 4 distinct clades. In addition, *Carollia perspicillata* bats, the most sampled species in our study, carried *Bartonella* with sequences from 6 distinct clades. This finding suggests that >1 *Bartonella* strain is circulating within bat species, even within the same cave.

When assessing spillover risk to humans and domestic animals, we found that the *Bartonella* sequences we detected did not cluster with *Bartonella* species known to cause infection in humans and other animals and did not significantly overlap with sequences from any globally identified species (Figure). To fully assess potential for *Bartonella* spillover from bat and bat fly species to other animals and humans, further analyses should be conducted.

In conclusion, we found *Bartonella* species to be diverse, prevalent, and potentially widely shared among species of bats and bat flies in Costa Rica and Mesoamerica. We expanded existing scientific knowledge on the prevalence and diversity of *Bartonella* in bats and bat flies in Costa Rica by including species that were not previously tested and described as positive by PCR for these bacteria. We also described 2 new *Bartonella* genotypes through phylogenetic analysis. Information about the dynamics of *Bartonella* in its natural hosts can be used to predict and avert further *Bartonella* emergence.

Acknowledgments

We thank the Anthros Speleology Group and Paula Ledezma-Campos for their assistance in the field and Hunter Seabolt and Christopher Phipps for guidance with molecular and phylogenetic analyses.

This investigation was funded by the American Museum of Natural History, the Fulbright Association, the American Society of Mammalogists, the Cave Research Foundation, the University of Costa Rica, the Emory University Global Health Institute, and the Emory University Department of Environmental Sciences.

About the Author

Ms. Mitchell is an ORISE Fellow at the Centers for Disease Control and Prevention, Agency for Toxic Substances and Disease Registry. Her primary research interests include environmental health, infectious disease epidemiology, molecular biology, public health assessment, and bioinformatics.

References

1. Harms A, Dehio C. Intruders below the radar: molecular pathogenesis of *Bartonella* spp. Clin Microbiol Rev. 2012;25:42–78. https://doi.org/10.1128/CMR.05009-11
2. McKee CD, Bai Y, Webb CT, Kosoy MY. Bats are key hosts in the radiation of mammal-associated *Bartonella* bacteria. Infect Genet Evol. 2021;89:104719. https://doi.org/10.1016/j.meegid.2021.104719
3. Stuckey MJ, Chomel BB, de Fleurieu EC, Aguilar-Setién A, Boulouis HJ, Chang CC. *Bartonella*, bats and bugs: a review. Comp Immunol Microbiol Infect Dis. 2017;55:20–9.
4. York HA, Rodríguez-Herrera B, LaVal RK, Timm RM, Lindsay KE. Field key to the bats of Costa Rica and Nicaragua. J Mammal. 2019;100:1726–49. https://doi.org/10.1093/jmammal/gyz150
5. Wenzel RL. The streblid batflies of Venezuela (Diptera: Streblidae). Brigham Young Univ Sci Bull. 1976;20:1–177.
6. Wenzel RL, Tipton VJ. Ectoparasites of Panama. In: Chicago, Field Museum of Natural History. Chicago: University of Illinois Urbana-Champaign; 1966. p. 882.
7. Billeter SA, Hayman DTS, Peel AJ, Baker K, Wood JLN, Cunningham A, et al. *Bartonella* species in bat flies (Diptera: Nycteribiidae) from western Africa. Parasitology. 2012;139:324–9. https://doi.org/10.1017/S0031182011002113
8. Judson SD, Frank HK, Hadly EA. *Bartonellae* are prevalent and diverse in Costa Rican bats and bat flies. Zoonoses Public Health. 2015;62:609–17. https://doi.org/10.1111/zph.12188
9. Bai Y, Kosoy M, Recuenco S, Alvarez D, Moran D, Turmelle A, et al. *Bartonella* spp. in bats, Guatemala. Emerg Infect Dis. 2011;17:1269–72. https://doi.org/10.3201/eid1707.101867

Address for correspondence: Thomas Gillespie, Emory University, Ste E510, 400 Dowman Dr, Atlanta, GA 30222, USA; email: thomas.gillespie@emory.edu

COMMENT LETTERS

Predictors of Nonseroconversion after SARS-CoV-2 Infection

Benjamin Davido, Karim Jaffal, Djillali Annane, Christine Lawrence, Elyanne Gault, Pierre De Truchis

Author affiliations: Université Versailles-Saint-Quentin, Versailles, France (B. Davido, K. Jaffal, D. Annane); Maladies infectieuses, Université Paris-Saclay, Garches, France (B. Davido, K. Jaffal, E. Gault, P. De Truchis); Médecine Intensive et réanimation, Université Paris-Saclay, Boulogne-Billancourt, France (D. Annane); Virologie, Université Paris-Saclay, AP-HP Hôpital Ambroise Paré, Boulogne-Billancourt (C. Lawrence, E. Gault)

DOI: https://doi.org/10.3201/eid2802.211971

To the Editor: Recently, Liu et al. (*1*) described the predictors of nonseroconversion after severe acute respiratory syndrome coronavirus 2 (SARS-CoV-2) infection (36.1% of cases), where nonresponders had significant higher cycle threshold (C_t) and were younger. Although a recent study showed that 1 dose of mRNA vaccine is sufficiently effective in previously infected persons (*2*), Reynolds et al. reported a previously infected vaccinee who never seroconverted (*3*). We report the case of a previously infected vaccinee who did not seroconvert and was subsequently reinfected.

In April 2020, a 55-year-old female nursing manager had mild SARS-CoV-2 pneumonia diagnosed that did not require admission, confirmed by weakly positive genes E and RNA-dependent RNA polymerase PCR testing (both C_t >33, near the limit of detection using homemade techniques). Concomitantly, her husband experienced symptoms and also tested positive, supporting that the woman's case was not a false-positive. One month later, SARS-CoV-2 serology revealed no detectable antibodies to nucleocapsid or spike (S) proteins.

Despite a low risk for SARS-CoV-2 reinfection in a healthcare worker without underlying conditions (*4*) and having been vaccinated with 1 dose of mRNA BNT162b2 (Pfizer-BioNTech, https://www.pfizer.com) in April 2021, as recommended for previously infected persons, the woman was reinfected in September 2021 by the Delta variant. She had mild symptoms and a high estimated viral load (C_t 26 for genes E and N2). Serologic testing at the time of the first detection of reinfection revealed a relatively low titer of 20 binding antibody units/mL of S antibodies, which then increased to 243 BAU/mL 1 month after reinfection. Testing to rule out immune deficiency (serum protein electrophoresis, quantitative immunoglobulin assay, and assessment for complement deficiency) detected no abnormalities.

Our findings support a 2-dose vaccine policy for previously infected persons, as applied in the United States. This cautious approach is even more relevant because neutralizing antibody titers are substantially reduced in patients infected with the Delta variant (*5*) and in light of efforts to promote a third dose of vaccine, to ensure a stable antibody level over time in

persons at high risk of being hospitalized for severe coronavirus disease.

B.D., C.L., K.J., and E.G. conceptualized and designed the manuscript; coordinated and drafted the initial manuscript; and reviewed the manuscript. P.D.T., D.A., and B.D. reviewed and revised the manuscript. All authors approved the final manuscript as submitted and agree to be accountable for all aspects of the work in ensuring that questions related to the accuracy or integrity of any part of the work are appropriately investigated and resolved.

References

1. Liu W, Russell RM, Bibollet-Ruche F, Skelly AN, Sherrill-Mix S, Freeman DA, et al. Predictors of nonseroconversion after SARS-CoV-2 infection. Emerg Infect Dis. 2021;27:2454–8. https://doi.org/10.3201/eid2709.211042
2. Hirotsu Y, Amemiya K, Sugiura H, Shinohara M, Takatori M, Mochizuki H, et al. Robust antibody responses to the BNT162b2 mRNA vaccine occur within a week after the first dose in previously infected individuals and after the second dose in uninfected individuals. Front Immunol. 2021;12:722766. https://doi.org/10.3389/fimmu.2021.722766
3. Reynolds CJ, Pade C, Gibbons JM, Butler DK, Otter AD, Menacho K, et al.; UK COVIDsortium Immune Correlates Network. UK COVIDsortium Investigators. Prior SARS-CoV-2 infection rescues B and T cell responses to variants after first vaccine dose. Science. 2021;372:1418–23. https://doi.org/10.1126/science.abh1282
4. Davido B, De Truchis P, Lawrence C, Annane D, Domart-Rancon M, Gault E, et al. SARS-CoV-2 reinfections among hospital staff in the greater Paris area. Travel Med. 2021;28:taab058. https://doi.org/10.1093/jtm/taab058
5. Planas D, Veyer D, Baidaliuk A, Staropoli I, Guivel-Benhassine F, Rajah MM, et al. Reduced sensitivity of SARS-CoV-2 variant Delta to antibody neutralization. Nature. 2021;596:276–80. https://doi.org/10.1038/s41586-021-03777-9

Address for correspondence: B. Davido, Infectious Diseases Department, Raymond Poincaré Teaching Hospital, Garches 92380, France; email: benjamin.davido@aphp.fr

High Infection Attack Rate after SARS-CoV-2 Delta Surge, Chattogram, Bangladesh

Sonia T. Hegde,[1] Taufiqur Rahman Bhuiyan,[1] Marjahan Akhtar, Taufiqul Islam, Juan Dent Hulse, Zahid Hasan Khan, Ishtiakul Islam Khan, Shakeel Ahmed, Mamunur Rashid, Rumana Rashid, Emily S. Gurley, Tahmina Shirin, Ashraful Islam Khan, Andrew S. Azman[2], Firdausi Qadri[2]

Author affiliations: Johns Hopkins Bloomberg School of Public Health, Baltimore, MD, USA (S.T. Hegde, J. Dent Hulse, E.S. Gurley, A.S. Azman); International Centre for Diarrhoeal Disease Research, Bangladesh (T.R. Bhuiyan, M. Akhtar, T. Islam, Z.H. Khan, I.I. Khan, A.I. Khan, F. Qadri); Bangladesh Institute of Tropical and Infectious Diseases, Chattogram, Bangladesh (S. Ahmed, M. Rashid, R. Rashid); Institute of Epidemiology, Disease Control and Research, Dhaka, Bangladesh (T. Shirin); Institute of Global Health, University of Geneva, Geneva, Switzerland (A.S. Azman)

DOI: https://doi.org/10.3201/eid2802.212417

To the Editor: After an initial serosurvey (*1*) to understand the prevalence of total antibodies to severe acute respiratory syndrome coronavirus 2 (SARS-CoV-2) in residents of the Sitakunda subdistrict was completed, a large epidemic wave hit the area, and nearly all publicly available samples genotyped via GISAID (https://www.gisaid.org) were the SARS-CoV-2 Delta variant (*2*,*3*). Of the total confirmed infections during the entire pandemic from the Chattogram District, 48.4% (48,253) were reported June 14–August 31, 2021. During September 21–October 9, 2021, we revisited all enrolled households and collected blood from 84% (1,938/2,307) of those tested in our initial serosurvey (Appendix Figure, https://wwwnc.cdc.gov/EID/article/28/2/21-2417-App1.pdf).

We tested 721 of the initially seronegative participants who agreed to a second blood draw using the same Wantai total Ab receptor-binding domain assay and found that 68% (492/721) had seroconverted in the approximately 3-month period between survey rounds (Appendix Table 1). Participation in the second round was not associated with serostatus in the first round. Among seropositive participants, 87 (18%) had received ≥1 dose of SARS-CoV-2 vaccine, and 28.3% (140/492) of those who seroconverted reported having had a sud-

[1]These first authors contributed equally to this article.

[2]These senior authors contributed equally to this article.

den onset of ≥1 coronavirus disease–related symptom since the first serosurvey. Assuming no seroreversion between rounds, 88.2% (1,709/1,938) of participants providing blood in both rounds were seropositive by the second serosurvey. Using our previous methods (*1*), we estimated an adjusted seroprevalence after the Delta wave of 88.2% (95% CrI 85.4%–90.8%) for all participants and 87.9% (95% CrI 85.2%–90.6%) when including only unvaccinated participants (Appendix Table 2). Seroprevalence among children 1–9 years of age remained significantly lower when compared with 25–34 year olds (28% reduced risk for 1–4 and 16% for 5–9 year age groups; p<0.00001), unlike other age groups (Appendix Table 2). Mirroring evidence from around the world, the Delta variant led to a significant increase in SARS-CoV-2 transmission in Bangladesh, leaving the vast majority of people with detectable serum antibodies.

Acknowledgements

The authors thank the Ministry of Health and Family Welfare (MOHFW) of Bangladesh. The authors also thank the staff of icddr,b for their dedicated work in the field and laboratory during this pandemic situation. icddr,b is thankful to and supported by the governments of Bangladesh, Canada, Sweden, and the United Kingdom.

This work was supported by the Bill and Melinda Gates Foundation (grant number INV-021879).

References

1. Bhuiyan TR, Hulse JD, Hegde ST, Akhtar M, Islam T, Khan ZH, et al. SARS-CoV-2 seroprevalence before Delta variant surge, Chattogram, Bangladesh, March–June 2021. Emerg Infect Dis. 2022 Feb [cited 2021 Nov 29]. https://doi.org/10.3201/eid2802.211689
2. dashboard: Bangladesh [cited 2021 Nov 21]. https://covid19.who.int/region/searo/country/bd
3. GISAID. COVID-19 lineages and variants [cited 2021 Nov 21]. http://www.gisaid.org

Address for correspondence: Andrew S. Azman, Johns Hopkins Bloomberg School of Public Health, 615 N. Wolfe St, Baltimore, MD 21205, USA; email: azman@jhu.edu

Legionellosis: Diagnosis and Control in the Genomic Era

Jacob Moran-Gilad and Rachel E. Gibbs, editors; Caister Academic Press, 2020, Poole, UK; ISBN: 978-1-913652-53-1 (paperback); 978-1-913652-54-8 (e-book) Pages: 336; Price: $250

DOI: http://doi.org/10.3201/eid2802.212055

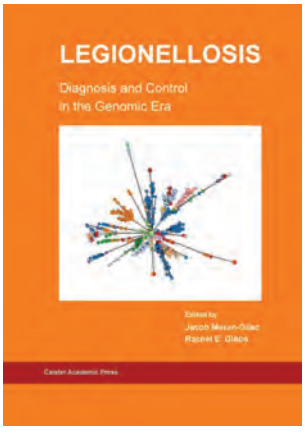

Hundreds of books and textbook chapters, and thousands of journal review articles, have been published on Legionnaires' disease and *Legionella* spp. bacteria over the past 45 years, making it important to decide whether this new and quite expensive compilation of reviews is worth acquiring. The field has become so specialized that even those who know one aspect of it may need a good review of other aspects to easily catch up on recent trends. The book contains chapters on the freshwater ecology of the bacterium; molecular and pathogenic aspects of virulence-associated bacterial secretion systems; very selected aspects of epidemiology; clinical aspects and treatment; laboratory diagnosis; and strain typing methods from serologic to whole-genome sequencing. Some chapters are more current than others. The most recent references for several chapters were published in 2016, and only 1 chapter cites references published in 2020. The book is lightly edited; some of the chapters contain overlapping material, but overall it has few typographical or spelling errors. Not all of the figures are properly labeled; for example, the figure legends in chapter 6 are reversed, and not all of the figure legends in chapter 3 fully explain the meanings of different colors and abbreviations.

I found that several of the chapters contained quite useful information that would be hard to find elsewhere, including a thorough review of *L. pneumophila* virulence secretory systems, as well as a review of the freshwater ecology of the bacterium, the clinical microbiology and clinical significance of *Legionella* spp. other than *L. pneumophila*, and regulatory and risk management strategies for control of the disease. Other readers, depending on their fields of interest and expertise, will find other chapters of particular interest. The chapter on non–whole-genome sequencing methods for strain typing for epidemiologic investigation is well done and could be of interest for those trying to dissect the older literature. Missing from the book, presumably by design, are chapters reviewing in detail the ecology of the bacterium in the built environment, practical guidance on outbreak investigation, advanced techniques in epidemiologic source investigation, molecular and cellular pathogenesis other than secretion systems, and the molecular evolution of the bacterium, all of which can be found in other sources.

Is this book good value for money? Perhaps not for those who have a narrow interest in a specific field, because there are more up-to-date reviews on many of the topics in journal articles and some textbooks. For those who want to gain an overview of the topics covered in the book, some of which are more comprehensive than those found in textbooks or recent reviews, this may be a useful addition to their libraries.

Paul H. Edelstein

Author affiliation: University of Pennsylvania, Philadelphia, Pennsylvania, USA; University of Cambridge, Cambridge, UK

Address for correspondence: Paul H. Edelstein, University of Pennsylvania, 3400 Spruce St, Philadelphia, PA 19104-4222, USA; email: paul.edelstein@pennmedicine.upenn.edu

P. R. Morley Horder, designer (1870–1944); J. Starkie Gardner Ltd, fabricator (years active 1884–1976). ***Gilded Vectors of Disease*****, 1912**. Gilded bronze and iron railings. 10.2 in x 10.6 in/26 cm x 27 cm. Images courtesy of Library & Archives Service, London School of Hygiene & Tropical Medicine, London, United Kingdom.

Deadly, Dangerous, and Decorative Creatures

Byron Breedlove

According to the World Health Organization, vectorborne diseases account for more than 17% of all infectious diseases, lead to more than 700,000 deaths annually, and contribute to a large overall global burden of debilitating disease. Mosquitoes, ticks, and fleas are among the arthropods responsible for transmitting many of the myriad bacteria, viruses, and parasites that cause vectorborne diseases—as are some mammals.

In terms of infectious disease transmission, mosquitoes are considered the most dangerous animals on earth. They are vectors that can spread the *Plasmodium* parasites that cause malaria, as well as chikungunya, West Nile, yellow fever, and Zika viruses, plus 4 types of dengue virus. Ticks, responsible for causing most vectorborne diseases in the United

Author affiliation: Centers for Disease Control and Prevention, Atlanta, Georgia, USA

DOI: https://doi.org/10.3201/eid2802.AC2802

Figure: Missing from the cover collage of the bronze figures is this bedbug. Although a worldwide problem, bedbugs are not a disease vector.

States and Europe, are vectors for agents causing Lyme disease, ehrlichiosis, babesiosis, anaplasmosis, Rocky Mountain spotted fever, Crimean-Congo hemorrhagic fever, and Heartland virus disease. Fleas carry pathogens that cause diseases such as plague and murine typhus. Other vectors include the body louse, which spreads louse-borne relapsing fever; the tsetse fly, which transmits African trypanosomiasis (sleeping sickness); and sand flies, which transmit the pathogen that causes leishmaniasis. Small mammals, particularly rodents, are vectors for the agents of plague, hantavirus infection, rat-bite fever, Lassa fever, and salmonellosis.

This month's cover features a collage of images arrayed like mug shots for a number of these creatures responsible for many vectorborne diseases across the globe. To many involved in the disciplines of public health and infectious disease, these images will be familiar as the "Gilded Vectors of Disease," an ornate, Art-Deco bestiary of sculpted bronze figures bracketing each side of 15 iron balconies located across the front and sides of the London School of Hygiene & Tropical Medicine. Each of these relatively small sculptures, measuring approximately 26 cm × 27 cm, appears three times across the various balconies and is bolted onto an iron square that encompasses much of the vector's body. Various wings, legs, and tails that extend in all directions help distinguish one vector from the other.

The bronze figures included in the cover collage are seven arthropods—six insects and one arachnid—one mammal, and one reptile. The insects are an *Aedes* mosquito, *Anopheles* mosquito (the one with its tail pointing upward), body louse, flea, tsetse fly, and housefly; the arachnid is a tick, and the mammal a rat. The snake, an Indian cobra, was included because it makes the cover image symmetrical, and snakes and other reptiles carry a range of pathogens including bacteria, viruses, parasites, and worms. Although reptiles are not considered disease vectors, their possible role as reservoirs of zoonotic parasites has garnered new attention among some researchers, including Mendoza-Roldan et al.

Precise details on whether an individual or a committee approved the creation and installation of the 10 animals that festoon the school's balconies are lost to history. Researcher and writer Ann Datta notes, "The actual selection process that led to the particular choice of animals in the frieze is unknown." She recounts that during 1926–1928, architects Percy Morley Horder and Verner Rees designed "the steel-framed building with a Portland stone façade" and that Horder was responsible for designing the frieze. The iron balconies, and presumably the bronzed creatures, were the handiwork of J. Starkie Gardner Ltd., Decorative Metal Workers, from the Southfields district of inner London (the firm ceased operations in 1976).

Datta states that "All the animal figures are somewhat stylized although most retain the essential characters for scientific identification to genus level." Created nearly a century ago, the Gilded Vectors of Disease are enduring symbols of the importance of national and international public health efforts to detect, understand, prevent, and track vectorborne diseases.

Bibliography

1. Campbell-Lendrum D, Manga L, Bagayoko M, Sommerfeld J. Climate change and vector-borne diseases: what are the implications for public health research and policy? Philos Trans R Soc Lond B Biol Sci. 2015;370:20130552. https://doi.org/10.1098/rstb.2013.0552
2. Datta A. The gilded vectors of disease: sculptures at the London School of Hygiene & Tropical Medicine [cited 2021 Dec 3]. https://blogs.lshtm.ac.uk/library/2019/05/10/the-gilded-vectors-of-disease-sculptures-at-the-london-school-of-hygiene-tropical-medicine
3. Gates B. The deadliest animal in the world [cited 2021 Dec 13]. https://www.gatesnotes.com/Health/Most-Lethal-Animal-Mosquito-Week
4. London School of Hygiene & Tropical Medicine. The building [cited 2021 Dec 3]. https://www.lshtm.ac.uk/aboutus/introducing/history/building
5. Mendoza-Roldan JA, Modry D, Otranto D. Zoonotic parasites of reptiles: a crawling threat. Trends Parasitol. 2020;36:677–87. https://doi.org/10.1016/j.pt.2020.04.014
6. Rochlin I, Ninivaggi DV, Benach JL. Malaria and Lyme disease–the largest vector-borne US epidemics in the last 100 years: success and failure of public health. BMC Public Health. 2019;19:804. https://doi.org/10.1186/s12889-019-7069-6
7. World Health Association. Vector-borne diseases [cited 2021 Dec 13]. https://www.who.int/news-room/fact-sheets/detail/vector-borne-diseases

Address for correspondence: Byron Breedlove, EID Journal, Centers for Disease Control and Prevention, 1600 Clifton Rd NE, Mailstop H16-2, Atlanta, GA 30329-4027, USA; email: wbb1@cdc.gov

EMERGING INFECTIOUS DISEASES®

Upcoming Issue, March 2022 • Mycobacterial Infections

- Eight-Year Retrospective Study of Healthcare- and Aesthetic Procedure–Associated Infections Caused by Nontuberculous Mycobacteria, France
- Airborne Transmission of SARS-CoV-2 Delta Variant within Tightly Monitored Isolation Facility, New Zealand (Aotearoa)
- Rising Incidence of Legionnaires' Disease and Associated Epidemiologic Patterns, United States, 1992–2018
- Vertical Transmission of SARS-CoV-2 and Death of Neonate
- Overseas Treatment of Latent Tuberculosis Infection in US–Bound Immigrants
- Effectiveness of 3 COVID-19 Vaccines in Preventing SARS-CoV-2 Infections in a Cohort of Inhabitants in Aragon, Spain, January–May 2021
- Infection Control Measures and Prevalence of Severe Acute Respiratory Syndrome Coronavirus-2 IgG among 4,554 University Hospital Employees, Munich, Germany
- SARS-CoV-2 Period Seroprevalence and Related Factors, Hillsborough County, Florida, October 2020–March 2021
- COVID-19 Vaccination Coverage, Behaviors, and Intentions among Previously Infected Adults, United States
- Novel Hendra Virus Variant Detected by Sentinel Surveillance of Horses in Australia
- Neutralizing Enterovirus D68 Antibodies in Children after 2014 Outbreak, Kansas City, Missouri, USA
- Genomic and Phenotypic Insights for Toxigenic Clinical *Vibrio cholerae* O141
- Competitive Advantage of SARS-CoV-2 Variant of Concern over Variant of Interest as Indicated by Spatiotemporal Analyses, New York, New York, USA
- Nowcasting (Short-Term Forecasting) of COVID-19 Hospitalizations Using Syndromic Healthcare Data, Sweden, 2020
- Development and Evaluation of Statewide Prospective Spatiotemporal Legionellosis Cluster Surveillance, New Jersey, USA
- SARS-CoV-2 from Rapid Antigen Test–Negative, Reverse Transcription PCR–Positive Specimen Pairs of Symptomatic Persons
- Transovarial Transmission of Heartland Virus by Invasive Asian Longhorned Ticks under Laboratory Conditions
- Epidemiology of COVID-19 after Emergence of SARS-CoV-2 Gamma Variant, Brazilian Amazon, 2020–2021
- Long-Term Symptoms among COVID-19 Survivors in Prospective Cohort Study, Brazil
- *Encephalitozoon cuniculi* and Extraintestinal Microsporidiosis in Bird Owners
- *Mycobacterium leprae* Infection in a Wild Nine-Banded Armadillo, Nuevo Leon, Mexico
- *Mycobacterium mageritense* Lymphadenitis in Child
- Restaurant-Based Measures to Control Community Transmission of COVID-19, Hong Kong

Complete list of articles in the March issue at https://wwwnc.cdc.gov/eid/#issue-286

Earning CME Credit

To obtain credit, you should first read the journal article. After reading the article, you should be able to answer the following, related, multiple-choice questions. To complete the questions (with a minimum 75% passing score) and earn continuing medical education (CME) credit, please go to http://www.medscape.org/journal/eid. Credit cannot be obtained for tests completed on paper, although you may use the worksheet below to keep a record of your answers.

You must be a registered user on http://www.medscape.org. If you are not registered on http://www.medscape.org, please click on the "Register" link on the right hand side of the website.

Only one answer is correct for each question. Once you successfully answer all post-test questions, you will be able to view and/or print your certificate. For questions regarding this activity, contact the accredited provider, CME@medscape.net. For technical assistance, contact CME@medscape.net. American Medical Association's Physician's Recognition Award (AMA PRA) credits are accepted in the US as evidence of participation in CME activities. For further information on this award, please go to https://www.ama-assn.org. The AMA has determined that physicians not licensed in the US who participate in this CME activity are eligible for *AMA PRA Category 1 Credits*™. Through agreements that the AMA has made with agencies in some countries, AMA PRA credit may be acceptable as evidence of participation in CME activities. If you are not licensed in the US, please complete the questions online, print the AMA PRA CME credit certificate, and present it to your national medical association for review.

Article Title

Clinical and Laboratory Characteristics and Outcome of Illness Caused by Tick-Borne Encephalitis Virus without Central Nervous System Involvement

CME Questions

1. Which one of the following statements best describes the normal disease course of tick-borne encephalitis virus (TBEV)?

A. At least 70% of patients infected with TBEV are asymptomatic
B. The initial phase of illness without central nervous system (CNS) inflammation usually lasts 10 to 14 days
C. Meningitis is rare in children with TBEV with CNS symptoms
D. Encephalitis occurs in less than 10% of adults with TBEV with CNS symptoms

2. Which one of the following statements regarding clinical characteristics of patients with TBEV in the current study is most accurate?

A. Less than one quarter of patients reported a history of tick bite
B. The median time from any known tick bite to illness onset was 14 days
C. The median total duration of illness was 16 days
D. Slightly more than one third of patients were hospitalized

3. Which one of the following trends were noted in laboratory values during infection with TBEV in the current study?

A. Leukopenia improved over the course of infection
B. Thrombocytopenia improved over the course of infection
C. Transaminitis improved over the course of infection
D. Most patients had a positive immunoglobulin M (IgM) test for TBEV at the time of positive polymerase chain reaction (PCR)

4. What approximate percentage of patients in the current study with a positive TBEV PCR test developed overt signs of CNS infection?

A. 12%
B. 33%
C. 51%
D. 84%

Earning CME Credit

To obtain credit, you should first read the journal article. After reading the article, you should be able to answer the following, related, multiple-choice questions. To complete the questions (with a minimum 75% passing score) and earn continuing medical education (CME) credit, please go to http://www.medscape.org/journal/eid. Credit cannot be obtained for tests completed on paper, although you may use the worksheet below to keep a record of your answers.

You must be a registered user on http://www.medscape.org. If you are not registered on http://www.medscape.org, please click on the "Register" link on the right hand side of the website.

Only one answer is correct for each question. Once you successfully answer all post-test questions, you will be able to view and/or print your certificate. For questions regarding this activity, contact the accredited provider, CME@medscape.net. For technical assistance, contact CME@medscape.net. American Medical Association's Physician's Recognition Award (AMA PRA) credits are accepted in the US as evidence of participation in CME activities. For further information on this award, please go to https://www.ama-assn.org. The AMA has determined that physicians not licensed in the US who participate in this CME activity are eligible for *AMA PRA Category 1 Credits*™. Through agreements that the AMA has made with agencies in some countries, AMA PRA credit may be acceptable as evidence of participation in CME activities. If you are not licensed in the US, please complete the questions online, print the AMA PRA CME credit certificate, and present it to your national medical association for review.

Article Title

Epidemiology of Hospitalized Patients with Babesiosis, United States, 2010–2016

CME Questions

1. Which one of the following statements regarding the pathology and outcomes of babesiosis is most accurate?

A. There are no reports of subclinical babesiosis
B. *Babesia* spp. primarily infect respiratory epithelial cells
C. Complications of babesiosis include anemia, renal failure, and cardiorespiratory failure
D. Transfusion-transmitted babesiosis has a better prognosis than tick-related infection

2. Which one of the following trends in babesiosis were noted in the current study?

A. The rate of severe babesiosis requiring hospital admission remained stable over time
B. The median age of patients admitted with babesiosis was 32 years
C. Nearly two thirds of patients with babesiosis were male
D. Nearly half of patients with babesiosis were Black

3. Where and when was babesiosis most common in the current study?

A. Spring; Midwest
B. Fall; Southeast
C. Summer; Rocky Mountains
D. Summer; New England

4. What was the most common complication of babesiosis in the current study?

A. Acute renal failure
B. Respiratory failure
C. Cardiac failure
D. Hepatic failure

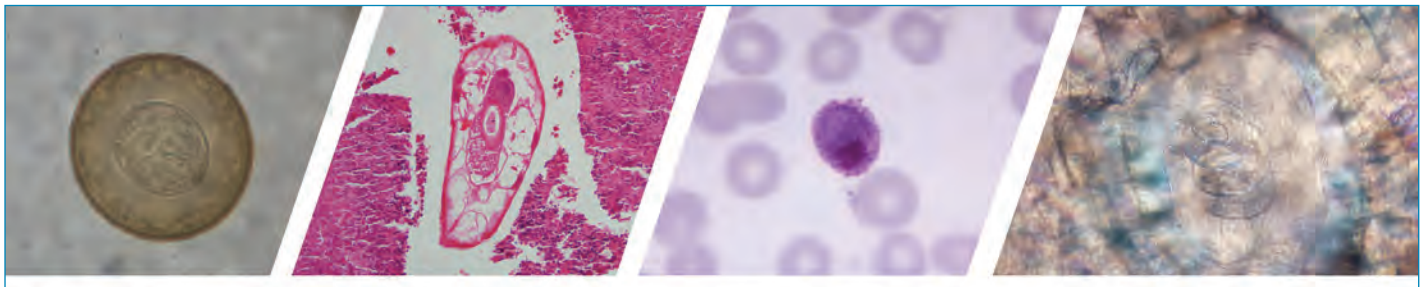

DPDx

Diagnostic Assistance and Training in Laboratory Identification of Parasites

A free service of CDC available to laboratorians, pathologists, and other health professionals in the United States and abroad

- Diagnosis from photographs of worms, histological sections, fecal, blood, and other specimen types
- Expert diagnostic review
- Formal diagnostic laboratory report
- Submission of samples via secure file share

Visit the DPDx website for information on laboratory diagnosis, geographic distribution, clinical features, parasite life cycles, and training via Monthly Case Studies of parasitic diseases.

www.cdc.gov/dpdx
dpdx@cdc.gov

CS272346-DE

U.S. Department of Health and Human Services
Centers for Disease Control and Prevention